University of Alberta

Age, origin and composition of the Attawapiskat lithospheric mantle and its diamonds (western Superior craton, Canada)

by

Karen Vena Smit

A thesis submitted to the Faculty of Graduate Studies and Research in partial fulfillment of the requirements for the degree of

Doctor of Philosophy

Department of Earth and Atmospheric Sciences

Fall 2013
Edmonton, Alberta

Abstract

This study reports results from peridotitic and eclogitic xenoliths and diamond samples from the Attawapiskat area to understand the processes of craton formation and modification in the Superior lithospheric mantle. These diamondiferous kimberlites also provide an opportunity to study the association of a primary diamond deposit (Victor) with a post-Archaean rift system - the Midcontinent Rift which impacted the southern Superior at $\sim$ 1.1 Ga. Existence of a depleted mantle reservoir beneath the Attawapiskat area since the Palaeoarchaean is indicated by T_{RD} ages in sulphides and PGE's trapped in olivine. Mg# up to 93.6 in olivine indicates high degrees of partial melting leading to harzburgitic - dunitic residues. High Cr# in garnet and positive slopes in depleted garnet $HREE_N$, indicate that melting occurred during fractional polybaric melt extraction ending at low pressures. Low-Mg eclogites have shallow origins as plagioclase-bearing protoliths likely in former oceanic crust, emplaced into the SCLM by subduction during the Archaean. Partial melting of low-Mg eclogites and interaction of these melts with overlying peridotite in the mantle wedge resulted in the formation of the high-Mg eclogites and pyroxenites. T_{RD} ages of $\sim$2.7 Ga in peridotite with residual PGE_N patterns also indicate melting in the mantle related to subduction - accretion and hydrous melts infiltrating the overlying mantle wedge led to I-PGE alloy

formation. Diamond destruction occurred in the Attawapiskat lithospheric mantle due to the thermal impact of the Midcontinent Rift - seen in an elevated geotherm and narrow "diamond window" in 1.1 Ga kimberlites - with high mantle residence temperatures recorded in pre-rift diamonds. Rift basalts interacted with variably depleted peridotite, leading to P-PGE-enrichment and Mesoproterozoic T_{RD} ages. Older depleted domains are, however preserved. After the thermal impact of the rift subsided, diamond-stable conditions were extended to shallower depths in the lithosphere and diamonds sampled by post-rift kimberlites, formed after the Midcontinent Rift. These diamonds are likely to be both lherzolitic and eclogitic - pyroxenitic, as indicated by their $\delta^{13}C$ compositions, and favourable high pressure compositions in both lherzolitic and high-Mg eclogitic - pyroxenitic garnets at Attawapiskat.

Acknowledgements

Thank you to my PhD supervisor, Thomas Stachel, for his guidance during the past 4 years. His German precision greatly improved my writing and I thank him for being timely with edits to many drafts of this thesis, especially during the summer when much else was happening. Thank you also for paying me for half the time I was at U of A, so that I wouldn't have to TA...

Thank you also to Graham Pearson for all always having an open door and for the many discussions during my final year that helped me shape some of the ideas presented here.

De Beers Canada is thanked for collecting and donating samples from their Victor and Delta kimberlites. Stephan Kurszlaukis along with Alexandrina Fulop are thanked for making a sampling trip to the De Beers core shed in Sudbury possible.

Chuck Fipke and Chad Ulansky from Metalex Ventures are thanked for donating diamonds from their T1 and U2 kimberlites. Thank you also to Herman Grütter for his help in obtaining the diamonds from Metalex.

Sergei Matveev and Guangcheng Chen are thanked for support in the electron microprobe and quadrupole mass spectrometer laboratories. Jingao Liu, Krystle Moore, David van Acken, Sarah Woodland and Barbara Ziger kindly and patiently assisted in the clean and TIMS laboratories. Kathy Mather kindly offered her help with Fitplot geotherms.

Research funding was provided through the Geomapping for Energy and Minerals Programme (Diamonds) of the Geological Survey of Canada and an associated NSERC CRD grant with contributions from De Beers Canada. Through Thomas Stachel, funding was received from a NSERC Discovery Grant and the Canada Research Chairs Programme. Through Graham Pearson, funding for some data in Chapter 5 was received through the Canada Excellence Research Chairs Programme. Scholarships I received through the U of A are gratefully acknowledged.

My supervisors during my MSc research - John Gurney, Steve Shirey, Steve

Richardson and Anton le Roex - without whose friendly encouragement I probably wouldn't have considered a PhD. Thank you also for providing good (?) reference letters, because, I know I didn't study hard enough during my undergrad to make it to U of A without your support...

Thank you to everyone in Edmonton and at U of A for making my stay so memorable. In particular, my officemates at various times during my PhD - Katie Smart and Josh Davies - proved to be willing and able drinking buddies, and also valuable sounding boards for many ideas in this thesis. I appreciate you both allowing me to crash at your respective places during the beginning and end of my time in Edmonton!

Contents

List of Tables

List of Figures

List of Symbols and Abbreviations

$\sim$	approximately
e.g.	for example
‰	parts per thousand or per mille
%B	Percentage of nitrogen in a diamond in B centres
δ^{13}C	Carbon isotope composition relative to the international V-PDB standard
CCIM	Canadian centre for isotopic microanalysis
CL	Cathodoluminescence
cps	counts per second
Cr#	100 x Cr/(Cr+Al)
EPMA	Electron probe micro analysis
Eu/Eu*	Eu anomaly calculated as calculated as $Eu_N/\sqrt{Sm_N X Gd_N}$
ϵ_{Hf}	Deviation of $^{176}Hf/^{177}Hf$ from a bulk earth reservoir
$\varepsilon_{\mathrm{Nd}}$	Deviation of $^{143}Nd/^{144}Nd$ from a bulk earth reservoir
γ_{Os}	Deviation of $^{187}Os/^{188}Os$ from a bulk earth reservoir
G1	Classification for mantle-derived megacrystic garnets
G3	Classification for mantle-derived eclogitic garnets
G4	Classification for mantle-derived eclogitic / pyroxenitic garnets

G5	Classification for mantle-derived pyroxenitic garnets
G9	Classification for mantle-derived lherzolitic garnets
G10	Classification for mantle-derived harzburgitic garnets
G11	Classification for mantle-derived Ti-metasomatised garnets
G12	Classification for mantle-derived wehrlitic garnets
G*D	"D" suffix denotes strong probability that garnet originates from the diamond stability field
Ga	Billions of years ago
GPa	Gigapascal
ICP-MS	Inductively coupled plasma-mass spectrometry
i.e.	that is
FTIR	Fourier transform infrared spectroscopy
HREE	Heavy rare earth element
HSE	Highly siderophile element
INAA	Instrumental neutron activation analysis
I-PGE	Iridium-group PGE's - Os, Ir, Ru
LILE	Large ion lithophile element
LREE	Light rare earth element
Ma	Millions of years ago
Mg#	100 x Mg/(Mg+Fe)
MORB	Mid-ocean ridge basalts
MREE	Middle rare earth element
N	Acid normality
$_N$	Subscript to indicate normalised values
NIST	National institute of standards and technology
$\delta^{18}O$	Oxygen isotope composition relative to the international V-SMOW standard
OIB	Ocean island basalt
PGE	Platinum group element
P-PGE	Platinum-group PGE's - Pt, Pd
ppb	parts per billion
ppm	parts per million

PT	Pressure and temperature
PUM	Primitive upper mantle
REE	Rare earth element
σ	Sigma or one standard deviation of the mean
SE	Standard error of the mean
SECP	Southeastern Churchill Province
SEM	Scanning electron microscope
SIMS	Secondary ion mass spectrometry
SCLM	Sub-continental lithospheric mantle
TIMS	Thermal ionisation mass spectrometry
T_{MA}	Re-Os model age
T_{RD}	Rhenium depletion age
Type IaA	Nitrogen aggregated in diamond A centres
Type IaAB	Nitrogen concentrated in diamond A and B centres
Type IaB	Nitrogen aggregated in diamond B centres
Type II	Nitrogen-free diamonds
UML	Ultramafic lamprophyres
V-PDB	Vienna-Pee-Dee-belemnite standard
V-SMOW	Vienna-standard-mean-ocean-water standard
wt%	Weight percent

Chapter 1

Introduction

1.0.1 The sub-continental lithospheric mantle

Old portions of continents that have been stable since the Archaean are known as cratons. Their longevity is due to presence of thick lithospheric roots, that have distinct thermal, chemical and seismic properties to the underlying asthenosphere. The sub-continental lithospheric mantle (SCLM) is predominantly composed of peridotite, that has been depleted through high degrees of melt extraction (removal of Al, Ca, Fe) to highly magnesian harzburgitic and dunitic residues (e.g., Boyd and Mertzman, 1987; Baker and Stolper, 1994; Walter, 1998). During melt extraction, the radiogenic elements (Th, U, K) and H_2O are also efficiently removed, resulting in a residue that is cooler and has increased buoyancy and viscosity, and a lower density relative to the asthenosphere. These combined attributes contribute to the SCLM's long-term isolation from mantle convection (e.g., Jordan, 1975; Boyd and McCallister, 1976).

There are competing models for the formation of cratonic lithospheric roots. Melt depletion may have occurred at high pressures in a plume setting (e.g., Boyd, 1989; Arndt et al., 1998; Herzberg, 1999; Aulbach, 2012) or at lower pressures with initial melting at a mid-ocean ridge followed by later subduction-accretion (e.g., Helmstaedt and Schulze, 1989; Bulatov et al., 1991; Canil and Wei, 1992; Stachel et al., 1998; Canil, 2004; Bernstein et al., 2007; Pearson and Wittig, 2008; Herzberg and Rudnick, 2012).

Although mainly composed of depleted peridotite, the SCLM also contains a minor mafic component - in the form of eclogite, which consists of omphacitic clinopyroxene and garnet, with or without minor kyanite and coesite (e.g., Coleman et al., 1965; Carswell, 1990). Many kimberlite localities worldwide sample both low-Mg and high-Mg varieties, for example, Bellsbank and Premier on the Kaapvaal craton (Taylor and Neal, 1989; Neal et al., 1990; Dludla et al., 2006), Koidu (Man craton; Barth et al., 2001, 2002a), Udachnaya (Siberian craton; Jerde et al., 1993; Beard et al., 1996; Snyder et al., 1997) and Diavik (Slave craton; Aulbach et al., 2007).

Eclogite can have variable origins, as high pressure mantle melts or former oceanic crust that was emplaced to the SCLM by subduction (e.g., O'Hara and Yoder, 1967; Caporuscio and Smyth, 1990; Helmstaedt and Doig, 1975; Jacob, 2004), therefore, the nature of it's origin in the SCLM can provide important insights into the formation and evolution of the SCLM.

The Superior is the largest exposure of Archaean crust on Earth (see map of worldwide cratonic regions in Bleeker, 2003). However, its SCLM has not been studied to the same extent as, for example, the Kaapvaal, Slave and Siberian cratons, and consequently, details of the composition of the lithospheric root and the mechanism of its formation are sparce (see for example, reviews on craton formation by Pearson et al., 2003; Carlson et al., 2005; Pearson and Wittig, 2013).

1.0.2 Attawapiskat kimberlites

Here we study samples from the Jurassic Attawapiskat kimberlites in the western Superior Province, including Victor which is the first diamond mine on the Superior craton. These diamondiferous kimberlites provide an opportunity to study the association of a primary diamond deposit with a post-Archaean rift system. The cratonic root in the the southern Superior is significantly thinned compared to the rest of the craton (Kopylova et al., 2011; Miller et al., 2012; Schaeffer and Lebedev, 2013; Zartman et al., 2013) and may be due to the Midcontinent Rift which affected the southern margin of the Superior Craton at ∼1.1 Ga (e.g., White, 1972; van Schmus and Hinze, 1985).

Kimberlites on the Superior craton that erupted syn- and post- rift sample distinctive lithosphere compositions. The Kyle Lake kimberlites, which are coeval with the Midcontinent Rift, sample predominantly harzburgitic lithosphere with an elevated geothermal gradient and a resulting small diamond window (Sage, 2000; Grütter, 2009). The nearby kimberlites at Attawapiskat were emplaced during the Jurassic, subsequent to the Rift. These kimberlites sample a lithosphere with a cooler geotherm and a larger diamond window. Garnet xenocrysts at Victor have predominantly lherzolitic compositions - perhaps due to refertilisation related to Midcontinent Rift magmas (Sage, 2000; Scully et al., 2004).

Samples from the Attawapiskat area include: Victor eclogite and pyroxenite xenoliths, Delta peridotite xenoliths, Victor peridotite xenocrysts, and diamonds from the T1 and U2 kimberlites (which are the same age as the Kyle Lake and Attawapiskat kimberlites, respectively).

During the course of this study, the main aims were to address the following:

1.) What was the process for melt extraction to form the proto-cratonic lithospheric root? Did initial melt extraction occur at high pressures in a plume-like setting or at low pressures in a setting similar to modern Mid-Ocean Ridges? How depleted were these residues? Are the lherzolitic compositions at Attawapiskat due to refertilisation or did the lithosphere below Attawapiskat never experience high degrees of melting to the point of clinopyroxene exhaustion (leading to depleted harzburgitic or dunitic residues)?

2.) How old is the lithosphere below the Superior? Palaeoarchaean crustal rocks have been identified at Assean Lake in Manitoba and at Inuukjuak in Quebec. Complimentary compositional relationships between cratonic residues and non-arc basalts found in Archaean greenstone belts has been suggested by Herzberg et al. (2010) and Herzberg and Rudnick (2012) and complimentary age relationships should therefore also exist (e.g., Pearson et al., 2007).

On the Kaapvaal craton, however, the majority of peridotite Re-Os T_{RD} ages are between ~2.9 and 2.7 Ga (Pearson et al., 1995; Carlson et al., 1999; Menzies et al., 1999; Irvine et al., 2001; Carlson and Moore, 2004; Simon et al., 2007) - significantly younger than crustal ages (3.7 - 3.2 Ga; Armstrong et al., 1990; Kroner et al., 1993). These T_{RD} ages, however, overlap with the ∼ 2.9 Ga collision of the Witwatersrand and Kimberley blocks of the Kaapvaal (Schmitz et al., 2004). This suggests that (additional?) mantle melting, to create residual peridotite, occurred at this time, likely in an arc environment.

Through combined PGE analyses and T_{RD} determinations of Delta peridotite xenoliths, the aims here are to assess depletion and enrichment processes in the Attawapiskat lithosphere and to provide constraints on the timing of these processes.

3.) What was the role of eclogite in craton formation / modification? Seismic profiles in the Abitibi-Grenville (Calvert et al., 1995) and western Superior (White et al., 2003; Musacchio et al., 2004) that trace dipping subduction zones in the lower crust and upper mantle have provided firm support for craton formation involving subducted slabs (Helmstaedt and Schulze, 1989). However, there is evidence from other cratons that subduction may contribute to craton destruction through the release of fluids from the subducting slab into the overlying mantle wedge (e.g., the eastern block of the North China craton; Peng et al., 1986; Ling et al., 2013). Here the aim is to investigate whether the Victor eclogites provide any evidence for subduction of oceanic crust into the Superior lithospheric mantle and to understand how subduction may have modified the compositions of the Attawapiskat SCLM.

4.) What was the impact of the Midcontinent Rift on the Superior lithosphere? The lithosphere in the southern Superior may have been thinned, but the impact of the Midcontinent Rift on the lithosphere below Attawapiskat is not fully understood. Here we investigate to what extent basaltic melts related to the Midcontinent Rift may have overprinted the lithosphere. Are depleted domains still preserved?

Some diamond destruction must have occurred due to the thermal impact of the rift and the narrowing of the diamond window at 1.1 Ga (Sage, 2000; Grütter, 2009); however, diamonds at Attawapiskat are mined from Jurassic kimberlites. Are these old diamonds that survived any melt metasomatic impact of the Midcontinent Rift? Or are they a younger generation of lherzolitic or eclogitic - pyroxenitic diamonds that formed after 1.1 Ga?

5. What are the diamond stable portions in the lithosphere? Victor is a productive diamond mine, yet the typical depleted harzburgite signature that is normally expected (e.g. Sobolev, 1977; Gurney, 1984a), is missing. The xenocryst population is predominantly lherzolitic and eclogitic - pyroxenitic (Sage, 2000). Here we investigate whether depleted peridotite compositions such as harzburgite and dunite are present at Attawapiskat, and discuss the likely diamond stable portions of the lithosphere.

1.0.3 Layout

An overview of the crustal geology of the Superior craton and previous studies on the underlying lithospheric mantle is given in Chapter 2. The main part of this thesis is formed by three scientific papers, submitted (or to be submitted) to peer-reviewed journals.

Chapter 3: Major element, trace element and isotopic study of eclogite and pyroxenite xenoliths from Victor to assess their formation processes and emplacement into the SCLM.

A modified version of this chapter has been submitted to Geochimica et Cosmochimica Acta: *Smit, K.V., Stachel, T., Creaser, R.A., Ickert, R.B., Dufrane, S.A., Stern, R.A. and Seller, M. Origin of eclogite and pyroxenite xenoliths from the Victor kimberlite, Canada, and implications for Superior craton formation.*

Chapter 4: Nitrogen aggregation characteristics and carbon isotopic compositions of diamonds from Attawapiskat in order to constrain their timing of formation relative to the Midcontinent Rift.

A modified version of this chapter is intended to be submitted as: *Smit, K.V., Stachel, T. and Stern, R. A. Multiple generations of diamond in the Attawapiskat area of the Superior craton (Canada).*

Chapter 5: Major element, trace element and Re-Os-PGE study of peridotite xenocrysts and xenoliths to constrain the nature of melt depletion and enrichment processes of the SCLM and their timing.

A modified version of this chapter is intended to be submitted as: *Smit, K.V., Pearson, G.P., Stachel, T. and Seller, M. Attawapiskat peridotites preserve evidence for the Palaeoarchaean origin and Proterozoic reworking of lithospheric mantle below the Northern Superior Superterrane, Canada.*

References

Armstrong, R. A., Compston, W., de Wit, M. J. and Williams, I. S.: 1990, The stratigraphy of the 3.5-3.2 Ga Barberton Greenstone Belt revisited: a single zircon ion microprobe study, *Earth and Planetary Science Letters* **101**, 90–106.

Arndt, N., Ginibre, C., Chauvel, C., Albarede, F., Cheadle, M., Herzberg, C., Jenner, G. and Lahaye, Y.: 1998, Were komatiites wet?, *Geology* **26**(8), 739–742.

Aulbach, S.: 2012, Craton nucleation and formation of thick lithospheric roots, *Lithos* **149**, 16–30.

Aulbach, S., Pearson, N. J., O'Reilly, S. Y. and Doyle, B. J.: 2007, Origins of Xenolithic Eclogites and Pyroxenites from the Central Slave Craton, Canada, *Journal of Petrology* **48**(10), 1843–1873.

Baker, M. B. and Stolper, E. M.: 1994, Determining the composition of high-pressure mantle melts using diamond aggregates, *Geochimica et Cosmochimica Acta* **58**(13), 2811–2827.

Barth, M. G., Rudnick, R. L., Horn, I., McDonough, W. F., Spicuzza, M. J., Valley, J. W. and Haggerty, S. E.: 2001, Geochemistry of xenolithic eclogites from West Africa, Part I: A link between low MgO eclogites and Archean crust formation, *Geochimica et Cosmochimica Acta* **65**(9), 1499–1527.

Barth, M. G., Rudnick, R. L., Horn, I., McDonough, W. F., Spicuzza, M. J., Valley, J. W. and Haggerty, S. E.: 2002a, Geochemistry of xenolithic eclogites from West Africa, Part 2: origins of the high MgO eclogites, *Geochimica et Cosmochimica Acta* **66**(24), 4325–4345.

Beard, B. L., Fraracci, K. N., Taylor, L. A., Snyder, G. A., Clayton, R. A., Mayeda, T. K. and Sobolev, N. V.: 1996, Petrography and geochemistry of eclogites from the Mir kimberlite, Yakutia, Russia, *Contributions to Mineralogy and Petrology* **125**, 293–310.

Bernstein, S., Kelemen, P. B. and Hanghøj, K.: 2007, Consistent olivine Mg# in cratonic mantle reflects Archean mantle melting to the exhaustion of orthpyroxene, *Geology* **35**(5), 459–462.

Bleeker, W.: 2003, The late Archaean record: a puzzle in ca. 35 pieces, *Lithos* **71**, 99–134.

Boyd, F. R.: 1989, Compositional distinction between oceanic and cratonic lithosphere, *Earth and Planetary Science Letters* **96**, 15–26.

Boyd, F. R. and McCallister, R. H.: 1976, Densities of fertile and sterile garnet peridotites, *Geophysical Research Letters* **3**, 509–512.

Boyd, F. R. and Mertzman, S. A.: 1987, Composition and structure of the Kaapvaal lithosphere, Southern Africa, *in* B. Mysen (ed.), *Magmatic Processes: Physicochemical Principles*, Vol. 1, The Geochemical Society, Houston, pp. 3–12.

Bulatov, V., Brey, G. P. and Foley, S. F.: 1991, Origin of low-Ca, high-Cr garnets by recrystallisation of low-pressure harzburgites, *Extended Abstracts of the 5th International Kimberlite Conference* pp. 29–31.

Calvert, A. J., Sawyer, E. W., Davis, W. J. and Ludden, J. N.: 1995, Archaean subduction inferred from seismic images of a mantle suture in the Superior Province, *Nature* **375**, 670–674.

Canil, D.: 2004, Mildly incompatible elements in peridotites and the origins of mantle lithosphere, *Lithos* **77**, 375–393.

Canil, D. and Wei, K. J.: 1992, Constraints on the origin of mantle-derived low Ca garnets., *Contributions to Mineralogy and Petrology* **109**, 421–430.

Caporuscio, F. A. and Smyth, J. R.: 1990, Trace element crystal chemistry of mantle eclogites, *Contributions to Mineralogy and Petrology* **105**, 550–561.

Carlson, R. W. and Moore, R. O.: 2004, Age of the Eastern Kaapvaal mantle: Re-Os isotope data for peridotite xenoliths from the Monastery mine, *South African Journal of Geology* **107**, 81–90.

Carlson, R. W., Pearson, D. G., Boyd, F. R., Shirey, S. B., Irvine, G., Menzies, A. H. and Gurney, J. J.: 1999, Re-Os systematics of lithosphere peridotites: Implications for lithosphere formation and preservation, *in* J. Gurney, J. Gurney, M. Pascoe and S. Richardson (eds), *Proceedings of the 7th International Kimberlite Conference, Cape Town, 1998*, Vol. 1, Red Roof Design, pp. 99–108.

Carlson, R. W., Pearson, D. G. and James, D. E.: 2005, Physical, Chemical, and Chronological Characteristics of Continental Mantle, *Reviews of Geophysics* **43**, RG1001.

Carswell, D. A.: 1990, Eclogites and the eclogite facies: definitions and classifications, *in* D. A. Carswell (ed.), *Eclogite facies rocks*, Blackie, pp. 1–13.

Coleman, R. G., Lee, E. D., Beatty, L. B. and Brannock, W. W.: 1965, Eclogites and eclogites: their differences and similarities, *Geological Society of America Bulletin* **76**, 483–508.

Dludla, S., le Roex, A. P. and Gurney, J. J.: 2006, Eclogite xenoliths from the Premier kimberlite, South Africa: geochemical evidence for a subduction origin, *South African Journal of Geology* **109**, 353–368.

Grütter, H. S.: 2009, Pyroxene xenocryst geotherms: Techniques and application, *Lithos* **112S**, 1167–1178.

Gurney, J. J.: 1984a, A correlation between garnets and diamonds in kimberlites, *Kimberlite occurrence and origin: A basis for conceptual models in exploration, Geology Department and University Extension, University of Western Australia, Publication 8*, Blackwell Scientific Publications, Perth, pp. 143–166.

Helmstaedt, H. and Doig, R.: 1975, Eclogite nodules and Kimberlite pipes of the Colorado Plateau - Samples of subducted Franciscan-type oceanic lithosphere, *Physics and Chemistry of the Earth* **9**, 95–111.

Helmstaedt, H. and Schulze, D. J.: 1989, Southern African kimberlites and their mantle sample: implications for Archaean tectonics and lithosphere evolution, *Kimberlites and Related Rocks I: Their Composition, Occurrence, Origin and Emplacement. Proceedings of the 4th International Kimberlite Conference, Perth 1986. Geological Society of Australia Special Publication 14.*, pp. 358–368.

Herzberg, C., Condie, K. and Korenaga, K.: 2010, Thermal history of the Earth and its petrological expression, *Earth and Planetary Science Letters* **292**, 79–88.

Herzberg, C. and Rudnick, R.: 2012, Formation of cratonic lithosphere: An integrated thermal and petrological model, *Lithos* **149**, 4–15.

Herzberg, C. T.: 1999, Phase equilibrium constraints on the formation of cratonic mantle, *in* Y. Fei, C. M. Bertka and B. O. Mysen (eds), *Mantle Petrology: Field Observations and High Pressure Experimentation: a Tribute to Francis R. (Joe) Boyd*, The Geochemical Society, Special Publication, pp. 241–257.

Irvine, G. J., Pearson, D. G. and Carlson, R. W.: 2001, Lithospheric mantle evolution in the Kaapvaal craton: a Re-Os isotope study of peridotite xenoliths from Lesotho kimberlites, *Geophysical Research Letters* **28**, 2505–2508.

Jacob, D. E.: 2004, Nature and origin of eclogite xenoliths from kimberlites, *Lithos* **77**, 295–316.

Jerde, E. A., Taylor, L. A., Crozaz, G., Sobolev, N. V. and Sobolev, V. N.: 1993, Diamondiferous eclogites from Yakutia, Siberia: evidence for a diversity of protoliths, *Contributions to Mineralogy and Petrology* **114**, 189–202.

Jordan, T. H.: 1975, The continental tectosphere, *Reviews of Geophysics* **13**, 1–12.

Kopylova, M. G., Afanasiev, V. P., Bruce, L. F., Thurston, P. C. and Ryder, J.: 2011, Metaconglomerate preserves evidence for kimberlite, diamondiferous root and medium grade terrane of a pre-2.7 Ga Southern Superior protocraton, *Earth and Planetary Science Letters* **312**, 213–225.

Kroner, A., Hegner, E., Wendt, J. I. and Byerly, G. R.: 1993, The oldest part of the Barberton granitoid-greenstone terrain, South Africa: evidence for crust formation between 3.5 and 3.7 Ga, *Precambrian Research* **78**, 105–124.

Ling, M.-X., Li, Y., Ding, X., Teng, F. Z., Yaang, X. Y., Fan, W. M., Xu, Y. G. and Sun, W.: 2013, Destruction of the North China Craton Induced by Ridge Subductions, *The Journal of Geology* **121**, 197–213.

Menzies, A. H., Shirey, S. B., Carlson, R. W. and Gurney, J. J.: 1999, Re-Os systematics of Newlands peridotite xenoliths: implications for diamond and lithosphere formation, *in* J. J. Gurney, J. L. Gurney, M. D. Pascoe and S. H. Richardson (eds), *Proceedings of the 7th International Kimberlite Conference*, Red Roof Design, Cape Town, pp. 566–583.

Miller, C. E., Kopylova, M. G. and Ryder, J.: 2012, Vanished diamondiferous cratonic root beneath the Southern Superior province: evidence from diamond inclusions in the Wawa metaconglomerate, *Contributions to Mineralogy and Petrology* **164**(4), 697–714.

Musacchio, G., White, D. J., Asudeh, I. and Thomson, C. J.: 2004, Lithospheric structure and composition of the Archean western Superior Province from seismic refraction/wide- angle reflection and gravity modeling, *Journal of Geophysical Research* **109**, B03304.

Neal, C. R., Taylor, L. A., Davidson, J. P., Holden, P., Halliday, A. N., Nixon, P. H., Paces, J. B., Clayton, R. N. and Mayeda, T. K.: 1990, Eclogites with oceanic crustal and mantle signatures from the Bellsbank kimberlite, South Africa, Part 2: Sr, Nd, and O isotope geochemistry, *Earth and Planetary Science Letters* **99**, 362–379.

O'Hara, M. J. and Yoder, H. S.: 1967, Formation and fractionation of basic magmas at high pressures, *Scottish Journal of Geology* **3**, 67–117.

Pearson, D. G., Canil, D. and Shirey, S. B.: 2003, Mantle Samples Included in Volcanic Rocks: Xenoliths and Diamonds, *Treatise on Geochemistry* **2**, 171–275.

Pearson, D. G., Carlson, R. W., Shirey, S. B., Boyd, F. R. and Nixon, P. H.: 1995, Stabilisation of Archaean lithospheric mantle: A Re-Os isotope study of peridotite xenoliths from the Kaapvaal Craton, *Earth and Planetary Science Letters* **134**(3-4), 341–357.

Pearson, D. G., Parman, S. W. and Nowell, G. M.: 2007, A link between large mantle melting events and continent growth seen in osmium isotopes, *Nature* **449**, 202–205.

Pearson, D. G. and Wittig, N.: 2008, Formation of Archaean continental lithosphere and its diamonds: the root of the problem, *Journal of the Geological Society, London* **165**, 1–20.

Pearson, D. G. and Wittig, N.: 2013, The Formation and Evolution of Cratonic Mantle Lithosphere – Evidence from Mantle Xenoliths, *Treatise on Geochemistry* **2**.

Peng, Z. C., Zartman, R. E., Futa, K. and Chen, D. G.: 1986, Pb-, Sr- and Nd-isotopic systematics and chemical characteristics of Cenozoic basalts, eastern China, *Chemical Geology* **59**, 3–33.

Sage, R. P.: 2000, Kimberlites of the Attawapiskat area, James Bay Lowlands, northern Ontario, *Ontario Geological Survey, Open File Report* **6019**(341), 341.

Schaeffer, A. J. and Lebedev, S.: 2013, Global shear speed structure of the upper mantle, *Geophysics Journal International* **submitted**.

Schmitz, M. D., Bowring, S. A., de Wit, M. J. and Gartz, V.: 2004, Subduction and terrane collisions stabilize the western Kaapvaal craton tectosphere 2.9 billion years ago, *Earth and Planetary Science Letters* **222**, 363–376.

Scully, K. R., Canil, D. and Schulze, D. J.: 2004, The lithospheric mantle of the Archean Superior Province as imaged by garnet xenocryst geochemistry, *Chemical Geology* **207**, 189–221.

Simon, N., Carlson, R. W., Pearson, D. G. and Davies, G. R.: 2007, The origin and evolution of the Kaapvaal cratonic lithospheric mantle, *Journal of Petrology* **48**, 589–625.

Snyder, G. A., Taylor, L. A., Crozaz, G., Halliday, A. N., Beard, B. L., Sobolev, V. N. and Sobolev, N. V.: 1997, The Origins of Yakutian Eclogite Xenoliths, *Journal of Petrology* **38**(1), 85–113.

Sobolev, N. V.: 1977, *Deep Seated Inclusions in Kimberlites and the Problems of the Composition of the Upper Mantle (translated by D.A. Brown)*, American Geophysical Union, Washington, D.C.

Stachel, T., Harris, J. W. and Brey, G. P.: 1998, Rare and unusual mineral inclusions in diamonds from Mwadui, Tanzania, *Contributions to Mineralogy and Petrology* **132**, 34–47.

Taylor, L. A. and Neal, C. R.: 1989, Eclogites with Oceanic Crustal and Mantle Signatures from the Bellsbank Kimberlite, South Africa, Part I: Mineralogy, Petrography, and Whole Rock Chemistry, *Journal of Geology* **97**, 551–567.

van Schmus, W. R. and Hinze, W. J.: 1985, The Midcontinent Rift System, *Annual Review of Earth and Planetary Sciences* **13**, 345–383.

Walter, M. J.: 1998, Melting of Garnet Peridotite and the Origin of Komatiite and Depleted Lithosphere, *Journal of Petrology* **39**(1), 29–60.

White, D. J., Musacchio, G., Helmstaedt, H. H., Harrap, R. M., Thurston, P. C., van der Velden, A. and Hall, K.: 2003, Images of a lower-crustal oceanic slab: Direct evidence for tectonic accretion in the Archean western Superior Province, *Geology* **31**(11), 997–1000.

White, W. S.: 1972, Keweenawan flood basalts and continental rifting, *Geological Association of America, Abstracts with Programs* **4**, 732–734.

Zartman, R. E., Kempton, P. D., Paces, J. B., Downes, H., Williams, I. S., Dobosi, G. and Futa, K.: 2013, Lower-Crustal Xenoliths from Jurassic Kimberlite Diatremes, Upper Michigan (USA): Evidence for Proterozoic Orogenesis and Plume Magmatism in the Lower Crust of the Southern Superior Province, *Journal of Petrology* **54**(3), 575–608.

Chapter 2

Superior craton

2.1 Evolution of the Superior craton

The Superior craton is the largest exposure of Archaean crust on Earth, with several continental nuclei separated by numerous terranes of plutonic complexes and magmatic arc material (e.g., the Berens River subprovince of the North Caribou superterrane), and turbidite sequences (e.g., the English River terrane) (Figure 2.1). Continental nuclei of the Superior craton include the Northern Superior superterrane (3.8-3.5 Ga - Böhm et al., 2000; Skulski et al., 2000); the Inukjuak domain of the northeastern Superior superterrane (∼3.8 Ga - David et al., 2002, 2009); the Winnipeg River terrane (∼3.4 Ga - Beakhouse, 1991; Tomlinson et al., 2004); the Marmion terrane (3.0-2.8 Ga - Davis and Jackson, 1988; Stone et al., 2002; Tomlinson et al., 2003, 2004); the Minnesota River Valley terrane (3.5-2.8 Ga - Goldich et al., 1984; Bickford et al., 2006; Schmitz et al., 2006) and the North Caribou superterrane (3.0-2.9 Ga - Corfu and Wood, 1986; Thurston et al., 1991; Stevenson, 1995).

An accretionary model for Superior craton amalgamation was first suggested by Langford and Morin (1976) due to similarity of the geologic features with those of the Canadian Cordillera. The Superior craton amalgamated between 2.72 and 2.68 Ga during several discrete orogenies, which in the past have been collectively termed the Kenoran orogeny (e.g., Langford and Morin, 1976, and references therein). In the western Superior Province, tectonism started in the North and continued southward over a period of 40 million years (e.g., Stott and Corfu, 1988, 1991; Percival et al., 2006b).

The Northern Superior superterrane contains the oldest rocks in the Western Superior province - the 3.8 - 3.5 Ga gneisses at Assean Lake in Manitoba (Böhm et al., 2000; Skulski et al., 2000). Their correlation with the Inukjuak domain of the northeastern Superior province of Quebec (~3.8 Ga - David et al., 2002, 2009) is speculative and has not been established. The Northern Superior superterrane subducted southward below the combined Oxford Stull domain and North Caribou superterrane during the Northern Superior orogeny (2.72-2.71 Ga; Corkery et al., 2000; Skulski et al., 2000; Craven et al., 2004; Parks et al., 2006). The North Kenyon Fault marks the current boundary between the Northern Superior and the Oxford-Stull domain to the south. The Oxford-Stull, along with the Molson Lake and Island Lake domains, have oceanic crust affinities that presumably developed on the margin of the North Caribou superterrane (Skulski et al., 2000; Parks et al., 2006).

The North Caribou superterrane is subdivided into the Sachigo, Berens River and Uchi subprovinces. It comprises ~ 3.0 - 2.8 Ga granite-greenstones which were substantially reworked during ~ 2.7 Ga continental arc magmatism (Thurston et al., 1991; Stevenson, 1995; Henry et al., 2000; Percival et al., 2006b). To the north-east and east the combined Oxford Stull and North Caribou terrane is bounded by the Winisk River Fault (e.g., Sage, 2000), a dextral strike-slip fault that developed in response to the ~1.8 Ga Trans Hudson Orogen (Gibb, 1983). However, other authors suggest that the North Caribou superterrane persists to the east of the Winisk River fault (Stott and Berdusco, 2000).

The English River terrane to the south of the North Caribou superterrane is considered to be the suture zone for the northward accretion of the ~ 3.4 Ga Winnipeg River terrane beneath the North Caribou superterrane during the Uchian Orogeny (Beakhouse, 1991; Corfu et al., 1995; Tomlinson et al., 2004). Arc magmatism as a precursor to the Uchian Orogeny is evident in the Berens River subprovince of the North Caribou superterrane (~2.75-2.71 Ga; e.g., Corfu and Stone, 1998).

The Shebandowanian orogeny subducted the Abitibi-Wawa terrane beneath the composite terranes to the North at ~2.7 Ga (Corfu and Stott, 1986; Stott, 1997), with final amalgamation of the Minnesota River Valley oceanic terrane to the composite Superior superterrane occuring during the ~2.68 Ga Minnesotan Orogeny (e.g., Percival et al., 2006b, and references therein). These composite terranes of the Superior craton have since remained a coherent unit.

This plate tectonic model has been accepted for the Superior craton, due also to seismic profiles in the Abitibi-Grenville (Calvert et al., 1995) and western Superior (White et al., 2003), that trace dipping subduction zones to depths of at least 30 km, and is in agreement with the generalised model for Archaean terrane formation by imbrication of subducted oceanic lithosphere, advocated by e.g., Helmstaedt and Schulze (1989). A schematic figure illustrating the accretionary growth of the western Superior Province is given in Percival et al. (2006b). The interpreted seismic section of the western Superior Province, illustrating the inferred subduction polarities during craton amalgamation, is shown in Figure 2.2.

2.2 Proterozoic orogenies marginal to the Superior craton

The Superior craton, together with the Nain, Churchill and Slave cratons and their bounding Proterozoic orogens comprise the Canadian Shield (e.g., Hoffman, 1990). The Superior craton is bounded on all sides by Proterozoic orogens, namely the Trans-Hudson, New Quebec, Penokean and Grenville orogens (e.g., Hoffman, 1990). These are briefly outlined below.

The Trans-Hudson orogen extends along the western and northern margin of the Superior craton and marks its collision with the composite Churchill province to the north-west, between 1.83 and 1.80 Ga (e.g., Bickford et al., 1990). Seismic profiling below the Trans-Hudson orogen has identified the Sask craton at depth, and traced it to the surface where it outcrops in small areas in the Glennie and Flin Flon Domains (Lucas et al., 1993). Subduction polarity of the Trans-Hudson orogen has been difficult to decipher, with early seismic reflection profiles showing dip to both the northwest and southeast beneath the bounding cratons (Lewry et al., 1994). Subsequently, the southeast dipping reflectors have been related to an early accretionary phase, whereas the northwest dipping reflectors relate to terminal collision of the Churchill, Sask and Superior cratons (Corrigan et al., 2005; Hajnal et al., 2005). A cross-section illustrating the tectonic evolution of both the accretionary and collisional phases in the Trans-Hudson orogen is given in Corrigan et al. (2005).

Along the northeastern boundary of the Superior craton is the southeastern Churchill Province (SECP). The SECP comprises the New Quebec and Torngat orogens as well as an Archaean block, termed the Core Zone (∼3.0-2.7 Ga tonalitic to granitic gneisses; Wardle et al., 2002, and references therein), which has previously been considered a continuation of the Rae craton (e.g., Hoffman, 1990; Scott, 1998). The Torngat orogen formed by collision and subduction of the Core Zone under the Nain craton between ∼1.9 and 1.85 Ga; the New Quebec orogen formed during 1.82-1.77 Ga collision between the Core Zone and the Superior craton (Wardle et al., 2002).

The Penokean orogen along the Southern margin of the Superior craton formed between 1.89 and 1.83 Ga (Hoffman, 1988; Schulz and Cannon, 2007). This orogen marks the end of southward subduction and the subsequent collision of the Superior craton with the Pembine-Wausau magmatic arc terrane, and the Archaean Marshfield Terrane (Schulz and Cannon, 2007, and references therein). The Grenville orogen along the south-eastern margin of the Superior craton, is part of an orogenic belt which runs from southern Greenland in the north to Mexico in the south (e.g., Rankin et al., 1993). It is part of a world-wide series of orogenic belts related to the formation of the Rodinia supercontinent at ∼1.1 Ga (e.g., Hoffman, 1988). The Grenville Orogeny lasted more than 100 million years, with peak metamorphism at ∼1.09-1.02 Ga and final collision and contraction at 1.00-0.98 Ga (Hynes and Rivers, 2010, and references therein). A schematic illustrating the plate tectonic model for the Grenville Orogeny is given in Hynes and Rivers (2010).

2.3 The Midcontinent Rift

The Midcontinent Rift is a tectonothermal event that impacted the Superior craton at ∼1.1 Ga, after accretion of the Superior craton. It is one the worlds major continental rifts, extending for 2300 km through central North America, though rifting ceased before significant crustal separation occurred (White, 1972; Halls, 1978; Wold and Hinze, 1982; van Schmus and Hinze, 1985). Exposures of rift successions are found only in the Lake Superior region, though the length of the rift can be traced through the presence of arcuate gravity and magnetic anomalies from Kansas to Michigan.

The rift successions are composed of two major suites: a volcanic sequence with an overlying clastic sedimentary sequence, the Midcontinent Rift Intrusive Supersuite and Keweenawan Supergroup, respectively (Morey and Grenn, 1952; Miller et al., 2002). The volcanics comprise a bimodal sequence of tholetiitic flood basalts (90%) and rhyolite (10%), with magmatism occurring in two major pulses, from 1109 to 1105 Ma and from 1100 to 1094 Ma (U-Pb zircon; Paces and Miller, 1993). The main phase of rifting is also characterised by coeval alkaline intrusions (e.g., ∼1105 Ma Nemegosenda carbonatite, ∼1100 Ma Lackner Lake carbonatite, ∼1108 Ma Coldwell alkaline gabbro; Heaman and Machado, 1992; Heaman et al., 2007). Also related to the Midcontinent Rift is ultramafic lamprophyre (UML) magmatism, occurring a few million years prior to the main phase of rift volcanism. These are recognised in the Wawa area and, on the basis of U-Pb perovskite and Rb-Sr phlogopite dating, intruded at 1147 to 1141 Ma (Queen et al., 1996). The Pele Mountain UMLs, also in the Wawa area, are slightly older, with an age of ∼1172 Ma (Heaman et al., 2004).

Initiation of Midcontinent rifting has been related to the Keweenawan hot spot, on the basis of both geophysical and geochemical evidence (e.g., Hinze et al., 1972; Burke and Dewy, 1973; Green, 1983; Hutchinson et al., 1990; Nicholson and Shirey, 1990; Cannon and Hinze, 1992), with failure of the rift due to coeval compression related to the Grenville orogeny (e.g., Cannon, 1994; Manson and Halls, 1997). The ∼1141 Ma Abitibi diabase dyke swarm (Krogh et al., 1987), which is of similar age to the early stages of UML magmatism, further supports the involvement of a mantle plume in the rift formation (e.g., Ernst and Bleeker, 2010, and references therein). Donaldson and Irving (1972), as well as Gordon and Hempton (1986) supported an alternative, collision-induced origin for rifting, possibly in a back-arc setting related to the Grenville orogeny.

In the southern Superior craton, basalts related to the Midcontinent Rift are found along the shores of Lake Superior and include the the Mamainse Point Formation - the most complete record of igneous activity in the Midcontinent Rift (e.g., Paces and Bell, 1989; Klewin and Berg, 1991; Shirey et al., 1994).

From the Nd isotopic composition and trace element chemistry of these basalts, Shirey et al. (1994) concluded that the early stage melts (high MgO picrites with low Al and enriched/unradiogenic $^{143}Nd/^{144}Nd$) have mainly lithospheric sources, whereas the late stage melts (tholeiitic basalts with higher Al and depleted/radiogenic $^{143}Nd/^{144}Nd$) have plume and asthenospheric sources.

The shear wave velocity structure for the mantle below the Superior craton shows lower velocities in the southern Superior which may be related to the effect of the Midcontinent Rift (Schaeffer and Lebedev, 2013). In the Attawapiskat area, the thermal impact of the Midcontinent Rift on the lithospheric mantle is evident in the elevated local geotherm determined from clinopyroxene xenocrysts from the 1.1 Ga Kyle Lake kimberlites (Sage, 2000; Heaman et al., 2004).

2.4 Kimberlites on the Superior craton

The Superior craton is host to several kimberlite fields, which, can be divided into three broad groups on the basis of their age (e.g., Heaman et al., 2004). The oldest kimberlites are the ∼1.1 Ga Kyle Lake and Bachelor Lake clusters, in Ontario and Quebec, respectively, which have been linked to the failed Midcontinent Rift (Heaman et al., 2004, and references therein). The Renard and Lac Beaver kimberlite clusters of the Otish mountains in Quebec, intrude the Opinaca Subprovince at ∼640-630 Ma and ∼550 Ma, respectively, and are associated with rifting and opening of the Iapetus Ocean (Moorhead et al., 2003; Birkett et al., 2004; Fitzgerald et al., 2009).

The Timiskaming (155-127 Ma; Heaman and Kjarsgaard, 2000), Kirkland Lake (157-152 Ma; Heaman and Kjarsgaard, 2000) and Attawapiskat (180-155Ma; Kong et al., 1999; Heaman and Kjarsgaard, 2000; Januszczak et al., 2013) kimberlite fields have been temporally linked to the track of the Great Meteor hotspot. Kimberlite magmatism along this track can be traced for over 2000 km, with the youngest kimberlites intruding the southern Superior province and the oldest kimberlites intruding the Churchill province at Rankin Inlet (214-196 Ma; Miller et al., 1998; Heaman and Kjarsgaard, 2000).

2.4.1 Attawapiskat and Kyle Lake kimberlites

The Attawapiskat kimberlite field is a cluster of 21 known kimberlites that occur ∼100 km west of the Attawapiskat community in the James Bay Lowlands, northern Ontario. They were first discovered in 1987 by De Beers Canada Exploration (then Monopros Limited) (Kong et al., 1999). The kimberlites were emplaced during the Jurassic between 180 and 156 Ma (Rb-Sr phlogopite; U-Pb perovskite; Kong et al., 1999; Heaman and Kjarsgaard, 2000; Januszczak et al., 2013), near the boundary of the North Caribou and Northern Superior superterranes, and are orientated on strike with the Winisk River Fault (Figure 2.1b). The nearby Kyle Lake kimberlites (∼100 km west of the Attawapiskat cluster) are much older than the Attawapiskat kimberlites and erupted during the Proterozoic at ∼1.1 Ga (Rb-Sr phlogopite; U-Pb perovskite; Heaman et al., 2004). These kimberlites intrude the North Caribou superterrane to the west of the Winisk River Fault (Figure 2.1b).

The T1 and U2 kimberlites at Attawapiskat were discovered in 2005 by Metalex Ventures after core drilling of aeromagnetic anomalies. Bulk sampling of these kimberlites is currently underway. There is no published age information on the T1 and U2 kimberlites, their age can, however, be inferred from stratigraphic relationships. The Kyle Lake Mesoproterozoic kimberlites are overlain by Palaeozoic limestone cover; whereas the younger Jurassic kimberlites at Attawapiskat, including Victor, break through this cover (Figure 2.3). Identical stratigraphic relationships suggest that T1 belongs to the Kyle Lake (1.1 Ga) kimberlite field and U2 to the Attawapiskat field (180 - 156 Ma).

2.5 Lithospheric mantle beneath the Superior craton

The Superior craton is underlain by relatively cold, high velocity, lithospheric mantle to depths of more than 200 km (e.g., Grand, 1987; Hoffman, 1990; van der Lee and Nolet, 1997). In the northwestern Superior Province, the North Caribou and Northern Superior superterranes are characterised by lithospheric mantle with higher velocity than the terranes to the southwest (e.g., Percival et al., 2006b, and references therein). Seismic anisotropy in the lithosphere is inherited from late Archaean tectonism and occurs sub-parallel to Archaean crustal subprovinces (Silver and Chan, 1988, 1991).

Considering the size of the Superior craton, the composition of the lithospheric mantle is still poorly constrained, largely due to the scarcity of large suites of mantle xenoliths. Sage (2000) analysed xenocrysts from several Superior craton kimberlites, including Kyle Lake and Attawapiskat. The Kyle Lake kimberlites are the only intrusion on the Superior craton that contain abundant harzburgitic garnets, though these may represent garnets derived from just a few xenoliths or disaggregated grains. A subset of this collection was analysed for trace elements by Scully et al. (2004), who concluded that younger kimberlite pipes on the Superior craton (Kirkland Lake, Timiskaming and Lake Ellen) sampled SCLM compositions that become more fertile with depth whereas the Proterozoic Kyle Lake kimberlite shows depleted portions to greater depths.

Numerous peridotites (and two eclogite) xenoliths from Attawapiskat were described by Schulze and Hetman (1997) and Scully (2000) and analysed for their major elements. Along with harzburgitic garnets, olivine grains with Mg# from 90.1 to 92.7, indicate a highly depleted lithosphere. Heavy mineral concentrate from the AT56 kimberlite, part of the Attawapiskat cluster, is predominantly lherzolitic, but also includes minor diamond-stable harzburgite and pyroxenite (Armstrong et al., 2004).

Garnet lherzolite xenoliths from the Kirkland Lake kimberlites in the Abitibi terrane were analysed for their petrography and major elements (Meyer et al., 1994; Vicker, 1997), along with $^{187}Os/^{188}Os$ for three xenoliths that indicate Palaeoproterozoic T_{RD} ages (Pearson et al., 1997). Peridotitic diamond inclusions from Wawa indicate the presence of a pre-2.7 Ga diamondiferous SCLM below this area that was subsequently destroyed (Stachel et al., 2006; Miller et al., 2012). Other evidence for the presence of a depleted SCLM in the Wawa terrain are ∼2.7 Ga sanukitoids that were derived from depleted mantle that experienced LILE-enrichment prior to eruption (Shirey and Hanson, 1984). In the eastern Superior, Hunt et al. (2012a) constrained a minimum age of 2.7 Ga for the SCLM below the Opinaca terrain based on Pb-Pb isotopic compositions of Renard clinopyroxene xenocrysts.

Previous work on eclogitic material from Attawapiskat included major element analyses of garnet xenocrysts from the AT56 kimberlite (Armstrong et al.,

2004) as well as petrography, major element analyses and geothermobarometry on four eclogite xenoliths (forming part of a predominantly peridotitic xenolith collection; Schulze and Hetman, 1997; Scully, 2000). Eclogite and pyroxenite xenoliths also occur at Renard in the Opinaca subprovince of the eastern Superior province (major/trace element analyses of eight xenoliths; Hunt et al., 2012b) (Figure 2.1). U-Pb crystallisation ages of $\sim$ 2.8 - 2.6 Ga have been reported for zircon from lower crustal granulite xenoliths from the Attawapiskat and Kirkland Lake kimberlites (Moser et al., 1997; Moser and Heaman, 1997). These may be the equivalent to eclogite and pyroxenite at lower metamorphic grade (e.g., Green and Ringwood, 1972; Toft et al., 1989) and suggest eclogites may have been emplaced into the SCLM below Attawapiskat at this time.

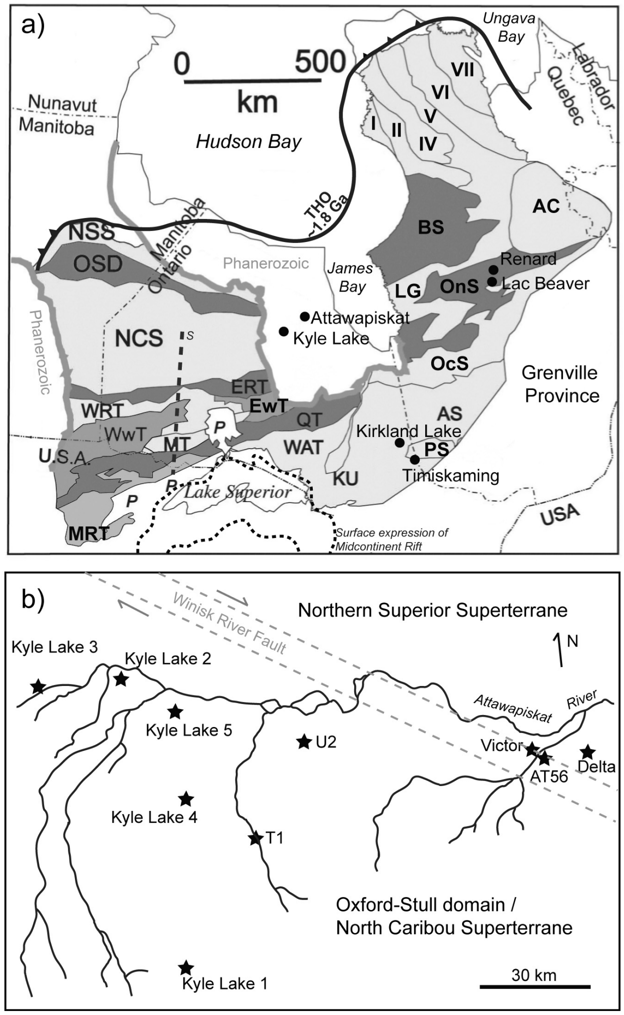

Figure 2.1: a) Subdivisions of the Superior craton (after Percival et al., 2006b, and references therein), with kimberlite localities indicated. Surface expression of the Midcontinent Rift from Ojakangas et al. (2001). Location and subduction polarity of the ∼1.8 Ga Trans Hudson Orogen (THO) from Berman et al. (2005). "s" indicates the approximate location of the seismic profile in Figure 2.2. Abbreviations used: AC - Ashuanipi complex; AS - Abitibi subprovince; BS - Bienville subprovince; ERT - English River terrane; EwT - East Wabigoon terrane; KU - Kapuskasing uplift; LG - La Grande subprovince; MT - Marmion terrane; MRT - Minnesota River Valley terrane; NCS - North Caribou superterrane; NSS - Northern Superior superterrane; OcS - Opatica subprovince; OnS - Opinaca subprovince; OSD - Oxford-Stull domain; PS - Pontiac subprovince; QT - Quetico terrane; WAT - Wawa-Abitibi terrane; WRT - Winnipeg River terrane; WwT - West Wabigoon terrane; I - Inukjuak domain; II - Tikkerutuk domain; IV - L. Minto domain; V - Goudalie domain; VI - Utsalik domain; VII - Douglas Harbour domain. b) Locations for selected Attawapiskat and Kyle Lake kimberlites, in relation to the Attawapiskat river. Kimberlite co-ordinates from Sage (2000) and the Ontario Geological Survey website at *www.geologyontario.mndm.gov.on.ca*.

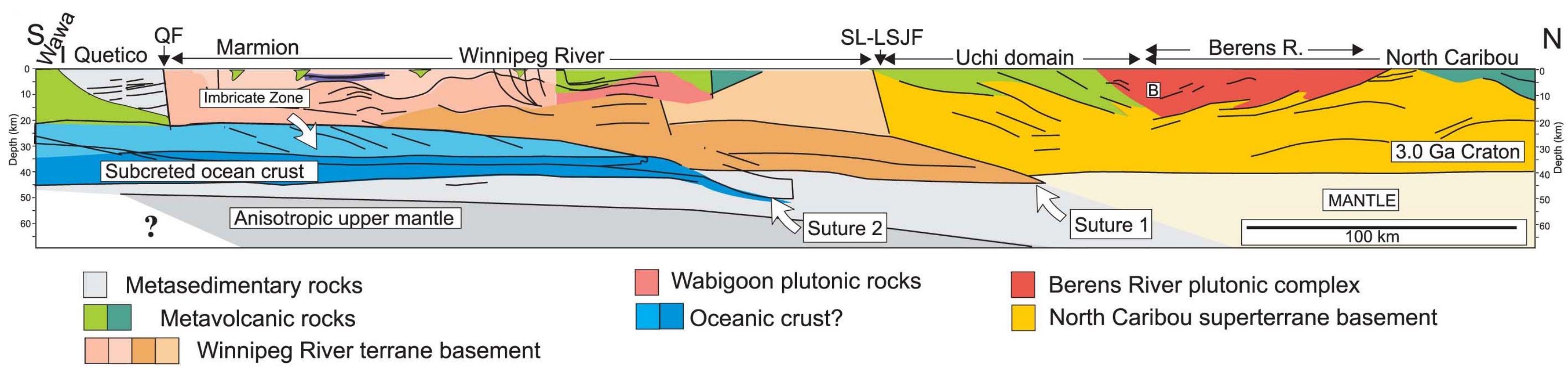

Figure 2.2: Tectonic interpretation of seismic data (Percival et al., 2006b, using seismic data from White et al. (2003)) for a section through the western Superior Province, from the Wawa-Abitibi terrane in the south to the North Caribou superterrane in the north. The Uchi and Berens River domains are part of the North Caribou superterrane shown in Figure 2.1. Suture 1 and Suture 2 are interpreted to represent the northward subduction of the Uchian and Minnesotan Orogens, respectively.

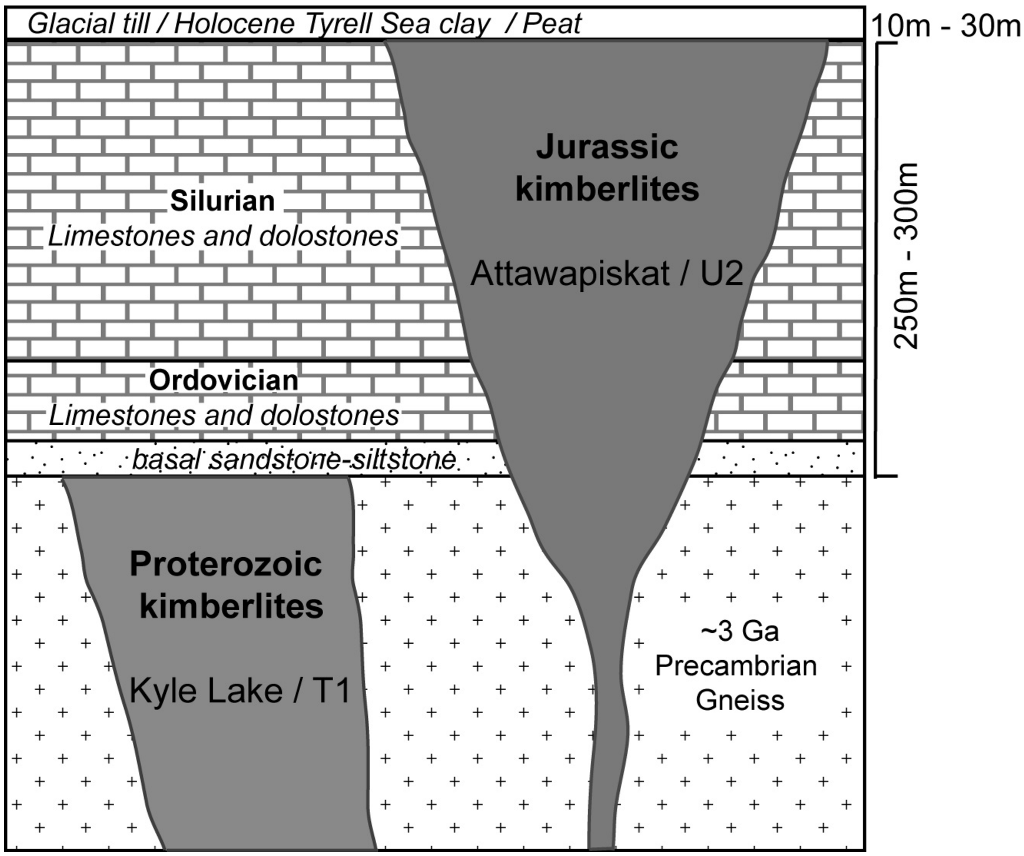

Figure 2.3: Simplified stratigraphic relationships for the Proterozoic Kyle Lake and Jurassic Attawapiskat kimberlites (not to scale) modified after Webb et al. (2004), Thomas (2004) and Hattori and Hamilton (2008). The kimberlites at Attawapiskat (including Victor) were emplaced between 180 and 156 Ma (Rb-Sr phlogopite; U-Pb perovskite; Kong et al., 1999; Heaman and Kjarsgaard, 2000) and intrude through the Palaeozoic sediments. The older Kyle Lake kimberlites do not penetrate the Palaeozoic cover, with kimberlite emplacement dated at ∼1.1 Ga (Rb-Sr phlogopite; U-Pb perovskite; Heaman et al., 2004). Though no published age information exists for the T1 and U2 kimberlites, stratigraphic relationships suggest that they are similar age as the Kyle Lake and Attawapiskat kimberlites, respectively.

References

Armstrong, K. A., Nowicki, T. E. and Read, G. H.: 2004, Kimberlite AT-56: a mantle sample from the north central Superior craton, Canada, *Lithos* **77**, 695–704.

Beakhouse, G. P.: 1991, Winnipeg River subprovince, *in* P. C. Thurston, H. R. Williams, R. H. Sutcliffe and G. M. Stott (eds), *Geology of Ontario*, Vol. Special Volume 4, Part 1, Ontario Geological Survey, pp. 279–301.

Berman, R. G., Sanborn-Barrie, M., Stern, R. A. and Carson, C. J.: 2005, Tectonometamorphism at ca. 2.35 and 1.85 Ga in the Rae Domain, Western Churchill Province, Nunavut, Canada: Insights from Structural, Metamorphic and in-situ Geochronological analysis of the Southwestern Committee Bay Belt, *The Canadian Mineralogist* **43**, 409–442.

Bickford, M. E., Collerson, K. D., Lewry, J. F., van Schmus, W. R. and Chiarenzelli, J. R.: 1990, Proterozoic collisional tectonism in the Trans-Hudson orogen, Saskatchewan, *Geology* **18**, 14–18.

Bickford, M. E., Wooden, J. L. and Bauer, R. L.: 2006, SHRIMP study of zircons from the Early Archaean rocks in the Minnesota River Valley: Implications for the tectonic history of the Superior Province, *Geological Society of America Bulletin* **118**, 94–108.

Birkett, T. C., McCandless, T. E. and Hood, C. T.: 2004, Petrology of the Renard igneous bodies: host rocks for diamond in the northern Otish Mountains region, Quebec, *Lithos* **76**(1-4), 475–490.

Böhm, C. O., Heaman, L. M., Creaser, R. A. and Crockery, M. T.: 2000, Discovery of pre-3.5 Ga exotic crust at the northwestern Superior Province margin, Manitoba, *Geology* **28**(1), 75–78.

Burke, K. and Dewy, J. F.: 1973, Plume-generated triple junctions: Key indicators in applying plate tectonics to old rocks, *The Journal of Geology* **81**(4), 406–433.

Calvert, A. J., Sawyer, E. W., Davis, W. J. and Ludden, J. N.: 1995, Archaean subduction inferred from seismic images of a mantle suture in the Superior Province, *Nature* **375**, 670–674.

Cannon, W. F.: 1994, Closing of the Midcontinent Rift - A far-field effect of Grenvillian compression, *Geology* **22**(2), 155–158.

Cannon, W. F. and Hinze, W. F.: 1992, Speculations on the origin of the North American Midcontinent rift, *Tectonphysics* **213**, 49–55.

Corfu, F. and Stone, D.: 1998, Age structure and orogenic significance of the Berens River composite batholiths, western Superior Province, *Canadian Journal of Earth Sciences* **35**, 1089–1109.

Corfu, F. and Stott, G. M.: 1986, U-Pb ages for late magmatism and regional deformation in the Shebandowan belt, Superior Province, Canada, *Canadian Journal of Earth Sciences* **23**, 1075–1082.

Corfu, F., Stott, G. M. and Breaks, F. W.: 1995, U-Pb geochronology and evolution of the English River Subprovince, an Archean low P-high T metasedimentary belt in the Superior Province, *Tectonics* **14**(5), 1220–1233.

Corfu, F. and Wood, J.: 1986, U-Pb zircon ages in supracrustal and plutonic rocks; North Spirit Lake area, northwestern Ontario, *Canadian Journal of Earth Sciences* **23**, 967–977.

Corkery, M. T., Cameron, H. D. M., Lin, S., Skulski, T., Whalen, J. B. and Stern, R. A.: 2000, Geological investigations in the Knee Lake belt (Parts of NTS 53L), *Report of Activities 2000, Manitoba Industry, Trade and Mines*, Manitoba Geological Survey, pp. 129–136.

Corrigan, D., Hajnal, Z., Nemeth, B. and Lucas, S. B.: 2005, Tectonic framework of a Paleoproterozoic arc-continent to continent-continent collisional zone, Trans-Hudson Orogen, from geological and seismic reflection studies, *Canadian Journal of Earth Sciences* **42**(4), 421–435.

Craven, J. A., Skulski, T. and White, D. W.: 2004, Lateral and vertical growth of cratons: seismic and magnetotelluric evidence from the western Superior transect, *Lithoprobe Celebratory Conference*, Vol. Lithoprobe Report 86, Lithoprobe Secretariat, The University of British Columbia.

David, J., Godin, L., Stevenson, R., O'Neil, J. and Francis, D.: 2009, U-Pb ages (3.8-2.7 Ga) and Nd isotope data from the newly identified Eoarchean

Nuvvuagittuq supracrustal belt, Superior Craton, Canada, *GSA Bulletin* **121**(1/2), 150–163.

David, J., Parent, M., Stevenson, R., Nadeau, P. and Godin, L.: 2002, The Porpoise Cove supracrustal sequence, Inukjuak area: A unique example of Paleoarchean crust (c.a 3.8 Ga) in the Superior Province, *Ministère des Ressources Naturelles de Québec* **DV**, 2002–10.

Davis, D. W. and Jackson, M.: 1988, Geochronology of the Lumby Lake greenstone belt: a 3 Ga complex within the Wabigoon Subprovince, northwest Ontario, *Geological Society of America Bulletin* **100**, 818–824.

Donaldson, J. A. and Irving, E.: 1972, Grenville Front and rifting of the Canadian Shield, *Nature* **237**, 139–140.

Ernst, R. and Bleeker, W.: 2010, Large igneous provinces (LIPs), giant dyke swarms, and mantle plumes: significance for breakup events within Canada and adjacent regions from 2.5 Ga to the Present, *Canadian Journal of Earth Sciences* **47**, 695–739.

Fitzgerald, C. E., Hetman, C. M., Lepine, I., Skelton, D. S. and McCandless, T. E.: 2009, The internal geology and emplacement history of the Renard 2 kimberlite, Superior Province, Quebec, Canada, *Lithos* **112**, 513–528.

Gibb, R. A.: 1983, Model for suturing of Superior and Churchill plates: An example of double indentation tectonics, *Geology* **11**, 413–417.

Goldich, S. S., Wooden, J. L., Ankenbauer, G. A., Levy, T. M. and Suda, R. U.: 1984, Origin of the Morton Gneiss, southwestern Minnesota: Part I, Lithology, *in* G. B. Morey and G. N. Hanson (eds), *Selected Studies of Archean gneisses and lower Proterozoic rocks, Southern Canadian Shiel*, Vol. Special Paper 182, Geological Society of America, pp. 45–50.

Gordon, M. B. and Hempton, M. R.: 1986, Collision-induced rifting: The Grenville Orogeny and the Keweenawan Rift of North America, *Tectonophysics* **127**, 1–25.

Grand, S. P.: 1987, Tomographic inversion for shear velocity beneath the North American plate, *Journal of Geophysical Research* **92**, 14 065 – 14 090.

Green, D. H. and Ringwood, A. E.: 1972, A Comparison of Recent Experimental Data on the Gabbro-Garnet Granulite-Eclogite Transition, *Journal of Geology* **80**, 277–288.

Green, J. C.: 1983, Geologic and Geochemical evidence for the nature and development of the Middle Proterozoic (Keweenawan) Midcontinent Rift of North America, *Tectonophysics* **94**, 413–437.

Hajnal, Z., Lewry, J., White, D., Ashton, K., Clowes, R., Stauffer, M., Gyorfi, I. and Takacs, E.: 2005, The Sask Craton and Hearne Province margin: Seismic reflection studies in the western Trans-Hudson Orogen, *Canadian Journal of Earth Sciences* **42**(4), 403–419.

Halls, H. C.: 1978, The late Precambrian Central North American Rift System - a survey of recent geological and geophysical investigations, *in* I. B. Ramberg and E. R. Neumann (eds), *Tectonics and Geophysics of Continental Rifts*, Reidel, Dordrecht, pp. 111–123.

Hattori, K. and Hamilton, S.: 2008, Geochemistry of peat over kimberlites in the Attawapiskat area, James Bay Lowlands, northern Canada, *Applied Geochemistry* **23**, 3767–3782.

Heaman, L. M., Easton, R. M., Hart, T. R., Hollings, P., MacDonald, C. A. and Smyk, M.: 2007, Further refinement to the timing of Mesoproterozoic magmatism, Lake Nipigon region, Ontario, *Canadian Journal of Earth Sciences* **44**, 1055–1086.

Heaman, L. M. and Kjarsgaard, B. A.: 2000, Timing of eastern North American kimberlite magmatism: continental extension of the Great Meteor hotspot track?, *Earth and Planetary Science Letters* **178**, 253–268.

Heaman, L. M., Kjarsgaard, B. A. and Creaser, R. A.: 2004, The temporal evolution of North American kimberlites, *Lithos* **76**, 377–397.

Heaman, L. M. and Machado, N.: 1992, Timing and origin of midcontinent rift alkaline magmatism, North America: evidence from the Coldwell Complex, *Contributions to Mineralogy and Petrology* **110**, 289–303.

Helmstaedt, H. and Schulze, D. J.: 1989, Southern African kimberlites and their mantle sample: implications for Archaean tectonics and lithosphere evolution, *Kimberlites and Related Rocks I: Their Composition, Occurrence, Origin and Emplacement. Proceedings of the 4th International Kimberlite Conference, Perth 1986. Geological Society of Australia Special Publication 14.*, pp. 358–368.

Henry, P., Stevenson, R. K., Larbi, Y. and Gariépy, C.: 2000, Nd isotopic evidence for Early to Late Archean (3.4-2.7 Ga) crustal growth in the Western Superior Province (Ontario, Canada), *Tectonophysics* **322**, 135–151.

Hinze, W. J., Roy, R. F. and Davidson, D. M.: 1972, The origin of Late Precambrian Rifts, *Geological Society of America, Abstracts with Program* **4**, 723.

Hoffman, P. F.: 1988, United Plates of America, The Birth of a Craton: Early Proterozoic Assembly and Growth of Laurentia, *Annual Review of Earth and Planetary Sciences* **16**, 543–603.

Hoffman, P. F.: 1990, Geological constraints on the origin of the mantle root beneath the Canadian shield, *Philosophical Transactions of the Royal Society* **A 331**, 523–532.

Hunt, L. C., Stachel, T., Grütter, H., Armstrong, J., McCandless, T. E., Simonetti, A. and Tappe, S.: 2012a, Small Mantle Fragments from the Renard Kimberlites, Quebec: Powerful Recorders of Mantle Lithosphere Formation and Modification Beneath the Eastern Superior Craton, *Journal of Petrology* .

Hunt, L. C., Stachel, T., McCandless, T. E., Armstrong, J. and Muehlenbachs, K.: 2012b, Diamonds and their mineral inclusions from the Renard kimberlites in Quebec, *Lithos* **142-143**, 267–284.

Hutchinson, D. R., White, R. S., Cannon, W. F. and Schulz, K. J.: 1990, Keweenaw hot spot: evidence for a 1.1 Ga mantle plume beneath the Midcontinent Rift system, *Journal of Geophysical Research* **95**(B7), 10869–10884.

Hynes, A. and Rivers, T.: 2010, Protracted continental collision - evidence from the Grenville Orogen, *Canadian Journal of Earth Sciences* **47**, 591–620.

Januszczak, N., Seller, M. H., Kurszlaukis, S., Murphy, C., Delgaty, J., Tappe, S., Ali, K., Zhu, J. and Ellemers, P.: 2013, A Multidisciplinary Approach to the Attawapiskat Kimberlite Field, Canada: Accelerating the Discovery-to-Production Pipeline, *Proceedings of the 10th International Kimberlite Conference* .

Klewin, K. W. and Berg, J. H.: 1991, Geochemistry of the Mamainse Point volcanics, Ontario: Petrogenesis and continental rift evolution, *Journal of Geophysical Research* **96**, 457–474.

Kong, J. M., Boucher, D. R. and Scott-Smith, B. H.: 1999, Exploration and Geology of the Attwapiskat kimberlites, James Bay Lowland, Northern Ontario, Canada, *Extended Abstracts of the 7th International Kimberlite Conference, Cape Town* pp. 446–448.

Krogh, T. E., Corfu, F., Davis, D. W., Dunning, G. R., Heaman, L. H., Kamo, S. L., Machado, N., Greenough, J. D. and Nakamura, E.: 1987, Precise U-Pb isotopic ages of diabase dykes and mafic to ultramafic dykes and mafic to ultramafic rocks using trace amounts of baddelyie and zircon, *in* H. C. Halls (ed.), *Mafic dyke swarms*, Vol. Special Paper 34, Geological Survey of Canada, pp. 147–152.

Langford, F. F. and Morin, J. A.: 1976, The development of the Superior Province of Northwestern Ontario by merging Island Arcs, *American Journal of Science* **270**, 1023–1034.

Lewry, J. F., Hajnal, Z., Green, A., Lucas, S. B., White, D., Stauffer, M. R., Ashton, K. E., Weber, W. and Clowes, R.: 1994, Structure of a Palaeoproterozoic continent-continent collision zone: a LITHOPROBE seismic reflection profile across the Trans-Hudson Orogen, Canada, *Tectonophysics* **232**, 143–160.

Lucas, S. B., Green, A., Hajnal, Z., White, D., Lewry, J., Ashton, K., Weber, W. and Clowes, R.: 1993, Deep seismic profile across a Proterozoic collision zone: surprises at depth, *Nature* **363**, 339–342.

Manson, M. L. and Halls, H. C.: 1997, Proterozoic reactivation of the southern Superior Province and its role in the evolution of the Midcontinent rift, *Canadian journal of Earth Sciences* **34**(4), 562–575.

Meyer, H. O. A., Waldman, M. A. and Garwood, B. L.: 1994, Mantle xenoliths from kimberlite near Kirkland Lake, Ontario, *The Canadian Mineralogist* **32**, 295–306.

Miller, A. R., Seller, M. H., Armitage, A. E., Davis, W. J. and Barnett, R. L.: 1998, Late Triassic kimberlitic magmatism, western Churchill Stuctural Province, Canada, *Extended Abstracts of the 7th International Kimberlite Conference, Cape Town* pp. 591–593.

Miller, C. E., Kopylova, M. G. and Ryder, J.: 2012, Vanished diamondiferous cratonic root beneath the Southern Superior province: evidence from diamond inclusions in the Wawa metaconglomerate, *Contributions to Mineralogy and Petrology* **164**(4), 697–714.

Miller, J. D., Green, J. C. and Severson, M. J.: 2002, Terminology, nomenclature and classification of Keweenawan igneous rocks of northeastern Minnesota, *Geology and mineral potential of the Duluth Complex and realted rocks of northeastern Minnesota*, Vol. 58, Minnesota Geological Survey, Report of Investigations, pp. 5–20.

Moorhead, J., Beaumier, M., Girard, R. and Heaman, L. M.: 2003, Distribution, structural controls and ages of kimberlite fields in the Superior Province of Québec, *Proceedings of the 8th International Kimberlite Conference* p. 128.

Morey, G. B. and Grenn, J. C.: 1952, Status of the Keweenawan as a stratigraphic unit in the Lake Superior region, *in* R. J. Wold and W. J. Hinze (eds), *Geology and Tectonics of the Lake Superior basin*, Vol. 156, Geological Society of America, Memoir, pp. 15–26.

Moser, D., Amelin, Y., Schulze, D. and Krogh, T.: 1997, Progress in Understanding the Geology of the Lithosphere beneath the Eastern Sachigo Subprovince, *in* R. M. Harrap and H. H. Helmstaedt (eds), *1997 Western Superior Transect Third Annual Workshop, April 11-12, 1997. Lithoprobe Report #63*, Lithoprobe Secretariat, The University of British Columbia, pp. 102–103.

Moser, D. E. and Heaman, L. M.: 1997, Proterozoic zircon growth in Archean lower crustal xenoliths, southern Superior craton - a consequence of Matachewan ocean opening, *Contributions to Mineralogy and Petrology* **128**, 164–175.

Nicholson, S. W. and Shirey, S. B.: 1990, Midcontinent Rift volcanism in the Lake Superior region - Sr, Nd and Pb isotopic evidence for a mantle plume origin, *Journal of Geophysical Research - Solid Earth and Planets* **95**(B7), 10851–10868.

Ojakangas, R. W., Morey, G. B. and Green, J. C.: 2001, The Mesoproterozoic Midcontinent Rift System, Lake Superior Region, USA, *Sedimentary Geology* **141-142**, 421–442.

Paces, J. B. and Bell, K.: 1989, Non-depleted sub-continental mantle beneath the Superior Province of the Canadian Shield: Nd-Sr isotopic and trace element evidence from Midcontinent Rift basalts, *Geochimica et Cosmochimica Acta* **53**, 2023–2035.

Paces, J. B. and Miller, J. D.: 1993, Precise U-Pb ages of Duluth Complex and related mafic intrusions, northeastern Minnesota: geochronological insights to physical, petrogenetic, paleomagnetic and tectonomagmatic processes associated with the 1.1 Ga Midcontinent Rift System, *Journal of Geophysical Research* **98**, 13997–14013.

Parks, J., Lin, S., Davis, D. W. and Corkery, M. T.: 2006, New high-precision U-Pb ages for the Island Lake greenstone belt, north-western Superior Province: implications for regional stratigraphy and the extent of the North Caribou terrane, *Canadian Journal of Earth Sciences* **43**, 789–803.

Pearson, D. G., Meyer, H. O. A., Boyd, F. R., Shirey, S. B. and Carlson, R. W.: 1997, Re-Os isotope evidence for late Archaean stabilisation of a thick lithospheric mantle keel beneath the Kirkland Lake area, Superior Province, Canada. Further evidence for long-term crust-mantle coupling, *Russian Geology and Geophysics, Special Issue: Proceedings of the 6th International Kimberlite Conference* **2**, 427–429.

Percival, J. A., Sanborn-Barrie, M., Skulski, T., Stott, G. M., Helmstaedt, H. and White, D. J.: 2006b, Tectonic evolution of the western Superior Province from NATMAP and Lithoprobe studies, *Canadian Journal of Earth Sciences* **43**, 1085–1117.

Queen, M., Heaman, L. M., Hanes, J. A., Archibald, D. A. and Farrar, E.: 1996, ^{40}Ar/^{39}Ar phlogopite and U-Pb perovskite dating of lamprophyre dykes from the eastern Lake Superior region: evidence for a 1.14 Ga magmatic precursor to Midcontinent Rift volcanism, *Canadian Journal of Earth Sciences* **33**, 958–965.

Rankin, D. W., Chiarenzelli, J. R., Drake, A. A., Goldsmith, R., Hall, L. M., Hinze, W. J., Isachsen, Y. W., Lidiak, E. G., McLelland, J., Mosher, S., Ratcliffe, N. M., Secor, D. and Whitney, P. R.: 1993, Proterozoic rocks of east and southeast of the Grenville Front, *in* J. C. Reed, M. E. Bickford, R. S. Houston, P. K. Link, D. W. Rankin, P. K. Sims and W. R. van Schmus (eds), *Precambrian: Conterminous US. The Geology of North America*, Vol. C-2, Geological Society of America, pp. 335–461.

Sage, R. P.: 2000, Kimberlites of the Attawapiskat area, James Bay Lowlands, northern Ontario, *Ontario Geological Survey, Open File Report* **6019**(341), 341.

Schaeffer, A. J. and Lebedev, S.: 2013, Global shear speed structure of the upper mantle, *Geophysics Journal International* **submitted**.

Schmitz, M. D., Bowring, S. A., Southwick, D. L., Boerboom, T. J. and Wirth, K. R.: 2006, High precision U-Pb geochronology in the Minnesota River Valley subprovince and its bearing on the Neoarchean to Paleoproterozoic evolution of the southern Superior Province, *GSA Bulletin* **118**(1/2), 82–93.

Schulz, K. J. and Cannon, W. F.: 2007, The Penokean orogeny in the Lake Superior region, *Precambrian Research* **157**, 4–25.

Schulze, D. J. and Hetman, C. M.: 1997, Mantle xenoliths from the Attawapiskat kimberlites, *in* R. M. Harrap and H. H. Helmstaedt (eds), *1997 Western Superior Transect Third Annual Workshop, April 11-12, 1997. Lithoprobe Report #63*, Lithoprobe Secretariat, The University of British Columbia, pp. 62–66.

Scott, D. J.: 1998, An overview of the U-Pb geochronology of the Paleoproterozoic Torngat Orogen, Northeastern Canada, *Precambrian Research* **91**, 91–107.

Scully, K. R.: 2000, *Mantle xenoliths from the Attawapiskat kimberlite field*, Master's thesis, University of Toronto.

Scully, K. R., Canil, D. and Schulze, D. J.: 2004, The lithospheric mantle of the Archean Superior Province as imaged by garnet xenocryst geochemistry, *Chemical Geology* **207**, 189–221.

Shirey, S. B. and Hanson, G. N.: 1984, Mantle-derived Archean monzodiorites and trachyandesites, *Nature* **310**(5974), 222–224.

Shirey, S. B., Klewin, K. W., Berg, J. H. and Carlson, R. W.: 1994, Temporal changes in the sources of flood basalts: Isotopic and trace element evidence from the 1100 Ma old Keweenawan Mamainse Point Formation, Ontario, Canada, *Geochimica et Cosmochimica Acta* **58**(20), 4475–4490.

Silver, P. G. and Chan, W. W.: 1988, Implications for continental structure and evolution from seismic anisotropy, *Nature* **335**, 34–39.

Silver, P. G. and Chan, W. W.: 1991, Shear-wave splitting and subcontinental mantle deformation, *Journal of Geophysical Research-Solid Earth* **96**(B10), 16429–16454.

Skulski, T., Corkery, M. T., Stone, D., Whalen, J. B. and Stern, R. A.: 2000, Geological and geochronological investigations in the Stull Lake - Edmund Lake greenstone belt and granitoid rocks of the northwestern Superior Province, *Report of Activities 2000, Manitoba Industry, Trade and Mines*, Manitoba Geological Survey, pp. 117–128.

Stachel, T., Banas, A., Muehlenbachs, K., Kurszlaukis, S. and Walker, E. C.: 2006, Archean diamonds from Wawa (Canada): samples from deep cratonic roots predating cratonization of the Superior Province, *Contributions to Mineralogy and Petrology* **151**, 737–750.

Stevenson, R. K.: 1995, Crust and mantle evolution in the late Archaean: Evidence from a Sm-Nd isotopic study of the North Spirit Lake greenstone belt, northwestern Ontario, *Geological Society of America Bulletin* **107**, 1458–1467.

Stone, D., Tomlinson, K. Y., Davis, D. W., Fralick, P., Hallé, J., Percival, J. A. and Pufahl, P.: 2002, Geology and tectonostratigraphic assemblages, south-central Wabigoon Subprovince, *Geological Survey of Canada, Open File* **4284**.

Stott, G. M.: 1997, The Superior Province, Canada, *in* M. J. de Wit and L. D. Ashwal (eds), *Greenstone Belts*, Vol. 35, Oxford Monograph of Geology and Geophysics, pp. 480–507.

Stott, G. M. and Berdusco, B. J.: 2000, Precambrian Features under the James Bay and Hudson Bay Lowlands, *Ontario Geological Survey, Open File Report* **6032**, 14–1 to 14–5.

Stott, G. M. and Corfu, F.: 1988, Whither the Kenoran orogeny?, *Annual Meeting of the Geological Association of Canada* **Abstracts Volume 13**(A120).

Stott, G. M. and Corfu, F.: 1991, Uchi Subprovince, *in* P. C. Thurston, H. R. Williams, R. H. Sutcliffe and G. M. Stott (eds), *Geology of Ontario*, Vol. Special Volume 4, Part 1, Ontario Geological Survey, pp. 145–238.

Thomas, R. D.: 2004, Spider #1 and #3 Projects (James Bay Joint Venture), James Bay, Ontario, *Technical Report prepared for Spider Resources and KWG Resources* p. pp. 76.

Thurston, P. C., Osmani, I. A. and Stone, D.: 1991, Northwestern Superior Province: Review and terrane analysis, *in* P. C. Thurston, H. R. Williams, R. H. Sutcliffe and G. M. Stott (eds), *Geology of Ontario*, Vol. Special Volume 4, Part 1, Ontario Geological Survey, pp. 81–144.

Toft, P. B., Hills, D. V. and Haggerty, S. E.: 1989, Crustal evolution and the granulite to eclogite transition in xenoliths from kimberlites in the West African Craton, *Tectonophysics* **161**, 213–231.

Tomlinson, K. Y., Davis, D. W., Stone, D. and Hart, T.: 2003, New U-Pb and Nd isotopic evidence for crustal recycling and Archean terrane development in the south-central Wabigoon Subprovince, Canada, *Contributions to Mineralogy and Petrology* **144**, 684–702.

Tomlinson, K. Y., Stott, G. M., Percival, J. A. and Stone, D.: 2004, Basement terrane correlations and crustal recycling in the western Superior Province:

Nd isotopic character of granitoid and felsic volcanic rocks in the Wabigoon subprovince, N. Ontario, Canada, *Precambrian Research* **132**, 245–274.

van der Lee, S. and Nolet, G.: 1997, Upper mantle S velocity of North America, *Journal of Geophysical Research* **102**(B10), 22815–22838.

van Schmus, W. R. and Hinze, W. J.: 1985, The Midcontinent Rift System, *Annual Review of Earth and Planetary Sciences* **13**, 345–383.

Vicker, P. A.: 1997, *Garnet peridotite xenoliths from kimberlite near Kirkland Lake, Canada*, Master's thesis, University of Toronto.

Wardle, R. J., James, D. T., Scott, D. J. and Hall, J.: 2002, The southeastern Churchill Province: synthesis of a Paleoproterozoic transpressional orogen, *Canadian Journal of Earth Sciences* **39**, 639–663.

Webb, K. J., Smith, B. H. S., Paul, J. L. and Hetman, C. M.: 2004, Geology of the Victor Kimberlite, Attawapiskat, Northern Ontario, Canada: cross-cutting and nested craters, *Lithos* **76**, 29–50.

White, D. J., Musacchio, G., Helmstaedt, H. H., Harrap, R. M., Thurston, P. C., van der Velden, A. and Hall, K.: 2003, Images of a lower-crustal oceanic slab: Direct evidence for tectonic accretion in the Archean western Superior Province, *Geology* **31**(11), 997–1000.

White, W. S.: 1972, Keweenawan flood basalts and continental rifting, *Geological Association of America, Abstracts with Programs* **4**, 732–734.

Wold, R. J. and Hinze, W. J.: 1982, Geology and Tectonics of the Lake Superior basin, *Geological Association of America Memoirs* **156**, 280.

Chapter 3

Origin of eclogite and pyroxenite xenoliths from Victor and implications for Superior craton formation

3.1 Introduction

The origin and development of sub-continental lithospheric mantle (SCLM) is still debated, with arguments for both subduction-accretion models (Helmstaedt and Doig, 1975; Helmstaedt and Schulze, 1989; Stachel et al., 1998; Canil, 2004; Pearson and Wittig, 2008) and mantle plume residue models (MacGregor and Carter, 1970; Griffin et al., 1999; Wyman and Kerrich, 2002; Aulbach, 2012). In the Superior craton, an accretionary tectonic model has been widely accepted based on numerous studies of crustal geology (e.g., Langford and Morin, 1976; Card, 1990; Percival et al., 2006b); however, there are no detailed studies on mantle eclogite xenoliths from the Superior craton to verify a possible subduction origin.

Eclogites are a minor component of the SCLM and are brought up as xenoliths in the majority of kimberlites worldwide. Despite their paucity, the study of eclogites can provide important insights into the composition and evolution of the SCLM. Two main competing models for eclogite formation are generally considered: an *in situ* origin from high pressure mantle melts (e.g., O'Hara and Yoder, 1967; Caporuscio and Smyth, 1990) and an origin as former oceanic crust, emplaced into the SCLM during subduction (e.g., Helmstaedt and Doig, 1975; Jacob, 2004).

Strong support for the latter model comes from stable oxygen isotopes. Eclogite xenoliths have a more diverse range in δ^{18}O than peridotite xenoliths, which have a narrow range corresponding to the accepted value for the upper mantle ($\delta^{18}O = 5.5 \pm 0.2$ ‰; Mattey et al., 1994). Significant fractionation of oxygen isotopes cannot occur at high temperatures in the mantle (e.g., Eiler, 2001), but occurs only due to water-rock interactions at crustal temperatures (Muehlenbachs and Clayton, 1972a,b). Jagoutz et al. (1984) and MacGregor and Manton (1986) were the first to recognise eclogites as rocks with a crustal prehistory based on the similar range in δ^{18}O of Roberts Victor eclogites to ophiolites that had undergone alteration by seawater (Muehlenbachs and Clayton, 1976).

In this contribution we present major and trace element analyses of a suite of eclogite and pyroxenite xenoliths from the Victor kimberlite (Superior craton), along with their oxygen, strontium and osmium isotopic compositions. Through these combined analyses, we aim to understand the formation of eclogites and pyroxenites - from either oceanic crustal protoliths or high pressure melts - and their emplacement into the SCLM. This suite of xenoliths provides an opportunity for the first time to evaluate the involvement of crustal components in the genesis of the lithospheric mantle below the Superior craton.

3.2 Samples and analytical techniques

The sample suite comprises 30 non-diamondiferous eclogite and pyroxenite xenoliths. These are mostly bimineralic composed of clinopyroxene and garnet; eight xenoliths are additionally orthopyroxene-bearing. Accessory rutile, ilmenite and sulphides are present in most samples. The majority of the samples were large enough for thin section preparation (ranging between ~ 2 and 5 cm in diameter), whereas six eclogite samples were too small (<1.5 cm in diameter) and grain mounts of constituent garnet and clinopyroxene were prepared. The samples have no layering at the scale observed and generally display granoblastic textures. Garnet and clinopyroxene grain boundaries display 120° angles, although these may vary to more rounded grain boundaries throughout each sample. Photos of representative thin sections are shown in Figure 3.1.

3.2.1 Major elements

Major element compositions were measured using a JEOL8900R electron microprobe at the University of Alberta, operating at 20 kV accelerating voltage, 20 nA probe current and 1 μm beam diameter. Peak count times varied between 30 and 60 seconds, and half that for background count times (Table A.1). Both natural and synthetic standards were used for calibration with matrix corrections following Armstrong (1995) (Table A.2). Multiple analyses for each mineral grain were averaged after those with low totals (< 98.5 %) and poor stoichiometry were removed. Detection limits were below 100 ppm for all oxides, apart from 200 ppm for Na_2O and 250 ppm for P_2O_5.

3.2.2 Trace elements

Microbeam trace element analyses were carried out at the University of Alberta, using a Nd:YAG UP213 nm laser ablation system (New Wave Research) connected to a Perkin Elmer Elan 6000 Quadrupole ICP-MS. The NIST612 glass standard was used for calibration and optimisation of instrument parameters. Samples were typically ablated for 50 seconds, with a spot size of 150 μm , 5 Hz repetition rate and energy density of $\sim$ 13 J/cm^2. Backgrounds were measured for 20 seconds prior to each analysis. Garnet grains (PN1 and PN2) that have been well characterised using several techniques (INAA, SIMS, LA-ICP-MS; Tappert et al., 2005) were ran as secondary standards. Average concentration values obtained for these garnets overlap within error to the recommended values (Tappert et al., 2005). Data reduction and concentration determinations, using EPMA-determined Ca concentrations in garnet as internal standard, were obtained using GLITTER laser ablation software (van Achterbergh et al., 2001).

3.2.3 Strontium isotopes

Chemical dissolution and TIMS

Strontium isotopic compositions of clinopyroxene picked from six samples were measured by isotope dilution thermal ionisation mass spectrometry (ID-TIMS). Between $\sim$3 mg and $\sim$30 mg clinopyroxene were picked, depending on Rb and Sr concentrations in individual samples (determined though laser ablation ICP-MS). These grains were leached for two hours in 1 ml cold 2N HCl, to remove any grain boundary contamination (e.g., Wittig et al., 2009). After pipetting the leachate and rinsing three times with MilliQ, a spike solution was added and the samples digested on a hotplate for one day in 1 ml HF / 1 ml HNO_3. Following dry down, HCl was added overnight and subsequently dried down, which brings the digested sample into chloride form ready for column chemistry. Rubidium and Sr were separated by conventional column chromatographic techniques using AG50W-X8 cation resin and then loaded on Re filaments with Ta activator and analysed on a Thermo Scientific Triton at the University of Alberta. The ^{85}Rb signal was used to correct for the isobaric interference of ^{87}Rb, using the normal ^{85}Rb/^{87}Rb ratio of 2.5906. Analyses were corrected for minimum procedural blanks of 243 pg Sr and 1270 pg Rb. Strontium blank contributions range between 0.001 and 0.008 % and Rb blank contributions between 0.6 and 5 %. 2 standard error (SE) uncertainties are reported as the in-run precision and are in the range 0.004 to 0.15%.

***In situ* MC-ICP-MS**

Strontium isotopic compositions for nine samples were obtained using a Nd:YAG UP213 nm laser ablation system (New Wave Research) coupled to a NuPlasma multicollector-ICP-MS, following procedures modified from Schmidberger et al. (2003). Line scans were ablated on clinopyroxene and collected in static multi-collector mode using Faraday detectors. The ^{85}Rb signal was used to correct for the isobaric interference of ^{87}Rb. Durango apatite, analysed by both TIMS and LA-ICP-MS (^{87}Sr/^{86}Sr (TIMS) = 0.706327; ^{87}Sr/^{86}Sr (LA-ICP-MS) = 0.70680 ± 0.00002 (2SD) Horstwood et al., 2008), was used as a secondary standard. Eleven analyses of Durango apatite on the first day of analyses gave ^{87}Sr/^{86}Sr = 0.70620 ± 0.0006 (2SE) and five analyses on the second day gave ^{87}Sr/^{86}Sr = 0.70632 ± 0.00066 (2SE). The apatite data were corrected for REE^{2+} interferences offline, whereas the clinopyroxene data were not, due to much lower REE contents. The weighted average for n line scans per sample are reported along with the in-run precision (2SE), which is typically between 0.001 and 0.033 %.

3.2.4 Oxygen isotopes

Oxygen isotopic analyses on garnet were performed on a IMS1280 multi-collector ion microprobe at the Canadian Centre for Isotopic Microanalysis

(CCIM) at the University of Alberta. Garnet grains about ~300 μm and less, were picked under the microscope and mounted in epoxy. Analytical protocols and data correction follow methods outlined in Ickert and Stern (2013).

$^{18}O/^{16}O$ data were collected during a one-day session, using a 15 μm diameter Cs^{+} primary beam and dual Faraday cups. During the analytical session, the primary beam intensity was $\sim$ 2.8 nA, yielding $\sim$ 3.3 x 10^{9} counts per second ^{16}O. The energy slit was fully opened. Data collection consisted of a 30 second raster (pre-sputtering), followed by secondary beam centering in the field aperture, and twenty, 5 second integrations for a total count time of 100 seconds. Amplifier baselines were measured before the session and subtracted from the ion beam intensities of each analysis.

The primary reference material to correct for instrumental mass fractionation (IMF) is UAG, a pyrope garnet from Gore Mountain with $\delta^{18}O$ of 5.72 ± 0.13 ‰ (2σ; Ickert and Stern, 2013). All results are reported relative to the international VSMOW standard. During the analytical session, the repeatability of UAG on the same mount as the unknown garnet material was 0.38 ‰ (2SD, n=32).

Any mineral that has wide variation in major element compositions, may exhibit variation in matrix-controlled instrumental mass fractionation (IMF). Vielzeuf et al. (2005) and Page et al. (2010) have documented the effect of Ca content (X_{Ca} = Ca/(Ca+Mg+Fe)) of garnet on instrument fractionation. We utilise a matrix correction substantially similar to Page et al. (2010), described by Ickert and Stern (2013) to correct for matrix effects based on the relative Ca abundances. The magnitude of the matrix correction varies from -0.25 ‰ to +1.71 ‰, but is mainly <1 ‰. The uncertainty on the matrix correction is propagated onto the final results. Secondary reference material S0088B, a near end-member Ca-Al (grossular) garnet was embedded in the same mount as the unknown garnet to check the accuracy of the matrix correction. Eight analyses of S0088B during the analytical session yielded a mean $\delta^{18}O$ value of +4.05 ± 0.16 ‰ (2 SE; n=8) after a matrix correction of +2.96 ‰, which agree with the value determined by laser fluorination of 4.13 ± 0.09 ‰ (2σ).

Two to three analyses per sample were performed. The total uncertainty

(2σ) on each analytical spot varies between ± 0.36 and ± 0.55 ‰ and is the combination of uncertainty on the mean UAG value for the session and uncertainty in the matrix correction. Analyses for each sample were averaged, with the uncertainty for each sample given as the largest error of the single spot analyses.

3.2.5 Rhenium and osmium isotopes

Each sample was broken into small fragments and then powdered using an agate mill. Quartz was powdered as a pre-clean and the milling equipment cleaned between samples using water, ethanol and compressed air. Between 0.5 and 1 g sample powders were added to Carius tubes with a mixed ^{190}Os - ^{185}Re spike and digested in reverse Aqua Regia (1:2 HCL:HNO_3) for five days at 240 °C (following Shirey and Walker, 1995). This was followed by solvent extraction of Os, first into $CHCl_3$ and then by back-extraction into HBr (Cohen and Waters, 1996). Re was recovered from the reverse Aqua Regia split after the first extraction, dried down and then separated by anion exchange chromatography (Morgan and Walker, 1989; Walker, 1988) using Eichrom AG1-X8 resin, followed by a single bead extraction. Os was purified using micro distillation techniques (Roy-Barman and Allègre, 1994; Birck et al., 1997). 20 μL HBr was added to the tip of a conical beaker and 30 μL CrO_3/H_2SO_4 solution to the dried down Os fraction. The inverted beaker was placed on a hotplate for three hours at 75 °C . The HBr drop was dried down and the distillation procedure repeated.

Isotopic compositions of Re and Os were measured by negative thermal ionisation mass spectrometry (N-TIMS) on a Thermo Scientific Triton at the University of Alberta. Rhenium and Os were loaded on Ni and Pt filaments, respectively. Barium, as $Ba(NO_3)_2$ or $Ba(OH)_2$ was added onto the filaments as an electron donor to aid with ionisation. Oxygen was leaked into the source during Os runs in order to improve ionisation efficiency. Rhenium isotopes were collected using Faraday cups and Os isotopes using an electron multiplier. Mass spectrometer fractionation was corrected by normalising ^{192}Os/^{188}Os to 3.08261 (Creaser et al., 1991). As Re and Os were run as negative oxides, data were corrected for interferences from three O isotopes, with $^{17}O/^{16}O = 0.0003$ and $^{18}O/^{16}O = 0.0020$. Analyses were corrected for procedural blanks of 0.37

pg Os and 0.67 pg Re.

$^{187}Re/^{188}Os$ and $^{187}Os/^{188}Os$ 2SE errors include the in-run precision, the uncertainty in the concentration and isotopic composition of the blank and the uncertainty in the spike calibration. 2SE uncertainties in $^{187}Os/^{188}Os$ are typically between ± 0.4 and 0.7%, with $^{187}Re/^{188}Os$ uncertainties between ± 0.4 and 1.4%.

3.3 Results

3.3.1 Mineral major and trace element chemistry

Eclogites and pyroxenites from Victor were classified based on clinopyroxene composition - 16 pyroxenites contain diopside (Na/Na+Ca < 0.2) whereas 17 eclogites contain omphacite (Na/Na+Ca > 0.2), consistent with commonly used definitions for eclogite (e.g., Coleman et al., 1965; Carswell, 1990; Pearson et al., 2003).

The samples in this study have a wide compositional range, comprising both low-Mg and high-Mg varieties, common for eclogite suites from many localities worldwide. For example, Bellsbank and Premier on the Kaapvaal craton (Taylor and Neal, 1989; Neal et al., 1990; Dludla et al., 2006), Koidu (Man craton; Barth et al., 2001, 2002a), Udachnaya (Siberian craton; Jerde et al., 1993; Beard et al., 1996; Snyder et al., 1997) and Diavik (Slave craton; Aulbach et al., 2007). Major and trace element compositions are given in Table A.3 to Table A.11 and Table B.1 to Table B.6. In addition to division into eclogites and pyroxenites, eclogites are also sub-divided into three groups based on similar major (Figure 3.2 and Figure 3.3) and trace element compositions (Figure 3.4).

High-Ca eclogites

The single calcium-rich sample has garnet with CaO = 15.7 wt%, MgO = 9.9 wt%, FeO = 10.9 wt%, Cr_2O_3 = 0.1 wt% (Figure 3.2 and Figure 3.3) and the lowest REE abundances in the suite (Figure 3.4). Garnet trace element patterns are extremely LREE depleted with $Ce_N/Sm_N = 0.003$, have a positive Eu anomaly ($Eu/Eu^* = 1.45$) and decrease again to the HREE ($Lu_N/Gd_N =$

0.44) (Figure 3.4). Eu/Eu* is calculated as $Eu_N/\sqrt{Sm_N X Gd_N}$ (e.g., Kemp and Hawkesworth, 2003) and REE_N refers to normalisation to CI chondrite (Sun and McDonough, 1989).

Omphacite has ~7 wt% Na_2O (Figure 3.2) and is LREE depleted with Ce_N/Sm_N = 0.03. It has a negative slope in the MREE to HREE (with an upward kink to Lu) and a slight positive Eu anomaly (Eu/Eu* = 1.17) (Figure 3.4). This sample has accessory kyanite. The temperature of last equilibration is 980 °C , based on Fe-Mg exchange between clinopyroxene and garnet and calculated at 5 GPa (Krogh, 1988).

Low-Mg eclogites

Eight samples classify as low-Mg eclogites. Garnets are Fe-rich with FeO = 17.5-24.4 wt%, MgO = 6.7-10.3 wt% and CaO = 5.7-10.6 wt%. They have the lowest Cr_2O_3 content of the entire suite (0.01-0.04 wt%). Garnets have normal REE_N patterns with depleted LREE (average La_N/Sm_N = 0.006), relatively flat MREE to HREE (average Lu_N/Gd_N = 1.32), and slight negative Eu anomalies (average Eu/Eu* = 0.96; range Eu/Eu* = 0.86-1.12). Clinopyroxenes have omphacitic compositions with 3.5-6.8 wt% Na_2O. They show LREE enrichment, a negative slope in the HREE (average Lu_N/Gd_N = 0.15) and a range in Eu/Eu* between 0.63-1.12 (with average Eu/Eu* = 0.92). Temperatures of last equilibration for the low-Mg eclogites range between 780 and 930 °C (calculated at 5 GPa; Krogh, 1988).

High-Mg eclogites

Eight high-Mg eclogites have garnet with MgO between 11.6-18.4 wt%, CaO between 4.0-8.5 wt% and FeO between 13.3-17.9 wt%. Cr_2O_3 varies between 0.05 and 0.18 wt%. Garnets are LREE depleted with Ce_N/Sm_N between 0.02-0.08 and have flat to slightly fractionated MREE to HREE (Lu_N/Gd_N = 0.5-3.7). Samples have both slightly negative and slightly positive Eu anomalies, with Eu/Eu* between 0.81 to 1.15 (Average Eu/Eu* = 0.99). Omphacitic clinopyroxenes have Na_2O between 2.7 and 4.7 wt%, LREE enrichment (average La_N/Sm_N = 2.69) and a negative slope in the HREE (average Lu_N/Gd_N = 0.04). Clinopyroxene has Eu/Eu* between 0.9 and 1.1; with average Eu/Eu* = 1.01. The high-Mg eclogites have temperatures of last equilibration between

835 and 975 °C (calculated at 5 GPa; Krogh, 1988).

Pyroxenites

Sixteen pyroxenites have garnet with MgO = 15.0-20.9 wt%, CaO = 4.0-8.0 wt% and FeO = 8.2-14.1 wt%. Cr_2O_3 ranges from ~ 0.1 to 0.9 wt%. Garnet is LREE depleted with $La_N/Sm_N < 0.1$ and has flat to slightly fractionated MREE to HREE, with Lu_N/Gd_N between 0.9 and 3.9. Eu/Eu* range between 0.93 and 1.17. Diopsidic clinopyroxene has between 0.9-2.7 wt% Na_2O and is LREE enriched (La_N/Sm_N between 2.3 and 20.8). It displays a negative slope in the HREE with average Lu_N/Gd_N = 0.07 and Eu/Eu* between 0.9 and 1.2. Eight of the pyroxenites contain enstatite, with a range in Mg# from 90.4 to 93.6 and 0.6-0.9 wt% Al_2O_3. Orthopyroxene was not analysed for trace elements, as it is not considered to be a major host for trace elements in the SCLM (e.g., Pearson et al., 2003).

The orthopyroxene-free pyroxenites yield temperatures between 770 and 860 °C (calculated at 5 GPa; Krogh, 1988).. The eight orthopyroxene-bearing samples allowed for both pressure and temperature calculations. Temperatures for Fe-Mg exchange between orthopyroxene and clinopyroxene (Taylor, 1998) were calculated iteratively with Al-in-orthopyroxene pressures (Nickel and Green, 1985) - yielding temperatures between 610 and 1030 °C and pressures between 2.0 and 4.7 GPa.

3.3.2 Strontium isotopic compositions

Strontium isotopic compositions for clinopyroxene from 12 samples were determined (Table C.1). Six samples were analysed by TIMS and nine samples by *in situ* MC-ICP-MS. Three samples were analysed by both techniques.

The high-Ca eclogite has clinopyroxene with the lowest Sr concentration (~30 ppm) in the suite. Clinopyroxene in the three low-Mg eclogites have ~ 150 to 300 ppm Sr; whereas clinopyroxene in the three high-Mg eclogites have slightly higher Sr concentrations, ranging from ~ 130 to 600 ppm Sr (Table C.1). The pyroxenites have clinopyroxene with the highest average Sr concentrations - the orthopyroxene-free pyroxenites range between ~ 250 and 690 ppm Sr; and the orthopyroxene-bearing pyroxenites between ~550 and 900 ppm Sr (Table C.1). Rb concentrations are low (< 5 ppm) and are below detection in half the samples. The six samples measured by TIMS have $^{87}Rb/^{86}Sr < 0.01924$.

The $^{87}Sr/^{86}Sr$ for clinopyroxene in the different eclogite groups is broadly similar and all are less radiogenic than the present-day bulk Earth composition ($^{87}Sr/^{86}Sr = 0.7045$; DePaolo and Wasserburg, 1976). Clinopyroxene in the three low-Mg eclogites analysed have a measured, present-day $^{87}Sr/^{86}Sr$ ranging between 0.7021 and 0.7031, the three high-Mg eclogites between 0.7020 and 0.7031, the three opx-free pyroxenites between 0.7020 and 0.7029 and the two opx-bearing pyroxenites between 0.7027 and 0.7039. The single high-Ca kyanite-bearing eclogite has clinopyroxene with $^{87}Sr/^{86}Sr$ of 0.7019. Three samples that were analysed by both TIMS and MC-ICP-MS have measured present-day $^{87}Sr/^{86}Sr$ ratios within error of each other (Table C.1). Due to low Rb contents, the calculated initial $^{87}Sr/^{86}Sr$ (at the time of kimberlite eruption, ∼180 Ma; Januszczak et al., 2013) for all samples are within error of their measured present-day values (Table C.1).

3.3.3 Oxygen isotopic compositions

Oxygen isotopic composition in garnet from all 33 samples was collected by SIMS. The majority of garnets have $\delta^{18}O$ values between ∼ 5 to 6 ‰, within error of the pristine mantle average ($\delta^{18}O = 5.5 \pm 0.2$ ‰; Mattey et al., 1994), with $\delta^{18}O$ in garnet ≈ $\delta^{18}O$ in the whole rock (Eiler, 2001, and references therein). Garnet in three of the low-Mg eclogites is more enriched in ^{18}O and has $\delta^{18}O$ values outside of error of the pristine mantle average (7.0 ± 0.5 ‰; 6.3 ± 0.4 ‰ and 6.3 ± 0.4 ‰) (2σ). The results from the oxygen isotope analyses are given in Table C.2 and Figure 3.5.

3.3.4 Rhenium and osmium isotopic compositions

Whole rock Re-Os isotopic compositions were obtained for 10 samples, considered to be representative of the different sample groups. Results are given in Table C.3. Rhenium and Os concentrations are plotted together with MORB and peridotite samples world-wide in Figure 3.6.

The single high-Ca eclogite has Re = 0.08 ppb and Os = 0.08 ppb. The three low-Mg eclogites have Re concentrations ranging from 0.10 to 0.56 ppb and Os from 0.10 to 0.14 ppb. The three high-Mg eclogites range between 0.03 and 0.16 ppb Re, with 0.17 to 0.21 ppb Os. The three pyroxenites have 0.03 to 1.53 ppb Re and 0.21 to 0.64 ppb Os.

The $^{187}Os/^{188}Os$ for all samples, apart from one pyroxenite, are radiogenic relative to the composition for O-chondrites (0.1283; Walker et al., 2002). This is expressed in their γ_{Os} , which is defined as the percentage deviation from a specific reservoir (O-chondrite in this case) at a certain time (e.g., Walker et al., 1989). The high-Ca eclogite has present day $\gamma_{Os} = 60$, the three low-Mg eclogites range from 153 to 1737 and the three high-Mg eclogites from 188 to 852. The three pyroxenites have a wide range in γ_{Os} , with one unradiogenic sample (γ_{Os} = -9) and two radiogenic samples (γ_{Os} = 152 and 623). The pyroxenite with the undradiogenic γ_{Os} composition is also the sample with the highest Re concentration (1.53 ppb) and is orthopyroxene-free.

The γ_{Os} values are shown in Figure 3.7 in relation to other mantle lithologies, ocean island basalts, continental crust and Archaean komatiites and basalts. Initial γ_{Os} , calculated for the time of kimberlite eruption (~180 Ma), is within 1 to 3 % of the present day γ_{Os} values (Table C.3).

The Re and Os isotopic compositions do not show any isochronous relationships and their model ages (T_{MA}), or mantle extraction ages, have a wide range between ~ 1 Ga and 41 Ga. The majority of model ages are older than the age of the Earth - these unrealistic ages typically reflect Re/Os ratios too low to account for the high measured $^{187}Os/^{188}Os$.

3.4 Discussion

3.4.1 Reconstructed bulk rock chemistry

Due to kimberlite infiltration in eclogitic / pyroxenitic xenoliths, original bulk incompatible trace element compositions cannot be measured directly, but need to be reconstructed using the modal proportions and analyses of clean mineral separates. Meaningful mineral modes could not be determined for these samples due to their small size, and approximate bulk rocks were reconstructed using modes of garnet 50% and clinopyroxene 50%. For the orthopyroxene-bearing pyroxenites, modes of garnet 45%, clinopyroxene 45% and orthopyroxene 10% were used. Previous studies have shown that the reconstructed trace element patterns for eclogites are relatively insensitive to the exact modes of constituent minerals (e.g., Jerde et al., 1993; Aulbach et al., 2007; Smart et al., 2009).

The bulk rock compositions of all eclogites and pyroxenites are shown in Figure 3.8, along with field for N-MORB (Sun and McDonough, 1989) and oceanic crust gabbro (Bach et al., 2001). The high-Ca eclogite has HREE abundances comparable to oceanic crust gabbro. The presence of the highly aluminous phase, kyanite, and a positive Eu anomaly (Eu/Eu* = 1.45) in the high-Ca eclogite, provide additional support for a gabbroic protolith. Positive Eu anomalies along with positive Sr anomalies (seen relative to Pr and Nd in Figure 3.8) are generally attributed to plagioclase accumulation and typical for cumulate gabbros of the lower oceanic crust. Strontium anomalies are generally considered to be more robust support for plagioclase accumulation since Eu anomalies may not be substantial if plagioclase crystallised together with a large proportion of clinopyroxene (Schmickler et al., 2004).

The low-Mg eclogites have flat to slightly negative slopes in whole rock $HREE_N$ patterns, with higher HREE abundances than gabbro, more comparable to average N-MORB as well as basalts from the Superior craton (e.g., tholeiites from several greenstone belts). However, the low-Mg eclogites do show positive Sr anomalies (Figure 3.8). Basalts typically possess neither positive Eu or Sr anomalies (see for example, N-MORB of Sun and McDonough (1989) and Klein (2003)), both of which are attributed to plagioclase fractionation/accumulation and therefore expected in a gabbro.

The low-Mg eclogites may be considered to have an intermediate REE composition between MORB and gabbro, that is more representative of bulk oceanic crust. For example, Viljoen et al. (2010) calculated 50:50 mixtures between N-MORB (composition from Klein, 2003) and a gabbro sample (sample 92OG53 from Benoit et al., 1996). This intermediate trace element composition has strong positive Sr anomalies, no Eu anomalies and HREE abundances between the two end-members - very similar to the REE composition of the low-Mg eclogites.

3.4.2 Formation of low-Mg and high-Ca eclogites

Petrogenetic models for mantle eclogites include an origin as high pressure cumulates of mantle melts (e.g., O'Hara and Yoder, 1967; MacGregor and Carter, 1970; Hatton and Gurney, 1987; Smyth et al., 1989; Caporuscio and Smyth, 1990) and an origin as high pressure metamorphic products of oceanic crust, emplaced into the SCLM by subduction processes (Helmstaedt and Doig, 1975; Helmstaedt and Schulze, 1989; Jacob et al., 1994). An extension of the subduction model is that some eclogites may be residues after TTG (tonalite-trondhjemite-granodiorite) extraction from former oceanic crust in the garnet stability field (Ireland et al., 1994; Rollinson, 1997; Barth et al., 2001). These different models and their applicability to the formation of Victor eclogites are discussed below.

Origin as high pressure mantle melts

A high pressure origin for the low-Mg eclogites is considered unlikely due to a number of reasons. Reconstructed bulk rock compositions of the low-Mg eclogites do not overlap with the composition of experimental melts of peridotite at 3-7 GPa (Walter, 1998, Figure 3.9). High pressure melts are too high in MgO and too low in Al_2O_3 to match these low-Mg eclogitic bulk compositions and, additionally, have olivine as a liquidus phase (e.g., O'Hara and Yoder, 1963), a phase not present in eclogites. Kyanite, found as an accessory phase in the single high-Ca eclogite, is not in equilibrium with a high pressure peridotite-derived melt composition. Additionally, clinopyroxenes in these low-Mg eclogites are jadeitic, whereas high pressure liquidus clinopyroxenes are predominantly Ca-Tschermaks (experimental compositions of Eggins, 1992).

We considered the possibility that the eclogites at Attawapiskat are Midcontinent Rift basalts that have crystallised at depth in the SCLM to form eclogites. The bulk compositions of the Mamainse Point basalts (Shirey et al., 1994) show some similarity to the low-Mg eclogites (Figure 3.9). However, if these eclogites were products of single-stage melting related to the Midcontinent Rift, coherent Re-Os isochron and model age relationships should be present, indicating extraction from the convecting mantle at ~ 1.1 Ga. The lack of any Re-Os isochron or model age relationships in the eclogites, preclude a single-stage melt model for their genesis, but rather require a more complex multi-stage model. Furthermore, the high δ^{18}O in three low-Mg eclogites requires surficial alteration, as oxygen isotopes cannot be appreciably fractionated at high temperatures in the mantle (e.g., Clayton et al., 1975; Eiler, 2001).

Origin as low pressure melts

Support for plagioclase-bearing protoliths comes from the presence of kyanite (not in equlibrium with high pressure peridotitic melt compositions), and the positive Eu (Eu/Eu* = 1.45 in the high-Ca, kyanite-bearing sample) and Sr anomalies (in all low-Mg and high-Ca samples) and the generally flat MREE to HREE patterns in the low-Mg eclogites (e.g., Green, 1994; Jacob et al., 2003b; Jacob, 2004). These flat REE patterns can be neither garnet-rich cumulates (which would have higher HREE abundances in garnet) nor melts with garnet in the residue and instead resemble the REE patterns of MORB / plagioclase, thereby suggesting a metamorphic origin for garnet from lower pressure protoliths.

Compared to Archaean tholeiites and komatiites, the whole rock compositions of the low-Mg eclogites are lower in SiO_2 and higher in CaO and Al_2O_3. They do, however, show overlap with oceanic gabbros (Bach et al., 2001), apart from their slightly lower SiO_2 content (Figure 3.10). The low-Mg eclogites (including the kyanite-bearing sample) are LREE depleted, which together with their lower bulk SiO_2 content (relative to basalts and oceanic crust gabbro) indicate that they may be residues of a secondary partial melting event.

Also, their Re concentrations are low relative to MORB (Figure 3.6; Gannoun et al., 2007) - too low to account for the radiogenic Os isotopic compositions - consistent with Re loss during dehydration/partial melting of a subducting slab (e.g., Dale et al., 2007). This, along with their variation in model age and isochron systematics, provides further support that the low-Mg eclogites are residues after partial melting.

As has been proposed for other localities, TTG's and eclogites show a complementary melt-residue relationship (Ireland et al., 1994; Rollinson, 1997; Barth et al., 2001; Tappe et al., 2011), with the major element composition of greenstone-belt basalts lying on a broadly linear trend between the eclogites and TTG's (Figure 3.10).

This complementary relationship between TTG and low-Mg eclogite is also seen in the rare earth elements (Figure 3.11a) - tonalites are LREE-enriched and HREE-depleted (e.g., Kemp and Hawkesworth, 2003), whereas the low-Mg eclogites studied here are LREE-depleted and HREE-enriched. As a further test of a possible melt-residue relationship between low-Mg eclogites and TTG's, compositions of residue and melt during batch melting of former pillow basalt were calculated. For these calculations, basalts from greenstone belts in the western Superior Province and partition co-efficients for eclogite in equilibrium with a tonalite melt (Barth et al., 2002c) were used. Residue and melt compositions at varying melt fractions are plotted in Figure 3.11b. The LREE-depleted composition of the low-Mg eclogites can be reproduced with $\sim$ 25-40% melt extraction, and the co-existing melt composition overlaps with that of tonalite. These results are consistent with experimental studies that produced TTG melts at $\sim$ 25-40% partial melting of metabasalt at high pressures (2.2 - 3.2 GPa) (Rapp et al., 1991; Rapp and Watson, 1995). The experimental residues at 3.2 GPa are eclogitic and contain garnet with MgO = 8.5 - 10.4 wt%, FeO = 19.9 - 21.1 wt%, CaO = 5.6 - 9.0 wt% and clinopyroxene with MgO = 8.7 wt%, CaO = 11.3 wt%, Na_2O = 6.6 wt% (Table 5 and 6 in Rapp and Watson, 1995). These major element compositions overlap with those of the Victor low-Mg eclogites (Table A.3 to Table A.10).

The tectonic setting for formation of TTG magmas, and by inference, emplacement of the low-Mg eclogites in the SCLM, is still debated. TTG's may be products of fluid-present melting of altered mafic rocks in a subducting slab (e.g., Rapp and Watson, 1995; Prouteau et al., 1999) or fluid-absent melting of mafic rocks in a thickened crust at higher temperatures (e.g., Rapp et al., 2003). To explain the HREE-depleted nature of TTG's, they are considered to be the melt products of mafic rocks with garnet in the residue - either garnet amphibolite or eclogite (e.g., Jahn et al., 1981; Rapp et al., 1991; Foley et al., 2002).

The $\delta^{18}O$ values of the low-Mg eclogites constrains the tectonic setting for melt extraction. Their fractionated values cannot be produced at high temperatures in the mantle, but only at low temperatures due to seafloor weathering

(Muehlenbachs and Clayton, 1972a,b). A study of basaltic glasses at Macquarie Island by Bindeman et al. (2012), confirmed that the oxygen isotopic composition of the mantle stays within a narrow range, even under a wide range of melting conditions. Additionally, it has been shown that Archaean granitoids on the Superior craton that are derived from a mantle source have a narrow range in $\delta^{18}O$ (5.5 ± 0.4 ‰), whereas those with crustal contributions to the source regions have a higher $\delta^{18}O$ (6.4 ± 0.2 ‰), outside the pristine mantle range (King et al., 1998). $\delta^{18}O$ in garnet of three low-Mg eclogites are higher than the typical mantle value, which is considered strong evidence that these eclogites had shallow oceanic crust precursors that were affected by low-temperature seafloor alteration processes and subsequently subducted and emplaced into the SCLM.

Summary

We have argued that the low-Mg eclogites have a shallow origin as plagioclase-bearing protoliths that were subsequently subducted and emplaced into the SCLM. This is supported by their generally flat MREE to HREE compositions, the presence of kyanite and a positive Eu anomaly in the high-Ca sample, and $\delta^{18}O$ in three low-Mg eclogites that are higher than the pristine mantle value. LREE depletion in the low-Mg eclogites, along with unradiogenic $^{87}Sr/^{86}Sr$ (less than present-day bulk Earth $^{87}Sr/^{86}Sr = 0.7045$; DePaolo and Wasserburg, 1976) indicate that they were not affected by widespread metasomatism after emplacement in the SCLM.

3.4.3 Formation of high-Mg eclogites and pyroxenites

The high-Mg eclogites and pyroxenites have several compositional characteristics that require a distinct origin to the low-Mg eclogites. These include 1.) bulk rock compositions which are broadly similar to < 3 GPa peridotite-derived melts and massif pyroxenites (Baker and Stolper, 1994; Pearson et al., 1993), 2.) LREE-enriched compositions, 3.) mantle-like $\delta^{18}O$ and 4.) a wide range in Os isotopic compositions from unradiogenic to radiogenic (relative to the $^{187}Os/^{188}Os$ of O-chondrites = 0.1283; Walker et al., 2002).

The LREE's are not typically considered in petrogenetic models for eclogite xenoliths suites, as any enrichment may be due to secondary processes after emplacement in the SCLM. Metasomatism by kimberlitic/carbonatitic mantle melts with high Mg content and strong LREE enrichment (le Roex et al., 2003) has previously been suggested for some eclogite suites. For example, the Udachnaya eclogites show an increase in MgO and incompatible trace elements compared to inclusions in diamonds (e.g., Ireland et al., 1994; Snyder et al., 1997).

The LREE enrichment in the Victor high-Mg eclogites and pyroxenites could support this carbonatite/kimberlite metasomatism model, for example, if 5% average carbonatite (from Tappe et al., 2006) is mixed with the low-Mg eclogites, the REE compositions of the high-Mg eclogites can be reproduced (Figure 3.12). However, 5% addition of kimberlite or carbonatite does not significantly alter the major element compositions and even higher degrees of metasomatism do not provide sufficient enrichment in SiO_2 or MgO to match the compositions of the high-Mg eclogites and pyroxenites. Additionally, these samples all have unradiogenic $^{87}Sr/^{86}Sr$, uncharacteristic for samples that have undergone metasomatism by fluids/melts originating in an ancient enriched SCLM, which would typically impose radiogenic $^{87}Sr/^{86}Sr$ and unradiogenic $^{143}Nd/^{144}Nd$ (e.g., Richardson et al., 1984).

The metasomatic model is therefore not suitable for the Victor high-Mg eclogites and pyroxenites. The LREE enrichment observed in these samples is not considered to be a secondary feature in these rocks, but rather a primary characteristic that needs to be accounted for in any model that satisfactorily explains their genesis.

Several other models for pyroxenite (and high Mg eclogites) petrogenesis have been proposed. These include 1.) the *in situ* crystallisation of partial melts of peridotite (e.g., Dick and Sinton, 1979; Sinigoi et al., 1983; Voshage et al., 1988); 2.) mafic to intermediate melts infiltrating depleted peridotite and forming a mixing product (e.g., Kelemen et al., 1993; Yaxley and Green, 1998; Garrido and Bodinier, 1999; Rapp et al., 1999; Aulbach et al., 2002; Taylor et al., 2003; Smart et al., 2009) and 3.) similar to the model proposed for eclogites, residues of melting of oceanic crust in the mantle (e.g., Dick and Sinton, 1979; Polvé and Allègre, 1980; Loubet and Allègre, 1982; Allègre and Turcotte, 1986; Blichert-Toft et al., 1999). The applicability of these models to the high Mg eclogites and pyroxenites at Victor is discussed below.

Origin as residues of melting of oceanic crust

The high-Mg eclogites and pyroxenites have only slight negative / positive Eu and Sr anomalies (Figures 3.4 and 3.8). Although eclogite protoliths with significant plagioclase crystallisation may not necessarily show large Eu anomalies, the lack of strong positive Sr anomalies does not support plagioclase accumulation in the protoliths (e.g., Schmickler et al., 2004). Additionally, their LREE enrichment relative to chondrite/NMORB argues against a residual origin (e.g., after partial melting during subduction) (Figure 3.8).

Origin as high pressure mantle melts

Calculated pressures for the orthopyroxene-bearing assemblages indicate they originated between 2 and 5 GPa. At these pressures, melts generated from peridotite would be basaltic-picritic (e.g Takahashi, 1986; Takahashi et al., 1993), which does not correspond with the bulk compositions of these eclogites and pyroxenites in terms of their MgO content.

Higher MgO melts, such as komatiites typically originate from higher pressures (5-7 GPa; Takahashi, 1986; Takahashi et al., 1993). However, the bulk compositions of the Victor high-Mg eclogites and pyroxenites are not similar to either high pressure peridotite melts (3-7 GPa experimental melts of Walter, 1998) or natural komatiites from greenstone belts on the Superior (Figure 3.10). The high-Mg eclogites and pyroxenites are also more strongly LREE-enriched (up to 100 times chondrite) and have higher HREE abundances than komatiites from greenstone belts in the Superior, which have flat REE patterns at < 10 times chondritic abundance (Hollings et al., 1999).

The whole rock compositions of the high-Mg eclogites and pyroxenites are similar to peridotite melts at intermediate pressure - they fall between $\sim$1 GPa peridotite melts (experimental melts of Baker and Stolper, 1994) and $\sim$ 3-7 GPa peridotite melts (experimental melts of Walter, 1998, Figure 3.9) - suggesting that they may have an origin as deeper portions of oceanic lithosphere, that were subsequently displaced to slightly greater depths. Additionally, these compositions overlap with Beni Bousera pyroxenites (Pearson et al., 1993) and high-Mg eclogites from Koidu. For the latter, Barth et al. (2002a) suggested an origin as deeper portions of oceanic lithosphere, as gabbroic cumulates or pyroxenitic veins. Pyroxenitic veins in the deeper oceanic lithosphere have also been suggested as protoliths for eclogitic diamond inclusions at Jericho (Smart et al., 2012).

An origin as melts emplaced in the deeper portions of the oceanic lithosphere, however, does not account for the unradiogenic Os isotopic composition in pyroxenite - unless the melt had interacted / equilibrated with a depleted component (e.g., peridotitic wall rock), as discussed in the next section.

Origin as reaction products between melt and peridotite

Formation of pyroxenite and Mg/Si-rich eclogites by mixing/reaction between peridotite and siliceous melts has been proposed by various authors since the 1970's (e.g., Ringwood, 1974; Sekine and Wyllie, 1982; Kelemen, 1986) and supported by the experimental studies of Yaxley and Green (1998), Rapp et al. (1999) and Mallik and Dasgupta (2012). Siliceous melts generated from eclogite will react with surrounding peridotite and therefore cannot percolate upwards (Yaxley and Green, 1998, and references therein). This reaction is at the expense of olivine.

This mode of origin has been proposed for several eclogite/pyroxenite massif and xenolith localities. For example, formation of websterites in the Ronda massif has been related to melt-rock reactions, whereby upwelling asthenospheric melts infiltrate the lithosphere and react with peridotite (Garrido and Bodinier, 1999). Formation of the LREE-enriched pyroxenites in the Cabo Ortegal massif (Santos et al., 2002) has been linked to the introduction of melts from a subducting slab. The involvement of slab melts was also suggested for the genesis of websteritic inclusions in Venetia diamonds (Aulbach et al., 2002) and the petrogenesis of high-Mg eclogites and pyroxenites in Yakutia (Taylor et al., 2003). Origin of the high-Mg eclogites at Jericho has been attributed to similar processes involving partial melting of low-Mg eclogites and the surrounding peridotite which facilitates elemental exchange and equilibration between the two rock types (Smart et al., 2009).

There are several compositional characteristics of the high-Mg eclogites and pyroxenites that are consistent with this origin:

- The LREE enrichment in the high-Mg eclogites and pyroxenites is consistent with the involvement of a low degree partial melt in their genesis. This is similar to the suggested formation mode for LREE-enriched spinel pyroxenites as crystal cumulates of mafic magmas within the lithospheric mantle. These are not necessarily cumulates by gravitational settling, but by crystal plating onto the side of a flowing magma conduit (e.g., Frey, 1980; Vaselli et al., 1995; Witt-Eickschen and Kramm, 1998; Dobosi et al., 1998). This scenario is consistent with low-degree melts from a subducting slab infiltrating the overlying peridotitic mantle wedge, with the crystals plating onto the side of the conduit forming hybridised reaction products between melt and wall rock.

- Reconstructed whole rock compositions of the high-Mg eclogites and pyroxenites are intermediate between eclogite-derived melts and an average fertile peridotitic composition (pyrolite) (Figure 3.9), suggesting that they may be the result of mixing between these two end-members. In addition, their compositions are broadly similar to experimentally produced mixtures of partial melts of MORB-eclogite and fertile peridotite at 3 GPa (Mallik and Dasgupta, 2012) and 3.5 GPa (Yaxley and Green, 1998).

- Higher Cr contents in garnet from the high-Mg eclogites and pyroxenites than in the low-Mg eclogites indicate equilibration with surrounding peridotite (Figure 3.3). Chromium is present in higher concentrations in peridotites than pyroxenites and eclogites (e.g., Gurney and Switzer, 1973; Pearson et al., 2003). High Cr/Al in peridotites is attributed to a protolith that experienced melt depletion in the spinel stability field (Bulatov et al., 1991; Trønnes et al., 1992; Canil and Wei, 1992; Stachel et al., 1998). Therefore reaction of depleted peridotite with a melt can explain the elevated Cr contents in garnet from the high-Mg eclogites and pyroxenites compared to low-Mg eclogites.

- The Osmium isotopic compositions of the high-Mg eclogites and pyroxenites range from unradiogenic (γ_{Os} = -10) to radiogenic (Figure 3.7). The unradiogenic $^{187}Os/^{188}Os$ requires the involvement of a depleted component during formation. During melting Re is moderately compatible and Os is incompatible, in time leading to highly radiogenic $^{187}Os/^{188}Os$ in the former melt (e.g., MORB) and unradiogenic $^{187}Os/^{188}Os$ in the depleted residue. Therefore, the most likely scenario for mixing between radiogenic and unradiogenic components involves melts from oceanic crust and depleted SCLM.

Experimental reaction products between eclogite-derived melts with intermediate compositions and peridotite are similar to those of the Victor eclogites. Layered run 9117 of Yaxley and Green (1998) sandwiched equal proportions of coesite-eclogite and pyrolite as starting materials. The reaction products at 1300 °C and 3.5 GPa were in four distinct zones, with the mineral compositions in each analagous to the compositions of certain Victor samples: Zone 1.) The products of the former coesite eclogite layer are almandine-rich garnet, omphacite and a dacitic melt. The mineral compositions of garnet and omphacite in this layer overlap with the Victor low-Mg eclogites (garnet with 12 wt% MgO, 17 wt% FeO and 6.6 wt% CaO; omphacite with 3.8 wt% Na_2O and 9 wt% MgO). Zone 2.) Layer of bimineralic eclogite. Garnet with 19.9 wt% MgO and 0.4 wt% Cr_2O_3, indicating increasing equilibration with peridotite. Clinopyroxene is diopsidic with 1.3 wt% Na_2O and 19.1 wt% MgO. These mineral compositions are similar to those of the high-Mg eclogites and pyroxenites. Zone 3.) Layer with a high proportion of orthopyroxene and minor olivine, clinopyroxene and garnet. This layer could be the equivalent to the orthpyroxene-bearing pyroxenites, although orthopyroxene is not a major phase in Victor samples. Zone 4.) Layer of enriched former pyrolite (garnet lherzolite). Garnet has 20 wt% MgO and 1.3 wt% Cr_2O_3 and the diopside has 1.2 wt% Na_2O and 19.2 wt% MgO.

The similarity of these experimental products to our samples is strong support for a model whereby the low-Mg eclogites are residues after partial melt extraction from former MORB, and the high-Mg eclogites and pyroxenites are reaction products between such melts and peridotitic wall rock.

Summary

The high-Mg eclogites and pyroxenites have compositional characteristics that require a distinct origin to the low-Mg eclogites. Their bulk compositions, $LREE_N$-enriched trace element patterns and in particular, occurrence of unradiogenic $^{187}Os/^{188}Os$ (less than the $^{187}Os/^{188}Os$ of O-chondrites = 0.1283; Walker et al., 2002), is consistent with formation by reaction of broadly siliceous melts (generated from the melting of low-Mg eclogites) with depleted peridotite.

3.4.4 Relative age constraints

The timing of eclogite and pyroxenite formation could not be constrained, as the Re-Os isotopic compositions of the eclogites and pyroxenites do not have any coherent isochron or model age relationships. The radiogenic $^{187}Os/^{188}Os$ of the majority of the samples - similar to Archaean komatiites and basalts (Figure 3.7) - do, however, require long term isolation of a high Re/Os component from the convecting mantle after melt extraction. Therefore a Neoarchaean age for the formation of these eclogites is likely, consistent with $\sim$ 2.8-2.6 Ga U-Pb crystallisation ages for lower crustal granulite xenoliths from Attawapiskat (Moser et al., 1997), which may be the lower grade metamorphic equivalent to the eclogites discussed here.

3.4.5 Implications for Superior craton assembly

Models for the formation of cratonic roots include: 1.) subcretion of mantle plumes (e.g., Wyman and Kerrich, 2002; Griffin et al., 2003), 2.) stacking of oceanic lithosphere (Helmstaedt and Schulze, 1989; Helmstaedt and Gurney, 1995) with possible additional fluid-fluxed melting of residual peridotite in the mantle wedge to produce highly depleted dunitic residues (e.g., Hirschmann et al., 1999; Bernstein et al., 2006; Pearson and Wittig, 2008), 3.) melting at the base of oceanic plateaus to form TTG's with delamination of the high density resititic eclogite (Bédard, 2006) and 4.) diapiric ascent of foundered shallow melting residues (Herzberg and Rudnick, 2012).

The low-Mg eclogites have been shown in this paper to require low pressure protoliths, which is consistent with emplacement into the SCLM by subduction, as is now the preferred model for Superior craton formation (see references above). This precludes the viability of plume models for craton assembly. The three remaining models all predict shallow basaltic precursors for mantle eclogites. Consistent with a low pressure origin, the high $\delta^{18}O$ values in the low-Mg eclogites require an origin as seafloor-altered oceanic crust.

A subduction origin of the eclogites studied here is consistent with numerous terranes in the western Superior which have submarine basalt sequences (i.e. ocean floor) (e.g., Hollings et al., 1999; Rogers, 2002) and magmatic arc assemblages (i.e. melting in the mantle-wedge above a subducting slab) (e.g., Corfu and Stone, 1998). Various field-based studies have reported terrane accretion by successive subduction of the west-east orientated terranes in the western Superior Province (e.g., Corfu and Stott, 1986; Stott and Corfu, 1988; Corkery et al., 2000; Skulski et al., 2000). This is supported by seismic profiles in the Abitibi-Grenville (Calvert et al., 1995) and western Superior (White et al., 2003) that have dipping structures interpreted to represent Neoarchaean subduction zones. These are seen to depths of at least 30 km, corresponding to a pressure of 1 GPa, the minimum for eclogite stability (e.g., Green and Ringwood, 1972).

3.5 Conclusions

Eclogites and pyroxenites sampled by the Victor kimberlite have large compositional variability. Distinct origins are required for low-Mg eclogites and high-Mg eclogites (and pyroxenites). The low-Mg eclogites have oceanic crust precursors that were emplaced into the SCLM by subduction and are residues after extraction of a broadly siliceous melt (TTG?). The high-Mg eclogites and pyroxenites are shown to likely result from interaction between a siliceous melt and surrounding peridotite.

These two processes, i.e., partial melting leaving low-Mg eclogitic residues and subsequent reaction of these melts with peridotite to form high-Mg eclogites and pyroxenites, may be temporally related. We consider two plausible scenarios:

Scenario 1 involves the melting of meta-basalt (former oceanic crust) in a downgoing subducting slab. Slab melting is possible due to higher heat flow in the Archaean (e.g., Sleep and Windley, 1982; Martin, 1986). Melt extraction leaves the low-Mg eclogites as residues. The broadly tonalitic melt reacts with the overlying peridotitic mantle to form eclogites with elevated Mg# and orthpyroxene-bearing layers.

Scenario 2 involves the emplacement of undepleted low-Mg eclogites into the

SCLM by subduction, without significant slab-melting. A later heating event (perhaps upwelling of asthenospheric mantle, e.g., during the Midcontinent Rift at 1.1 Ga (Paces and Miller, 1993)) causes the eclogites to melt, due to the lower hydrous solidus of eclogite compared to peridotite (Yasuda et al., 1994). This eclogite-derived melt, which is broadly tonalitic to granodioritic in composition, then reacts with the surrounding peridotite to form Mg- and Cr-rich eclogite as well as orthpyroxene-bearing layers, similar to experimental products in Yaxley and Green (1998).

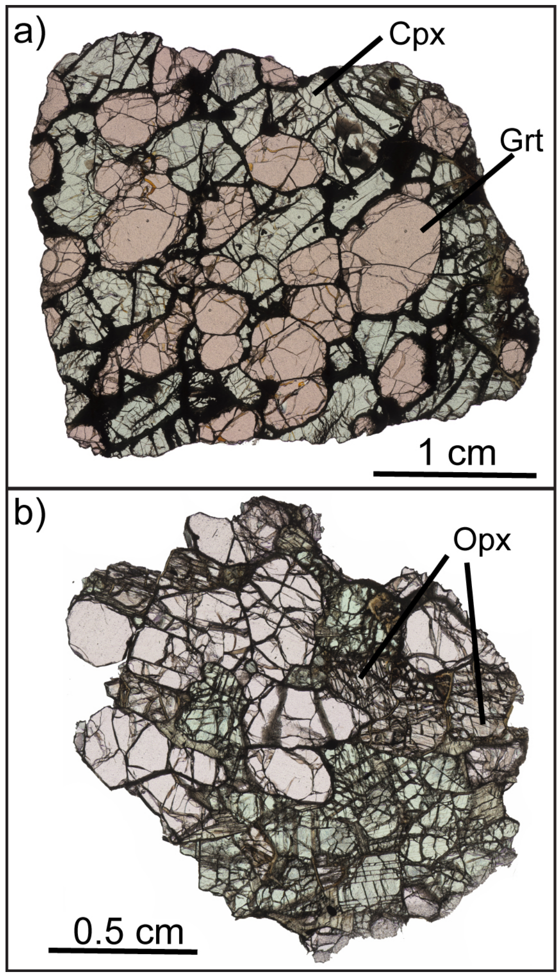

Figure 3.1: Representative samples in thin section (plane-polarised light). a.) Bimineralic low-Mg eclogite with omphacite and garnet. b.) Pyroxenite with diopside, garnet and enstatite.

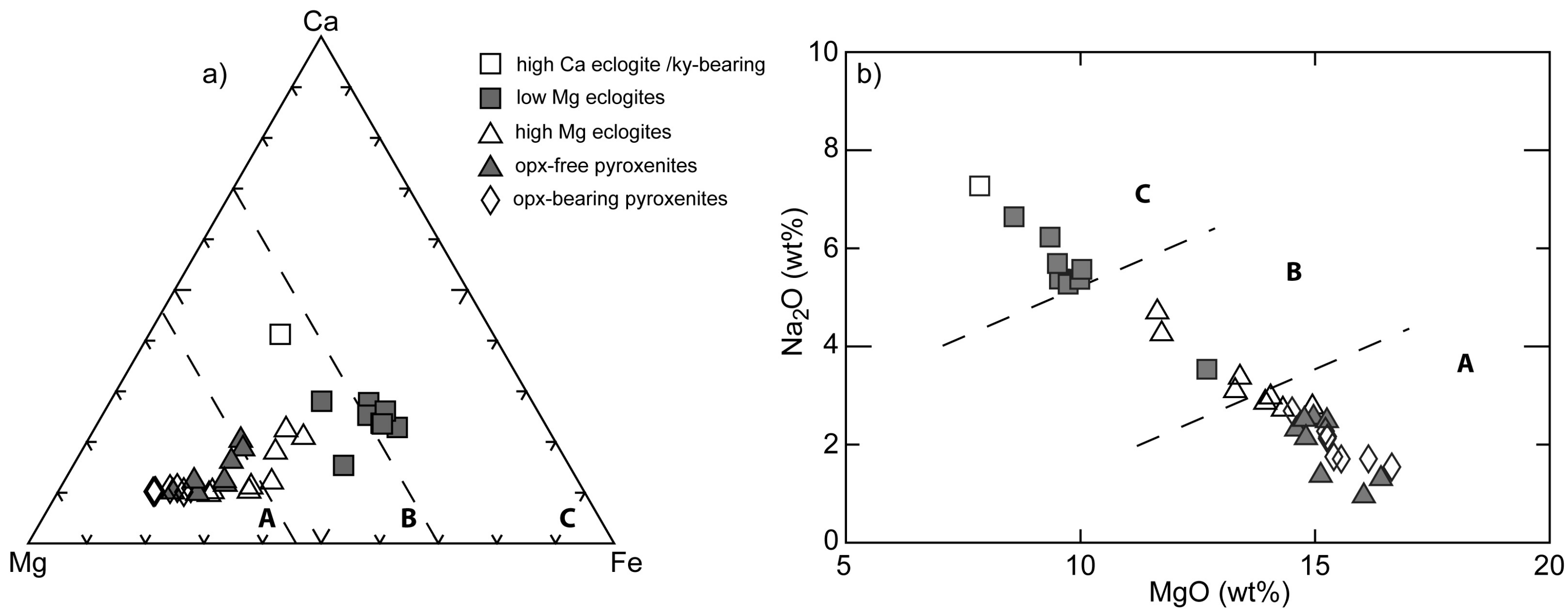

Figure 3.2: a.) Ca-Mg-Fe compositions of garnet in eclogite and pyroxenite xenoliths. b.) Clinopyroxene compositions. Both figures show the A-B-C eclogite classification scheme of Coleman et al. (1965). Garnet and clinopyroxene may lead to different classifications; for example, the high-Ca eclogite falls in the group B field according to garnet compositions and in group C according to clinopyroxene.

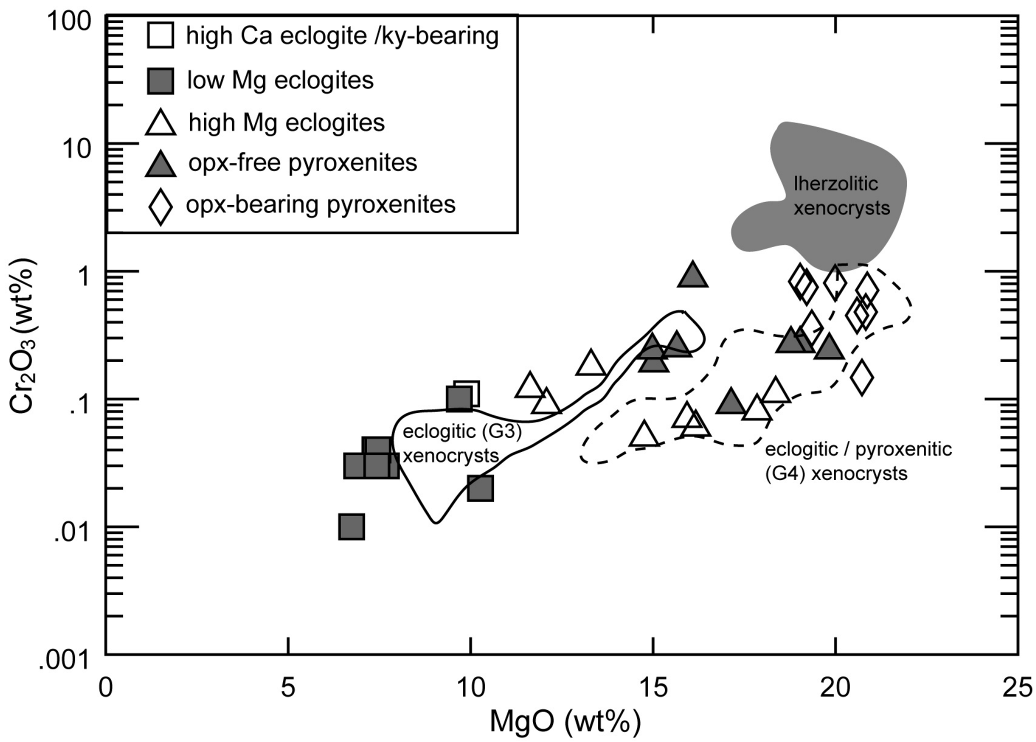

Figure 3.3: Garnet MgO and Cr_2O_3 in eclogite and pyroxenite xenoliths compared to xenocryst compositions from Victor (Chapter 5). G3 / G4 classification for eclogitic and pyroxenitic xenocrysts after Grütter et al. (2004). Garnet from pyroxenitic xenoliths and xenocrysts have similar MgO but lower Cr_2O_3 content compared to Victor lherzolitic xenocrysts.

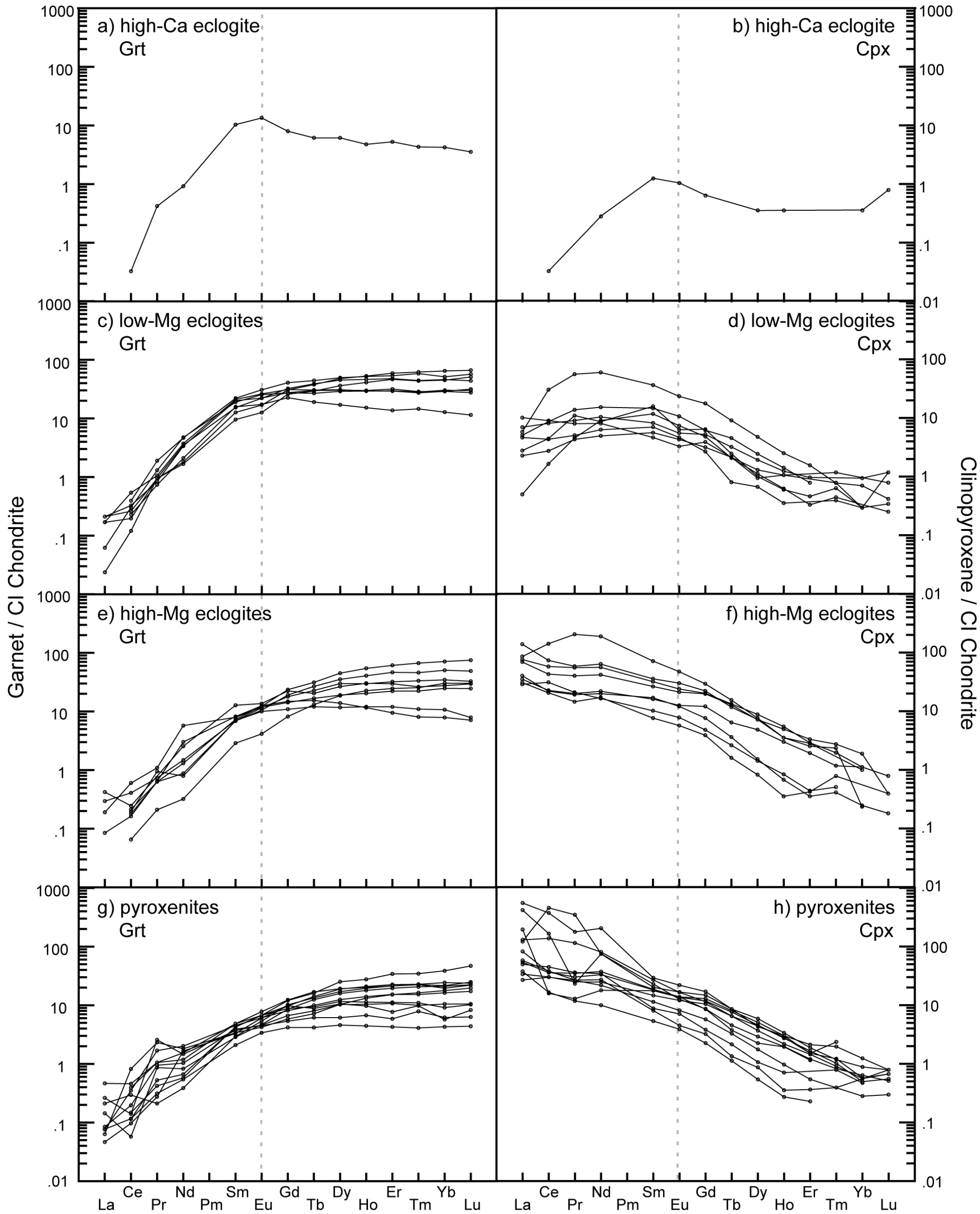

Figure 3.4: Garnet and clinopyroxene REE compositions, for the different compositional groups, normalised to CI chondrite (Sun and McDonough, 1989).

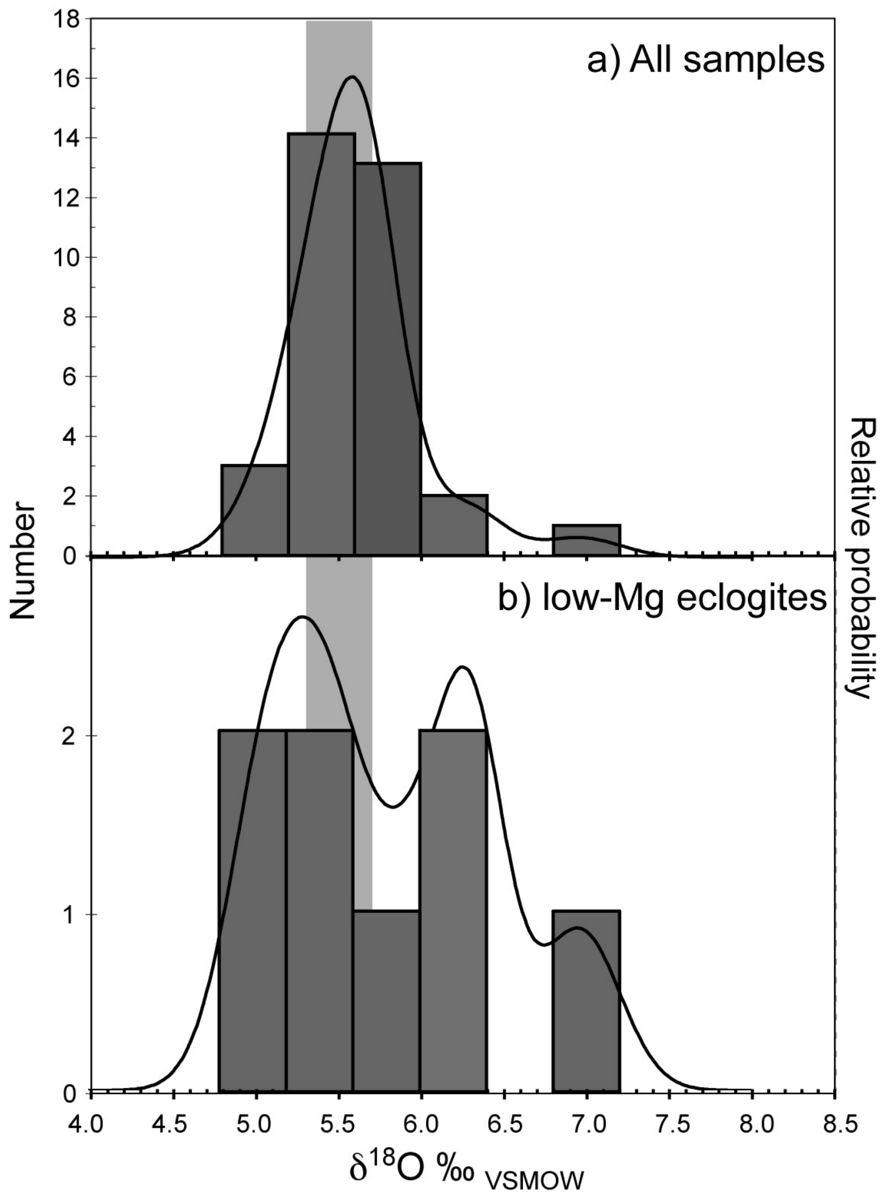

Figure 3.5: a) Oxygen isotope data for all samples in the study, showing a normal distribution around the mantle average (grey field; $\delta^{18}O = 5.5 \pm 0.2$ ‰; Mattey et al., 1994). b) low-Mg eclogites with 3 samples that have values higher than pristine mantle. Bin sizes for the histograms are 0.4 ‰, equivalent to the average error on the analyses. The probability distributions were plotted in Isoplot (Ludwig, 1991).

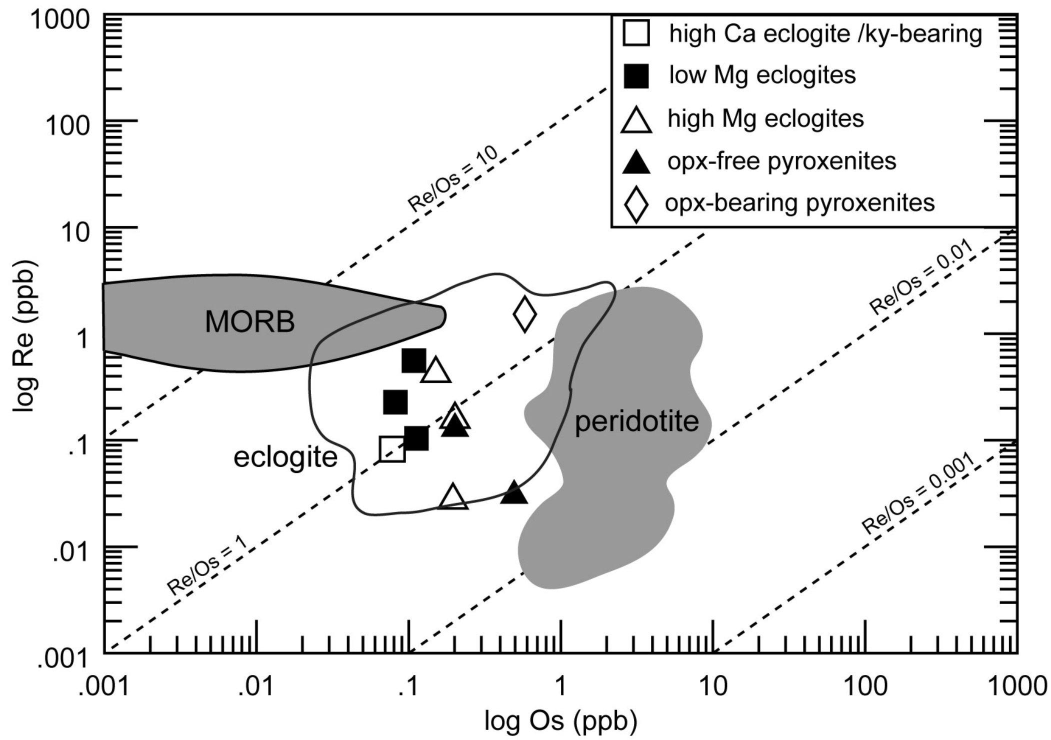

Figure 3.6: Rhenium and Os concentrations of the samples in this study compared to MORB (Gannoun et al., 2007) and worldwide mantle xenoliths (Pearson et al., 1995a,b; Graham et al., 1999; Barth et al., 2002b; Irvine et al., 2003; Menzies et al., 2003; Westerlund, 2005; Aulbach et al., 2009; Luguet et al., 2009; Wittig et al., 2010). "Common Os" - the Os concentration after in-grown ^{187}Os is subtracted - is plotted for eclogites and MORB. The low-Mg eclogites have lower Re contents than MORB (at the same Os concentration), in agreement with the interpretation that they are residues of melting of subducted oceanic crust. In such a scenario, Re would have been lost (along with the other incompatible elements) during dehydration and partial melting of the subducting slab (e.g., Becker, 2000; Dale et al., 2007).

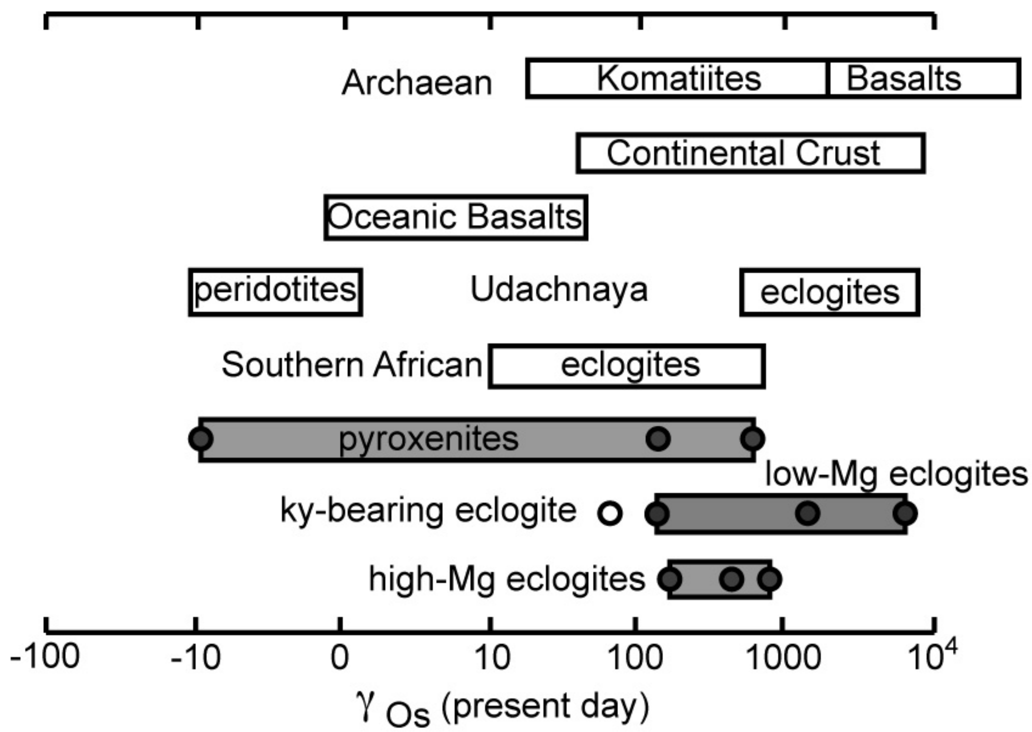

Figure 3.7: Comparison of present day γ_{Os} for Victor eclogites and pyroxenites (shaded) with other eclogite suites and a variety of mafic magmas. γ_{Os} was calculated as the percentage deviation from O-chondrite (Walker et al., 2002). Literature data from Pearson et al. (2003, and references therein).

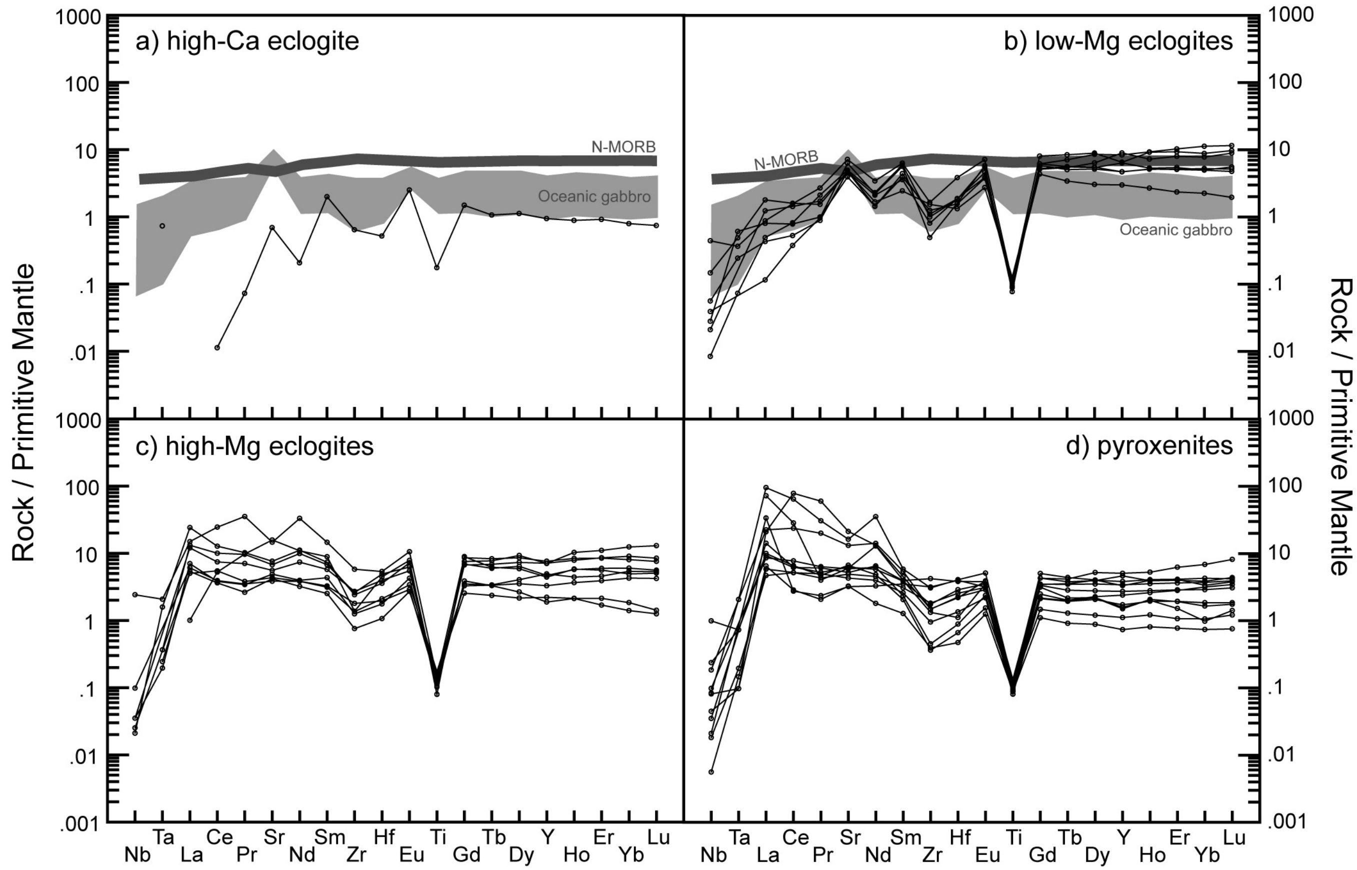

Figure 3.8: a) and b) Reconstructed whole rock extended trace element compositions of the Victor high-Ca and low-Mg eclogites, compared to oceanic gabbro (Bach et al., 2001) and N-MORB (Sun and McDonough, 1989). c) and d) Reconstructed whole rock extended trace element compositions of the Victor high-Mg eclogites and pyroxenites. Whole rock compositions were reconstructed using modes of 50% garnet and 50% clinopyroxene. Normalised to primitive mantle (Sun and McDonough, 1989).

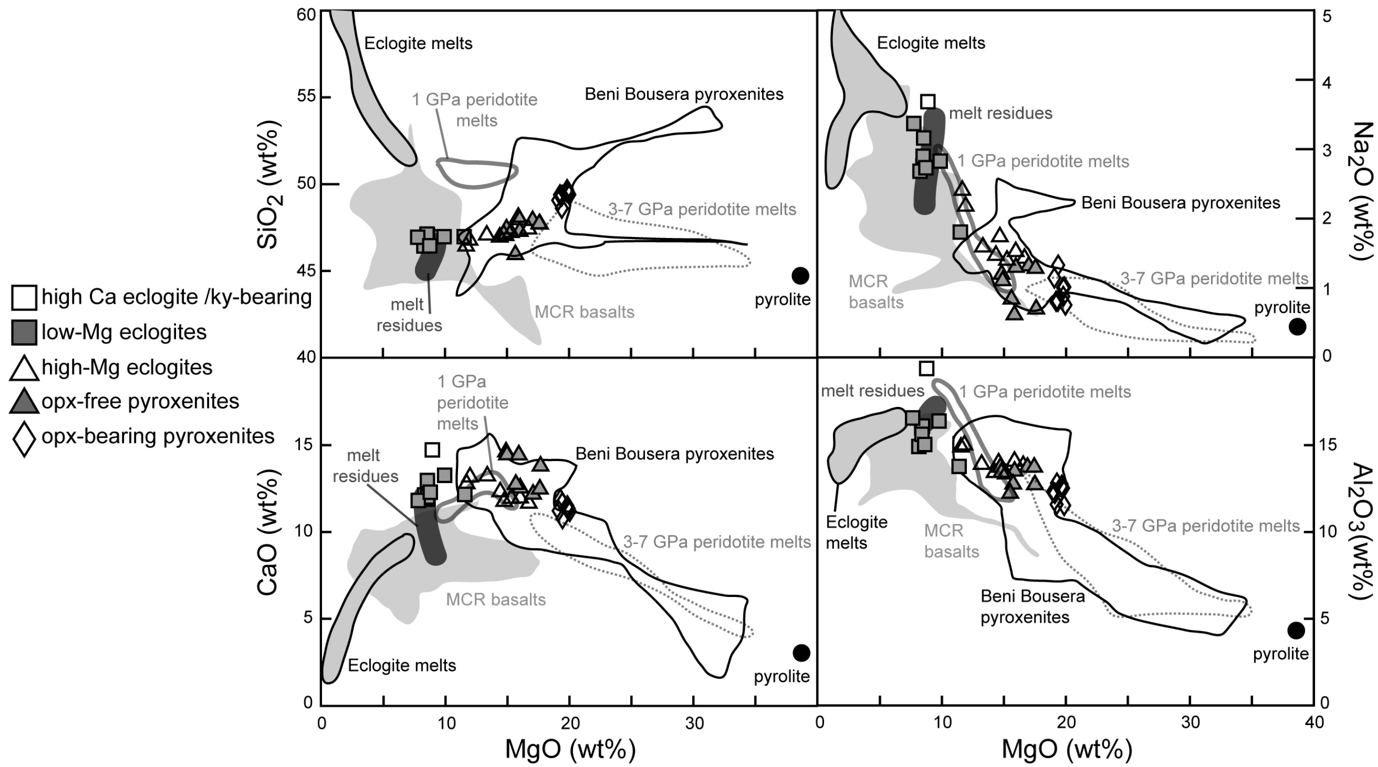

Figure 3.9: Reconstructed xenolith whole rock compositions compared to experimental mantle melts, massif pyroxenites (Beni Bousera; Pearson et al., 1993) and Midcontinent Rift basalts (Shirey et al., 1994). Eclogite-derived melts from Rapp and Watson (1995) and Spandler et al. (2008), 1 GPa peridotite-derived melts from Baker and Stolper (1994) and 3-7 GPa peridotite-derived melts from Walter (1998). Pyrolite (MPY90) from Green et al. (1979). The composition of the low-Mg eclogites overlaps with residues of melting of metabasalt at 3.2 GPa from Rapp and Watson (1995). The high-Mg eclogites and pyroxenites have compositions intermediate between eclogite-derived melts and pyrolite - supporting the interpretation that they may be reaction products between these two end-members. See text for discussion.

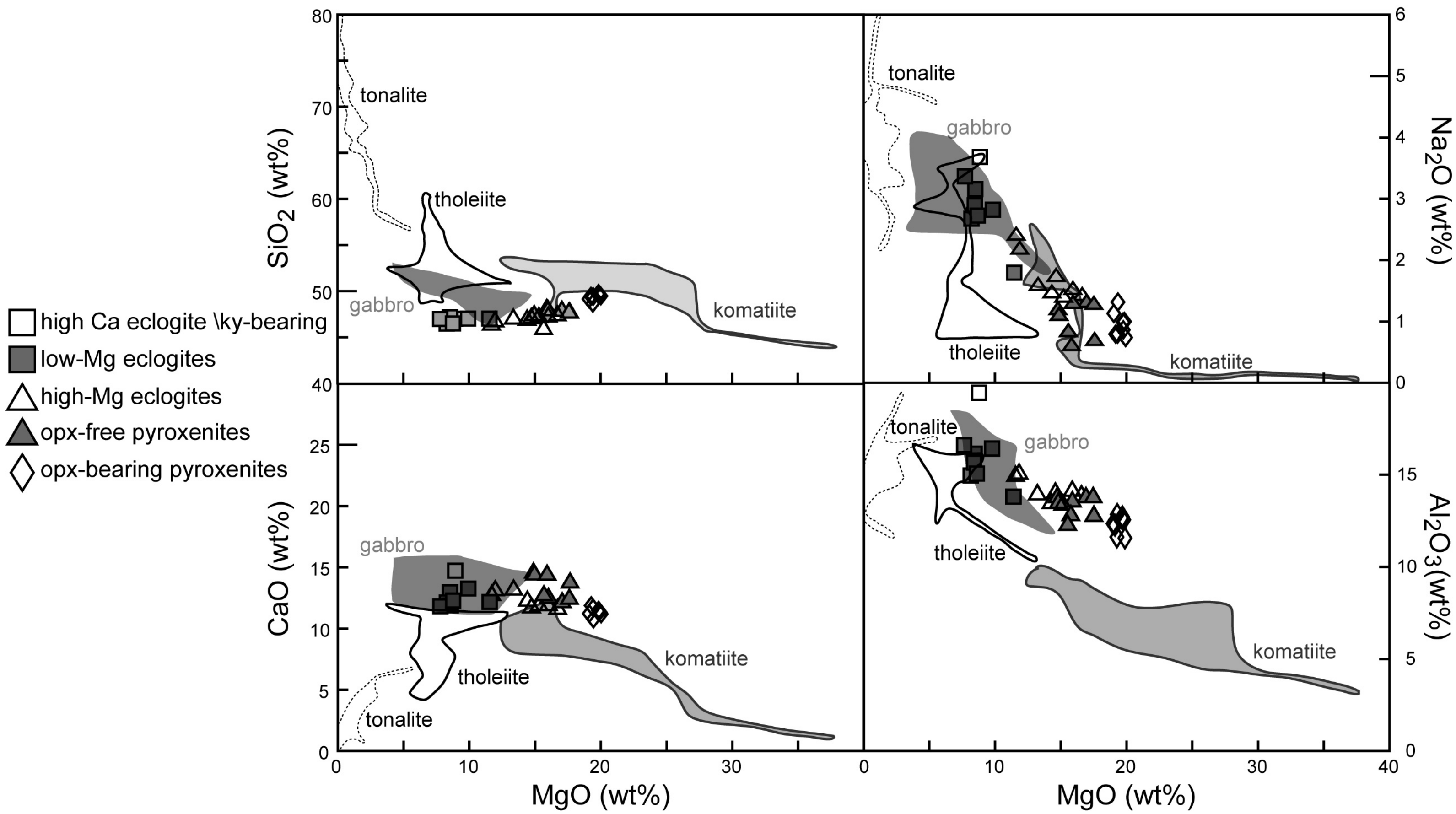

Figure 3.10: Reconstructed xenolith whole rock compositions compared to various rock types in greenstone belts from the Superior craton and oceanic crust gabbro (Bach et al., 2001). Tonalite compositions are from the Birch-Uchi and North Caribou greenstone belts (Rogers, 2002; Wyman et al., 2011). Tholeiite and komatiite compositions are from the Lumby Lake, Red Lake, Rice Lake and North Caribou greenstone belts (Hollings et al., 1999).

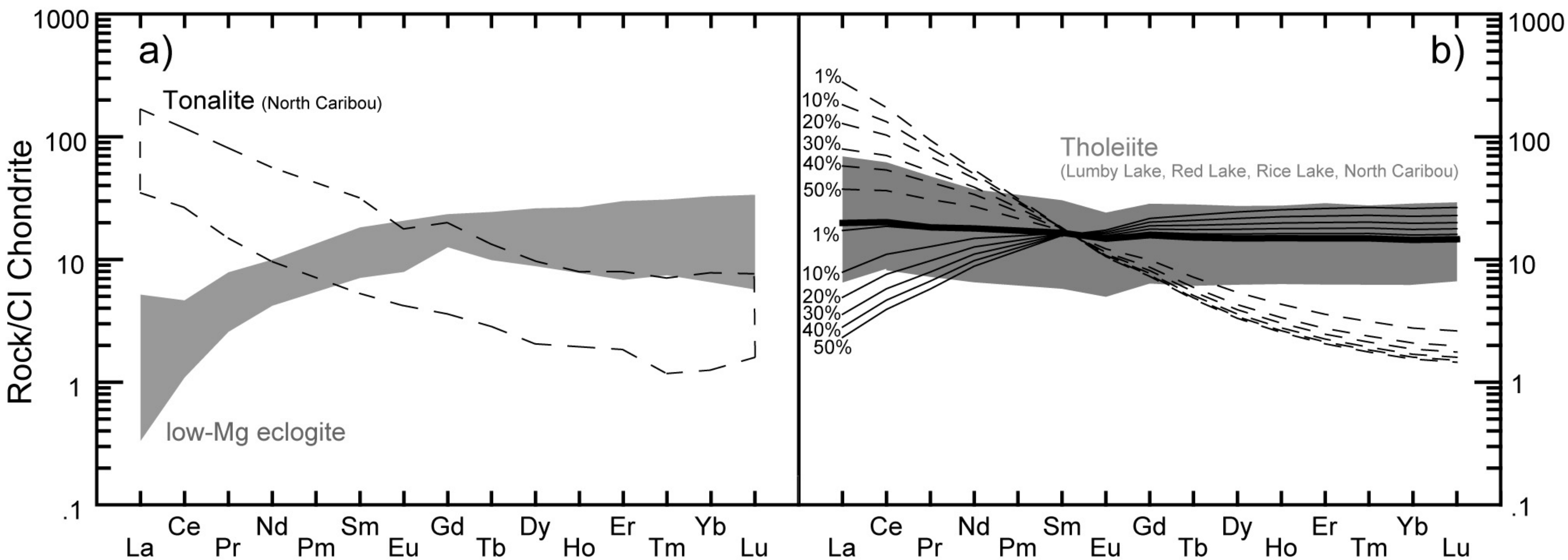

Figure 3.11: a) Complementary REE compositions of low-Mg eclogite and tonalite (North Caribou greenstone belt; Wyman et al., 2011). b) Batch melting calculations for average basalt (bold line) (Lumby Lake, Red Lake, Rice Lake and North Caribou greenstone belts; Hollings et al., 1999). Solid lines are residual compositions for 1-50% partial melting, with the dashed lines indicating the co-existing melt compositions. Partition co-efficients from Barth et al. (2002c). The compositions of Victor low-Mg eclogite xenoliths and tonalites from the North Caribou greenstone belt can be reproduced with $\sim$ 30% melting.

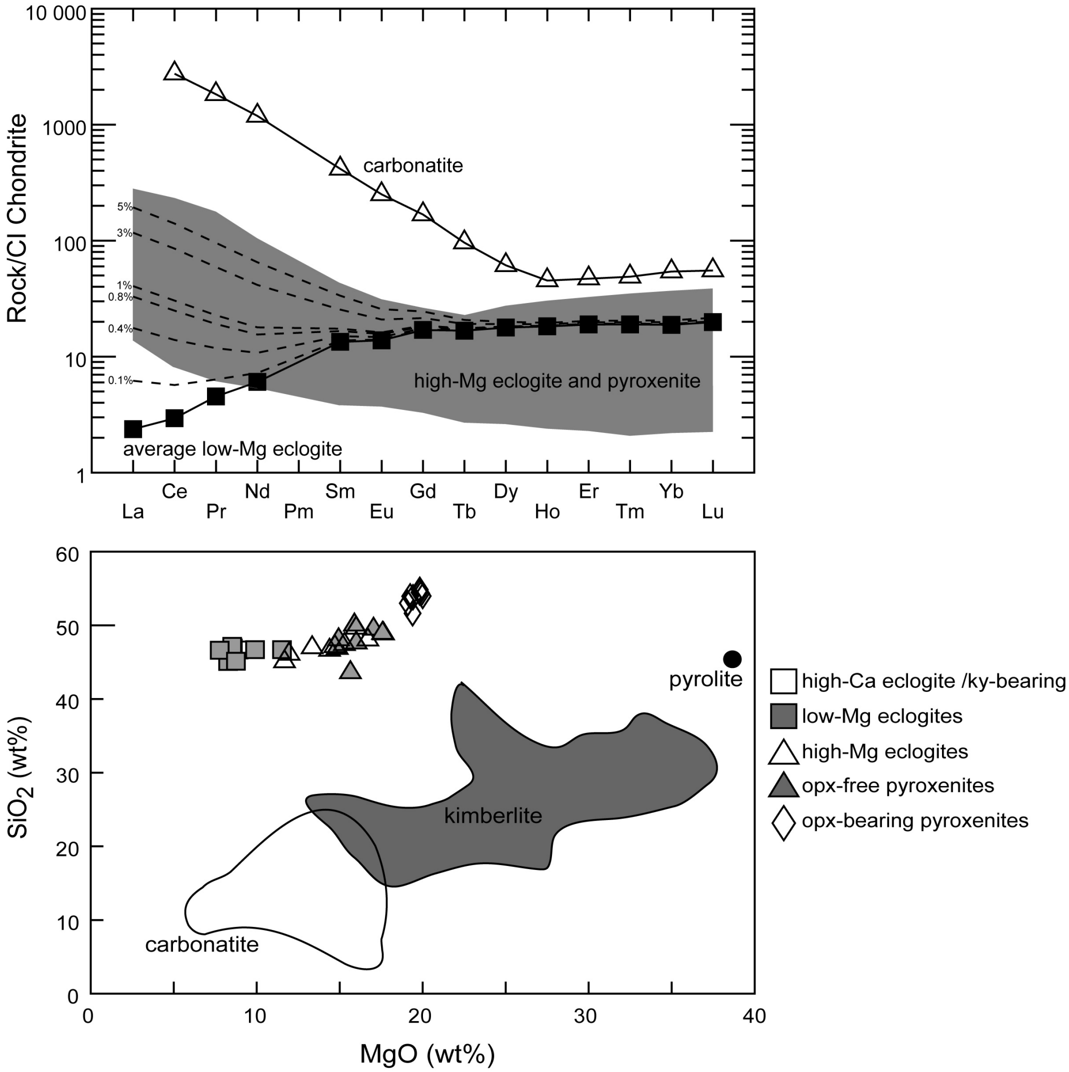

Figure 3.12: a) The REE compositions of the high-Mg eclogites can be reproduced by adding a low volume melt, e.g., 5% average carbonatite from Tappe et al. (2006), to the low-Mg eclogites. Dashed lines indicate mixing of low-Mg eclogite with 0.1%, 0.4%, 0.8%, 1%, 3% and 5% carbonatite. b) Addition of kimberlite or carbonatite would not provide sufficient enrichment in SiO_2 to account for the major element compositions of the high-Mg eclogites and pyroxenites. Carbonatite compositions from Wallace and Green (1988); Tappe et al. (2006); kimberlite compositions from Kaminsky et al. (2002); le Roex et al. (2003); Birkett et al. (2004); Nielsen et al. (2009); Patterson et al. (2009); pyrolite composition (MPY90) from Green et al. (1979).

References

Allègre, C. J. and Turcotte, D. L.: 1986, Implications of a two-component marble-cake mantle, *Nature* **323**, 123–127.

Armstrong, J. T.: 1995, Citzaf - A Package Of Correction Programs For The Quantitative Electron Microbeam X-Ray-Analysis Of Thick Polished Materials, Thin-Films, And Particles, *Microbeam Analysis* **4**(3), 177–200.

Aulbach, S.: 2012, Craton nucleation and formation of thick lithospheric roots, *Lithos* **149**, 16–30.

Aulbach, S., Pearson, N. J., O'Reilly, S. Y. and Doyle, B. J.: 2007, Origins of Xenolithic Eclogites and Pyroxenites from the Central Slave Craton, Canada, *Journal of Petrology* **48**(10), 1843–1873.

Aulbach, S., Stachel, T., Creaser, R. A., Heaman, L. M., Shirey, S. B., Muehlenbachs, K., Eichenberg, D. and Harris, J. W.: 2009, Sulphide survival and diamond genesis during formation and evolution of Archaean subcontinental lithosphere: A comparison between the Slave and Kaapvaal cratons, *Lithos* **112S - Proceedings of the 9th International Kimberlite Conference**, 747–757.

Aulbach, S., Stachel, T., Viljoen, K. S., Brey, G. P. and Harris, J. W.: 2002, Eclogitic and websteritic diamond sources beneath the Limpopo Belt - is slab-melting the link?, *Contributions to Mineralogy and Petrology* **143**, 56–70.

Bach, W., Alt, J. C., Niu, Y., Humphris, S. E., Erzinger, J. and Dick, H. J. B.: 2001, The geochemical consequences of late-stage low-grade alteration of lower ocean crust at the SW Indian Ridge: Results from ODP Hole 735B (Leg 176), *Geochimica et Cosmochimica Acta* **65**(19), 3267–3287.

Baker, M. B. and Stolper, E. M.: 1994, Determining the composition of high-pressure mantle melts using diamond aggregates, *Geochimica et Cosmochimica Acta* **58**(13), 2811–2827.

Barth, M. G., Foley, S. F. and Horn, I.: 2002c, Partial melting in Archean subduction zones: Constraints from experimentally determined trace element partition coefficients between eclogitic minerals and tonalitic melts under upper mantle conditions, *Precambrian Research* **113**, 323–340.

Barth, M. G., Rudnick, R. L., Horn, I., McDonough, W. F., Spicuzza, M. J., Valley, J. W. and Haggerty, S. E.: 2001, Geochemistry of xenolithic eclogites from West Africa, Part I: A link between low MgO eclogites and Archean crust formation, *Geochimica et Cosmochimica Acta* **65**(9), 1499–1527.

Barth, M. G., Rudnick, R. L., Horn, I., McDonough, W. F., Spicuzza, M. J., Valley, J. W. and Haggerty, S. E.: 2002a, Geochemistry of xenolithic eclogites from West Africa, Part 2: origins of the high MgO eclogites, *Geochimica et Cosmochimica Acta* **66**(24), 4325–4345.

Barth, M., Rudnick, R. L., Carlson, R. W., Horn, I. and McDonough, W. F.: 2002b, Re-Os and U-Pb geochronological constraints on the eclogite-tonalite connection in the Archean Man Shield, West Africa, *Precambrian Research* **118**, 267–283.

Beard, B. L., Fraracci, K. N., Taylor, L. A., Snyder, G. A., Clayton, R. A., Mayeda, T. K. and Sobolev, N. V.: 1996, Petrography and geochemistry of eclogites from the Mir kimberlite, Yakutia, Russia, *Contributions to Mineralogy and Petrology* **125**, 293–310.

Becker, H.: 2000, Re-Os fractionation in eclogites and blueschists and the implications for recycling of oceanic crust into the mantle, *Earth and Planetary Science Letters* **177**, 287–300.

Bédard, J. H.: 2006, A catalytic delamination-driven model for coupled genesis of Archaean crust and sub-continental lithospheric mantle, *Geochimica et Cosmochimica Acta* **70**, 1188–1214.

Benoit, M., Polve, M. and Ceuleneer, G.: 1996, Trace element and isotopic characterisation of mafic cumulates in a fossil mantle diapir (Oman Ophiolite), *Chemical Geology* **134**(1-3), 199–214.

Bernstein, S., Hanghøj, K., Kelemen, P. B. and Brooks, C. K.: 2006, Ultra-depleted, shallow cratonic mantle beneath West Grenland: dunitic xenoltihs from Ubekendt Ejland, *Contributions to Mineralogy and Petrology* **152**, 335–347.

Bindeman, I. N., Kamenetsky, V. S., Palandri, J. and Vennemann, T.: 2012, Hydrogen and oxygen isotope behaviours during variable degrees of upper mantle melting: Example from the basaltic glasses from Macquarie Island, *Chemical Geology* **310-311**, 126–136.

Birck, J. L., Barman, M. R. and Capmas, F.: 1997, Re-Os Isotopic Measurements at the Femtomole Level in Natural Samples, *Geostandards Newsletter* **20**(1), 19–27.

Birkett, T. C., McCandless, T. E. and Hood, C. T.: 2004, Petrology of the Renard igneous bodies: host rocks for diamond in the northern Otish Mountains region, Quebec, *Lithos* **76**(1-4), 475–490.

Blichert-Toft, J., Albarede, F. and Kornprobst, J.: 1999, Lu-Hf isotope systematics of garnet pyroxenites from Beni Bousera, Morocco: implications for basalt origin, *Science* **283**, 1303–1306.

Bulatov, V., Brey, G. P. and Foley, S. F.: 1991, Origin of low-Ca, high-Cr garnets by recrystallisation of low-pressure harzburgites, *Extended Abstracts of the 5th International Kimberlite Conference* pp. 29–31.

Calvert, A. J., Sawyer, E. W., Davis, W. J. and Ludden, J. N.: 1995, Archaean subduction inferred from seismic images of a mantle suture in the Superior Province, *Nature* **375**, 670–674.

Canil, D.: 2004, Mildly incompatible elements in peridotites and the origins of mantle lithosphere, *Lithos* **77**, 375–393.

Canil, D. and Wei, K. J.: 1992, Constraints on the origin of mantle-derived low Ca garnets., *Contributions to Mineralogy and Petrology* **109**, 421–430.

Caporuscio, F. A. and Smyth, J. R.: 1990, Trace element crystal chemistry of mantle eclogites, *Contributions to Mineralogy and Petrology* **105**, 550–561.

Card, K. D.: 1990, A review of the Superior Province of the Canadian Shield, a product of Archean accretion, *Precambrian Research* **48**, 99–156.

Carswell, D. A.: 1990, Eclogites and the eclogite facies: definitions and classifications, *in* D. A. Carswell (ed.), *Eclogite facies rocks*, Blackie, pp. 1–13.

Clayton, R. N., Goldsmith, J. R., Karel, K. J., Mayeda, T. K. and Newton, R. C.: 1975, Limits on the effect of pressure on isotopic fractionation, *Geochimica et Cosmochimica Acta* **39**, 1197–1201.

Cohen, A. S. and Waters, F. G.: 1996, Separation of osmium from geological materials by solvent extraction for analysis by thermal ionisation mass spectrometry, *Analytica Chimica Acta* **332**, 269–275.

Coleman, R. G., Lee, E. D., Beatty, L. B. and Brannock, W. W.: 1965, Eclogites and eclogites: their differences and similarities, *Geological Society of America Bulletin* **76**, 483–508.

Corfu, F. and Stone, D.: 1998, Age structure and orogenic significance of the Berens River composite batholiths, western Superior Province, *Canadian Journal of Earth Sciences* **35**, 1089–1109.

Corfu, F. and Stott, G. M.: 1986, U-Pb ages for late magmatism and regional deformation in the Shebandowan belt, Superior Province, Canada, *Canadian Journal of Earth Sciences* **23**, 1075–1082.

Corkery, M. T., Cameron, H. D. M., Lin, S., Skulski, T., Whalen, J. B. and Stern, R. A.: 2000, Geological investigations in the Knee Lake belt (Parts of NTS 53L), *Report of Activities 2000, Manitoba Industry, Trade and Mines*, Manitoba Geological Survey, pp. 129–136.

Creaser, R. A., Papanastassiou, D. A. and Wasserburg, G. J.: 1991, Negative thermal ion mass spectrometry of osmium, rhenium and iridium, *Geochimica et Cosmochimica Acta* **55**, 397–401.

Dale, C. W., Gannoun, A., Burton, K. W., Argles, T. W. and Parkinson, I. J.: 2007, Rhenium-Osmium isotope and elemental behaviour during subduction of oceanic crust and implications for mantle recycling, *Earth and Planetary Science Letters* **253**, 211–225.

DePaolo, D. J. and Wasserburg, G. J.: 1976, Inferences about magma sources and mantle structure from variations of $^{143}Nd/^{144}Nd$, *Geophysical Research Letters* **3**(12), 743–746.

Dick, H. J. B. and Sinton, J. M.: 1979, Compositional layering in Alpine peridotites: evidence for pressure solution creep in the mantle, *Journal of Geology* **87**, 403–416.

Dludla, S., le Roex, A. P. and Gurney, J. J.: 2006, Eclogite xenoliths from the Premier kimberlite, South Africa: geochemical evidence for a subduction origin, *South African Journal of Geology* **109**, 353–368.

Dobosi, G., Downes, H., Mattey, D. and Embey-Isztin, A.: 1998, Oxygen isotope ratios of phenocrysts from alkaki basalts of the Pannonian Basin: evidence for an O-isotopically homogeneous upper mantle beneath a subduction-influenced area, *Lithos* **42**, 213–223.

Eggins, S. M.: 1992, Petrogenesis of Hawaiin tholeiites: 1. Phase equilibria constraints, *Contributions to Mineralogy and Petrology* **110**, 387–397.

Eiler, J. M.: 2001, Oxygen Isotope Variations of Basaltic Lavas and Upper Mantle Rocks, *in* J. W. Valley and D. R. Cole (eds), *Stable Isotope Geochemistry, Reviews in Mineralogy and Petrology*, Vol. 43, Mineralogical Society of America, pp. 319–364.

Foley, S., Tiepolo, M. and Vannucci, R.: 2002, Growth of early continental crust controlled by melting of amphibolite in subduction zones, *Nature* **417**, 837–840.

Frey, F. A.: 1980, The origin of pyroxenites and garnet pyroxenites from Salt Lake Crater, Oahu, Hawaii: trace element evidence, *American Journal of Science* **280-A**, 427–449.

Gannoun, A., Burton, K. W., Parkinson, I. J., Alard, O., Schiano, P. and Thomas, L. E.: 2007, The scale and origin of the osmium isotope variations in mid-ocean ridge basalts, *Earth and Planetary Science Letters* **259**, 541–556.

Garrido, C. J. and Bodinier, J.-L.: 1999, Diversity of Mafic Rocks in the Ronda Peridotite: Evidence for Pervasive Melt-Rock Reaction during Heating of Subcontinental Lithosphere by Upwelling Asthenosphere, *Journal of Petrology* **40**(5), 729–754.

Graham, S., Lambert, D. D., Shee, S. R., Smith, C. B. and Reeves, S.: 1999, Re-Os isotopic evidence for Archean lithospheric mantle beneath the Kimberley block, Western Australia, *Geology* **27**(5), 431–434.

Green, D. H., Hibberson, W. O. and Jacques, A. L.: 1979, Petrogenesis of mid-ocean ridge basalts, *in* M. W. McElhinny (ed.), *The Earth: its origin, structure and evolution*, Academic Press, London, pp. 265–299.

Green, D. H. and Ringwood, A. E.: 1972, A Comparison of Recent Experimental Data on the Gabbro-Garnet Granulite-Eclogite Transition, *Journal of Geology* **80**, 277–288.

Green, T.: 1994, Experimental studies of trace-element partitioning applicable to igneous petrogenesis—Sedona 16 years later, *Chemical Geology* **117**, 1–36.

Griffin, W. L., O'Reilly, S. Y., Abe, N., Aulbach, S., Davies, R. M., Pearson, N. J., Doyle, B. J. and Kivi, K.: 2003, The origin and evolution of Archean lithospheric mantle, *Precambrian Research* **127**, 19–41.

Griffin, W. L., O'Reilly, S. Y. and Ryan, C. G.: 1999, The composition and origin of sub-continental lithospheric mantle, *in* Y. Fei, C. Bertka and B. Mysen (eds), *Mantle Petrology: Field Observations and High Pressure Experimentation: a Tribute to Francis R. (Joe) Boyd*, The Geochemical Society, Special Publication, pp. 13–45.

Grütter, H. S., Gurney, J. J., Menzies, A. H. and Winter, F.: 2004, An updated classification scheme for mantle-derived garnet, for use by diamond explorers, *Lithos* **77 - Proceedings of the 8th International Kimberlite Conference**, 841–857.

Gurney, J. J. and Switzer, G. S.: 1973, The discovery of garnets closely related to diamonds in the Finsch Pipe, South Africa, *Contributions to Mineralogy and Petrology* **39**, 103–116.

Hatton, C. J. and Gurney, J. J.: 1987, Roberts Victor eclogites and their relation to the mantle, *in* P. H. Nixon (ed.), *Mantle xenoliths*, Wiley, London, pp. 453–463.

Helmstaedt, H. and Doig, R.: 1975, Eclogite nodules and Kimberlite pipes of the Colorado Plateau - Samples of subducted Franciscan-type oceanic lithosphere, *Physics and Chemistry of the Earth* **9**, 95–111.

Helmstaedt, H. H. and Gurney, J. J.: 1995, Geotectonic controls of primary diamond deposits: Implications for area selection, *Journal of Geochemical Exploration* **53**, 125–144.

Helmstaedt, H. and Schulze, D. J.: 1989, Southern African kimberlites and their mantle sample: implications for Archaean tectonics and lithosphere evolution, *Kimberlites and Related Rocks I: Their Composition, Occurrence, Origin and Emplacement. Proceedings of the 4th International Kimberlite Conference, Perth 1986. Geological Society of Australia Special Publication 14.*, pp. 358–368.

Herzberg, C. and Rudnick, R.: 2012, Formation of cratonic lithosphere: An integrated thermal and petrological model, *Lithos* **149**, 4–15.

Hirschmann, M. M., Asimov, P. D., Ghiorso, M. S. and Stolper, E. M.: 1999, Calculation of peridotite partial melting from thermodynamic models of minerals and melts. III. Controls on isobaric melt production and the effect of water on melt production, *Journal of Petrology* **40**(5), 831–851.

Hollings, P., Wyman, D. A. and Kerrich, R.: 1999, Komatiite-basalt-rhyolite volcanic associations in Northern Superior Province greenstone belts: significance of plume-arc interaction in the generation of the proto-continental Superior Province, *Lithos* **46**, 137–161.

Horstwood, M. S. A., Evans, J. A. and Montgomery, J.: 2008, Determination of Sr isotopes in calcium phosphates using laser ablation inductively coupled plasma mass spectrometry and their application to archaeological tooth enamel, *Geochimica et Cosmochimica Acta* **72**, 5659–5674.

Ickert, R. B. and Stern, R. A.: 2013, Matrix Corrections and Error Analysis in High-Precision SIMS $^{18}O/^{16}O$ Measurements of Ca-Mg-Fe Garnet , *Geostandards and Geoanalytical Research* **doi: 10.1111/j.1751-908X.2013.00222.x**.

Ireland, T. R., Rudnick, R. L. and Spetsius, Z.: 1994, Trace elements in diamond inclusions from eclogites reveal link to Archean granites, *Earth and Planetary Science Letters* **128**, 199–213.

Irvine, G. J., Pearson, D. G., Kjarsgaard, B. A., Carlson, R. W., Kopylova, M. G. and Dreibus, G.: 2003, A Re-Os isotope and PGE study of kimberlite-derived peridotite xenoliths from Somerset Island and a comparison to the Slave and Kaapvaal cratons, *Lithos* **71**, 461–488.

Jacob, D. E.: 2004, Nature and origin of eclogite xenoliths from kimberlites, *Lithos* **77**, 295–316.

Jacob, D. E., Schmickler, B. and Schulze, D. J.: 2003b, Trace element geochemistry of coesite-bearing eclogites from the Roberts Victor kimberlite, Kaapvaal craton, *Lithos* **71**, 337–351.

Jacob, D., Jagoutz, E., Lowry, D., Mattey, D. and Kudrjavtseva, G.: 1994, Diamondiferous eclogites from Siberia: Remnants of Archean oceanic crust, *Geochimica et Cosmochimica Acta* **58**(23), 5191–5207.

Jagoutz, E., Dawson, J. B., Hoernes, S., Spettel, B. and Wänke, H.: 1984, Anorthositic Oceanic Crust in the Archean Earth, *Abstracts of the 15th Lunar and Planetary Science Conference*, pp. 395–396.

Jahn, B. M., Glikson, A. Y., Peucat, J. J. and Hickman, A. H.: 1981, REE Geochemistry and Isotopic Data of Archean Silicic Volcanics and Granitoids from the Pilbara Block, Western Australia - Implications for the early Crustal Evolution, *Geochimica et Cosmochimica Acta* **45**(9), 1633–1652.

Januszczak, N., Seller, M. H., Kurszlaukis, S., Murphy, C., Delgaty, J., Tappe, S., Ali, K., Zhu, J. and Ellemers, P.: 2013, A Multidisciplinary Approach to the Attawapiskat Kimberlite Field, Canada: Accelerating the Discovery-to-Production Pipeline, *Proceedings of the 10th International Kimberlite Conference* .

Jerde, E. A., Taylor, L. A., Crozaz, G., Sobolev, N. V. and Sobolev, V. N.: 1993, Diamondiferous eclogites from Yakutia, Siberia: evidence for a diversity of protoliths, *Contributions to Mineralogy and Petrology* **114**, 189–202.

Kaminsky, F. V., Sablukov, S. M., Sablukova, L. I., Shchukin, V. S. and Canil, D.: 2002, Kimberlites from the Wawa area, Ontario, *Canadian Journal of Earth Sciences* **39**, 1819–1838.

Kelemen, P. B.: 1986, Assimilation of ultramafic rocks in subdction-related magmatic arcs, *Journal of Geology* **94**, 829–843.

Kelemen, P. B., Shimizu, N. and Dunn, T.: 1993, Relative depletion of niobium in some arc magmas and the continental crust: partitioning of K, Nb, La and Ce during melt/rock reaction in the upper mantle, *Earth and Planetary Science Letters* **120**, 111–134.

Kemp, A. I. S. and Hawkesworth, C. J.: 2003, Granitic Perspectives on the Generation and Secular Evolution of the Continental Crust, *Treatise on Geochemistry* **3**, 349–410.

King, E. M., Valley, J. W., Davis, D. W. and Edwards, G. R.: 1998, Oxygen isotope ratios of Archean plutonic zircons from granite-greenstone belts of the Superior Province: indicator of magmatic source, *Precambrian Research* **92**, 365–387.

Klein, E. M.: 2003, Geochemistry of the Igneous Oceanic Crust, *in* R. L. Rudnick, H. D. Holland and K. K. Turekian (eds), *Treatise on Geochemistry, Volume 3, The Crust*, Elsevier-Pergamon, Oxford, pp. 433–463.

Krogh, E.: 1988, The garnet-clinopyroxene Fe-Mg geothermometer - a reinterpretation of existing experimental data, *Contributions to Mineralogy and Petrology* **99**, 44–48.

Langford, F. F. and Morin, J. A.: 1976, The development of the Superior Province of Northwestern Ontario by merging Island Arcs, *American Journal of Science* **270**, 1023–1034.

le Roex, A. P., Bell, D. R. and Davis, P.: 2003, Petrogenesis of group I kimberlites from Kimberley, South Africa: Evidence from bulk-rock geochemistry, *Journal of Petrology* **44**(12), 2261–2286.

Loubet, M. and Allègre, C. J.: 1982, Trace elements in orogenic lherzolites reveal the complex history of the upper mantle, *Nature* **298**, 809–814.

Ludwig, K. R.: 1991, ISOPLOT: A Plotting and Regression Program for Radiogenic-isotope Data, *US Geological Survey Open File Report* p. 39.

Luguet, A., Jaques, A. L., Pearson, D. G., Smith, C. B., Bulanova, G. P., Roffey, S. L., Rayner, M. J. and Lorand, J.-P.: 2009, An integrated petrological, geochemical and Re-Os isotope study of peridotite xenoliths from the Argyle lamproite, Western Australia and implications for cratonic diamond occurrences, *Lithos* **112S - Proceedings of the 9th International Kimberlite Conference**, 1096–1108.

MacGregor, I. D. and Carter, J. L.: 1970, The chemistry of clinopyroxenes and garnets of eclogite and peridotite xenoliths from the Roberts Victor mine, South Africa, *Physics of the Earth and Planetary Interiors* **3**, 391–397.

MacGregor, I. D. and Manton, W. I.: 1986, Robert Victor eclogites: Ancient oceanic crust, *Journal of Geophysical Research* **91**, 14 063 – 14 079.

Mallik, A. and Dasgupta, R.: 2012, Reaction between MORB-eclogite derived melts and fertile peridotite and generation of ocean island basalts, *Earth and Planetary Science Letters* **329-330**, 97–108.

Martin, H.: 1986, Effect of steeper Archean geothermal gradient on geochemistry of subduction zone magmas, *Geology* **14**, 753–756.

Mattey, D. P., Lowry, D., Macpherson, C. G. and Chazot, G.: 1994, Oxygen isotope composition of mantle minerals by laser fluorination analysis: homogeneity in peridotites, heterogeneity in eclogites, *Mineralogical Magazine* **58A**, 573–574.

Menzies, A. H., Carlson, R. W., Shirey, S. B. and Gurney, J. J.: 2003, Re-Os systematics of diamond-bearing eclogites from Newlands kimberlite, *Lithos* **71**, 323–336.

Morgan, J. W. and Walker, R. J.: 1989, Isotopic determinations of rhenium and osmium in meteorites by using fusion, distillation and ion-exchange separations, *Analytica Chimica Acta* **222**, 291–300.

Moser, D., Amelin, Y., Schulze, D. and Krogh, T.: 1997, Progress in Understanding the Geology of the Lithosphere beneath the Eastern Sachigo Subprovince, *in* R. M. Harrap and H. H. Helmstaedt (eds), *1997 Western Superior Transect Third Annual Workshop, April 11-12, 1997. Lithoprobe Report #63*, Lithoprobe Secretariat, The University of British Columbia, pp. 102–103.

Muehlenbachs, K. and Clayton, R. N.: 1972a, Oxygen isotope geochemistry of submarine greenstones, *Canadian Journal of Earth Sciences* **9**, 471–478.

Muehlenbachs, K. and Clayton, R. N.: 1972b, Oxygen isotope studies of fresh and weathered submarine basalts, *Canadian Journal of Earth Sciences* **9**, 172–184.

Muehlenbachs, K. and Clayton, R. N.: 1976, Oxygen Isotope Composition of the Oceanic Crust and Its Bearing on Seawater, *Journal of Geophysical Research* **81**(23), 4365–4369.

Neal, C. R., Taylor, L. A., Davidson, J. P., Holden, P., Halliday, A. N., Nixon, P. H., Paces, J. B., Clayton, R. N. and Mayeda, T. K.: 1990, Eclogites with oceanic crustal and mantle signatures from the Bellsbank kimberlite, South Africa, Part 2: Sr, Nd, and O isotope geochemistry, *Earth and Planetary Science Letters* **99**, 362–379.

Nickel, K. G. and Green, D. H.: 1985, Empirical geothermobarometry for garnet peridotites and implications for the nature of the lithosphere, kimberlites and diamonds., *Earth and Planetary Science Letters* **73**, 158–170.

Nielsen, T. F. D., Jensen, S. M., Secher, K. and Sand, K. K.: 2009, Distribution of kimberlite and aillikite in the Diamond Province of southern West Greenland: A regional perspective based on groundmass mineral chemistry and bulk compositions, *Lithos* **112**, 358–371.

O'Hara, M. J. and Yoder, H. S.: 1963, Partial melting of the mantle, *Carnegie Institution of Washington Yearbook* **62**, 66–71.

O'Hara, M. J. and Yoder, H. S.: 1967, Formation and fractionation of basic magmas at high pressures, *Scottish Journal of Geology* **3**, 67–117.

Paces, J. B. and Miller, J. D.: 1993, Precise U-Pb ages of Duluth Complex and related mafic intrusions, northeastern Minnesota: geochronological insights to physical, petrogenetic, paleomagnetic and tectonomagmatic processes associated with the 1.1 Ga Midcontinent Rift System, *Journal of Geophysical Research* **98**, 13997–14013.

Page, F. Z., Kita, N. T. and Valley, J. W.: 2010, Ion microprobe analysis in garnets of complex chemistry, *Chemical Geology* **270**(1-4), 9–19.

Patterson, M., Francis, D. and McCandless, T.: 2009, Kimberlites: Magmas or mixtures?, *Lithos* **112**, 191–200.

Pearson, D. G., Canil, D. and Shirey, S. B.: 2003, Mantle Samples Included in Volcanic Rocks: Xenoliths and Diamonds, *Treatise on Geochemistry* **2**, 171–275.

Pearson, D. G., Davies, G. R. and Nixon, P. H.: 1993, Geochemical Constraints on the Petrogenesis of Diamond Facies Pyroxenites from the Beni Bousera Peridotite Massif, North Morocco, *Geochimica et Cosmochimica Acta* **34**(1), 125–172.

Pearson, D. G., Shirey, S. B., Carlson, R. W., Boyd, F. R., Pokhilenko, N. P. and Shimizu, N.: 1995a, Re-Os, Sm-Nd, and Rb-Sr isotope evidence for thick Archaean lithospheric mantle beneath the Siberian craton modified by multistage metasomatism, *Geochimica et Cosmochimica Acta* **59**(5), 959–977.

Pearson, D. G., Snyder, G. A., Shirey, S. B., Taylor, L. A., Carlson, R. W. and Sobolev, N. V.: 1995b, Archaean Re-Os age for Siberian eclogites and constraints on Archaean tectonics, *Nature* **374**, 711–713.

Pearson, D. G. and Wittig, N.: 2008, Formation of Archaean continental lithosphere and its diamonds: the root of the problem, *Journal of the Geological Society, London* **165**, 1–20.

Percival, J. A., Sanborn-Barrie, M., Skulski, T., Stott, G. M., Helmstaedt, H. and White, D. J.: 2006b, Tectonic evolution of the western Superior Province from NATMAP and Lithoprobe studies, *Canadian Journal of Earth Sciences* **43**, 1085–1117.

Polvé, M. and Allègre, C. J.: 1980, Orogenic lherzolite complexes studies by ^{87}Rb-^{87}Sr: a clue to understand the mantle convection processes?, *Earth and Planetary Science Letters* **51**, 71–93.

Prouteau, G., Scaillet, B., Pichavant, M. and Maury, R. C.: 1999, Fluid-present melting of ocean crust in subuction zones, *Geology* **27**(12), 1111–1114.

Rapp, R. P., Shimizu, N. and Norman, M. D.: 2003, Growth of early continental crust by partial melting of eclogite, *Nature* **425**(6958), 605–609.

Rapp, R. P., Shimizu, N., Norman, M. D. and Applegate, G. S.: 1999, Reaction between slab-derived melts and peridotite in the mantle wedge: experimental constraints at 3.8 GPa, *Chemical Geology* **160**, 335–356.

Rapp, R. P. and Watson, E. B.: 1995, Dehydration Melting of Metabasalt at 8-32 kbar: Implications for Continental Growth and Crust-Mantle Recycling, *Journal of Petrology* **36**(4), 891–931.

Rapp, R. P., Watson, E. B. and Miller, C. F.: 1991, Partial melting of amphibolite/eclogite and the origin of Archean trondhjemites and tonalites, *Precambrian Research* **51**, 1–25.

Richardson, S. H., Gurney, J. J., Erlank, A. J. and Harris, J. W.: 1984, Origin of diamonds in old enriched mantle, *Nature* **310**, 198–202.

Ringwood, A. E.: 1974, The petrological evolution of island arc systems, *Journal of Geological Society of London* **130**, 183–204.

Rogers, N.: 2002, Whole-rock chemical analyses from the Birch-Uchi greenstone belt, Superior Province, *Geological Survey of Canada, Open File* **4271**.

Rollinson, H.: 1997, Eclogite xenoliths in west African kimberlites as residues from Archaean granitoid crust formation, *Nature* **389**, 173–176.

Roy-Barman, M. and Allègre, C. J.: 1994, $^{187}Os/^{186}Os$ ratio of mid-ocean ridge basalts and abyssal peridotites, *Geochimica et Cosmochimica Acta* **58**(22), 5043–5054.

Santos, J. F., Schärer, U., Ibarguchi, J. I. G. and Girardeau, J.: 2002, Genesis of pyroxenite-rich peridotite at Cabo Ortegal (NW Spain): Geochemical and Pb-Sr-Nd isotope data, *Journal of Petrology* **43**, 17–43.

Schmickler, B., Jacob, D. E. and Foley, S. F.: 2004, Eclogite xenoliths from the Kuruman kimberlites, South Africa: geochemical fingerprinting of deep subduction zone and cumulate processes, *Lithos* **75**, 173–207.

Schmidberger, S. S., Simonetti, A. and Francis, D.: 2003, Small-scale Sr investigation of clinopyroxenes from peridotite xenoliths by laser ablation MC-ICP-MS - implications for mantle metasomatism, *Chemical Geology* **199**, 317–329.

Sekine, T. and Wyllie, P.: 1982, The system granite-peridotite-H_2O at 30 kbar with applications to hybridization in subduction zone magmatism, *Contributions to Mineralogy and Petrology* **81**, 190–202.

Shirey, S. B., Klewin, K. W., Berg, J. H. and Carlson, R. W.: 1994, Temporal changes in the sources of flood basalts: Isotopic and trace element evidence from the 1100 Ma old Keweenawan Mamainse Point Formation, Ontario, Canada, *Geochimica et Cosmochimica Acta* **58**(20), 4475–4490.

Shirey, S. B. and Walker, R. J.: 1995, Carius tube digestions for low-blank rhenium-osmium analysis, *Analytical Chemistry* **67**, 2136–2141.

Sinigoi, S., Comin-Chiaramonti, P., Demarchi, G. and Siena, F.: 1983, Differentiation of partial melts in the mantle: evidence from the Balmuccia peridotite, Italy, *Contributions to Mineralogy and Petrology* **82**, 351–359.

Skulski, T., Corkery, M. T., Stone, D., Whalen, J. B. and Stern, R. A.: 2000, Geological and geochronological investigations in the Stull Lake - Edmund Lake greenstone belt and granitoid rocks of the northwestern Superior Province, *Report of Activities 2000, Manitoba Industry, Trade and Mines*, Manitoba Geological Survey, pp. 117–128.

Sleep, N. H. and Windley, B. F.: 1982, Archaean plate tectonics: constraints and inferences, *Journal of Geology* **90**, 363–379.

Smart, K. A., Chacko, T., Stachel, T., Tappe, S., Stern, R. A., Ickert, R. B. and EIMF: 2012, Eclogite formation beneath the northern Slave craton constrained by diamond inclusions: Oceanic lithosphere origin without a crustal signature, *Earth and Planetary Science Letters* **319-320**, 165–177.

Smart, K. A., Heaman, L. M., Chacko, T., Simonetti, A., Kopylova, M., Mah, D. and Daniels, D.: 2009, The origin of high-MgO diamond eclogites from the Jericho Kimberlite, Canada, *Earth and Planetary Science Letters* **284**, 527–537.

Smyth, J. R., Caporuscio, F. A. and McCormick, T. C.: 1989, Mantle eclogites: evidence of igneous fractionation in the mantle, *Earth and Planetary Science Letters* **93**, 133–141.

Snyder, G. A., Taylor, L. A., Crozaz, G., Halliday, A. N., Beard, B. L., Sobolev, V. N. and Sobolev, N. V.: 1997, The Origins of Yakutian Eclogite Xenoliths, *Journal of Petrology* **38**(1), 85–113.

Spandler, C., Yaxley, G., Green, D. H. and Rosenthal, A.: 2008, Phase Relations and Melting of Anhydrous K-bearing Eclogite from 1200 to 1600 °C and 3 to 5 GPa, *Journal of Petrology* **49**(4), 771–795.

Stachel, T., Harris, J. W. and Brey, G. P.: 1998, Rare and unusual mineral inclusions in diamonds from Mwadui, Tanzania, *Contributions to Mineralogy and Petrology* **132**, 34–47.

Stott, G. M. and Corfu, F.: 1988, Whither the Kenoran orogeny?, *Annual Meeting of the Geological Association of Canada* **Abstracts Volume 13**(A120).

Sun, S.-S. and McDonough, W. F.: 1989, Chemical and isotopic systematics of oceanic basalts: implications for mantle compositions and processes., *in* A. D. Saunders and M. J. Norry (eds), *Magmatism in the ocean basins*, Geological Society, London, pp. 313–345.

Takahashi, E.: 1986, Melting of a dry peridotite KLB-1 up to 14 GPa: implications on the origin of peridotite upper mantle., *Journal of Geophysical Research* **91**, 9367–9382.

Takahashi, E., Shimazaki, T., Tsuzaki, Y. and Yoshido, H.: 1993, Melting study of peridotite KLB-1 to 6.5 GPa and the origin of basaltic magmas, *Philosophical Transactions of the Royal Society* **A 342**, 105–120.

Tappe, S., Foley, S. F., Genner, G. A., Heaman, L. M., Kjarsgaard, B. A., Romer, R. L., Stracke, A., Joyce, N. and Hoefs, J.: 2006, Genesis of ultramafic lamprophyres and carbonatites at Ailik Bay, Labrador: A consequence of incipient lithospheric thinning beneath the North Atlantic craton, *Journal of Petrology* **47**(7), 1261–1315.

Tappe, S., Smart, K. A., Pearson, D. G., Steenfelt, A. and Simonetti, A.: 2011, Craton formation in Late Archaean subduction zones revealed by first Greenland eclogites, *Geology* **39**(12), 1103–1106.

Tappert, R., Stachel, T., Harris, J. W., Muehlenbachs, K., Ludwig, T. and Brey, G. P.: 2005, Diamonds from Jagersfontein (South Africa): messengers from the sublithospheric mantle, *Contributions to Mineralogy and Petrology* **150**(5), 505–522.

Taylor, L. A. and Neal, C. R.: 1989, Eclogites with Oceanic Crustal and Mantle Signatures from the Bellsbank Kimberlite, South Africa, Part I: Mineralogy, Petrography, and Whole Rock Chemistry, *Journal of Geology* **97**, 551–567.

Taylor, L. A., Snyder, G. A., Keller, R., Remley, D. A., Anand, M., Wiesli, R., Valley, J. and Sobolev, N. V.: 2003, Petrogenesis of group A eclogites and websterites: evidence from the Obnazhennaya kimberlite, Yakutia, *Contributions to Mineralogy and Petrology* **145**, 424–443.

Taylor, W. R.: 1998, An experimental test of some geothermometer and geobarometer formulations for upper mantle peridotites with application to the thermobarometry of fertile lherzolite and garnet websterite, *Neues Jahrbuch Mineralogie Abhandlungen* **172**, 381–408.

Trønnes, R. G., Canil, D. and Wei, K. J.: 1992, Element partitioning between silicate minerals and coexisting melts at pressures of 1-27 GPa, and implications for mantle evolution, *Earth and Planetary Science Letters* **111**(2-4), 241–255.

van Achterbergh, E., Ryan, C., Jackson, S. and Griffin, W.: 2001, Appendix 3 Data reduction software for LA-ICP-MS, *in* P. Sylvester (ed.), *Laser-Ablation-ICPMS in the Earth Sciences*, Vol. 29, Mineralogical Association of Canada Short Course, pp. 239–243.

Vaselli, O., Downes, H., Thirlwall, M. F., Dobosi, G., Coradossi, N., Seghedi, I., Szackacs, A. and Vannucci, R.: 1995, Ultramafic xenoliths from Plio-Pleistocene alkali basalts from the Eastern Transylvanian Basin: depleted mantle enriched by vein metasomatism, *Journal of Petrology* **38**, 23–54.

Vielzeuf, D., Champenois, M., Valley, J. W., Brunet, F. and Devidal, J. L.: 2005, SIMS analyses of oxygen isotopes: Matrix effects in Fe-Mg-Ca garnets, *Chemical Geology* **223**(4), 208–226.

Viljoen, K. S., Dobbe, R., Harris, J. and Smit, B.: 2010, Trace element chemistry of mineral inclusions in eclogitic diamonds from the Premier (Cullinan) and Finsch kimberlites, South Africa: Implications for the evolution of their mantle source, *Lithos* **118**, 156–168.

Voshage, H., Sinigoi, S., Mazzuccelli, M., Demarchi, G. and Rivalenti, G.: 1988, Isotopic constraints on the origin of ultramafic and mafic dikes in the

Balmuccia peridotite (Ivrea Zone), *Contributions to Mineralogy and Petrology* **100**, 261–267.

Walker, R., Carlson, R., Shirey, S. and Boyd, F.: 1989, Os, Sr, Nd, and Pb isotope systematics of southern African peridotite xenoliths and implications for the chemical evolution of the subcontinental mantle, *Geochimica et Cosmochimica Acta* **53**, 1583–1595.

Walker, R. J.: 1988, Low-blank chemical separation of rhenium and osmium from gram quantities of silicate rock for measurement by resonance ionization mass spectrometry, *Analytical Chemistry* **60**, 1231–1234.

Walker, R. J., Horan, M. F., Morgan, J. W., Becker, H., Grossman, J. N. and Rubin, A. E.: 2002, Comparative ^{187}Re-^{187}Os systematics of chondrites: Implications regarding early solar system processes, *Geochimica et Cosmochimica Acta* **66**(23), 4187–4201.

Wallace, M. E. and Green, D. H.: 1988, An experimental-determination of primary carbonatite magma composition, *Nature* **335**(6188), 343–346.

Walter, M. J.: 1998, Melting of Garnet Peridotite and the Origin of Komatiite and Depleted Lithosphere, *Journal of Petrology* **39**(1), 29–60.

Westerlund, K. J.: 2005, *A Geochemical Study of Diamonds, Sulfide Inclusions in Diamonds and Mantle Xenoliths from the Panda Kimberlite, Slave Craton*, PhD thesis, University of Cape Town.

White, D. J., Musacchio, G., Helmstaedt, H. H., Harrap, R. M., Thurston, P. C., van der Velden, A. and Hall, K.: 2003, Images of a lower-crustal oceanic slab: Direct evidence for tectonic accretion in the Archean western Superior Province, *Geology* **31**(11), 997–1000.

Witt-Eickschen, G. and Kramm, U.: 1998, Evidence for the multiple stage evolution of the subcontinental lithospheric mantle beneath the Eifel (Germany) from pyroxenite and composite pyroxenite/peridotite xenoliths, *Contributions to Mineralogy and Petrology* **131**, 258–272.

Wittig, N., Pearson, D. G., Downes, H. and Baker, J. A.: 2009, The U, Th and Pb elemental and isotopes compositions of mantle clinopyroxenes and their grain boundary contamination derived from leaching and digestion experiments, *Geochimica et Cosmochimica Acta* **73**, 469–488.

Wittig, N., Pearson, D. G., Duggen, S., Baker, J. A. and Hoernle, K.: 2010, Tracing the metasomatic and magmatic evolution of continental mantle roots with Sr, Nd, Hf and Pb isotopes: A case study of Middle Atlas (Morocco) peridotite xenoliths, *Geochimica et Cosmochimica Acta* **74**, 1417–1435.

Wyman, D. A., Hollings, P. and Biczok, J.: 2011, Crustal evolution in a cratonic nucleus: Granitoids and felsic volcanic rocks of the North Caribou Terrane, Superior Province Canada, *Lithos* **123**, 37–49.

Wyman, D. A. and Kerrich, R.: 2002, Formation of Archean continental lithospheric roots: the role of mantle plumes, *Geology* **30**, 543–546.

Yasuda, A., Fujii, T. and Kurita, K.: 1994, Melting phase relations of an anhydrous mid-ocean ridge basalt from 3 to 20 GPa: implications for the behaviour of subducted oceanic crust in the mantle., *Journal of Geophysical Research* **99**, 9401–9414.

Yaxley, G. M. and Green, D. H.: 1998, Reactions between eclogite and peridotite: mantle refertilisation by subduction of oceanic crust, *Schweizer Mineralogische und Petrographische Mitteilungen* **78**, 243–255.

Chapter 4

Multiple generations of diamond in the Attawapiskat area

4.1 Introduction

The Attawapiskat diamondiferous kimberlites on the Superior craton, Canada, provide an opportunity to study the association of a primary diamond deposit with a post-Archaean rift system. The southern margin of the Superior craton was affected by the Midcontinent Rift at ~1.1 Ga (e.g. White, 1972; van Schmus and Hinze, 1985) and kimberlites that erupted syn- and post- rift sample distinctive lithosphere compositions.

The Kyle Lake kimberlites, which are coeval with the Midcontinent Rift, sample predominantly harzburgitic lithosphere with an elevated geothermal gradient and a resulting small diamond window (Sage, 2000; Grütter, 2009). The nearby kimberlites at Attawapiskat, including Victor - the first diamond mine on the Superior craton - were emplaced during the Jurassic, subsequent to the Rift. These kimberlites sample a lithosphere with a cooler geotherm and a larger diamond window. Garnet xenocrysts at Victor have refertilised lherzolitic compositions - perhaps related in origin to the Midcontinent Rift - depleted domains are, however, still preserved (Sage, 2000, and Chapter 5 of this thesis).

Here we study diamonds from the T1 and U2 diamondiferous kimberlites in the Attawapiskat area, in order to gain a better understanding of the diamond growth events in the lithosphere. These kimberlites are of similar age to Kyle Lake and Victor, respectively, and will allow us to investigate the timing of diamond formation relative to the Midcontinent Rift. Through comparison of nitrogen aggregation characteristics and carbon isotopic compositions in T1 and U2 diamonds, we aim to answer the following questions: Are the diamonds sampled by post-rift kimberlites (e.g., Victor / U2) an older generation of harzburgitic / lherzolitic diamonds which survived any melt metasomatic impact of the Midcontinent Rift? Or are they a younger generation (<1.1 Ga) of lherzolitic or eclogitic / pyroxenitic diamonds?

4.2 Analytical Techniques

4.2.1 Nitrogen concentration and aggregation state by FTIR

One hundred microdiamonds each from the T1 and the U2 kimberlite were analysed. All 100 diamonds from T1 were in the size range 0.425 to 0.600 mm; 49 diamonds from U2 ranged between 0.425 and 0.600 mm, with 51 diamonds between 0.600 and 0.850 mm. Diamonds were mounted along the side of a glass slide with double-sided tape. Absorption spectra were measured with a Thermo-Nicolet Nexus 470 Fourier Transform Infrared (FTIR) spectrometer coupled with a Nicolet Continuum infrared microscope and attached to a KBr beam splitter and a MCT detector that was cooled with liquid nitrogen.

The sample stage was purged continuously with dry nitrogen-oxygen. All spectra were recorded for 200 seconds over the mid-infrared range (650 to 4000 cm^{-1}), with resolution set at 4 cm^{-1} and a square aperture of 50 μm . Background spectra were recorded repeatedly (every 2 hours) during the analytical session and subtracted from the diamond spectra to correct for non-sample contributions. The OMNIC software was used for baseline correction and the subtraction and normalisation to a pure Type II diamond spectrum. The Type II diamond spectrum was normalised to 11.94 cm^{-1} at 1995 cm^{-1} prior to subtraction from sample spectra. After sample spectra were baselined, the peak area tool in the OMNIC software was used to measure the intensities of the platelet peak (1350 to 1380 cm^{-1}) and a hydrogen-related peak at 3107 cm^{-1}.

Spectral decomposition to quantify nitrogen content and aggregation state was done on a spreadsheet provided by David Fisher of the DTC Research Centre in Maidenhead, UK. Nitrogen concentration is calculated from absorption co-efficients at 1282 cm^{-1}: [N_A] = 16.5 X μA (Boyd et al., 1994) and [N_B] = 79.4 X μB (Boyd et al., 1995). Typically, two analyses per diamond were performed. As the nitrogen characteristics of these two analyses may be significantly different due to the heterogeneous nature of diamond, they were not averaged.

4.2.2 Carbon isotopes and nitrogen content by SIMS

A subset of diamonds from the T1 and U2 kimberlites (44 diamonds from T1 / 46 diamonds from U2) were sectioned for cathodoluminesence (CL) imaging of growth zones and multi-collector secondary ion mass spectrometry (MC-SIMS) analyses of δ^{13}C and N content. Whole diamonds were mounted in epoxy, at random orientations, and polished with a series of diamond-embedded metal plates. The final polish used a plate with 3 μm embedded diamonds. The epoxy mounts were coated with 5 nm of gold for backscatter electron (BSE) and CL imaging, using a Zeiss EVO 15 Scanning Electron Microscope (SEM) equipped with a CL detector from ETP Semra, Pty. Ltd. Epoxy mounts were subsequently embedded in indium along with two reference materials - synthetic carbon (S00233a) and synthetic diamond (S0011Bd and S0011Cd) - and coated with 25 nm gold, prior to SIMS analyses.

Carbon isotopic ratios

^{13}C/^{12}C ratios were measured using a Cameca IMS1280 ion microprobe. A $^{133}Cs^{+}$ primary ion beam with ~3.5 to 4.0 nA current was used for carbon isotopic analyses, with a mass resolution of 2950, sufficient to remove any hydride interferences. Samples were pre-sputtered for 30 seconds to remove surface contaminants and for automated tuning of the secondary ion beam. Carbon isotopes were measured with a 10 μm raster, with collection of secondary C^{-} ions on dual Faraday cups, and counting of 15 ratios at 5 seconds per ratio.

Analyses of S0011Bd and S0011Cd diamond were performed after every three to four unknowns in order to correct for instrumental mass fractionation and for error analysis. For each analytical session a polynomial fit was applied to the analyses of S0011Bd and S0011Cd in order to correct for instrumental mass fractionation. The reference material used in this study has $\delta^{13}C$ = -22.78 ± 0.05 ‰, established through conventional bulk analysis. Uncertainties on the unknowns vary between ±0.1 to ±0.2 ‰(2σ) and include in-run precision (internal error), between spot error and uncertainty related to instrumental mass fractionation and reference material composition (external error). All results are reported relative to the international Vienna Pee-Dee Belemnite standard (V-PDB).

Nitrogen abundances

Nitrogen abundances were determined as $^{12}C^{14}N^-/^{12}C_2{}^-$ on the same analytical spots as the carbon isotope analyses, however only a subset of the spots were analysed for their nitrogen content. Spots were pre-rastered for 60 to 120 seconds to remove surficial contamination. High mass resolution (7000) was needed in order to resolve $^{13}C_2{}^-$, $^{12}C^{13}C^1H^-$ and $^{12}C^{14}N^-$ interferences. $^{12}C_2{}^-$ and $^{12}C^{14}N^-$ were measured on dual Faraday cups or a Faraday cup / Electron Multiplier combination, depending on nitrogen concentration. Ten ratios were collected with a counting time of 5 seconds per ratio.

Nitrogen concentrations from the unknowns were referenced back to diamond (S0011G) for which FTIR nitrogen abundance is known. Uncertainties reported in the tables include the within-spot counting statistics and the error in the nitrogen abundance calibration. An additional error of ∼10% (2σ) is associated with uncertainty in the FTIR-determined nitrogen abundance, and should be used when comparing data with nitrogen concentrations determined elsewhere (i.e., this error does not apply to relative differences between analytical spots).

4.3 Nitrogen aggregation characteristics of whole diamonds

Nitrogen is the main impurity in diamond, and its principal significance in diamond studies is the temperature-time dependence of the conversion of nitrogen from A centres (pairs of N atoms) to B centres (4 N atoms distributed around a vacancy) (Bursill and Glaisher, 1985). This conversion allows derivation of time-averaged mantle residence temperatures for given mantle residence times (Evans and Qi, 1982; Taylor et al., 1990). Any temperatures calculated from nitrogen aggregation are time-averaged temperatures and therefore may not necessarily correlate with those calculated from silicate inclusions, as ambient mantle temperatures may fluctuate over a billion year timescale.

During formation of B nitrogen aggregates, carbon atoms are expelled from the diamond lattice and form platelets (Humble, 1982; Woods, 1986). In diamond zones with low nitrogen content, platelet nucleation and growth are slow, whereas the opposite is true for higher nitrogen zones (Woods, 1986). In 'regular' diamonds the amount of nitrogen in B aggregates is strictly proportional to the platelet peak strength. However, platelet degradation may occur due to transient thermal events and/or deformation, with the result that this proportional relationship breaks down - leading to 'irregular' diamonds (Woods, 1986; Evans et al., 1995; Kiflawi and Bruley, 2000). For cuboid growth sectors the linear relationship between B aggregates and platelet peak area does not hold (Howell et al., 2012), implying that apparent platelet degradation may relate to the presence of cuboid growth sectors not necessarily recognisable from external morphology. For diamonds where no CL images are available to investigate internal growth zoning, high hydrogen content could be an indication for cuboid growth, where diamonds with ≥ 20 cm^{-2} hydrogen at 3107 cm^{-1} may have cuboid sectors (Howell et al., 2012).

4.3.1 T1

A high proportion (93 %) of the T1 diamonds analysed with FTIR are Type II, with no measurable nitrogen. The 7 % of diamonds that contain nitrogen, have nitrogen contents between 23 and 920 at. ppm, with a median of 50 at. ppm (average = 145 at. ppm; Table D.1). T1 diamonds are highly aggregated, with all N-bearing diamonds showing >70 % B aggregates. The majority of N-bearing diamonds from T1 show an irregular relationship between %B aggregates and platelet peak area (Figure 4.2a,b).

4.3.2 U2

U2 has a greater percentage (25 %) of nitrogen-bearing diamonds than T1. Nitrogen contents are also significantly higher than in T1 diamonds, varying between 24 at. ppm and 1740 at. ppm, with a median of 266 at. ppm (average of 512 at. ppm; Table D.2). The nitrogen aggregation state in U2 diamonds varies from 0 to 100 % B. In general, the diamonds from U2 are characterised by lower aggregation states (Type IaA, with <10 % B aggregation) at higher average nitrogen contents than the diamonds from T1 (Figure 4.1). 29 % of U2 diamonds show a hydrogen peak at 3107 cm^{-1}. Unlike the samples from T1, the greatest hydrogen peak area, is not found in the diamonds with the highest nitrogen content (Table D.2).

4.4 Carbon isotopes and nitrogen content by SIMS

4.4.1 T1

The 44 analysed diamonds (158 point analyses) from T1 have a narrow distribution in $\delta^{13}C$ from -4.0 to -0.9 ‰, with a sharply defined mode at -3.4 ‰ (Figure 4.3 and Figure 4.4). Nitrogen content in the 44 diamonds (104 analyses) varies from 0.3 at. ppm to 121 at. ppm, with a median of 5.4 at. ppm (Table D.3). This is significantly lower than the median determined from FTIR analyses ($\sim$ 50 at. ppm).

Zoning in some T1 diamonds reveals that earlier growth is associated with less negative $\delta^{13}C$ (-2.0 to -0.9 ‰) followed by later growth with more negative $\delta^{13}C$ values (-4.0 to -2.5 ‰) (Figure 4.5). No systematic co-variations in $\delta^{13}C$ and nitrogen content could be established within individual growth zones or within the individual diamonds as diamond growth is interrupted by numerous resorption surfaces.

4.4.2 U2

The 46 analysed diamonds (203 point analyses) from U2 have a wide variation of $\delta^{13}C$ from -17.7 to 0.6 ‰, with a mode at -5.7 ‰ (Figure 4.3). Nitrogen content (103 analyses) ranges between 1.15 at. ppm and 1593 at. ppm, with a median of 5.4 at. ppm (Table D.4). This is lower than the median nitrogen from FTIR analyses (266 at. ppm). Overall, U2 diamonds have significantly higher nitrogen than the diamonds from T1.

The $\delta^{13}C$ distribution for U2 diamonds is represented by 3 different populations: 1.) One diamond has lighter carbon isotopic compositions than the rest of the U2 population. The central portion of this diamond has $\delta^{13}C$ from -15.8 to -17.7 ‰ and low nitrogen contents (105 to 220 at. ppm; n=4), surrounded by diamond growth more enriched in ^{13}C, with $\delta^{13}C$ from -6.7 to -9.4 ‰ and higher nitrogen (720 to 780 at. ppm) (Figure 4.4 and Figure 4.6f). 2.) Five diamonds have compositions that are more ^{13}C-enriched than average mantle, with $\delta^{13}C$ >-4 ‰ (Figure 4.4 and CL images in Figure 4.6). 3.) The remaining diamonds from U2 have $\delta^{13}C$ ranging from -7.8 to -4.2 ‰ with a mean of -6.0 ‰. This population has two distinct peaks - with modes of -6.7 ‰ and -5.3 ‰ - which could potentially represent sub-populations of diamonds.

Diamonds from U2 show both more negative $\delta^{13}C$ and more positive $\delta^{13}C$ compositions towards the rim (Figure 4.6c and 4.7). However, as with T1 diamonds, no correlation between $\delta^{13}C$ and nitrogen content could be established for individual growth zones, or across zones with apparently uninterrupted diamond growth.

4.5 Discussion

4.5.1 Nitrogen aggregation state and relative timing of diamond formation

T1

For T1 diamonds, isotherms for a mantle residence time of 2.1 billion years were constructed, assuming Mesoarchaean diamond formation and Mesoproterozoic kimberlite eruption (Figure 4.1). T1 diamonds experienced high temperatures during their mantle residency (>1200°C) (Figure 4.1) and also show high levels of platelet degradation (Figure 4.2). These diamonds were evaluated for possible cuboid growth sectors, for which the linear relationship between platelet peak area and B aggregation may not hold (Howell et al., 2012). The three nitrogen-bearing diamonds that underwent SIMS analyses, have no cuboid growth zones evident in their CL images. The sample with the highest nitrogen concentration in the T1 suite (average 656 at. ppm, with two analyses at 391 to 920 at. ppm, no CL image available) (Table D.1), also has the highest hydrogen contents. The two FTIR spectra for this sample exhibit hydrogen peak areas at 3107 cm^{-1} of 70 and 82 cm^{-2}. One of these analyses plots along the 'regular' trend, whereas the other is 'irregular' (Figure 4.2a), suggesting this diamond may have some cuboid growth sectors and should be excluded during platelet evaluation. The remainder of the N-bearing diamonds (all irregular), have 3107 cm^{-1} peak areas <10 cm^{-2}, which suggests absence of cuboid growth sectors. Therefore, with one exception, the irregular relationship between B centre concentration and platelet peak strength (Figure 4.2a,b) is interpreted to reflect platelet degradation during mantle residence (after Woods, 1986).

Platelet degradation typically occurs in response to thermal pulses and/or deformation events in the lithospheric mantle. Platelet degradation in T1 diamonds may relate to the Midcontinent Rift event, which affected the Superior craton around 1.1 Ga close to the time of kimberlite eruption. Elevated temperatures associated with the Midcontinent Rift are evident in the higher geotherm determined from clinopyroxene xenocrysts from the Proterozoic Kyle Lake kimberlites. This is not a perturbed geotherm and indicates that the heating event has already been conducted through the sampled SCLM (Figure 4.8). This elevated geotherm results in a narrow 'diamond window' of only about 25 km thickness, where diamonds are only stable above ~1060 °C . Any previously existing diamonds at depths less than 140 km must have been graphitised due to this thermal effect of the Midcontinent Rift.

U2

For U2 diamonds, isotherms reflect possible mantle residence times of both 3.0 billion years (assuming Archaean diamond formation and kimberlite eruption at 180 Ma) and 0.9 billion years (assuming diamond formation after the Midcontinent Rift) (Figure 4.1). Calculated residence temperatures for U2 diamonds are between 1050 °C and 1300 °C .

The relationship between %B aggregates and platelet peak area for U2 diamonds is shown in Figure 4.2c. In this plot, diamonds that have low aggregation states (< 1%) were excluded, as platelet development is associated with B centre formation. The one diamond with the highest aggregation state (100 % B aggregation) was also excluded as platelets disappear over time once nitrogen aggregation is completed. The remaining diamonds were grouped according to their nitrogen aggregation and temperature.

Seven analyses plot along or above the 'regular' trend (after Woods, 1986), whereas the remaining diamonds all display an irregular relationship between %B aggregates and platelet peak area (Figure 4.2c). None of the irregular diamonds have high hydrogen contents indicative of cuboid growth zoning (Howell et al., 2012). Three analyses that plot along and above the 'regular' trend have high hydrogen contents, with 3107 cm−1 hydrogen peak areas between 10.4 and 17.6 cm^{-2}; however these values are below the cutoff for cuboid growth sectors ($\geq$ 20 cm^{-2}) suggested by Howell et al. (2012).

A subgroup of U2 diamonds have low levels of nitrogen aggregation, with some diamonds showing 0 % B, which indicate that these diamonds resided at low mantle temperatures (< 1050 °C) and/or that these diamonds had an even shorter mantle residency time than 0.9 Ga (Figure 4.1). The lack of pervasive B aggregation compared to T1 indicates that these U2 diamonds never experienced the thermal conditions that are reflected by the high time average mantle residence temperatures for T1 diamonds. Therefore U2 diamonds must have formed after T1 diamonds acquired their high nitrogen aggregation states and likely postdate the Midcontinent Rift.

IaAB diamonds (1100 - 1200 °C) from U2 are platelet degraded (Figure 4.2), indicating that a minor population of U2 diamonds may have survived the impact of the Midcontinent Rift. Five diamonds from U2 have less negative $\delta^{13}C$ (> -3.7 ‰) similar to T1 (Figures 4.3 and 4.4). Only one of these diamonds has sufficient nitrogen for FTIR analyses. While $\delta^{13}C$ of this diamond is -2.83 to -1.95 ‰ overlapping with T1; it has much lower nitrogen aggregation around 55 %, suggesting mantle storage at lower average temperatures than the diamonds from T1 (>70 % B aggregation; temperatures >1200 °C). This does not exclude the possibility that the other 4 Type II diamonds from U2 with less negative $\delta^{13}C$ compositions may be inherited from the pre-rift lithosphere (sampled at T1).

The majority of U2 diamonds are Type IaA though and have more negative $\delta^{13}C$ compositions than T1 diamonds, indicating they are clearly younger and unrelated to T1 diamonds. Under a normal cratonic geotherm, the range in residence temperatures for U2 diamonds indicates diamond derivation from a wide depth range, similar to that seen in xenoliths and xenocrysts from Attawapiskat (Figure 4.8).

4.5.2 Carbon isotopic composition and diamond paragenesis

Background

Diamonds worldwide display a large range in $\delta^{13}C$ (∼-41 to ∼ +5 ‰), with the lowest $\delta^{13}C$ values dominated by diamonds from Jericho in the northern Slave craton (Deines, 1980; Kirkley et al., 1991; Stachel et al., 2009; de Stefano et al., 2009; Smart et al., 2011). Eclogitic paragenesis diamonds are typically associated with $\delta^{13}C$ distributions skewed towards light values ($\delta^{13}C$ < -10 ‰), whereas peridotitic diamonds have $\delta^{13}C$ distributions between -10 and 0 ‰. This overlaps with the pristine mantle value, which has a similar range and a mean around -5 ‰, as determined from analyses of MORB, kimberlites and carbonatites (e.g., Deines and Gold, 1973; Pineau et al., 1973; Sheppard and Dawson, 1975; Marais and Moore, 1984; Mattey et al., 1984; Exley et al., 1986; Marty and Zimmermann, 1999).

However, diamonds with $\delta^{13}C$ that overlap with mantle derived $\delta^{13}C$ should not be used as firm evidence for a peridotitic source parageneses, as some eclogitic diamond populations also have narrow $\delta^{13}C$ around ∼-5 ‰, without a tail to ^{13}C-depleted values. For example, diamonds in Siberian eclogite xenoliths have $\delta^{13}C$ from -7 to -1 ‰ (Sobolev et al., 1994; Snyder et al., 1995), Premier diamonds with eclogitic inclusions have $\delta^{13}C$ with a narrow range from -6.0 to -2.5 ‰ (database of Stachel and Harris, 2008) and diamonds hosted in low-Mg eclogites from Jericho have $\delta^{13}C$ from -6.0 to -2.7 ‰ (Smart et al., 2011).

The full range in $\delta^{13}C$ values observed for eclogitic diamonds can be reconciled with carbon input from several sources, including unaltered MORB (∼-5 ‰) and subducted sedimentary carbon which comprise both carbonates and organic carbon. Carbonates are ^{13}C-enriched relative to MORB and precipitate from reaction of CO_2-bearing seawater and basaltic crust. They have an average $\delta^{13}C$ around 0 ‰ (e.g., Coggon et al., 2006). Organic carbon has ^{13}C-depleted compositions with $\delta^{13}C$ <-15 ‰ and can be produced through reduction of magmatic CO_2 by both biogenic and abiogenic processes (e.g., Blank et al., 1993; Lilley et al., 1993; Nisbet et al., 1994; McCandless and Gurney, 1997; Delacour et al., 2008; Shilobreeva et al., 2011).

Extreme isotopic signatures of organic carbon are not always retained during high pressure metamorphism and subduction (e.g., McKirdy and Powell, 1974; Hoefs and Frey, 1976). The carbon isotopic composition of carbonate and organic carbon equilibrates with increasing temperature causing homogenisation after subduction into the mantle (e.g., Deines, 2002; Satish-Kumar et al., 2002; Cartigny, 2005). Therefore, if extremely ^{13}C-depleted domains are to be preserved after subduction, they need to be essentially free of carbonate. One example is eclogite in the Monviso ophiolite (Italy) that contains reduced carbon with an average $\delta^{13}C$ of -24.2 ±1.2 ‰ and negligible carbonates in the overall carbon budget of the rocks (Nadeau et al., 1993).

T1/U2 diamond parageneses

Less than 1 % of worldwide peridotitic diamonds have $\delta^{13}C <$ -10 ‰ (Stachel and Harris, 2008). Therefore, the ^{13}C-depleted composition for one diamond from U2 (with $\delta^{13}C$ ranging from -18 to -7 ‰) strongly indicates an eclogitic / pyroxenitic paragenesis for this sample. The strong mode around -5.7 ‰ for the main population at U2, however, resembles $\delta^{13}C$ distributions for peridotitic diamond productions world-wide. As some eclogite productions (see above) show mantle-like values around -5 ‰ (suggesting input from mantle carbon or unaltered homogenised basaltic oceanic crust), a clear distinction between parageneses can, however, not be made without evidence from inclusions.

The predominantly lherzolitic compositions of garnet xenocrysts at Victor (Sage, 2000, and Chapter 5 in this thesis), suggest that, if peridotitic, the U2 diamonds are likely to be lherzolitic. Some lherzolitic garnets from Victor have sinusoidal REE_N patterns (Section 5.12.3), typical for both harzburgitic and lherzolitic garnet inclusions in diamonds worldwide (e.g., Stachel et al., 2004).

The restricted range in carbon isotopic compositions and a lack of light $\delta^{13}C$ values in T1 diamonds suggest that they represent one paragenesis, likely peridotitic. This is supported by xenocrystic garnets from the Kyle Lake kimberlite (~ coeval to T1) that are both harzburgitic and lherzolitic, and lack abundant eclogitic compositions (Sage, 2000).

4.5.3 Diamond growth processes inferred from internal variations in δ^{13}C

T1 diamonds have a narrow range in δ^{13}C with a mode at -3.4 ‰. This is more enriched in ^{13}C than average mantle (~ -5 ‰) but corresponds well to the ranges in carbon isotopic composition of other diamond localities on the Superior craton. Peridotitic diamonds from Renard in the eastern Superior have δ^{13}C between -5.4 to -1.2 ‰ (Hunt et al., 2012b) and Wawa harzburgitic diamonds have δ^{13}C from -5.5 to -1.1 ‰ (Stachel et al., 2006; Miller et al., 2012).

The positive skewness of the probability density plot for T1 diamonds may look compatible with closed system Rayleigh fractionation from an oxidised source, where δ^{13}C becomes more positive with progressive diamond crystallisation (Deines, 1980) (Figure 4.4). However, diamond growth zones revealed through CL imaging, show the opposite. Early growth in the core of diamond crystals is characterised by slightly less negative δ^{13}C (-2.0 to -0.9 ‰) and later growth zones have more negative δ^{13}C (-4.0 to -2.5 ‰) (Figure 4.5). Additionally, no systematic co-variations in δ^{13}C and nitrogen content were observed within individual diamonds and multiple stages of resorption and growth are evident in CL images (Figure 4.5). This suggests that T1 diamond growth did not occur in one continuous event (involving Raleigh fractionation of a single diamond forming fluid/melt), but rather during multiple growth events (e.g., Boyd et al., 1987; Harte et al., 1999; WiggersdeVries et al., 2013; Palot et al., 2013).

U2 diamonds have several characteristics that suggest diamond growth occurred during multiple stages, likely from multiple melts/fluids. U2 diamonds display core to rim δ^{13}C trends that become both less negative (Figure 4.6c; Figure 4.7a,b) and more negative (Figure 4.7c), which may suggest diamond growth from both oxidised and reduced sources (e.g. Deines, 1980). However, no systematic internal compositional co-variations were observed, and due to the presence of numerous resorption surfaces, diamond growth must not be modelled through a single Rayleigh fractionation process.

Additionally, the diamonds in Figure 4.7a-c have different core compositions of -6.9, -7.3 and -4.9 ‰, respectively, suggesting that diamonds at U2 grew from multiple melts/fluids, with substantially different $\delta^{13}C$ compositions. This is consistent with the overall $\delta^{13}C$ distribution in the main population of U2 diamonds (excluding the one diamond with light $\delta^{13}C$) that can be unmixed into at least three distinct populations (Figure 4.4).

4.5.4 Origin of carbon isotopic compositions in T1 and U2 diamonds

Low $\delta^{13}C$ values at U2

One diamond from U2 has lower $\delta^{13}C$ than the rest of the population (-17.7 to -8.1 ‰). Possible explanations for the origin of such low carbon isotopic values include open system fractionation, by CO_2 escape from a carbonate melt (Cartigny et al., 2001) and subduction of oceanic crust containing ^{13}C depleted material (McCandless and Gurney, 1997).

The CO_2 escape model can explain $\delta^{13}C$ values down to -14 ‰, if fractionated from a mantle source with average carbon around -5 ‰ (Cartigny et al., 2001). If the starting composition is -9 ‰ (lower range of mantle carbonatites), modelling indicates that diamonds with $\delta^{13}C$ as low as -18 ‰ could be precipitated, but only after >99 % CO_2 separation from the carbonatite fluid/melt (e.g., Smart et al., 2011). However, this single diamond's growth zones do not seem to represent one continuously fractionating melt, but rather distinct growth events (Figure 4.6f). Therefore the role of subducted sediments and oceanic crust needs to be considered in order to explain the low $\delta^{13}C$ of ~-18 ‰ in this diamond.

The carbon isotopic composition of average altered oceanic crust is ~-4.7 ‰ (Shilobreeva et al., 2011) and is due to mixing between organic ($\delta^{13}C >$ -27 ‰; Javoy et al., 1986; Strauss, 1986) and carbonate components ($\delta^{13}C \approx$ 0 ‰; Javoy et al., 1986; Schidlowski and Aharon, 1992). Subducted oceanic crust with varying proportions of oceanic crust, organic matter and carbonates can, therefore, account for a wide range in $\delta^{13}C$ values (e.g., McCandless and

Gurney, 1997; Westerlund, 2005).

δ^{13}C values from -7.8 to 0.6 ‰ at T1 and U2

Source reservoirs for the generation of fluids/melts that could precipitate diamonds with δ^{13}C compositions between -7.8 and 0.6 ‰ observed for T1 and U2, can be generated in three ways described below.

1.) Carbonates in the oceanic crust have an average δ^{13}C value of 0 ‰ (Javoy et al., 1986; Schidlowski, 2001; Coggon et al., 2006). With progressive subduction (e.g., during ~2.7 Ga amalgamation of the Superior; Langford and Morin, 1976) these carbonates would undergo devolatilisation and consequent isotopic fractionation leading to more negative δ^{13}C compositions (Kirkley et al., 1991, and references therein).

For diamonds at U2 that are younger than the Midcontinent Rift (~1.1 Ga), a modified version of this subduction model is considered as there are no subduction events documented below the North Caribou superterrane after Superior craton amalgamation at ~2.7 Ga (Langford and Morin, 1976) to directly account for fluids/melts generated from the subduction of carbonated oceanic crust. However, CO_2-rich fluids/melts from an Archaean (2.7 Ga) subducting slab would have reacted with olivine in overlying peridotite to form carbonates (e.g., Wyllie and Huang, 1976). Later thermal events (e.g., the Midcontinent Rift at 1.1 Ga) could raise the local geotherm and carbonated peridotites could melt to form CO_3-bearing melts (e.g., van Groos, 1975; Eggler, 1978; Wendlandt and Mysen, 1980; Brey et al., 2008) which then infiltrate more reduced portions of the lithosphere and precipitate diamond.

2.) A fractionated mantle carbon reservoir, that is more enriched in ^{13}C, but still within the range of mantle values. For example, carbonatite melts have δ^{13}C ranging from -9 to -1 ‰ (Deines and Gold, 1973; Pineau et al., 1973; Sheppard and Dawson, 1975). Carbonatite magmatism in the Superior lithosphere occurred at 1.8 Ga; around 1.1 Ga (related to the Midcontinent Rift) and between 570 - 550 Ma (related to break-up of Rodinia and opening of the Iapetus ocean) (Doig, 1970; Bell and Blenkinsop, 1987; Rukhlov and Bell, 2010, and references therein).

3.) CH_4-bearing fluids remobilised in the lithosphere or originating from the underlying asthenosphere will have $\delta^{13}C$ within the mantle range. Diamond formation from reduced fluids ascending along a typical cratonic P-T-fO_2 path was demonstrated by Huizenga et al. (2012). This process was also invoked by Thomassot et al. (2007) for ~1.9 Ga Premier lherzolitic diamonds based on $\delta^{13}C$ -N co-variations; and Stachel et al. (2009), who, based on $\delta^{13}C$ frequency distributions, suggested that harzurgitic diamonds worldwide frequently precipitated during CH_4 oxidation.

However, a single carbon source is not considered likely for T1 and U2 diamonds, as their internal growth zoning suggests multiple growth events involving isotopically distinct melts/fluids (Section 4.5.3).

4.6 Summary

T1 diamonds. Pre-1.1 Ga diamonds sampled at T1 have a narrow range in $\delta^{13}C$, with a mode of -3.4 ‰, corresponding to other diamond localities on the Superior. T1 diamonds have highly aggregated nitrogen and exhibit platelet degradation, possibly due to the thermal effect of the Midcontinent Rift. The probability density curve for $\delta^{13}C$ in T1 diamonds is skewed towards less negative values; however, this is not indicative of crystallisation from an oxidised source. CL imaging reveals that earlier core growth has higher $\delta^{13}C$, whereas later diamond growth towards the rims has lower $\delta^{13}C$.

U2 diamonds. A high proportion of diamonds sampled by the Jurassic U2 kimberlite - including a likely eclogitic diamond with low $\delta^{13}C$ - are Type IaA. Their unaggregated nature - compared to the highly aggregated T1 diamonds - indicate that they formed after thermal impact of the Midcontinent Rift at 1.1 Ga. The overall $\delta^{13}C$ distribution for U2 diamonds is distinct to T1 and other Superior diamonds, further suggesting that U2 diamonds are not related to the older pre-rift diamonds. Three distinct peaks in the U2 $\delta^{13}C$ distribution, varying $\delta^{13}C$ in diamond cores and lack of consistent internal $\delta^{13}C$ and nitrogen variations suggest that U2 diamonds likely crystallised from fluids/melts derived from multiple sources.

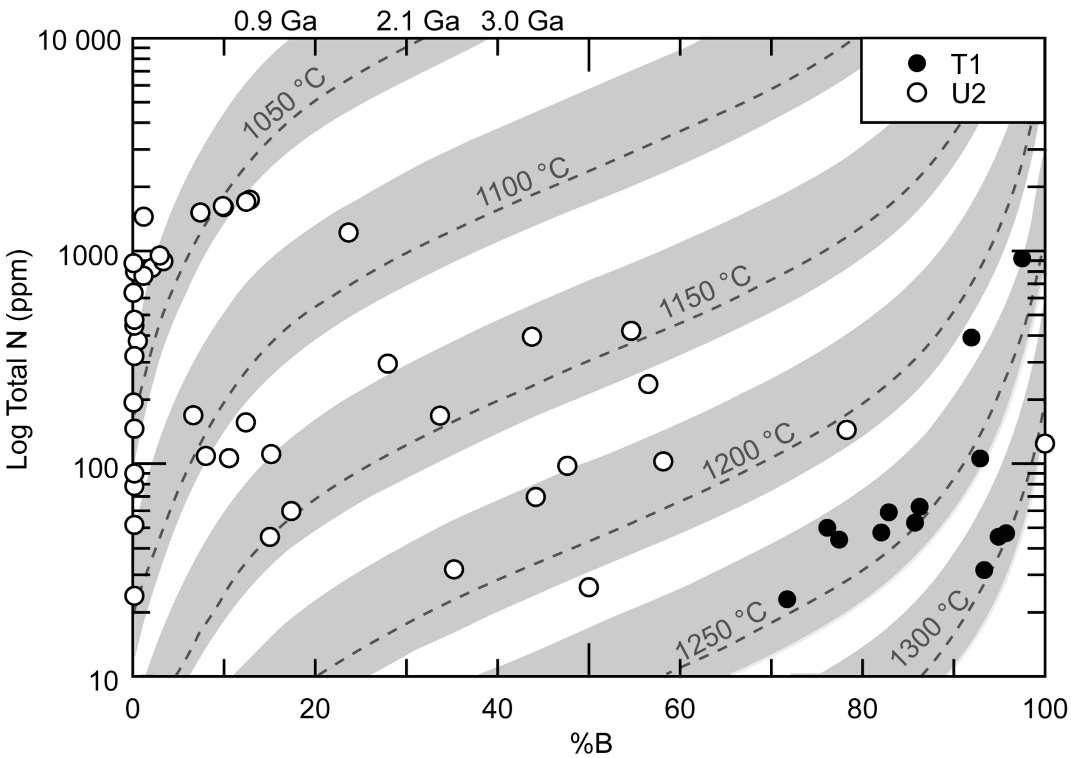

Figure 4.1: Nitrogen content plotted against the percentage of B aggregation (100B / [A + B]) for diamonds from T1 and U2. Only 13 FTIR analyses of T1 diamonds, and 43 analyses of U2 diamonds had measurable nitrogen contents. T1 diamonds are characterised by high levels of B aggregation (>70 %). U2 diamonds have a wide variation of aggregation states, including a high proportion of Type IaA and Type IaAB diamonds with <20 % B aggregation. Isotherms for mantle residence times of 3.0 billion years, 2.1 billion years and 0.9 billion years, were constructed after Leahy and Taylor (1997) (see Section 4.5.1 for details on mantle residence times for T1 and U2 diamonds).

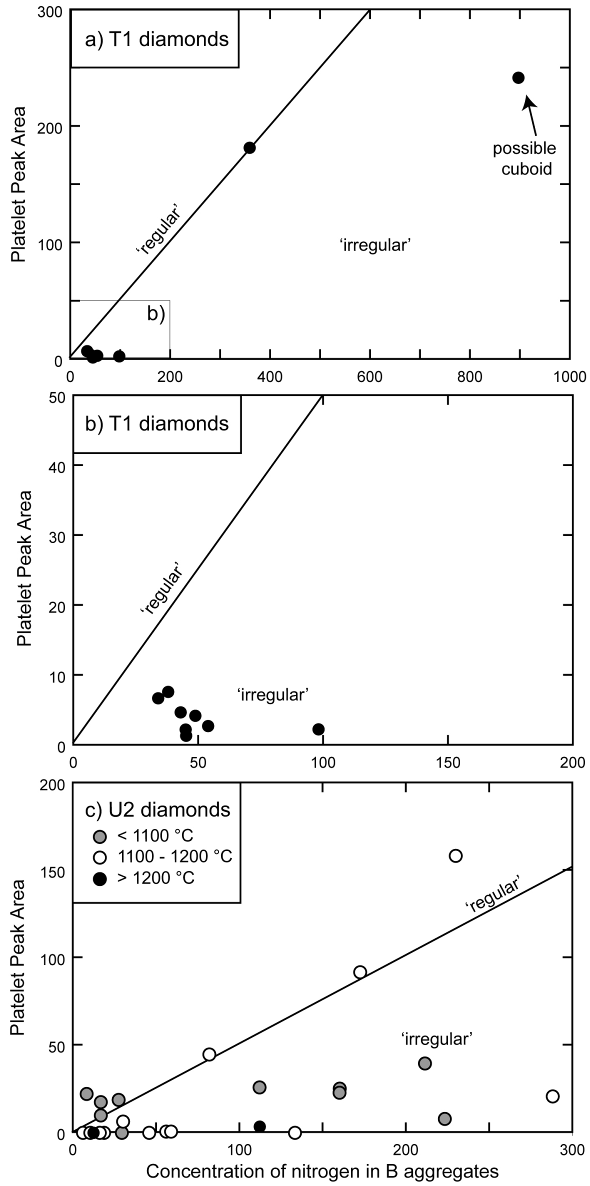

Figure 4.2: Platelet peak area vs B aggregation for Type IaAB diamonds from T1 and U2. Only diamonds with between 1 and 99 % B aggregation were plotted. Diamonds that have a proportional relationship between platelet peaks and %B aggregation fall along a 'regular' linear trend (after Woods, 1986). Platelet degradation may occur due to transient thermal events and/or deformation, with the result that this proportional relationship breaks down - leading to 'irregular' diamonds. For diamonds with cuboid growth, a linear relationship between B aggregates and platelet peak area may not exist (Howell et al., 2012).

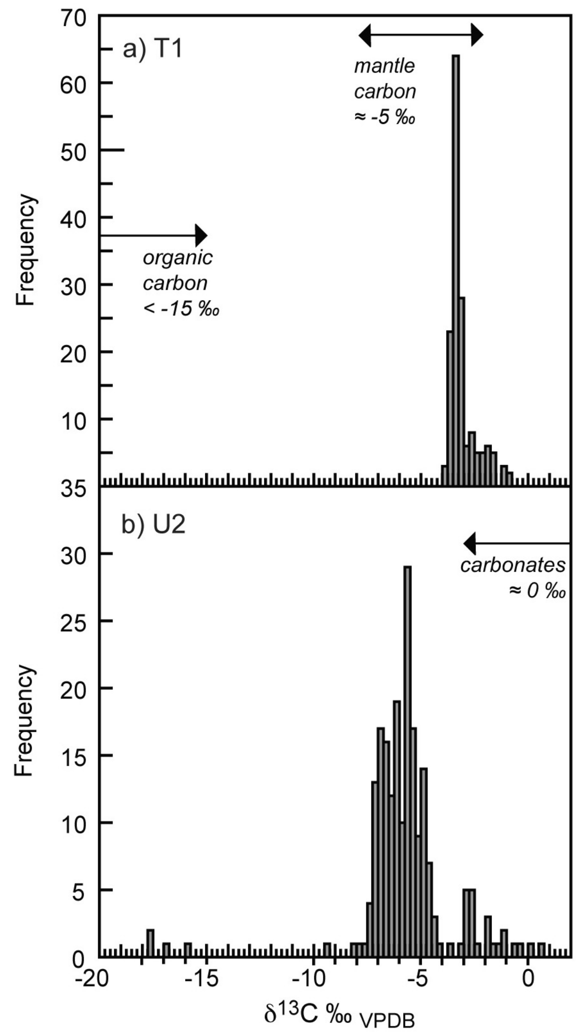

Figure 4.3: Histograms of SIMS analyses of $\delta^{13}C$ for diamonds from T1 and U2. T1 diamonds (158 analyses, 44 diamonds) have a mode around -3.4 ‰, and 203 analyses from U2 (46 diamonds) have a mode around -5.7 ‰. Also shown are the carbon isotopic compositions of possible mantle and sedimentary carbon sources. Mantle carbon ranges from about -8 to -2 ‰, with a mean around -5 ‰; as determined from analyses of mid ocean ridge basalts, kimberlites and carbonatites. Organic carbon has $<$ -15 ‰ and carbonates have a mean of $\approx$ 0 ‰. Refer to Section 4.5.2 for references.

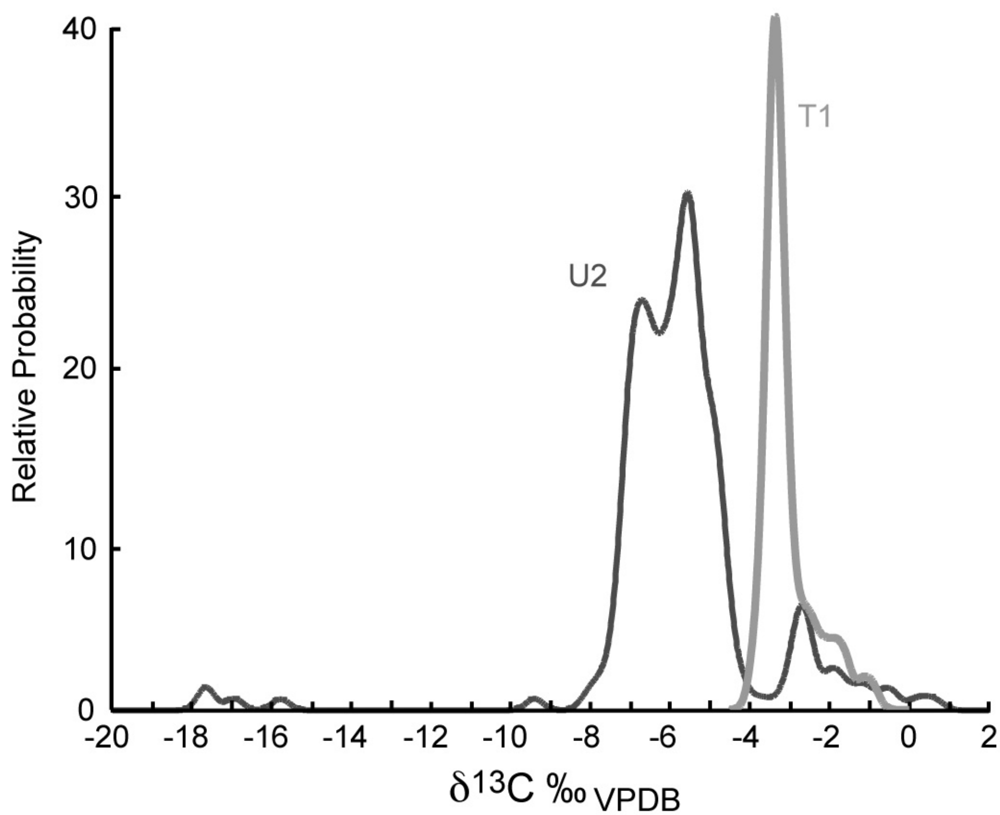

Figure 4.4: Probability density plots of δ^{13}C for diamonds from T1 and U2. T1 diamonds have a narrow distribution that is skewed to more positive δ^{13}C, resembling diamond growth by Rayleigh fractionation from oxidised sources (e.g., Deines, 1980). However, growth zoning in T1 diamonds suggest that early diamond growth was characterised by more positive δ^{13}C, whereas later diamond growth had more negative δ^{13}C (Figure 4.5). The distribution for U2 diamonds is represented by 3 to 4 different populations (see Section 4.4 for details).

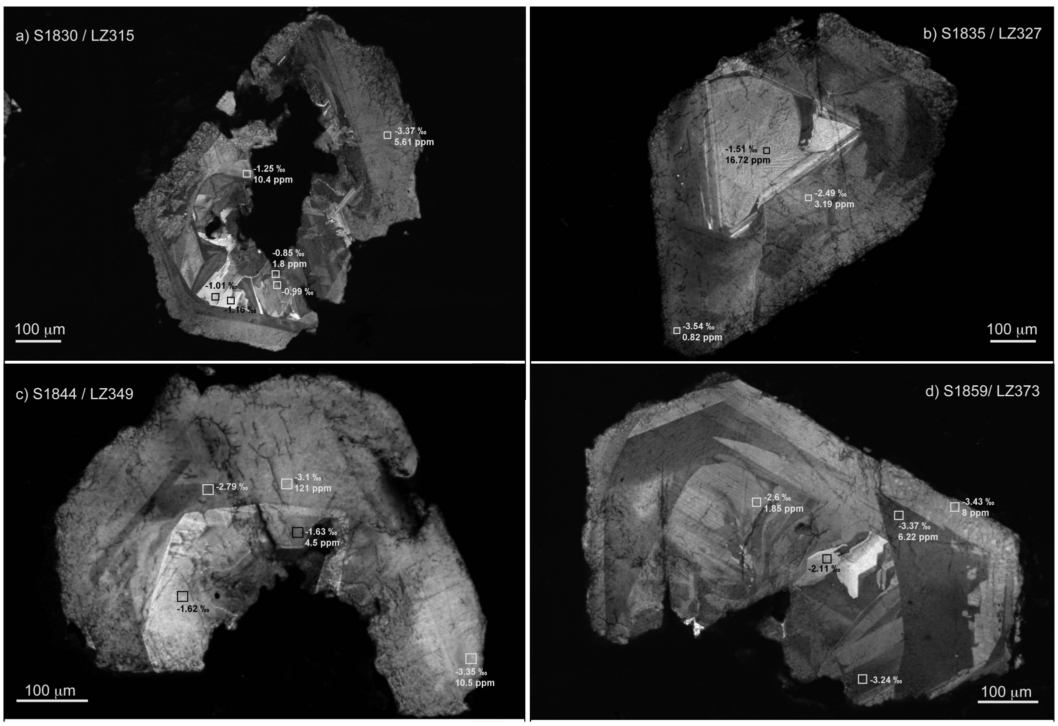

Figure 4.5: Cathodoluminesence images for diamonds from T1. Spot analyses with $\delta^{13}C$ and nitrogen content (at. ppm) are indicated. Earlier diamond growth has slightly less negative $\delta^{13}C$ values (-2 to -0.9 ‰), followed by later overgrowths with more negative $\delta^{13}C$ values (-4.0 to -2.5 ‰). These diamonds have multiple growth zones and resorption surfaces precluding a single diamond growth event with continuous Rayleigh fractionation.

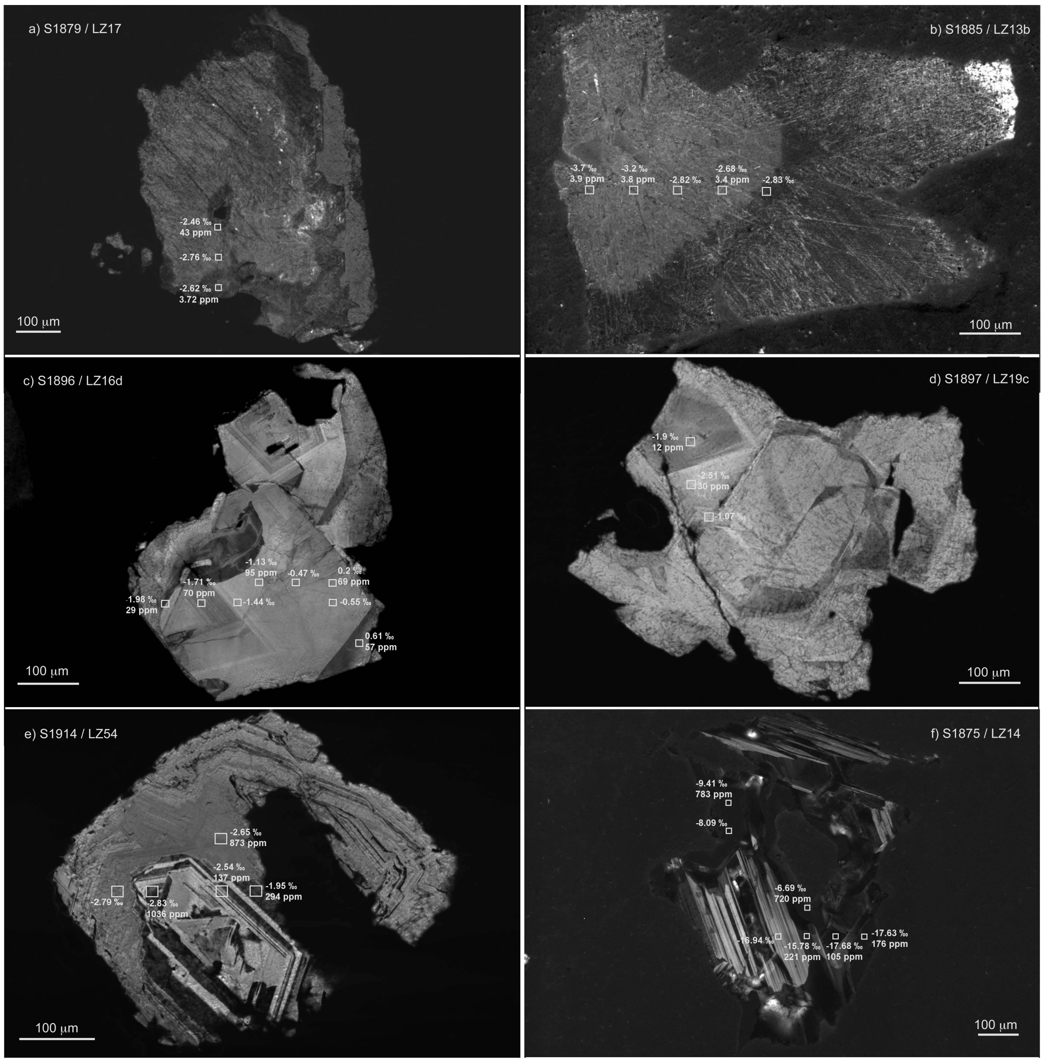

Figure 4.6: Cathodoluminesence images for U2 diamonds that have δ^{13}C deviating from the main population in Figure 4.3. a-e.) five diamonds that have ^{13}C-enriched carbon isotopic compositions (δ^{13}C > -4 ‰) and f.) the only diamond from U2 that has ^{13}C-depleted carbon isotopic compositions (δ^{13}C ≈ -7 to -18 ‰). Spot analyses with δ^{13}C and nitrogen content (at. ppm) are indicated.

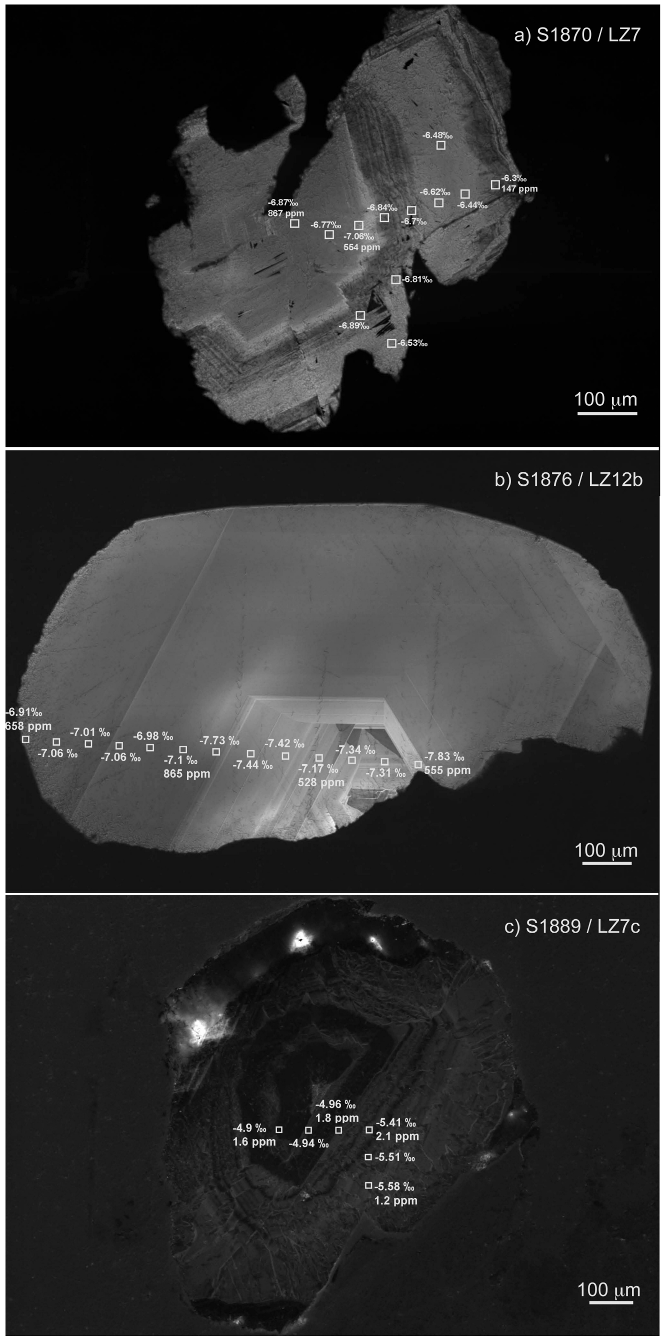

Figure 4.7: Cathodoluminesence images for diamonds from U2 that have δ^{13}C within the main population in Figure 4.3. Analytical spots with δ^{13}C and nitrogen content (at. ppm) are indicated. a) and b) have increasing δ^{13}C from core to rim; whereas in c) δ^{13}C becomes more negative from core to rim, which may suggest diamond growth from oxidised and reduced sources, respectively. However, these diamonds have multiple resorption surfaces, which preclude modelling diamond growth through a continuous Rayleigh fractionation process.

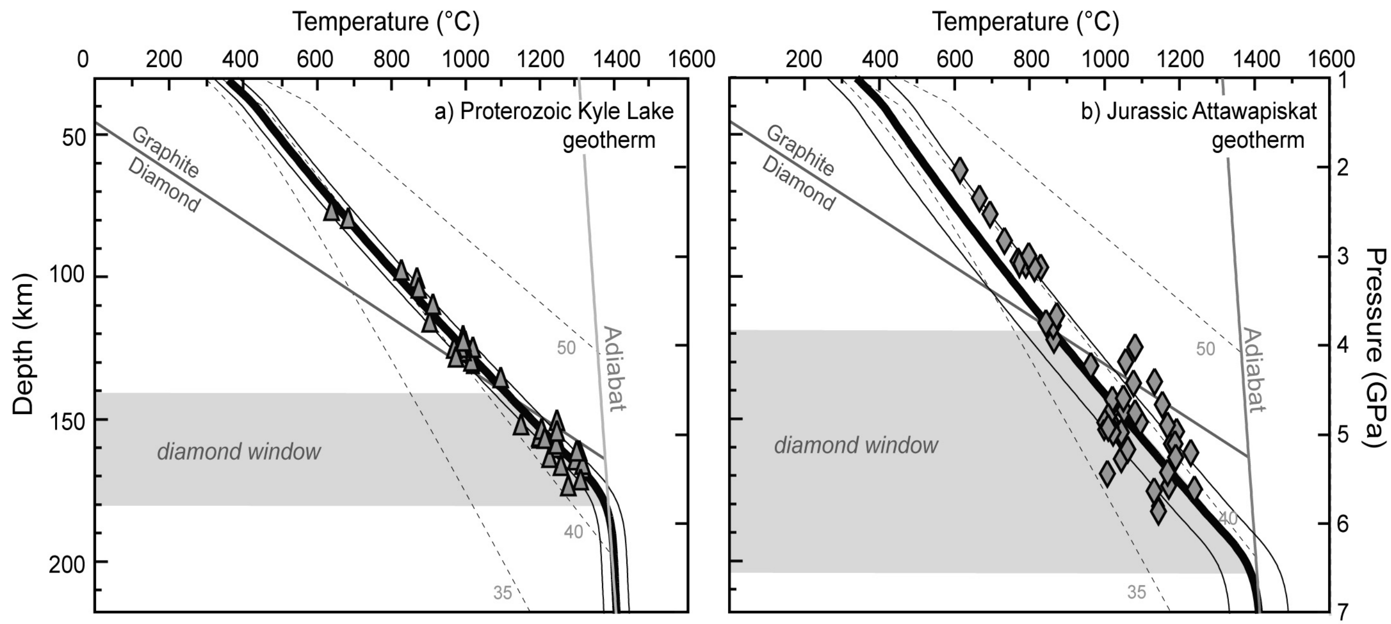

Figure 4.8: Fitplot (e.g., Mather et al., 2011) geotherms (and their error envelopes) for the lithosphere in the Attawapiskat area. Grey dashed lines are geotherms that correspond to 35, 40 and 50 mW/m^2 surface heat flow (Hasterok and Chapman, 2011). Graphite-diamond transition from Day (2012). Pressure (GPa) was converted to depth (km) using a constant density conversion of 0.0324. a.) PT calculations for Kyle Lake single clinopyroxene grains after Nimis and Taylor (2000) and data from Sage (2000). Lithosphere thickness, calculated as the intersection of the conducting geotherm and the mantle adiabat, is ∼180 km. Kyle Lake has a narrow "diamond window" of < 30 km, with diamond stability above 1060 °C / 140 km. Nitrogen-based temperatures in T1 diamonds are all above 1200 °C . b.) Victor single clinopyroxene xenocrysts combined with lherzolite, pyroxenite and harzburgite xenoliths from both Victor and Delta (Section 5.8.3). PT calculations after Nickel and Green (1985), Taylor (1998), Nimis and Taylor (2000) and Nimis and Grütter (2009). Lithosphere thickness is ∼200 km. Attawapiskat has a broad "diamond window" of ∼70 km, with diamond stability above 860 °C / 120 km. Nitrogen-based temperatures calculated for U2 diamonds are >1050°C .

References

Bell, K. and Blenkinsop, J.: 1987, Nd and Sr isotopic compositions of East African carbonatites: Implications for mantle heterogeneity, *Geology* **15**(2), 99–102.

Blank, J. G., Delaney, J. R. and Marais, D. J. D.: 1993, The concentration and isotopic composition of carbon in basaltic glasses from the Juan de Fuca Ridge, Pacific Ocean, *Geochimica et Cosmochimica Acta* **57**, 875.

Boyd, S. R., Kiflawi, I. and Woods, G. S.: 1994, The relationship between infrared absorption and the A defect concentration in diamond, *Philosophical Magazine B* **69**(6), 1149–1153.

Boyd, S. R., Kiflawi, I. and Woods, G. S.: 1995, Infrared absorption by the B nitrogen aggregate in diamond, *Philosophical Magazine B* **72**(3), 351–361.

Boyd, S. R., Mattey, D. P., Pillinger, C. I., Milledge, H. J., Mendelssohn, M. and Seal, M.: 1987, Multiple growth events during diamond genesis: an integrated study of carbon and nitrogen isotopes and nitrogen aggregation state in coated stones, *Earth and Planetary Science Letters* **86**, 341–353.

Brey, G. P., Bulatov, V. K., Girnis, A. V. and Lahaye, Y.: 2008, Experimental Melting of Carbonated Peridotite at 6–10 GPa, *Journal of Petrology* **49**(4), 797–821.

Bursill, L. A. and Glaisher, R. W.: 1985, Aggregation and dissolution of small and extended defect structures in Type Ia diamond, *American Mineralogist* **70**(5-6), 608–618.

Cartigny, P.: 2005, Stable isotopes and the origin of diamond, *Elements* **1**, 79–84.

Cartigny, P., Harris, J. W. and Javoy, M.: 2001, Diamond genesis, mantle fractionations and mantle nitrogen content: a study of δ^{13}C-N concentrations in diamonds, *Earth and Planetary Science Letters* **185**, 85–98.

Coggon, R. M., Teagle, D. A. H., Cooper, M. J., Hayes, T. E. F. and Green, D. R. H.: 2006, Data report: compositions of calcium carbonate veins from superfast spreading rate crust, ODP Leg 206, *Proceedings of the Ocean Drilling Program, Scientific Results* **206**, 1–6.

Day, H. W.: 2012, A revised diamond-graphite transition curve, *American Mineralogist* **97**, 52–62.

de Stefano, A., Kopylova, M. G., Cartigny, P. and Afanasiev, V.: 2009, Diamonds and eclogites of the Jericho kimberlite (Northern Canada), *Contributions to Mineralogy and Petrology* **158**(3), 295–315.

de Vries, D. F. W., Bulanova, G. P., de Corte, K., Pearson, D. G., Craven, J. A. and Davies, G. R.: 2013, Micron-scale couple carbon isotope and nitrogen abundance variations in diamonds: Evidence for episodic diamond formation beneath the Siberian Craton, *Geochimica et Cosmochimica Acta* **100**, 176–199.

Deines, P.: 1980, The carbon isotopic composition of diamonds: relationship to diamond shape, colour, occurrence and vapour deposition, *Geochimica et Cosmochimica Acta* **44**, 943–961.

Deines, P.: 2002, The carbon isotope geochemistry of mantle xenoliths, *Earth-Science Reviews* **58**, 247–278.

Deines, P. and Gold, D. P.: 1973, The isotopic composition of carbonatite and kimberlite carbonate and their bearing on the isotopic composition of deep-seated carbon, *Geochimica et Cosmochimica Acta* **37**, 1709–1733.

Delacour, A., Früh-Green, G. L., Bernasconi, S. M., Schaeffer, P. and Kelley, D. S.: 2008, Carbon geochemistry of serpentinites in the Lost City Hydrothermal System (30N, MAR), *Geochimica et Cosmochimica Acta* **72**, 3681–3702.

Doig, R.: 1970, An alkaline rock province linking Europe and North America, *Canadian Journal of Earth Sciences* **7**(1), 22–26.

Eggler, D. H.: 1978, The effect of CO_2 upon partial melting of peridotite in the system Na_2O-CaO-Al_2O_3-MgO-SiO_2-CO_2 to 35kbar, with an analysis of melting in a peridotite-H_2O-CO_2 system, *American Journal of Science* **278**, 305–343.

Evans, T., Kiflawi, I., Luyten, W., van Tendeloo, G. and Woods, G. S.: 1995, Conversion of platelets into dislocation loops and voidite formation in Type

IaB diamonds, *Proceedings of the Royal Society of London, Ser A* **449**, 295–313.

Evans, T. and Qi, Z.: 1982, The kinetics of aggregation of nitrogen in diamond, *Proceedings of the Royal Society of London, Ser A* **361**, 109–127.

Exley, R. A., Mattey, D. P., Clague, D. A. and Pillinger, C. T.: 1986, Carbon isotope systematics of a mantle "Hot Spot": A comparison of Loihi Seamount and MORB glasses, *Earth and Planetary Science Letters* **78**, 189–199.

Grütter, H. S.: 2009, Pyroxene xenocryst geotherms: Techniques and application, *Lithos* **112S**, 1167–1178.

Harte, B., Fitzsimons, I. C. W., Harris, J. W. and Otter, M. L.: 1999, Carbon isotope ratios and nitrogen abundances in relation to cathodoluminesence characteristics for some diamonds from the Kaapvaal Province, S. Africa, *Mineralogical Magazine* **63**(6), 829–856.

Hasterok, D. and Chapman, D. S.: 2011, Heat production and geotherms for the continental lithosphere, *Earth and Planetary Science Letters* **307**, 59–70.

Hoefs, J. and Frey, M.: 1976, The isotopic composition of carbonaceous matter in a metamorphic profile from the Swiss Alps, *Geochimica et Cosmochimica Acta* **40**, 945.

Howell, D., O'Neill, C. J., Grant, K. J., Griffin, W. L., O'Reilly, S. Y., Pearson, N. J., Stern, R. A. and Stachel, T.: 2012, Platelet development in cuboid diamonds: insights from micro-FTIR mapping, *Contributions to Mineralogy and Petrology* **164**, 1011–1025.

Huizenga, J. M., Crossingham, A. and Viljoen, F.: 2012, Diamond precipitation from ascending reduced fluids in the Kaapvaal lithosphere: Thermodynamic constraints, *Comptes Rendus Geoscience* **344**, 67–76.

Humble, P.: 1982, The structure and mechanism of formation of platelets in natural type Ia diamond, *Proceedings of the Royal Society of London, Ser A* **381**, 65–81.

Hunt, L. C., Stachel, T., McCandless, T. E., Armstrong, J. and Muehlenbachs, K.: 2012b, Diamonds and their mineral inclusions from the Renard kimberlites in Quebec, *Lithos* **142-143**, 267–284.

Javoy, M., Pineau, F. and Delorme, H.: 1986, Carbon and nitrogen isotopes in the mantle, *Chemical Geology* **57**(1-2), 41–62.

Kiflawi, I. and Bruley, J.: 2000, The nitrogen aggregation sequence and the formation of voidites in diamond, *Diamond and Related Materials* **9**, 87–93.

Kirkley, M. B., Gurney, J. J., Otter, M. L., Hill, S. J. and Daniels, L. R.: 1991, The application of C isotope measurements to the identification of the sources of C in diamonds: a review, *Applied Geochemistry* **6**, 477–494.

Langford, F. F. and Morin, J. A.: 1976, The development of the Superior Province of Northwestern Ontario by merging Island Arcs, *American Journal of Science* **270**, 1023–1034.

Leahy, K. and Taylor, W. R.: 1997, The influence of the Glennie domain deep structure on the diamonds in Saskatchewan kimberlites, *Russian Geology and Geophysics* **38**(2), 481–491.

Lilley, M. D., Butterfield, D. A., Olson, E. J., Lupton, J. E., Macko, S. A. and McDuff, R. E.: 1993, Anomalous CH_4 and NH_4^+ concentrations at an unsedimented mid-ocean-ridge hydrothermal system, *Nature* **364**, 45–47.

Marais, D. J. D. and Moore, J. G.: 1984, Carbon and its isotopes in mid-oceanic basaltic glasses, *Earth and Planetary Science Letters* **62**, 43–57.

Marty, B. and Zimmermann, L.: 1999, Volatiles (He, C, N, Ar) in mid-ocean ridge basalts: Assesment of shallow-level fractionation and characterization of source composition, *Geochimica et Cosmochimica Acta* **63**(21), 3619–3633.

Mather, K. A., Pearson, D. G., McKenzie, D., Kjarsgaard, B. A. and Priestley, K.: 2011, Constraints on the depth and thermal history of cratonic lithosphere from peridotite xenoliths, xenocrysts and seismology, *Lithos* **125**, 729–742.

Mattey, D. P., Carr, R. H., Wright, I. P. and Pillinger, C. T.: 1984, Carbon isotopes in submarine basalts, *Earth and Planetary Science Letters* **70**, 196–206.

McCandless, T. E. and Gurney, J. J.: 1997, Diamond eclogites: comparison with carbonaceous chondrites, carbonaecous shales, and microbial carbon-enriched MORB, *Russian Geology and Geophysics, Special Issue: Proceedings of the 6th International Kimberlite Conference* **2**, 394–404.

McKirdy, D. M. and Powell, T. G.: 1974, Metamorphic alteration of carbon isotopic composition in ancient sedimentary organic matter: new evidence from Australia and South Africa, *Geology* **2**, 591.

Miller, C. E., Kopylova, M. G. and Ryder, J.: 2012, Vanished diamondiferous cratonic root beneath the Southern Superior province: evidence from diamond inclusions in the Wawa metaconglomerate, *Contributions to Mineralogy and Petrology* **164**(4), 697–714.

Nadeau, S., Philippot, P. and Pineau, F.: 1993, Fluid inclusion and mineral isotopic compositions (H-C-O) in eclogite rocks as tracers of local fluid migration during high-pressure metamorphism, *Earth and Planetary Science Letters* **114**, 431.

Nickel, K. G. and Green, D. H.: 1985, Empirical geothermobarometry for garnet peridotites and implications for the nature of the lithosphere, kimberlites and diamonds., *Earth and Planetary Science Letters* **73**, 158–170.

Nimis, P. and Grütter, H.: 2009, Internally consistent geothermometers for garnet peridotites and pyroxenites, *Contributions to Mineralogy and Petrology* **159**(3), 411–427.

Nimis, P. and Taylor, W. R.: 2000, Single clinopyroxene thermobarometry for garnet peridotites. Part I. Calibration and testing of a Cr-in-Cpx barometer and an enstatite-in-Cpx thermometer, *Contributions to Mineralogy and Petrology* **139**, 541–554.

Nisbet, E. G., Mattey, D. P. and Lowry, D.: 1994, Can diamonds be dead bacteria?, *Nature* **367**, 694.

Palot, M., Pearson, D. G., Stern, R. A., Stachel, T. and Harris, J. W.: 2013, Multiple growth events, processes and fluid sources involved in diamond genesis: A micro-analytical study of sulphide-bearing diamonds from the Finsch mine, RSA, *Geochimica et Cosmochimica Acta* **106**, 51–70.

Pineau, F., Javoy, M. and Allègre, C. J.: 1973, Ètude systématique des isotopes de l'oxygène, du carbone et du strontium dans les carbonatites, *Geochimica et Cosmochimica Acta* **37**, 2363–2377.

Rukhlov, A. S. and Bell, K.: 2010, Geochronology of carbonatites from the Canadian and Baltic shields, and the Canadian Cordillera: clues to mantle evolution, *Mineralogy and Petrology* **98**(1-4), 11–54.

Sage, R. P.: 2000, Kimberlites of the Attawapiskat area, James Bay Lowlands, northern Ontario, *Ontario Geological Survey, Open File Report* **6019**(341), 341.

Satish-Kumar, M., Wada, H. and Santosh, M.: 2002, Constraints on the application of carbon isotope thermometry in high-to ultrahigh-temperature metamorphic terranes, *Journal of Metamorphic Geology* **20**(3), 335–350.

Schidlowski, M.: 2001, Carbon isotopes as biogeochemical recorders of life over 3.8 Ga of Earth history: evolution of a concept, *Precambrian Research* **106**, 117–134.

Schidlowski, M. and Aharon, P.: 1992, Carbon cycle and isotope record: Geochemical impact of life over 3.8 Ga of Earth history, *in* M. Schidlowski, S. Golubic, M. M. Kimberley, D. M. McKirdy and P. A. Trudinger (eds), *Early Organic Evolution: Implications for Mineral and Energy Resources*, Springer, Berlin, pp. 147–175.

Sheppard, S. M. F. and Dawson, J. B.: 1975, Hydrogen, carbon and oxygen isotope studies of megacryst and matrix minerals from Lesothan and South African kimberlites, *in* L. Ahrens, H. C. Urey and S. K. Runcorn (eds), *Physics and Chemistry of the Earth*, Vol. 9, Pergamon Press, Oxford, pp. 747–763.

Shilobreeva, S., Martinex, I., Busigny, V., Agrinier, P. and Laverne, C.: 2011, Insights into C and H storage in the altered ocean crust: Results fromODP/IODP Hole 1256D/, *Geochimica et Cosmochimica Acta* **75**(2237-2255).

Smart, K. A., Chacko, T., Stachel, T., Muehlenbachs, K., Stern, R. A. and Heaman, L. M.: 2011, Diamond growth from oxidized carbon sources beneath the Northern Slave Craton, Canada: A δ^{13}C-N study of eclogite-hosted diamonds from the Jericho kimberlite, *Geochimica et Cosmochimica Acta* **75**, 6027–6047.

Snyder, G. A., Taylor, L. A., Jerde, E. A., Clayton, R. N., Mayeda, T. K., Deines, P., Rossman, G. R. and Sobolev, N. V.: 1995, Archean mantle heterogeneity and origin of diamondiferous eclogites, Siberia: evidence from stable isotopes and hydroxyl in garnet, *American Mineralogist* **80**, 799.

Sobolev, V. N., Taylor, L. A. and Snyder, G. A.: 1994, Diamondiferous eclogites from the Udachnaya kimberlite pipe, Yakutia, *International Geology Review* **36**, 42.

Stachel, T., Aulbach, S., Brey, G. P., Harris, J. W., Leost, I., Tappert, R. and Viljoen, K. S.: 2004, The trace element composition of silicate inclusions in diamonds: a review, *Lithos* **77**, 1–20.

Stachel, T., Banas, A., Muehlenbachs, K., Kurszlaukis, S. and Walker, E. C.: 2006, Archean diamonds from Wawa (Canada): samples from deep cratonic roots predating cratonization of the Superior Province, *Contributions to Mineralogy and Petrology* **151**, 737–750.

Stachel, T. and Harris, J. W.: 2008, The origin of cratonic diamonds - constraints from mineral inclusions, *Ore Geology Reviews* **34**(1-2), 5–32.

Stachel, T., Harris, J. W. and Muehlenbachs, K.: 2009, Sources of carbon in inclusion-bearing diamonds, *Lithos* **112S - Proceedings of the 9th International Kimberlite Conference**, 625–637.

Strauss, H.: 1986, Carbon and sulphur isotopes in Precambrian sediments from the Canadian Shield, *Geochimica et Cosmochimica Acta* **50**, 2653–2662.

Taylor, W. R.: 1998, An experimental test of some geothermometer and geobarometer formulations for upper mantle peridotites with application to the thermobarometry of fertile lherzolite and garnet websterite, *Neues Jahrbuch Mineralogie Abhandlungen* **172**, 381–408.

Taylor, W. R., Jaques, A. L. and Ridd, M.: 1990, Nitrogen-defect aggregation characteristics of some Australasian diamonds: Time-temperature constraints on the source regions of pipe and alluvial diamonds, *American Mineralogist* **75**, 1290–1310.

Thomassot, E., Cartigny, P., Harris, J. W. and Viljoen, K. S.: 2007, Methane-related diamond crystallisation in the Earth's mantle: Stable isotope evidences from a single diamond-bearing xenolith, *Earth and Planetary Science Letters* **257**, 362–371.

van Groos, A. F. K.: 1975, The effect of high CO_2 pressures on alkalic rock and its bearing on the formation of alkalic ultrabasic rocks and the associated carbonatites, *American Journal of Science* **275**, 163–185.

van Schmus, W. R. and Hinze, W. J.: 1985, The Midcontinent Rift System, *Annual Review of Earth and Planetary Sciences* **13**, 345–383.

Wendlandt, R. F. and Mysen, B. O.: 1980, Melting phase relations of natural peridotite + CO_2 as a function of degreee of partial melting at 15 and 30 kbar, *American Mineralogist* **65**, 37–44.

Westerlund, K. J.: 2005, *A Geochemical Study of Diamonds, Sulfide Inclusions in Diamonds and Mantle Xenoliths from the Panda Kimberlite, Slave Craton*, PhD thesis, University of Cape Town.

White, W. S.: 1972, Keweenawan flood basalts and continental rifting, *Geological Association of America, Abstracts with Programs* **4**, 732–734.

Woods, G.: 1986, Platelets and the infrared absorption of type Ia diamonds, *Proceedings of the Royal Society* **A407**, 219–238.

Wyllie, P. J. and Huang, W.-L.: 1976, Carbonation and melting reactions in the system CaO-MgO-SiO_2-CO_2 at mantle pressures with geophysical and petrological applications, *Contributions to Mineralogy and Petrology* **54**, 79–107.

Chapter 5

Mesoproterozoic reworking of Palaeoarchaean lithospheric mantle beneath the Northern Superior superterrane

5.1 Introduction

Old continental crust is underlain by sub-continental lithospheric mantle (SCLM) that has undergone high degrees of melt depletion (removal of Ca, Al, Fe, H_2O) leading to a residue with low density and high viscosity compared to the underlying asthenosphere (e.g., Jordan, 1975; Boyd and McCallister, 1976). Melt depletion is key for the long term survival of the lithospheric mantle root of a craton, however the process by which the lithosphere attained its highly depleted nature is still debated.

Melt depletion may have occurred at high pressures in a plume setting (e.g., Boyd, 1989; Arndt et al., 1998; Herzberg, 1999; Aulbach et al., 2007; Aulbach, 2012) or at lower pressures with initial melting at a mid-ocean ridge (e.g., Bulatov et al., 1991; Canil and Wei, 1992; Stachel et al., 1998; Canil, 2004; Bernstein et al., 2007; Herzberg and Rudnick, 2012). Regardless of the exact setting, the SCLM must have undergone high degrees of melting, in part to the point of orthopyroxene exhaustion and dunitic residues (Bernstein et al., 2006, 2007; Herzberg and Rudnick, 2012). This suggests that other minerals were introduced into the SCLM after the initial depletion event. Evidence for secondary addition of not only orthopyroxene, but also garnet, olivine and clinopyroxene, to the SCLM has been widely documented (e.g., Kelemen, 1990a; Kelemen et al., 1992; Shimizu et al., 1997; Grégoire et al., 2003; Simon et al., 2003; Bell et al., 2005; Rehfeldt et al., 2008; Hunt et al., 2012a).

Major tectonothermal events may result in lithosphere removal (e.g., the North China and Wyoming cratons Gao et al., 2002; Carlson et al., 2004; Yang et al., 2010; Liu et al., 2011, 2012), gradual melt metasomatism however may refertilise the SCLM. Melt metasomatism (and accompanying oxidation) may be detrimental to diamond preservation (e.g., McCammon et al., 2001) and may increase the water content in mantle minerals, thereby lowering the viscosity in the lithosphere (Peslier et al., 2010, 2012) which may contribute to the eventual demise of lithospheric roots. However, these enrichment events may also lead to lherzolitic diamond formation, for example Premier and Venetia on the Kaapvaal craton (Richardson et al., 1993, 2009), Ellendale on the Kimberley craton (Smit et al., 2010) and Udachnaya in Siberia (Richardson and Harris, 1997).

The Superior craton was affected by a major tectonothermal event, the Midcontinent Rift, at 1.1 Ga (White, 1972; Halls, 1978; Wold and Hinze, 1982; van Schmus and Hinze, 1985), which may have thinned the cratonic root in the southern Superior (Kopylova et al., 2011; Miller et al., 2012; Schaeffer and Lebedev, 2013; Zartman et al., 2013). Any effect of the Midcontinent Rift, or other thermal events on the SCLM in the Northern Superior province below Attawapiskat is not yet fully understood. Previous studies have suggested that the thermal effect of the Rift may be seen in the elevated geotherm at Kyle Lake (clinopyroxene xenocrysts; Sage, 2000; Grütter, 2009). Additionally, the lithosphere at 1.1 Ga, as sampled by Kyle Lake, is predominantly harzburgitic in composition; whereas the lithosphere sampled by younger kimberlites, including the Attawapiskat kimberlites (180 Ma) is predominantly lherzolitic (Sage, 2000). This may have been due to melt/fluid infiltration related to the Midcontinent Rift (Sage, 2000; Scully et al., 2004).

In this study, we analyse peridotitic xenocrysts and xenoliths from Attawapiskat on the Superior craton. We aim to answer the following questions: To what extent and in what setting did primary melt depletion occur during SCLM formation in the Archaean? What was the timing of initial depletion? How thick is the lithosphere and what are the diamond-stable lithologies? To what extent was the peridotitic lithosphere affected by the major Midcontinent Rift event?

In addition to major and trace element evidence, we present PGE analyses for sulphide / alloy inclusions in olivine from peridotite xenoliths. Due to fractionation of I-PGE's (Os, Ir, Ru; Barnes et al., 1985) and P-PGE's (Pt, Pd; Barnes et al., 1985) between residues and mantle melts (e.g., Bockrath et al., 2004), PGE analyses are a powerful tool for tracing depletion and enrichment processes in the lithosphere (Pearson et al., 2004; Wittig et al., 2010; Maier et al., 2012). Combining these PGE results with T_{RD} age determinations for these xenoliths - the first for the Superior craton - we aim to provide constraints on the timing of these processes.

5.2 Samples

5.2.1 Victor

Samples for this study include eclogite/pyroxenite xenoliths and mixed parageneses mineral concentrate from Victor Mine. We analysed a suite of 33 xenoliths - 17 bimineralic eclogite xenoliths and 16 pyroxenite xenoliths, five of which are orthopyroxene-bearing. The formation of the eclogite and pyroxenite xenoliths from Victor has been fully described in Chapter 3, however their PT conditions of last equilibration and origin in either the graphite or diamond stability fields are discussed here in context with the peridotites. Garnet, clinopyroxene, orthopyroxene and olivine xenocrysts were picked from Victor mineral concentrate and analysed for their major and trace elements.

5.2.2 Delta

Samples analyses from Delta include seven harzburgites, five lherzolites, three dunites, three pyroxenites and one garnet dunite that were sawed out of kimberlite core. Due to the small size of most samples, they were not classified on mineral modal abundances but on the basis of their garnet chemistry, where garnet was present. Samples that contained that no clinopyroxene were classified as harzburgite and samples containing only olivine as dunite. The majority of the xenoliths show substantial modal metasomatism, with secondary amphibole, mica and clinopyroxene (summarised in Table E.1). Kimberlite infiltration and serpentinisation in olivine-bearing samples is common and kimberlite rims around the xenoliths are visible in thin section (Figure 5.1).

In this study, only the primary mantle mineralogy is discussed and xenoliths were analysed for their major elements and geothermobarometry. Olivine was picked from crushed peridotite xenoliths and analysed for its Re-Os isotopic composition and platinum group element (PGE) content.

5.3 Analytical techniques

5.3.1 Major elements

Major element compositions were measured using a JEOL8900R electron microprobe at the University of Alberta, operating at 20 kV accelerating voltage, 20 nA probe current and 1 μm beam diameter. Peak count times varied between 30 and 60 seconds, and half that for background count times (Table A.1). Both natural and synthetic standards were used for calibration with matrix corrections following Armstrong (1995) (Table A.2). Multiple analyses for each mineral grain were averaged after those with low totals (< 98.5 %) and poor stoichiometry were removed. Detection limits were below 100 ppm for all oxides, apart from 200 ppm for Na_2O and 250 ppm for P_2O_5.

5.3.2 Trace elements

In-situ trace element analyses were carried out using a Nd:YAG UP213 nm laser ablation system (New Wave Research) connected to a Perkin Elmer Elan 6000 Quadrupole ICP-MS. The NIST612 glass standard was used for calibration and optimisation of instrument parameters. Samples were typically ablated for 50 seconds, with a spot size of 150 μm and the background analysed for 20 seconds prior to each analysis. Garnet grains (PN1 and PN2) that have been well characterised using several techniques (INAA, SIMS, LA-ICP-MS; Tappert et al., 2005) were analysed as secondary standards. Average concentration values obtained for these garnets overlap within error to the recommended values for these standards. Data reduction and concentration determinations, using EPMA-determined Ca concentrations in garnet as internal standard, were obtained using GLITTER laser ablation software (van Achterbergh et al., 2001).

5.3.3 Re-Os isotopic compositions and PGE content

Due to small sample size and the extensive nature of kimberlite infiltration in many xenoliths, olivine separates were analysed to ensure analyses of peridotite with the least contamination. Xenoliths were sawed out of kimberlite drill core using a low speed diamond saw, after which xenoliths were crushed (in a plastic bag to avoid metal contamination) and olivine picked under a binocular microscope. Olivine was rinsed three times and ultrasonically cleaned in milli-Q H_2O for about 30 minutes. After dry down overnight on a hotplate, olivine was weighed and then attacked in 12N HCL at 80 °C overnight to start break down of the olivine lattice. Olivine was digested in reverse Aqua Regia for 16 hours at 290 °C and 120 bar in an Anton Paar high pressure Asher, sufficient to allow for equilibration with a mixed ^{190}Os-^{191}Ir-^{99}Ru-^{194}Pt-^{106}Pd-^{185}Re spike.

Osmium isotopic composition and concentration

Osmium was separated by solvent extraction into either $CHCl_3$ (chloroform) or CCL_4 (carbon tetrachloride), with back extraction into HBr (following Cohen and Waters, 1996) and purification using micro distillation techniques (Roy-Barman and Allègre, 1994; Birck et al., 1997). For the distillation, 15 μl HBr was added to the tip of a conical beaker and 30 μl CrO_3/H_2SO_4 solution to the dried down Os fraction. The inverted beaker was placed on a hotplate for two hours at 85 °C . The HBr drop was partially dried down and loaded onto platinum ribbon filaments, along with $Ba(OH)_2$. The osmium isotopic compositions were analysed by negative thermal ionisation mass spectrometry (N-TIMS) on a Thermo Scientifc Triton Plus using an electron multiplier in peak jumping mode. Air was bled in during the sample run to ensure more efficient ionisation.

Mass spectrometer fractionation was corrected by normalising ^{192}Os/^{188}Os to 3.08261 (Creaser et al., 1991). As Re and Os were run as negative oxides, data were corrected for interferences from three O isotopes, with $^{17}O/^{16}O = 0.0003$ and $^{18}O/^{16}O = 0.0020$. Analyses were corrected for procedural blanks of 0.2 $\pm$ 0.1 pg Os. ^{187}Os/^{188}Os standard errors (SE) include the in-run precision, the uncertainty in the concentration and isotopic composition of the blank and the uncertainty in the spike calibration (Table I.3 and I.4). 2SE uncertainties in

$^{187}Os/^{188}Os$ are between ± 0.3 and 3.7%. Uncertainties in the Os concentration include the in-run precision, uncertainty in the blank concentration and error magnification due to overspiking.

Rhenium isotopic composition and PGE concentration

Following Os extraction, the Re and PGE fractions were further separated by column chromatography, following methods similar to Pearson and Woodland (2000) and Becker et al. (2006). Aqua Regia fractions were dried down overnight, re-dissolved in 6N HCL overnight and dried down to remove all remaining HNO_3. Samples were dissolved in 1N HCL, centrifuged and loaded onto columns containing ~2 ml pre-cleaned Biorad AG1X-8 anion exchange resin. After matrix elution in 10 ml 1N HCL and 6 ml 0.8N HNO_3, Re + Ru were collected in 12 ml 6N HCL, Pt + Ir in 15 ml concentrated HNO_3 and Pd in 14 ml concentrated HCL. Following dry-down, Pt + Ir and Pd fractions were dried down in Aqua Regia to remove any organic material. All fractions were dissolved in 1 ml 0.8N HNO_3 and centrifuged for ICP-MS analyses.

PGE and Re fractions were analysed on a Thermo Scientific Element 2 XR magnetic sector ICP-MS. Solutions were aspirated into the plasma at a flow rate of 0.05 ml/min and signals detected using an electron multiplier. Single element standards containing 1 ppb of the analyte in question were measured at the beginning, during and end of each analytical session to allow for mass fractionation correction. Standards were also prepared to measure oxide production rates in order to correct for possible isobaric interferences. For Pd analyses - ZrO/Zr was less than 4% and YO/Y less than 2.5%. For Pt+Ir analyses - HfO/Hf was less than 2.25% and LuO/Lu less than 0.35%. For Re analyses - YbO/Y was less than 0.06% and TmO/Tm less than 0.14%. For Ru analyses, ^{95}Mo was monitored to correct for ^{100}Mo on ^{100}Ru.

Background signals were monitored before each analysis, with wash-out times between samples of about 2 minutes. PGE concentrations were corrected using procedural blanks of 1 ± 1 pg Ir, 0.49 ± 0.48 pg Pt, 2 ± 2 pg Ru, 0.45 ± 0.25 pg Pd and 1 ± 0.5 pg Re. 2σ uncertainties in the concentration of Re and PGE's include the in-run precision and the uncertainty in the blank concentration. 2σ uncertainties in $^{187}Re/^{188}Os$ include in-run precision, the uncertainty in the concentration and isotopic compositions of the blanks.

5.4 Victor xenocryst major element chemistry

5.4.1 Garnet

According to the classification outlined in Grütter et al. (2004), 70% of the 375 Victor garnets analysed are lherzolitic (G9), 16% are eclogitic/pyroxenitic (G3/G4), 12% are megacrystic (G1), 2% classified as being derived from a high TiO_2 peridotitic source (G11) and 1% are harzburgitic (G10) (Figure 5.2a,b; Table F.1 to Table F.6).

Lherzolitic (G9) garnets have CaO = 3.71 - 7.51 wt% and Cr_2O_3 = 1.05 - 9.83 wt%, with TiO_2 = 0 - 0.48 wt% and Mg# between 70.6 and 84.9 with an average of 82.2. MnO content varies from 0.33 to 0.62 wt%. Eclogitic (G3) garnets have CaO = 6.03 - 13.1 wt%, Cr_2O_3 = $\leqslant$0.01 - 0.36 wt% and Mg# between 39.1 and 73.0, with average of 57.1. Na_2O content varies from 0 to 0.22 wt%. Eclogitic / pyroxenitic (G4) garnets have CaO = 3.66 - 5.82 wt%, Cr_2O_3 = 0.03 - 0.98 wt% and Mg# between 54.95 and 85.24, with average of 70.84. Na_2O content varies from $\leqslant$0.02 to 0.36 wt%. Low-Cr megacrystic (G1) garnets have CaO = 4.09 - 4.91 wt%, Cr_2O_3 = 0.98 - 3.59 wt% and Mg# between 75.5 to 82.4, with an average of 80.3. High TiO_2 peridotitic (G11) garnets have CaO = 3.99 - 5.23 wt%, Cr_2O_3 = 3.02 - 5.39 wt% and TiO_2 = 0.39 - 0.52 wt%. Mg# range from 80.4 to 84.7, with an average of 83.5. Harzburgitic (G10) garnets are only marginally sub-calcic and plot near the boundary with lherzolitic garnets (Figure 5.2a). These garnets have CaO = 3.60 - 5.19 wt%, Cr_2O_3 = 1.54 - 7.29 wt% and Mg# from 78.6 to 85.6, with an average of 82.1.

5.4.2 Olivine

A total of 199 olivine grains were analysed, of which 171 remained after low analytical totals were removed. There are two populations of Victor olivine xenocrysts, differing in both colour and composition. 82 grains with a yellowish-green colour have more depleted compositions with Mg# ranging between 90.0 to 93.6 (average and median of Mg# 92.7) (Table F.7). These compositions correspond to the worldwide average for olivine from harzburgite xenoliths (Mg# = 92.8 ± 0.9; database of Stachel and Harris, 2008) (Figure 5.3).

Eighty-nine brownish-yellow grains have less depleted compositions. Mg# range from 88.1 to 91.7, with average and median of Mg# of 90.3 (Table F.8). These compositions are less depleted than the worldwide average for olivine from lherzolite xenoliths (Mg# = 91.8 ± 0.9; database of Stachel and Harris, 2008) (Figure 5.3). NiO in all olivine ranges between between 0.21 and 0.38 wt%.

5.4.3 Clinopyroxene

Two hundred and four clinopyroxene grains were mounted for analysis. After low analytical totals were removed 157 grains remained. These are all chromian diopside, with Na_2O = 0.86 to 4.03 wt%, MgO = 13.57 to 17.85 wt% and Cr_2O_3 = 0.60 and 3.09 wt% (Table F.9). The criteria of Sobolev et al. (1992) and Grütter (2009) were used to distinguish clinopyroxene with Tschermak components (typical in the spinel stability field) from clinopyroxene where Al and Na are predominantly in the jadeite and kosmochlor components (typical in the garnet stability field) (Figure 5.4a,b).

5.4.4 Orthopyroxene

All 102 orthopyroxenes from the mineral concentrate that were analysed are enstatites and range in Mg# from 90.6 to 93.1, with a mean Mg# of 91.1 (Table F.10). They are likely sourced from lherzolites, as harzburgitic orthopyroxene generally will have much lower Ca content with Ca/(Ca+Mg+Fe) typically less than 0.006 (Brey et al., 1999; Grütter, 2009) (Figure 5.5). This is consistent with the predominance of lherzolitic garnets in the concentrate.

Grütter (2009) has shown that a coexisting equilibrium assemblage of clinopyroxene and orthopyroxene in garnet lherzolite may record mutually consistent compositional arrays and therefore, that the graphite-diamond transition Kennedy and Kennedy (1976) and the mantle adiabat (T = 1300 °C) can be interpolated into orthopyroxene compositional space. These are shown for reference on Figure 5.5, where it can be seen that orthopyroxene compositions straddle the graphite-diamond transition.

5.5 Xenoliths major element chemistry

5.5.1 Victor eclogite and pyroxenite xenoliths

The major element compositions of the 17 eclogite xenoliths and the 16 pyroxenite xenoliths are fully described in Chapter 3. They fall into four categories: 1.) High-Ca eclogite, 2.) Low-Mg eclogite, 3.) High-Mg eclogite and 4.) Pyroxenite ± orthopyroxene. The distinction between eclogite and pyroxenite was made based on clinopyroxene compositions - eclogites contain omphacite, whereas pyroxenites contain diopside - consistent with commonly used definitions for eclogite (e.g., Coleman et al., 1965; Carswell, 1990; Pearson et al., 2003). Omphacite was distinguished from diopside by having $0.2 \leqslant$ Na/(Na+Ca).

5.5.2 Delta pyroxenite xenoliths

Three orthopyroxene-bearing pyroxenite xenoliths from Delta were analysed. Garnet in these samples has CaO from 4.68 to 5.88 wt%, Cr_2O_3 from 0.78 to 3.05 wt% and Na_2O from 0.02 to 0.03 wt% (Table G.1). Only one pyroxenite has garnet with $Cr_2O_3 > 1$ wt%, thereby classifying as G5 (after Grütter et al., 2004). Diopsides have 0.51 to 0.97 wt% Na_2O and 16.3 to 17.1 wt% MgO (Table G.2). Enstatites have Mg# between 87.2 and 90.1 and Al_2O_3 = 0.54 to 0.58 wt% (Tables G.5 and G.6) The pyroxenite with G5 garnet is also olivine-bearing (with Mg# = 85.32) (Table G.3).

5.5.3 Delta peridotite xenoliths

Dunites

Three dunite xenoliths contain only olivine, with Mg# ranging between 91.2 and 92.7 (average Mg# = 91.9; median Mg# of 92.1) (Table G.3 and G.4). One of these dunites contain metasomatic clinopyroxene (non-texturally equilibrated and associated with mica and amphibole) that has high Na_2O and Cr_2O_3 compositions, (Table G.2) distinct to clinopyroxene found in lherzolite xenoliths, discussed below.

Lherzolites

Five xenoliths were classified as lherzolites based on their garnet CaO-Cr_2O_3 compositions (CaO = 4.27 - 6.22 wt% and Cr_2O_3 = 1.51 - 4.77 wt%; Table G.1). Four lherzolites contain olivine with Mg# between 90.1 and 92.5 (average Mg# = 91.3) (Table G.2) Enstatite occurs in four of the five lherzolites and has Mg# between 93.0 and 93.3 (average Mg# = 92.7; Table G.5 and G.6). Primary clinopyroxene in four lherzolites have diopsidic compositions with Na_2O = 1.25 to 2.18 wt% (Table G.2).

Harzburgites

Seven harzburgite xenoliths contain olivine ± enstatite ± garnet. Two of these harzburgites contain G10 garnets (CaO = 2.85 - 3.45 wt% and Cr_2O_3 = 3.04 - 3.41 wt%; Table G.1). Olivine in the harzburgite xenoliths have Mg# between 91.4 to 92.7 (average Mg# = 92.2; Table G.3 and G.4). Six of the seven samples contain enstatite with Mg# ranging from 92.5 to 93.5 (average Mg# = 93.1; Table G.5 and G.6). Two harzburgites contain metasomatic clinopyroxene, with similar compositions to those found in the dunite xenoliths (Table G.2).

Garnet dunite

One xenolith contains only olivine and garnet and no visible orthopyroxene or clinopyroxene. Olivine has Mg# = 92.1 (Table G.3 and G.4), however the garnet has a wehrlitic composition (G12) with CaO = 9.02 wt% and Cr_2O_3 = 2.12 wt% and Mg# = 77.6 (Table G.1).

5.6 Victor xenocryst trace element chemistry

5.6.1 Garnet

One hundred lherzolitic garnets (G9) from Victor were analysed for their trace elements (Table H.1 to H.13) These have sinusoidal or sloped chondrite-normalised (REE_N) patterns and can be divided into 4 main groups, based on their combined REE_N and trace element compositions (Figures 5.6 and 5.7):

1.) Twenty-nine grains have sinusoidal chondrite-normalised REE patterns.

These have positive slopes in the $LREE_N$, with a peak in Sm_N at ~ 7 x chondrite, followed by negative $MREE_N$ slopes with a trough in Dy_N at ~ 0.7 x chondrite. The HREE have a positive slope from Dy_N to Lu_N (~ 10 x chondritic). These garnets have the highest Mg# (82.0 to 84.9) and the lowest Y and Zr concentrations (Zr <18 ppm and Y <8 ppm), with Ti = 18 to 153 ppm.

2.) Eighteen garnets also have sinusoidal chondrite-normalised REE patterns, but with significantly more enrichment in the MREE. They have positive slopes in the $LREE_N$, with a peak in Sm_N at ~ 20 x chondrite. This is followed by a negative slope until a trough in Ho_N at ~ 3 x chondrite, and a positive slope in the $HREE_N$ to Lu_N at about 10-20 x chondrite. These grains have Mg# from 79.8 to 84.3 and the highest Zr content (25 to 73 ppm), with Ti = 22 to 252 ppm and Y = 3 to 10 ppm.

3.) Forty-eight garnets have LREE-depleted patterns, with a positive slope in $LREE_N$ peaking at Gd (10-20 x chondrite) and slightly fractionated to flat $MREE_N$ to $HREE_N$ (average $Lu_N/Gd_N = 1.66$) at approximately 10 x chondrite. These are considered to be 'normal' patterns for lherzolitic garnets. These garnets have Mg# from 79.6 to 84.9 and the highest average Ti content (43 to 368 ppm), with Zr = 3 to 74 ppm and Y = 6 to 23 ppm.

4.) Five garnets with 'sloped' patterns have a positive slope in $LREE_N$, with a peak in Tb at ~ 30 x chondrite. Four garnets have broadly flat patterns from Tb_N / Dy_N to Lu_N at ~ 30 x chondrite. One sample has a negative slope from Tb_N to Lu_N at about 9 x chondrite. These grains have the lowest average Mg#, ranging from 73.3 to 82.4 and the highest Y concentrations (39 to 47 ppm), wtih Ti = 38 to 90 ppm and Zr = 11 to 72 ppm.

5.6.2 Clinopyroxene

Thirty-three clinopyroxene xenocrysts from Victor were analysed for their trace elements (Table H.14 to H.18). They have enriched $LREE_N$ compositions with a negative slope from La_N at ~ 10 x chondrite to Lu_N at 1-3 times chondritic adundances (Figure 5.8). Eu/Eu* in clinopyroxene range from 0.71 and 1.27 (with average Eu/Eu* = 0.97).

5.7 Re-Os isotopic compositions and PGE content of peridotitic olivine

Olivine from 12 Delta xenoliths was analysed for its Re and Os isotopic composition and PGE content. Replicate digestions of the GP13 rock standard and replicate analyses of the DrOsS mass specrometry standard are given in Tables I.1 and I.2. Results for sulphide / alloy inclusions in Delta olivines are given in Table I.3 and I.4. The xenoliths display a range in $^{187}Os/^{188}Os$ ranging from unradiogenic (< present day $^{187}Os/^{188}Os$ of O-chondrite - 0.1283; Walker et al., 2002) to values more radiogenic than any estimate of the PUM. PGE contents and inter-element fractionation of the olivines are highly variable and can be grouped into several categories based on similar chondrite-normalised PGE patterns (PGE_N). For PGE normalisation, the CI chondrite values of Horan et al. (2003) were used.

1.) This group comprises two samples, with $^{187}Os/^{188}Os$ of 0.10921 ± 0.00069 and 0.11052 ± 0.00029. The first sample contains lherzolitic garnet and the second sample is a dunite. These have Neoarchaean T_{RD} ages of 2.7 ± 0.1 Ga and 2.47 ± 0.04 Ga, respectively (Figure 5.9).

Os content in these olivines are 1.1 and 1.44 ppb. Osmium is slightly fractionated compared to Ir in both samples - $(Os/Ir)_N$ is 1.38 in the lherzolitic sample, and 0.73 in the dunitic sample. Both samples are depleted in Pd compared to the I-PGE's (Os, Ir, Ru; Barnes et al., 1985) (Figure 5.10a). The dunitic sample exhibits extreme depletion with a $(Pd/Ir)_N$ ratio of 0.01. Olivine from the lherzolitic sample does not show the Pd depletion relative to Ir ($(Pd/Ir)_N$ of 1), however it is depleted relative to Ru ($(Pd/Ru)_N$ of 0.16).

Both samples show Re enrichment relative to Pd, with $(Re/Pd)_N$ of 1.6 and 22.8. $(Re/Os)_N$ for the dunitic sample is low (0.31) and slightly enriched for the lherzolitic sample (1.15). Overall, PGE abundances in this group overlap those of whole rock cratonic peridotites (Figure 5.10a) and show similar P-PGE fractionation compared to I-PGE ratios (e.g., Pearson et al., 2004).

2.) Olivines in this group includes two samples with the most unradiogenic $^{187}Os/^{188}Os$ in the suite: 0.10222 ± 0.00082 and 0.1012 ± 0.0037 (garnet dunite and harzburgite, respectively).

Rhenium depletion ages (T_{RD}) are Palaeo-Archaean - 3.6 ± 0.1 Ga and 3.7 ± 0.5 Ga, respectively. Olivines from these two samples have low Os content - the garnet dunite, 0.14 ppb and the harzburgite, 0.17 ppb. Osmium is depleted relative to Ir in the harzburgite ($(Os/Ir)_N$ of 0.54), but slightly enriched over Ir in the garnet dunite ($(Os/Ir)_N$ of 1.75) (Figure 5.10b).

The harzburgite is enriched in Pd ($(Pd/Ir)_N$ of 24) and depleted in Re ($(Re/Pd)_N$ of 0.25). The garnet dunite does not show the same levels of Pd enrichment, with $(Pd/Ir)_N$ of 1.86. Rhenium is slightly enriched with $(Re/Pd)_N$ of 1.46. $(Re/Os)_N$ for both samples are high - the harzburgite has the lowest $^{187}Os/^{188}Os$ and has the highest $(Re/Os)_N$ in the suite (10.53); and the garnet dunite sample, 1.55. The PGE_N pattern for olivine from the garnet dunite is approximately flat, with slight enrichment in Os over Ir ($(Os/Ir)_N$ of 1.75), Pd over Ir ($(Pd/Ir)_N$ of 1.86) and Re over Pd ($(Re/Pd)_N$ of 1.46).

3.) Olivine from the pyroxenite sample has $^{187}Os/^{188}Os$ of 0.1137 ± 0.0039 and a similar PGE_N pattern to the Palaeoarchaean harzburgite, discussed above. This pyroxenite has a Proterozoic T_{RD} age of 2.0 ± 0.5 Ga (Figure 5.9) and the lowest Os content in the suite (0.09 ppb). Osmium is depleted relative to Ir ($(Os/Ir)_N$ of 0.73) (Figure 5.10b). This sample is enriched in Pd ($(Pd/Ir)_N$ of 11) and depleted in Re ($(Re/Pd)_N$ of 0.56). $(Re/Os)_N$ is high with $(Re/Os)_N$ of 8.58.

4.) Olivine from two samples have radiogenic $^{187}Os/^{188}Os$ of 0.16093 ± 0.00441 and 0.18213 ± 0.00190. One is from a dunite (containing only olivine) and the other is from a peridotite containing harzburgitic garnet. These samples have the highest Os content (2.30 and 3.52 ppb), compared to Os contents of less than 1.50 ppb in the rest of the suite. Os is enriched over Ir and $(Os/Ir)_N$ values are 87.00 and 12.07, respectively (Figure 5.10c).

Both samples are extremely depleted in Pd and Pt - with $(Pd/Ir)_N$ of 0.50 and 0.05; and show enrichment of Re over Pd ($(Re/Pd)_N$ of 14.21 and 18.35). They have the lowest $(Re/Os)_N$ in the suite (0.11 and 0.06).

5.) Olivines from this group comprise three samples (2 harzburgites and 1 lherzolite) that have Proterozoic T_{RD} ages ranging from 1.43 to 1.58 Ga; with $^{187}Os/^{188}Os$ of 0.11700 ± 0.00030; 0.11812 ± 0.00127 and 0.11724 ± 0.00100 (Figure 5.9). Os contents in these olivines are 0.51, 0.73 and 1.17 ppb. Osmium in the two harzburgitic olivines are fractionated relative to Ir, with $(Os/Ir)_N$ of 2.7 and 2.8. The lherzolitic sample has $(Os/Ir)_N$ of 0.94 (Figure 5.10d).

Two samples are depleted in Pt compared to the I-PGE's (and also Pd with $(Pd/Ir)_N$ of 0.26), however, these PGE_N patterns do show enrichment in the P-PGE's (Pt, Pd, Re Barnes et al., 1985) with $(Re/Pd)_N$ of 8.56 to 14.15. One harzburgite has a different PGE_N pattern, with a negative trend in the P-PGE. Pt is enriched to similar levels as the estimate for the primitive upper mantle (PUM; Becker et al., 2006) and Re is depleted relative to Pd ($(Re/Pd)_N$ of 0.39). $(Re/Os)_N$ for these samples have a wide range. One harzburgite has low $(Re/Os)_N$ of 0.36. The other harzburgite has a high $(Re/Os)_N$ of 6.61, whereas the lherzolitic sample has an intermediate $(Re/Os)_N$ of 2.37.

6.) Two olivines have extremely low Os contents and $^{187}Os/^{188}Os$ could not be measured by N-TIMS. This is reflected in their severely depleted Ir compositions. These samples also have negligible Pt content - indicated by the dotted line connecting Ru and Pd in Figure 5.10e. Re is enriched over Pd, with $(Re/Pd)_N$ of 18.17 and 35.89.

5.8 Geothermobarometry

5.8.1 Single clinopyroxene geothermobarometry

Compositional suitability

The enstatite-in-clinopyroxene thermometer and Cr-in-clinopyroxene barometer combination of Nimis and Taylor (2000) can be applied to single Cr-diopside grains to obtain pressure and temperature (PT) conditions of last equilibration. Equilibrium with orthopyroxene and garnet is essential and is established through a series of compositional filters. Only Cr-diopside that classified as being derived from garnet lherzolite (compositional constraints after Sobolev et al. (1992), Ramsay and Tompkins (1994) and Ramsay (1995); Figure 5.4a,b,c,d) were selected for geothermobarometry.

Although Al in clinopyroxene is typically considered a good indicator for pressure (with concentrations dropping sharply over the spinel to garnet peridotite transition), clinopyroxenes affected by carbonatite metasomatism have lower Al content (e.g., Rudnick et al., 1994; Nimis, 1998) and therefore grains derived from spinel-bearing lherzolites may erroneously plot in the garnet-bearing field. These low-Al grains may cause pressure overestimates and were excluded by means of the MgO - Al_2O_3 plot of Nimis (1998) (Figure 5.4e,f). 79% of the clinopyroxenes analysed were eliminated due to their low-Al content. Further compositional filters outlined in the online supplementary data to Grütter (2009) were applied to ensure suitability. After all filters were applied only 31 out of 157 grains remained for geothermobarometry calculations.

Xenocryst geotherm

The enstatite-in-clinopyroxene thermometer (Nimis and Taylor, 2000) can be applied to both xenolith and xenocryst populations, as it accurately (±40 °C) reproduces experimental temperatures over a wide range of PT conditions. However, the Cr-in-clinpyroxene barometer (Nimis and Taylor, 2000) has been shown by Nimis (2002) and Grütter and Moore (2003) to overestimate pressures at low PT conditions and underestimate pressures at high PT conditions, compared to the modified opx - grt barometer (Nickel and Green, 1985; Taylor, 1998). The single crystal thermobarometer combination of Nimis and Taylor (2000) therefore yields geothermal arrays with significantly more scatter than geotherms created with the combination of the enstatite-in-clinopyroxene thermometer (Nimis and Taylor, 2000) and the modified orthopyroxene - garnet barometer (Nickel and Green, 1985; Taylor, 1998). Grütter (2009) has suggested, however, that these single clinopyroxene geotherms are still useful in "relative" comparative studies between localities, but traditional xenolith-based geotherms may still be preferred for more precise and accurate PT arrays.

Palaeogeotherms were calculated from PT data using the Fitplot program (McKenzie and Bickle, 1988; McKenzie et al., 2005; Mather et al., 2011). This program quantifies the lithosphere thickness, calculated as the intersection of the conductive geotherm (numerically fitted to the PT array) with the adiabatic geotherm of the convecting mantle ('thermal' definition of the base of the lithosphere after Rudnick et al., 1998; Rudnick and Nyblade, 1999), as well as the "diamond-in" parameter - the point at which the graphite-diamond transition intersects the conductive geotherm.

PT results from single clinopyroxene grains and the resulting Fitplot geotherm is shown in Figure 5.11a. Lithosphere thickness was calculated between 190 and 210 km and diamond stability above 850 °C / 118 km (using graphite-diamond transition of Day, 2012). The resulting diamond window is $\sim$ 85 km thick. These Victor clinopyroxenes are mainly derived from depths between 120 and 180 km, i.e., dominantly in the diamond stability field.

5.8.2 Xenolith geothermobarometry

Pressures and temperatures of last equilibration were calculated iteratively for eight orthopyroxene-bearing xenoliths from Victor, as well as three orthopyroxene-bearing xenoliths and four lherzolite xenoliths from Delta.

Temperatures for Fe-Mg exchange between orthopyroxene and clinopyroxene were calculated using the formulation of Taylor (1998). Al-in-orthopyroxene pressures were calculated after Nickel and Green (1985). Modification of this barometer by Taylor (1998) was recommended for fertile lherzolites and websterites at $P < 3.5$ GPa, especially those with high Ti contents. However, the Ti content in our samples is much lower than the pyroxenes in the HPY40 experimental dataset of Taylor (1998), which was shown to overlap with fertile lherzolites and websterites.

Equilibrium between the two pyroxenes was asessed by evaluating the temperature differences between the two pyroxene thermometer of Taylor (1998) and the Ca-in-orthopyroxene thermometer of Brey and Köhler (1990) (modified by Nimis and Grütter (2009) for low temperatures). Pyroxene-garnet equilibrium was evaluated through the difference between the two pyroxene thermometer of Taylor (1998) and Fe-Mg orthopyroxene-garnet thermometer of Nimis and Grütter (2009). A summary of the calculated temperatures and the equilibrium evaluations is shown in Table J.1 and J.2. Three pyroxenites from Victor were found to be in disequilibrium and were not used for the geotherm calculations.

One sample from Delta had an assemblage of only garnet, orthopyroxene and olivine but no co-existing clinopyroxene. For this sample, temperatures for Fe-Mg exchange between orthopyroxene and garnet were calculated (Nimis and Grütter, 2009) in combination with Al-in-orthopyroxene pressures (Nickel and Green, 1985).

The Fitplot palaeogeotherm using the combined PT results for lherzolite, pyroxenite and harzburgite xenoliths is given in Figure 5.11b. All samples, except one, plot within the graphite stability field. Lithosphere thickness was calculated to be between 185 and 195 km and diamond stability above 930 °C / 125 km (using graphite-diamond transition of Day, 2012). The resulting diamond window is $\sim$ 75 km thick.

5.8.3 Combined xenolith / xenocryst geotherm

All xenolith and xenocryst PT data were combined to produce the Fitplot geotherm in Figure 5.11c. Results compare well to the individual xenolith and xenocryst geotherms, with the calculated lithosphere thickness between 190 and 205 km and diamond stability above 860 °C / 120 km (using graphite-diamond transition of Day, 2012). The resulting diamond window is $\sim$ 85 km thick, compared to the much smaller diamond window of $\sim$ 30 km at Kyle Lake.

The bimineralic eclogites and pyroxenites yield temperatures of last equilibration between 770 °C and 980 °C (calculated at 5 GPa; Krogh, 1988). Projecting the temperatures for these bimineralic eclogites and pyroxenites onto the combined xenolith/xenocryst palaeogeotherm places them on the boundary between the graphite and diamond stability fields (Figure 5.11c).

5.9 Depletion of the SCLM below Attawapiskat

The Kyle Lake kimberlites, about 100 km west of Attawapiskat, are the oldest kimberlites in the western Superior province and the only kimberlites on the Superior craton that sample lithospheric mantle with abundant harzburgitic compositions. The younger kimberlites at Kirkland Lake, Timiskaming and Attawapiskat, sample predominantly lherzolitic compositions with minor harzburgite (Sage, 2000; Scully, 2000; Armstrong et al., 2004).

The apparent temporal change in SCLM composition, the coincidence in age of Kyle Lake kimberlite eruption to the Midcontinent Rift (1.1 Ga), as well as the elevated geotherm seen in the clinopyroxene xenocrysts at Kyle Lake (Figure 5.11), have led to the suggestion that the lower portions of the SCLM below this region have been refertilised from harzburgite to lherzolite, perhaps by melt infiltration related to the Midcontinent Rift (Sage, 2000; Scully et al., 2004). Alternatively, the lithosphere below Attawapiskat, including Victor and Delta, never experienced high degrees of melting to the point of clinopyroxene exhaustion (leading to depleted harzburgitic or dunitic residues).

Our sample set comprises mainly lherzolitic garnet xenocrysts, consistent with previous studies. However, xenoliths from Delta have a wider range in peridotitic compositions, including lherzolite, harzburgite and dunite. In this section, we investigate evidence for high degrees of partial melting still preserved in the SCLM below Attawapiskat.

5.9.1 Residues after high degrees of melting

Approximately half of the Victor olivine xenocrysts have highly depleted compositions with an average Mg# of 92.6 and Mg# up to 93.6 (Table F.7). The mode for Victor olivine overlaps that shown for Slave, Kaapvaal and North Atlantic cratons (compilation of Pearson and Wittig, 2008) (Figure 5.3a).

Mg#'s in olivine of 92.8 - 93.0 can only be produced after extensive melting - after 50 % at 3 GPa or after 37 % melting at 7 GPa (garnet lherzolite melting experiments - Walter, 1998). Natural analogues, such as the Iwaidake peridotite massif (a Phanerozoic ophiolite; Kubo, 2002), show that at Mg#'s of 92.8 the resultant rock type is dunite.

Lower olivine Mg#'s are produced by lower extents of melting and yield harzburgitic residues, i.e., after 20 % melting at 3 GPa (Walter, 1998), corresponding to the point of clinopyroxene exhaustion. At higher pressures, these Mg#'s are produced after 15 % melting and clinopyroxene is only exhausted after 40 % melting (7 GPa; garnet lherzolite melting experiments of Walter, 1998). Experiments that have more clinopyroxene-rich starting compositions may have clinopyroxene remain in the residue to much higher degrees of melting (e.g., Kinzler and Grove, 1999).

Therefore, depending on depth of melting, Mg#'s between 91 and 92 at Victor may correspond to lherzolitic or harzburgitic residual compositions. The depleted olivine at Victor, with Mg# up to 93.6, requires that the lithospheric mantle underwent high degrees of melting (>37 %) to produce dunitic residual compositions (see also Bernstein et al., 2007; Pearson and Wittig, 2008). High degrees of melting indicated by the olivine compositions, suggests that the other minerals in the Attawapiskat peridotitic lithosphere (i.e., clinopyroxene, garnet, orthopyroxene, less depleted olivine) may have been introduced by secondary enrichment processes in the SCLM, as also suggested for other cratonic roots (e.g., Kelemen et al., 1992; Shimizu et al., 1997; Grégoire et al., 2003; Bell et al., 2005; Rehfeldt et al., 2008; Gibson et al., 2013).

5.9.2 Melting in a low-pressure environment

Mg#'s up to 93.6 in Victor olivine require high degrees of partial melting of at least 40%, irrespective of the depth of melting. However, combined evidence from both Cr/Al ratios and HREE content in garnet may provide additional constraints as to the depth of melting - i.e., whether melting occurred in either the garnet or spinel stability fields. The spinel-garnet transition occurs between 1.7 and 2.2 GPa in peridotite with low bulk rock Cr# (where Cr# is the molar proportion of Cr/(Cr+Al)) (Robinson and Wood, 1998). Spinel can however be stable to much higher pressures (7.0 GPa) in peridotites with increased bulk rock Cr#, which results from higher degrees of depletion (e.g., O'Neill, 1981).

1.) Cr/Al ratios. Victor lherzolitic garnets with the most depleted compositions (sinusoidal REE_N; lowest Y and Zr; discussed in Section 5.12.3) have Cr# up to 30. The Cr/Al ratios are the highest in these depleted sinusoidal garnets and the lowest in the garnets with normal and sloped REE_N patterns (Figure 5.12).

Melt extraction in the garnet stability field is unable to explain high Cr/Al ratios, as shown experimentally by Bulatov et al. (1991), since the partition coefficient of Cr/Al between garnet and ultramafic liquid decreases with pressure and would require numerous melt extraction processes to achieve high Cr contents in garnet (e.g., Trønnes et al., 1992; Canil and Wei, 1992). Residual garnets after experimental melting of garnet lherzolite at 3 - 7 GPa have Cr_2O_3 content between 1.01 and 1.71 wt% (Walter, 1998), significantly lower than the range of compositions seen in Victor lherzolitic garnets which reach up to 10 wt% Cr_2O_3 (Figure 5.2). The partition coefficient for Cr/Al between spinel and ultramafic liquid is ~ 40 and therefore high Cr content in garnet can be explained through initial melt extraction at low pressures in the spinel stability field, followed by metamorphic conversion to garnet (Stachel et al., 1998).

2.) Positive slopes in HREE$_N$. The most depleted Victor lherzolitic garnets have positive slopes in the HREE$_N$ and display depletion in HREE relative to the primitive mantle, as seen when the REE are normalised to J4, a garnet from a "primitive" lherzolite (Stachel et al., 1998, and references therein) (Figure 5.6a,b) .

Garnets with low HREE content and positive slopes in the HREE$_N$ have been linked to low pressure melt extraction that starts in the garnet stability field and ends in the spinel stability field (e.g., Kelemen et al., 1998; Stachel et al., 1998). These HREE$_N$ signatures cannot be explained by melting only in spinel stability field. The partition coefficients of Yb in spinel (and also orthopyroxene and olivine) is low and during partial melting, Yb behaves as an incompatible element and will not be retained in the residue. Therefore, some melting must have occurred in the presence of garnet that would account for the positive slopes observed in the HREE$_N$ of depleted garnets (Figure 5.6a,b).

To reconcile the Cr# in garnet that indicates melting in the spinel stability field and the positive HREE$_N$ slopes, indicative of melting in the garnet stability field, fractional polybaric melting starting at high and ending at low pressures is required (e.g., Stachel et al., 1998). The most depleted Victor lherzolitic garnet have slopes in their HREE$_N$ that correspond to 20% melting in the spinel stability field and 5 to 15% melting in the garnet stability field (Figure 16 in Simon et al., 2007). Although these melting calculations in Simon et al. (2007) are based on whole rock compositions, the slope in the $HREE_N$ (rather than their absolute concentrations) can still be used, as the HREE budget in the whole rock is dominated by the garnet.

5.9.3 Comparison to Kyle Lake

Twenty-five olivine xenocrysts from Kyle Lake have a range in Mg# from 90.5 to 93.5, with an average Mg# of 92.2 (Sage, 2000), also indicating that they are residues after high degrees of melting to harzburgitic and dunitic residues (Section 5.9.1; Figure 5.3c).Trace element analyses on a subset of the Kyle Lake garnet samples (Scully et al., 2004) show that harzburgitic and lherzolitic garnet xenocrysts have Yb_N between ~ 0.8 and 10, similar in range to those from Victor (distinct REE_N patterns for harzburgite vs lherzolite not given).

Whereas Yb concentrations in garnets from Kyle Lake and Victor are similar, harzburgitic garnets from Kyle Lake have significantly higher Cr/Al ratios, with a pronounced mode at Cr# >30 (Figure 5.13; Victor Cr# < 30). This mainly indicates sampling from deeper lithosphere with elevated Cr/Al at Kyle Lake. The mode for lherzolitic garnets from Kyle Lake (Cr# between 10 and 15) overlaps with the mode for lherzolitic garnets from Victor.

Other explanations for the difference in Cr# between Kyle Lake and Attawapiskat garnets include: 1.) High Cr#'s in garnet may reflect higher extents of melt depletion. This would suggest that the lithosphere sampled at 1.1 Ga at Kyle Lake had not yet undergone refertilisation to the same extent as the lithosphere sampled during the Jurassic at Attawapiskat. Clinopyroxene introduction and conversion to lherzolite may have occurred around 1.1 Ga due to silicate and UML magmatism related to the Midcontinent Rift, or due to kimberlite metasomatism, either at 1.1 Ga or later during the Jurassic (e.g., Foley et al., 2002b, 2006; Simon et al., 2003). Melt infiltration and conversion from harzburgite to lherzolitic, leading to lower Cr# due to influx of Al in the melt, has also been suggested for some Diavik diamondiferous lherzolite xenoliths (Creighton et al., 2008). 2.) The difference in Cr# between Kyle Lake and Attawapiskat could represent sampling of different lithospheres. The

Attawapiskat kimberlites erupted near the boundary of the North Caribou and Northern Superior superterrane, and therefore could conceivably sample lithosphere from either terrane. The Kyle Lake kimberlites erupt further west in the North Caribou superterrane and could be sampling just North Caribou lithosphere (Figure 2.1).

5.9.4 Geodynamic setting for initial melting

Extensive melting in the Attawapiskat lithosphere is indicated by both Mg# in olivine and $HREE_N$ in garnet, resulting in harzburgitic to dunitic residual compositions. Modelling of garnet $HREE_N$ (after Simon et al., 2007) indicates at least >25 % total melting at high and low pressures. High Cr# in garnet require that significant melting must have taken place in the spinel stability field.

The geodynamic setting that is most consistent with these compositional characteristics is decompression melting of upwelling mantle, akin to a Mid-Ocean Ridge setting. Melting would start at high pressures in the garnet stability field (3-6 GPa) proceeding to low pressures in the spinel stability field (< 3 GPa) (e.g., Kelemen et al., 1998; Stachel et al., 1998; Bernstein et al., 2007; Herzberg et al., 2010; Herzberg and Rudnick, 2012). During the Archaean (>2.5 Ga), high degrees of melting (30 - 40 %) were possible due to higher mantle potential temperatures, around 1600 °C (Korenaga, 2008).

5.9.5 Palaeoarchaean melt depletion

PGE-rich phases encapsulated in depleted olivine from two Delta peridotites record Palaeoarchaean T_{RD} ages - olivine from a garnet harzburgite has $T_{RD} = 3.73 \pm 0.49$ Ga and olivine from a garnet dunite has $T_{RD} = 3.59 \pm 0.11$ Ga. The harzburgitic sample does not have a typical depleted PGE_N pattern, as may be expected for olivine with high Mg# (92.4) and of Palaeoarchaean age. Rather, the positive slope in the PGE_N pattern, along with high $(Pd/Ir)_N$ and high $(Re/Os)_N$, is frequently seen in metasomatic sulphides that result from melt infiltration (Lorand et al., 1993; Luguet et al., 2003, 2004). Since Re>Os, some radiogenic ingrowth is likely and it indicates that the Palaeoarchaen T_{RD} age in the harzburgite is definately a *minimum* age and the 'real' age of the trapped sulphide/PGE's is even older.

The garnet dunite has a PGE_N pattern that is approximately similar to the estimate for the primitive upper mantle (PUM) (Becker et al., 2006), albeit at lower absolute concentrations (Figure 5.10a,b). This is likely due to these PGE's being diluted by their olivine host, which because of very high sulphide-silicate partition coefficients (>10 000; e.g., Bezmen et al., 1994; Peach et al., 1994; Fleet et al., 1996, 1999; Sattari et al., 2002) is not considered a likely host for PGE's.

These old depletion ages in *metasomatic* sulphides/PGE's require the existence of a depleted mantle reservoir beneath Attawapiskat since at least the Palaeoarchaean. There are no crustal ages in the North Caribou superterrane older than 3.0 Ga, however these Palaeoarchaean depletion ages correspond with gneisses in the Pikwitonei domain of the Northern Superior superterrane that were dated to about 3.6 Ga (Böhm et al., 2000; Skulski et al., 2000).

Other evidence for a Palaeoarchaean depleted mantle reservoir below the Superior craton is mainly from the southern Superior: 1.) Archaean zircons from the Winnipeg River and Quetico Terranes in the south-western Superior province have ϵ_{Hf} compositions that require extraction from the convecting mantle in the Palaeoarchaean (3.8 - 3.2 Ga) (Davis et al., 2005). 2.) The oldest detrital zircons in Quetico metasediments are 3.45 Ga (Fralick and Davis, 1999). 3.) Zircon cores in lower crustal xenoliths of the Minnesota River Valley Terrane have 3.5 Ga ages (Zartman et al., 2013).

5.10 Mantle processes associated with ~2.7 Ga subduction

5.10.1 Depleted residual patterns with Neoarchaean T_{RD} ages

Two samples record Neoarchaean T_{RD} ages (including errors these range between 2.8 and 2.4 Ga) and have PGE_N patterns that are typical for depleted cratonic residues (Figure 5.10a). These residual PGE_N patterns are complimentary to that of basaltic melt (e.g., Bockrath et al., 2004), due to the different partitioning behaviour of the I-PGE's and P-PGE's during mantle melting. P-PGE's have lower partition coefficients between monosulphide solid solution (mss) and sulphide melt and therefore behave incompatibly; whereas the I-PGE's, due to their higher partition coefficients, remain in the mss residue (Fleet et al., 1993; Li et al., 1996; Sinyakova et al., 2001; Ballhaus et al., 2001; Brenan, 2002; Mungall et al., 2005; Barnes et al., 2006).

The PGE_N patterns for these two Delta samples are similar to those of Lesotho depleted peridotites, that were P-PGE depleted during partial melting (with $(Pd/Ir)_N = 0.01$ in one sample), followed by Re enrichment during later melt/kimberlite infiltration (Pearson et al., 2004) (Figure 5.10a). Apart from their Re enrichment, these Pd-depleted patterns, are also comparable to the residues calculated for komatiite melts in the Abitibi greenstone belt (Superior craton) (Puchtel et al., 2004).

Their T_{RD} ages correlate with the timing of subduction-accretion of the Northern Superior and North Caribou superterranes at ~ 2.7 Ga and associated continental arc magmatism (see Section 2.1), and suggests that melting took place in the mantle wedge during this time. These ages also overlap with a 2.6 Ga whole-rock T_{RD} age for a peridotite xenolith from Kirkland Lake in the Wawa-Abitibi Terrane (Pearson et al., 1997) (Figure 5.9).

The majority of Kaapvaal peridotite xenoliths have Re-Os T_{RD} ages between 2.9 and 2.7 Ga (Pearson et al., 1995; Carlson et al., 1999; Menzies et al., 1999; Irvine et al., 2001; Carlson and Moore, 2004; Simon et al., 2007), which overlap with the 2.9 Ga collision of the Witwatersrand and Kimberley blocks of the Kaapvaal (Schmitz et al., 2004), suggesting that mantle melting in an arc environment during collisional tectonics took place, similar to that proposed for the Attawapiskat peridotites analysed here.

5.10.2 I-PGE alloy formation in a supra-subduction zone

Olivine from two samples have radiogenic $^{187}Os/^{188}Os$ (0.16093 to 0.18213) and high Os content (2.3 to 3.5 ppb). Due to their extremely low Re/Os (0.06 to 0.11) (Figure 5.10c), these isotopic compositions must be an inherent attribute of the phase/s hosting Os in these olivines (i.e., the radiogenic $^{187}Os/^{188}Os$ did not develop as a result of radiogenic ingrowth from high

Re/Os).

The Os-rich nature of these olivines could be indicative of I-PGE-alloy or sulphide inclusions. These are highly refractive grains which remain after extensive melting has depleted the protolith of its sulphide budget ($\sim 25\%$ melting; Barnes et al., 1985) and should normally preserve depleted $^{187}Os/^{188}Os$ indicative of the time of melting. However, the radiogenic $^{187}Os/^{188}Os$ of the Os-rich PGE grains suggest the possibility of another influence.

I-PGE-rich alloys can form in conjunction with chromite from hydrous melts (Matveev and Ballhaus, 2002). During exsolution of fluid from the melt, chromite and I-PGE's are strongly partitioned into the hydrous fluid. A likely setting for generation of radiogenic $^{187}Os/^{188}Os$ would be during dehydration and melting of a subducting slab, with hydrous melts percolating through the overlying mantle wedge where PGE alloys are formed (e.g., Brenker et al., 2003; Pearson et al., 2007). The very high $(Os/Ir)_N$ of these olivines from the Delta peridotites, and their high Ru, indicate the inclusion of Os-Ru alloys in these alloys. The relative enrichment in Re may derive from the olivine itself.

5.10.3 Pyroxenite formation

Similarity of the PGE_N pattern in a harzburgitc sample to that in a pyroxenitic sample with significantly younger T_{RD} age of 2.0 ± 0.5 Ga, is consistent with the petrogenetic model for Victor pyroxenites, whereby melts generated from the melting of low-Mg eclogites infiltrate and react with surrounding depleted peridotites to form pyroxenites (Chapter 3). A melt generated from a low-Mg eclogite (recycled oceanic crust) is expected to have high Re/Os due to long-term isolation from the convecting mantle, and is observed in the high $(Re/Os)_N$ seen in this harzburgite and pyroxenite (10.53 and 8.58, respectively), the highest observed in this suite (Figure 5.10).

The process of P-PGE enrichment in wallrock peridotite is analagous to melt infiltration from pyroxenite layers to surrounding perdidotites, documented in ultramafic massifs (e.g., van Acken et al., 2008, 2010). If the percolating silicate melt is close to S saturation (e.g., with progressive fractional crystallisation; Li and Ripley, 2005, and references therein), it may not be saturated in clinopyroxene. Therefore HSE enrichment could occur in a depleted harzburgite without the simultaneous addition of Al and Ca, as shown for harzburgites from the Samail ophiolite, Oman (Lorand et al., 2009).

5.11 PGE_N patterns resulting from the Midcontinent Rift

Three samples have Meso-proterozoic T_{RD} ages between 1.6 and 1.4 ± 0.2 Ga and correlate with 1.5 and 1.1 Ga whole-rock T_{RD} age for two peridotite xenoliths from Kirkland Lake in the Wawa-Abitibi Terrane (Pearson et al., 1997) (Figure 5.9).

A major tectonothermal event that affected the Superior during the Proterozoic is basaltic and alkaline magmatism related to the Midcontinent Rift (~1.1 Ga; Paces and Miller, 1993; Heaman and Machado, 1992; Heaman et al., 2007). Ultramafic lamprophyre (UML) magmatism occurred prior to the main phase of rift volcanism from 1172 to 1141 Ma (Queen et al., 1996; Heaman et al., 2004).

These Proterozoic T_{RD} ages could reflect mixing of older, unradiogenic Os (>> 1.6 Ga) from depleted peridotite with that of younger, more radiogenic $^{187}Os/^{188}Os$ from Midcontinent Rift basalts ($\gamma_{Os} = 5.7$ at 1.13 Ga; Shirey, 1997). There are no published PGE data for the Midcontinent Rift basalts, however, the enrichment in P-PGE's and Re seen in olivine from these three Delta samples (Figure 5.10d) is similar to that of other basalts, including mid-ocean ridge basalts (MORB), and both tholeiitic and alkali ocean island basalts (OIB) (Figure 5.10f).

The strong Mesoproterozoic imprint of Midcontinent Rift melt infiltration on the deep mantle lithosphere beneath the Attawapiskat region is constistent with that seen in the southern Superior lower crust. Granulites from Minnesota River Valley Terrane in Michigan, shown to be the metamorphic equivalent of Midcontinent Rift basalts, contain 1104 ± 42 Ma zircons and also have a 1046 ± 100 Ma Sm-Nd whole-rock errorchron (Zartman et al., 2013). Rift basalts also led to the formation of magmatic sulphide deposits in the southern Superior (1107 Ma; U-Pb baddeleyite; Ding et al., 2010, 2012).

5.12 Other enrichment processes in the SCLM below Attawapiskat

Metasomatism is common in the continental lithosphere and even ancient harzburgitic garnets that have sinusoidal chondrite-normalised REE patterns, are affected by early fluid metasomatism (e.g., Richardson et al., 1984; Stachel et al., 1998). The best example of highly depleted cratonic lithosphere, without significant enrichment processes,is the North Atlantic / West Greenland peridotites (e.g., Bernstein et al., 1998, 2006; Wittig et al., 2008). The effect of silica addition (orthopyroxene) and incompatible element enrichment is widely seen in Kaapvaal peridotites (Boyd et al., 1999; Simon et al., 2003), where enrichment may be due to fluids/melts from the subducting slabs infiltrating the overlying mantle wedge (Kelemen et al., 1998; Yaxley and Green, 1998; Simon et al., 2007). In this section we discuss evidence for enrichment processes that impacted the Superior lithosphere at Attawapiskat.

5.12.1 Modal metasomatism in Delta peridotite xenoliths

There are abundant secondary (or non-texturally equilibrated) mica, amphibole and clinopyroxene in the xenoliths from Delta. Modal metasomatic phases present in each xenolith is summarised in Table E.1 and could derive from enrichment that began during formation of the Midcontinent Rift, or could have formed a few million years prior to Jurassic kimberlites, similar to Kaapvaal craton metasomites (Hamilton et al., 1998; Konzett et al., 2000).

5.12.2 ”Less depleted” olivine compositions

Approximately half of the Victor olivine xenocrysts analysed have ”less depleted” compositions, which are not seen at Kyle Lake (Sage, 2000) (Figure 5.3a,c). The average Mg# for these olivines (90.3) is lower than the 'less depleted' (i.e., lherzolite) mode in Slave craton olivine (Figure 5.3 and olivine from worldwide lherzolite xenoliths, that have Mg# = 91.8 ± 0.9 (2σ) (database of Stachel and Harris, 2008).

Even though these olivines have Mg# that overlap with kimberlitic olivine, they are probably not kimberlitic as they have higher average Ni contents (Ni from 0.30 to 0.40 wt%) than a compilation of kimberlitic olivines (average Ni between 0.25 and 0.30 wt%) (Kaminsky et al., 2002; Armstrong et al., 2004; Birkett et al., 2004; Kamenetsky et al., 2008; Matveev and Stachel, 2009; Patterson et al., 2009; de Hoog et al., 2010).

Cratonic olivine with lower forsterite contents than typical SCLM (Section 5.9.1), is associated with melt metasomatism (e.g., Green and Ringwood, 1967; Quick and Gregory, 1995). For example, Fe-rich lherzolites from Siberia with Mg# from 84 to 89 formed due to percolation of melts into depleted peridotites (Ionov et al., 2005). In the Trinity peridotite in California, infiltrating melts reacted with clinopyroxene to form orthopyroxene and olivine with Mg# from 89 to 91 (Quick, 1981; Kelemen et al., 1992).

For the North China craton, Liu et al. (2011) showed that "less depleted" olivine compositions (Mg# 87.4 - 92.2) in the Northern region are associated with Proterozoic T_{RD} ages, whereas more refractory compositions in the Southern Region have older 2.5 - 2.1 Ga depletion ages. For the Delta xenoliths however, there is no correlation between "less depleted" Mg# and younger T_{RD} ages for olivine. Olivine from the two samples with the oldest T_{RD} ages of 3.7 - 3.6 Ga have Mg# 92.1 and 92.4. However, olivine with the youngest T_{RD} age of 1.4 Ga also has Mg# of 92.1 (Tables I.3 and I.4).

The presence of economic diamond grades at Victor, indicates that melt infiltration resulting in these "less depleted" olivine compositions is not necessarily detrimental to diamond formation or preservation in the SCLM. Although rare, a number of worldwide localities have olivine diamond inclusions with these compositions. For example, olivine diamond inclusions with Mg# of 88 have been documented at both Premier and Ellendale (Gurney et al., 1985; Jaques et al., 1989); and olivine inclusions with Mg# of 86 were reported in diamonds from Yubileinaya and Internacionalnaya (Sobolev et al., 2008).

5.12.3 Metasomatism in lherzolitic garnet (G9) and clinopyroxene xenocrysts

In this section the metasomatic characteristics of the Victor garnet and clinopyroxene xenocrysts are discussed, and hypothetical liquids in equilibrium with these minerals calculated. Liquids were calculated using partition coefficients for minerals in equilibrium with both basaltic and carbonatite melts (Green et al., 2000; Dasgupta et al., 2009; Girnis et al., 2013) and their correlation with compositions of natural basaltic and carbonatite melts evaluated. Also, melts in equilibrium with Si-rich tonalitic melts (partition coefficients of Barth et al., 2002c) were calculated to evaluate whether the peridotitic lithosphere was metasomatised by melts of low-Mg eclogites subducted into the SCLM, as proposed for the origin of high-Mg eclogites and pyroxenites at Victor (Chapter 3).

Fluid and melt metasomatism in lherzolitic garnet

All lherzolitic garnet xenocrysts from Victor, even those that retain depleted signatures in the $HREE_N$ (discussed in Section 5.9.2), show some form of enrichment in their REE_N and other trace elements.

1. Fluid-dominated metasomatism in sinusoidal garnets. Garnets that have sinusoidal chondrite-normalised REE patterns (Section 5.6 and Figure 5.6a) fall into both the depleted and low temperature metasomatism fields, defined by Y-Zr systematics (Figure 5.7; Griffin and Ryan, 1995). Sinusoidal garnets in the depleted field have low Y and Zr contents (< 5 ppm and 25 ppm, respectively) and low Ti contents, which indicates that they were only affected by mild, fluid-dominated metasomatism.

With these REE characteristics and the modest levels of Y-Zr re-enrichment, these "depleted" lherzolitic garnets from Victor resemble garnets from diamondiferous lherzolite xenoliths from the Diavik Mine (Creighton et al., 2008). They are also similar to harzburgitic and lherzolitic garnets from Kyle Lake (Scully et al., 2004). Only a small subset of lherzolitic garnets from AT56 (also at Attawapiskat; see Figure 2.1) have sinusoidal REE_N patterns (Armstrong et al., 2004). Calculated equilibrium basaltic and carbonatitic melts for these sinusoidal garnets (figure not shown) have extremely fractionated REE_N patterns where LREE >> HREE, and are not a match for any natural mantle melts, further suggesting these garnets were metasomatised by fluids (CH_4 / CO_2?) or extremely low-degree <<1% melts.

2. Melt-dominated metasomatism. Garnets that have 'normal' REE_N compositions, with relatively flat $MREE_N$ to $HREE_N$ (Section 5.6 and Figure 5.6c) show an enrichment in Y, Ti and Zr content, compared to the most depleted compositions (Figure 5.7). These compositions are consistent with silicate melt-dominated metasomatism and overlap with those seen in harzburgitic and lherzolitic garnets at AT56, however Ti content in AT56 garnets also extend to much higher concentrations up to 2485 ppm (Armstrong et al., 2004).

Garnets with 'sloped' REE_N compositions (Section 5.6 and Figure 5.6d) display enrichment in Y but not in Zr or Ti (Figure 5.7). Calculated equilibrium liquids for these 'sloped' garnets are not a match for silicate melts - calculated basaltic melts are too LREE-enriched to match Midcontinent Rift basalts (Shirey, 1997) (Figure 5.14a) and calculated tonalitic melts have positive Eu anomalies not seen in natural tonalites (Rogers, 2002) (figure not shown). They do, however, have similar compositions to carbonatites and kimberlites. In particular, carbonated silicate melts calculated using the Girnis et al. (2013) partition coefficients are strongly depleted in Zr and Hf and have LREE and Nb concentrations similar to natural carbonatites (Bizimis et al., 2003; Tappe et al., 2006) (Figure 5.14b).

During percolation through the garnet peridotite lithosphere, this melt may become progressively depleted in HREE and Y and will evolve to more LREE and volatile-rich compositions (e.g., Navon and Stolper, 1987; Bedini et al., 1997). Therefore both the melt-dominated and fluid-dominated metasomatic signatures in Victor garnets can potentially be explained by the percolation of a single metasomatic agent, represented here by the melt in equilibrium with the 'sloped' garnet (Figure 5.14), as also suggested for Renard peridotites (Superior craton) by Hunt et al. (2012a) and for Slave peridotites (Aulbach et al., 2013).

Metasomatism of clinopyroxene xenocrysts

Victor clinopyroxene xenocrysts are strongly LREE-enriched (Figure 5.8), unlike depleted peridotites, which are residual after melt extraction and typically have LREE-depleted compositions (e.g., residual abyssal peridotites; Johnson and Dick, 1992; Warren and Shimizu, 2010). This suggests either their secondary metasomatic origin or cryptic metasomatism of primary clinopyroxene by percolating low-degree melts.

However, major element compositions for these clinopyroxene xenocrysts are distinct to metasomatic clinopyroxene in dunite and harzburgite xenoliths that is not texturally equilibrated and have high Na and Cr compositions. They have similar major element compositions to texturally equilibrated clinopyroxene in Delta lherzolitic xenoliths (Section 5.5.3 and Table G.2), which suggests their LREE-enriched compositions are the result of cryptic metasomatism.

Calculated silicate liquids (basaltic and tonalitic) in equilibrium with clinopyroxene do not resemble either basalts from the Midcontinent Rift (Shirey, 1997) or natural tonalites (Rogers, 2002). A better compositional match is found between calculated carbonated silicate melts (Girnis et al., 2013) and kimberlite-carbonatite. These calculated melts have compositions intermediate between kimberlite and carbonatite - they have LREE content and Nb, Ta contents higher than those present in kimberlite and Zr, Hf anomalies similar to carbonatite melts. However, these calculated melts are not a perfect match to carbonatite melts as they do have corresponding Nb and Ta anomalies. A clear distinction between kimberlite and carbonatite melt metasomatism could therefore, not be made. Crystallisation from kimberlite-like melts just prior to eruption would, however, explain the apparent trace element disequilibrium between garnet and clinopyroxene (i.e., clinopyroxene melt compositions are a match to none of the garnet melt compositions).

5.13 Diamond stable portions of the lithosphere

Victor is a productive diamond mine, yet the typical depleted harzburgite signature that is normally expected at almost all kimberlite-hosted diamond deposits (e.g., Sobolev, 1977; Gurney, 1984a), is missing. The xenocryst population is predominantly lherzolitic and eclogitic / pyroxenitic; even though more depleted compositions, including dunite and harzburgite, are sampled in the xenoliths. In the following section, we discuss the likely diamond stable portions of the Victor lithosphere and their possible relation to the Victor diamond production.

5.13.1 Diamond stable lherzolite

Several compositional characteristics suggest that a thick cool diamond stable lherzolitic SCLM persisted below Attawapiskat after the Midcontinent Rift and into the Jurassic. The strongest evidence is from high shear wave velocities below Attawapiskat (Darbyshire et al., 2007, 2013; Faure et al., 2011; Schaeffer and Lebedev, 2013) that indicates the present-day lithosphere is about 220 km thick. During the Jurassic, the geotherm calculated from both xenolith and xenocryst data, indicates that the lithosphere was $\sim$ 200 km thick with a relatively broad "diamond window" of $\sim$ 70 km thickness. This geotherm is constrained by a very high proportion of diamond stable Cr-diopside xenocrysts (Figure 5.11a,c). After all the compositional filters of Nimis (1998, 2002) and Grütter (2009) (see Section 5.8.1) were applied, 74% (23 of the remaining 31) Cr-diopside grains originate inside the diamond stability field.

The mantle geotherm at Attawapiskat corresponds to between 35 and 40 mW/m^2 surface heat flow (Hasterok and Chapman, 2011) (Figure 5.11c). This is slightly "cooler" than the geotherm at Kyle Lake, which corresponds to 40 mW/m^2 (and slightly higher) surface heat flow resulting in a smaller "diamond window" of $<$ 30 km. Indicated depths for Victor lherzolitic garnets are predominantly in the graphite stability field $<$4 GPa (Cr-in-grt barometry; Grütter et al., 2006) (Figure 5.2a). However, their Cr-in-garnet pressures are *minimum* pressures, as bulk peridotite at Attawapiskat has not been shown to be Cr-saturated (i.e., precipitate chromite).

Similarly, MnO contents in only $\sim$5% of lherzolitic garnets are $<$ 0.36 wt% (Figure 5.17a), an approximate cutoff for diamond stable conditions by Grütter et al. (2004), based on Mn-in-garnet thermometry (Grütter et al., 1999). The thermometric expression of Grütter et al. (1999) does, however, ignore crystal chemical effects and, as a consequence, a number of lherzolitic garnet inclusions in diamond with elevated grossular content and relatively low Mg-number fall above the 0.36 wt% MnO cut-off. Therefore, the 5% diamond stable lherzolitic garnets indicated by MnO contents is considered a minimum value.

Ni-in-garnet temperatures for lherzolitic garnets range between 690 °C and 1036 °C (using the formulation of Canil, 1999). 87% of these lherzolitic garnets have temperatures above 860 °C , the minimum temperature for diamond stability on the combined xenolith and xenocryst geotherm (Figure 5.11c). Nearly half of Victor lherzolitic garnets analysed in this study have depleted compositions and display sinusoidal REE_N patterns (Figure 5.6), which are considered typical for peridotitic garnet inclusions in diamonds worldwide (e.g., Stachel et al., 2004). These combined results indicate that a high proportion of Victor lherzolitic garnets are diamond-stable and are consistent with the results reported in Januszczak et al. (2013).

5.13.2 Diamond stable eclogites and pyroxenites

The majority of eclogite and pyroxenite xenoliths have Fe-Mg exchange temperatures <980 °C (Section 5.8.3) which according to the established geotherm for Attawapiskat, places them near the boundary between the graphite and diamond stability field (Figure 5.11). Additionally, Na_2O in garnet and K_2O in clinopyroxene in the majority of eclogite and pyroxenite xenoliths are low (< 0.09 wt% and < 0.08 wt%, respectively) (Figure 5.17b), which is usually taken as an indication that they are not derived from high pressures in the diamond stability field (McCandless and Gurney, 1989). Only one of the 17 eclogite xenoliths has garnet with elevated Na contents (Na_2O = 0.1 wt%). However, garnet from five of the 19 pyroxenite xenoliths and 26% of the high Ca-eclogitic (G3) and low Ca-eclogitic/pyroxenitic (G4) garnets picked from mineral concentrate have Na_2O > 0.09 wt% (Figure 5.17b).

As bulk rock chemistry exerts a major control on Na_2O in garnet, many high Mg# garnets originating in the diamond stability field may have low Na_2O (Grütter and Quadling, 1999). For example, garnet from diamondiferous high-Mg eclogites at Jericho do not classify as diamond stable on the basis of their low Na_2O (0.04 to 0.06%), even though garnet diamond inclusions at Jericho do have high Na_2O (Smart et al., 2009). Therefore, it is possible that more pyroxenite and eclogite xenoliths at Victor are derived from the diamond stability field, even if it is not indicated in their Na_2O content. High Na content in several high Mg pyroxenitic garnet xenocrysts can be taken as strong indication of their derivation from diamond-stable portions of the lithosphere.

5.14 Summary

Initial Melting in the Palaeoarchaean

Initial melting to form the proto-craton occurred at low pressures, likely in a mid-ocean ridge setting. This led to highly depleted harzburgitic and dunitic residues, with Mg#'s in olivine up to 93.6 (average Mg# 92.6). This depletion event likely occurred during the Palaeoarchaean, with preservation of >3.2 Ga depletion ages in two xenoliths. There are no Palaeoarchaean ages in the North Caribou superterrane, however these old ages do correlate with old crustal ages (3.8 - 3.5 Ga) at Assean Lake in Manitoba and the Inukjuak domain in Quebec (Böhm et al., 2000; Skulski et al., 2000; David et al., 2002, 2009). This supports the assertion that Attawapiskat is underlain by the Northern Superior superterrane, i.e., that the Winisk River Fault is the boundary between the North Caribou and Northern Superior superterranes (Sage, 2000).

Subduction at 2.7 Ga

Further mantle melting, likely in an arc environment during subduction - accretion, occurred at 2.7 Ga with PGE_N residual patterns preserved in two xenoliths. Hydrous melts infiltrating the overlying mantle wedge led to I-PGE alloy formation with radiogenic $^{187}Os/^{188}Os$ (e.g., Matveev and Ballhaus, 2002; Brenker et al., 2003).

Midcontinent Rift at 1.1 Ga

Midcontinent Rift basalts interacted with variably depleted peridotite. This led to P-PGE-enrichment and T_{RD} ages ranging between 1.6 and 1.4 ± 0.2 Ga. Basaltic melts did not overprint the lithosphere and older, depleted domains are preserved (e.g., depleted sinusoidal garnets). Calculated basaltic equilibrium melts from neither garnet or clinopyroxene xenocrysts is similar to that of Midcontinent Rift basalts. The thermal impact of the rift is seen in the elevated geotherm at the 1.1 Ga Kyle Lake kimberlite, which due to extreme narrowing of the diamond window (Figure 4.8), must have led to some diamond destruction.

Diamond stable portions of the lithosphere

Diamond-stable conditions were prevalent in the lithosphere after the thermal impact of the rift subsided and was present during the Jurassic when the Attawapiskat kimberlites erupted. This is indicated in the thick lithosphere of about 200 km, with a large diamond window compared to the PT conditions prevalent in the Proterozoic at nearby Kyle Lake.

Lherzolitic garnets have favourable compositions for diamond, in both their MnO content and Ni-in-garnet temperatures. Their sinusoidal REE_N patterns are typical for harzburgitic and lherzolitic garnet inclusions in diamonds worldwide (e.g., Stachel et al., 2004). High Na content in high Mg eclogite and pyroxenite indicate that these lithologies also have the potential to be an important mantle source of diamonds in this region, as previously suggested for the AT56 kimberlite at Attawapiskat (Armstrong et al., 2004).

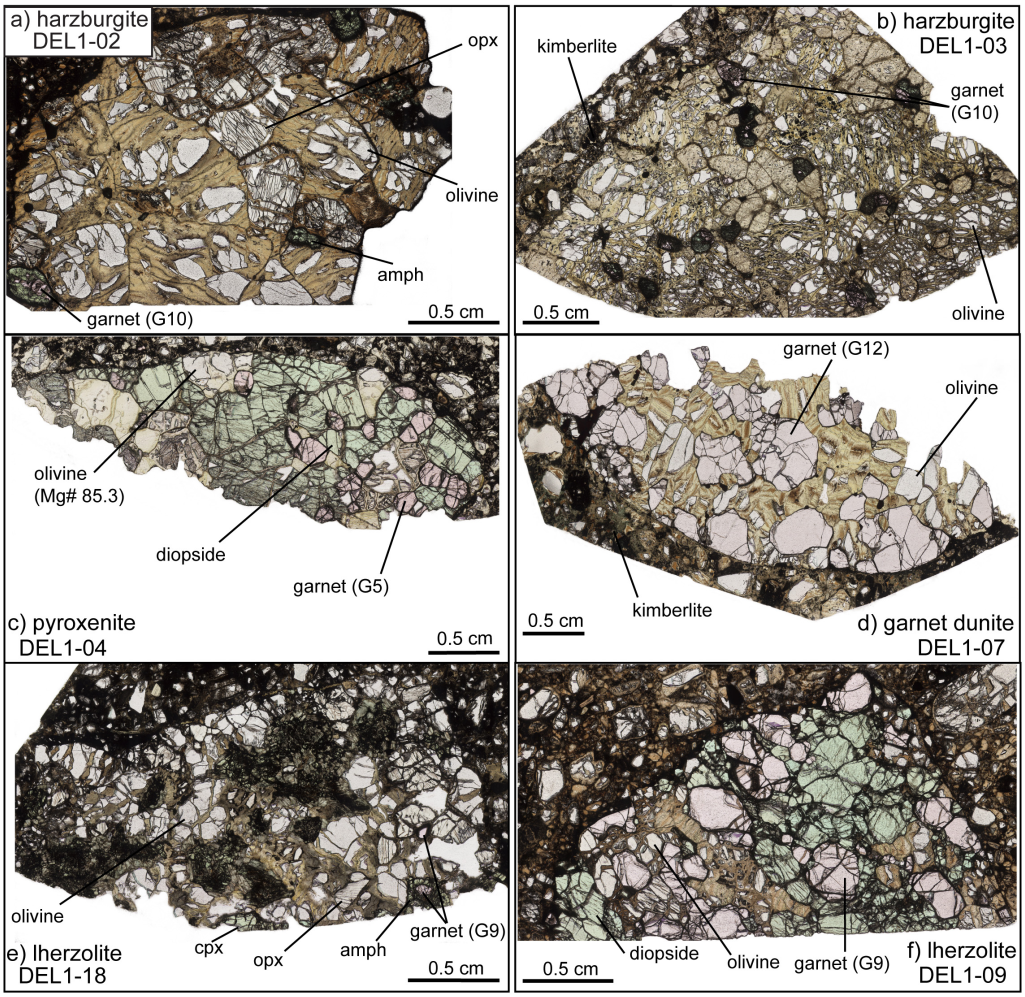

Figure 5.1: Thin sections of selected Delta xenoliths in plane-polarised light. Due to the small size of most the samples, they were not classified on modal abundance but rather on garnet chemistry.

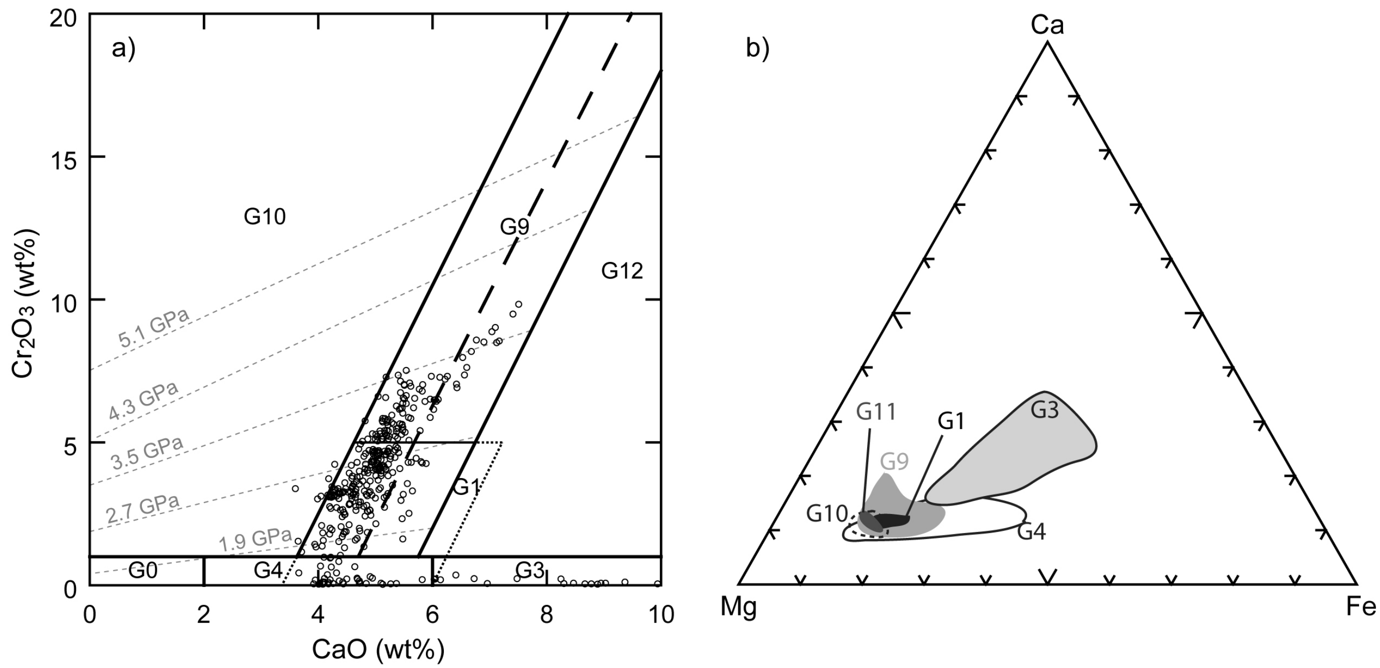

Figure 5.2: a) Victor garnet xenocryst compositions in Ca-Cr space with classification from Grütter et al. (2004) and Cr-saturation arrays (grey dashed lines) that indicate minimum pressure where peridotite does not contain chromite (Grütter et al., 2006). b) Garnet xenocryst Mg-Ca-Fe compositions.

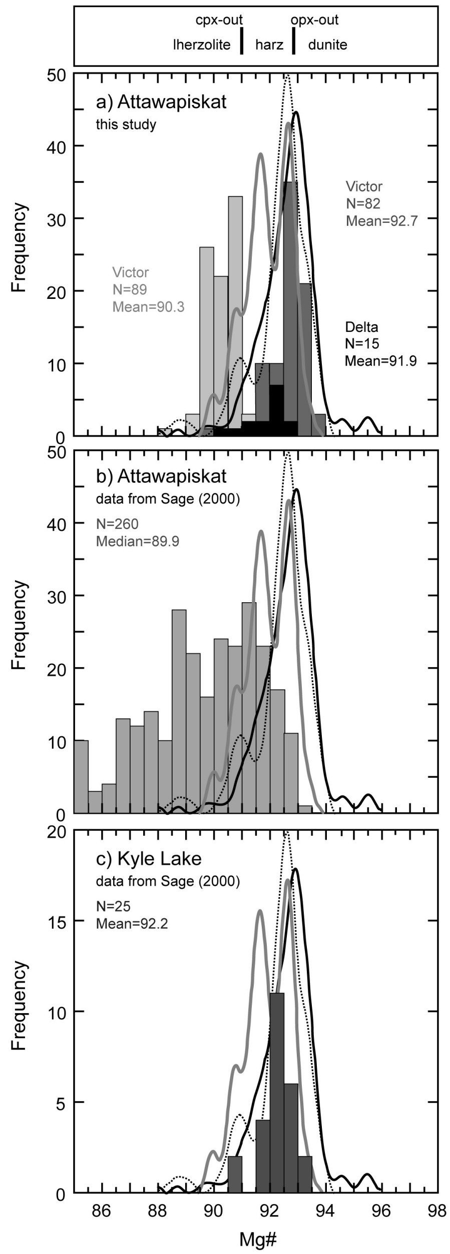

Figure 5.3: Histogram of olivine Mg# from this study compared to those of Kyle Lake and Attawapiskat reported in Sage (2000). a) Two populations of Victor olivine xenocrysts and olivine from Delta peridotite xenoliths; b) Compilation of olivine xenocrysts from several Attawapiskat kimberlites (Sage, 2000) and c) Kyle Lake olivine xenocrysts (Sage, 2000). Relative probability curves for olivine from the Slave (grey), Kaapvaal (black) and North Atlantic (dashed) cratons are shown for reference (compilation of Pearson and Wittig, 2008).

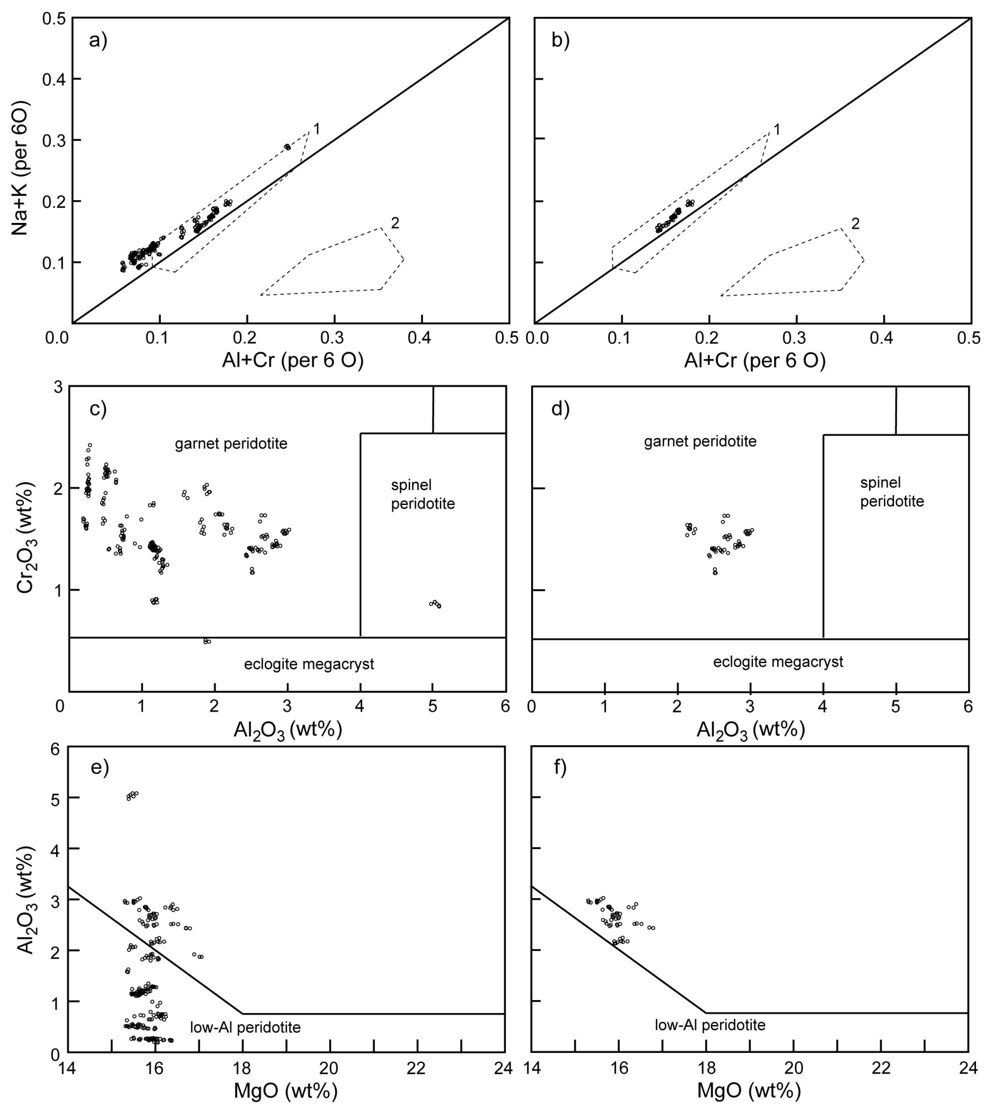

Figure 5.4: Compositional filters applied to clinopyroxene grains prior to geothermobarometry calculations. a) and b) Filter to distinguish between jadeite (field 1 for garnet stability field) and Tschermak (field 2 for spinel stability field) components (Sobolev et al., 1992). c) and d) Cr_2O_3 and Al_2O_3 compositions, used to distinguish different mantle lithologies after Ramsay and Tompkins (1994) and Ramsay (1995). e and f) Low-Al and low-Mg grains were removed as they may be due to carbonatite metasomatism (Nimis, 1998).

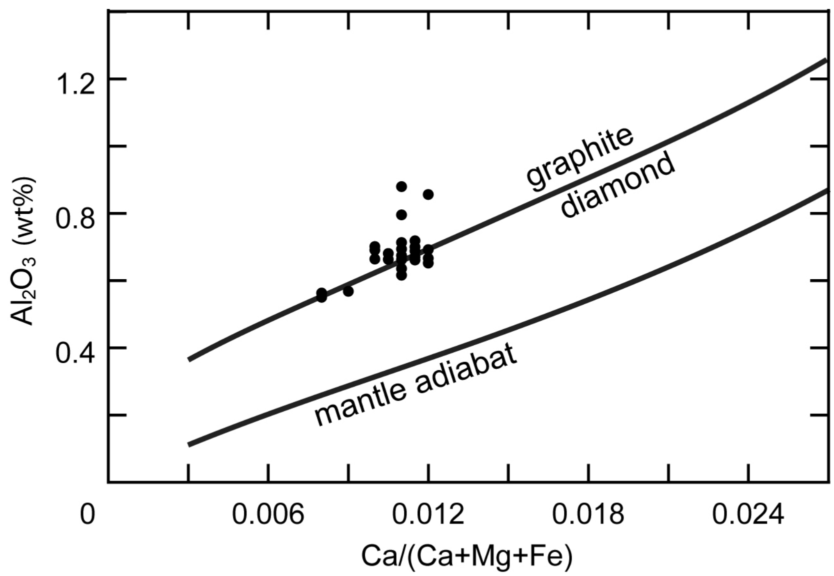

Figure 5.5: Al_2O_3 vs Ca/(Ca+Mg+Fe) for Victor orthopyroxene xenocrysts. Grütter (2009) has shown that a coexisting equilibrium assemblage of cpx and opx in garnet lherzolite may record mutually consistent compositional arrays and therefore, that the graphite-diamond transition (Kennedy and Kennedy, 1976) and the mantle adiabat (T = 1300 °C) can be interpolated into orthopyroxene compositional space. These orthopyroxenes are lherzolitic and straddle the graphite-diamond transition.

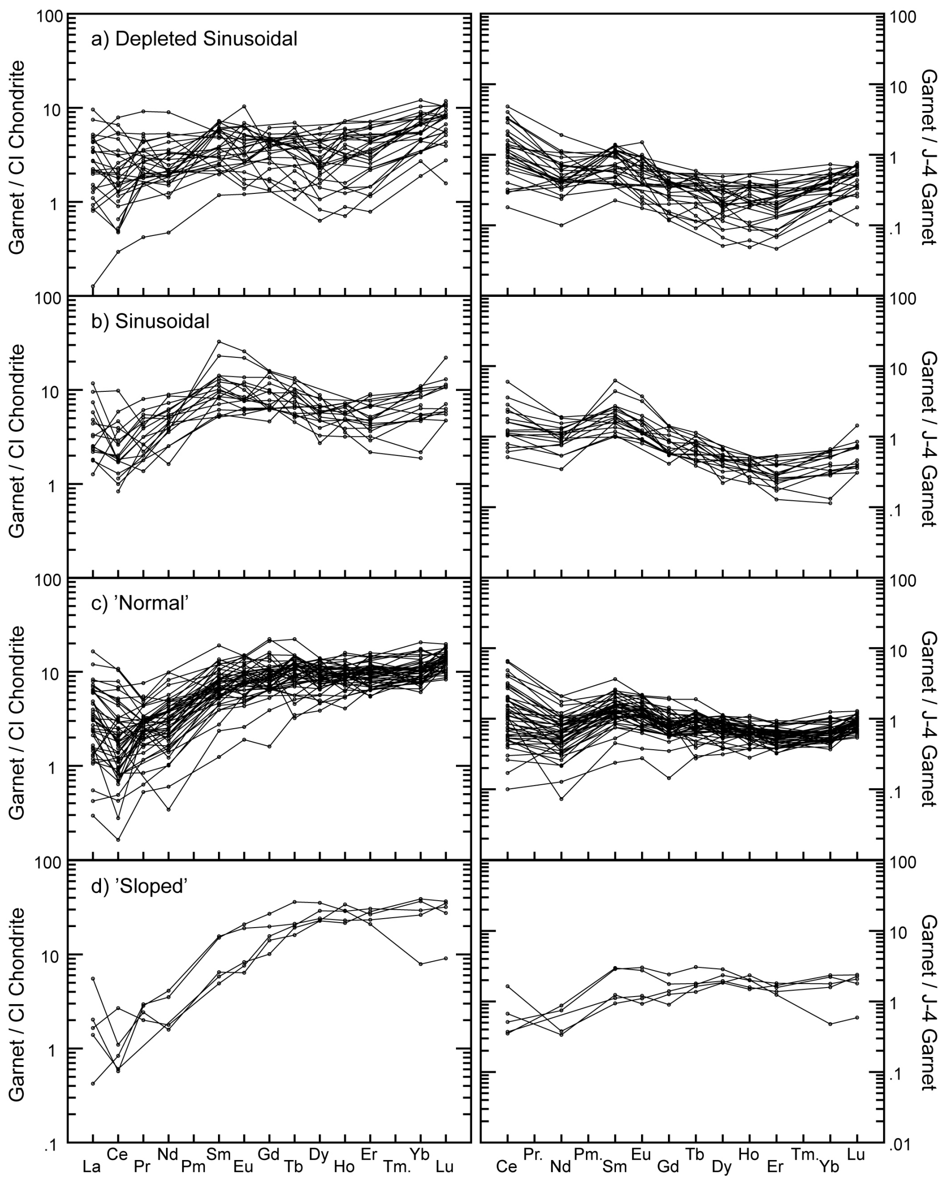

Figure 5.6: REE compositions for garnet xenocrysts normalised to chondrite Sun and McDonough (1989) and J4 (a Jagersfontein garnet with a primitive mantle composition (Stachel et al., 1998, and references therein). a) Sinusoidal garnets with the most depleted Y and Zr concentrations. These concentrations overlap with those of harzurgitic and lherzolitic garnets from Kyle Lake (Scully et al., 2004). b) Sinusoidal garnets with more Zr enrichment indicative of mild fluid-metasomatism. These garnets still show good overlap with those from Kyle Lake (Scully et al., 2004) c) "Normal" garnet with approximately flat chondrite normalised MREE to HREE. The J4 normalised plot show that these are at primitive mantle concentrations. d) Melt metasomatised garnet with enriched MREE to HREE relative to both chondrite and J4.

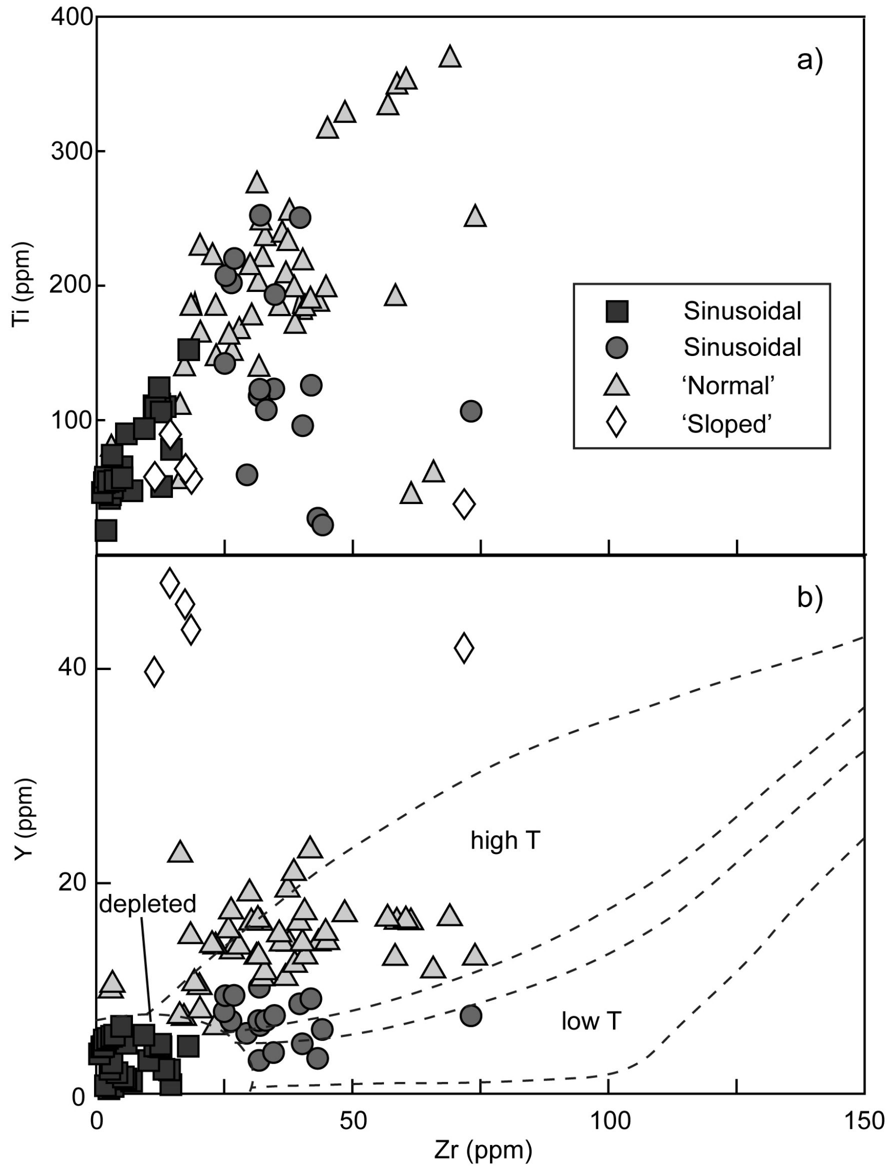

Figure 5.7: Garnet Ti-Y-Zr compositions for the four main groups of lherzolitic garnets, with divisions based on their combined REE_N and trace element compositions. Fields for depleted and low temperature (fluid) and high temperature (melt) metasomatism from Griffin and Ryan (1995).

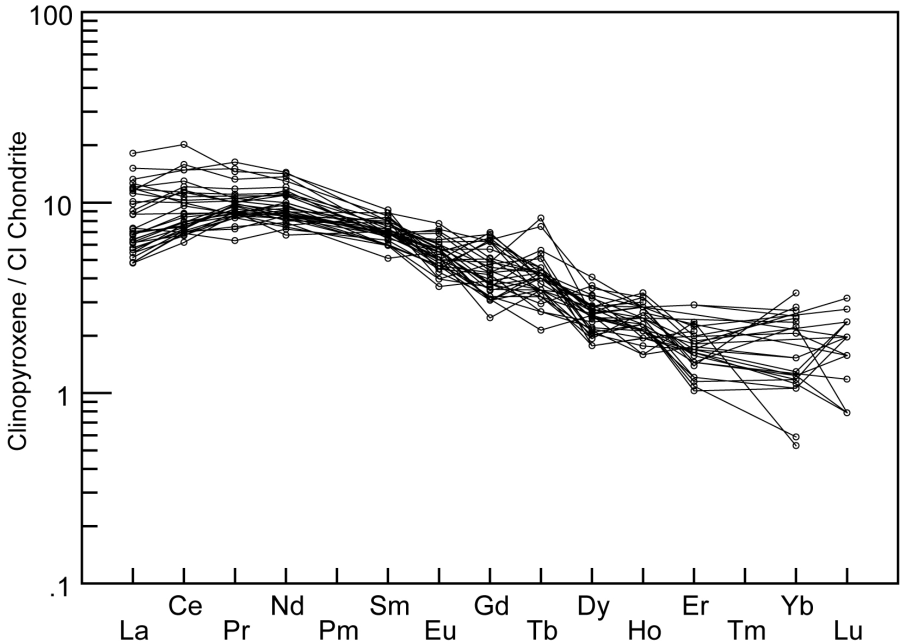

Figure 5.8: REE compositions for clinopyroxene xenocrysts. All data normalised to Sun and McDonough (1989).

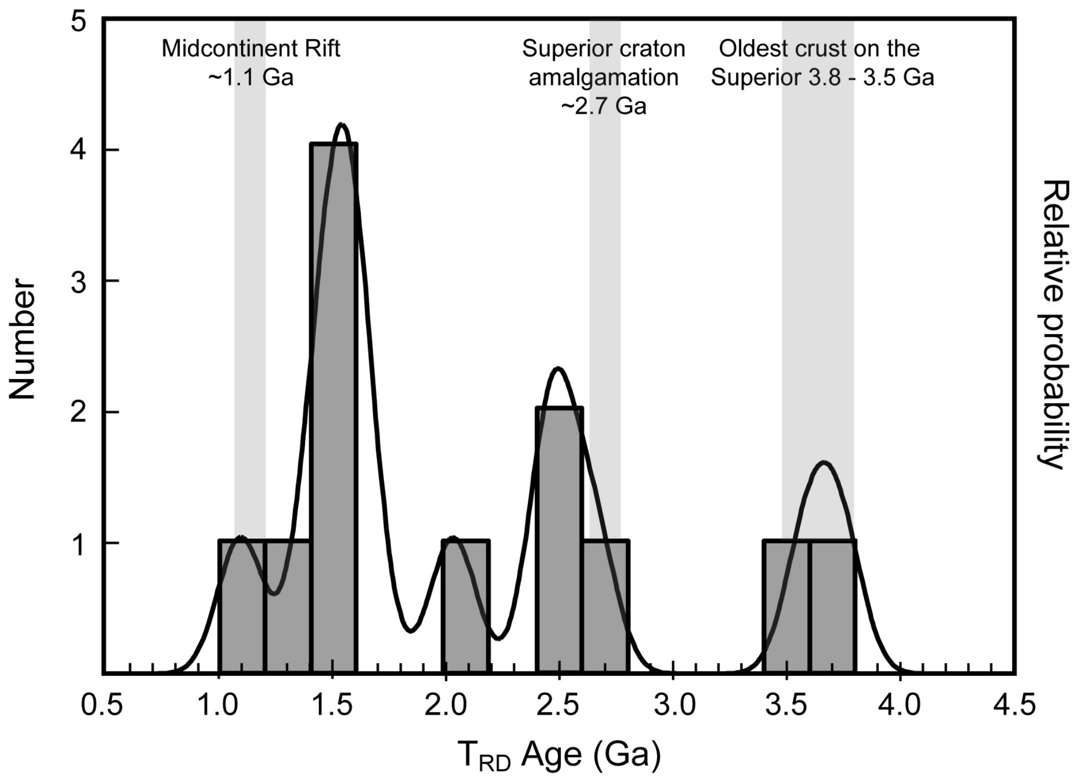

Figure 5.9: Relative probability plot for the T_{RD} ages for olivine from Delta xenoliths with unradiogenic $^{187}Os/^{188}Os$, calculated using equations given in Shirey and Walker (1995) and the O-chondrite reservoir ($^{187}Os/^{188}Os = 0.1283$; Walker et al., 2002). Also included are a whole-rock T_{RD} age for a pyroxenite from Victor (Chapter 3) and three peridotite whole rocks from Kirkland Lake (Pearson et al., 1997). A uniform error on all T_{RD} ages was used, to avoid any over-emphasis on samples with higher analytical precision.

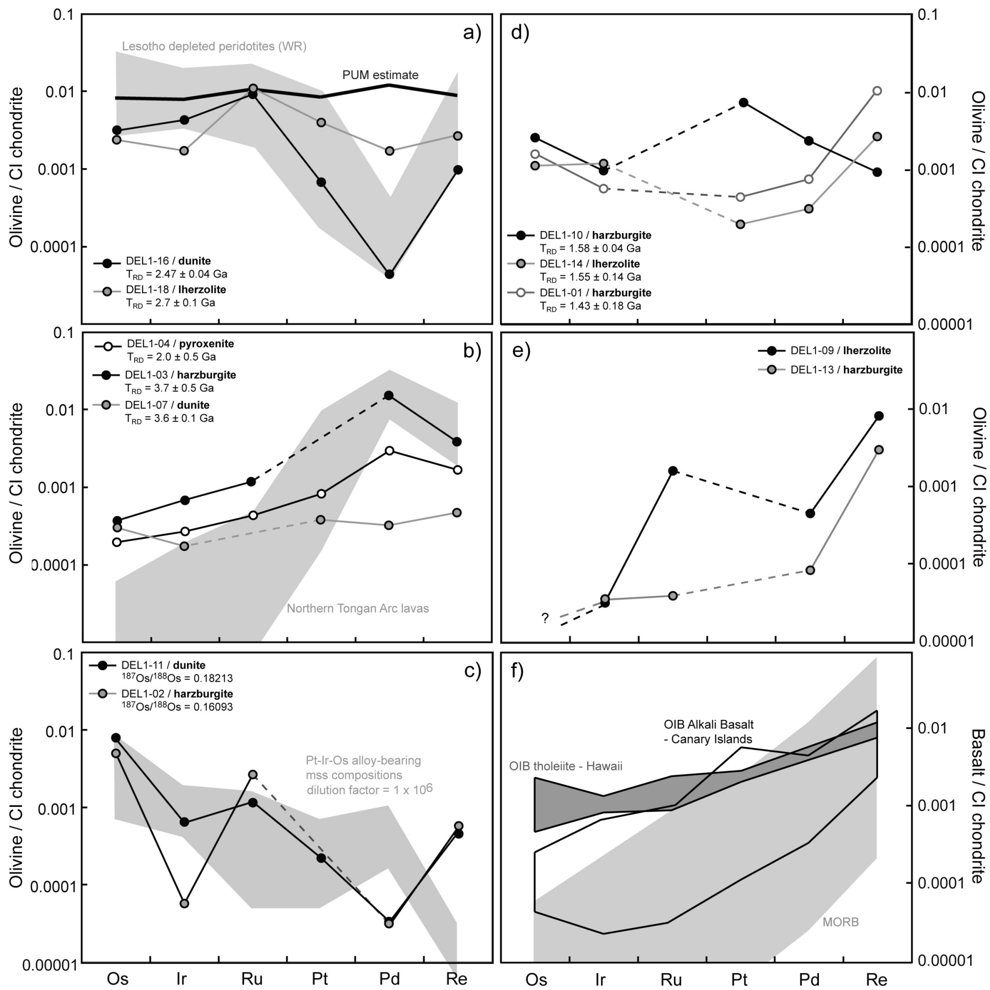

Figure 5.10: PGE compositions for samples grouped according to their $^{187}Os/^{188}Os$ and calculated T_{RD} ages. a.) Samples with 2.7 to 2.5 Ga T_{RD} ages. Compositions for Lesotho depleted peridotites (WR) from Pearson et al. (2004) and the PUM estimate from Becker et al. (2006). b.) Samples with Palaeoarchaean T_{RD} ages, and pyroxenite with a Proterozoic T_{RD} age. Composition for Northern Tongan Arc lavas from Dale et al. (2012). c.) Os-rich samples with radiogenic $^{187}Os/^{188}Os$. Composition for Pt-Ir-Os alloy-bearing monosulphide solid solution (mss) from Griffin et al. (2002), which had to be diluted by a factor of $1x10^6$ to be comparable to inclusions in olivine. d.) Samples with 1.6 to 1.4 Ga T_{RD} ages, with P-PGE and Re enrichment similar to the basalts in e. e.) Two samples with extremely low Os content, for which no $^{187}Os/^{188}Os$ and T_{RD} determinations could be made. f.) Basalt PGE_N compositions compiled from the literature. Range for tholeiitic ocean island basalts (OIB) from Ireland et al. (2009) and alkali OIB from Day et al. (2010). Day (2013) reports the average and standard deviations for both these localities. Mid-ocean ridge basalts (MORB) from Rehkämper et al. (1999), Bezos et al. (2005), Gannoun et al. (2007) and Dale et al. (2008). All compositions normalised to CI Chondrite of Horan et al. (2003).

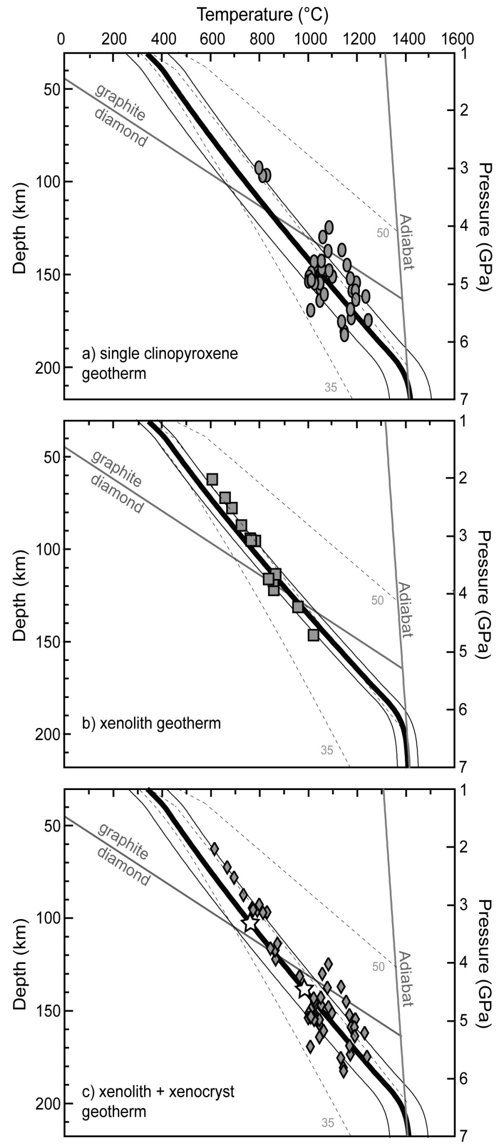

Figure 5.11: Fitplot geotherms calculated using both xenoliths and xenocrysts from Attawapiskat. Grey dashed lines are geotherms that correspond to 35, 40 and 50 mW/m^2 surface heat flow (Hasterok and Chapman, 2011). Graphite-diamond transition from Day (2012). Pressure (GPa) was converted to depth (km) using a constant density conversion of 0.0324. a) Geotherm for single clinopyroxenes from Victor b) Harzburgite, lherzolite and pyroxenite xenolith geotherm from Delta and Victor. c) Combined xenolith and xenocryst geotherm, which corresponds to between 35 and 40 mW/m^2 surface heat flow. Bimineralic eclogites and pyroxenites have temperatures between 770 and 980 °C (range indicated by stars); which places them around the transition between the graphite and diamond stability fields when plotted on this combined xenocryst/xenolith geotherm.

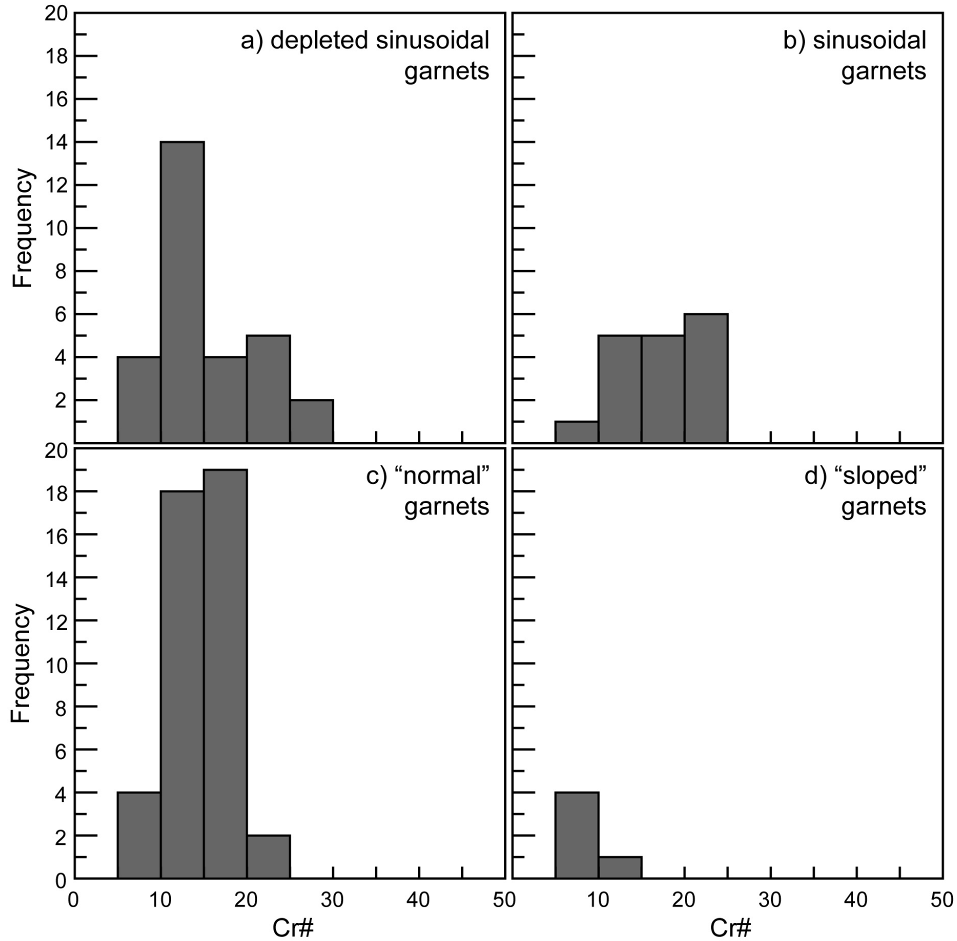

Figure 5.12: Cr#, given as Cr/(Cr+Al) x 100, for different groupings of lherzolitic garnet xenocrysts from Victor. Garnets with the most depleted compositions that were only affected by mild fluid-metasomatism (Section 5.12.3) have the highest Cr# up to to 30. ”Sloped” garnets, that were affected by melt metasomatism have the lowest average Cr#.

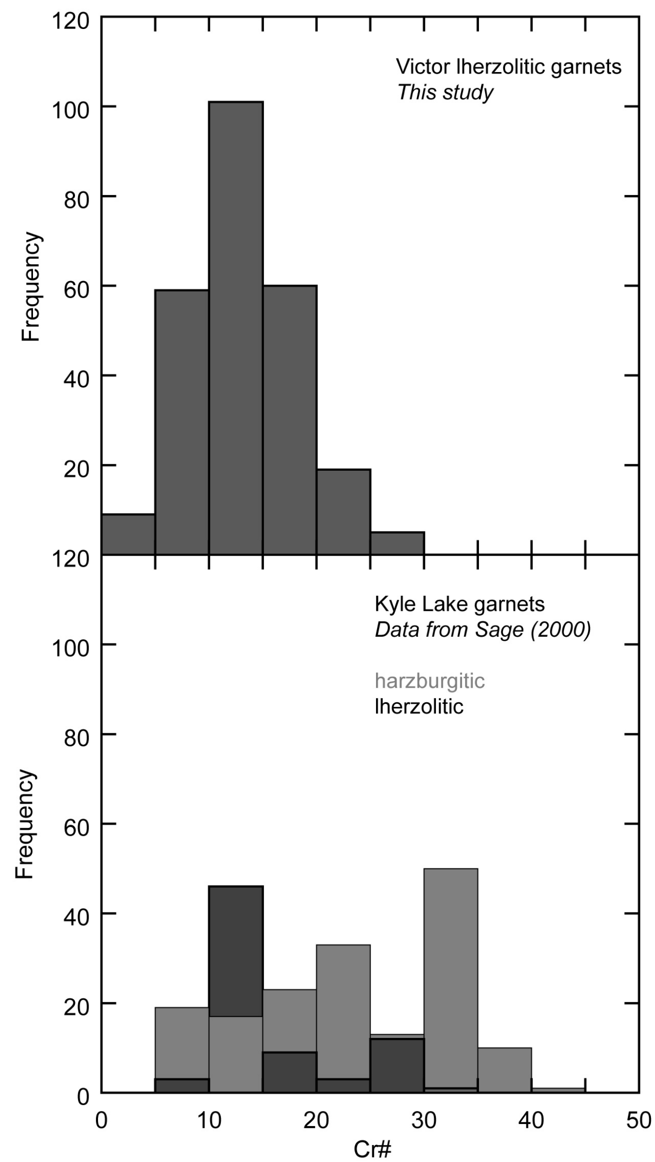

Figure 5.13: Cr#, given as Cr/(Cr+Al) x 100, for lherzolitic garnets from Victor compared to harzburgitic and lherzolitic garnets from Kyle Lake (Sage, 2000). Cr# in the Kyle Lake harzburgites have a higher mode than Victor, whereas the mode for Cr# in Kyle Lake lherzolites is similar to lherzolites at Victor.

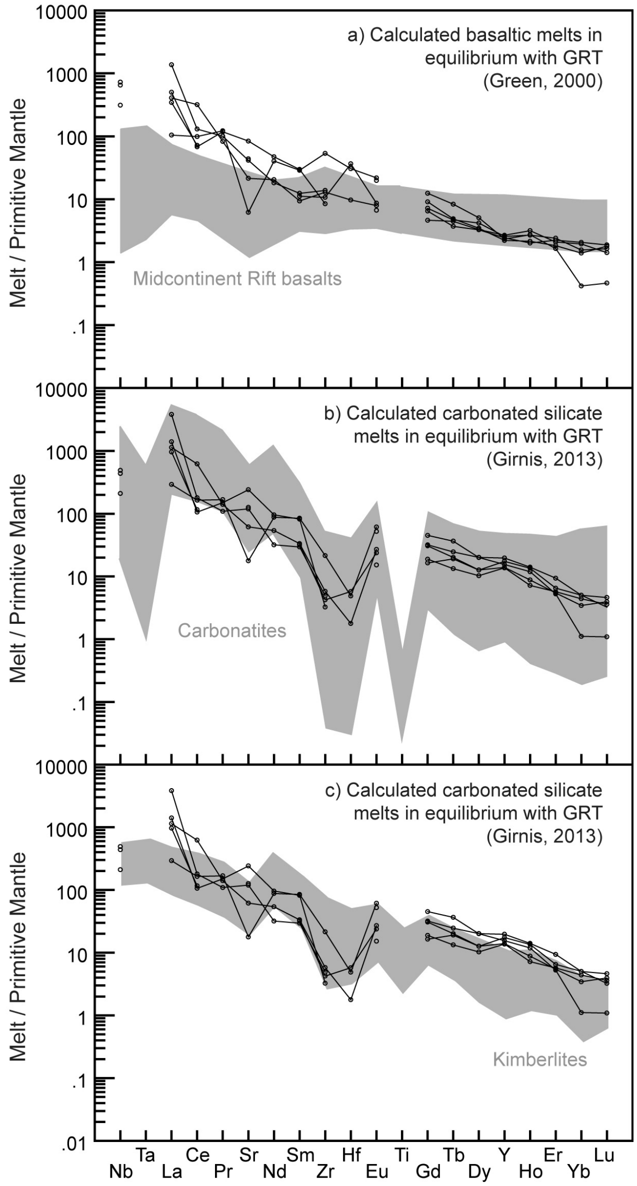

Figure 5.14: Calculated liquids in equilibrium with the 'sloped' lherzolitic garnet xeoncrysts, normalised to the primitive mantle composition of (Sun and McDonough, 1989). a) Basaltic melts using partition coefficients for garnet and basaltic melt (Green et al., 2000). These are not a good compositional match for Midcontinent Rift basalts (Shirey, 1997). b and c) Carbonatitic / kimberlitic melts calculated using partition coefficients for garnet and carbonated silicate melt (Girnis et al., 2013). These calculated melts have a closer compositional match to natural carbonatites (Bizimis et al., 2003; Tappe et al., 2006) than to kimberlites (Kaminsky et al., 2002; le Roex et al., 2003; Birkett et al., 2004; Nielsen et al., 2009; Patterson et al., 2009).

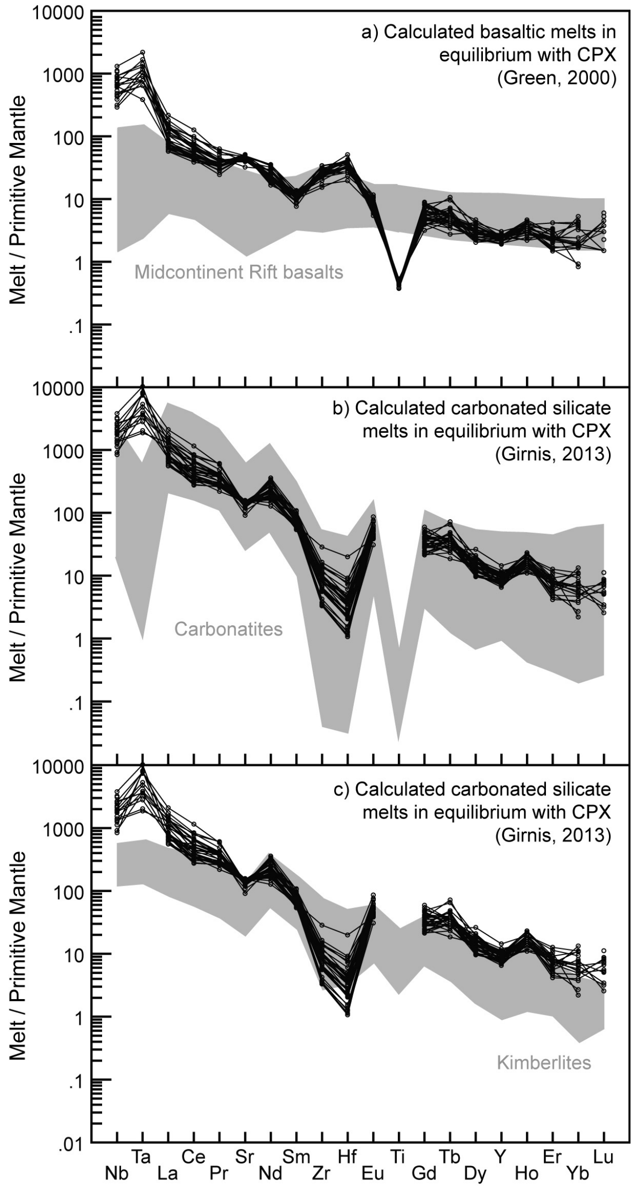

Figure 5.15: Calculated melts in equilibrium with clinopyroxene xenocrysts, normalised to the primitive mantle composition of (Sun and McDonough, 1989). a) Basaltic melts using partition coefficients for clinopyroxene and basaltic melt (Green et al., 2000). These are not a good compositional match for Midcontinent Rift basalts (Shirey, 1997). b and c) Carbonatitic / kimberlitic melts calculated using partition coefficients for clinopyroxene and carbonated silicate melt (Girnis et al., 2013). These calculated melts have an intermediate composition between kimberlite (Kaminsky et al., 2002; le Roex et al., 2003; Birkett et al., 2004; Nielsen et al., 2009; Patterson et al., 2009) and carbonatite (Bizimis et al., 2003; Tappe et al., 2006).

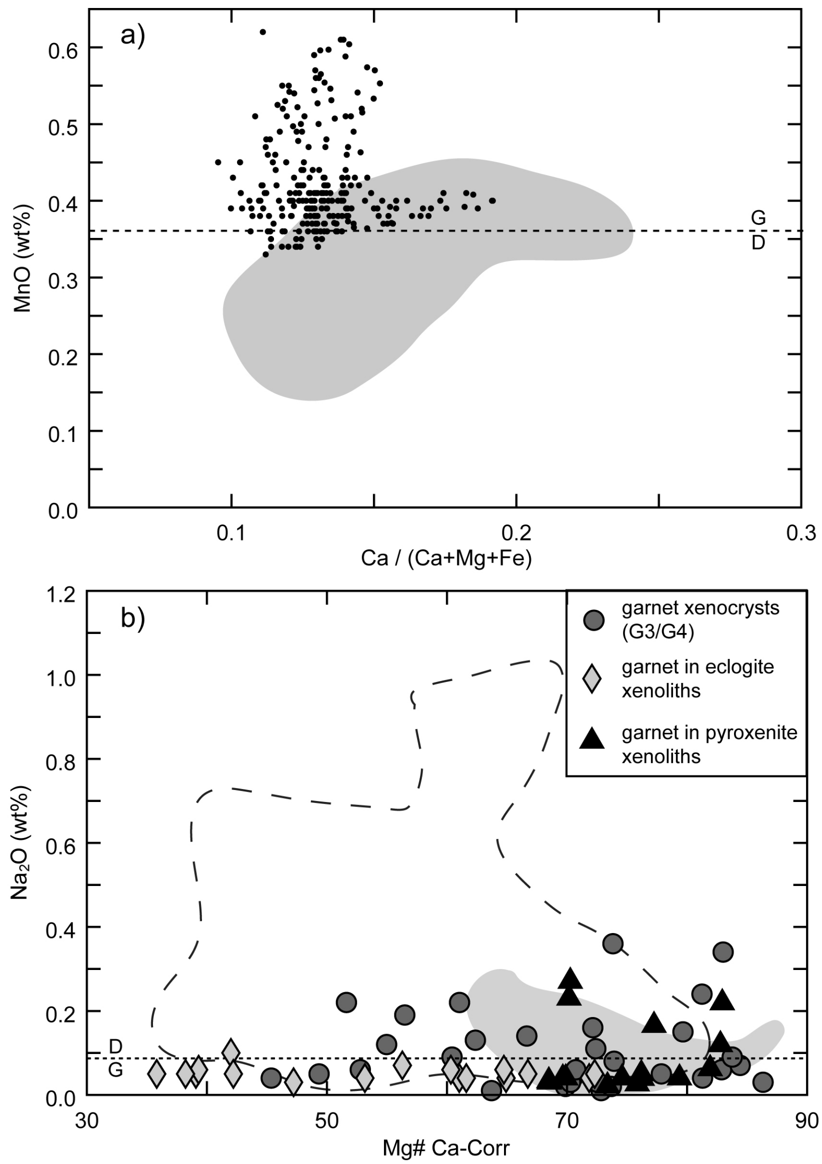

Figure 5.16: a) MnO vs Ca/(Ca+Mg+Fe) in lherzolitic garnet xenocrysts. Dashed line is the traditional cut-off for diamond-stable lherzolitic garnets (MnO < 0.36 wt%; Grütter et al., 2004). Shaded field for garnet diamond inclusions (database of Stachel and Harris, 2008). b) Na content vs Ca-corrected Mg# in xenocryst garnets and garnets from eclogite and pyroxenite xenoliths. The dashed line is the cut-off for diamond stable eclogitic garnets (Na_2O > 0.09 wt%; McCandless and Gurney, 1989). The shaded field is for pyroxenitic garnet diamond inclusions and the dashed field for eclogitic diamond inclusions (database of Stachel and Harris, 2008). 'D' is for diamond stability field and 'G' is for graphite stability field.

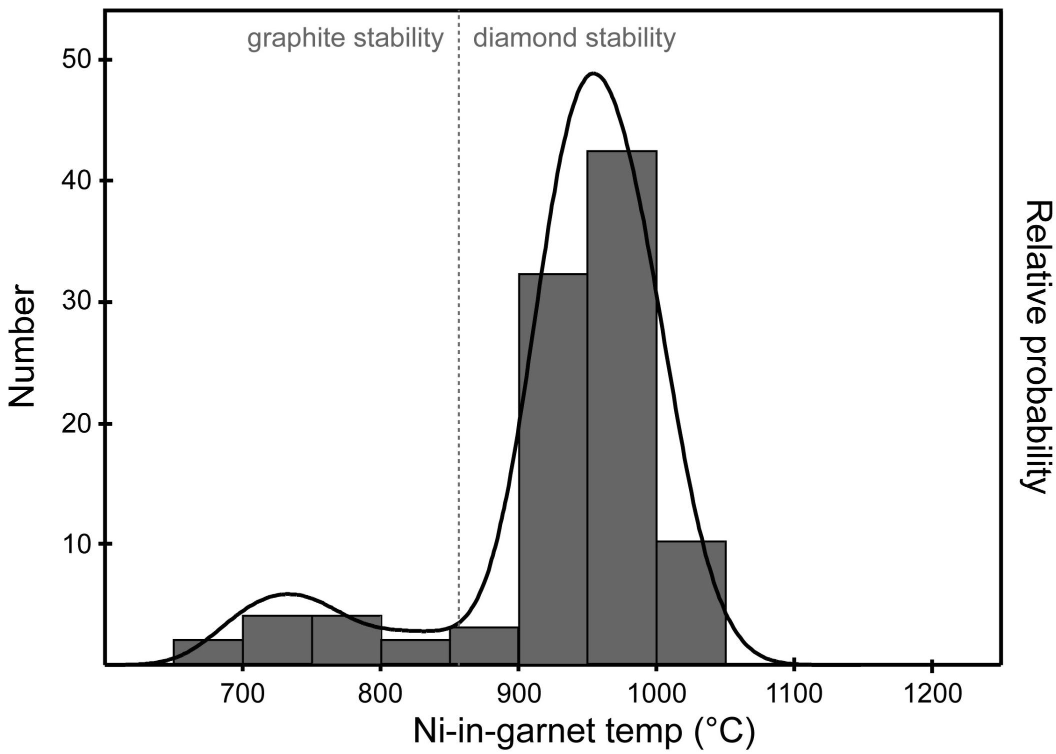

Figure 5.17: Ni-in-garnet thermometry for lherzolitic garnet xenocrysts, using the formulation of Canil (1999). 87% of these lherzolitic garnet xenocrysts have temperatures above 860 °C , the minimum for diamond stability as indicated by the combined xenolith and xenocryst geotherm in Figure 5.11c. Bin sizes for the histogram are 50 °C , equivalent to the average error on mantle geothermometers. The probability distribution was plotted in Isoplot (Ludwig, 1991).

References

Armstrong, J. T.: 1995, Citzaf - A Package Of Correction Programs For The Quantitative Electron Microbeam X-Ray-Analysis Of Thick Polished Materials, Thin-Films, And Particles, *Microbeam Analysis* **4**(3), 177–200.

Armstrong, K. A., Nowicki, T. E. and Read, G. H.: 2004, Kimberlite AT-56: a mantle sample from the north central Superior craton, Canada, *Lithos* **77**, 695–704.

Arndt, N., Ginibre, C., Chauvel, C., Albarede, F., Cheadle, M., Herzberg, C., Jenner, G. and Lahaye, Y.: 1998, Were komatiites wet?, *Geology* **26**(8), 739–742.

Aulbach, S.: 2012, Craton nucleation and formation of thick lithospheric roots, *Lithos* **149**, 16–30.

Aulbach, S., Griffin, W. L., Pearson, N. J. and O'Reilly, S. Y.: 2013, Nature and Timing of Metasomatism in the Stratified Mantle Lithosphere Beneath the Central Slave Craton (Canada), *Chemical Geology* **in press**.

Aulbach, S., Griffin, W. L., Pearson, N. J., O'Reilly, S. Y. and Doyle, B. J.: 2007, Lithosphere formation in the Central Slave Craton (Canada): plume accretion or lithosphere accretion, *Contributions to Mineralogy and Petrology* **154**, 409–428.

Ballhaus, C., Tredoux, M. and Spath, A.: 2001, Phase relations in the Fe-Ni-Cu-PGE-S system at magmatic temperature and application to the massive sulphide ores of the Sudbury igneous complex, *Journal of Petrology* **42**, 1911–1926.

Barnes, S. J., Cox, R. A. and Zientek, M. K.: 2006, Platinum-group element, Gold, Silver and Base Metal distribution in compositionally zoned sulfide droplets from the Medvezky Creek Mine, Noril'sk, Russia, *Contributions to Mineralogy and Petrology* **152**, 187–200.

Barnes, S. J., Naldrett, A. J. and Gorton, M. P.: 1985, The origin of the fractionation of platinum-group elements in terrestrial magmas, *Chemical Geology* **53**, 303–323.

Barth, M. G., Foley, S. F. and Horn, I.: 2002c, Partial melting in Archean subduction zones: Constraints from experimentally determined trace element partition coefficients between eclogitic minerals and tonalitic melts under upper mantle conditions, *Precambrian Research* **113**, 323–340.

Becker, H., Horan, M. F., Walker, R. J., Gao, S., Lorand, J.-P. and Rudnick, R. L.: 2006, Highly siderophile element composition of the Earth's primitive upper mantle: Constraints from new data on peridotite massifs and xenoliths, *Geochimica et Cosmochimica Acta* **70**, 4528–4550.

Bedini, R. M., Bodinier, J. L., Dautria, J.-M. and Morten, L.: 1997, Evolution of LILE-enriched small melt fractions in the lithospheric mantle: a case study from the East African Rift, *Earth and Planetary Science Letters* **153**, 67–83.

Bell, D. R., Grégoire, M., Grove, T. L., Chatterjee, N., Carlson, R. W. and Buseck, P. R.: 2005, Silica and volatile-element metasomatism of Archean mantle: a xenolith-scale example from the Kaapvaal Craton, *Contributions to Mineralogy and Petrology* **150**, 251–267.

Bernstein, S., Hanghøj, K., Kelemen, P. B. and Brooks, C. K.: 2006, Ultra-depleted, shallow cratonic mantle beneath West Grenland: dunitic xenoltihs from Ubekendt Ejland, *Contributions to Mineralogy and Petrology* **152**, 335–347.

Bernstein, S., Kelemen, P. B. and Brooks, C. K.: 1998, Depleted spinel harzburgite xenoltihs in Tertiary dykes from East Greenland restites from high melting degrees, *Earth and Planetary Science Letters* **154**(1-4), 221–235.

Bernstein, S., Kelemen, P. B. and Hanghøj, K.: 2007, Consistent olivine Mg# in cratonic mantle reflects Archean mantle melting to the exhaustion of orthpyroxene, *Geology* **35**(5), 459–462.

Bezmen, N. I., Asif, M., Brügmann, G., Romanenko, I. M. and Naldrett, A. J.: 1994, Distribution of Pd, Rh, Ru, Ir, Os and Au between sulphide and silicate metals, *Geochimica et Cosmochimica Acta* **58**(4), 1251–1260.

Bezos, A., Lorand, J. P., Humler, E. and Gros, M.: 2005, Platinum-group element systematics in mid-oceanic ridge basaltic glasses from the Pacific, Atlantic, and Indian Oceans, *Geochimica et Cosmochimica Acta* **69**, 2613–2627.

Birck, J. L., Barman, M. R. and Capmas, F.: 1997, Re-Os Isotopic Measurements at the Femtomole Level in Natural Samples, *Geostandards Newsletter* **20**(1), 19–27.

Birkett, T. C., McCandless, T. E. and Hood, C. T.: 2004, Petrology of the Renard igneous bodies: host rocks for diamond in the northern Otish Mountains region, Quebec, *Lithos* **76**(1-4), 475–490.

Bizimis, M., Salters, V. J. M. and Dawson, J. B.: 2003, The brevity of carbonatite sources in the mantle: evidence from Hf isotopes, *Contributions to Mineralogy and Petrology* **145**, 281–300.

Bockrath, C., Ballhaus, C. and Holzheid, A.: 2004, Fractionation of the Platinum-Group Elements During Mantle Melting, *Science* **305**, 1951–1953.

Böhm, C. O., Heaman, L. M., Creaser, R. A. and Crockery, M. T.: 2000, Discovery of pre-3.5 Ga exotic crust at the northwestern Superior Province margin, Manitoba, *Geology* **28**(1), 75–78.

Boyd, F. R.: 1989, Compositional distinction between oceanic and cratonic lithosphere, *Earth and Planetary Science Letters* **96**, 15–26.

Boyd, F. R. and McCallister, R. H.: 1976, Densities of fertile and sterile garnet peridotites, *Geophysical Research Letters* **3**, 509–512.

Boyd, F. R., Pearson, D. G. and Mertzman, S. A.: 1999, Spinel-facies peridotites from the Kaapvaal root, *in* J. J. Gurney, J. L. Gurney, M. D. Pascoe and S. H. Richardson (eds), *Proceedings of the 7th International Kimberlite Conference, Cape Town, 1998*, Vol. 1, Red Roof Design, Cape Town, pp. 40–48.

Brenan, J. M.: 2002, Re-Os fractionation in magmatic sulphide melt by monosulphide solid solution, *Earth and Planetary Science Letters* **199**, 257–268.

Brenker, F. E., Meibom, A. and Frei, R.: 2003, On the formation of peridotite-derived Os-rich PGE alloys, *American Mineralogist* **88**, 1731–1740.

Brey, G. P., Doroshev, A. M., Girnis, A. V. and Turkin, A. I.: 1999, Garnet-spinel-olivine-orthopyroxene equilibria in the FeO-MgO-Al_2O_3-SiO_2-Cr_2O_3 system: I. Composition and molar volumes of minerals, *European Journal of Mineralogy* **11**, 599–617.

Brey, G. P. and Köhler, T.: 1990, Geothermobarometry in four-phase lherzolites II. New Thermobarometers, and Practical Assessment of Existing Thermobarometers, *Journal of Petrology* **31**, 1353–1378.

Bulatov, V., Brey, G. P. and Foley, S. F.: 1991, Origin of low-Ca, high-Cr garnets by recrystallisation of low-pressure harzburgites, *Extended Abstracts of the 5th International Kimberlite Conference* pp. 29–31.

Canil, D.: 1999, The Ni-in-garnet geothermometer: calibration at natural abundances, *Contributions to Mineralogy and Petrology* **136**, 240–246.

Canil, D.: 2004, Mildly incompatible elements in peridotites and the origins of mantle lithosphere, *Lithos* **77**, 375–393.

Canil, D. and Wei, K. J.: 1992, Constraints on the origin of mantle-derived low Ca garnets., *Contributions to Mineralogy and Petrology* **109**, 421–430.

Carlson, R. W., Irving, A. J., Schulze, D. J. and Jr., B. C. H.: 2004, Timing of Precambrian melt depletion and Phanerozoic refertilization events in the lithospheric mantle of the Wyoming craton and adjacent Central Plains Orogen, *Lithos* **77**, 453–472.

Carlson, R. W. and Moore, R. O.: 2004, Age of the Eastern Kaapvaal mantle: Re-Os isotope data for peridotite xenoliths from the Monastery mine, *South African Journal of Geology* **107**, 81–90.

Carlson, R. W., Pearson, D. G., Boyd, F. R., Shirey, S. B., Irvine, G., Menzies, A. H. and Gurney, J. J.: 1999, Re-Os systematics of lithosphere peridotites: Implications for lithosphere formation and preservation, *in* J. Gurney, J. Gurney, M. Pascoe and S. Richardson (eds), *Proceedings of the 7th International Kimberlite Conference, Cape Town, 1998*, Vol. 1, Red Roof Design, pp. 99–108.

Carswell, D. A.: 1990, Eclogites and the eclogite facies: definitions and classifications, *in* D. A. Carswell (ed.), *Eclogite facies rocks*, Blackie, pp. 1–13.

Cohen, A. S. and Waters, F. G.: 1996, Separation of osmium from geological materials by solvent extraction for analysis by thermal ionisation mass spectrometry, *Analytica Chimica Acta* **332**, 269–275.

Coleman, R. G., Lee, E. D., Beatty, L. B. and Brannock, W. W.: 1965, Eclogites and eclogites: their differences and similarities, *Geological Society of America Bulletin* **76**, 483–508.

Creaser, R. A., Papanastassiou, D. A. and Wasserburg, G. J.: 1991, Negative thermal ion mass spectrometry of osmium, rhenium and iridium, *Geochimica et Cosmochimica Acta* **55**, 397–401.

Creighton, S., Stachel, T., McLean, H., Muehlenbachs, K., Simonetti, A., Eichenberg, D. and Luth, R.: 2008, Diamondiferous peridotitic microxenoliths from the Diavik Diamond Mine, NT, *Contributions to Mineralogy and Petrology* **155**, 541–554.

Dale, C. W., Luguet, A., Macpherson, C. G., Pearson, D. G. and Hickey-Vargas, R.: 2008, Extreme platinum-group element fractionation and variable Os isotope compositions in Philippine Sea Plate basalts: tracing mantle source heterogeneity, *Chemical Geology* **248**, 213–238.

Dale, C. W., Macpherson, C. G., Pearson, D. G., Hammond, S. J. and Arculus, R. J.: 2012, Inter-element fractionation of highly siderophile elements in the Tonga Arc due to flux melting of a depleted source, *Geochimica et Cosmochimica Acta* **89**, 202–225.

Darbyshire, F. A., Eaton, D. W. and Bastow, I. D.: 2013, Seismic imaging of the lithosphere beneath Hudson Bay: Episodic growth of the Laurentian mantle keel, *Earth and Planetary Science Letters* **373**, 179–193.

Darbyshire, F. A., Eaton, D. W., Fredericksen, A. W. and Ertolahti, L.: 2007, New insights into the lithosphere beneath the Superior Province from Rayleigh wave dispersion and receiver function analysis, *Geophysics Journal International* **169**, 1043–1068.

Dasgupta, R., Hirschmann, M. M., McDonough, W. F., Spiegelman, M. and Withers, A. C.: 2009, Trace element partitioning between garnet lherzolite and carbonatite at 6.6 and 8.6 GPa with applications to the geochemistry of the mantle and of mantle-derived melts, *Chemical Geology* **262**, 57–77.

David, J., Godin, L., Stevenson, R., O'Neil, J. and Francis, D.: 2009, U-Pb ages (3.8-2.7 Ga) and Nd isotope data from the newly identified Eoarchean Nuvvuagittuq supracrustal belt, Superior Craton, Canada, *GSA Bulletin* **121**(1/2), 150–163.

David, J., Parent, M., Stevenson, R., Nadeau, P. and Godin, L.: 2002, The Porpoise Cove supracrustal sequence, Inukjuak area: A unique example of Paleoarchean crust (c.a 3.8 Ga) in the Superior Province, *Ministère des Ressources Naturelles de Québec* **DV**, 2002–10.

Davis, D. W., Amelin, Y., Nowell, G. M. and Parrish, R. R.: 2005, Hf isotopes in zircon from the western Superior province, Canada: Implications for Archean crustal development and evolution of the depleted mantle reservoir, *Precambrian Research* **140**, 132–156.

Day, H. W.: 2012, A revised diamond-graphite transition curve, *American Mineralogist* **97**, 52–62.

Day, J. M. D.: 2013, Hotspot volcanism and highly siderophile elements, *Chemical Geology* **341**, 50–74.

Day, J. M. D., Pearson, D. G., Macpherson, C. G., Lowry, D. and Carracedo, J. C.: 2010, Evidence for distinct proportions of subducted oceanic crust and lithosphere in HIMU-type mantle beneath El Hierro and La Palma, Canary Islands, *Geochimica et Cosmochimica Acta* **74**, 6565–6589.

de Hoog, J. C. M., Gall, L. and Cornell, D. H.: 2010, Trace-element geochemistry of mantle olivine and application to mantle petrogenesis and geothermobarometry, *Chemical Geology* **270**, 196–215.

Ding, X., Li, C., Ripley, E. M., Rossell, D. and Kamo, S.: 2010, The Eagle and East Eagle sulfide orebearing mafic ultramafic intrusions in the Midcontinent Rift System, upper Michigan: Geochronology and petrologic evolution, *Geochemistry, Geophysics and Geosystems* **11**(3), ISSN: 1525–2027.

Ding, X., Ripley, E. M., Shirey, S. B. and Li, C.: 2012, Os, Nd, O and S isotope constraints on country rock contamination in the conduit-related Eagle Cu–Ni–(PGE) deposit, Midcontinent Rift System, Upper Michigan, *Geochimica et Cosmochimica Acta* **89**, 10–30.

Faure, S., Godey, S., Fallara, F. and Trepanier, S.: 2011, Seismic architecture of the Archean North American mantle and its relationship to diamondiferous kimberlite fields, *Economic Geology* **106**(2), 223–240.

Fleet, M., Chryssoulis, S. L., Stone, W. E. and Weisener, C. G.: 1993, Partioning of platinum-group elements and Au in the Fe-Ni-Cu-S system: experiments on the fractional crystallisation of sulphide melt, *Contributions to Mineralogy and Petrology* **115**, 36–44.

Fleet, M. E., Crocket, J. H., Liu, M. and Stone, W. E.: 1999, Laboratory partitioning of platinum-group elements (PGE) and gold with application to magmatic sulphide-PGE deposits, *Lithos* **47**, 127–142.

Fleet, M. E., Crocket, J. H. and Stone, W. E.: 1996, Partitioning of platinum-group elements (Os, Ir, Ru, Pt, Pd) and gold between sulphide liquid and basalt melt, *Geochimica et Cosmochimica Acta* **60**(13), 2397–2412.

Foley, S. F., Andronikov, A. V., Jacob, D. E. and Melzer, S.: 2006, Evidence from Antarctic mantle peridotite xenoliths for changes in mineralogy, geochemistry and geothermal gradients beneath a developing rift, *Geochimica et Cosmochimica Acta* **70**, 3096–3120.

Foley, S. F., Andronikov, A. V. and Melzer, S.: 2002b, Petrology, geochemistry, and mineral chemistry of ultramafic lamprophyres from the Jetty Peninsula area of the Lambert-Amery Rift, Eastern Antarctica, *Mineralogy and Petrology* **74**, 361–384.

Fralick, P. and Davis, D.: 1999, The Seine-Coutchiching problem revisited: sedimentology, geochronology and geochemistry of sedimentary units in the Rainy Lake and Sioux Lookout areas, *in* R. M. Harrap and H. H. Helmstaedt (eds), *Western Superior Transect Fifth Annual Workshop*, Vol. Lithoprobe Report 70, Lithoprobe Secretariat, The University of British Columbia, pp. 66–75.

Gannoun, A., Burton, K. W., Parkinson, I. J., Alard, O., Schiano, P. and Thomas, L. E.: 2007, The scale and origin of the osmium isotope variations in mid-ocean ridge basalts, *Earth and Planetary Science Letters* **259**, 541–556.

Gao, S., Rudnick, R. L., Carlson, R. W., McDonough, W. F. and Liu, Y.-S.: 2002, Re-Os evidence for replacement of ancient mantle lithosphere beneath the North China craton, *Earth and Planetary Science Letters* **198**, 307–322.

Gibson, S. A., McMahon, S. C., Day, J. A. and Dawson, J. B.: 2013, Highly Refractory Lithospheric Mantle beneath the Tanzanian Craton: Evidence from Lashaine Pre-metasomatic Garnet-bearing Peridotites, *Journal of Petrology* **54**(8), 1503–1546.

Girnis, A. V., Bulatov, V. K., Brey, G. P., Gerdes, A. and Höfer, H. E.: 2013, Trace element partitioning between mantle minerals and silico-carbonate melts at 6–12 GPa and applications to mantle metasomatism and kimberlite genesis, *Lithos* **160-161**, 183–200.

Green, D. H. and Ringwood, A. E.: 1967, The Genesis of Basaltic Magmas, *Contributions to Mineralogy and Petrology* **15**, 103–190.

Green, T. H., Blundy, J. D., Adam, J. and Yaxley, G. M.: 2000, SIMS determination of trace element partitioning coefficients between garnet, clinopyroxene and hydrous basaltic liquids at 2-7.5 GPa and 1080-1200 °C, *Lithos* **53**, 165–187.

Grégoire, M., Bell, D. R. and le Roex, A. P.: 2003, Garnet lherzolites from the Kaapvaal Craton (South Africa): trace element evidence for a metasomatic history, *Journal of Petrology* **44**, 629–657.

Griffin, W. L. and Ryan, C. G.: 1995, Trace elements in indicator minerals: area selection and target evaluation in diamond exploration, *Journal of Geochemical Exploration* **53**, 311–337.

Griffin, W. L., Spetsius, Z. V., Pearson, N. J. and O'Reilly, S. Y.: 2002, In situ Re-Os analysis of sulphide inclusions in kimberlitic olivine: new constraints on depletion events in the Siberian lithospheric mantle, *Geochemistry, Geophysics and Geosystems* **3**(11), ISSN: 1525–2027.

Grütter, H. S.: 2009, Pyroxene xenocryst geotherms: Techniques and application, *Lithos* **112S**, 1167–1178.

Grütter, H. S., Apter, D. B. and Kong, J.: 1999, Crust-Mantle Coupling: Evidence from Mantle-Derived Xenocrystic Garnets., *in* J. J. Gurney, J. L.

Gurney, M. D. Pascoe and S. H. Richardson (eds), *Proceedings of the 7th International Kimberlite Conference, Cape Town, 1998*, Vol. 1, Red Roof Design, Cape Town, pp. 307–313.

Grütter, H. S., Gurney, J. J., Menzies, A. H. and Winter, F.: 2004, An updated classification scheme for mantle-derived garnet, for use by diamond explorers, *Lithos* **77 - Proceedings of the 8th International Kimberlite Conference**, 841–857.

Grütter, H. S., Latti, D. and Menzies, A. H.: 2006, Cr-saturation arrays in concentrate garnet compositions from kimberlite and their use in mantle barometry, *Journal of Petrology* **47**, 801–820.

Grütter, H. S. and Moore, R. O.: 2003, Pyroxene geotherms revisited - an empirical approach based on Canadian xenoliths, *Extended Abstracts of the 8th International Kimberlite Conference, Victoria* p. 272.

Grütter, H. S. and Quadling, K. E.: 1999, Can sodium in garnet be used to monitor eclogitic diamond potential?, *in* J. J. Gurney, J. L. Gurney, M. D. Pascoe and S. H. Richardson (eds), *Proceedings of the 7th International Kimberlite Conference, Cape Town, 1998*, Vol. 1, Red Roof Design, Cape Town, pp. 314–320.

Gurney, J. J.: 1984a, A correlation between garnets and diamonds in kimberlites, *Kimberlite occurrence and origin: A basis for conceptual models in exploration, Geology Department and University Extension, University of Western Australia, Publication 8*, Blackwell Scientific Publications, Perth, pp. 143–166.

Gurney, J. J., Harris, J. W., Rickard, R. and Moore, R.: 1985, Inclusions in Premier mine diamonds, *Transactions of the Geological Society of South Africa* **88**, 301–310.

Halls, H. C.: 1978, The late Precambrian Central North American Rift System - a survey of recent geological and geophysical investigations, *in* I. B. Ramberg and E. R. Neumann (eds), *Tectonics and Geophysics of Continental Rifts*, Reidel, Dordrecht, pp. 111–123.

Hamilton, M. A., Pearson, D. G., Stern, R. A. and Boyd, F. R.: 1998, Constraints on MARID petrogenesis: SHRIMP II U-Pb zircon evidence for preeruptive metasomatism at Kamfersdam, *Extended Abstracts of the 7th International Kimberlite Conference, Cape Town* pp. 296–298.

Hasterok, D. and Chapman, D. S.: 2011, Heat production and geotherms for the continental lithosphere, *Earth and Planetary Science Letters* **307**, 59–70.

Heaman, L. M., Easton, R. M., Hart, T. R., Hollings, P., MacDonald, C. A. and Smyk, M.: 2007, Further refinement to the timing of Mesoproterozoic magmatism, Lake Nipigon region, Ontario, *Canadian Journal of Earth Sciences* **44**, 1055–1086.

Heaman, L. M., Kjarsgaard, B. A. and Creaser, R. A.: 2004, The temporal evolution of North American kimberlites, *Lithos* **76**, 377–397.

Heaman, L. M. and Machado, N.: 1992, Timing and origin of midcontinent rift alkaline magmatism, North America: evidence from the Coldwell Complex, *Contributions to Mineralogy and Petrology* **110**, 289–303.

Herzberg, C., Condie, K. and Korenaga, K.: 2010, Thermal history of the Earth and its petrological expression, *Earth and Planetary Science Letters* **292**, 79–88.

Herzberg, C. and Rudnick, R.: 2012, Formation of cratonic lithosphere: An integrated thermal and petrological model, *Lithos* **149**, 4–15.

Herzberg, C. T.: 1999, Phase equilibrium constraints on the formation of cratonic mantle, *in* Y. Fei, C. M. Bertka and B. O. Mysen (eds), *Mantle Petrology: Field Observations and High Pressure Experimentation: a Tribute to Francis R. (Joe) Boyd*, The Geochemical Society, Special Publication, pp. 241–257.

Horan, M. F., Walker, R. J., Morgan, J. W., Grossman, J. N. and Rubin, A. E.: 2003, Highly siderophile elements in chondrites, *Chemical Geology* **196**, 5–20.

Hunt, L. C., Stachel, T., Grütter, H., Armstrong, J., McCandless, T. E., Simonetti, A. and Tappe, S.: 2012a, Small Mantle Fragments from the Renard Kimberlites, Quebec: Powerful Recorders of Mantle Lithosphere

Formation and Modification Beneath the Eastern Superior Craton, *Journal of Petrology* .

Ionov, D. A., Chanefo, I. and Bodinier, J. L.: 2005, Origin of Fe-rich lherzolites and wehrlites from Tok, SE Siberia by reactive melt percolation in refractory mantle peridotites, *Contributions to Mineralogy and Petrology* **150**(3), 335–353.

Ireland, T. J., Walker, R. J. and Garcia, M. O.: 2009, Highly siderophile element and Os-187 isotope systematics of Hawaiian picrites: implications for parental melt composition and source heterogeneity, *Chemical Geology* **260**, 112–128.

Irvine, G. J., Pearson, D. G. and Carlson, R. W.: 2001, Lithospheric mantle evolution in the Kaapvaal craton: a Re-Os isotope study of peridotite xenoliths from Lesotho kimberlites, *Geophysical Research Letters* **28**, 2505–2508.

Januszczak, N., Seller, M. H., Kurszlaukis, S., Murphy, C., Delgaty, J., Tappe, S., Ali, K., Zhu, J. and Ellemers, P.: 2013, A Multidisciplinary Approach to the Attawapiskat Kimberlite Field, Canada: Accelerating the Discovery-to-Production Pipeline, *Proceedings of the 10th International Kimberlite Conference* .

Jaques, A. L., Hall, A. E., Sheraton, J. W., Smith, C. B., Sun, S.-S., Drew, R. M., Foudoulis, C. and Ellingsen, K.: 1989, Composition of crystalline inclusions and C-isotopic composition of Argyle and Ellendale diamonds, *Proceedings of the 4th International Kimberlite Conference, Perth, 1986, Geological Society of Australia Special Publication*, Vol. 14, pp. 966–989.

Johnson, K. T. M. and Dick, H. J. B.: 1992, Open system melting and temporal and spatial variation of peridotite and basalt at the Atlantis II Fracture Zone, *Journal of Geophysical Research* **97**(B6), 9219–9241.

Jordan, T. H.: 1975, The continental tectosphere, *Reviews of Geophysics* **13**, 1–12.

Kamenetsky, V. S., Kamenetsky, M. B., Sobolev, A. V., Golovin, A. V., Demouchy, S., Faure, K., Sharygin, V. V. and Kuzmin, D. V.: 2008, Olivine in the udachnaya-east kimberlite (Yakutia, Russia): Types, compositions and origins, *Journal of Petrology* **49**(4), 823–839.

Kaminsky, F. V., Sablukov, S. M., Sablukova, L. I., Shchukin, V. S. and Canil, D.: 2002, Kimberlites from the Wawa area, Ontario, *Canadian Journal of Earth Sciences* **39**, 1819–1838.

Kelemen, P. B.: 1990a, Reaction between ultramafic rock and fractionating basaltic magma: I. Phase relations, the origin of calc-alkaline magma series, and the formation of discordant dunite, *Journal of Petrology* **31**, 51–98.

Kelemen, P. B., Dick, H. J. B. and Quick, J. E.: 1992, Formation of harzburgite by pervasive melt/rock reaction in the upper mantle, *Nature* **342**(6388), 635–641.

Kelemen, P. B., Hart, S. R. and Bernstein, S.: 1998, Silica enrichment in the continental upper mantle via melt/rock interaction, *Earth and Planetary Science Letters* **164**, 387–406.

Kennedy, C. S. and Kennedy, G. C.: 1976, The equilibrium boundary between graphite and diamond, *Journal of Geophysical Research* **81**, 2467 – 2470.

Kinzler, R. J. and Grove, T. L.: 1999, *Origin of Depleted Cratonic Harzburgite by Deep Fractional Melt Extractino and Shallow Olivine Cumulate Infusion*, Red Roof Design, Cape Town, pp. 437–443.

Konzett, J., Armstong, R. A. and Günther, D.: 2000, Modal metasomatism in the Kaapvaal craton lithosphere: constraints on timing and genesis from U-Pb zircon dating of metasomatized peridotites and MARID-type xenoliths, *Contributions to Mineralogy and Petrology* **139**, 704–719.

Kopylova, M. G., Afanasiev, V. P., Bruce, L. F., Thurston, P. C. and Ryder, J.: 2011, Metaconglomerate preserves evidence for kimberlite, diamondiferous root and medium grade terrane of a pre-2.7 Ga Southern Superior protocraton, *Earth and Planetary Science Letters* **312**, 213–225.

Korenaga, J.: 2008, Urey ratio and the structure and evolution of Earth's mantle, *Reviews of Geophysics* **46**(RG2007), doi:10.1029/2007RG000241.

Krogh, E.: 1988, The garnet-clinopyroxene Fe-Mg geothermometer - a reinterpretation of existing experimental data, *Contributions to Mineralogy and Petrology* **99**, 44–48.

Kubo, K.: 2002, Dunite Formation Processes in Highly Depleted Peridotite: Case study of the Iwanaidake Peridotite, Hokkaido, Japan, *Journal of Petrology* **43**(3), 423–448.

le Roex, A. P., Bell, D. R. and Davis, P.: 2003, Petrogenesis of group I kimberlites from Kimberley, South Africa: Evidence from bulk-rock geochemistry, *Journal of Petrology* **44**(12), 2261–2286.

Li, C., Barnes, S. J., Makovicky, E., Rose-Hansen, J. and Makovicky, M.: 1996, Partitioning of Ni, Cu, Ir, Rh, Pt and Pd between monosulphide solid solution and sulphide liquid: effects of compositions and temperature, *Geochimica et Cosmochimica Acta* **60**, 1231–1238.

Li, C. and Ripley, E. M.: 2005, Empirical equations to predict the sulfur content of mafic magmas at sulfide saturation and applications to magmatic sulfide deposits, *Mineralium Deposita* **40**, 218–230.

Liu, J., Carlson, R. W., Rudnick, R. L., Walker, R. J., Gao, S. and Wu, F.: 2012, Comparitive Sr-Nd-Hf-Os-Pb isotope systematics of xenolithic peridotites from Yangyuan, North China Craton: Additional evidence for a Paleoproterozoic age, *Chemical Geology* **332-333**, 1–14.

Liu, J., Rudnick, R. L., Walker, R. J., Gao, S., yuan Wu, F., Piccoli, P. M., Yuan, H., liang Xu, W. and Xu, Y.-G.: 2011, Mapping lithospheric boundaries using Os isotopes of mantle xenoliths: An example from the North China Craton, *Geochimica et Cosmochimica Acta* **75**(13), 3881–3902.

Lorand, J. P., Alard, O. and Godard, M.: 2009, Platinum-group element signature of the primitive mantle rejuvenated by melt-rock reactions: evidence from Sumail peridotites (Oman Ophiolite), *Terra Nova* **21**, 35–40.

Lorand, J. P., Keays, R. R. and Bodinier, J. L.: 1993, Copper and noble metal across the lithosphere-asthenosphere boundary of mantle diapirs: evidence from the Lanzo lherzolite massif, *Journal of Petrology* **34**, 1111–1140.

Ludwig, K. R.: 1991, ISOPLOT: A Plotting and Regression Program for Radiogenic-isotope Data, *US Geological Survey Open File Report* p. 39.

Luguet, A., Lorand, J. P., Alard, O. and Cottin, J.-V.: 2004, A multi-technique study of platinum group element systematic in some Ligurian ophiolitic peridotites, Italy, *Chemical Geology* **208**, 175–194.

Luguet, A., Lorand, J. P. and Seyler, M.: 2003, Sulfide petrology and highly siderophile element geochemistry of abyssal peridotites: A coupled study of samples from the Kane Fracture Zone (45 °W 23 °20N, MARK Area, Atlantic Ocean), *Geochimica et Cosmochimica Acta* **67**(8), 1553–1570.

Maier, W. D., Peltonen, P., McDonald, I., Barnes, S. J., Hatton, C. and Viljoen, F.: 2012, The concentration of platinum-group elements and gold in southern African and Karelian kimberlite-hosted mantle xenoliths: Implications for the noble metal content of the Earth's mantle, *Chemical Geology* **302-303**, 119–135.

Mather, K. A., Pearson, D. G., McKenzie, D., Kjarsgaard, B. A. and Priestley, K.: 2011, Constraints on the depth and thermal history of cratonic lithosphere from peridotite xenoliths, xenocrysts and seismology, *Lithos* **125**, 729–742.

Matveev, S. and Ballhaus, C.: 2002, Role of water in the origin of podiform chromite deposits, *Earth and Planetary Science Letters* **203**, 235–243.

Matveev, S. and Stachel, T.: 2009, Evaluation of kimberlite diamond potential using MR spectroscopy of xenocrystic olivine, *Lithos* **112**, 36–40.

McCammon, C., Griffin, W. L., Shee, S. R. and O'Neill, H. S. C.: 2001, Oxidation during metasomatism in ultramafic xenoliths from the Wesselton kimberlite, South Africa: implications for the survival of diamond, *Contributions to Mineralogy and Petrology* **141**, 287–296.

McCandless, T. E. and Gurney, J. J.: 1989, Sodium in garnet and potassium in clinopyroxene: criteria for classifying mantle eclogites, *Proceedings of the 4th International Kimberlite Conference, Perth, 1986, Geological Society of Australia Special Publication* **14**(2), 827–832.

McKenzie, D. and Bickle, M. J.: 1988, The volume and composition of melt generated by extension of the lithosphere, *Journal of Petrology* **29**, 625–679.

McKenzie, D., Jackson, J. and Priestley, K.: 2005, Thermal structure of oceanic and continental lithosphere, *Earth and Planetary Science Letters* **233**, 337–349.

Menzies, A. H., Shirey, S. B., Carlson, R. W. and Gurney, J. J.: 1999, Re-Os systematics of Newlands peridotite xenoliths: implications for diamond and lithosphere formation, *in* J. J. Gurney, J. L. Gurney, M. D. Pascoe and S. H. Richardson (eds), *Proceedings of the 7th International Kimberlite Conference*, Red Roof Design, Cape Town, pp. 566–583.

Miller, C. E., Kopylova, M. G. and Ryder, J.: 2012, Vanished diamondiferous cratonic root beneath the Southern Superior province: evidence from diamond inclusions in the Wawa metaconglomerate, *Contributions to Mineralogy and Petrology* **164**(4), 697–714.

Mungall, J. E., Andrews, D. R. A., Cabri, L. J., Sylvester, P. J. and Turbrett, M.: 2005, Partitioning of Cu, Ni, Au, and platinum-group elements between monosulphide solid solution and sulphide melt under controlled oxygen and sulphur fugacities, *Geochimica et Cosmochimica Acta* **69**, 4349–4360.

Navon, O. and Stolper, E.: 1987, Geochemical consequences of melt percolation: the upper mantle as a chromatographic column, *The Journal of Geology* **95**(3), 285–307.

Nickel, K. G. and Green, D. H.: 1985, Empirical geothermobarometry for garnet peridotites and implications for the nature of the lithosphere, kimberlites and diamonds., *Earth and Planetary Science Letters* **73**, 158–170.

Nielsen, T. F. D., Jensen, S. M., Secher, K. and Sand, K. K.: 2009, Distribution of kimberlite and aillikite in the Diamond Province of southern West Greenland: A regional perspective based on groundmass mineral chemistry and bulk compositions, *Lithos* **112**, 358–371.

Nimis, P.: 1998, Evaluation of diamond potential from the composition of peridotitic chromian diopside, *European Journal of Mineralogy* **10**, 505–519.

Nimis, P.: 2002, The pressures and temperatures of formation of diamond based on thermobarometry of chromian diopside inclusions, *The Canadian Mineralogist* **40**, 871–884.

Nimis, P. and Grütter, H.: 2009, Internally consistent geothermometers for garnet peridotites and pyroxenites, *Contributions to Mineralogy and Petrology* **159**(3), 411–427.

Nimis, P. and Taylor, W. R.: 2000, Single clinopyroxene thermobarometry for garnet peridotites. Part I. Calibration and testing of a Cr-in-Cpx barometer and an enstatite-in-Cpx thermometer, *Contributions to Mineralogy and Petrology* **139**, 541–554.

O'Neill, H. S. C.: 1981, The transition between spinel lherzolite and garnet lherzolite, and its use as a geobarometer, *Contributions to Mineralogy and Petrology* **77**, 185–194.

Paces, J. B. and Miller, J. D.: 1993, Precise U-Pb ages of Duluth Complex and related mafic intrusions, northeastern Minnesota: geochronological insights to physical, petrogenetic, paleomagnetic and tectonomagmatic processes associated with the 1.1 Ga Midcontinent Rift System, *Journal of Geophysical Research* **98**, 13997–14013.

Patterson, M., Francis, D. and McCandless, T.: 2009, Kimberlites: Magmas or mixtures?, *Lithos* **112**, 191–200.

Peach, C. I., Mathez, E. A., Keays, R. R. and Reeves, S. J.: 1994, Experimentally determined sulphide melt-silicate melt partition co-efficients for iridium and platinum, *Chemical Geology* **117**, 361–377.

Pearson, D. G., Canil, D. and Shirey, S. B.: 2003, Mantle Samples Included in Volcanic Rocks: Xenoliths and Diamonds, *Treatise on Geochemistry* **2**, 171–275.

Pearson, D. G., Carlson, R. W., Shirey, S. B., Boyd, F. R. and Nixon, P. H.: 1995, Stabilisation of Archaean lithospheric mantle: A Re-Os isotope study of peridotite xenoliths from the Kaapvaal Craton, *Earth and Planetary Science Letters* **134**(3-4), 341–357.

Pearson, D. G., Irvine, G. J., Ionov, D. A., Boyd, F. R. and Dreibus, G. E.: 2004, Re-Os isotope systematics and platinum group element fractionation during mantle melt extraction: a study of massif and xenolith peridotite suites, *Chemical Geology* **208**, 29–59.

Pearson, D. G., Meyer, H. O. A., Boyd, F. R., Shirey, S. B. and Carlson, R. W.: 1997, Re-Os isotope evidence for late Archaean stabilisation of a thick lithospheric mantle keel beneath the Kirkland Lake area, Superior Province, Canada. Further evidence for long-term crust-mantle coupling, *Russian Geology and Geophysics, Special Issue: Proceedings of the 6th International Kimberlite Conference* **2**, 427–429.

Pearson, D. G., Parman, S. W. and Nowell, G. M.: 2007, A link between large mantle melting events and continent growth seen in osmium isotopes, *Nature* **449**, 202–205.

Pearson, D. G. and Wittig, N.: 2008, Formation of Archaean continental lithosphere and its diamonds: the root of the problem, *Journal of the Geological Society, London* **165**, 1–20.

Pearson, D. G. and Woodland, S. J.: 2000, Solvent extraction / anion exchange separation and determination of PGEs (Os, Ir, Pt, Pd, Ru) and Re-Os isotopes in geological samples by isotope dilution ICP-MS, *Chemical Geology* **165**, 87–107.

Peslier, A. H., Woodland, A. B., Bell, D. R. and Lazarov, M.: 2010, Olivine water contents in the continental lithosphere and the longevity of cratons, *Nature* **467**, 78–U108.

Peslier, A. H., Woodland, A. B., Bell, D. R., Lazarov, M. and Lapen, T. J.: 2012, Metasomatic control of water contents in the Kaapvaal cratonic mantle, *Geochimica et Cosmochimica Acta* **97**, 213–246.

Puchtel, I. S., Humayun, M., Campbell, A. J., Sproule, R. A. and Lesher, C. M.: 2004, Platinum group element geochemistry of komatiites from the Alexo and Pyke Hill areas, Ontario, Canada, *Geochimica et Cosmochimica Acta* **68**(6), 1361–1383.

Queen, M., Heaman, L. M., Hanes, J. A., Archibald, D. A. and Farrar, E.: 1996, $^{40}Ar/^{39}Ar$ phlogopite and U-Pb perovskite dating of lamprophyre dykes from the eastern Lake Superior region: evidence for a 1.14 Ga magmatic precursor to Midcontinent Rift volcanism, *Canadian Journal of Earth Sciences* **33**, 958–965.

Quick, J. E.: 1981, The Origin and Significance of Large, Tabular Dunite Bodies in the Trinity Peridotite, Northern California, *Contributions to Mineralogy and Petrology* **78**, 413–422.

Quick, J. E. and Gregory, R. T.: 1995, Significance of Melt-Wall Rock Reaction: A Comparitive Anatomy of Three Ophiolites, *Journal of Geology* **103**, 187–198.

Ramsay, R. R.: 1995, *Geochemistry of diamond indicator minerals*, PhD thesis, University of Western Australia, Perth.

Ramsay, R. R. and Tompkins, L. A.: 1994, The geology, heavy mineral concentrate mineralogy, and diamond prospectivity of the Boa Esperanca and Cana Verde pipes, Corrga D'anta, Minas Gerais, Brazil, *in* H. O. A. Meyer and O. H. Leonardos (eds), *Diamonds: Characterization, Genesis and Exploration. Proceedings of the 5th International Kimberlite Conference, Brazil, 1991*, pp. 329–345.

Rehfeldt, T., Foley, S. F., Jacob, D. E., Carlson, R. W. and Lowry, D.: 2008, Contrasting types of metasomatism in dunite, wehrlite and websterite xenoliths from Kimberley, South Africa, *Geochimica et Cosmochimica Acta* **72**, 5722–5756.

Rehkämper, M., Halliday, A. N., Alt, J., Fitton, J. G., Zipfel, J. and Takazawa, E.: 1999, Non-chondritic platinum-group element ratios in oceanic mantle lithosphere: petrogenetic signature of melt percolation?, *Earth and Planetary Science Letters* **172**, 65–81.

Richardson, S. H., Gurney, J. J., Erlank, A. J. and Harris, J. W.: 1984, Origin of diamonds in old enriched mantle, *Nature* **310**, 198–202.

Richardson, S. H. and Harris, J. W.: 1997, Antiquity of peridotitic diamonds from the Siberian craton, *Earth and Planetary Science Letters* **151**, 271–277.

Richardson, S. H., Harris, J. W. and Gurney, J. J.: 1993, Three generations of diamond from old continental mantle, *Nature* **366**, 256–258.

Richardson, S. H., Pöml, P. F., Shirey, S. B. and Harris, J. W.: 2009, Age and origin of peridotitic diamonds from Venetia, Limpopo Belt, Kaapvaal-Zimbabwe Craton, *Lithos* **112S - Proceedings of the 9th International Kimberlite Conference**, 785–792.

Robinson, J. A. C. and Wood, B. J.: 1998, The depth of the garnet/spinel transition in fractionally melting peridotite, *Earth and Planetary Science Letters* **164**, 277–284.

Rogers, N.: 2002, Whole-rock chemical analyses from the Birch-Uchi greenstone belt, Superior Province, *Geological Survey of Canada, Open File* **4271**.

Roy-Barman, M. and Allègre, C. J.: 1994, $^{187}Os/^{186}Os$ ratio of mid-ocean ridge basalts and abyssal peridotites, *Geochimica et Cosmochimica Acta* **58**(22), 5043–5054.

Rudnick, R. L., McDonough, W. F. and O'Connell, R. H.: 1998, Thermal structure, thickness and composition of continental lithosphere, *Chemical Geology* **145**, 395–411.

Rudnick, R. L., McDonough, W. F. and Orpin, A.: 1994, Northern Tanzanian peridotite xenoliths: A comparison with Kaapvaal peridotites and inferences on metasomatic interactions, *in* H. Meyer and O. Leonardos (eds), *Kimberlites, Related Rocks and Mantle Xenoliths. Proceedings of the 5th International Kimberlite Conference, Brazil, 1991*, Brazil Companhia de Pesquisa de Recursos Minerais, pp. 336–353.

Rudnick, R. L. and Nyblade, A. A.: 1999, The thickness and heat production of Archaean lithosphere: constraints from xenolith thermobarometry and surface heat flow, *in* Y. Fei, C. Bertka and B. Mysen (eds), *Mantle Petrology: Field Observations and High Pressure Experimentation: a Tribute to Francis R. (Joe) Boyd*, Vol. 6, The Geochemical Society, Houston, pp. 3–12.

Sage, R. P.: 2000, Kimberlites of the Attawapiskat area, James Bay Lowlands, northern Ontario, *Ontario Geological Survey, Open File Report* **6019**(341), 341.

Sattari, P., Brenan, J. M., Horn, I. and McDonough, W. F.: 2002, Experimental constraints on the sulphide-and chromite-silicate melt partitioning of rhenium and platinum-group elements, *Economic Geology* **97**, 385–398.

Schaeffer, A. J. and Lebedev, S.: 2013, Global shear speed structure of the upper mantle, *Geophysics Journal International* **submitted**.

Schmitz, M. D., Bowring, S. A., de Wit, M. J. and Gartz, V.: 2004, Subduction and terrane collisions stabilize the western Kaapvaal craton tectosphere 2.9 billion years ago, *Earth and Planetary Science Letters* **222**, 363–376.

Scully, K. R.: 2000, *Mantle xenoliths from the Attawapiskat kimberlite field*, Master's thesis, University of Toronto.

Scully, K. R., Canil, D. and Schulze, D. J.: 2004, The lithospheric mantle of the Archean Superior Province as imaged by garnet xenocryst geochemistry, *Chemical Geology* **207**, 189–221.

Shimizu, N., Sobolev, N. V. and Yefimova, E. S.: 1997, Chemical heterogeneity of garnet inclusions and juvenility of peridotite diamonds from Siberia, *Geologiya i Geofizika* **38**(2), 337–352.

Shirey, S. B.: 1997, Re-Os isotopic compositions of Midcontinent rift system picrites: implications for plume-lithosphere interaction and enriched mantle sources, *Canadian Journal of Earth Sciences* **34**, 489–503.

Shirey, S. B. and Walker, R. J.: 1995, Carius tube digestions for low-blank rhenium-osmium analysis, *Analytical Chemistry* **67**, 2136–2141.

Simon, N., Carlson, R. W., Pearson, D. G. and Davies, G. R.: 2007, The origin and evolution of the Kaapvaal cratonic lithospheric mantle, *Journal of Petrology* **48**, 589–625.

Simon, N. S. C., Irvine, G. J., Davies, G. R., Pearson, D. G. and Carlson, R. W.: 2003, The origin of garnet and clinopyroxene in "depleted" Kaapvaal peridotites, *Lithos* **71**, 289–322.

Sinyakova, E. F., Kosyakov, V. I. and Kolonin, G. R.: 2001, Behaviour of PGE on the cross-section of melts in the system Fe-Ni-S, *Russian Journal of Geology and Geophysics* **42**, 1287–1304.

Skulski, T., Corkery, M. T., Stone, D., Whalen, J. B. and Stern, R. A.: 2000, Geological and geochronological investigations in the Stull Lake - Edmund Lake greenstone belt and granitoid rocks of the northwestern Superior Province, *Report of Activities 2000, Manitoba Industry, Trade and Mines*, Manitoba Geological Survey, pp. 117–128.

Smart, K. A., Heaman, L. M., Chacko, T., Simonetti, A., Kopylova, M., Mah, D. and Daniels, D.: 2009, The origin of high-MgO diamond eclogites from the Jericho Kimberlite, Canada, *Earth and Planetary Science Letters* **284**, 527–537.

Smit, K. V., Shirey, S. B., Richardson, S. H., le Roex, A. P. and Gurney, J. J.: 2010, Re-Os isotopic composition of peridotitic sulphide inclusions in diamonds from Ellendale, Australia: Age constraints on Kimberley cratonic lithosphere, *Geochimica et Cosmochimica Acta* **74**(11), 3292–3306.

Sobolev, N. V.: 1977, *Deep Seated Inclusions in Kimberlites and the Problems of the Composition of the Upper Mantle (translated by D.A. Brown)*, American Geophysical Union, Washington, D.C.

Sobolev, N. V., Logvinova, A. M., Zedgenizov, D. A., Pokhilenko, N. P., Kuzmin, D. V. and Sobolev, A. V.: 2008, Olivine inclusions in Siberian diamonds: high-precision approach to minor elements, *European Journal of Mineralogy* **20**, 305–315.

Sobolev, N. V., Pokhilenko, N. P., Grib, V. P., Skripnichenko, V. A. and Titova, V. E.: 1992, Specific composition and conditions of formation of deep-seated minerals in explosion pipes of the Onega Peninsula and kimberlites of the Zimnii Coast in the Arkhangelsk province, *Soviet Geology and Geophysics* **33**(10), 71–78.

Stachel, T., Aulbach, S., Brey, G. P., Harris, J. W., Leost, I., Tappert, R. and Viljoen, K. S.: 2004, The trace element composition of silicate inclusions in diamonds: a review, *Lithos* **77**, 1–20.

Stachel, T. and Harris, J. W.: 2008, The origin of cratonic diamonds - constraints from mineral inclusions, *Ore Geology Reviews* **34**(1-2), 5–32.

Stachel, T., Harris, J. W. and Brey, G. P.: 1998, Rare and unusual mineral inclusions in diamonds from Mwadui, Tanzania, *Contributions to Mineralogy and Petrology* **132**, 34–47.

Sun, S.-S. and McDonough, W. F.: 1989, Chemical and isotopic systematics of oceanic basalts: implications for mantle compositions and processes., *in* A. D. Saunders and M. J. Norry (eds), *Magmatism in the ocean basins*, Geological Society, London, pp. 313–345.

Tappe, S., Foley, S. F., Genner, G. A., Heaman, L. M., Kjarsgaard, B. A., Romer, R. L., Stracke, A., Joyce, N. and Hoefs, J.: 2006, Genesis of ultramafic lamprophyres and carbonatites at Ailik Bay, Labrador: A consequence of incipient lithospheric thinning beneath the North Atlantic craton, *Journal of Petrology* **47**(7), 1261–1315.

Tappert, R., Stachel, T., Harris, J. W., Muehlenbachs, K., Ludwig, T. and Brey, G. P.: 2005, Diamonds from Jagersfontein (South Africa): messengers from the sublithospheric mantle, *Contributions to Mineralogy and Petrology* **150**(5), 505–522.

Taylor, W. R.: 1998, An experimental test of some geothermometer and geobarometer formulations for upper mantle peridotites with application to the thermobarometry of fertile lherzolite and garnet websterite, *Neues Jahrbuch Mineralogie Abhandlungen* **172**, 381–408.

Trønnes, R. G., Canil, D. and Wei, K. J.: 1992, Element partitioning between silicate minerals and coexisting melts at pressures of 1-27 GPa, and implications for mantle evolution, *Earth and Planetary Science Letters* **111**(2-4), 241–255.

van Achterbergh, E., Ryan, C., Jackson, S. and Griffin, W.: 2001, Appendix 3 Data reduction software for LA-ICP-MS, *in* P. Sylvester (ed.), *Laser-Ablation-ICPMS in the Earth Sciences*, Vol. 29, Mineralogical Association of Canada Short Course, pp. 239–243.

van Acken, D., Becker, H. and Walker, R. J.: 2008, Refertilization of Jurassic oceanic peridotites from the Tethys Ocean - Implications for the Re-Os systematics of the upper mantle, *Earth and Planetary Science Letters* **268**(1-2), 171–181.

van Acken, D., Becker, H., Walker, R. J., McDonough, W. F., Wombacher, F., Ash, R. D. and Piccoli, P. M.: 2010, Formation of pyroxenite layers in the Totalp ultramafic massif (Swiss Alps) - Insights from highly siderophile elements and Os isotopes, *Geochimica et Cosmochimica Acta* **74**(2), 661–683.

van Schmus, W. R. and Hinze, W. J.: 1985, The Midcontinent Rift System, *Annual Review of Earth and Planetary Sciences* **13**, 345–383.

Walker, R. J., Horan, M. F., Morgan, J. W., Becker, H., Grossman, J. N. and Rubin, A. E.: 2002, Comparative ^{187}Re-^{187}Os systematics of chondrites: Implications regarding early solar system processes, *Geochimica et Cosmochimica Acta* **66**(23), 4187–4201.

Walter, M. J.: 1998, Melting of Garnet Peridotite and the Origin of Komatiite and Depleted Lithosphere, *Journal of Petrology* **39**(1), 29–60.

Warren, J. M. and Shimizu, N.: 2010, Cryptic variations in Abyssal Peridotite Compositions: Evidence for Shallow-level Melt Infiltration in the Oceanic Lithosphere, *Journal of Petrology* **51**(1/2), 395–423.

White, W. S.: 1972, Keweenawan flood basalts and continental rifting, *Geological Association of America, Abstracts with Programs* **4**, 732–734.

Wittig, N., Pearson, D. G., Duggen, S., Baker, J. A. and Hoernle, K.: 2010, Tracing the metasomatic and magmatic evolution of continental mantle roots with Sr, Nd, Hf and Pb isotopes: A case study of Middle Atlas (Morocco) peridotite xenoliths, *Geochimica et Cosmochimica Acta* **74**, 1417–1435.

Wittig, N., Pearson, D., Webb, M., Ottley, C., Irvine, G., Kopylova, M., Jensen, S. and Nowell, G.: 2008, Origin of cratonic lithospheric mantle roots: A geochemical study of peridotites from the North Atlantic Craton, West Greenland, *Earth and Planetary Science Letters* **274**, 24–33.

Wold, R. J. and Hinze, W. J.: 1982, Geology and Tectonics of the Lake Superior basin, *Geological Association of America Memoirs* **156**, 280.

Yang, J.-H., O'Reilly, S. Y., Walker, R. J., Griffin, W., Wu, F.-Y., Zhang, M. and Pearson, N. J.: 2010, Diachronous decratonization of the Sino-Korean craton: Geochemistry of mantle xenoliths from North Korea, *Geology* **38**(9), 799–802.

Yaxley, G. M. and Green, D. H.: 1998, Reactions between eclogite and peridotite: mantle refertilisation by subduction of oceanic crust, *Schweizer Mineralogische und Petrographische Mitteilungen* **78**, 243–255.

Zartman, R. E., Kempton, P. D., Paces, J. B., Downes, H., Williams, I. S., Dobosi, G. and Futa, K.: 2013, Lower-Crustal Xenoliths from Jurassic Kimberlite Diatremes, Upper Michigan (USA): Evidence for Proterozoic Orogenesis and Plume Magmatism in the Lower Crust of the Southern Superior Province, *Journal of Petrology* **54**(3), 575–608.

Chapter 6

Conclusions

6.1 Composition of the SCLM below the Attawapiskat area

Similar to the results in Sage (2000) and Scully (2000), Victor xenocrysts analysed during this study are predominantly lherzolitic (G9 garnets, clinopyroxene and orthopyroxene), however, more depleted compositions are also present. One population of Victor olivine xenocrysts has high Mg# from 92.0 up to 93.6, indicating their origin from highly depleted harzburgite to dunite, comparable to many xenoliths from Delta, as well as the nearby Kyle Lake kimberlites (Sage, 2000). A second population of Victor olivine xenocrysts with lower Mg# around 89-90, likely represent melt infiltration into the SCLM. Attawapiskat has a higher proportion of eclogite and pyroxenite, in both the xenocrysts and xenoliths, than the lithosphere sampled by the Kyle Lake kimberlites (Sage, 2000).

6.2 Formation of the western Superior SCLM

Shallow versus deep melting

High Cr# in garnet and positive slopes in depleted garnet $HREE_N$ indicate that initial melting to form the proto-cratonic root must have occurred in both the garnet and spinel stability fields, similar to fractional polybaric melting occuring at modern mid-ocean ridges (e.g., Kelemen et al., 1998; Stachel et al., 1998). This rules out plume subcretion processes (e.g., Boyd, 1989; Arndt et al., 1998; Aulbach, 2012) as a viable mechanism for Superior lithosphere formation. High degrees of partial melting ($\sim$40%) are indicated by olivines with high Mg# up to 93.6, resulting in harzburgitic to dunitic residues (e.g., Kubo, 2002; Bernstein et al., 2007).

Age of the lithosphere

T_{RD} ages of 3.7 ± 0.5 Ga and 3.6 ± 0.1 Ga in sulphides or PGE inclusions in olivine, require the existence of a depleted mantle reservoir beneath the Attawapiskat area since at least the Palaeoarchaean. These ages do not correspond to crustal ages in the North Caribou superterrane, which are <3.0 Ga (e.g., Thurston et al., 1991; Stevenson, 1995); however they correspond with gneisses in the Pikwitonei domain of the Northern Superior superterrane that were dated to about 3.6 Ga (Böhm et al., 2000; Skulski et al., 2000). Since the Attawapiskat kimberlites erupt near the boundary of the North Caribou and Northern Superterranes (Figure 2.1), these Palaeoarchaean ages in Attawapiskat peridotites support the notion that these kimberlites mainly sampled lithospheric mantle from the Northern Superior superterrane.

Role of eclogites in SCLM formation

The low-Mg eclogites have a shallow origin as plagioclase-bearing protoliths likely in former oceanic crust. This is supported by their generally flat MREE to HREE compositions, the presence of kyanite and a positive Eu anomaly in the high-Ca sample, and $\delta^{18}O$ values in three low-Mg eclogites that are higher than the pristine mantle value. The origin of these eclogites as oceanic crust requires that they were emplaced into the SCLM by subduction, in general agreement with seismic studies in the western Superior (White et al., 2003; Musacchio et al., 2004) that image dipping subducting slabs into the lower crust and upper mantle. Moreover, there is abundant evidence from crustal geology that suggests subduction - accretion processes and associated arc magmatism contributed to the amalgamation of the western Superior craton (see references in Chapter 2), similar to mechanisms for craton formation and stabilisation advocated by Helmstaedt and Schulze (1989) and Pearson and Wittig (2008).

The radiogenic $^{187}Os/^{188}Os$ of the majority of eclogites - similar to Archaean komatiites and basalts - requires long term isolation of a high Re/Os component from the convecting mantle after melt extraction. A Neoarchaean age for the formation of these eclogites is therefore likely, consistent with the timing of ~2.7 Ga subduction and amalgamation of the Superior craton (e.g., Langford and Morin, 1976) and $\sim$ 2.8-2.6 Ga U-Pb crystallisation ages for lower crustal granulite xenoliths from Atttawapiskat (Moser et al., 1997), which may be the lower grade metamorphic equivalent to the low-Mg eclogites (e.g., Green and Ringwood, 1972; Toft et al., 1989).

Impact of subduction on the SCLM
Partial melting of the low-Mg eclogites and interaction of these melts with overlying peridotite in the mantle wedge resulted in the formation of the high-Mg eclogites and pyroxenites. Their bulk compositions, $LREE_N$-enriched trace element patterns and in particular, occurrence of unradiogenic $^{187}Os/^{188}Os$ (less than the $^{187}Os/^{188}Os$ of O-chondrites = 0.1283; Walker et al., 2002), are consistent with formation by reaction of broadly siliceous melts (generated from the melting of low-Mg eclogites) with depleted peridotite.

T_{RD} ages of $\sim$2.7 Ga are preserved in two samples that have residual PGE_N patterns, which indicates that additional melting occurred at this time, likely corresponding to subduction events, similar to that inferred for samples from the Kaapvaal craton (see references in Section 5.10). Hydrous melts infiltrating the overlying mantle also, in some cases, introduced radiogenic Os. While these results indicate that some melt / fluid percolation into the overlying mantle took place as a result of subduction, this was not sufficient to lead to craton destruction, as suggested for the North China craton (e.g., Peng et al., 1986; Ling et al., 2013).

6.3 Impact of the Midcontinent Rift

In the Attawapiskat area, the thermal impact of the Midcontinent Rift is seen in the elevated palaeogeotherm derived for the 1.1 Ga Kyle Lake kimberlite (Figure 4.8). Some diamond destruction must have occurred in response to thermal impact of the rift and is indicated by extreme narrowing of the diamond window at 1.1 Ga and high mantle residence temperatures recorded in T1 diamonds. These diamonds also preserve evidence for platelet degradation, which typically occurs due to thermal pulses and / or deformation events in the SCLM (Woods, 1986), and may relate to the Midcontinent Rift, which affected the Superior craton around the time of kimberlite eruption.

In the Delta peridotite xenoliths, there is evidence that magmas related to the Midcontinent Rift interacted with variably depleted peridotite. This led to P-PGE-enrichment and T_{RD} ages ranging between 1.6 and 1.4 ± 0.2 Ga. These melts did not overprint the lithosphere though, and older depleted domains are preserved (e.g., depleted sinusoidal garnets). In particular, it is significant that the trace element compositions of calculated equilibrium melts from neither garnet or clinopyroxene (Victor xenocrysts) are similar to that of Midcontinent Rift basalts.

6.4 Diamonds in the Attawapiskat lithosphere

Diamond-stable conditions were prevalent in the lithospheric mantle after the thermal impact of the rift subsided, i.e., during the Jurassic when the Attawapiskat kimberlites erupted. This is indicated in the thick lithosphere of about 200 km, with a large diamond window of 80 km, compared to the PT conditions prevalent in the Mesoproterozoic at the nearby Kyle Lake kimberlites.

The ^{13}C-depleted composition for one diamond from U2 indicates an eclogitic or pyroxenitic paragenesis. The strong mode around -5.7 ‰ for the main population at U2, however, may represent both peridotitic and eclogitic parageneses, as also suggested by the compositions of Victor garnet xenocrysts. Lherzolitic garnets have diamond-favourable compositions, in both their MnO contents and their sinusoidal REE_N patterns, which are typical for harzburgitic and lherzolitic garnet inclusions in diamonds worldwide (e.g., Stachel et al., 2004). These results are consistent with the high proportion of Victor diamond-stable peridotitic garnets reported in Januszczak et al. (2013). Additionally, high Na content in several high Mg pyroxenitic garnet xenocrysts from Victor can be taken as strong indication of their derivation from diamond-stable portions of the lithosphere.

These results are contrary to the prevalent mindset in diamond exploration that depleted harzburgitic compositions need to be present in order for a diamondiferous kimberlite to be productive (e.g., Sobolev, 1977; Gurney, 1984a). However, this study clearly shows that diamondiferous kimberlites sampling lherzolitic compositions should not be overlooked.

Diamonds sampled at Attawapiskat likely formed after the Midcontinent Rift, as indicated by their low degrees of nitrogen aggregation compared to diamonds from the Mesoproterozoic T1 kimberlite. The overall $\delta^{13}C$ distribution for U2 diamonds is distinct to T1 diamonds (and other Superior diamond sources), further suggesting that U2 diamonds are not related to the older pre-rift diamonds.

Diamond growth after a major tectonothermal event is not unique to the Superior. Examples from other cratons are Premier and Venetia on the Kaapvaal craton, where lherzolitic diamond formation (1.93 Ga and 2.0 Ga, respectively; Richardson et al., 1993, 2009) post-date magmatism of the Bushveld Igneous Complex at ∼2.05 Ga. At Artemisia in the northern Slave craton, diamonds were sampled at ∼616 Ma (U-Pb perovskite; Armstrong et al., 2012), after the plume impact associated with the MacKenzie large igneous province (∼1.27 Ga; LeCheminant and Heaman, 1989). The lherzolitic diamond population at Ellendale on the Kimberley craton has an age of ∼1.4 Ga, younger and unrelated to Archaean craton formation (Graham et al., 1999; Luguet et al., 2009; Smit et al., 2010) and likely associated with later reworking events in the lithospheric mantle.

References

Armstrong, J. P., Fitzgerald, C. E., Kjarsgaard, B. A., Heaman, L. and Tappe, S.: 2012, Kimberlites of the Coronation Gulf Field, Northern Slave Craton, Nunavut Canada, *10th International Kimberlite Conference Extended Abstracts* (170).

Arndt, N., Ginibre, C., Chauvel, C., Albarede, F., Cheadle, M., Herzberg, C., Jenner, G. and Lahaye, Y.: 1998, Were komatiites wet?, *Geology* **26**(8), 739–742.

Aulbach, S.: 2012, Craton nucleation and formation of thick lithospheric roots, *Lithos* **149**, 16–30.

Bernstein, S., Kelemen, P. B. and Hanghøj, K.: 2007, Consistent olivine Mg# in cratonic mantle reflects Archean mantle melting to the exhaustion of orthpyroxene, *Geology* **35**(5), 459–462.

Böhm, C. O., Heaman, L. M., Creaser, R. A. and Crockery, M. T.: 2000, Discovery of pre-3.5 Ga exotic crust at the northwestern Superior Province margin, Manitoba, *Geology* **28**(1), 75–78.

Boyd, F. R.: 1989, Compositional distinction between oceanic and cratonic lithosphere, *Earth and Planetary Science Letters* **96**, 15–26.

Graham, S., Lambert, D. D., Shee, S. R., Smith, C. B. and Reeves, S.: 1999, Re-Os isotopic evidence for Archean lithospheric mantle beneath the Kimberley block, Western Australia, *Geology* **27**(5), 431–434.

Green, D. H. and Ringwood, A. E.: 1972, A Comparison of Recent Experimental Data on the Gabbro-Garnet Granulite-Eclogite Transition, *Journal of Geology* **80**, 277–288.

Gurney, J. J.: 1984a, A correlation between garnets and diamonds in kimberlites, *Kimberlite occurrence and origin: A basis for conceptual models in exploration, Geology Department and University Extension, University of Western Australia, Publication 8*, Blackwell Scientific Publications, Perth, pp. 143–166.

Helmstaedt, H. and Schulze, D. J.: 1989, Southern African kimberlites and their mantle sample: implications for Archaean tectonics and lithosphere evolution, *Kimberlites and Related Rocks I: Their Composition, Occurrence, Origin and Emplacement. Proceedings of the 4th International Kimberlite Conference, Perth 1986. Geological Society of Australia Special Publication 14.*, pp. 358–368.

Januszczak, N., Seller, M. H., Kurszlaukis, S., Murphy, C., Delgaty, J., Tappe, S., Ali, K., Zhu, J. and Ellemers, P.: 2013, A Multidisciplinary Approach to the Attawapiskat Kimberlite Field, Canada: Accelerating the Discovery-to-Production Pipeline, *Proceedings of the 10th International Kimberlite Conference* .

Kelemen, P. B., Hart, S. R. and Bernstein, S.: 1998, Silica enrichment in the continental upper mantle via melt/rock interaction, *Earth and Planetary Science Letters* **164**, 387–406.

Kubo, K.: 2002, Dunite Formation Processes in Highly Depleted Peridotite: Case study of the Iwanaidake Peridotite, Hokkaido, Japan, *Journal of Petrology* **43**(3), 423–448.

Langford, F. F. and Morin, J. A.: 1976, The development of the Superior Province of Northwestern Ontario by merging Island Arcs, *American Journal of Science* **270**, 1023–1034.

LeCheminant, A. N. and Heaman, L. M.: 1989, Mackenzie igneous events, Canada: Middle Proterozoic hotspot magmatism associated with ocean opening, *Earth and Planetary Science Letters* **96**, 38–48.

Ling, M.-X., Li, Y., Ding, X., Teng, F. Z., Yaang, X. Y., Fan, W. M., Xu, Y. G. and Sun, W.: 2013, Destruction of the North China Craton Induced by Ridge Subductions, *The Journal of Geology* **121**, 197–213.

Luguet, A., Jaques, A. L., Pearson, D. G., Smith, C. B., Bulanova, G. P., Roffey, S. L., Rayner, M. J. and Lorand, J.-P.: 2009, An integrated petrological, geochemical and Re-Os isotope study of peridotite xenoliths from the Argyle lamproite, Western Australia and implications for cratonic diamond occurrences, *Lithos* **112S - Proceedings of the 9th International Kimberlite Conference**, 1096–1108.

Moser, D., Amelin, Y., Schulze, D. and Krogh, T.: 1997, Progress in Understanding the Geology of the Lithosphere beneath the Eastern Sachigo Subprovince, *in* R. M. Harrap and H. H. Helmstaedt (eds), *1997 Western Superior Transect Third Annual Workshop, April 11-12, 1997. Lithoprobe Report #63*, Lithoprobe Secretariat, The University of British Columbia, pp. 102–103.

Musacchio, G., White, D. J., Asudeh, I. and Thomson, C. J.: 2004, Lithospheric structure and composition of the Archean western Superior Province from seismic refraction/wide- angle reflection and gravity modeling, *Journal of Geophysical Research* **109**, B03304.

Pearson, D. G. and Wittig, N.: 2008, Formation of Archaean continental lithosphere and its diamonds: the root of the problem, *Journal of the Geological Society, London* **165**, 1–20.

Peng, Z. C., Zartman, R. E., Futa, K. and Chen, D. G.: 1986, Pb-, Sr- and Nd-isotopic systematics and chemical characteristics of Cenozoic basalts, eastern China, *Chemical Geology* **59**, 3–33.

Richardson, S. H., Harris, J. W. and Gurney, J. J.: 1993, Three generations of diamond from old continental mantle, *Nature* **366**, 256–258.

Richardson, S. H., Pöml, P. F., Shirey, S. B. and Harris, J. W.: 2009, Age and origin of peridotitic diamonds from Venetia, Limpopo Belt, Kaapvaal-Zimbabwe Craton, *Lithos* **112S - Proceedings of the 9th International Kimberlite Conference**, 785–792.

Sage, R. P.: 2000, Kimberlites of the Attawapiskat area, James Bay Lowlands, northern Ontario, *Ontario Geological Survey, Open File Report* **6019**(341), 341.

Scully, K. R.: 2000, *Mantle xenoliths from the Attawapiskat kimberlite field*, Master's thesis, University of Toronto.

Skulski, T., Corkery, M. T., Stone, D., Whalen, J. B. and Stern, R. A.: 2000, Geological and geochronological investigations in the Stull Lake - Edmund Lake greenstone belt and granitoid rocks of the northwestern Superior Province, *Report of Activities 2000, Manitoba Industry, Trade and Mines*, Manitoba Geological Survey, pp. 117–128.

Smit, K. V., Shirey, S. B., Richardson, S. H., le Roex, A. P. and Gurney, J. J.: 2010, Re-Os isotopic composition of peridotitic sulphide inclusions in diamonds from Ellendale, Australia: Age constraints on Kimberley cratonic lithosphere, *Geochimica et Cosmochimica Acta* **74**(11), 3292–3306.

Sobolev, N. V.: 1977, *Deep Seated Inclusions in Kimberlites and the Problems of the Composition of the Upper Mantle (translated by D.A. Brown)*, American Geophysical Union, Washington, D.C.

Stachel, T., Aulbach, S., Brey, G. P., Harris, J. W., Leost, I., Tappert, R. and Viljoen, K. S.: 2004, The trace element composition of silicate inclusions in diamonds: a review, *Lithos* **77**, 1–20.

Stachel, T., Harris, J. W. and Brey, G. P.: 1998, Rare and unusual mineral inclusions in diamonds from Mwadui, Tanzania, *Contributions to Mineralogy and Petrology* **132**, 34–47.

Stevenson, R. K.: 1995, Crust and mantle evolution in the late Archaean: Evidence from a Sm-Nd isotopic study of the North Spirit Lake greenstone belt, northwestern Ontario, *Geological Society of America Bulletin* **107**, 1458–1467.

Thurston, P. C., Osmani, I. A. and Stone, D.: 1991, Northwestern Superior Province: Review and terrane analysis, *in* P. C. Thurston, H. R. Williams, R. H. Sutcliffe and G. M. Stott (eds), *Geology of Ontario*, Vol. Special Volume 4, Part 1, Ontario Geological Survey, pp. 81–144.

Toft, P. B., Hills, D. V. and Haggerty, S. E.: 1989, Crustal evolution and the granulite to eclogite transition in xenoliths from kimberlites in the West African Craton, *Tectonophysics* **161**, 213–231.

Walker, R. J., Horan, M. F., Morgan, J. W., Becker, H., Grossman, J. N. and Rubin, A. E.: 2002, Comparative ^{187}Re-^{187}Os systematics of chondrites: Implications regarding early solar system processes, *Geochimica et Cosmochimica Acta* **66**(23), 4187–4201.

White, D. J., Musacchio, G., Helmstaedt, H. H., Harrap, R. M., Thurston, P. C., van der Velden, A. and Hall, K.: 2003, Images of a lower-crustal oceanic slab: Direct evidence for tectonic accretion in the Archean western Superior Province, *Geology* **31**(11), 997–1000.

Woods, G.: 1986, Platelets and the infrared absorption of type Ia diamonds, *Proceedings of the Royal Society* **A407**, 219–238.

Appendix A

Major element data for Victor eclogite and pyroxenite xenoliths

All major element data in weight %. "-" indicates not measured or below detection.
2σ for the major element data is the standard deviation of the mean of 'n' analytical spots per xenolith.
FeO tot as ferrous iron.

Table A.1: JEOL JXA-8900 spectrometer setup for silicate analysis, with peak and background counting times

PET crystal			TAP crystal			PETH crystal			TAP crystal			LIFH crystal		
Element	Peak	Bkg	Element	Peak	Bkg	Element	Peak	Bkg	Element	Peak	Bkg	Element	Peak	Bkg
Cr	40	20	Al	60	30	P	50	25	Mg	50	25	Ni	40	20
Ti	50	25	Si	60	30	K	60	30	Na	60	30	Fe	30	15
Ca	40	20										Mn	30	15
												V	30	15

Table A.2: Standards used for silicate analysis

Element	Standard	Locality	Source	Reference
Na	Albite	Casedero, CA, USA	U of A collection	
P	Apatite	Durange, Mexico	Smithsonian Institute	Jarosewich, 2002
Cr	Chromite		U of A collection	
Si	Diopside	Wakefield, QB	U of A collection	
Ca	Diopside	Wakefield, QB	U of A collection	
Fe	Fayalite	Rockport, MA	Smithsonian Institute	Jarosewich, 2002
Mg	Fo93		U of A collection	
Mn	Mn_2O_3	synthetic	Smithsonian Institute	Jarosewich, 2002
Ni	Nickel	synthetic	U of A collection	
K	Orthoclase		U of A collection	
Al	Pyrope	Kakanui, New Zealand	Smithsonian Institute	Jarosewich, 2002
Ti	Rutile		U of A collection	
V	V metal		U of A collection	

Table A.3: Garnet major element compositions of Victor high-Ca and low-Mg eclogites

Sample	VIC0608	VIC0502	VIC0504	VIC0604	VIC0703	VIC0704	VIC0705	VIC1104	VIC1305
	high-Ca	low-Mg	low-Mg	low-Mg	low-Mg	low-Mg	low-Mg	low-Mg	low-Mg
n	21	18	11	31	23	12	47	24	8
SiO_2	40.46	38.70	40.65	40.32	42.50	39.38	39.60	40.23	39.39
2σ	1.05	0.53	0.34	0.38	0.33	0.58	0.85	0.29	0.12
TiO_2	0.07	0.05	0.08	0.09	0.06	0.07	0.14	0.13	0.09
2σ	0.05	0.02	0.02	0.05	0.05	0.04	0.04	0.03	0.04
Al_2O_3	23.46	22.04	23.18	22.76	24.10	22.46	22.56	22.84	22.16
2σ	0.16	0.25	0.10	0.27	0.23	0.31	0.33	0.17	0.11
Cr_2O_3	0.12	0.01	0.09	0.18	0.71	0.03	0.12	0.11	0.04
2σ	0.03	0.02	0.02	0.05	0.17	0.02	0.03	0.03	0.03
V_2O_3	0.01	0.03	0.02	0.01	0.01	0.02	0.01	0.01	0.02
2σ	0.02	0.02	0.01	0.02	0.02	0.02	0.02	0.01	0.02
FeO tot	13.34	24.37	14.12	16.14	8.42	21.27	17.85	10.91	23.13
2σ	0.24	0.68	0.08	0.26	0.07	0.76	0.20	0.23	0.33
MnO	0.37	0.61	0.40	0.37	0.44	0.55	0.39	0.20	0.49
2σ	0.02	0.03	0.01	0.16	0.03	0.12	0.02	0.02	0.02
MgO	18.35	6.74	17.14	13.30	20.87	7.69	11.63	9.89	7.46
2σ	0.26	0.13	0.10	0.21	0.18	0.17	0.23	0.25	0.20
CaO	3.87	8.46	4.64	6.90	4.13	9.29	7.99	15.72	8.86
2σ	0.10	0.34	0.10	0.22	0.07	0.48	0.17	0.40	0.11
Na_2O	0.05	0.05	0.04	0.04	0.03	0.05	0.07	0.05	0.06
2σ	0.02	0.05	0.01	0.02	0.02	0.03	0.02	0.02	0.03
P_2O_5	0.03	0.03	0.03	0.03	0.01	0.02	0.04	0.04	0.03
2σ	0.02	0.02	0.02	0.03	0.01	0.02	0.02	0.03	0.03
NiO	-	-	-	-	-	-	-	-	-
2σ	-	-	-	-	-	-	-	-	-
Total	100.11	101.11	100.39	100.14	101.27	100.82	100.41	100.13	101.72
2σ	1.20	0.75	0.49	0.65	0.44	1.27	0.94	0.61	0.27

Table A.4: Garnet major element compositions of Victor high-Mg eclogites

Sample	VIC0101	VIC0107	VIC0201	VIC0302	VIC0506	VIC0607	VIC0707	VIC1601
	high-Mg	high-Mg	high-Mg	high-Mg	high-Mg	high-Mg	high-Mg	high-Mg
n	8	15	48	13	13	15	12	13
SiO_2	41.35	40.34	41.38	40.22	41.53	41.41	40.41	39.15
2σ	0.40	0.63	0.35	0.65	0.20	0.44	0.46	0.40
TiO_2	0.07	0.10	0.08	0.06	0.05	0.08	0.06	0.04
2σ	0.03	0.03	0.03	0.04	0.02	0.02	0.03	0.03
Al_2O_3	23.06	23.19	23.60	23.00	23.42	23.31	23.12	22.30
2σ	0.27	0.14	0.20	0.13	0.15	0.14	0.12	0.54
Cr_2O_3	0.83	0.07	0.08	0.05	0.27	0.27	0.19	0.04
2σ	0.19	0.03	0.06	0.02	0.04	0.03	0.03	0.03
V_2O_3	0.01	0.02	0.02	0.02	0.01	0.01	0.01	0.01
2σ	0.03	0.01	0.01	0.01	0.01	0.01	0.01	0.02
FeO tot	11.35	16.45	13.24	17.85	12.32	11.37	13.08	20.88
2σ	0.41	0.45	0.19	0.19	0.16	0.14	0.68	0.19
MnO	0.43	0.46	0.43	0.46	0.38	0.35	0.33	0.45
2σ	0.19	0.03	0.02	0.02	0.02	0.02	0.03	0.03
MgO	19.03	15.93	17.85	14.76	19.03	18.78	15.02	7.38
2σ	0.35	0.28	0.22	0.26	0.12	0.14	0.45	0.30
CaO	4.37	4.43	4.03	4.75	3.99	4.95	8.00	10.26
2σ	0.07	0.15	0.14	0.24	0.06	0.11	0.12	0.11
Na_2O	0.04	0.06	0.04	0.04	0.04	0.05	0.04	0.10
2σ	0.01	0.03	0.02	0.02	0.03	0.04	0.02	0.23
P_2O_5	0.04	0.04	0.04	0.03	0.02	0.03	0.02	0.04
2σ	0.02	0.03	0.03	0.03	0.02	0.03	0.02	0.06
NiO	-	-	-	-	-	-	-	-
2σ	-	-	-	-	-	-	-	-
Total	100.58	101.09	100.78	101.25	101.06	100.61	100.28	100.65
2σ	0.63	0.53	0.65	0.61	0.28	0.54	0.29	0.59

Table A.5: Garnet major element compositions of Victor orthopyroxene-free pyroxenites

Sample	VIC0303	VIC0304	VIC0406	VIC0505	VIC1106	VIC1303	VIC2412	VIC2418
	opx-free	opx-free	opx-free	opx-free	opx-free	opx-free	opx-free	opx-free
n	15	11	30	30	15	3	20	31
SiO_2	42.25	42.11	42.01	42.58	41.48	41.50	42.61	42.14
2σ	0.16	0.34	0.47	0.28	0.34	0.14	0.36	0.56
TiO_2	0.06	0.06	0.07	0.09	0.07	0.06	0.06	0.23
2σ	0.03	0.04	0.06	0.07	0.03	0.02	0.05	0.03
Al_2O_3	24.11	24.11	23.71	24.33	23.46	22.98	24.11	23.38
2σ	0.13	0.19	0.21	0.26	0.32	0.13	0.18	0.19
Cr_2O_3	0.36	0.48	0.75	0.15	0.25	0.87	0.45	0.81
2σ	0.06	0.27	0.12	0.06	0.06	0.06	0.14	0.11
V_2O_3	0.01	0.01	0.02	0.01	0.01	0.01	0.02	0.03
2σ	0.02	0.02	0.01	0.02	0.02	0.01	0.02	0.02
Fe_{tot}	10.01	8.30	10.79	8.17	12.98	12.95	8.30	9.53
2σ	0.10	0.14	0.17	0.13	0.22	0.06	0.13	0.23
MnO	0.40	0.42	0.41	0.37	0.34	0.39	0.44	0.38
2σ	0.02	0.02	0.03	0.03	0.02	0.01	0.03	0.03
MgO	19.35	20.83	19.21	20.73	15.65	16.68	20.59	19.99
2σ	0.28	0.23	0.17	0.31	0.47	0.07	0.28	0.17
CaO	4.31	4.02	4.00	4.05	6.23	4.73	4.07	4.31
2σ	0.06	0.08	0.08	0.08	0.24	0.08	0.09	0.12
Na_2O	0.04	0.22	0.16	0.05	0.23	-	0.12	0.06
2σ	0.02	0.23	0.38	0.02	0.56	-	0.42	0.03
P_2O_5	0.02	0.02	0.03	0.04	0.02	0.03	0.02	0.04
2σ	0.01	0.03	0.02	0.07	0.02	0.02	0.02	0.03
NiO	-	0.08	0.02	-	-	-	0.01	-
2σ	-	0.23	0.11	-	-	-	0.06	-
Total	100.92	100.67	101.19	100.57	100.72	100.21	100.79	100.92
2σ	0.38	0.79	0.90	0.72	1.20	0.23	1.01	0.54

Table A.6: Garnet major element compositions of Victor orthopyroxene-bearing pyroxenites

Sample	VIC0106	VIC0507	VIC1703	VIC2001	VIC2002	VIC2302	VIC2501	VIC8401
	opx-bearing	opx-bearing	opx-bearing	opx-bearing	opx-bearing	opx-bearing	opx-bearing	opx-bearing
n	14	14	41	7	81	21	44	15
SiO_2	39.72	39.21	39.88	38.97	40.91	41.29	39.76	40.50
2σ	0.18	0.27	0.84	0.29	0.25	0.49	0.73	0.53
TiO_2	0.05	0.08	0.15	0.08	0.07	0.08	0.07	0.08
2σ	0.03	0.04	0.05	0.04	0.03	0.03	0.04	0.03
Al_2O_3	22.56	22.22	22.62	22.17	23.14	23.46	22.73	23.00
2σ	0.17	0.15	0.42	0.25	0.16	0.29	0.27	0.35
Cr_2O_3	0.02	0.03	0.09	0.03	0.24	0.24	0.10	0.06
2σ	0.02	0.02	0.03	0.03	0.03	0.04	0.04	0.02
V_2O_3	0.01	0.02	0.02	0.03	0.01	0.02	0.02	0.02
2σ	0.02	0.01	0.02	0.02	0.01	0.01	0.02	0.02
Fe_{tot}	22.05	22.80	15.84	23.27	13.59	9.90	17.45	16.45
2σ	0.31	0.32	0.37	0.73	0.32	0.14	0.35	0.31
MnO	0.60	0.46	0.43	0.54	0.34	0.35	0.29	0.38
2σ	0.14	0.05	0.16	0.03	0.03	0.01	0.02	0.02
MgO	10.27	6.88	12.05	7.43	14.98	19.81	9.69	16.17
2σ	0.20	0.13	0.31	0.24	0.30	0.21	0.22	0.20
CaO	5.76	9.70	8.48	8.85	7.22	4.02	10.65	4.08
2σ	0.14	0.16	0.23	0.53	0.13	0.09	0.25	0.07
Na_2O	0.03	0.05	0.06	0.05	0.03	0.04	0.04	0.04
2σ	0.02	0.02	0.03	0.02	0.01	0.01	0.02	0.02
P_2O_5	0.03	0.04	0.03	0.03	0.02	0.02	0.03	0.03
2σ	0.03	0.02	0.03	0.03	0.02	0.02	0.03	0.02
NiO	-	-	-	-	-	-	-	-
2σ	-	-	-	-	-	-	-	-
Total	101.10	101.49	99.66	101.44	100.54	99.24	100.83	100.80
2σ	0.66	0.34	1.40	0.43	0.49	0.87	1.06	0.87

Table A.7: Clinopyroxene major element compositions of Victor high-Ca and low-Mg eclogites

Sample	VIC0608	VIC0502	VIC0504	VIC0604	VIC0703	VIC0704	VIC0705	VIC1104	VIC1305
Description	high-Ca	low-Mg	low-Mg	low-Mg	low-Mg	low-Mg	low-Mg	low-Mg	low-Mg
n	30	23	18	24	9	11	18	16	47
SiO_2	53.76	54.54	54.26	54.89	54.94	54.31	55.06	54.00	54.24
2σ	0.45	0.45	0.26	0.78	0.25	0.22	1.19	0.46	0.70
TiO_2	0.41	0.12	0.14	0.16	0.13	0.12	0.17	0.26	0.20
2σ	0.03	0.02	0.02	0.02	0.02	0.04	0.05	0.08	0.07
Al_2O_3	15.92	9.62	7.73	9.88	9.01	4.91	11.51	7.83	9.98
2σ	0.54	0.23	0.30	0.58	0.25	0.37	2.91	0.44	0.77
Cr_2O_3	0.12	0.04	0.02	0.04	0.04	0.02	0.04	0.03	0.12
2σ	0.03	0.04	0.02	0.03	0.02	0.03	0.02	0.02	0.03
V_2O_3	0.02	0.07	0.12	0.07	0.07	0.04	0.07	0.11	0.06
2σ	0.02	0.02	0.02	0.04	0.02	0.02	0.02	0.05	0.03
FeO_{tot}	1.32	3.87	6.29	4.64	5.01	5.02	4.20	5.75	3.12
2σ	0.15	0.15	0.30	0.46	0.12	0.29	1.01	0.17	0.59
MnO	0.01	0.03	0.05	0.09	0.04	0.10	0.05	0.04	0.02
2σ	0.02	0.01	0.02	0.14	0.01	0.21	0.05	0.02	0.01
MgO	7.85	9.53	9.74	9.34	9.51	12.69	8.12	9.99	10.02
2σ	0.14	0.23	0.09	1.13	0.06	0.18	2.02	0.25	0.38
CaO	13.42	15.36	15.50	13.96	14.88	18.26	12.85	15.43	15.56
2σ	0.26	0.28	0.10	0.87	0.11	0.36	3.14	0.27	0.27
Na_2O	7.27	5.34	5.27	6.33	5.69	3.53	6.78	5.37	5.56
2σ	0.22	0.34	0.10	0.38	0.10	0.16	0.50	0.23	0.47
P_2O_5	0.01	0.01	0.01	0.01	0.01	-	0.01	0.02	0.01
2σ	0.02	0.02	0.03	0.02	0.02	-	0.01	0.02	0.02
NiO	0.04	0.01	0.01	-	0.01	-	0.01	0.02	0.04
2σ	0.01	0.02	0.02	-	0.01	-	0.01	0.01	0.01
Total	100.16	98.54	99.12	99.41	99.35	99.00	98.89	98.84	98.93
2σ	0.81	0.79	0.39	1.82	0.35	0.59	1.63	0.53	1.36

Table A.8: Clinopyroxene major element compositions of Victor high-Mg eclogites

Sample	VIC0101	VIC0107	VIC0201	VIC0302	VIC0506	VIC0607	VIC0707	VIC1601
Description	high-Mg	high-Mg	high-Mg	high-Mg	high-Mg	high-Mg	high-Mg	high-Mg
n	18	13	144	11	25	78	34	16
SiO_2	54.40	53.93	54.59	53.71	53.64	53.33	52.93	54.00
2σ	0.71	0.47	0.50	0.62	0.78	0.69	1.47	0.33
TiO_2	0.15	0.21	0.22	0.16	0.20	0.38	0.36	0.16
2σ	0.04	0.05	0.66	0.04	0.10	0.09	0.20	0.03
Al_2O_3	4.10	4.65	4.46	3.74	4.94	7.12	7.04	3.59
2σ	0.59	0.24	0.43	0.25	0.28	0.34	0.71	0.40
Cr_2O_3	0.13	0.08	0.15	0.04	0.20	0.15	0.09	0.06
2σ	0.02	0.02	0.05	0.02	0.04	0.02	0.04	0.02
V_2O_3	0.06	0.08	0.08	0.08	0.04	0.05	0.08	0.08
2σ	0.04	0.02	0.02	0.04	0.02	0.02	0.05	0.02
FeO_{tot}	3.04	4.27	3.17	4.60	3.41	4.21	3.55	4.16
2σ	0.75	0.18	0.13	0.22	0.26	0.32	0.32	0.13
MnO	0.04	0.07	0.05	0.06	0.08	0.03	0.08	0.05
2σ	0.03	0.09	0.02	0.04	0.15	0.02	0.13	0.01
MgO	14.92	13.41	14.05	13.93	13.33	11.64	11.80	14.31
2σ	3.10	0.16	0.38	0.17	0.31	0.20	0.39	0.18
CaO	19.16	18.73	19.57	19.52	19.05	17.25	17.34	19.49
2σ	2.98	0.38	0.48	0.30	0.63	0.21	0.55	0.34
Na_2O	2.76	3.36	2.96	2.85	3.12	4.70	4.26	2.71
2σ	0.44	0.10	0.25	0.09	0.17	0.14	0.20	0.16
P_2O_5	0.01	0.01	0.01	0.01	0.01	0.01	0.01	0.01
2σ	0.02	0.02	0.02	0.02	0.02	0.02	0.02	0.02
NiO	0.04	0.02	0.02	0.03	0.02	0.03	0.01	0.03
2σ	0.03	0.02	0.01	0.02	0.04	0.02	0.02	0.01
Total	98.80	98.83	99.34	98.74	98.06	98.90	97.55	98.66
2σ	0.72	0.73	0.66	1.10	1.16	0.81	2.16	0.37

Table A.9: Clinopyroxene major element compositions of Victor orthopyroxene-free pyroxenites

Sample	VIC0303	VIC0304	VIC0406	VIC0505	VIC1106	VIC1303	VIC2412	VIC2418
Description	opx-free	opx-free	opx-free	opx-free	opx-free	opx-free	opx-free	opx-free
n	14	16	15	13	144	36	16	12
SiO_2	54.34	54.05	53.74	54.00	54.01	54.19	54.78	51.95
2σ	0.42	0.45	0.51	0.41	0.37	0.72	0.44	3.08
TiO_2	0.26	0.12	0.13	0.21	0.17	0.27	0.11	0.11
2σ	0.02	0.03	0.02	0.07	0.03	0.04	0.02	0.03
Al_2O_3	3.94	2.05	4.24	3.69	3.63	3.87	1.97	2.06
2σ	0.05	0.32	0.09	0.47	0.22	0.11	0.16	0.21
Cr_2O_3	0.29	0.16	0.15	0.12	0.18	0.18	0.15	0.52
2σ	0.03	0.04	0.02	0.04	0.03	0.03	0.05	0.06
V_2O_3	0.07	0.03	0.04	0.08	0.03	0.07	0.03	0.04
2σ	0.02	0.02	0.03	0.02	0.02	0.02	0.02	0.01
FeO_{tot}	2.26	2.22	2.33	3.17	2.68	1.81	2.34	2.60
2σ	0.09	0.07	0.12	0.29	0.15	0.08	0.04	0.10
MnO	0.05	0.04	0.03	0.05	0.03	0.05	0.04	0.05
2σ	0.06	0.02	0.01	0.04	0.02	0.02	0.02	0.02
MgO	14.97	16.40	14.60	14.80	14.81	15.25	16.04	15.12
2σ	0.10	0.18	0.18	0.28	0.30	0.19	0.18	0.40
CaO	20.03	22.33	20.89	20.13	21.35	20.60	22.32	20.56
2σ	0.30	0.25	0.18	0.34	0.24	0.17	0.31	0.63
Na_2O	2.55	1.30	2.31	2.49	2.13	2.48	0.95	1.36
2σ	0.07	0.13	0.06	0.22	0.14	0.07	0.64	0.66
P_2O_5	0.02	0.01	0.02	0.02	0.01	0.02	0.02	0.02
2σ	0.02	0.02	0.02	0.02	0.02	0.03	0.02	0.02
NiO	0.03	0.05	0.06	0.03	0.05	0.03	0.01	0.03
2σ	0.02	0.02	0.02	0.02	0.02	0.01	0.04	0.06
Total	98.82	98.77	98.53	98.79	99.07	98.82	98.75	94.42
2σ	0.56	0.41	0.70	0.55	0.66	0.84	0.83	4.20

Table A.10: Clinopyroxene major element compositions of Victor orthopyroxene-bearing pyroxenites

Sample	VIC0106	VIC0507	VIC1703	VIC2001	VIC2002	VIC2302	VIC2501	VIC8401
Description	opx-bearing	opx-bearing	opx-bearing	opx-bearing	opx-bearing	opx-bearing	opx-bearing	opx-bearing
n	6	18	32	17	15	36	20	49
SiO_2	54.15	54.75	54.79	54.36	54.86	54.78	54.98	54.91
2σ	0.28	1.08	0.22	0.48	0.40	0.40	0.44	0.62
TiO_2	0.15	0.46	0.13	0.13	0.26	0.19	0.20	0.22
2σ	0.04	2.12	0.05	0.02	0.08	0.05	0.03	0.04
Al_2O_3	2.45	3.48	2.82	3.39	4.13	3.63	3.50	2.02
2σ	0.29	0.41	0.20	0.37	0.26	0.22	0.35	0.42
Cr_2O_3	0.64	0.76	0.25	0.65	0.80	0.20	0.37	0.33
2σ	0.04	0.14	0.07	0.08	0.12	0.07	0.12	0.05
V_2O_3	0.06	0.10	0.06	0.09	0.10	0.06	0.09	0.05
2σ	0.03	0.07	0.03	0.06	0.03	0.03	0.01	0.03
FeO_{tot}	2.35	1.68	2.04	1.69	2.12	1.51	1.54	3.05
2σ	0.20	0.07	0.07	0.04	0.12	0.12	0.08	0.18
MnO	0.17	0.05	0.04	0.05	0.05	0.04	0.05	0.09
2σ	0.06	0.02	0.02	0.02	0.02	0.02	0.02	0.03
MgO	16.14	15.27	15.56	15.22	14.51	15.26	15.40	16.64
2σ	0.11	0.29	0.22	0.35	0.17	0.18	0.25	0.30
CaO	21.22	20.73	21.73	20.57	19.55	21.15	20.73	20.15
2σ	0.07	0.56	0.22	0.34	0.46	0.16	0.38	0.85
Na_2O	1.71	2.16	1.70	2.27	2.68	2.12	1.75	1.54
2σ	0.15	0.17	0.10	0.17	0.71	0.09	0.46	0.29
P_2O_5	-	0.01	0.02	0.01	0.02	0.02	0.02	0.03
2σ	0.01	0.02	0.02	0.02	0.02	0.02	0.02	0.04
NiO	-	0.03	0.03	0.05	0.03	0.03	0.02	0.04
2σ	-	0.01	0.01	0.22	0.09	0.01	0.10	0.02
Total	99.03	99.47	99.18	98.49	99.10	98.99	98.64	99.07
2σ	0.60	0.74	0.44	0.77	0.87	0.58	1.14	0.86

Table A.11: Orthopyroxene major element compositions of Victor pyroxenites

Sample	VIC0106	VIC0507	VIC1703	VIC2001	VIC2002	VIC2302	VIC2501	VIC8401
n	11	13	7	11	18	31	15	28
SiO_2	56.79	57.95	57.59	57.44	57.49	57.85	58.08	57.63
2σ	0.47	0.45	0.27	0.41	0.71	0.30	0.46	0.57
TiO_2	0.05	0.09	0.05	0.04	0.05	0.05	0.05	0.11
2σ	0.02	0.29	0.06	0.02	0.02	0.01	0.03	0.02
Al_2O_3	0.66	0.75	0.68	0.73	0.67	0.69	0.76	0.58
2σ	0.11	0.11	0.09	0.06	0.09	0.08	0.08	0.02
Cr_2O_3	0.08	0.09	0.03	0.07	0.08	0.02	0.06	0.05
2σ	0.02	0.03	0.02	0.03	0.02	0.01	0.02	0.02
V_2O_3	0.01	0.01	0.01	0.01	0.01	0.01	0.01	0.01
2σ	0.02	0.01	0.01	0.01	0.01	0.01	0.02	0.01
FeO tot	6.66	4.57	5.60	4.53	6.10	4.36	4.49	6.21
2σ	0.19	0.05	0.09	0.05	0.15	0.04	0.05	0.17
MnO	0.08	0.10	0.09	0.10	0.09	0.08	0.10	0.12
2σ	0.15	0.02	0.01	0.01	0.02	0.01	0.01	0.02
MgO	35.21	36.08	34.94	35.67	34.71	35.71	35.86	34.72
2σ	0.28	0.20	0.29	0.39	0.22	0.25	0.30	0.19
CaO	0.22	0.16	0.17	0.16	0.17	0.16	0.18	0.40
2σ	0.25	0.03	0.01	0.10	0.05	0.02	0.03	0.02
Na_2O	0.03	0.04	0.04	0.26	-	0.04	0.15	0.10
2σ	0.02	0.02	0.01	0.28	-	0.01	0.42	0.02
P_2O_5	0.00	0.00	0.01	0.00	0.00	0.00	0.00	0.01
2σ	0.01	0.01	0.01	0.01	0.01	0.00	0.01	0.02
NiO	-	0.06	0.06	0.04	0.02	0.07	0.03	0.08
2σ	-	0.02	0.01	0.15	0.03	0.01	0.08	0.02
Total	99.80	99.89	99.25	99.06	99.39	99.06	99.77	100.01
2σ	0.65	0.47	0.13	0.66	0.78	0.49	1.01	0.61

Appendix B

Trace element data for Victor eclogite and pyroxenite xenoliths

Data are averages for "n" analyses per xenolith, given in ppm. "-" indicates below detection. 2σ errors given as the average of the in-run precision for "n" analyses.

Table B.1: Garnet trace element compositions of Victor high-Ca and low-Mg eclogites

Sample	VIC0608	VIC0502	VIC0504	VIC0604	VIC0703	VIC0704	VIC0705	VIC1104	VIC1305
	high-Ca	low-Mg	low-Mg	low-Mg	low-Mg	low-Mg	low-Mg	low-Mg	low-Mg
n	3	6	3	5	3	6	3	3	3
Li7	0.89	0.97	-	0.65	-	0.60	0.57	0.57	0.49
2σ	0.92	0.69	-	0.51	-	0.50	0.44	0.30	0.54
Sc45	40.69	43.84	66.39	55.28	68.84	46.07	56.73	63.52	38.64
2σ	3.30	3.32	6.49	4.29	5.38	3.51	4.93	5.06	3.19
Ti48	140.20	62.67	67.34	76.17	98.94	43.85	91.55	86.99	81.48
2σ	9.99	3.92	6.35	4.81	6.36	2.75	5.88	5.53	6.09
V51	31.28	94.96	116.09	90.27	83.22	51.70	88.28	101.70	65.62
2σ	2.57	8.97	12.09	9.13	6.79	5.02	7.03	7.79	5.40
Ni60	9.44	5.79	1.36	3.78	1.50	1.18	1.37	1.08	5.32
2σ	1.57	1.07	0.87	0.84	0.57	0.43	0.77	0.49	1.09
Co59	41.52	50.90	43.10	53.95	35.53	45.99	29.06	27.73	41.13
2σ	4.33	4.46	7.11	4.93	4.35	4.08	3.19	2.85	4.65
Zn64	60.52	120.89	76.37	67.17	59.43	68.15	31.92	40.74	71.42
2σ	5.49	37.63	9.09	24.04	12.76	22.24	6.42	6.89	6.60
Ga69	5.48	9.48	8.46	8.42	6.64	9.41	6.35	5.44	6.98
2σ	0.61	1.22	1.29	1.21	0.78	1.24	0.78	0.61	0.78
Rb85	-	0.07	-	0.88	-	0.09	26.93	-	-
2σ	-	0.04	-	0.13	-	0.04	3.72	-	-
Sr88	0.54	9.58	0.21	0.42	0.33	0.29	0.66	0.29	0.35
2σ	0.11	0.75	0.08	0.06	0.10	0.05	0.16	0.11	0.08
Y89	8.45	41.93	74.82	42.02	58.10	66.08	56.88	79.90	26.79
2σ	1.02	4.34	13.59	4.80	12.43	7.04	10.75	13.84	3.37
Zr90	9.89	2.00	2.55	5.70	9.55	2.76	5.19	6.67	9.79
2σ	1.05	0.27	0.50	0.71	2.01	0.35	1.11	1.27	1.07
Nb93	-	-	-	-	0.04	-	-	0.13	0.04
2σ	-	-	-	-	0.03	-	-	0.11	0.04
Cs133	-	-	-	0.24	-	-	-	-	-

Continued on next page...

Table B.1 – continued

Sample	VIC0608	VIC0502	VIC0504	VIC0604	VIC0703	VIC0704	VIC0705	VIC1104	VIC1305
	high-Ca	low-Mg	low-Mg	low-Mg	low-Mg	low-Mg	low-Mg	low-Mg	low-Mg
n	3	6	3	5	3	6	3	3	3
2σ	-	-	-	0.04	-	-	-	-	-
Ba138	0.01	0.18	0.01	0.60	0.02	0.09	-	-	-
2σ	0.01	0.03	0.01	0.07	0.02	0.02	-	-	-
La139	-	0.04	0.04	0.01	-	0.01	0.05	0.05	-
2σ	-	0.02	0.03	0.01	-	0.00	0.04	0.04	-
Ce140	0.02	0.33	0.12	0.19	0.24	0.07	0.20	0.16	0.14
2σ	0.02	0.04	0.06	0.03	0.07	0.02	0.07	0.08	0.05
Pr141	0.04	0.10	0.09	0.12	0.18	0.09	0.08	0.09	0.07
2σ	0.02	0.02	0.04	0.02	0.06	0.02	0.05	0.06	0.03
Nd142	0.43	0.82	0.84	0.55	2.17	0.54	1.57	0.78	0.98
2σ	0.14	0.54	0.27	0.40	0.39	0.39	0.32	0.23	0.23
Sm152	1.58	3.22	1.93	2.89	3.38	2.34	3.06	1.46	2.41
2σ	0.35	0.35	0.53	0.34	0.60	0.27	0.57	0.37	0.47
Eu153	0.78	1.51	0.98	1.47	1.78	1.28	1.29	0.73	1.00
2σ	0.18	0.15	0.28	0.15	0.29	0.13	0.24	0.17	0.21
Gd158	1.64	6.37	6.28	5.60	8.34	6.62	5.64	5.32	4.63
2σ	0.42	0.76	1.68	0.74	1.35	0.80	0.99	0.93	0.91
Tb159	0.23	1.14	1.41	1.00	1.65	1.45	1.12	1.09	0.71
2σ	0.07	0.14	0.35	0.13	0.24	0.17	0.19	0.19	0.14
Dy164	1.56	7.81	12.12	7.35	12.52	11.43	7.66	9.15	4.32
2σ	0.37	0.89	3.02	0.92	2.07	1.31	1.27	1.42	0.84
Ho165	0.27	1.66	2.98	1.65	2.93	2.61	1.69	2.32	0.86
2σ	0.08	0.20	0.65	0.22	0.43	0.31	0.26	0.34	0.16
Er166	0.87	4.83	9.73	4.89	8.82	7.86	5.23	7.67	2.26
2σ	0.25	0.63	2.61	0.70	1.29	1.04	0.83	1.09	0.49
Tm169	0.11	0.69	1.57	0.72	1.48	1.13	0.73	1.11	0.37
2σ	0.05	0.10	0.39	0.11	0.21	0.16	0.14	0.19	0.09
Yb173	0.72	4.90	10.95	5.13	8.70	7.79	4.93	7.63	2.17
2σ	0.36	0.69	3.01	0.78	1.81	1.06	1.13	1.53	0.59

Continued on next page. . .

Table B.1 – continued

Sample	VIC0608	VIC0502	VIC0504	VIC0604	VIC0703	VIC0704	VIC0705	VIC1104	VIC1305
	high-Ca	low-Mg	low-Mg	low-Mg	low-Mg	low-Mg	low-Mg	low-Mg	low-Mg
n	3	6	3	5	3	6	3	3	3
Lu175	0.09	0.70	1.68	0.76	1.44	1.11	0.80	1.29	0.29
2σ	0.06	0.10	0.41	0.12	0.25	0.16	0.17	0.23	0.08
Hf180	0.14	0.05	0.05	0.07	0.15	0.07	0.11	-	0.10
2σ	0.10	0.03	0.06	0.04	0.11	0.03	0.08	-	0.08
Ta181	0.06	-	-	-	0.03	-	-	0.01	0.04
2σ	0.04	-	-	-	0.03	-	-	0.02	0.03
Pb208	-	5.88	0.10	1.29	-	0.72	0.11	-	-
2σ	-	1.68	0.08	0.44	-	0.22	0.06	-	-
Th232	-	0.01	0.04	0.00	-	0.01	0.02	0.02	-
2σ	-	0.01	0.03	0.00	-	0.01	0.02	0.03	-
U238	0.03	0.03	-	0.02	-	0.01	0.03	0.02	0.02
2σ	0.02	0.01	-	0.01	-	0.01	0.02	0.02	0.02

Table B.2: Garnet trace element compositions of Victor high-Mg eclogites

Sample	VIC0101	VIC0107	VIC0201	VIC0302	VIC0506	VIC0607	VIC0707	VIC1601
	high-Mg	high-Mg	high-Mg	high-Mg	high-Mg	high-Mg	high-Mg	high-Mg
n	2	3	3	3	5	3	5	3
Li7	-	0.29	-	0.47	0.52	0.58	0.58	0.27
2σ	-	0.25	-	0.60	0.39	0.58	0.41	0.18
Sc45	48.05	63.65	74.62	74.11	29.69	51.26	49.19	54.42
2σ	12.05	26.39	6.41	6.29	2.24	4.11	3.63	15.34
Ti48	45.46	87.50	55.52	72.36	81.98	117.47	127.85	67.94
2σ	3.78	9.35	4.52	4.85	5.10	8.54	7.92	5.95
V51	46.43	83.45	65.23	105.88	60.95	49.87	110.44	93.31
2σ	4.33	9.40	5.89	9.59	5.64	4.05	10.04	8.81
Ni60	7.76	3.06	4.29	5.60	12.19	4.34	7.43	6.45
2σ	3.00	2.00	1.21	1.71	1.78	1.07	1.18	2.79
Co59	37.78	33.31	25.43	47.81	61.31	44.84	54.08	41.71
2σ	8.35	11.21	3.41	7.96	5.24	4.81	4.60	10.20
Zn64	16.32	31.70	19.75	39.87	64.83	45.55	42.06	31.88
2σ	6.51	20.28	2.51	12.11	19.04	4.33	12.06	13.87
Ga69	5.53	7.85	5.77	9.09	8.75	5.69	9.05	8.89
2σ	0.80	0.95	0.77	1.22	1.07	0.63	1.08	0.99
Rb85	2.49	2.30	-	-	0.06	-	0.42	1.63
2σ	0.68	0.59	-	-	0.04	-	0.07	0.52
Sr88	0.12	0.10	0.05	0.11	0.17	0.21	0.26	0.11
2σ	0.08	0.05	0.03	0.05	0.03	0.06	0.04	0.06
Y89	35.52	58.72	39.65	58.99	16.30	19.47	29.03	38.05
2σ	3.47	7.10	5.78	14.95	1.64	2.33	2.84	3.89
Zr90	22.61	13.67	7.61	12.45	7.78	4.94	9.34	10.85
2σ	2.86	2.25	0.98	2.98	0.83	0.61	0.96	1.57
Nb93	0.09	-	-	-	0.02	-	0.02	-
2σ	0.07	-	-	-	0.02	-	0.01	-
Cs133	-	-	0.02	-	-	-	0.06	-
2σ	-	-	0.02	-	-	-	0.02	-

Continued on next page...

Table B.2 – continued

Sample	VIC0101	VIC0107	VIC0201	VIC0302	VIC0506	VIC0607	VIC0707	VIC1601
	high-Mg	high-Mg	high-Mg	high-Mg	high-Mg	high-Mg	high-Mg	high-Mg
n	2	3	3	3	5	3	5	3
Ba138	-	-	-	0.03	0.12	-	0.09	-
2σ	-	-	-	0.03	0.02	-	0.02	-
La139	0.10	-	-	-	0.02	0.07	0.05	-
2σ	0.08	-	-	-	0.01	0.04	0.01	-
Ce140	-	0.11	0.04	0.13	0.10	0.25	0.37	0.12
2σ	-	0.06	0.03	0.05	0.02	0.07	0.04	0.08
Pr141	-	0.06	0.02	0.06	0.06	0.07	0.10	0.09
2σ	-	0.04	0.02	0.03	0.02	0.03	0.02	0.08
Nd142	1.28	0.41	0.15	0.61	0.40	0.69	0.49	0.37
2σ	0.42	0.19	0.09	0.18	0.30	0.17	0.32	0.25
Sm152	2.05	1.05	0.44	1.12	1.25	1.07	1.21	1.06
2σ	0.71	0.39	0.16	0.31	0.16	0.27	0.15	0.45
Eu153	0.79	0.61	0.24	0.71	0.72	0.58	0.69	0.67
2σ	0.32	0.21	0.09	0.17	0.08	0.15	0.08	0.27
Gd158	4.62	3.92	1.68	4.83	3.05	2.24	2.92	3.67
2σ	1.47	1.43	0.47	0.95	0.38	0.51	0.36	1.25
Tb159	0.80	1.00	0.49	1.17	0.58	0.45	0.63	0.85
2σ	0.28	0.32	0.12	0.20	0.07	0.10	0.08	0.27
Dy164	6.46	8.96	4.72	11.42	3.52	2.97	4.82	7.59
2σ	2.17	3.78	1.05	2.19	0.42	0.59	0.54	2.68
Ho165	1.73	2.30	1.28	3.07	0.66	0.68	1.15	1.68
2σ	0.57	0.92	0.26	0.50	0.08	0.14	0.13	0.58
Er166	4.58	7.68	4.07	10.11	1.57	1.98	3.68	5.31
2σ	1.39	2.67	0.95	1.64	0.22	0.44	0.46	1.63
Tm169	0.71	1.17	0.65	1.70	0.21	0.28	0.57	0.85
2σ	0.34	0.52	0.16	0.25	0.04	0.08	0.08	0.35
Yb173	4.51	8.57	5.14	12.06	1.34	1.82	4.21	5.88
2σ	1.91	3.67	1.30	2.77	0.24	0.51	0.56	2.29
Lu175	0.89	1.24	0.77	1.90	0.18	0.20	0.62	0.83

Continued on next page. . .

Table B.2 – continued

Sample	VIC0101	VIC0107	VIC0201	VIC0302	VIC0506	VIC0607	VIC0707	VIC1601
	high-Mg	high-Mg	high-Mg	high-Mg	high-Mg	high-Mg	high-Mg	high-Mg
n	2	3	3	3	5	3	5	3
2σ	0.39	0.59	0.18	0.35	0.03	0.07	0.09	0.37
Hf180	-	0.32	0.13	0.21	0.10	0.13	0.13	-
2σ	-	0.30	0.09	0.12	0.03	0.09	0.04	-
Ta181	0.10	-	-	0.03	0.01	0.02	-	0.13
2σ	0.10	-	-	0.03	0.01	0.02	-	0.14
Pb208	-	-	-	-	2.47	-	0.96	-
2σ	-	-	-	-	0.69	-	0.27	-
Th232	-	-	0.01	-	0.01	-	0.01	-
2σ	-	-	0.01	-	0.00	-	0.01	-
U238	-	-	0.01	0.04	0.04	0.07	0.08	0.05
2σ	-	-	0.01	0.02	0.01	0.04	0.02	0.05

Table B.3: Garnet trace element compositions of Victor pyroxenites

Sample	VIC0303	VIC0304	VIC0406	VIC0505	VIC1106	VIC1303	VIC2412	VIC2418	VIC0106	VIC2001	VIC2002	VIC2501
	opx-free	opx-free	opx-free	opx-free	opx-free	opx-free	opx-free	opx-free	opx-bearing	opx-bearing	opx-bearing	opx-bearing
n	3	3	3	3	3	3	5	9	6	5	7	5
Li7	-	0.28	0.32	-	-	0.36	0.60	0.48	0.66	-	-	0.48
2σ	-	0.17	0.42	-	-	0.56	0.49	0.43	0.52	-	-	0.42
Sc45	53.66	67.23	70.13	75.86	79.83	71.29	60.75	61.40	85.38	92.57	78.75	84.00
2σ	19.55	21.57	5.86	7.25	6.70	6.42	5.06	4.94	7.25	8.56	7.00	7.63
Ti48	46.83	74.00	70.41	78.48	71.78	70.99	70.82	55.31	66.25	63.66	54.37	53.76
2σ	4.69	6.91	4.66	7.09	5.60	6.17	4.59	3.55	4.33	4.30	3.62	3.61
V51	54.51	60.62	50.62	103.85	46.26	63.45	81.26	100.32	115.83	98.96	104.45	105.24
2σ	5.87	6.15	4.54	10.40	4.10	6.11	9.36	10.83	13.86	13.43	13.37	13.88
Ni60	6.86	9.09	7.90	6.48	6.22	7.12	8.00	10.52	6.91	7.57	9.53	8.47
2σ	3.69	4.32	2.09	1.91	1.59	1.56	1.57	1.88	1.43	1.70	1.96	1.84
Co59	32.74	42.97	55.21	42.34	56.35	25.73	61.18	48.82	35.75	31.71	37.37	31.61
2σ	9.96	11.75	7.42	6.57	6.81	3.78	6.11	4.68	3.72	3.64	4.09	3.56
Zn64	14.78	12.82	32.67	25.12	31.69	8.91	21.68	20.39	15.37	8.19	15.58	8.67
2σ	8.51	6.61	8.11	3.55	3.64	1.51	9.79	8.29	7.43	4.86	8.35	4.93
Ga69	6.72	6.13	5.59	9.48	5.25	6.51	7.77	8.50	7.46	6.18	7.78	5.07
2σ	0.92	0.89	0.81	1.40	0.73	0.90	1.33	1.34	1.36	1.33	1.54	1.08
Rb85	1.51	2.27	-	0.40	-	-	0.13	0.85	-	-	-	0.55
2σ	0.67	0.74	-	0.30	-	-	0.09	0.40	-	-	-	0.18
Sr88	0.14	0.14	0.20	0.17	0.12	0.06	0.14	0.06	0.07	0.13	0.08	0.22
2σ	0.07	0.06	0.10	0.07	0.07	0.04	0.04	0.03	0.03	0.04	0.03	0.05
Y89	27.05	13.27	13.15	42.15	9.58	37.31	6.37	14.48	31.21	21.90	27.39	19.36
2σ	3.15	1.54	3.07	7.25	1.37	6.07	0.89	1.82	4.48	3.72	4.30	3.17
Zr90	11.40	13.06	3.92	9.80	3.31	21.92	4.71	8.53	14.53	10.00	13.89	9.16
2σ	1.83	1.96	1.01	1.41	0.54	2.66	0.69	1.12	2.13	1.74	2.23	1.55
Nb93	-	0.05	-	-	0.05	-	-	0.03	-	-	-	0.03
2σ	-	0.05	-	-	0.05	-	-	0.02	-	-	-	0.03
Cs133	-	0.06	0.03	0.02	0.02	0.02	-	0.01	-	-	-	0.01
2σ	-	0.05	0.03	0.01	0.02	0.01	-	0.01	-	-	-	0.01

Continued on next page...

Table B.3 – continued

Sample	VIC0303	VIC0304	VIC0406	VIC0505	VIC1106	VIC1303	VIC2412	VIC2418	VIC0106	VIC2001	VIC2002	VIC2501
	opx-free	opx-free	opx-free	opx-free	opx-free	opx-free	opx-free	opx-free	opx-bearing	opx-bearing	opx-bearing	opx-bearing
n	3	3	3	3	3	3	5	9	6	5	7	5
Ba138	0.02	-	-	0.02	-	-	0.15	0.31	0.20	0.03	0.12	0.02
2σ	0.03	-	-	0.02	-	-	0.03	0.04	0.03	0.01	0.03	0.01
La139	0.11	-	-	-	0.02	0.05	0.02	0.06	0.01	0.02	0.03	0.02
2σ	0.07	-	-	-	0.02	0.03	0.01	0.02	0.01	0.01	0.02	0.01
Ce140	0.28	0.07	0.24	0.09	0.12	0.18	0.07	0.09	0.06	0.21	0.04	0.50
2σ	0.11	0.05	0.10	0.05	0.06	0.06	0.02	0.02	0.02	0.04	0.01	0.07
Pr141	0.10	0.05	0.10	0.04	0.09	0.02	0.03	0.24	0.03	0.16	0.08	0.22
2σ	0.07	0.05	0.06	0.03	0.04	0.02	0.01	0.04	0.01	0.03	0.02	0.04
Nd142	0.55	0.31	0.72	0.27	0.48	0.18	0.50	0.41	0.56	-	0.41	0.40
2σ	0.24	0.19	0.27	0.14	0.16	0.09	0.40	0.34	0.42	-	0.34	0.34
Sm152	0.74	0.65	0.74	0.66	0.60	0.45	0.32	0.57	0.50	0.69	0.44	0.52
2σ	0.33	0.33	0.29	0.25	0.23	0.17	0.08	0.11	0.10	0.14	0.10	0.12
Eu153	0.45	0.39	0.39	0.39	0.26	0.31	0.20	0.27	0.35	0.36	0.27	0.25
2σ	0.19	0.19	0.15	0.15	0.10	0.11	0.04	0.05	0.06	0.06	0.05	0.05
Gd158	2.53	2.01	1.81	2.47	1.10	2.09	0.86	1.37	2.00	1.66	1.76	1.20
2σ	0.98	0.81	0.57	0.77	0.37	0.58	0.18	0.24	0.36	0.34	0.34	0.26
Tb159	0.63	0.33	0.35	0.60	0.23	0.50	0.16	0.30	0.53	0.37	0.47	0.27
2σ	0.22	0.15	0.11	0.17	0.08	0.13	0.03	0.05	0.09	0.07	0.08	0.06
Dy164	4.86	2.67	2.95	6.39	1.56	4.33	1.16	2.60	4.79	3.16	4.03	2.62
2σ	2.03	1.13	0.75	1.59	0.43	1.03	0.21	0.39	0.75	0.58	0.69	0.48
Ho165	1.14	0.55	0.64	1.56	0.38	1.10	0.25	0.59	1.18	0.79	1.01	0.75
2σ	0.45	0.25	0.17	0.35	0.11	0.25	0.05	0.09	0.19	0.15	0.18	0.14
Er166	3.70	1.27	1.85	5.65	0.97	3.53	0.71	1.77	3.72	2.53	3.23	2.51
2σ	1.31	0.57	0.50	1.51	0.31	0.91	0.15	0.30	0.67	0.54	0.64	0.52
Tm169	0.57	0.25	0.28	0.88	0.20	0.57	0.10	0.25	0.58	0.39	0.53	0.41
2σ	0.26	0.16	0.10	0.23	0.07	0.15	0.03	0.05	0.11	0.09	0.11	0.09
Yb173	3.32	0.97	1.55	6.57	1.05	3.67	0.73	1.78	4.13	2.76	3.59	3.02
2σ	1.57	0.76	0.67	1.85	0.43	1.03	0.19	0.34	0.77	0.61	0.73	0.64
Lu175	0.56	0.21	0.26	1.19	0.16	0.63	0.11	0.27	0.60	0.44	0.57	0.50

Continued on next page...

Table B.3 – continued

Sample	VIC0303	VIC0304	VIC0406	VIC0505	VIC1106	VIC1303	VIC2412	VIC2418	VIC0106	VIC2001	VIC2002	VIC2501
	opx-free	opx-free	opx-free	opx-free	opx-free	opx-free	opx-free	opx-free	opx-bearing	opx-bearing	opx-bearing	opx-bearing
n	3	3	3	3	3	3	5	9	6	5	7	5
2σ	0.27	0.15	0.12	0.30	0.06	0.16	0.03	0.05	0.12	0.10	0.12	0.11
Hf180	0.24	0.15	0.05	0.21	0.14	0.21	0.09	0.15	0.23	0.15	0.19	0.12
2σ	0.20	0.17	0.08	0.13	0.09	0.10	0.04	0.05	0.07	0.06	0.06	0.05
Ta181	0.13	0.06	-	-	0.01	-	0.01	0.02	-	-	-	-
2σ	0.13	0.07	-	-	0.02	-	0.01	0.01	-	-	-	-
Pb208	-	-	-	-	0.09	0.05	0.98	0.11	2.42	0.03	1.32	1.79
2σ	-	-	-	-	0.07	0.04	0.40	0.05	1.03	0.02	0.61	0.86
Th232	-	-	-	0.01	0.02	0.03	0.01	0.01	0.01	0.01	0.01	-
2σ	-	-	-	0.02	0.02	0.02	0.01	0.01	0.01	0.01	0.01	-
U238	-	0.04	0.03	0.05	0.05	0.01	0.05	0.01	0.02	0.01	0.01	0.02
2σ	-	0.04	0.03	0.03	0.04	0.01	0.01	-	0.01	0.01	0.01	0.01

Table B.4: Clinopyroxene trace element compositions of Victor high-Ca and low-Mg eclogites

Sample	VIC0608	VIC0502	VIC0504	VIC0604	VIC0703	VIC0704	VIC0705	VIC1104	VIC1305
	high-Ca	low-Mg	low-Mg	low-Mg	low-Mg	low-Mg	low-Mg	low-Mg	low-Mg
n	3	6	3	9	3	6	3	3	3
Li7	4.37	20.11	7.58	7.67	1.36	7.28	7.61	6.51	3.34
2σ	2.13	7.76	6.29	3.29	0.62	3.03	2.31	1.53	1.97
Sc45	7.17	25.50	45.40	25.71	38.41	29.72	26.75	35.11	13.34
2σ	0.72	1.92	4.39	2.01	2.97	2.27	2.61	3.00	1.21
Ti48	314.94	138.56	163.58	166.39	190.10	162.78	173.78	242.43	189.48
2σ	22.53	8.61	15.35	10.45	12.09	10.17	10.99	15.13	14.35
V51	94.70	403.84	553.32	364.52	353.16	234.34	338.50	437.62	249.91
2σ	7.38	37.31	56.74	36.15	27.65	22.48	25.73	32.01	20.42
Ni60	144.51	105.45	62.28	117.51	42.26	87.95	37.22	36.95	168.79
2σ	13.64	12.73	8.87	15.43	6.43	11.16	5.17	4.46	17.12
Co59	11.75	25.54	27.89	24.31	15.02	26.07	12.40	15.63	16.72
2σ	1.30	2.24	4.60	2.23	1.79	2.33	1.41	1.57	1.99
Zn64	40.22	131.98	93.87	78.29	65.25	88.86	35.75	37.40	61.30
2σ	3.65	39.95	10.62	27.32	13.24	29.06	6.65	5.96	5.67
Ga69	15.24	22.73	16.93	18.02	14.28	15.83	11.59	8.30	14.96
2σ	1.44	2.71	2.38	2.41	1.44	2.02	1.14	0.85	1.55
Rb85	-	0.06	-	0.17	0.15	0.03	3.49	5.05	-
2σ	-	0.03	-	0.04	0.11	0.02	0.83	1.07	-
Sr88	28.64	256.22	198.15	209.78	302.51	665.70	199.29	197.19	165.70
2σ	2.54	18.87	25.39	16.29	49.42	50.33	29.71	25.79	15.88
Y89	0.10	0.75	1.55	0.90	1.27	3.23	1.00	1.77	0.47
2σ	0.04	0.09	0.32	0.12	0.29	0.36	0.24	0.37	0.10
Zr90	4.47	9.09	15.55	16.70	27.40	27.91	19.53	27.75	18.31
2σ	0.51	0.96	2.06	1.92	5.36	3.03	3.57	4.44	1.85
Nb93	-	0.06	0.03	0.01	0.59	-	0.08	0.08	-
2σ	-	0.03	0.02	0.01	0.17	-	0.07	0.05	-
Cs133	-	-	-	0.02	-	-	-	-	0.01

Continued on next page...

Table B.4 – continued

Sample	VIC0608	VIC0502	VIC0504	VIC0604	VIC0703	VIC0704	VIC0705	VIC1104	VIC1305
	high-Ca	low-Mg	low-Mg	low-Mg	low-Mg	low-Mg	low-Mg	low-Mg	low-Mg
n	3	6	3	9	3	6	3	3	3
2σ	-	-	-	0.01	-	-	-	-	0.01
Ba138	0.00	0.06	0.04	0.05	0.11	0.10	0.06	-	0.04
2σ	0.01	0.01	0.03	0.01	0.04	0.02	0.03	-	0.02
La139	-	0.12	1.65	0.66	1.20	1.37	0.54	2.40	1.10
2σ	-	0.02	0.41	0.07	0.19	0.13	0.12	0.35	0.21
Ce140	0.02	1.01	4.96	2.72	5.32	18.55	1.68	5.51	2.65
2σ	0.02	0.09	1.12	0.23	0.61	1.43	0.23	0.59	0.43
Pr141	-	0.43	0.86	1.04	1.31	5.30	0.41	0.76	0.48
2σ	-	0.05	0.22	0.10	0.20	0.46	0.08	0.13	0.10
Nd142	0.13	17.05	4.86	6.52	7.13	6.18	2.31	3.77	2.95
2σ	0.06	4.64	1.22	2.14	0.93	1.93	0.37	0.53	0.55
Sm152	0.19	1.80	1.26	2.42	2.24	5.57	0.86	0.71	1.07
2σ	0.09	0.20	0.33	0.27	0.38	0.55	0.23	0.21	0.24
Eu153	0.06	0.43	0.32	0.37	0.62	1.36	0.25	0.19	0.27
2σ	0.04	0.05	0.10	0.05	0.12	0.12	0.08	0.08	0.08
Gd158	0.13	0.99	1.08	1.32	1.27	3.64	0.65	0.80	0.55
2σ	0.11	0.15	0.33	0.20	0.29	0.46	0.24	0.26	0.19
Tb159	-	0.08	0.12	0.09	0.17	0.34	0.08	0.08	0.03
2σ	-	0.02	0.04	0.02	0.04	0.05	0.04	0.04	0.02
Dy164	0.09	0.28	0.49	0.26	0.62	1.21	0.33	0.24	0.17
2σ	0.06	0.06	0.17	0.06	0.17	0.17	0.13	0.16	0.08
Ho165	0.02	0.04	0.07	0.03	0.08	0.14	0.06	0.06	0.02
2σ	0.02	0.01	0.03	0.01	0.03	0.03	0.04	0.03	0.02
Er166	0.01	0.05	0.16	0.08	0.13	0.26	-	-	-
2σ	0.02	0.03	0.08	0.03	0.09	0.06	-	-	-
Tm169	-	0.01	-	0.02	-	0.02	0.03	0.02	0.01
2σ	-	0.01	-	0.01	-	0.01	0.02	0.02	0.01
Yb173	0.06	-	0.16	0.05	-	0.12	-	0.05	0.05
2σ	0.06	-	0.10	0.04	-	0.06	-	0.07	0.05

Continued on next page...

Table B.4 – continued

Sample	VIC0608	VIC0502	VIC0504	VIC0604	VIC0703	VIC0704	VIC0705	VIC1104	VIC1305
	high-Ca	low-Mg	low-Mg	low-Mg	low-Mg	low-Mg	low-Mg	low-Mg	low-Mg
n	3	6	3	9	3	6	3	3	3
Lu175	0.02	0.01	0.03	0.01	-	0.01	0.02	0.03	-
2σ	0.01	0.01	0.02	0.01	-	0.01	0.02	0.02	-
Hf180	0.18	0.94	1.11	1.07	2.23	2.69	1.04	0.82	0.87
2σ	0.09	0.15	0.29	0.18	0.35	0.40	0.25	0.23	0.20
Ta181	-	-	-	0.01	-	-	0.02	0.03	0.01
2σ	-	-	-	0.01	-	-	0.02	0.03	0.01
Pb208	0.09	0.43	0.58	1.18	0.75	1.08	0.25	0.37	0.24
2σ	0.06	0.13	0.16	0.38	0.18	0.33	0.12	0.17	0.09
Th232	0.02	-	0.03	0.06	0.02	0.01	-	-	-
2σ	0.02	-	0.02	0.01	0.02	0.01	-	-	-
U238	-	-	0.02	0.02	0.03	0.03	0.02	0.03	-
2σ	-	-	0.01	0.01	0.02	0.01	0.02	0.02	-

Table B.5: Clinopyroxene trace element compositions of Victor high-Mg eclogites

Sample	VIC0101	VIC0107	VIC0201	VIC0302	VIC0506	VIC0607	VIC0707	VIC1601
	high-Mg	high-Mg	high-Mg	high-Mg	high-Mg	high-Mg	high-Mg	high-Mg
n	4	3	3	3	6	3	4	4
Li7	0.62	1.69	2.32	0.89	3.06	0.94	1.75	1.26
2σ	0.24	0.77	1.67	1.13	1.29	0.74	0.80	0.43
Sc45	29.06	34.71	38.08	39.43	15.13	25.32	23.83	28.77
2σ	7.23	13.49	3.29	3.32	1.16	2.06	1.78	7.79
Ti48	259.12	227.13	252.71	200.95	184.56	289.23	322.59	197.45
2σ	21.05	23.31	20.77	13.25	11.44	21.17	19.96	16.73
V51	225.96	354.48	335.11	400.76	270.93	202.65	455.23	375.33
2σ	19.74	38.01	29.79	34.99	24.74	16.03	41.16	33.85
Ni60	153.22	86.98	92.27	132.74	295.42	108.96	165.28	160.38
2σ	49.98	44.62	10.61	29.03	34.59	10.70	18.97	57.58
Co59	22.30	10.90	8.33	19.37	27.06	16.70	21.96	16.40
2σ	4.90	3.51	1.16	3.09	2.35	1.87	1.91	3.89
Zn64	18.86	25.60	19.03	39.54	72.87	37.80	43.92	31.20
2σ	7.20	15.34	2.09	11.33	21.43	3.49	12.62	12.90
Ga69	8.52	11.05	9.03	11.68	15.66	10.81	19.74	11.07
2σ	0.87	1.06	1.07	1.44	1.85	1.07	2.27	1.00
Rb85	1.94	2.90	-	-	-	-	0.04	2.04
2σ	0.44	0.55	-	-	-	-	0.03	0.50
Sr88	461.87	234.84	161.77	284.64	206.06	176.34	183.11	324.68
2σ	42.05	27.27	17.53	56.13	15.03	16.01	13.26	31.06
Y89	12.40	6.05	5.20	5.10	0.81	0.68	0.94	4.49
2σ	1.27	0.76	0.81	1.29	0.10	0.12	0.11	0.52
Zr90	85.94	47.07	32.61	45.75	20.38	12.00	21.02	43.10
2σ	9.72	6.99	3.56	10.49	2.07	1.19	2.09	5.21
Nb93	2.54	0.05	0.14	-	0.03	-	0.02	0.03
2σ	0.39	0.03	0.06	-	0.02	-	0.01	0.03
Cs133	-	-	-	-	0.01	-	0.23	-

Continued on next page. . .

Table B.5 – continued

Sample	VIC0101	VIC0107	VIC0201	VIC0302	VIC0506	VIC0607	VIC0707	VIC1601
	high-Mg	high-Mg	high-Mg	high-Mg	high-Mg	high-Mg	high-Mg	high-Mg
n	4	3	3	3	6	3	4	4
2σ	-	-	-	-	0.01	-	0.03	-
Ba138	3.06	0.15	0.32	0.22	0.94	0.07	0.18	0.41
2σ	0.68	0.06	0.08	0.06	0.08	0.03	0.03	0.14
La139	20.32	16.42	8.32	18.02	9.56	7.29	6.83	33.62
2σ	4.95	5.36	1.64	2.65	0.79	1.13	0.56	8.90
Ce140	65.09	26.26	13.89	35.44	13.44	12.61	19.05	45.95
2σ	11.50	6.23	2.55	4.37	1.00	1.83	1.40	8.89
Pr141	19.49	3.82	1.91	5.27	1.82	1.38	2.00	5.60
2σ	3.54	0.94	0.39	0.85	0.16	0.23	0.17	1.14
Nd142	66.53	19.55	10.22	26.20	2.61	8.02	1.48	30.07
2σ	10.90	4.29	2.09	3.75	0.84	1.31	0.54	5.40
Sm152	8.66	4.05	2.46	4.89	2.60	1.17	1.56	5.50
2σ	1.56	0.89	0.50	0.81	0.27	0.24	0.17	1.08
Eu153	2.27	1.23	0.73	1.39	0.70	0.33	0.45	1.77
2σ	0.53	0.32	0.17	0.23	0.07	0.08	0.05	0.41
Gd158	5.67	4.07	2.48	4.16	1.57	0.80	0.99	4.69
2σ	1.58	1.38	0.57	0.76	0.21	0.21	0.14	1.36
Tb159	0.60	0.48	0.24	0.50	0.14	0.06	0.10	0.48
2σ	0.19	0.16	0.06	0.09	0.02	0.03	0.02	0.15
Dy164	3.28	1.83	1.23	2.24	0.39	0.21	0.36	1.84
2σ	1.17	0.80	0.30	0.48	0.07	0.09	0.07	0.71
Ho165	0.57	0.28	0.17	0.31	0.04	0.02	0.05	0.19
2σ	0.24	0.13	0.05	0.07	0.01	0.02	0.01	0.11
Er166	1.74	0.55	0.32	0.48	0.06	0.07	0.07	0.42
2σ	0.61	0.26	0.11	0.14	0.03	0.06	0.03	0.26
Tm169	0.58	0.07	0.03	0.05	0.01	0.02	0.01	0.06
2σ	0.30	0.05	0.02	0.03	0.01	0.01	0.01	0.06
Yb173	2.60	0.32	0.19	0.19	0.04	-	-	0.04
2σ	1.16	0.22	0.11	0.16	0.04	-	-	0.08

Continued on next page. . .

Table B.5 – continued

Sample	VIC0101	VIC0107	VIC0201	VIC0302	VIC0506	VIC0607	VIC0707	VIC1601
	high-Mg	high-Mg	high-Mg	high-Mg	high-Mg	high-Mg	high-Mg	high-Mg
n	4	3	3	3	6	3	4	4
Lu175	0.46	0.01	0.02	0.02	-	0.01	-	-
2σ	0.32	0.01	0.02	0.01	-	0.01	-	-
Hf180	3.31	2.13	1.08	2.82	0.99	0.53	1.17	2.32
2σ	1.30	1.09	0.25	0.44	0.15	0.14	0.17	1.00
Ta181	0.07	-	-	-	-	-	-	-
2σ	0.08	-	-	-	-	-	-	-
Pb208	0.62	0.95	0.53	1.19	1.36	0.29	1.24	1.46
2σ	0.46	0.78	0.12	0.27	0.38	0.09	0.34	1.00
Th232	0.32	0.69	0.45	0.60	0.14	0.13	0.31	1.25
2σ	0.22	0.41	0.11	0.12	0.03	0.05	0.05	0.64
U238	0.11	0.06	0.03	0.05	0.07	0.03	0.05	0.16
2σ	0.08	0.05	0.02	0.03	0.01	0.02	0.01	0.12

Table B.6: Clinopyroxene trace element compositions of Victor pyroxenites

Sample	VIC0303	VIC0304	VIC0406	VIC0505	VIC1106	VIC1303	VIC2412	VIC2418	VIC0106	VIC2001	VIC2002	VIC2501
	opx-free	opx-free	opx-free	opx-free	opx-free	opx-free	opx-free	opx-free	opx-bearing	opx-bearing	opx-bearing	opx-bearing
n	3	3	3	3	3	3	6	8	5	3	6	4
Li7	0.71	0.73	0.54	1.04	1.33	-	1.33	1.51	1.21	1.11	1.02	0.70
2σ	0.34	0.30	0.65	1.09	0.98	-	0.87	0.88	0.75	0.79	0.69	0.55
Sc45	24.12	23.09	22.60	34.64	26.12	31.91	17.59	22.58	35.00	39.67	38.58	34.95
2σ	8.25	6.99	1.98	3.33	2.29	2.84	1.51	1.87	3.00	3.73	3.39	3.20
Ti48	261.70	193.15	174.18	270.82	203.95	236.99	158.44	154.26	190.03	171.09	266.59	218.32
2σ	25.05	17.33	11.35	24.14	16.05	19.92	10.19	9.85	12.38	11.54	17.50	14.56
V51	324.13	151.98	171.39	394.99	155.39	274.71	174.69	256.51	365.74	480.30	560.20	500.01
2σ	32.67	14.51	14.54	38.35	13.27	25.05	19.86	27.93	43.99	65.85	69.80	65.95
Ni60	174.43	267.18	261.08	158.97	218.18	133.90	274.14	288.81	191.79	167.77	204.54	184.43
2σ	79.02	107.21	49.82	20.36	23.21	15.72	41.86	41.97	31.34	31.91	34.81	33.57
Co59	11.16	17.03	21.95	16.22	22.57	8.70	27.68	20.67	13.05	9.93	13.13	10.65
2σ	3.25	4.45	3.17	2.53	2.83	1.25	2.78	2.03	1.39	1.19	1.44	1.23
Zn64	16.11	19.24	36.30	22.60	31.19	10.95	25.47	28.34	18.89	11.25	18.31	11.88
2σ	8.57	9.01	9.39	2.81	3.22	1.40	11.30	11.74	9.20	6.73	9.43	6.71
Ga69	11.62	4.50	7.09	11.15	6.68	8.50	5.97	7.57	7.38	7.77	12.97	7.02
2σ	1.10	0.63	0.87	1.51	0.79	1.05	1.02	1.19	1.33	1.66	2.42	1.44
Rb85	2.58	2.21	0.23	-	-	-	0.17	-	0.41	-	0.10	0.27
2σ	0.63	0.59	0.17	-	-	-	0.11	-	0.08	-	0.05	0.11
Sr88	688.54	220.04	249.64	264.80	281.95	255.69	137.84	181.55	208.21	555.70	135.93	898.95
2σ	74.83	22.43	46.83	31.91	28.67	28.57	11.93	15.17	18.91	56.83	12.74	88.65
Y89	3.17	1.17	0.56	4.08	0.58	5.03	0.34	1.21	3.67	2.95	3.77	2.50
2σ	0.41	0.19	0.17	0.73	0.12	0.81	0.06	0.17	0.54	0.52	0.59	0.43
Zr90	57.51	16.76	6.23	29.62	4.86	72.74	4.12	12.86	26.41	23.47	57.31	24.05
2σ	7.94	2.26	1.43	3.63	0.60	8.08	0.59	1.68	3.86	4.09	8.75	3.98
Nb93	0.12	0.29	0.14	0.05	1.37	-	0.01	-	0.11	0.26	0.03	0.03
2σ	0.08	0.10	0.08	0.04	0.25	-	0.01	-	0.03	0.05	0.02	0.02
Cs133	0.06	-	-	-	0.01	0.01	-	0.01	0.01	-	-	-
2σ	0.04	-	-	-	0.01	0.01	-	0.01	0.01	-	-	-

Continued on next page...

Table B.6 – continued

Sample	VIC0303	VIC0304	VIC0406	VIC0505	VIC1106	VIC1303	VIC2412	VIC2418	VIC0106	VIC2001	VIC2002	VIC2501
	opx-free	opx-free	opx-free	opx-free	opx-free	opx-free	opx-free	opx-free	opx-bearing	opx-bearing	opx-bearing	opx-bearing
n	3	3	3	3	3	3	6	8	5	3	6	4
Ba138	0.94	0.24	0.13	0.15	0.14	0.48	0.07	0.22	4.62	0.43	0.38	1.22
2σ	0.27	0.10	0.05	0.06	0.04	0.11	0.02	0.03	0.45	0.06	0.05	0.15
La139	130.76	12.76	11.80	19.48	13.69	98.92	8.91	6.37	8.00	30.77	46.20	28.75
2σ	40.27	3.71	1.70	4.33	2.49	20.05	0.93	0.64	0.88	3.86	5.21	3.45
Ce140	228.41	21.90	27.32	22.29	23.30	101.10	10.11	18.32	18.48	84.13	9.73	278.75
2σ	51.16	4.63	3.27	4.63	3.95	19.20	0.90	1.55	1.70	8.63	0.93	27.58
Pr141	16.86	3.32	3.42	2.86	2.53	2.20	1.12	2.51	2.36	10.90	1.22	32.96
2σ	3.88	0.75	0.54	0.66	0.48	0.47	0.13	0.26	0.27	1.37	0.15	3.96
Nd142	95.36	17.39	16.09	15.47	12.66	34.87	1.16	1.30	1.03	0.96	0.89	0.61
2σ	19.53	3.43	2.25	3.56	2.40	7.31	0.66	0.65	0.56	0.62	0.53	0.44
Sm152	4.46	2.84	1.34	2.78	1.23	3.07	0.82	1.74	2.24	4.12	2.69	3.50
2σ	0.95	0.65	0.30	0.63	0.27	0.63	0.13	0.22	0.29	0.59	0.36	0.49
Eu153	1.27	0.80	0.41	0.80	0.26	0.97	0.22	0.47	0.70	0.96	0.79	0.73
2σ	0.33	0.23	0.11	0.21	0.08	0.23	0.04	0.06	0.08	0.11	0.09	0.09
Gd158	3.49	1.75	0.78	2.65	0.66	3.04	0.46	1.17	2.14	2.35	2.41	1.77
2σ	1.16	0.64	0.25	0.70	0.21	0.72	0.11	0.20	0.36	0.45	0.42	0.34
Tb159	0.32	0.14	0.08	0.30	0.05	0.32	0.04	0.12	0.24	0.24	0.28	0.17
2σ	0.12	0.07	0.03	0.08	0.02	0.08	0.01	0.02	0.04	0.05	0.05	0.04
Dy164	1.09	0.57	0.27	1.29	0.22	1.49	0.14	0.44	1.12	0.93	1.16	0.74
2σ	0.49	0.30	0.14	0.37	0.10	0.36	0.05	0.09	0.19	0.19	0.21	0.15
Ho165	0.17	0.11	0.04	0.17	0.02	0.19	0.02	0.05	0.16	0.12	0.15	0.11
2σ	0.10	0.06	0.03	0.05	0.02	0.05	0.01	0.02	0.03	0.03	0.03	0.03
Er166	0.25	0.19	-	0.35	0.06	0.31	0.04	0.09	0.25	0.24	0.27	0.20
2σ	0.18	0.15	-	0.15	0.05	0.11	0.03	0.04	0.06	0.07	0.07	0.06
Tm169	0.06	-	0.02	0.05	0.01	0.03	-	-	0.03	0.02	0.03	0.02
2σ	0.04	-	0.01	0.03	0.01	0.02	-	-	0.01	0.01	0.01	0.01
Yb173	-	-	0.08	0.21	-	0.15	-	0.05	0.10	0.09	0.08	0.11
2σ	-	-	0.08	0.14	-	0.10	-	0.04	0.06	0.05	0.05	0.05
Lu175	-	-	-	0.02	0.02	0.02	-	0.01	0.02	0.02	0.01	0.01

Continued on next page...

Table B.6 – continued

Sample	VIC0303	VIC0304	VIC0406	VIC0505	VIC1106	VIC1303	VIC2412	VIC2418	VIC0106	VIC2001	VIC2002	VIC2501
	opx-free	opx-free	opx-free	opx-free	opx-free	opx-free	opx-free	opx-free	opx-bearing	opx-bearing	opx-bearing	opx-bearing
n	3	3	3	3	3	3	6	8	5	3	6	4
2σ	-	-	-	0.02	0.01	0.02	-	0.01	0.01	0.01	0.01	0.01
Hf180	2.28	0.54	0.50	1.58	0.27	2.16	0.20	0.69	1.36	1.21	2.29	1.28
2σ	1.11	0.33	0.16	0.39	0.11	0.47	0.06	0.14	0.28	0.29	0.48	0.30
Ta181	0.04	-	-	-	0.05	-	-	-	0.01	-	-	0.01
2σ	0.04	-	-	-	0.03	-	-	-	0.01	-	-	0.01
Pb208	1.30	1.10	0.84	1.01	0.75	0.71	1.61	1.40	1.43	1.79	1.29	1.29
2σ	1.01	0.83	0.24	0.24	0.17	0.16	0.63	0.52	0.60	0.88	0.57	0.61
Th232	0.59	0.64	0.05	1.31	0.15	0.21	0.50	0.10	0.34	0.10	1.04	0.04
2σ	0.35	0.37	0.04	0.31	0.06	0.06	0.09	0.02	0.07	0.03	0.21	0.01
U238	0.26	0.06	0.06	0.07	0.04	-	0.05	0.02	0.06	0.03	0.01	0.02
2σ	0.18	0.07	0.03	0.03	0.02	-	0.01	0.01	0.01	0.01	0.01	0.01

Appendix C

Isotopic data for Victor eclogite and pyroxenite xenoliths

Table C.1: Clinopyroxene strontium isotopic compositions of Victor eclogites and pyroxenites

Sample	Description	Rb (ppm) (TIMS)	Sr (ppm) (TIMS)	Rb (ppm) (ICP-MS)	Sr (ppm) (ICP-MS)	$^{87}Rb/^{86}Sr$ (TIMS)	$^{87}Sr/^{86}Sr$ measured (TIMS)	2SE	$^{87}Sr/^{86}Sr$ measured (ICP-MS)	2SE	n	$^{87}Sr/^{86}Sr$ initial (TIMS)
VIC0608	high-Ca ecl	0.21	31.85	-	28.64	0.01924	0.70193	0.00106	-	-	-	0.70188
VIC0703	low-Mg ecl	-	-	0.15	302.51	-	-	-	0.70308	0.00021	4	-
VIC1104	low-Mg ecl	-	186.44	5.05	197.19	-	0.70213	0.00003	-	-	-	0.70213
VIC1305	low-Mg ecl	0.02	149.73	-	165.7	0.00048	0.70210	0.00003	0.70193	0.00019	12	0.70210
VIC0101	high-Mg ecl	-	-	1.94	615.78	-	-	-	0.70312	0.00014	4	-
VIC0201	high-Mg ecl	-	133.65	-	161.77	-	0.70201	0.00006	-	-	-	0.70201
VIC1601	high-Mg ecl	-	250.04	1.26	320.95	-	0.70230	0.00004	0.70244	0.00014	9	0.70231
VIC0303	opx-free px	-	-	2.58	688.54	-	-	-	0.70288	0.00021	5	-
VIC1106	opx-free px	0.43	229.53	-	281.95	0.00544	0.70191	0.00003	0.70196	0.00009	9	0.70189
VIC1303	opx-free px	-	-	-	255.69	-	-	-	0.70225	0.00007	12	-
VIC2001	opx-bearing px	-	-	-	555.7	-	-	-	0.70391	0.00023	3	-
VIC2501	opx-bearing px	-	-	0.27	898.95	-	-	-	0.70265	0.00021	7	-

MC-ICP-MS $^{87}Sr/^{86}Sr$ are reported as the weighted average of "n" number of line scans. 2 standard errors (SE) report the in-run precision. Calculated $^{87}Sr/^{86}Sr$ are for the time of kimberlite eruption (~180 Ma; Januszczak et al., 2013). "-" indicates not measured or below detection.

Table C.2: Garnet oxygen isotopic compositions of Victor eclogites and pyroxenites

Sample		n	$\delta^{18}O$	2σ
VIC0608	high-Ca eclogite	2	5.18	0.55
VIC0502	low-Mg eclogite	2	6.96	0.48
VIC0504	low-Mg eclogite	3	6.29	0.44
VIC0604	low-Mg eclogite	2	5.54	0.47
VIC0703	low-Mg eclogite	2	5.39	0.44
VIC0704	low-Mg eclogite	3	6.31	0.4
VIC0705	low-Mg eclogite	2	5.13	0.47
VIC1104	low-Mg eclogite	2	5.94	0.45
VIC1305	low-Mg eclogite	2	5.04	0.48
VIC0101	high-Mg eclogite	2	5.54	0.39
VIC0107	high-Mg eclogite	2	5.79	0.39
VIC0201	high-Mg eclogite	2	5.64	0.38
VIC0302	high-Mg eclogite	2	5.79	0.38
VIC0506	high-Mg eclogite	2	5.4	0.4
VIC0607	high-Mg eclogite	2	5.31	0.42
VIC0707	high-Mg eclogite	2	5.51	0.44
VIC1601	high-Mg eclogite	2	5.56	0.4
VIC0303	opx-free pyroxenite	2	5.58	0.4
VIC0304	opx-free pyroxenite	2	5.47	0.39
VIC0406	opx-free pyroxenite	2	5.22	0.43
VIC0505	opx-free pyroxenite	2	5.64	0.38
VIC1106	opx-free pyroxenite	2	5.33	0.4
VIC1303	opx-free pyroxenite	2	5.72	0.38
VIC2412	opx-free pyroxenite	2	5.21	0.43
VIC2418	opx-free pyroxenite	2	5.71	0.38
VIC0106	opx-bearing pyroxenite	2	5.68	0.39
VIC0507	opx-bearing pyroxenite	2	5.62	0.38
VIC1703	opx-bearing pyroxenite	2	5.39	0.37
VIC2001	opx-bearing pyroxenite	2	5.74	0.39
VIC2002	opx-bearing pyroxenite	2	5.46	0.39
VIC2302	opx-bearing pyroxenite	2	5.63	0.41
VIC2501	opx-bearing pyroxenite	2	5.66	0.39
VIC8401	opx-bearing pyroxenite	3	5.64	0.38

Oxygen isotope data is given in per mill () and as the average of "n" analytical spots. The total uncertainty on each analytical spot is the combination of uncertainty on the mean UAG value for the session, the standard deviation of UAG, and uncertainty in the matrix correction. Analyses for each sample were averaged, with the uncertainty for each sample given as the largest error of the single spot analyses.
These data relate to CCIM Project 1110.

Table C.3: Whole Rock Re-Os isotopic compositions of Victor eclogites and pyroxenites

Sample		Re (ppb)	Os (ppb)	Common Os (ppb)	$^{187}Re/^{188}Os$	2SE	$^{187}Os/^{188}Os$	2SE	T_{RD} (Ga)	T_{MA} (Ga)	γ_{Os} present day	γ_{Os} initial
VIC0608	high-Ca ecl	0.08	0.08	0.08	5.0853	0.0295	0.2057	0.0013	-	0.97	59	60
VIC0703	low-Mg ecl	0.56	0.14	0.11	24.8181	0.1139	2.3568	0.0121	-	5.25	1719	1737
VIC1104	low-Mg ecl	0.23	0.10	0.08	13.3141	0.0728	1.4961	0.0071	-	6.05	1054	1066
VIC1305	low-Mg ecl	0.10	0.12	0.11	4.4435	0.0367	0.3244	0.0020	-	2.85	150	153
VIC0101	high-Mg ecl	0.03	0.20	0.20	0.6695	0.0092	0.3689	0.0021	-	42.18	185	188
VIC0201	high-Mg ecl	0.42	0.17	0.15	13.4224	0.0644	1.2217	0.0050	-	4.85	843	852
VIC1601	high-Mg ecl	0.16	0.21	0.20	3.7273	0.0268	0.5534	0.0038	-	7.27	327	331
VIC1106	Opx-free px	0.13	0.21	0.20	3.0575	0.0215	0.3228	0.0015	-	4.27	149	152
VIC1303	Opx-free px	0.03	0.49	0.49	0.2941	0.0042	0.1167	0.0004	1.76	5.29	-10	-9
VIC1703	Opx-bearing px	1.52	0.64	0.58	12.6393	0.1679	0.9278	0.0034	-	3.80	616	623

Common Os is given as the Os concentration after in-grown ^{187}Os is subtracted. Initial γ_{Os} calculated at the time of kimberlite eruption (~180 Ma; Januszczak et al., 2013). 2 standard errors include the in-run precision, the uncertainty in the concentration and isotopic composition of the blank, and the uncertainty in the spike calibration.

Appendix D

FTIR and SIMS data for T1 and U2 diamonds

Table D.1: FTIR analyses of T1 diamonds

Diamond	N_A (ppm)	N_B (ppm)	N_{TOT} (ppm)	%B	Platelet Peak Area (cm^{-2})	Platelet Peak Position (cm^{-1})	Hydrogen Peak Area (cm^{-2})
LZ363-1	-	-	-	-	-	-	1.01
LZ363-2	-	-	-	-	-	-	1.66
LZ282-1	-	-	-	-	-	-	2.48
LZ282-2	-	-	-	-	-	-	1.54
LZ283-1	-	-	-	-	-	-	3.22
LZ283-2	-	-	-	-	-	-	3.03
LZ284-1	-	-	-	-	-	-	2.05
LZ284-2	-	-	-	-	-	-	1.68
LZ285-1	2.30	43.00	45.30	94.92	4.62	1359.67	4.28
LZ286-1	-	-	-	-	-	-	1.77
LZ286-2	-	-	-	-	-	-	0.75
LZ287-1	-	-	-	-	-	-	0.68
LZ287-2	-	-	-	-	-	-	0.72
LZ288-1	-	-	-	-	-	-	2.14
LZ288-2	-	-	-	-	-	-	1.38
LZ289-1	-	-	-	-	-	-	-
LZ290-1	-	-	-	-	-	-	0.89
LZ290-2	-	-	-	-	-	-	0.93
LZ291-1	-	-	-	-	-	-	1.63
LZ292-1	-	-	-	-	-	-	0.18
LZ292-2	-	-	-	-	-	-	0.19
LZ293-1	-	-	-	-	-	-	0.74
LZ293-2	-	-	-	-	-	-	1.80
LZ294-1	-	-	-	-	-	-	1.71
LZ294-2	-	-	-	-	-	-	1.71
LZ295-1	-	-	-	-	-	-	1.54
LZ295-2	-	-	-	-	-	-	1.12
LZ296-1	-	-	-	-	-	-	-
LZ296-2	-	-	-	-	-	-	-
LZ297-1	-	-	-	-	-	-	0.61
LZ297-2	-	-	-	-	-	-	0.70
LZ298-1	-	-	-	-	-	-	0.76
LZ298-2	-	-	-	-	-	-	0.93
LZ299-1	-	-	-	-	-	-	0.80
LZ299-2	-	-	-	-	-	-	0.72
LZ300-1	-	-	-	-	-	-	1.93
LZ300-2	-	-	-	-	-	-	-
LZ301-1	-	-	-	-	-	-	2.31
LZ301-2	-	-	-	-	-	-	0.70
LZ302-1	-	-	-	-	-	-	1.64
LZ302-2	-	-	-	-	-	-	2.26
LZ303-1	-	-	-	-	-	-	1.07
LZ303-2	-	-	-	-	-	-	0.77
LZ304-1	-	-	-	-	-	-	0.19
LZ304-2	-	-	-	-	-	-	-
LZ305-1	-	-	-	-	-	-	1.15
LZ305-2	-	-	-	-	-	-	0.41

Continued on next page. . .

Table D.1 – continued

Diamond	N_A (ppm)	N_B (ppm)	N_{TOT} (ppm)	%B	Platelet Peak Area (cm^{-2})	Platelet Peak Position (cm^{-1})	Hydrogen Peak Area (cm^{-2})
LZ306-1	-	-	-	-	-	-	0.63
LZ306-2	-	-	-	-	-	-	0.63
LZ307-1	-	-	-	-	-	-	1.13
LZ307-2	-	-	-	-	-	-	1.24
LZ308-1	-	-	-	-	-	-	1.10
LZ308-2	-	-	-	-	-	-	1.03
LZ309-1	-	-	-	-	-	-	1.51
LZ309-2	-	-	-	-	-	-	1.23
LZ310-1	23.00	897.30	920.30	97.50	241.23	1365.14	82.11
LZ310-2	31.40	359.30	390.80	91.94	181.18	1363.32	70.25
LZ311-1	-	-	-	-	-	-	1.43
LZ311-2	-	-	-	-	-	-	1.46
LZ312-1	-	-	-	-	-	-	0.81
LZ313-1	-	-	-	-	-	-	1.44
LZ313-2	-	-	-	-	-	-	0.53
LZ314-1	2.10	29.50	31.60	93.35	-	-	4.08
LZ314-2	-	-	-	-	-	-	2.41
LZ315-1	-	-	-	-	-	-	0.99
LZ315-2	-	-	-	-	-	-	0.64
LZ316-1	-	-	-	-	-	-	0.84
LZ316-2	-	-	-	-	-	-	0.81
LZ317-1	-	-	-	-	-	-	0.61
LZ317-2	-	-	-	-	-	-	1.29
LZ318-1	-	-	-	-	-	-	0.26
LZ318-2	-	-	-	-	-	-	0.56
LZ319-1	-	-	-	-	-	-	1.01
LZ319-2	-	-	-	-	-	-	1.47
LZ320-1	-	-	-	-	-	-	2.02
LZ320-2	-	-	-	-	-	-	1.57
LZ321-1	-	-	-	-	-	-	0.58
LZ321-2	-	-	-	-	-	-	0.40
LZ322-1	-	-	-	-	-	-	1.16
LZ322-2	-	-	-	-	-	-	0.86
LZ323-1	-	-	-	-	-	-	1.46
LZ323-2	-	-	-	-	-	-	1.01
LZ324-1	-	-	-	-	-	-	1.58
LZ324-2	-	-	-	-	-	-	0.76
LZ325-1	-	-	-	-	-	-	2.00
LZ325-2	-	-	-	-	-	-	2.39
LZ326-1	-	-	-	-	-	-	3.71
LZ327-1	-	-	-	-	-	-	1.75
LZ327-2	-	-	-	-	-	-	1.16
LZ328-1	-	-	-	-	-	-	-
LZ329-1	-	-	-	-	-	-	1.10
LZ329-2	-	-	-	-	-	-	0.60
LZ330-1	-	-	-	-	-	-	1.94
LZ330-2	-	-	-	-	-	-	1.54
LZ331-1	-	-	-	-	-	-	1.04

Continued on next page...

Table D.1 – continued

Diamond	N_A (ppm)	N_B (ppm)	N_{TOT} (ppm)	%B	Platelet Peak Area (cm^{-2})	Platelet Peak Position (cm^{-1})	Hydrogen Peak Area (cm^{-2})
LZ331-2	-	-	-	-	-	-	1.75
LZ332-1	-	-	-	-	-	-	2.08
LZ332-2	-	-	-	-	-	-	0.37
LZ333-1	11.90	38.00	49.90	76.15	7.55	1360.04	5.47
LZ333-2	7.50	98.20	105.70	92.90	2.20	1360.27	3.99
LZ334-1	-	-	-	-	-	-	3.65
LZ334-2	-	-	-	-	-	-	2.37
LZ335-1	-	-	-	-	-	-	0.31
LZ335-2	-	-	-	-	-	-	0.36
LZ336-1	-	-	-	-	-	-	1.31
LZ336-2	-	-	-	-	-	-	0.81
LZ337-1	-	-	-	-	-	-	1.15
LZ337-2	-	-	-	-	-	-	-
LZ338-1	-	-	-	-	-	-	1.38
LZ338-2	-	-	-	-	-	-	0.95
LZ339-1	-	-	-	-	-	-	1.55
LZ340-1	-	-	-	-	-	-	0.82
LZ340-2	-	-	-	-	-	-	1.58
LZ341-1	-	-	-	-	-	-	1.11
LZ341-2	-	-	-	-	-	-	-
LZ342-1	-	-	-	-	-	-	-
LZ343-1	-	-	-	-	-	-	0.68
LZ343-2	-	-	-	-	-	-	0.63
LZ344-1	-	-	-	-	-	-	0.67
LZ344-2	-	-	-	-	-	-	1.01
LZ345-1	-	-	-	-	-	-	1.10
LZ345-2	-	-	-	-	-	-	0.72
LZ346-1	-	-	-	-	-	-	1.11
LZ346-2	-	-	-	-	-	-	1.22
LZ347-1	-	-	-	-	-	-	2.64
LZ347-2	-	-	-	-	-	-	1.38
LZ348-1	-	-	-	-	-	-	1.69
LZ348-2	-	-	-	-	-	-	1.75
LZ349-1	-	-	-	-	-	-	1.18
LZ349-2	-	-	-	-	-	-	1.04
LZ350-1	-	-	-	-	-	-	0.60
LZ350-2	-	-	-	-	-	-	0.47
LZ351-1	-	-	-	-	-	-	-
LZ351-2	-	-	-	-	-	-	2.58
LZ352-1	-	-	-	-	-	-	0.52
LZ352-2	-	-	-	-	-	-	1.29
LZ353-1	-	-	-	-	-	-	1.44
LZ353-2	-	-	-	-	-	-	-
LZ354-1	-	-	-	-	-	-	4.87
LZ354-2	6.50	16.50	23.00	71.74	-	-	3.48
LZ355-1	-	-	-	-	-	-	-
LZ355-2	-	-	-	-	-	-	0.96
LZ356-1	-	-	-	-	-	-	1.39

Continued on next page. . .

Table D.1 – continued

Diamond	N_A (ppm)	N_B (ppm)	N_{TOT} (ppm)	%B	Platelet Peak Area (cm^{-2})	Platelet Peak Position (cm^{-1})	Hydrogen Peak Area (cm^{-2})
LZ356-2	-	-	-	-	-	-	0.47
LZ357-1	-	-	-	-	-	-	0.69
LZ358-1	8.50	38.90	47.40	82.07	-	-	8.65
LZ358-2	-	-	-	-	-	-	1.76
LZ359-1	-	-	-	-	-	-	0.45
LZ360-1	-	-	-	-	-	-	1.44
LZ360-2	-	-	-	-	-	-	1.22
LZ361-1	-	-	-	-	-	-	1.11
LZ361-2	-	-	-	-	-	-	0.84
LZ362-1	-	-	-	-	-	-	0.80
LZ362-2	-	-	-	-	-	-	1.11
LZ364-1	-	-	-	-	-	-	-
LZ365-1	-	-	-	-	-	-	0.51
LZ365-2	9.90	34.00	43.90	77.45	6.63	1359.69	5.74
LZ366-1	-	-	-	-	-	-	1.10
LZ366-2	-	-	-	-	-	-	0.63
LZ367-1	-	-	-	-	-	-	0.67
LZ367-2	-	-	-	-	-	-	-
LZ368-1	-	-	-	-	-	-	0.96
LZ368-2	-	-	-	-	-	-	0.94
LZ369-1	-	-	-	-	-	-	1.47
LZ369-2	-	-	-	-	-	-	1.30
LZ370-1	-	-	-	-	-	-	0.49
LZ370-2	-	-	-	-	-	-	1.15
LZ371-1	-	-	-	-	-	-	1.42
LZ371-2	-	-	-	-	-	-	1.23
LZ372-1	-	-	-	-	-	-	1.08
LZ372-2	-	-	-	-	-	-	1.69
LZ373-1	-	-	-	-	-	-	2.02
LZ373-2	-	-	-	-	-	-	0.45
LZ374-1	-	-	-	-	-	-	-
LZ374-2	-	-	-	-	-	-	1.69
LZ375-1	-	-	-	-	-	-	0.92
LZ375-2	-	-	-	-	-	-	1.57
LZ376-1	2.10	45.00	47.00	95.74	2.17	1359.21	1.35
LZ376-2	-	-	-	-	-	-	0.69
LZ377-1	10.10	48.90	59.00	82.88	4.13	1358.58	9.80
LZ377-2	8.60	54.00	62.60	86.26	2.67	1359.22	6.74
LZ378-1	-	-	-	-	-	-	1.11
LZ378-2	-	-	-	-	-	-	1.62
LZ379-1	-	-	-	-	-	-	1.20
LZ379-2	-	-	-	-	-	-	2.90
LZ380-1	-	-	-	-	-	-	3.55
LZ380-2	7.40	45.20	52.70	85.77	1.28	1360.65	3.77

'-' indicates below detection limit or not present.

Table D.2: FTIR analyses of U2 diamonds

Diamond	N_A (ppm)	N_B (ppm)	N_{TOT} (ppm)	%B	Platelet Peak Area (cm^{-2})	Platelet Peak Position (cm^{-1})	Hydrogen Peak Area (cm^{-2})
LZ2-1	-	-	-	-	-	-	0.81
LZ2-2	-	-	-	-	-	-	1.12
LZ3-1	-	-	-	-	-	-	-
LZ3-2	-	-	-	-	-	-	-
LZ4-1	-	-	-	-	-	-	-
LZ5-1	-	-	-	-	-	-	-
LZ5b-1	51.70	-	51.70	-	-	-	-
LZ5b-2	111.30	56.60	168.00	33.69	0.73	1364.63	-
LZ6b-1	78.90	-	78.90	-	-	-	0.33
LZ7-1	222.00	172.80	394.80	43.77	91.70	1362.89	17.64
LZ7-2	212.60	82.50	295.10	27.96	44.78	1361.69	10.41
LZ7b-1	23.90	-	23.90	-	-	-	-
LZ7c-1	-	-	-	-	-	-	-
LZ7c-2	-	-	-	-	-	-	-
LZ8-1	-	-	-	-	-	-	-
LZ8-2	-	-	-	-	-	-	-
LZ8b-1	-	-	-	-	-	-	-
LZ8b-2	-	-	-	-	-	-	-
LZ9-1	-	-	-	-	-	-	-
LZ9b-1	1429.30	17.50	1446.80	1.21	9.92	1376.75	1.66
LZ9b-2	1516.30	223.50	1739.70	12.85	7.93	1378.21	2.15
LZ9c-1	-	-	-	-	-	-	0.51
LZ9c-2	-	-	-	-	-	-	-
LZ10b-1	-	-	-	-	-	-	-
LZ11-1	1401.70	112.50	1514.30	7.43	25.97	1375.88	1.73
LZ11-2	1446.90	160.40	1607.30	9.98	22.84	1376.60	2.00
LZ11b-1	-	-	-	-	-	-	-
LZ11c-1	-	-	-	-	-	-	-
LZ11c-2	-	-	-	-	-	-	-
LZ11d-1	-	-	-	-	-	-	-
LZ12-1	-	-	-	-	-	-	-
LZ12-2	-	-	-	-	-	-	-
LZ12b-1	813.10	17.50	830.60	2.11	17.54	1373.07	-
LZ12b-2	797.40	2.10	799.50	0.26	12.88	1374.06	-
LZ12c-1	-	-	-	-	-	-	-
LZ12c-2	-	-	-	-	-	-	-
LZ12d-1	-	-	-	-	-	-	0.69
LZ12d-2	-	-	-	-	-	-	0.86
LZ12e-1	-	-	-	-	-	-	-
LZ12e-2	-	-	-	-	-	-	-
LZ13-1	-	-	-	-	-	-	-
LZ13-2	-	-	-	-	-	-	-
LZ13b-1	-	-	-	-	-	-	-
LZ13b-2	-	-	-	-	-	-	-
LZ13c-1	-	-	-	-	-	-	-
LZ13c-2	-	-	-	-	-	-	-
LZ13d-1	-	-	-	-	-	-	-

Continued on next page...

Table D.2 – continued

Diamond	N_A (ppm)	N_B (ppm)	N_{TOT} (ppm)	%B	Platelet Peak Area (cm^{-2})	Platelet Peak Position (cm^{-1})	Hydrogen Peak Area (cm^{-2})
LZ13d-2	-	-	-	-	-	-	-
LZ14-1	195.30	-	195.30	-	-	-	-
LZ14b-1	-	-	-	-	-	-	-
LZ14b-2	-	-	-	-	-	-	-
LZ14c-1	-	-	-	-	-	-	-
LZ14c-2	-	-	-	-	-	-	-
LZ14d-1	-	-	-	-	-	-	-
LZ15-1	136.80	19.40	156.30	12.41	-	-	0.42
LZ15-2	148.00	-	148.00	-	-	-	0.37
LZ15b-1	-	-	-	-	-	-	-
LZ15b-2	-	-	-	-	-	-	-
LZ15c-1	-	-	-	-	-	-	-
LZ15d-1	335.00	-	335.00	-	5.77	1374.06	0.46
LZ15d-2	441.70	-	441.70	-	-	-	-
LZ16-2	-	-	-	-	-	-	-
LZ16b-1	375.40	2.10	377.60	0.56	4.67	1374.61	0.50
LZ16b-2	325.10	-	325.10	-	3.71	1376.13	0.48
LZ16c-1	-	-	-	-	-	-	-
LZ16c-2	-	-	-	-	-	-	-
LZ16d-1	-	-	-	-	-	-	20.05
LZ16d-2	-	-	-	-	-	-	15.95
LZ16e-1	-	-	-	-	-	-	-
LZ16e-2	-	-	-	-	-	-	-
LZ17-1	90.90	-	90.90	-	1.08	1370.58	-
LZ17b-1	1488.60	211.60	1700.20	12.45	39.53	1376.53	2.68
LZ17b-2	1462.80	160.50	1623.30	9.89	25.26	1376.12	1.89
LZ17c-1	-	-	-	-	-	-	-
LZ17c-2	-	-	-	-	-	-	-
LZ17d-1	-	-	-	-	-	-	-
LZ17d-2	-	-	-	-	-	-	-
LZ18-1	38.40	6.80	45.20	15.04	-	-	-
LZ18-2	-	-	-	-	-	-	-
LZ18b-1	-	-	-	-	-	-	4.26
Lz18b-2	-	-	-	-	-	-	9.86
LZ18c-1	-	-	-	-	-	-	-
LZ18c-2	-	-	-	-	-	-	-
LZ18d-1	99.80	8.70	108.50	8.02	-	-	0.36
LZ18d-2	93.90	16.80	110.70	15.18	-	-	0.50
LZ19-1	20.70	11.20	31.80	35.22	-	-	-
LZ19-2	102.80	133.70	236.50	56.53	-	-	0.59
LZ19b-1	0.00	124.20	124.20	100.00	-	-	35.07
LZ19c-2	-	-	-	-	-	-	10.08
LZ19d-1	49.40	10.40	59.80	17.39	-	-	-
LZ19d-2	-	-	-	-	-	-	-
LZ20-1	-	-	-	-	-	-	-
LZ20-2	-	-	-	-	-	-	-
LZ20b-1	754.60	9.00	763.60	1.18	22.15	1372.44	0.29
LZ20b-2	886.10	-	886.10	-	16.38	1372.15	0.34

Continued on next page...

Table D.2 – continued

Diamond	N_A (ppm)	N_B (ppm)	N_{TOT} (ppm)	%B	Platelet Peak Area (cm^{-2})	Platelet Peak Position (cm^{-1})	Hydrogen Peak Area (cm^{-2})
LZ21-1	-	-	-	-	-	-	1.21
LZ21-2	-	-	-	-	-	-	0.78
LZ21b-1	-	-	-	-	-	-	0.22
LZ21b-2	-	-	-	-	-	-	-
LZ22-1	-	-	-	-	-	-	0.21
LZ22-2	-	-	-	-	-	-	0.24
LZ22b-1	-	-	-	-	-	-	0.25
LZ22b-2	-	-	-	-	-	-	-
LZ23-1	157.60	11.20	168.80	6.64	-	-	-
LZ23-2	-	-	-	-	-	-	4.60
LZ23b-1	640.70	-	640.70	-	-	-	3.14
LZ23b-2	863.90	30.10	894.00	3.37	-	-	6.32
LZ24-1	-	-	-	-	-	-	-
LZ24-2	13.10	13.10	26.20	50.00	-	-	-
LZ24b-1	-	-	-	-	-	-	-
LZ25-1	473.30	-	473.30	-	6.01	1369.45	0.68
LZ25-2	94.90	11.20	106.10	10.56	0.61	1350.56	-
LZ25b-1	-	-	-	-	-	-	-
Lz25b-2	-	-	-	-	-	-	-
LZ26-1	-	-	-	-	-	-	-
LZ27-1	-	-	-	-	-	-	-
LZ27-2	-	-	-	-	-	-	-
LZ27-3	-	-	-	-	-	-	-
LZ27b-1	-	-	-	-	-	-	-
LZ28-1	38.90	30.80	69.70	44.19	6.40	1379.03	0.34
LZ28-2	-	-	-	-	-	-	-
LZ28b-1	-	-	-	-	-	-	-
LZ28b-2	-	-	-	-	-	-	-
LZ29-1	42.80	59.50	102.30	58.16	0.69	1380.08	-
LZ29-2	31.20	112.70	144.00	78.26	3.49	1377.83	-
LZ30-1	-	-	-	-	-	-	-
LZ30-2	-	-	-	-	-	-	-
LZ31-1	-	-	-	-	-	-	-
LZ31-2	-	-	-	-	-	-	-
LZ32-1	-	-	-	-	-	-	0.58
LZ32-2	-	-	-	-	-	-	-
LZ33-1	-	-	-	-	-	-	-
LZ33-2	-	-	-	-	-	-	-
LZ34-1	-	-	-	-	-	-	-
LZ34-2	-	-	-	-	-	-	-
LZ35-1	-	-	-	-	-	-	-
LZ35-2	-	-	-	-	-	-	-
LZ36-1	929.70	288.10	1217.80	23.66	20.74	1374.15	0.83
LZ36-2	921.90	28.10	949.90	2.96	18.77	1373.72	0.96
LZ37-1	-	-	-	-	-	-	-
LZ37-2	-	-	-	-	-	-	-
LZ38-1	-	-	-	-	-	-	0.49
LZ38-2	-	-	-	-	-	-	-

Continued on next page. . .

Table D.2 – continued

Diamond	N_A (ppm)	N_B (ppm)	N_{TOT} (ppm)	%B	Platelet Peak Area (cm^{-2})	Platelet Peak Position (cm^{-1})	Hydrogen Peak Area (cm^{-2})
LZ38-3	-	-	-	-	-	-	-
LZ39-1	-	-	-	-	-	-	1.15
LZ39-2	-	-	-	-	-	-	0.28
LZ40-1	-	-	-	-	-	-	-
LZ40-2	-	-	-	-	-	-	-
LZ41-1	-	-	-	-	-	-	-
LZ41-2	-	-	-	-	-	-	-
LZ42-1	-	-	-	-	-	-	-
LZ43-1	-	-	-	-	-	-	0.58
LZ43-2	-	-	-	-	-	-	1.80
LZ44-1	-	-	-	-	-	-	-
LZ44-2	-	-	-	-	-	-	-
LZ45-1	-	-	-	-	-	-	-
LZ46-1	-	-	-	-	-	-	-
LZ46-2	51.20	46.50	97.60	47.64	-	-	-
LZ47-1	-	-	-	-	-	-	-
LZ47-2	-	-	-	-	-	-	-
LZ48-1	-	-	-	-	-	-	-
LZ48-2	-	-	-	-	-	-	-
LZ49-1	-	-	-	-	-	-	-
LZ50-1	-	-	-	-	-	-	-
LZ50-2	-	-	-	-	-	-	-
LZ51-1	-	-	-	-	-	-	-
LZ51-2	-	-	-	-	-	-	-
LZ52-1	-	-	-	-	-	-	-
LZ52-2	-	-	-	-	-	-	-
LZ53-1	-	-	-	-	-	-	-
LZ53-2	-	-	-	-	-	-	-
LZ54-1	190.90	230.00	420.90	54.64	158.11	1363.85	10.96

'-' indicates below detection limit or not present.

Table D.3: SIMS analyses of T1 diamonds

CCIM #	Diamond	Spot	δ^{13}C‰	2σ (internal)	2σ (external)	N (ppm)	2σ
S1816	LZ282	1	-1.71	0.16	0.21	12.38	1.4
S1816	LZ282	2	-3.11	0.16	0.21	1.75	0.2
S1816	LZ282	3	-3.56	0.16	0.21	4.78	0.54
S1816	LZ282	4	-3.05	0.16	0.21	-	-
S1816	LZ282	5	-3.64	0.16	0.21	6.23	0.68
S1817	LZ283	1	-2.52	0.16	0.21	2.1	0.23
S1817	LZ283	2	-3.02	0.15	0.2	-	-
S1817	LZ283	3	-2.65	0.16	0.21	5.51	0.69
S1817	LZ283	4	-3.25	0.16	0.21	-	-
S1818	LZ286	1	-3.4	0.16	0.21	11.05	1.15
S1818	LZ286	2	-2.34	0.16	0.21	0.98	0.1
S1818	LZ286	3	-3.53	0.16	0.21	-	-
S1819	LZ287	1	-3.52	0.17	0.22	-	-
S1819	LZ287	2	-3.6	0.16	0.21	1.24	0.14
S1819	LZ287	3	-3.6	0.16	0.21	4.89	0.51
S1820	LZ289	1	-3.19	0.16	0.21	9.36	1.09
S1820	LZ289	2	-2.36	0.16	0.21	4.81	0.53
S1820	LZ289	3	-2.16	0.16	0.21	-	-
S1821	LZ291	1	-1.82	0.16	0.21	0.44	0.05
S1821	LZ291	2	-3.25	0.15	0.2	-	-
S1821	LZ291	3	-3.21	0.16	0.21	4.58	0.49
S1821	LZ291	4	-2.24	0.16	0.21	-	-
S1822	LZ296	1	-3.23	0.15	0.2	-	-
S1822	LZ296	2	-3.68	0.16	0.21	1.26	0.14
S1822	LZ296	3	-2.12	0.16	0.21	-	-
S1822	LZ296	4	-1.96	0.16	0.21	8.44	0.86
S1823	LZ298	1	-3.4	0.17	0.22	4.35	0.49
S1823	LZ298	2	-2.02	0.15	0.2	0.66	0.07
S1823	LZ298	3	-2.96	0.16	0.21	-	-
S1823	LZ298	4	-3.66	0.15	0.2	-	-
S1823	LZ298	5	-3.65	0.16	0.21	1.88	0.22
S1825	LZ306	1	-1.98	0.16	0.21	10.22	1.09
S1825	LZ306	2	-1.76	0.17	0.22	101.15	10.72
S1825	LZ306	3	-1.92	0.16	0.21	14.81	1.64
S1825	LZ306	4	-3.72	0.16	0.21	-	-
S1825	LZ306	5	-3.19	0.16	0.21	-	-
S1826	LZ307	1	-3.15	0.16	0.21	-	-
S1826	LZ307	2	-3.3	0.16	0.21	14.22	1.63
S1826	LZ307	3	-3.41	0.16	0.21	0.74	0.08
S1827	LZ308	1	-3.49	0.16	0.21	6.56	0.83
S1827	LZ308	2	-3.31	0.16	0.21	-	-
S1827	LZ308	3	-3.52	0.15	0.2	7.21	0.83
S1828	LZ312	1	-3.6	0.16	0.21	9.02	1.02
S1828	LZ312	2	-3.38	0.15	0.2	-	-
S1828	LZ312	3	-3.41	0.1	0.15	13.84	1.48
S1829	LZ314	1	-2.34	0.11	0.16	1.74	0.19
S1829	LZ314	2	-3.38	0.11	0.16	0.68	0.08

Continued on next page. . .

Table D.3 – continued

CCIM #	Diamond	Spot	$\delta^{13}C$‰	2σ (internal)	2σ (external)	N (ppm)	2σ
S1829	LZ314	3	-2.53	0.12	0.17	1.28	0.14
S1830	LZ315	1	-3.37	0.1	0.15	5.61	0.62
S1830	LZ315	2	-1.25	0.11	0.16	10.35	1.24
S1830	LZ315	3	-0.85	0.11	0.16	1.8	0.19
S1830	LZ315	3 rep	-0.99	0.11	0.16	-	-
S1830	LZ315	4	-1.01	0.12	0.17	-	-
S1830	LZ315	4	-1.16	0.1	0.15	-	-
S1831	LZ318	1	-1.84	0.13	0.18	0.87	0.09
S1831	LZ318	1 rep	-2.62	0.11	0.16	-	-
S1831	LZ318	2	-2.73	0.12	0.17	3.81	0.44
S1831	LZ318	3	-2.51	0.11	0.16	-	-
S1832	LZ323	1	-3.49	0.1	0.15	-	-
S1832	LZ323	2	-3.27	0.12	0.17	0.65	0.07
S1832	LZ323	3	-3.61	0.1	0.15	5.43	0.55
S1833	LZ324	1	-3.11	0.13	0.18	3.33	0.38
S1833	LZ324	2	-3.4	0.1	0.15	0.29	0.03
S1833	LZ324	3	-3.32	0.1	0.15	-	-
S1833	LZ324	4	-3.38	0.11	0.16	-	-
S1834	LZ326	1	-3.41	0.1	0.15	-	-
S1834	LZ326	2	-3.39	0.11	0.16	9.25	1.04
S1834	LZ326	3	-3.39	0.1	0.15	0.69	0.08
S1835	LZ327	1	-1.51	0.16	0.21	16.72	1.72
S1835	LZ327	2	-2.49	0.16	0.21	3.19	0.36
S1835	LZ327	3	-3.54	0.16	0.21	0.82	0.1
S1837	LZ331	1	-3.39	0.12	0.17	4.5	0.49
S1837	LZ331	2	-3.42	0.11	0.16	-	-
S1837	LZ331	3	-3.19	0.11	0.16	6.06	0.65
S1837	LZ331	4	-3.38	0.13	0.18	-	-
S1837	LZ331	5	-3.31	0.11	0.16	1.81	0.2
S1838	LZ332	1	-3.05	0.1	0.15	1.93	0.2
S1838	LZ332	2	-3.47	0.1	0.15	-	-
S1838	LZ332	3	-3.36	0.11	0.16	-	-
S1838	LZ332	4	-3.39	0.11	0.16	2.08	0.25
S1839	LZ335	1	-3.21	0.11	0.16	5.3	0.59
S1839	LZ335	2	-3.61	0.12	0.17	7.38	0.8
S1839	LZ335	3	-3.27	0.11	0.16	0.65	0.07
S1839	LZ335	4	-3.7	0.11	0.16	-	-
S1840	LZ336	1	-3.16	0.11	0.16	0.3	0.03
S1840	LZ336	2	-3.4	0.11	0.16	-	-
S1840	LZ336	3	-3.13	0.11	0.16	0.28	0.03
S1840	LZ336	4	-3.48	0.1	0.15	15.95	1.78
S1841	LZ341	1	-3.46	0.11	0.16	5.62	0.57
S1841	LZ341	2	-3.39	0.11	0.16	-	-
S1841	LZ341	3	-3.27	0.12	0.17	6.97	0.85
S1842	LZ343	1	-3.34	0.12	0.17	4.6	0.48
S1842	LZ343	2	-3.12	0.1	0.15	3.72	0.42
S1842	LZ343	3	-3.45	0.12	0.17	0.32	0.04
S1842	LZ343	4	-3.36	0.11	0.16	-	-

Continued on next page...

Table D.3 – continued

CCIM #	Diamond	Spot	$\delta^{13}C$‰	2σ (internal)	2σ (external)	N (ppm)	2σ
S1843	LZ348	1	-3.36	0.11	0.16	19.58	2.07
S1843	LZ348	2	-3.34	0.11	0.16	10	1.04
S1843	LZ348	3	-3.44	0.1	0.15	-	-
S1844	LZ349	1	-1.63	0.11	0.16	4.53	0.49
S1844	LZ349	2	-3.1	0.11	0.16	121.04	13
S1844	LZ349	3	-2.79	0.12	0.17	-	-
S1844	LZ349	4	-1.62	0.12	0.17	-	-
S1844	LZ349	5	-3.35	0.11	0.16	10.49	1.13
S1845	LZ350	1	-3.2	0.12	0.17	3.88	0.42
S1845	LZ350	2	-3.56	0.11	0.16	0.35	0.04
S1845	LZ350	3	-3.33	0.11	0.16	-	-
S1845	LZ350	4	-3.43	0.1	0.15	5.06	0.6
S1846	LZ351	1	-3.1	0.11	0.16	-	-
S1846	LZ351	2	-3.15	0.11	0.16	3.41	0.36
S1846	LZ351	3	-3.33	0.12	0.17	-	-
S1846	LZ351	4	-3.43	0.12	0.17	0.63	0.07
S1847	LZ352	1	-2.84	0.11	0.16	8.89	1.03
S1847	LZ352	2	-3.16	0.12	0.17	-	-
S1847	LZ352	3	-3.51	0.11	0.16	9.29	0.97
S1848	LZ354	1	-3.35	0.13	0.18	12.43	1.36
S1848	LZ354	2	-3.95	0.1	0.15	0.29	0.04
S1848	LZ354	3	-3.37	0.11	0.16	-	-
S1849	LZ356	1	-3.5	0.1	0.15	8.44	0.9
S1849	LZ356	2	-3.38	0.11	0.16	11.75	1.35
S1849	LZ356	3	-3.4	0.16	0.21	-	-
S1850	LZ358	1	-3.41	0.15	0.2	19.04	2
S1850	LZ358	2	-3.34	0.15	0.2	-	-
S1850	LZ358	3	-3.75	0.14	0.19	6.66	0.79
S1851	LZ361	1	-3.32	0.15	0.2	-	-
S1851	LZ361	2	-3.11	0.15	0.2	3.68	0.4
S1851	LZ361	3	-3.63	0.15	0.2	16.03	1.76
S1852	LZ363	2	-3.34	0.15	0.2	3.48	0.41
S1852	LZ363	3	-3.37	0.15	0.2	10.53	1.18
S1852	LZ363	4	-3.35	0.14	0.19	-	-
S1853	LZ364	1	-2.47	0.14	0.19	9.09	0.98
S1853	LZ364	2	-1.56	0.14	0.19	8.69	0.89
S1854	LZ366	1	-3.42	0.15	0.2	-	-
S1854	LZ366	2	-3.37	0.16	0.21	5.47	0.61
S1854	LZ366	3	-3.48	0.16	0.21	9.02	1
S1855	LZ367	1	-3.46	0.14	0.19	6.51	0.73
S1855	LZ367	2	-3.61	0.14	0.19	4.27	0.45
S1855	LZ367	3	-3.91	0.14	0.19	14.92	1.68
S1856	LZ369	1	-2.91	0.14	0.19	39.62	4.31
S1856	LZ369	2	-2.67	0.15	0.2	-	-
S1856	LZ369	3	-2.83	0.15	0.2	2.59	0.32
S1856	LZ369	4	-3.23	0.16	0.21	3.63	0.44
S1857	LZ371	1	-3.52	0.15	0.2	7.03	0.81
S1857	LZ371	2	-3.55	0.15	0.2	-	-

Continued on next page. . .

Table D.3 – continued

CCIM #	Diamond	Spot	δ^{13}C‰	2σ (internal)	2σ (external)	N (ppm)	2σ
S1857	LZ371	3	-3.84	0.14	0.19	11.96	1.3
S1858	LZ372	1	-3.35	0.16	0.21	34.68	3.96
S1858	LZ372	2	-3.14	0.14	0.19	2.79	0.29
S1858	LZ372	3	-3.17	0.15	0.2	-	-
S1859	LZ373	1	-2.11	0.15	0.2	-	-
S1859	LZ373	2	-3.37	0.16	0.21	6.22	0.66
S1859	LZ373	3	-3.43	0.15	0.2	8	0.82
S1859	LZ373	4	-3.24	0.15	0.2	-	-
S1859	LZ373	5	-2.6	0.15	0.2	1.85	0.19
S1860	LZ374	1	-2.91	0.15	0.2	-	-
S1860	LZ374	2	-3.01	0.15	0.2	7.65	0.79
S1860	LZ374	3	-3.28	0.15	0.2	4.2	0.45
S1861	LZ375	1	-3.29	0.16	0.21	-	-
S1861	LZ375	2	-3.29	0.15	0.2	10.77	1.17
S1861	LZ375	3	-3.38	0.15	0.2	9.98	1.05

2σ uncertainties for δ^{13}C include in-run precision (internal error), between spot error and uncertainty related to instrumental mass fractionation and reference material composition (external error). All results are reported relative to the international Vienna Pee-Dee Belemnite standard (V-PDB).

2σ uncertainties for nitrogen concentration include within-spot counting statistics and the error in the nitrogen abundance calibration. An additional error of ~10% (2σ) is associated with uncertainty in the FTIR-determined nitrogen abundance, and should be used when comparing data with FTIR-determined concentrations. '-' indicates not measured.

These data relate to CCIM Project 1202.

Table D.4: SIMS analyses of U2 diamonds

CCIM #	Diamond	Spot	δ^{13}C‰	2σ (internal)	2σ (external)	N (ppm)	2σ
S1868	LZ3	1	-6.54	0.17	0.22	1.77	0.19
S1868	LZ3	2	-6.77	0.17	0.22	-	-
S1868	LZ3	3	-6.71	0.18	0.23	-	-
S1868	LZ3	4	-6.65	0.18	0.23	-	-
S1868	LZ3	5	-6.52	0.17	0.22	1.31	0.14
S1869	LZ5	1	-6.24	0.18	0.23	3.25	0.34
S1869	LZ5	2	-6.29	0.17	0.22	-	-
S1869	LZ5	3	-6.1	0.17	0.22	-	-
S1869	LZ5	4	-6.1	0.17	0.22	-	-
S1869	LZ5	5	-6.38	0.17	0.22	2.32	0.27
S1870	LZ7	1	-6.87	0.18	0.23	867.27	87.2
S1870	LZ7	2	-6.77	0.17	0.22	-	-
S1870	LZ7	3	-7.06	0.17	0.22	553.85	56.69
S1870	LZ7	4	-6.84	0.17	0.22	-	-
S1870	LZ7	5	-6.7	0.17	0.22	-	-
S1870	LZ7	6	-6.62	0.17	0.22	-	-
S1870	LZ7	7	-6.44	0.17	0.22	-	-
S1870	LZ7	8	-6.3	0.17	0.22	147.23	14.9
S1870	LZ7	9	-6.48	0.17	0.22	-	-
S1870	LZ7	10	-6.53	0.17	0.22	-	-
S1870	LZ7	11	-6.81	0.17	0.22	-	-
S1870	LZ7	12	-6.89	0.18	0.23	-	-
S1871	LZ9	1	-7.02	0.17	0.22	14.77	1.75
S1871	LZ9	2	-6.93	0.17	0.22	-	-
S1871	LZ9	3	-6.93	0.18	0.23	-	-
S1871	LZ9	4	-7.03	0.17	0.22	3.41	0.37
S1871	LZ9	5	-6.86	0.17	0.22	-	-
S1871	LZ9	6	-7.04	0.17	0.22	-	-
S1871	LZ9	7	-7.18	0.17	0.22	-	-
S1871	LZ9	8	-7.11	0.17	0.22	-	-
S1872	LZ8	1	-6.57	0.17	0.22	2.36	0.25
S1872	LZ8	2	-6.61	0.17	0.22	3.25	0.36
S1872	LZ8	3	-6.5	0.17	0.22	-	-
S1872	LZ8	4	-6.69	0.17	0.22	-	-
S1873	LZ12	1	-6.49	0.17	0.22	-	-
S1873	LZ12	2	-6.35	0.17	0.22	55.45	5.7
S1873	LZ12	3	-6.56	0.17	0.22	60.73	6.25
S1874	LZ13	1	-6.11	0.17	0.22	6.91	0.71
S1874	LZ13	2	-6.14	0.17	0.22	-	-
S1874	LZ13	3	-6.05	0.17	0.22	-	-
S1874	LZ13	4	-6.1	0.17	0.22	3.64	0.37
S1874	LZ13	5	-6.14	0.17	0.22	-	-
S1874	LZ13	6	-6.23	0.17	0.22	-	-
S1874	LZ13	7	-6.18	0.18	0.23	-	-
S1875	LZ14	1	-6.69	0.17	0.22	719.46	72.77
S1875	LZ14	2	-15.78	0.18	0.23	220.94	22.48
S1875	LZ14	3	-16.94	0.17	0.22	-	-

Continued on next page. . .

Table D.4 – continued

CCIM #	Diamond	Spot	$\delta^{13}C$‰	2σ (internal)	2σ (external)	N (ppm)	2σ
S1875	LZ14	4	-17.68	0.17	0.22	105.24	10.79
S1875	LZ14	5	-17.63	0.17	0.22	175.73	17.82
S1875	LZ14	6	-8.09	0.17	0.22	-	-
S1875	LZ14	7	-9.41	0.17	0.22	783.15	78.99
S1876	LZ12B	1	-7.83	0.17	0.22	555.44	55.88
S1876	LZ12B	2	-7.31	0.17	0.22	-	-
S1876	LZ12B	3	-7.34	0.17	0.22	-	-
S1876	LZ12B	4	-7.17	0.17	0.22	528.29	53.44
S1876	LZ12B	5	-7.42	0.17	0.22	-	-
S1876	LZ12B	6	-7.44	0.17	0.22	-	-
S1876	LZ12B	7	-7.73	0.17	0.22	-	-
S1876	LZ12B	8	-7.1	0.17	0.22	864.72	87.4
S1876	LZ12B	9	-6.98	0.17	0.22	-	-
S1876	LZ12B	10	-7.06	0.18	0.23	-	-
S1876	LZ12B	11	-7.01	0.17	0.22	-	-
S1876	LZ12B	12	-7.06	0.17	0.22	-	-
S1876	LZ12B	13	-6.91	0.17	0.22	657.96	66.5
S1877	LZ16	1	-6.01	0.18	0.23	5.64	0.58
S1877	LZ16	2	-5.96	0.17	0.22	-	-
S1877	LZ16	3	-6.03	0.18	0.23	-	-
S1877	LZ16	4	-6.09	0.18	0.23	15.64	2.32
S1877	LZ16	5	-6.01	0.17	0.22	-	-
S1878	LZ18	1	-6.69	0.17	0.22	165.5	16.75
S1878	LZ18	2	-6.53	0.17	0.22	-	-
S1878	LZ18	3	-6.34	0.17	0.22	172.06	17.41
S1879	LZ17	1	-2.46	0.18	0.23	42.9	4.62
S1879	LZ17	2	-2.76	0.17	0.22	-	-
S1879	LZ17	3	-2.62	0.18	0.23	3.72	0.41
S1880	LZ25	1	-5.36	0.17	0.22	263.48	27.25
S1880	LZ25	2	-4.94	0.17	0.22	-	-
S1880	LZ25	3	-4.75	0.17	0.22	524.79	53.4
S1880	LZ25	4	-4.18	0.17	0.22	307.54	31.3
S1880	LZ25	6	-4.47	0.17	0.22	-	-
S1880	LZ25	7	-4.5	0.18	0.23	-	-
S1881	LZ21	1	-4.64	0.17	0.22	5.36	0.59
S1881	LZ21	2	-4.73	0.17	0.22	-	-
S1881	LZ21	3	-4.73	0.17	0.22	4.67	0.51
S1882	LZ23	1	-6.24	0.17	0.22	249.1	25.29
S1882	LZ23	2	-5.82	0.17	0.22	-	-
S1882	LZ23	3	-5.74	0.17	0.22	50.6	5.2
S1882	LZ23	4	-5.94	0.17	0.22	-	-
S1882	LZ23	5	-6.11	0.17	0.22	317.03	32.06
S1883	LZ26	1	-5.52	0.17	0.22	3.46	0.4
S1883	LZ26	2	-5.33	0.18	0.23	-	-
S1883	LZ26	3	-5.25	0.17	0.22	2.94	0.3
S1884	LZ11B	1	-4.92	0.17	0.22	1.77	0.19
S1884	LZ11B	2	-4.81	0.17	0.22	-	-
S1884	LZ11B	3	-4.74	0.17	0.22	4.03	0.47

Continued on next page. . .

Table D.4 – continued

CCIM #	Diamond	Spot	$\delta^{13}C‰$	2σ (internal)	2σ (external)	N (ppm)	2σ
S1884	LZ11B	4	-4.72	0.17	0.22	-	-
S1884	LZ11B	5	-4.69	0.18	0.23	-	-
S1884	LZ11B	6	-4.26	0.18	0.23	3.39	0.37
S1885	LZ13B	1	-3.7	0.17	0.22	3.88	0.44
S1885	LZ13B	2	-3.2	0.17	0.22	3.75	0.46
S1885	LZ13B	3	-2.82	0.17	0.22	-	-
S1885	LZ13B	4	-2.68	0.18	0.23	3.36	0.37
S1885	LZ13B	5	-2.83	0.18	0.23	-	-
S1886	LZ14B	1	-5.13	0.18	0.23	4.5	0.53
S1886	LZ14B	2	-4.95	0.17	0.22	3.1	0.36
S1886	LZ14B	3	-4.97	0.18	0.23	-	-
S1887	LZ17B	1	-6.89	0.18	0.23	1565.37	158.61
S1887	LZ17B	2	-6.92	0.18	0.23	1554.66	157.48
S1887	LZ17B	3	-6.53	0.18	0.23	-	-
S1887	LZ17B	4	-6.43	0.17	0.22	1593.42	161.62
S1887	LZ17B	5	-6.49	0.17	0.22	-	-
S1887	LZ17B	6	-6.83	0.17	0.22	-	-
S1887	LZ17B	7	-6.66	0.17	0.22	1448.81	146.76
S1889	LZ7C	1	-5.58	0.17	0.22	1.15	0.12
S1889	LZ7C	2	-5.51	0.17	0.22	-	-
S1889	LZ7C	3	-5.41	0.17	0.22	2.13	0.26
S1889	LZ7C	4	-4.96	0.18	0.23	1.82	0.2
S1889	LZ7C	5	-4.94	0.17	0.22	-	-
S1889	LZ7C	6	-4.9	0.17	0.22	1.62	0.17
S1890	LZ8B	1	-5.48	0.17	0.22	2.87	0.33
S1890	LZ8B	2	-5.57	0.17	0.22	-	-
S1890	LZ8B	3	-5.54	0.17	0.22	2.53	0.29
S1890	LZ8B	4	-5.42	0.18	0.23	-	-
S1891	LZ10B	1	-5.62	0.18	0.23	1.86	0.2
S1891	LZ10B	2	-5.55	0.17	0.22	-	-
S1891	LZ10B	3	-5.74	0.17	0.22	-	-
S1891	LZ10B	4	-5.86	0.17	0.22	242.17	25.73
S1892	LZ16C	1	-5.38	0.17	0.22	2.47	0.26
S1892	LZ16C	2	-5.75	0.18	0.23	1.91	0.2
S1894	LZ11D	1	-5.62	0.19	0.24	1.81	0.19
S1894	LZ11D	2	-5.6	0.2	0.25	-	-
S1894	LZ11D	3	-5.41	0.19	0.24	3.15	0.33
S1895	LZ12E	1	-4.99	0.19	0.24	2.75	0.3
S1895	LZ12E	2	-4.89	0.19	0.24	2.77	0.3
S1896	LZ16D	1	-1.13	0.19	0.24	94.52	9.98
S1896	LZ16D	2	-1.44	0.2	0.25	-	-
S1896	LZ16D	3	-1.71	0.19	0.24	69.76	7.61
S1896	LZ16D	4	-1.98	0.19	0.24	28.48	3.18
S1896	LZ16D	5	-0.47	0.19	0.24	-	-
S1896	LZ16D	6	0.2	0.2	0.25	69.01	7.23
S1896	LZ16D	7	0.61	0.2	0.25	56.56	5.96
S1896	LZ16D	8	-0.55	0.19	0.24	-	-
S1897	LZ19C	1	-1.9	0.19	0.24	11.46	1.2

Continued on next page. . .

Table D.4 – continued

CCIM #	Diamond	Spot	$\delta^{13}C‰$	2σ (internal)	2σ (external)	N (ppm)	2σ
S1897	LZ19C	2	-2.51	0.19	0.24	30.23	3.28
S1897	LZ19C	3	-1.07	0.2	0.25	-	-
S1898	LZ17D	1	-6.43	0.19	0.24	7.67	0.9
S1898	LZ17D	2	-6.23	0.19	0.24	-	-
S1898	LZ17D	3	-5.74	0.2	0.25	-	-
S1898	LZ17D	4	-5.5	0.19	0.24	1.93	0.21
S1899	LZ22B	1	-5.03	0.19	0.24	-	-
S1899	LZ22B	2	-5.35	0.19	0.24	3.17	0.35
S1899	LZ22B	3	-5.3	0.19	0.24	-	-
S1899	LZ22B	4	-5.3	0.19	0.24	10.2	1.04
S1899	LZ22B	5	-5.32	0.19	0.24	-	-
S1900	LZ24B	1	-5.35	0.19	0.24	2.09	0.23
S1900	LZ24B	2	-5.24	0.19	0.24	-	-
S1900	LZ24B	3	-5.31	0.19	0.24	5.67	0.76
S1901	LZ25B	1	-5.09	0.19	0.24	2.68	0.28
S1901	LZ25B	2	-5.21	0.19	0.24	-	-
S1901	LZ25B	3	-5.56	0.19	0.24	5.42	0.58
S1902	LZ27B	1	-5.66	0.19	0.24	-	-
S1902	LZ27B	2	-5.63	0.19	0.24	1.65	0.17
S1902	LZ27B	3	-5.72	0.19	0.24	-	-
S1903	LZ28B	1	-4.95	0.19	0.24	4.05	0.48
S1903	LZ28B	2	-5.08	0.19	0.24	-	-
S1903	LZ28B	3	-5.43	0.19	0.24	3.41	0.36
S1904	LZ29	1	-5.56	0.19	0.24	27.78	3.04
S1904	LZ29	2	-5.25	0.2	0.25	-	-
S1905	LZ34	1	-5.75	0.19	0.24	1.46	0.16
S1905	LZ34	2	-5.78	0.19	0.24	-	-
S1905	LZ34	3	-5.77	0.19	0.24	-	-
S1906	LZ33	1	-5.56	0.19	0.24	-	-
S1906	LZ33	2	-5.74	0.19	0.24	3.06	0.32
S1906	LZ33	3	-5.64	0.19	0.24	-	-
S1907	LZ36	1	-6.97	0.19	0.24	-	-
S1907	LZ36	2	-6.79	0.2	0.25	907.35	91.62
S1907	LZ36	3	-6.94	0.19	0.24	-	-
S1907	LZ36	4	-7.17	0.19	0.24	923.13	93.57
S1907	LZ36	5	-7.09	0.19	0.24	-	-
S1908	LZ39	1	-4.76	0.19	0.24	3.61	0.39
S1908	LZ39	2	-4.85	0.2	0.25	-	-
S1908	LZ39	4	-4.85	0.2	0.25	-	-
S1908	LZ39	6	-5.11	0.19	0.24	4.45	0.46
S1909	LZ44	1	-5.46	0.19	0.24	-	-
S1909	LZ44	2	-5.53	0.19	0.24	1.76	0.18
S1909	LZ44	3	-5.56	0.19	0.24	-	-
S1910	LZ51	1	-5.96	0.2	0.25	3.78	0.41
S1910	LZ51	2	-6.06	0.19	0.24	3.54	0.37
S1910	LZ51	3	-6.02	0.19	0.24	-	-
S1911	LZ47	1	-5.7	0.19	0.24	4.63	0.48
S1911	LZ47	2	-5.73	0.19	0.24	-	-

Continued on next page. . .

Table D.4 – continued

CCIM #	Diamond	Spot	$\delta^{13}C$‰	2σ (internal)	2σ (external)	N (ppm)	2σ
S1911	LZ47	3	-5.58	0.19	0.24	6.62	0.68
S1912	LZ49	1	-5.84	0.19	0.24	3.4	0.4
S1912	LZ49	2	-5.8	0.2	0.25	-	-
S1913	LZ50	1	-5.89	0.19	0.24	3.83	0.47
S1914	LZ54	1	-1.95	0.19	0.24	294.22	30.1
S1914	LZ54	2	-2.54	0.19	0.24	137.32	14.36
S1914	LZ54	3	-2.65	0.19	0.24	872.92	88.29
S1914	LZ54	5	-2.83	0.19	0.24	1036.29	104.89
S1914	LZ54	6	-2.79	0.19	0.24	-	-
S1915	LZ53	1	-5.47	0.19	0.24	-	-
S1915	LZ53	2	-5.52	0.19	0.24	5.47	0.59
S1915	LZ53	3	-5.51	0.19	0.24	-	-

2σ uncertainties for $\delta^{13}C$ include in-run precision (internal error), between spot error and uncertainty related to instrumental mass fractionation and reference material composition (external error). All results are reported relative to the international Vienna Pee-Dee Belemnite standard (V-PDB).

2σ uncertainties for nitrogen concentration include within-spot counting statistics and the error in the nitrogen abundance calibration. An additional error of $\sim$10% (2σ) is associated with uncertainty in the FTIR-determined nitrogen abundance, and should be used when comparing data with FTIR-determined concentrations. '-' indicates not measured.

These data relate to CCIM Project 1202.

Appendix E

Mineralogy and calculated temperatures for the Delta and Victor xenoliths

Table E.1: Summary of the mineralogy and geothermobarometry for Delta and Victor xenoliths

Sample	Included in geotherm?	Description	Primary minerals	Secondary minerals	Temperature (°C) Taylor (1998)	Pressure (kbar) N and G (1985)*	Temperature (°C) N and G (2009)	Pressure (kbar) N and G (1985)*
DEL-01	no	dunite	ol	amph, cpx, mica	-	-	-	-
DEL1-01	no	harzburgite	ol, opx	amph	-	-	-	-
DEL1-02	yes	harzburgite	G10, ol, opx	amph, mica	-	-	769	31
DEL1-03	no	harzburgite	G10, ol	amph	-	-	-	-
DEL1-04	yes	pyroxenite	G5, ol, opx, cpx	-	866	40	-	-
DEL1-05	yes	lherzolite	G9, opx, cpx	-	966	42	-	-
DEL1-06	no	harzburgite	ol, opx	amph, cpx, mica	-	-	-	-
DEL1-07	no	wehrlite	G12, ol	-	-	-	-	-
DEL1-08	no	harzburgite	ol, opx	amph	-	-	-	-
DEL1-09	yes	lherzolite	G9, ol, opx, cpx	amph	790	31	-	-
DEL1-10	no	harzburgite	ol, opx	mica	-	-	-	-
DEL1-11	no	dunite	ol	cpx, mica	-	-	-	-
DEL1-12	yes	pyroxenite	G4, cpx, opx	-	864	38	-	-
DEL1-13	no	harzburgite	ol, opx	amph, mica	-	-	-	-
DEL1-14	no	lherzolite	G9, ol	-	-	-	-	-
DEL1-15	yes	lherzolite	G9, ol, opx, cpx	amph	874	37	-	-
DEL1-16	no	dunite	ol	amph, mica	-	-	-	-
DEL1-17	yes	pyroxenite	G4, opx, cpx	-	845	38	-	-
DEL1-18	yes	lherzolite	G9, ol, opx, cpx	amph	693	25	-	-
VIC0106	yes	pyroxenite	cpx, opx, grt	-	773	31	-	-
VIC0507	yes	pyroxenite	cpx, opx, grt	-	733	28	-	-
VIC1703	yes	pyroxenite	cpx, opx, grt	-	665	23	-	-
VIC2002	no	pyroxenite	cpx, opx, grt	-	680	31	-	-
VIC2001	no	pyroxenite	cpx, opx, grt	-	769	31	-	-
VIC2302	yes	pyroxenite	cpx, opx, grt	-	612	20	-	-
VIC2501	no	pyroxenite	cpx, opx, grt	-	891	39	-	-
VIC8401	yes	pyroxenite	cpx, opx, grt	-	1030	47	-	-

*modified by (Carswell, 1991). N and G (1985) refers to Nickel and Green (1985). N and G (2009) to Nimis and Grütter (2009).

Appendix F

Major element data for Victor xenocrysts

All major element data in weight %. ”-” indicates not measured or below detection.
FeO tot as ferrous iron.

Table F.1: Major element compositions of Victor G9 xenocrysts

Sample	SiO_2	TiO_2	Al_2O_3	Cr_2O_3	V_2O_3	FeO tot	MnO	MgO	CaO	Na_2O	K_2O	P_2O_5	NiO	Total
grt1-1	42.41	0.04	20.36	4.08	0.06	7.77	0.36	20.19	5.07	0.03	-	0.01	0.01	100.35
grt1-2	42.38	0.21	19.90	4.66	0.04	7.47	0.39	20.50	4.98	0.06	-	0.03	0.01	100.59
grt1-3	42.40	0.25	20.09	4.68	0.04	7.75	0.42	20.32	4.95	0.06	-	0.02	0.01	100.97
grt1-4	42.45	0.05	22.62	1.88	0.02	9.05	0.48	20.13	4.49	0.02	0.01	0.03	0.01	101.21
grt1-5	42.14	0.29	19.37	5.70	0.05	7.10	0.38	20.89	5.20	0.05	-	0.03	0.01	101.18
grt1-6	41.80	0.30	20.72	4.22	0.04	6.80	0.34	21.57	4.93	0.05	0.01	0.04	0.01	100.80
grt1-7	41.52	0.11	20.52	4.57	0.05	7.54	0.41	20.81	5.16	0.05	-	0.02	0.01	100.74
grt1-8	41.61	0.08	21.43	3.18	0.05	7.68	0.38	20.96	4.84	0.05	-	0.01	0.01	100.28
grt1-9	41.17	0.05	20.62	4.03	0.05	7.36	0.38	20.64	4.96	0.02	-	-	0.01	99.29
grt1-10	41.78	0.08	22.74	1.86	0.02	8.85	0.47	20.54	4.46	0.04	0.01	0.03	-	100.84
grt1-11	41.83	0.12	20.39	4.57	0.04	7.51	0.41	20.50	5.19	0.04	0.01	0.02	0.01	100.61
grt1-12	42.50	0.06	21.10	3.18	0.04	7.80	0.34	20.71	4.66	0.03	-	0.01	0.01	100.45
grt1-14	41.94	0.27	19.39	5.38	0.04	7.40	0.40	19.77	5.37	0.06	0.01	0.02	0.01	100.02
grt1-15	42.48	0.18	19.74	5.12	0.04	6.91	0.39	20.73	5.00	0.04	-	0.01	-	100.63
grt1-16	42.37	0.26	19.20	5.48	0.04	7.44	0.40	20.00	5.37	0.07	-	0.03	-	100.62
grt1-17	42.74	0.05	20.52	4.17	0.04	7.74	0.37	20.39	5.08	0.04	-	0.01	0.01	101.12
grt1-18	42.22	0.28	19.32	5.75	0.05	7.09	0.37	20.67	5.21	0.06	0.01	0.03	0.02	101.05
grt1-20	42.25	0.29	19.43	5.71	0.04	7.10	0.37	20.90	5.13	0.05	-	0.01	0.01	101.26
grt1-21	42.20	0.28	19.45	5.76	0.05	7.09	0.38	20.79	5.12	0.06	-	0.01	0.01	101.18
grt1-22	41.79	0.08	22.80	1.88	0.02	9.16	0.48	20.31	4.46	0.03	0.01	0.03	0.01	101.03
grt1-23	41.42	0.22	20.46	4.61	0.04	7.56	0.41	21.10	4.83	0.06	0.01	0.03	0.01	100.73
grt1-24	41.20	0.29	19.49	5.83	0.05	7.13	0.37	21.03	5.17	0.05	-	0.03	0.01	100.62
grt1-25	41.87	0.27	19.71	5.50	0.02	7.51	0.40	20.50	5.40	0.06	0.01	0.03	0.01	101.29
grt1-26	42.08	0.23	20.30	4.72	0.02	7.80	0.41	20.66	4.89	0.05	-	0.05	0.01	101.22
grt1-27	42.54	0.11	20.41	4.66	0.04	7.58	0.39	20.42	5.21	0.04	-	0.01	-	101.41
grt1-28	42.52	0.05	20.72	4.20	0.04	7.68	0.37	20.54	5.11	0.03	-	0.02	0.01	101.27
grt1-29	42.63	0.18	22.11	2.47	0.02	7.80	0.41	20.98	4.46	0.05	-	0.02	0.01	101.13
grt1-30	42.23	0.12	20.03	4.58	0.06	7.57	0.39	20.13	5.19	0.05	-	0.02	0.01	100.34
grt1-31	41.50	0.22	20.35	4.71	0.05	7.45	0.41	20.84	5.06	0.04	-	0.02	0.01	100.63
grt1-32	42.03	0.31	20.39	4.41	0.03	6.83	0.34	21.46	4.96	0.07	-	0.04	-	100.85

Continued on next page...

Table F.1 – continued

Sample	SiO_2	TiO_2	Al_2O_3	Cr_2O_3	V_2O_3	FeO tot	MnO	MgO	CaO	Na_2O	K_2O	P_2O_5	NiO	Total
grt1-33	42.07	0.07	21.79	2.85	0.03	7.87	0.37	21.19	4.56	0.02	-	0.02	0.01	100.83
grt1-34	42.16	0.17	19.89	5.28	0.04	6.86	0.39	20.73	5.01	0.05	0.01	0.03	-	100.57
grt1-35	42.51	0.30	20.68	4.11	0.05	6.82	0.35	21.27	4.91	0.06	-	0.03	0.01	101.07
grt1-36	42.56	0.31	20.54	4.35	0.06	6.84	0.34	21.28	4.97	0.05	-	0.03	0.01	101.31
grt1-37	42.22	0.04	20.84	4.13	0.05	7.67	0.37	20.37	5.07	0.03	-	0.02	-	100.79
grt1-38	42.52	0.06	21.76	2.86	0.03	7.82	0.35	21.14	4.55	0.03	-	0.01	-	101.11
grt1-39	42.06	0.19	22.13	2.55	0.03	7.76	0.41	21.14	4.45	0.05	-	0.03	0.01	100.79
grt1-40	41.93	0.18	22.33	2.40	0.03	7.77	0.42	21.20	4.42	0.04	0.01	0.03	0.01	100.76
grt2-1	41.77	0.06	22.29	2.81	0.02	8.08	0.51	20.56	4.72	0.03	-	0.02	0.01	100.87
grt2-2	41.37	0.15	20.44	4.75	0.05	7.58	0.42	20.84	4.96	0.05	-	0.04	0.01	100.63
grt2-3	40.97	0.14	20.13	5.21	0.04	7.62	0.40	20.65	5.24	0.04	0.01	0.02	0.01	100.46
grt2-4	41.48	0.06	22.19	2.92	0.04	8.00	0.53	20.70	4.74	0.03	-	0.02	0.01	100.69
grt2-5	41.28	0.03	22.27	2.33	0.03	10.59	0.61	18.35	5.47	0.03	-	0.02	0.01	100.99
grt2-6	41.00	0.01	22.09	2.97	0.02	8.38	0.61	19.74	5.45	0.03	-	0.04	0.01	100.30
grt2-7	40.67	0.06	22.34	2.62	0.02	8.32	0.55	20.50	4.66	0.03	-	0.02	-	99.76
grt2-8	40.97	0.08	22.15	2.91	0.03	7.89	0.52	20.75	4.71	0.03	-	0.01	0.01	100.03
grt2-9	41.44	0.07	22.26	2.76	0.02	7.94	0.49	20.77	4.66	0.04	-	0.02	0.01	100.45
grt2-10	39.86	0.14	20.14	5.13	0.04	7.63	0.40	20.63	5.23	0.04	-	0.03	0.01	99.25
grt2-11	40.72	0.15	20.16	5.22	0.05	7.64	0.41	20.73	5.20	0.05	-	0.02	0.01	100.33
grt2-12	39.64	0.10	19.35	6.19	0.05	7.23	0.40	20.69	5.44	0.03	-	0.03	-	99.13
grt2-13	39.42	0.09	19.54	6.02	0.04	7.03	0.36	20.85	5.48	0.05	0.01	0.03	0.01	98.88
grt2-14	39.79	0.03	20.98	4.07	0.04	7.68	0.37	20.81	5.00	0.03	-	0.02	0.02	98.80
grt2-15	40.27	0.34	19.15	6.27	0.06	6.93	0.38	20.84	5.37	0.06	-	0.03	0.01	99.68
grt2-16	40.66	0.28	20.00	5.12	0.03	7.44	0.40	21.10	4.87	0.06	-	0.03	0.02	99.98
grt2-17	41.57	0.27	20.46	4.50	0.05	7.84	0.40	20.63	5.00	0.07	0.01	0.04	0.01	100.81
grt2-19	41.27	0.23	21.11	3.82	0.02	7.82	0.42	21.04	4.60	0.05	-	0.03	0.02	100.40
grt2-20	40.28	0.14	20.45	4.61	0.04	7.37	0.41	21.05	4.96	0.04	0.01	0.03	0.01	99.37
grt2-21	41.31	0.08	21.94	2.82	0.05	7.78	0.36	21.30	4.54	0.04	0.01	0.02	0.01	100.22
grt2-22	40.83	0.30	20.50	3.99	0.04	7.42	0.38	20.66	4.72	0.07	-	0.02	0.02	98.92
grt2-23	41.43	0.27	20.98	3.95	0.05	7.32	0.40	21.10	4.81	0.07	-	0.04	0.01	100.41
grt2-24	41.24	0.37	19.66	5.30	0.04	7.21	0.38	20.81	5.08	0.07	0.01	0.01	0.01	100.17

Continued on next page. . .

Table F.1 – continued

Sample	SiO_2	TiO_2	Al_2O_3	Cr_2O_3	V_2O_3	FeO tot	MnO	MgO	CaO	Na_2O	K_2O	P_2O_5	NiO	Total
grt2-25	40.10	0.05	22.58	1.62	0.04	12.69	0.51	17.15	5.48	0.02	-	0.03	0.01	100.24
grt2-26	40.60	0.19	19.01	6.37	0.05	6.91	0.38	20.46	5.48	0.05	-	0.02	0.01	99.53
grt2-27	40.76	0.25	19.55	5.64	0.03	7.55	0.41	20.47	5.32	0.06	-	0.03	0.01	100.06
grt2-28	40.72	0.17	20.98	4.08	0.04	7.44	0.40	21.04	4.82	0.05	0.01	0.01	0.01	99.75
grt2-29	40.69	0.24	20.82	4.07	0.04	7.72	0.43	20.80	4.82	0.06	0.01	0.06	0.01	99.72
grt2-30	39.76	0.10	19.69	5.61	0.06	7.38	0.41	20.73	5.22	0.03	-	0.05	0.01	99.04
grt2-31	41.29	0.22	21.24	3.78	0.04	7.11	0.38	21.33	4.68	0.06	-	0.02	0.01	100.13
grt2-32	40.98	0.24	20.75	3.74	0.02	7.23	0.39	20.55	4.59	0.04	-	0.03	-	98.56
grt2-33	40.04	0.19	19.86	5.42	0.04	7.50	0.40	20.49	5.20	0.06	-	0.03	0.02	99.22
grt2-35	41.34	0.23	21.70	3.13	0.03	8.02	0.44	20.67	4.58	0.06	-	0.02	0.01	100.20
grt2-36	40.34	0.08	21.98	2.52	0.02	11.48	0.49	17.58	5.59	0.02	-	0.02	-	100.08
grt2-37	40.17	0.15	20.09	5.05	0.04	7.78	0.43	20.57	5.04	0.05	-	0.05	0.01	99.40
grt2-38	40.36	0.22	20.75	4.20	0.03	7.73	0.45	21.09	4.58	0.06	-	0.04	-	99.47
grt2-39	40.67	0.06	20.77	4.42	0.05	7.67	0.36	20.63	5.26	0.02	-	0.01	0.01	99.91
grt3-1	40.96	0.03	19.92	5.36	0.06	7.29	0.38	20.28	5.52	0.06	0.02	0.01	0.02	99.89
grt3-2	41.26	0.02	22.26	2.45	0.03	8.97	0.51	19.71	4.92	0.03	0.01	0.06	0.01	100.20
grt3-3	42.38	0.03	20.86	4.07	0.05	7.58	0.38	20.62	5.07	0.02	-	0.01	0.01	101.05
grt3-4	42.21	0.12	20.25	4.70	0.03	7.80	0.43	20.26	5.22	0.04	-	0.05	0.01	101.07
grt3-5	41.58	0.28	18.50	6.86	0.04	7.26	0.40	20.00	5.77	0.06	-	0.05	0.01	100.78
grt3-6	41.95	0.01	21.57	3.45	0.02	7.93	0.51	20.74	4.24	0.02	-	0.01	0.01	100.43
grt3-7	41.67	0.01	21.40	3.30	0.02	8.58	0.52	19.04	5.65	0.03	0.01	0.05	-	100.25
grt3-8	41.53	0.02	18.05	7.62	0.07	7.09	0.38	19.26	6.60	0.02	-	0.01	0.01	100.65
grt3-9	42.02	0.02	21.47	3.56	0.01	8.08	0.51	19.73	5.56	0.02	-	0.03	0.01	101.02
grt3-10	41.81	0.05	21.86	3.21	0.01	8.46	0.48	19.78	5.22	0.01	-	-	0.01	100.90
grt3-11	41.55	0.14	18.70	7.08	0.05	7.25	0.42	20.23	5.60	0.04	-	0.03	0.01	101.06
grt3-12	41.88	0.06	22.79	1.99	0.04	8.28	0.45	20.53	4.72	0.03	-	0.03	-	100.77
grt3-13	41.10	0.21	20.50	4.69	0.04	7.54	0.41	20.78	5.02	0.05	-	0.03	0.01	100.35
grt3-14	41.84	0.20	20.71	4.40	0.03	7.40	0.39	20.69	5.05	0.05	-	0.02	0.01	100.76
grt3-15	40.66	0.05	18.35	7.36	0.07	7.35	0.39	19.54	6.56	0.01	-	0.03	0.01	100.35
grt3-16	41.87	0.22	18.64	6.79	0.04	7.19	0.41	20.04	5.82	0.05	-	0.02	0.01	101.09
grt3-17	40.95	0.18	19.50	5.95	0.04	7.11	0.39	20.78	5.29	0.05	-	0.03	0.01	100.24

Continued on next page. . .

Table F.1 – continued

Sample	SiO_2	TiO_2	Al_2O_3	Cr_2O_3	V_2O_3	FeO tot	MnO	MgO	CaO	Na_2O	K_2O	P_2O_5	NiO	Total
grt3-18	41.61	0.24	18.41	7.14	0.04	7.57	0.41	20.16	5.44	0.06	-	0.03	0.01	101.10
grt3-19	41.94	0.17	18.90	6.57	0.04	7.32	0.44	20.50	5.18	0.05	-	0.05	-	101.16
grt3-20	41.58	0.06	20.22	5.10	0.03	8.09	0.50	20.13	5.12	0.03	0.01	0.05	0.02	100.89
grt3-21	42.23	0.14	20.64	4.18	0.05	7.69	0.34	20.55	5.15	0.03	-	0.01	0.01	101.01
grt3-22	42.08	0.07	20.91	4.06	0.05	7.64	0.37	20.82	5.03	0.03	-	0.02	0.01	101.08
grt3-23	40.95	0.04	17.39	8.51	0.07	7.17	0.39	19.23	6.90	0.01	-	0.02	0.01	100.67
grt3-24	41.95	0.24	19.06	6.36	0.04	7.62	0.43	20.15	5.54	0.06	-	0.04	0.01	101.47
grt3-25	40.69	0.22	18.90	6.51	0.05	7.51	0.39	19.97	5.96	0.05	-	0.03	0.01	100.27
grt3-26	40.84	0.28	19.06	6.56	0.03	7.40	0.42	20.29	5.49	0.07	0.01	0.04	0.01	100.48
grt3-27	41.70	0.06	22.32	2.64	0.02	8.58	0.50	20.12	4.90	0.04	-	0.03	-	100.88
grt3-28	41.51	0.19	18.73	7.00	0.04	6.76	0.39	20.46	5.51	0.06	-	0.02	0.02	100.67
grt3-29	40.82	0.03	16.44	9.83	0.07	7.18	0.40	18.77	7.51	0.02	-	0.02	0.01	101.07
grt3-30	41.59	0.13	19.07	6.21	0.06	7.38	0.37	20.24	5.67	0.04	-	0.02	-	100.76
grt3-31	42.18	0.03	21.29	3.50	0.05	7.68	0.35	20.56	5.30	0.02	-	0.02	0.01	100.96
grt3-32	41.64	0.17	16.86	9.02	0.06	7.21	0.41	18.88	7.10	0.03	-	0.04	-	101.41
grt4-2	40.62	0.18	19.55	5.87	0.05	7.41	0.39	20.51	5.58	0.04	-	0.03	0.01	100.19
grt4-4	40.05	0.14	20.27	5.22	0.03	7.21	0.39	21.07	5.13	0.04	0.01	0.02	0.01	99.54
grt4-5	40.32	0.31	18.19	7.31	0.07	7.60	0.40	19.83	6.26	0.04	-	0.01	0.01	100.33
grt4-6	40.65	0.06	21.44	3.65	0.05	7.71	0.38	21.14	4.91	0.03	-	0.01	0.01	100.01
grt4-7	40.11	0.34	20.78	4.24	0.04	7.09	0.34	21.54	4.83	0.06	-	0.04	0.01	99.37
grt4-9	40.64	0.11	18.31	7.52	0.04	7.16	0.44	20.39	5.54	0.05	-	0.05	0.01	100.23
grt4-10	41.10	0.28	18.98	6.52	0.05	7.71	0.41	20.08	5.51	0.06	-	0.03	0.01	100.71
grt4-11	41.91	0.21	19.98	5.26	0.05	7.29	0.40	20.72	5.20	0.06	0.01	0.05	-	101.11
grt4-12	42.27	0.24	20.36	4.62	0.05	7.47	0.40	20.64	5.05	0.07	0.01	0.03	0.01	101.17
grt4-13	42.05	0.26	19.65	5.53	0.04	7.07	0.38	20.59	5.48	0.04	-	0.02	0.01	101.09
grt4-14	42.15	0.06	20.82	4.13	0.05	7.67	0.37	20.66	5.16	0.04	-	0.02	0.01	101.11
grt4-15	41.99	0.25	20.56	4.51	0.04	7.54	0.40	20.95	4.80	0.06	-	0.02	0.01	101.11
grt4-16	41.35	0.18	19.60	5.80	0.04	7.66	0.42	20.36	5.22	0.05	-	0.01	-	100.67
grt4-17	40.83	0.18	19.77	5.69	0.04	7.63	0.41	20.53	5.29	0.05	-	0.01	0.01	100.41
grt4-19	41.09	0.17	21.25	3.65	0.05	7.68	0.36	21.10	4.78	0.05	-	0.01	0.01	100.17
grt4-20	41.13	0.15	20.14	5.22	0.04	6.99	0.36	20.99	5.35	0.03	-	0.01	0.01	100.41

Continued on next page. . .

Table F.1 – continued

Sample	SiO_2	TiO_2	Al_2O_3	Cr_2O_3	V_2O_3	FeO tot	MnO	MgO	CaO	Na_2O	K_2O	P_2O_5	NiO	Total
grt4-21	40.71	0.28	20.03	5.30	0.03	7.37	0.45	20.85	4.95	0.09	-	0.04	-	100.07
grt4-22	41.21	0.23	20.56	4.65	0.04	7.35	0.39	20.90	5.07	0.05	-	0.03	-	100.46
grt4-23	41.03	0.30	19.76	5.28	0.03	7.81	0.43	20.18	5.46	0.06	-	0.03	0.01	100.36
grt4-24	41.55	0.04	20.50	4.73	0.05	7.66	0.38	20.46	5.35	0.03	-	0.01	0.01	100.74
grt4-25	41.51	0.05	18.97	6.50	0.06	7.35	0.38	19.79	6.10	0.03	-	0.03	-	100.73
grt4-26	41.80	0.35	19.03	6.16	0.06	6.80	0.36	20.71	5.42	0.06	-	0.04	0.01	100.77
grt5-1	42.45	0.13	19.25	5.84	0.04	6.96	0.36	20.40	5.13	0.04	-	0.02	0.01	100.61
grt5-2	42.43	0.17	19.59	5.20	0.04	6.99	0.39	20.45	5.03	0.05	-	0.03	0.01	100.35
grt5-3	41.96	0.25	17.73	7.21	0.06	7.34	0.40	19.20	6.22	0.04	0.01	0.03	0.01	100.41
grt5-4	42.19	0.15	20.32	3.50	0.04	7.94	0.35	20.08	4.85	0.04	-	-	0.01	99.48
grt5-6	41.84	0.05	20.76	3.15	0.01	8.71	0.57	19.06	4.94	0.03	0.01	0.02	0.01	99.12
grt5-7	42.50	0.06	20.33	4.10	0.04	7.69	0.38	20.15	5.06	0.03	-	0.01	0.01	100.33
grt5-8	41.70	0.22	17.69	7.02	0.04	7.15	0.40	19.16	5.83	0.05	0.01	0.04	-	99.28
grt5-9	41.98	0.13	18.41	6.54	0.05	7.36	0.43	19.43	5.69	0.04	0.01	0.05	-	100.08
grt5-10	42.32	0.11	20.03	4.67	0.05	7.59	0.40	20.00	5.23	0.05	-	0.01	0.02	100.44
grt5-11	42.06	0.40	18.74	5.84	0.05	7.79	0.42	19.60	5.62	0.07	-	-	0.01	100.55
grt5-12	42.43	0.04	20.31	4.77	0.03	7.62	0.54	20.07	4.71	0.05	-	0.06	-	100.59
grt5-13	42.45	0.27	19.41	5.42	0.06	7.19	0.39	20.23	5.48	0.04	-	0.02	0.01	100.94
grt5-14	42.02	0.09	18.14	6.91	0.07	7.40	0.38	19.09	6.43	0.02	-	0.02	0.01	100.57
grt5-15	42.01	0.17	18.11	7.35	0.04	7.53	0.47	19.64	5.40	0.06	-	0.03	-	100.77
grt5-16	42.88	0.04	21.26	3.13	0.04	7.68	0.36	20.52	4.86	0.03	-	0.02	0.02	100.80
grt5-17	42.36	0.07	19.33	5.63	0.05	7.02	0.38	20.18	5.47	0.04	0.01	0.02	0.01	100.54
grt5-18	41.74	0.06	18.90	6.20	0.03	7.30	0.43	19.38	5.47	0.05	-	0.04	-	99.57
grt5-19	42.56	0.04	20.48	4.04	0.06	7.66	0.36	20.19	5.06	0.02	-	0.02	0.01	100.48
grt5-20	42.08	0.08	22.11	1.80	0.02	8.96	0.46	19.69	4.44	0.04	-	0.03	-	99.69
grt5-21	41.73	0.10	17.29	7.97	0.09	7.21	0.39	19.02	6.53	0.02	-	0.09	0.02	100.43
grt5-22	41.79	0.12	17.03	8.18	0.08	7.26	0.40	18.81	6.68	0.03	-	0.01	0.01	100.39
grt5-23	42.60	0.31	20.18	4.15	0.04	7.59	0.39	20.40	5.00	0.06	-	0.01	0.02	100.71
grt5-24	42.42	0.24	19.90	4.79	0.04	7.58	0.42	20.12	5.24	0.05	0.01	0.02	-	100.81
grt5-25	42.40	0.10	20.17	4.51	0.06	7.58	0.36	20.15	5.27	0.04	-	0.02	0.01	100.62
grt5-26	42.25	0.19	18.70	6.64	0.05	7.15	0.39	20.05	5.54	0.05	-	0.04	0.01	101.04

Continued on next page. . .

Table F.1 – continued

Sample	SiO_2	TiO_2	Al_2O_3	Cr_2O_3	V_2O_3	FeO tot	MnO	MgO	CaO	Na_2O	K_2O	P_2O_5	NiO	Total
grt5-27	42.44	0.13	20.14	4.69	0.04	7.96	0.42	19.88	5.16	0.05	-	0.04	0.01	100.93
grt5-28	42.33	0.06	21.46	3.08	0.03	7.78	0.36	20.66	4.65	0.03	-	-	0.01	100.42
grt5-29	42.55	0.21	20.58	4.11	0.04	7.43	0.40	20.66	4.91	0.06	-	0.04	0.01	100.95
grt5-30	42.15	0.10	22.22	1.90	0.02	11.62	0.49	17.94	4.73	0.05	-	0.03	-	101.22
grt5-31	42.15	0.15	20.37	4.53	0.05	7.81	0.44	20.18	5.03	0.05	-	0.03	0.01	100.76
grt6-5	42.37	0.32	22.91	1.05	0.03	10.10	0.33	19.46	4.39	0.00	-	0.02	-	100.97
grt6-17	42.79	0.22	23.24	1.37	0.03	7.63	0.39	20.86	4.07	0.01	-	0.03	-	100.65
grt6-19	42.33	0.34	22.49	1.43	0.04	10.07	0.43	19.70	3.94	0.00	-	0.02	-	100.80
BC24150-grt1-1	41.68	0.03	21.43	3.95	0.03	7.76	0.51	19.81	5.31	0.03	-	0.03	-	100.55
BC24150-grt1-2	41.65	0.01	21.45	4.01	0.01	8.20	0.57	19.64	5.10	0.04	-	0.02	-	100.67
BC24150-grt1-3	41.28	0.08	19.02	6.97	0.04	7.12	0.46	19.77	5.62	0.03	-	0.04	-	100.41
BC24150-grt1-4	41.45	0.01	21.30	4.09	0.02	8.38	0.59	19.28	5.43	0.03	-	0.01	-	100.57
BC24150-grt1-5	41.62	0.02	21.59	3.64	0.02	8.12	0.54	20.00	4.67	0.08	-	0.05	0.01	100.35
BC24150-grt1-6	41.48	0.01	21.89	3.35	0.02	7.78	0.53	19.96	5.07	0.02	0.01	0.03	0.01	100.13
BC24150-grt1-7	41.08	0.07	21.95	2.77	0.01	9.56	0.52	19.16	4.80	0.04	-	0.01	-	99.96
BC24150-grt1-8	41.21	0.04	20.97	4.30	0.01	7.84	0.55	20.24	4.68	0.00	-	0.06	0.01	99.89
BC24150-grt1-9	41.13	0.01	20.88	4.45	0.02	8.31	0.57	19.07	5.72	0.04	-	0.02	-	100.20
BC24150-grt1-10	41.80	0.01	21.15	4.30	0.03	8.12	0.54	19.22	5.58	0.09	-	0.02	-	100.84
BC24150-grt1-11	42.03	0.01	21.17	4.30	0.03	7.91	0.52	19.27	5.63	0.00	-	0.01	-	100.86
BC24150-grt1-12	42.05	0.02	21.43	4.07	0.03	8.27	0.55	19.32	5.19	0.06	-	0.02	0.01	100.98
BC24150-grt1-13	41.69	0.01	17.53	8.49	0.07	7.08	0.41	18.60	7.13	0.00	-	0.04	0.01	101.05
BC24150-grt1-14	42.25	0.03	22.09	3.12	0.02	8.34	0.60	19.43	5.20	0.12	-	0.02	0.01	101.20
BC24150-grt1-15	42.27	0.01	22.20	3.07	0.01	8.30	0.55	19.57	5.16	0.15	-	0.02	0.01	101.31
BC24150-grt1-16	42.39	0.00	22.58	2.72	0.01	8.18	0.62	20.29	4.33	0.05	-	0.01	0.01	101.18
BC24150-grt1-17	41.85	0.01	21.20	4.26	0.02	8.02	0.55	19.09	5.89	0.02	-	0.01	-	100.92
BC24150-grt1-18	42.19	0.01	21.59	3.81	0.02	7.91	0.50	20.14	4.73	0.09	0.01	-	-	100.96
BC24150-grt1-19	41.58	0.02	21.09	4.33	0.03	8.04	0.53	19.13	5.80	0.04	0.01	0.02	0.01	100.60
BC24150-grt1-20	41.87	0.12	20.47	5.04	0.03	7.05	0.39	20.77	4.78	0.00	-	0.04	0.02	100.56
BC24150-grt1-21	41.97	0.02	21.57	3.83	0.02	8.00	0.53	19.57	5.23	0.00	-	0.04	-	100.75
BC24150-grt1-22	42.08	0.02	20.10	5.41	0.06	7.40	0.36	19.87	5.79	0.00	-	0.02	0.02	101.10
BC24150-grt1-23	41.79	0.20	18.85	7.03	0.04	6.75	0.37	20.35	5.51	0.00	-	0.04	0.02	100.94

Continued on next page...

Table F.1 – continued

Sample	SiO_2	TiO_2	Al_2O_3	Cr_2O_3	V_2O_3	FeO tot	MnO	MgO	CaO	Na_2O	K_2O	P_2O_5	NiO	Total
BC24150-grt1-24	42.29	0.00	22.10	3.30	0.02	7.57	0.48	20.32	4.81	0.04	-	-	-	100.92
BC24150-grt1-25	42.34	0.05	20.78	4.47	0.05	7.42	0.37	20.23	5.35	0.01	-	0.02	0.01	101.09
BC24150-grt1-26	41.41	0.09	17.47	8.55	0.07	7.21	0.39	18.45	7.17	0.04	-	0.03	0.01	100.87
BC24150-grt1-28	42.11	0.00	21.89	3.41	0.02	8.56	0.60	19.44	5.09	0.05	-	0.03	0.01	101.19
BC24150-grt1-29	41.38	0.07	17.19	8.87	0.06	7.18	0.39	18.73	7.04	0.06	-	0.01	0.02	101.00
BC24150-grt1-30	42.03	0.03	20.27	5.07	0.06	7.45	0.37	19.91	5.59	0.08	-	0.03	0.01	100.88
BC24150-grt1-32	41.92	0.03	19.30	6.44	0.04	7.19	0.37	19.55	6.07	0.07	-	0.02	-	100.98
BC24150-grt1-33	41.82	0.02	21.01	4.33	0.02	7.96	0.54	19.57	4.95	0.02	0.01	0.06	0.01	100.30
BC24150-grt1-34	41.99	0.03	19.20	6.49	0.06	7.42	0.39	19.36	6.03	0.00	-	0.01	-	100.96
BC24150-grt1-35	42.41	0.04	21.54	3.93	0.01	7.39	0.53	20.72	4.55	0.07	-	0.08	0.01	101.25
BC24150-grt1-36	42.25	0.01	22.07	3.18	0.02	8.42	0.60	19.27	5.49	0.05	-	0.03	-	101.38
BC24150-grt2-1	41.69	0.14	20.14	5.32	0.04	7.36	0.43	20.22	5.17	0.23	-	0.05	0.01	100.79
BC24150-grt2-2	41.87	0.02	19.72	5.87	0.06	7.29	0.38	19.85	5.96	0.11	-	0.01	0.02	101.15
BC24150-grt2-3	41.91	0.14	20.50	4.71	0.04	7.57	0.40	20.41	5.05	0.13	-	0.03	0.01	100.89
BC24150-grt2-4	41.97	0.17	20.01	5.41	0.04	7.14	0.41	20.40	5.16	0.06	-	0.03	0.01	100.80
BC24150-grt2-5	42.03	0.05	20.59	4.80	0.04	7.24	0.37	20.41	5.39	0.11	-	0.02	-	101.07
BC24150-grt2-6	42.00	0.17	20.32	4.85	0.06	7.56	0.37	20.12	5.36	0.08	-	0.03	0.02	100.94
BC24150-grt2-7	42.38	0.01	22.23	3.05	0.02	8.40	0.59	19.68	5.00	0.20	-	0.04	0.01	101.60
BC24150-grt2-8	42.16	0.05	20.20	5.14	0.06	7.50	0.37	20.20	5.39	0.26	-	0.01	0.01	101.36
BC24150-grt2-9	41.71	0.14	18.36	7.31	0.05	7.39	0.37	19.59	5.98	0.20	-	0.03	0.02	101.16
BC24150-grt2-10	42.18	0.04	21.16	3.83	0.05	7.47	0.36	20.52	5.01	0.06	-	0.02	0.02	100.72
BC24150-grt2-11	41.27	0.03	18.89	6.49	0.07	7.13	0.37	19.43	6.05	0.09	-	0.02	0.01	99.86
BC24150-grt2-12	41.24	0.20	17.20	8.58	0.06	7.64	0.41	18.66	6.77	0.02	-	0.02	-	100.80
BC24150-grt2-13	41.46	0.04	20.83	4.28	0.03	8.39	0.56	19.53	5.04	0.03	-	0.06	-	100.23
BC24150-grt2-14	41.80	0.03	21.08	4.28	0.02	8.45	0.57	18.87	5.82	0.03	-	0.01	-	100.96
BC24150-grt2-15	41.90	0.06	19.88	5.65	0.05	6.93	0.36	20.31	5.43	0.07	-	0.02	-	100.67
BC24150-grt2-16	41.28	0.04	18.48	7.28	0.06	7.38	0.39	19.42	6.13	0.10	-	0.02	0.02	100.59
BC24150-grt2-17	42.03	0.05	21.03	4.05	0.03	7.56	0.35	20.36	5.19	0.21	-	0.03	0.01	100.90
BC24150-grt2-18	41.85	0.01	21.58	3.68	0.03	8.35	0.56	19.68	5.05	0.10	-	0.01	0.01	100.91
BC24150-grt2-19	41.87	0.29	19.80	5.40	0.04	6.66	0.35	20.89	5.08	0.12	-	0.03	0.01	100.54
BC24150-grt2-20	42.33	0.08	20.94	4.24	0.04	7.53	0.37	20.22	5.23	0.02	-	0.02	0.01	101.02

Continued on next page...

Table F.1 – continued

Sample	SiO_2	TiO_2	Al_2O_3	Cr_2O_3	V_2O_3	FeO tot	MnO	MgO	CaO	Na_2O	K_2O	P_2O_5	NiO	Total
BC24150-grt2-21	41.68	0.04	19.32	6.61	0.03	6.79	0.40	20.54	5.05	0.03	-	0.04	-	100.53
BC24150-grt2-22	41.93	0.10	20.68	4.40	0.04	7.73	0.41	20.16	5.10	0.04	-	0.03	-	100.62
BC24150-grt2-23	42.26	0.01	22.16	3.28	0.02	7.70	0.49	20.33	4.91	0.00	-	0.01	0.01	101.18
BC24150-grt2-24	41.72	0.11	19.12	6.43	0.04	7.15	0.39	19.84	5.87	0.15	-	0.02	0.02	100.87
BC24150-grt2-25	42.11	0.07	23.00	1.70	0.02	8.73	0.46	20.14	4.42	0.26	-	0.03	-	100.94
BC24150-grt2-26	40.85	0.06	16.58	9.49	0.09	7.13	0.40	18.49	7.41	0.12	-	0.01	-	100.63
BC24150-grt2-27	41.66	0.04	20.48	4.64	0.05	7.27	0.38	20.34	5.41	0.04	-	0.01	0.02	100.34
BC24150-grt2-28	42.27	0.01	22.96	2.09	0.02	7.46	0.45	21.04	4.06	0.09	-	-	0.01	100.44
BC24150-grt2-29	41.58	0.25	18.88	6.74	0.04	7.31	0.41	19.98	5.44	0.24	-	0.04	0.01	100.93
BC24150-grt2-30	41.88	0.02	22.16	2.73	0.02	8.59	0.47	19.47	5.16	0.14	-	0.02	-	100.67
BC24150-grt2-31	41.50	0.06	19.83	5.61	0.02	7.76	0.46	19.66	5.47	0.04	-	0.06	-	100.48
BC24150-grt2-32	41.52	0.03	19.33	6.15	0.06	7.32	0.37	19.57	6.02	0.13	-	0.01	-	100.52
BC24150-grt2-33	41.82	0.12	21.03	3.93	0.03	7.44	0.42	20.57	4.87	0.19	-	0.03	0.01	100.45
BC24150-grt2-34	41.25	0.03	18.54	7.04	0.07	7.26	0.38	19.43	6.42	0.00	-	0.01	0.01	100.46
BC24150-grt2-35	41.76	0.01	20.77	4.70	0.03	7.72	0.47	20.22	4.99	0.05	-	0.07	0.01	100.79
BC24150-grt2-36	41.82	0.15	20.90	3.92	0.05	7.58	0.36	20.47	5.10	0.05	-	0.01	0.01	100.41
BC24150-grt2-37	41.61	0.14	19.96	5.75	0.03	6.82	0.40	20.75	4.82	0.02	-	0.04	-	100.33
BC24150-grt2-38	41.88	0.04	21.24	3.83	0.04	7.50	0.36	20.39	5.10	0.00	-	0.01	0.01	100.41
BC24150-grt3-7	41.75	0.44	20.98	3.28	0.04	8.89	0.42	20.21	4.37	0.00	-	0.01	0.02	100.41
BC24150-grt3-12	42.47	0.35	22.29	1.53	0.03	9.59	0.40	19.83	4.36	0.03	-	0.01	-	100.90
BC24150-grt3-16	42.06	0.40	21.17	3.21	0.03	8.79	0.40	20.02	4.62	0.15	-	0.04	0.02	100.89
BC24150-grt3-17	42.46	0.43	21.15	3.08	0.04	8.63	0.38	20.38	4.23	0.37	-	0.04	0.01	101.20
BC24150-grt3-21	42.03	0.37	21.67	2.65	0.03	8.20	0.34	20.29	4.43	0.13	-	0.04	0.01	100.19
BC24150-grt3-23	42.15	0.48	21.43	2.15	0.05	9.63	0.40	19.14	5.01	0.09	-	0.02	0.01	100.58
BC24150-grt3-24	42.50	0.33	22.34	1.34	0.03	9.60	0.39	20.25	3.96	0.05	-	0.02	0.02	100.82
BC24150-grt3-38	42.67	0.24	23.08	1.31	0.03	7.43	0.38	20.93	4.46	0.14	-	0.03	0.01	100.71
BC24150-grt4-6	41.14	0.43	20.84	3.22	0.04	8.78	0.38	20.25	4.35	0.05	-	0.01	0.01	99.48
BC24150-grt4-8	41.02	0.44	20.87	3.12	0.04	8.85	0.40	20.32	4.32	0.30	-	0.02	-	99.69
BC24150-grt4-9	40.92	0.43	20.81	3.16	0.03	8.70	0.36	20.33	4.17	0.28	-	0.03	-	99.22
BC24150-grt4-17	42.25	0.30	22.03	2.63	0.03	7.65	0.36	20.63	4.39	0.14	-	0.03	-	100.43
BC24150-grt4-19	41.36	0.47	21.36	2.60	0.03	9.34	0.44	19.27	4.86	0.00	-	0.03	-	99.75

Continued on next page...

Table F.1 – continued

Sample	SiO_2	TiO_2	Al_2O_3	Cr_2O_3	V_2O_3	FeO tot	MnO	MgO	CaO	Na_2O	K_2O	P_2O_5	NiO	Total
BC24150-grt4-22	41.26	0.43	21.72	1.83	0.04	9.34	0.41	20.21	4.08	0.00	-	0.02	-	99.33
BC24150-grt4-24	41.78	0.44	21.39	2.75	0.03	8.85	0.40	20.30	4.20	0.24	-	0.02	0.01	100.39
BC24150-grt4-25	41.56	0.47	21.05	3.24	0.03	9.39	0.44	19.22	4.89	0.33	-	0.03	-	100.65
BC24150-grt4-29	41.99	0.44	21.10	3.15	0.03	8.76	0.39	20.14	4.20	0.00	-	0.03	-	100.23
BC24150-grt4-31	41.00	0.44	20.82	3.03	0.03	8.99	0.39	20.17	4.36	0.00	-	0.05	-	99.27
BC24150-grt5-8	42.05	0.42	22.61	1.17	0.02	9.85	0.45	19.98	3.71	0.11	-	0.02	-	100.39
average	41.67	0.15	20.43	4.61	0.04	7.78	0.42	20.18	5.19	0.06	0.01	0.03	0.01	100.54
min	39.42	0.00	16.44	1.05	0.01	6.66	0.33	17.15	3.71	0.00	0.01	0.01	0.01	98.56
max	42.88	0.48	23.24	9.83	0.09	12.69	0.62	21.57	7.51	0.37	0.02	0.09	0.02	101.60
2σ	1.33	0.24	2.72	3.38	0.03	1.61	0.13	1.41	1.23	0.11	0.00	0.03	0.01	1.13
n	253													

BC24150 in the sample name refers to grains from a different unit.

Table F.2: Major element compositions of Victor G10 xenocrysts

Sample	SiO_2	TiO_2	Al_2O_3	Cr_2O_3	V_2O_3	FeO tot	MnO	MgO	CaO	Na_2O	K_2O	P_2O_5	NiO	Total
grt2-18	40.44	0.24	20.73	4.23	0.02	7.43	0.44	21.61	4.29	0.09	0.01	0.04	0.01	99.53
BC24150-grt1-27	42.58	0.02	21.87	3.73	0.03	6.42	0.42	21.43	4.19	0.03	-	0.01	-	100.72
BC24150-grt1-31	41.75	0.25	18.62	7.29	0.04	7.29	0.43	20.13	5.19	0.20	-	0.04	0.02	101.22
BC24150-grt4-15	41.88	0.43	21.19	3.38	0.03	9.30	0.44	20.18	3.60	0.31	-	0.02	-	100.74
BC24150-grt4-30	41.90	0.34	22.26	1.54	0.04	9.80	0.43	20.20	3.65	0.00	-	0.03	0.01	100.20
average	41.71	0.26	20.93	4.03	0.03	8.05	0.43	20.71	4.18	0.13	0.01	0.03	0.01	100.48
min	40.44	0.02	18.62	1.54	0.02	6.42	0.42	20.13	3.60	0.00	0.01	0.01	0.01	99.53
max	42.58	0.43	22.26	7.29	0.04	9.80	0.44	21.61	5.19	0.31	0.01	0.04	0.02	101.22
2σ	1.56	0.30	2.85	4.17	0.01	2.87	0.02	1.48	1.28	0.25	-	0.03	0.01	1.29
n	5													

BC24150 in the sample name refers to grains from a different unit.

Table F.3: Major element compositions of Victor G3 xenocrysts

Sample	SiO_2	TiO_2	Al_2O_3	Cr_2O_3	V_2O_3	FeO tot	MnO	MgO	CaO	Na_2O	K_2O	P_2O_5	NiO	Total
grt6-8	39.75	0.12	22.80	0.04	0.01	21.55	0.46	7.76	8.89	-	-	0.05	-	101.44
grt6-11	41.46	0.07	23.72	0.23	0.01	12.63	0.31	15.33	7.48	-	-	0.05	-	101.30
grt6-12	41.20	0.06	23.88	-	0.01	13.00	0.22	12.69	10.22	-	-	0.02	-	101.30
grt6-16	40.63	0.19	23.11	0.01	0.04	15.19	0.24	8.99	13.06	-	-	0.02	-	101.47
BC24150-grt-27	40.68	0.09	23.13	0.06	0.02	16.17	0.31	10.46	10.85	-	-	0.03	0.01	101.80
BC24150-grt3-4	39.78	0.13	22.91	0.07	0.03	19.53	0.45	9.52	8.95	0.05	-	0.04	-	101.44
BC24150-grt3-9	41.89	0.25	23.57	0.22	0.02	11.43	0.51	17.27	6.05	-	-	0.02	0.02	101.24
BC24150-grt3-14	40.55	0.13	23.15	0.05	0.02	17.18	0.38	10.38	9.94	0.12	-	0.01	-	101.92
BC24150-grt3-33	40.04	0.10	22.88	0.07	0.03	19.81	0.45	8.04	10.56	0.04	-	0.05	-	102.06
BC24150-grt5-1	40.45	0.13	23.16	0.06	0.03	17.30	0.44	12.34	6.96	-	-	0.04	-	100.91
BC24150-grt5-13	41.20	0.06	23.65	0.22	0.01	12.55	0.32	14.50	8.25	0.02	-	0.03	-	100.80
BC24150-grt5-14	39.88	0.40	22.66	0.07	0.02	18.59	0.37	9.99	8.47	0.22	-	0.19	-	100.85
BC24150-grt5-17	41.12	0.09	23.64	0.23	0.02	11.97	0.30	16.21	6.73	0.02	-	0.02	-	100.35
BC24150-grt5-19	40.23	0.16	23.02	0.05	0.03	17.54	0.40	10.64	8.78	-	-	0.05	-	100.91
BC24150-grt5-20	39.96	0.08	22.98	0.05	0.03	19.73	0.42	9.09	8.67	-	-	0.04	-	101.06
BC24150-grt5-21	41.16	0.08	23.58	0.11	-	12.13	0.23	13.66	9.37	-	-	0.02	-	100.35
BC24150-grt5-22	39.77	0.11	22.74	0.07	0.02	18.94	0.44	9.21	9.03	-	-	0.02	-	100.35
BC24150-grt5-23	40.13	0.15	22.94	0.06	0.02	18.62	0.45	10.50	8.30	0.06	-	0.03	-	101.27
BC24150-grt5-26	40.65	0.09	23.29	0.21	0.02	12.91	0.32	16.00	6.03	-	-	0.01	0.01	99.53
BC24150-grt5-27	41.00	0.08	23.43	0.19	0.01	13.02	0.32	15.92	6.14	0.04	-	0.04	-	100.20
BC24150-grt5-29	40.48	0.13	23.28	0.03	0.02	13.97	0.25	10.50	12.01	0.22	-	0.03	-	100.91
BC24150-grt5-31	41.54	0.08	23.54	0.36	0.01	12.89	0.34	15.65	6.41	-	-	0.04	-	100.86
average	40.62	0.13	23.23	0.12	0.02	15.76	0.36	12.03	8.69	0.09	-	0.04	0.01	101.01
min	39.75	0.06	22.66	0.01	0.01	11.43	0.22	7.76	6.03	0.02	-	0.01	0.01	99.53
max	41.89	0.40	23.88	0.36	0.04	21.55	0.51	17.27	13.06	0.22	-	0.19	0.02	102.06
2σ	1.27	0.15	0.70	0.19	0.02	6.40	0.17	6.04	3.84	0.16	-	0.07	0.01	1.21
n	22.00													

BC24150 in the sample name refers to grains from a different unit.

Table F.4: Major element compositions of Victor G4 xenocrysts

Sample	SiO_2	TiO_2	Al_2O_3	Cr_2O_3	V_2O_3	FeO tot	MnO	MgO	CaO	Na_2O	K_2O	P_2O_5	NiO	Total
grt6-1	40.33	0.10	23.20	0.05	0.02	19.35	0.43	13.32	4.44	0.19	-	0.04	-	101.48
grt6-2	41.25	0.08	23.64	0.06	0.02	16.61	0.35	15.22	4.26	-	-	0.03	-	101.52
grt6-3	41.60	0.06	23.93	0.05	0.03	14.45	0.32	15.82	5.27	-	-	0.03	-	101.58
grt6-4	42.06	0.07	24.11	0.04	0.01	13.23	0.42	17.60	4.01	-	-	0.05	-	101.59
grt6-6	42.01	0.06	24.22	0.12	0.02	12.90	0.43	17.66	4.08	0.16	-	0.03	-	101.70
grt6-7	41.88	0.07	23.98	0.09	0.02	12.67	0.38	17.37	4.73	0.11	-	0.03	-	101.34
grt6-9	41.55	0.08	23.76	0.07	0.02	14.85	0.32	15.61	5.10	-	-	0.02	-	101.37
grt6-10	41.98	0.05	24.08	0.09	0.02	12.10	0.41	18.27	4.09	-	-	0.04	-	101.14
grt6-13	42.63	0.34	23.51	0.65	0.04	8.67	0.44	19.96	4.64	-	-	0.02	-	100.90
grt6-14	42.64	0.09	24.33	0.10	0.02	9.32	0.41	19.70	4.18	-	-	0.03	-	100.82
grt6-15	42.63	0.06	24.39	0.11	0.01	9.66	0.40	19.40	4.11	-	-	0.02	-	100.79
grt6-20	41.76	0.08	23.85	0.06	0.02	14.34	0.27	15.73	5.37	-	-	0.03	0.01	101.52
BC24150-grt-29	41.33	0.08	23.54	0.07	0.02	16.84	0.42	14.72	4.72	0.13	-	0.03	-	101.90
BC24150-grt3-2	41.36	0.08	23.63	0.25	0.01	13.38	0.33	16.87	4.95	0.06	-	0.01	0.01	100.93
BC24150-grt3-6	42.16	0.34	23.30	0.37	0.03	8.22	0.38	20.86	4.16	-	-	0.02	0.02	99.86
BC24150-grt3-8	41.53	0.27	23.50	0.19	0.02	12.69	0.34	17.91	4.21	0.01	-	0.02	-	100.68
BC24150-grt3-10	42.65	0.32	23.46	0.43	0.03	9.00	0.34	20.19	4.32	0.04	-	0.02	-	100.80
BC24150-grt3-13	42.62	0.35	23.33	0.83	0.03	7.87	0.36	20.75	4.36	0.09	-	0.02	0.01	100.63
BC24150-grt3-15	41.43	0.08	23.53	0.22	0.02	16.45	0.36	15.26	4.50	0.01	-	0.04	0.02	101.90
BC24150-grt3-25	41.14	0.08	23.39	0.05	0.02	17.82	0.44	14.47	4.18	0.09	-	0.03	-	101.72
BC24150-grt3-26	41.92	0.11	23.66	0.30	0.01	11.96	0.37	17.62	4.91	0.08	-	0.03	-	100.97
BC24150-grt3-28	42.40	0.09	24.06	0.11	0.03	10.45	0.41	19.10	4.43	0.05	-	0.03	-	101.16
BC24150-grt3-30	42.50	0.39	23.10	0.95	0.04	8.30	0.35	20.83	4.21	0.34	-	0.02	0.01	101.02
BC24150-grt3-31	42.47	0.24	23.44	0.64	0.03	9.03	0.40	20.23	4.23	0.24	-	0.02	0.01	100.98
BC24150-grt3-35	42.74	0.35	23.64	0.21	0.03	8.31	0.30	20.50	4.69	0.06	-	0.02	-	100.86
BC24150-grt3-37	42.55	0.34	22.73	0.98	0.02	9.76	0.41	19.89	4.10	0.15	-	0.02	0.01	100.96
BC24150-grt5-2	40.58	0.08	23.33	0.06	0.02	17.55	0.43	13.93	4.84	-	-	0.04	-	100.87
BC24150-grt5-4	40.99	0.07	23.44	0.08	0.02	17.85	0.39	14.46	4.03	-	-	0.03	-	101.37
BC24150-grt5-5	41.16	0.09	23.43	0.25	0.02	15.58	0.42	15.37	4.68	-	-	0.04	0.01	101.04
BC24150-grt5-6	41.39	0.27	23.23	0.15	0.04	12.15	0.38	17.62	4.72	-	-	0.05	0.02	100.03

Continued on next page...

Table F.4 – continued

Sample	SiO_2	TiO_2	Al_2O_3	Cr_2O_3	V_2O_3	FeO tot	MnO	MgO	CaO	Na_2O	K_2O	P_2O_5	NiO	Total
BC24150-grt5-7	41.61	0.06	23.79	0.18	0.02	13.61	0.42	17.06	3.95	0.03	-	0.05	-	100.77
BC24150-grt5-9	42.42	0.34	23.39	0.67	0.03	7.63	0.40	21.21	4.04	0.07	-	0.02	-	100.22
BC24150-grt5-12	40.84	0.08	23.43	0.04	0.01	17.39	0.44	14.65	4.08	-	-	0.04	-	101.01
BC24150-grt5-15	41.04	0.07	23.68	0.05	0.02	15.23	0.43	16.18	3.92	0.14	-	0.04	-	100.81
BC24150-grt5-16	42.44	0.32	23.64	0.43	0.03	6.81	0.31	22.04	3.66	0.03	-	0.03	-	99.73
BC24150-grt5-18	41.64	0.25	23.50	0.15	0.02	12.25	0.33	18.00	4.37	0.02	-	0.03	-	100.56
BC24150-grt5-24	40.99	0.09	23.58	0.20	0.02	12.23	0.31	16.58	5.82	0.03	-	0.02	-	99.87
BC24150-grt5-25	40.40	0.06	23.18	0.03	0.02	18.77	0.46	12.86	5.13	-	-	0.03	-	100.94
BC24150-grt5-28	41.44	0.26	23.29	0.24	0.03	12.30	0.37	18.25	4.11	0.36	-	0.04	-	100.68
average	41.75	0.16	23.60	0.25	0.02	12.76	0.38	17.51	4.45	0.11	-	0.03	0.01	100.97
min	40.33	0.05	22.73	0.03	0.01	6.81	0.27	12.86	3.66	0.01	-	0.01	0.01	99.73
max	42.74	0.39	24.39	0.98	0.04	19.35	0.46	22.04	5.82	0.36	-	0.05	0.02	101.90
2σ	1.37	0.24	0.70	0.52	0.02	7.07	0.09	4.91	0.93	0.19	-	0.02	0.01	1.08
n	39													

BC24150 in the sample name refers to grains from a different unit.

Table F.5: Major element compositions of Victor G11 xenocrysts

Sample	SiO_2	TiO_2	Al_2O_3	Cr_2O_3	V_2O_3	FeO tot	MnO	MgO	CaO	Na_2O	K_2O	P_2O_5	NiO	Total
grt1-13	42.06	0.49	19.79	4.33	0.04	7.11	0.35	20.68	4.93	0.07	-	0.03	0.01	99.86
grt1-19	42.25	0.48	20.15	4.54	0.04	7.18	0.36	21.03	5.06	0.07	-	0.04	0.01	101.17
grt2-34	40.64	0.39	19.65	4.94	0.03	7.07	0.29	21.02	4.74	0.07	-	0.03	0.02	98.89
grt2-40	41.26	0.52	20.11	4.63	0.05	7.13	0.36	21.07	5.08	0.07	-	0.03	0.01	100.29
grt4-1	41.28	0.45	20.48	4.33	0.06	7.05	0.33	21.38	4.98	0.07	-	0.05	-	100.46
grt4-3	41.67	0.39	19.85	5.13	0.05	6.81	0.36	21.29	5.11	0.07	-	0.03	0.01	100.72
grt4-8	40.19	0.41	20.80	4.02	0.04	7.09	0.35	21.54	4.86	0.07	0.01	0.02	0.01	99.39
grt4-18	40.87	0.46	19.65	5.39	0.04	6.94	0.36	21.11	5.23	0.08	-	0.02	0.01	100.14
BC24150-grt4-1	41.67	0.44	21.11	3.02	0.03	8.56	0.38	20.19	3.99	0.32	-	0.02	0.02	99.75
BC24150-grt4-10	42.34	0.48	21.09	3.12	0.04	8.71	0.39	19.96	4.05	0.34	-	0.02	0.02	100.56
average	41.42	0.45	20.27	4.35	0.04	7.37	0.35	20.93	4.80	0.12	0.01	0.03	0.01	100.12
min	40.19	0.39	19.65	3.02	0.03	6.81	0.29	19.96	3.99	0.07	0.01	0.02	0.01	98.89
max	42.34	0.52	21.11	5.39	0.06	8.71	0.39	21.54	5.23	0.34	0.01	0.05	0.02	101.17
2σ	1.42	0.09	1.14	1.57	0.02	1.36	0.05	1.02	0.87	0.22	-	0.02	0.01	1.34
n	10													

BC24150 in the sample name refers to grains from a different unit.

Table F.6: Major element compositions of Victor G1 xenocrysts

Sample	SiO_2	TiO_2	Al_2O_3	Cr_2O_3	V_2O_3	FeO tot	MnO	MgO	CaO	Na_2O	K_2O	P_2O_5	NiO	Total
grt6-18	42.19	0.46	20.83	3.59	0.04	8.63	0.39	19.93	4.47	0.01	-	0.03	0.01	100.59
BC24150-grt3-1	41.79	0.49	20.88	3.39	0.03	8.66	0.39	20.12	4.59	0.05	-	0.02	0.01	100.43
BC24150-grt3-3	41.89	0.46	20.97	3.27	0.03	8.77	0.39	20.14	4.65	0.07	-	0.03	0.01	100.68
BC24150-grt3-5	41.76	0.46	21.00	3.17	0.03	8.74	0.40	20.23	4.28	0.12	-	0.03	0.01	100.21
BC24150-grt3-7	41.78	0.45	21.04	3.21	0.04	8.89	0.40	20.30	4.39	-	-	0.04	0.01	100.51
BC24150-grt3-11	42.47	0.55	22.34	1.58	0.03	8.77	0.33	19.95	4.65	0.08	-	0.01	0.01	100.76
BC24150-grt3-17	42.48	0.44	21.20	3.09	0.04	8.59	0.38	20.37	4.24	0.28	-	0.03	0.01	101.13
BC24150-grt3-18	42.12	0.48	20.97	3.26	0.03	8.80	0.39	20.15	4.52	0.31	-	0.02	0.01	101.08
BC24150-grt3-19	42.09	0.49	20.84	3.35	0.04	8.92	0.40	19.97	4.66	0.24	-	0.03	0.01	101.04
BC24150-grt3-20	42.25	0.47	21.92	2.48	0.04	7.85	0.35	20.67	4.47	0.12	-	0.03	-	100.65
BC24150-grt3-22	42.53	0.43	22.15	2.12	0.03	7.89	0.36	20.63	4.54	0.11	-	0.03	-	100.82
BC24150-grt3-30	42.45	0.42	22.95	0.98	0.03	8.31	0.36	20.87	4.22	0.23	-	0.01	0.01	100.84
BC24150-grt3-32	41.89	0.48	20.69	3.54	0.04	8.76	0.40	20.07	4.62	0.07	-	0.03	0.01	100.58
BC24150-grt3-34	42.25	0.46	20.84	3.44	0.03	8.81	0.40	20.12	4.60	0.08	-	0.01	-	101.04
BC24150-grt3-34	42.16	0.47	20.84	3.48	0.04	8.79	0.40	20.11	4.60	0.12	-	0.02	0.01	101.02
BC24150-grt3-36	42.08	0.49	20.89	3.26	0.03	8.87	0.39	19.93	4.57	0.09	-	0.01	-	100.61
BC24150-grt4-2	42.00	0.46	20.96	3.54	0.03	7.99	0.36	20.20	4.72	0.30	-	0.02	0.01	100.59
BC24150-grt4-10	42.10	0.60	21.32	3.03	0.05	8.20	0.37	19.90	4.59	0.26	-	0.02	-	100.42
BC24150-grt4-11	42.03	0.49	21.07	3.24	0.03	8.85	0.39	20.04	4.27	0.08	-	0.02	-	100.52
BC24150-grt4-12	41.86	0.66	21.95	1.35	0.09	10.75	0.41	18.66	4.80	-	-	0.02	0.01	100.55
BC24150-grt4-13	42.12	0.49	20.95	3.33	0.05	8.60	0.37	20.17	4.28	0.15	-	0.01	-	100.52
BC24150-grt4-14	42.06	0.47	21.07	3.20	0.04	8.85	0.39	19.96	4.38	0.30	-	0.03	-	100.74
BC24150-grt4-16	41.88	0.57	21.56	1.85	0.06	10.22	0.40	18.96	4.86	0.07	-	0.02	-	100.47
BC24150-grt4-18	41.89	0.48	20.98	3.24	0.03	8.87	0.39	19.92	4.43	-	-	0.03	-	100.27
BC24150-grt4-19	41.70	0.50	21.39	2.58	0.04	9.32	0.45	19.34	4.87	-	-	0.01	-	100.20
BC24150-grt4-20	41.27	0.47	20.91	3.09	0.04	8.93	0.38	20.18	4.19	-	-	0.03	-	99.50
BC24150-grt4-21	41.66	0.48	22.00	2.05	0.03	7.93	0.35	20.76	4.40	-	-	0.03	-	99.69
BC24150-grt4-23	41.43	0.50	21.49	2.42	0.04	8.52	0.39	20.11	4.82	0.23	-	0.01	-	99.96
BC24150-grt4-24	41.75	0.45	21.40	2.69	0.03	8.86	0.39	20.29	4.22	0.22	-	0.01	0.03	100.34
BC24150-grt4-26	41.81	0.48	20.93	3.26	0.04	8.86	0.40	19.96	4.42	0.24	-	0.03	0.01	100.44

Continued on next page...

Table F.6 – continued

Sample	SiO_2	TiO_2	Al_2O_3	Cr_2O_3	V_2O_3	FeO tot	MnO	MgO	CaO	Na_2O	K_2O	P_2O_5	NiO	Total
BC24150-grt4-27	41.87	0.52	20.77	3.38	0.04	8.86	0.39	19.91	4.48	-	-	0.03	0.01	100.26
BC24150-grt4-28	41.88	0.54	21.10	2.62	0.05	9.49	0.41	19.26	4.91	0.04	-	0.03	-	100.33
BC24150-grt4-29	41.86	0.45	21.13	3.11	0.03	8.79	0.37	20.23	4.22	-	-	0.03	0.01	100.22
BC24150-grt4-3	41.57	0.48	20.72	3.38	0.03	8.72	0.38	20.01	4.35	0.06	-	0.03	-	99.73
BC24150-grt4-4	41.40	0.57	21.61	1.64	0.06	10.35	0.41	19.19	4.68	0.02	-	0.02	-	99.95
BC24150-grt4-5	41.22	0.50	20.69	3.27	0.04	8.78	0.38	20.10	4.45	-	-	0.02	0.01	99.46
BC24150-grt4-6	41.28	0.46	20.75	3.35	0.02	8.78	0.39	20.30	4.30	0.26	-	0.03	-	99.92
BC24150-grt4-7	41.30	0.44	21.11	2.80	0.04	8.53	0.40	20.00	4.85	0.41	-	0.03	-	99.91
BC24150-grt4-8	40.77	0.44	20.80	3.12	0.03	8.80	0.40	20.43	4.28	0.23	-	0.03	0.01	99.34
BC24150-grt4-9	40.93	0.44	20.73	3.12	0.04	8.74	0.41	20.56	4.19	0.27	-	0.01	-	99.44
BC24150-grt4-31	41.26	0.46	20.92	3.04	0.04	8.94	0.38	20.04	4.36	-	-	0.03	-	99.47
BC24150-grt4-32	40.66	0.46	20.54	3.17	0.03	8.85	0.40	20.06	4.61	-	-	0.02	0.01	98.81
BC24150-grt5-3	42.13	0.54	22.12	1.94	0.04	8.35	0.35	20.48	4.24	-	-	0.02	-	100.21
BC24150-grt5-10	41.94	0.48	22.50	1.57	0.03	8.48	0.36	20.51	4.09	0.28	-	0.03	-	100.27
BC24150-grt5-11	41.79	0.61	22.05	2.00	0.02	8.54	0.35	20.46	4.21	0.22	-	0.02	-	100.27
BC24150-grt5-30	42.09	0.48	22.34	1.79	0.02	8.35	0.35	20.40	4.20	-	-	0.02	0.01	100.04
average	41.82	0.49	21.27	2.81	0.04	8.79	0.38	20.09	4.47	0.17	-	0.02	0.01	100.30
min	40.66	0.42	20.54	0.98	0.02	7.85	0.33	18.66	4.09	0.01	-	0.01	0.01	98.81
max	42.53	0.66	22.95	3.59	0.09	10.75	0.45	20.87	4.91	0.41	-	0.04	0.03	101.13
2σ	0.86	0.10	1.16	1.38	0.02	1.10	0.04	0.87	0.44	0.21	-	0.02	0.01	1.03
n	46													

BC24150 in the sample name refers to grains from a different unit.

Table F.7: Major element compositions of "more depleted" Victor olivine xenocrysts

Sample	SiO_2	TiO_2	Al_2O_3	Cr_2O_3	V_2O_3	FeO tot	MnO	MgO	CaO	Na_2O	K_2O	P_2O_5	NiO	Total	Mg#
Ol1-1	39.74	0.01	0.01	0.01	-	7.49	0.14	51.41	0.01	0.02	-	0.01	0.35	99.18	92.63
Ol1-2	40.06	-	0.01	-	-	7.73	0.16	51.06	0.01	0.02	-	0.01	0.35	99.38	92.12
Ol1-3	39.92	0.01	0.01	0.01	0.01	8.08	0.15	50.82	0.01	0.01	0.01	0.03	0.35	99.38	91.63
Ol1-4	39.47	0.01	0.01	0.01	0.01	8.21	0.18	50.89	0.01	0.01	-	0.01	0.33	99.12	91.67
Ol1-5	39.70	0.02	0.01	0.01	-	6.87	0.10	52.09	-	0.02	-	0.02	0.37	99.18	93.15
Ol1-7	39.96	-	0.09	-	0.01	7.82	0.15	50.82	0.02	0.01	-	0.02	0.34	99.23	92.08
Ol1-8	39.50	0.01	0.03	0.01	0.01	6.84	0.10	52.76	0.01	0.02	0.01	-	0.37	99.63	93.20
Ol1-9	39.71	-	-	0.01	-	7.09	0.10	51.52	0.01	0.02	-	0.01	0.37	98.82	92.88
Ol1-10	39.57	0.01	-	-	-	8.26	0.18	50.29	0.01	0.01	0.01	-	0.34	98.67	91.63
Ol1-11	39.12	0.01	-	-	-	7.64	0.15	51.66	0.02	0.03	-	0.01	0.35	98.96	92.23
Ol1-12	39.84	-	0.25	-	-	7.05	0.10	50.93	-	0.01	-	0.02	0.34	98.54	92.57
Ol1-13	39.61	-	0.01	0.01	-	7.48	0.13	51.27	0.01	0.01	-	0.01	0.33	98.87	92.61
Ol1-14	39.36	0.01	0.04	-	0.01	7.04	0.11	51.90	-	0.02	-	0.02	0.36	98.82	92.93
Ol1-15	39.78	-	0.01	-	0.01	7.96	0.16	50.54	0.01	0.01	-	-	0.33	98.82	92.08
Ol1-16	39.34	-	-	-	-	7.71	0.14	51.13	0.01	0.02	0.01	0.04	0.34	98.74	92.16
Ol1-20	39.65	0.01	0.06	-	-	8.01	0.15	50.47	0.02	0.01	-	-	0.34	98.73	91.63
Ol1-22	39.54	0.01	-	-	-	6.80	0.11	52.00	0.01	0.01	-	-	0.35	98.83	93.17
Ol1-27	39.50	0.01	-	0.01	-	8.21	0.11	50.75	-	0.03	-	-	0.35	98.97	91.67
Ol1-29	39.72	-	-	-	0.02	6.42	0.11	51.92	-	0.02	-	0.02	0.36	98.58	93.60
Ol1-30	39.43	0.01	0.01	-	-	7.43	0.09	51.89	-	0.01	-	-	0.35	99.23	92.68
Ol2-1	40.06	0.01	0.01	-	0.01	8.12	0.12	51.30	0.01	0.01	-	-	0.36	99.98	91.65
Ol2-2	40.68	0.01	-	-	-	6.98	0.10	52.64	-	0.02	-	0.01	0.33	100.75	93.10
Ol2-3	40.47	0.01	0.03	0.02	0.01	6.99	0.10	51.96	0.01	0.02	0.01	0.01	0.35	99.94	93.07
Ol2-4	40.77	-	-	0.01	-	7.40	0.12	52.05	0.01	0.02	-	0.02	0.36	100.72	92.57
Ol2-5	40.56	-	0.01	-	-	7.17	0.10	51.98	0.02	0.03	-	0.03	0.36	100.22	92.82
Ol2-6	40.47	0.01	0.06	0.01	-	8.10	0.11	51.80	-	0.02	-	0.01	0.38	100.95	92.12
Ol2-7	40.75	0.01	0.01	-	-	6.98	0.11	52.29	-	0.01	-	0.02	0.36	100.51	93.09
Ol2-8	40.68	0.01	0.01	0.01	-	8.27	0.14	51.39	-	0.01	-	0.02	0.37	100.89	91.58
Ol2-9	40.67	0.01	-	-	-	6.72	0.11	52.16	0.01	0.01	-	-	0.38	100.04	93.09

Continued on next page...

Table F.7 – continued

Sample	SiO_2	TiO_2	Al_2O_3	Cr_2O_3	V_2O_3	FeO tot	MnO	MgO	CaO	Na_2O	K_2O	P_2O_5	NiO	Total	Mg#
Ol2-10	40.59	0.01	-	0.01	0.01	6.98	0.11	51.96	0.02	0.01	-	0.01	0.35	100.02	93.07
Ol2-11	40.05	0.01	-	0.01	0.01	8.06	0.13	51.14	-	0.02	0.01	-	0.37	99.78	91.87
Ol2-12	40.48	0.01	0.03	0.01	-	7.00	0.10	51.99	0.01	0.01	-	0.02	0.36	99.99	93.07
Ol2-13	39.83	-	0.07	0.01	0.01	7.10	0.10	51.34	0.01	0.01	0.01	0.02	0.34	98.81	92.61
Ol2-14	39.79	-	0.01	0.01	-	7.97	0.12	51.21	0.01	-	-	0.02	0.36	99.48	92.14
Ol2-15	40.27	0.01	0.03	0.01	-	7.13	0.12	51.57	0.01	0.05	-	0.01	0.36	99.52	92.61
Ol2-16	39.72	0.02	0.01	0.01	0.01	6.81	0.11	52.15	0.01	0.01	-	-	0.32	99.14	93.15
Ol2-17	39.88	0.01	0.03	-	-	7.07	0.10	51.97	-	0.01	-	0.01	0.37	99.43	93.10
Ol2-18	39.67	0.01	0.07	0.01	-	7.29	0.12	51.59	0.01	0.02	-	0.02	0.36	99.15	92.63
Ol2-19	40.25	-	0.01	0.01	0.01	7.07	0.10	51.39	0.01	0.02	-	0.01	0.34	99.18	92.82
Ol2-21	39.72	0.01	-	-	-	8.07	0.11	50.97	0.01	0.02	-	0.02	0.36	99.27	91.67
Ol2-22	39.98	0.01	0.01	0.01	-	6.76	0.12	51.94	0.01	0.02	0.01	0.01	0.32	99.15	93.12
Ol2-23	39.67	0.01	0.01	0.01	0.01	7.19	0.12	51.58	0.01	0.03	-	0.03	0.36	99.00	92.65
Ol2-24	39.99	0.01	0.01	0.01	0.01	7.15	0.10	52.25	-	0.01	-	0.01	0.37	99.89	92.68
Ol2-25	40.12	0.01	0.02	-	-	7.17	0.10	51.33	0.01	0.01	-	0.02	0.35	99.12	92.59
Ol2-26	39.93	0.01	0.01	-	-	7.13	0.10	51.60	0.01	0.02	-	0.03	0.36	99.16	92.63
Ol2-27	39.92	0.01	0.26	0.01	0.01	7.00	0.12	51.92	0.01	0.02	0.01	-	0.36	99.61	93.09
Ol2-28	40.10	-	0.05	-	0.01	7.04	0.10	51.70	0.01	0.01	-	-	0.34	99.35	93.07
Ol2-29	40.40	0.01	0.01	0.01	-	7.13	0.11	51.69	0.01	0.01	-	0.01	0.35	99.72	92.82
Ol2-30	39.97	0.01	0.02	-	-	7.22	0.12	51.41	-	0.01	0.01	-	0.34	99.08	92.61
Ol2-31	40.02	-	0.01	0.01	-	7.17	0.10	51.75	0.01	0.01	-	0.01	0.37	99.43	92.63
Ol2-32	40.14	0.01	0.06	0.01	0.01	7.99	0.13	51.18	0.01	0.02	-	0.03	0.36	99.91	92.08
Ol3-1	40.15	-	0.08	-	-	7.36	0.09	51.75	0.02	0.01	-	-	0.36	99.82	92.61
Ol3-2	41.10	0.01	0.04	-	-	6.28	0.10	52.13	0.01	0.02	0.01	0.02	0.33	100.02	93.53
Ol3-3	40.27	-	0.38	-	0.01	7.03	0.11	51.38	0.01	0.02	-	0.01	0.35	99.54	92.81
Ol3-4	41.59	0.01	0.02	-	-	6.99	0.11	51.48	0.01	0.02	-	0.01	0.36	100.57	92.96
Ol3-5	41.61	0.01	0.08	-	-	7.17	0.10	50.98	0.01	0.01	0.01	0.02	0.36	100.33	92.66
Ol3-6	41.07	0.02	-	0.01	-	7.02	0.11	52.05	-	0.01	-	0.05	0.36	100.69	93.04
Ol3-7	41.03	0.01	-	-	0.01	6.85	0.10	52.02	0.02	0.01	-	-	0.35	100.37	93.03
Ol3-8	40.03	0.01	0.09	0.02	0.01	7.27	0.10	53.15	-	0.02	-	0.04	0.38	101.11	92.72
Ol3-9	40.40	-	-	0.01	0.01	9.58	0.17	49.90	0.01	0.01	-	0.03	0.36	100.48	90.10

Continued on next page...

Table F.7 – continued

Sample	SiO_2	TiO_2	Al_2O_3	Cr_2O_3	V_2O_3	FeO tot	MnO	MgO	CaO	Na_2O	K_2O	P_2O_5	NiO	Total	Mg#
Ol3-10	40.83	0.01	0.01	-	-	7.31	0.11	51.90	0.02	0.02	-	0.02	0.37	100.56	92.57
Ol3-12	41.11	0.01	-	0.01	-	6.25	0.10	52.57	0.02	0.02	0.01	0.01	0.33	100.39	93.55
Ol3-13	41.50	0.01	-	-	-	7.15	0.12	51.56	-	0.02	-	-	0.36	100.72	92.97
Ol3-14	40.37	0.01	0.04	0.01	-	6.65	0.09	51.67	0.02	0.02	-	0.01	0.36	99.22	93.09
Ol3-15	41.24	-	0.02	-	0.01	6.79	0.11	51.32	0.01	0.01	0.01	0.01	0.33	99.85	92.98
Ol3-16	43.14	-	0.06	-	-	6.63	0.08	50.65	-	0.01	-	0.02	0.34	100.94	93.26
Ol3-17	39.80	-	0.01	-	-	8.65	0.18	51.48	0.02	0.02	-	0.02	0.35	100.53	91.22
Ol3-18	42.45	-	0.06	-	-	6.83	0.11	51.52	0.01	0.02	0.01	-	0.37	101.38	92.89
Ol3-19	41.01	0.01	0.02	-	0.01	9.59	0.18	49.27	0.01	0.02	-	0.01	0.38	100.47	89.98
Ol3-20	41.69	0.01	-	-	-	6.80	0.11	52.15	-	0.02	-	0.01	0.33	101.11	93.00
Ol3-21	40.96	0.01	0.05	0.01	-	6.75	0.10	51.64	0.01	0.01	0.01	0.01	0.36	99.90	93.02
Ol3-22	40.25	0.01	0.01	-	0.01	7.28	0.10	51.39	0.01	0.01	0.01	0.01	0.37	99.43	92.57
Ol3-23	40.47	-	0.01	-	0.01	7.40	0.12	51.37	0.01	0.01	-	-	0.32	99.71	92.57
Ol3-24	40.68	-	-	-	0.01	7.62	0.12	51.35	0.01	0.02	-	0.02	0.35	100.16	92.29
Ol3-25	40.58	-	0.02	0.01	-	7.25	0.11	51.44	-	0.01	-	0.01	0.36	99.78	92.56
Ol3-26	40.84	0.01	0.01	0.01	-	7.67	0.14	51.22	0.01	0.01	-	0.02	0.34	100.26	92.04
Ol3-28	41.47	-	-	-	-	7.25	0.10	51.85	0.01	0.01	-	0.01	0.35	101.05	92.54
Ol3-29	41.99	0.01	-	0.01	0.01	7.25	0.12	51.37	0.01	0.02	-	0.01	0.36	101.13	92.68
Ol3-30	41.06	-	-	0.01	0.01	7.54	0.13	51.20	0.01	0.02	0.01	0.03	0.37	100.36	92.50
Ol3-31	39.96	-	0.07	0.01	0.01	6.74	0.10	52.36	0.01	0.01	-	0.03	0.34	99.60	93.15
Ol3-32	40.58	0.01	0.06	-	0.01	7.48	0.12	51.06	0.01	0.01	-	0.03	0.36	99.69	92.52
Ol3-33	41.64	-	0.18	-	-	7.72	0.13	50.11	0.01	0.01	-	0.02	0.34	100.14	91.99
average	40.35	0.01	0.05	0.01	0.01	7.35	0.12	51.52	0.01	0.02	0.01	0.02	0.35	99.76	92.56
min	39.12	0.01	0.01	0.01	0.01	6.25	0.08	49.27	0.01	0.01	0.01	0.01	0.32	98.54	89.98
max	43.14	0.02	0.38	0.02	0.02	9.59	0.18	53.15	0.02	0.05	0.01	0.05	0.38	101.38	93.60
2σ	1.50	0.00	0.14	0.00	0.00	1.22	0.05	1.26	0.01	0.01	0.00	0.02	0.03	1.45	1.30
n	82														

Table F.8: Major element compositions of "less depleted" Victor olivine xenocrysts

Sample	SiO_2	TiO_2	Al_2O_3	Cr_2O_3	V_2O_3	FeO tot	MnO	MgO	CaO	Na_2O	K_2O	P_2O_5	NiO	Total	Mg#
2Ol1-1	40.03	0.02	0.02	0.03	0.01	10.20	0.12	49.12	0.03	0.03	0.01	0.01	0.33	99.92	89.58
2Ol1-2	40.56	0.04	0.01	0.02	-	9.07	0.12	50.57	0.03	0.02	0.01	-	0.33	100.76	91.07
2Ol1-3	39.98	0.05	-	0.03	-	9.27	0.12	50.09	0.03	0.02	0.01	0.02	0.33	99.93	90.62
2Ol1-4	39.41	0.03	0.01	0.02	0.01	9.60	0.13	50.18	0.03	0.02	0.01	-	0.31	99.74	90.22
2Ol1-5	39.91	0.03	0.01	0.02	-	10.19	0.12	49.73	0.03	0.03	0.01	0.02	0.33	100.41	89.66
2Ol1-6	39.39	0.02	0.02	0.03	-	10.17	0.14	49.28	0.03	0.03	-	0.02	0.34	99.43	89.68
2Ol1-7	39.71	0.01	0.01	0.02	-	10.23	0.13	49.57	0.04	0.04	-	0.03	0.32	100.09	89.66
2Ol1-8	39.76	0.03	0.01	0.02	-	9.70	0.11	50.11	0.03	0.03	-	0.01	0.31	100.10	90.17
2Ol1-9	40.00	0.03	0.01	0.03	-	9.13	0.13	50.27	0.02	0.02	-	0.01	0.34	99.97	90.62
2Ol1-10	39.74	0.04	0.01	0.03	-	9.07	0.14	50.52	0.02	0.03	-	0.02	0.33	99.91	90.66
2Ol1-11	39.97	0.05	0.04	0.02	0.01	9.10	0.12	50.50	0.02	0.03	-	0.01	0.32	100.17	90.66
2Ol1-12	39.60	0.03	0.02	0.02	-	10.19	0.14	49.64	0.03	0.04	-	0.02	0.34	100.04	89.68
2Ol1-13	39.60	0.04	0.01	0.04	0.01	9.05	0.12	50.67	0.02	0.03	0.01	-	0.33	99.89	90.93
2Ol1-14	40.62	0.02	-	0.01	0.01	9.02	0.16	50.27	0.01	0.02	-	0.01	0.30	100.45	91.05
2Ol1-15	40.28	0.03	0.01	0.03	0.01	10.25	0.13	49.98	0.03	0.03	-	0.02	0.32	101.08	89.63
2Ol1-16	39.38	0.03	0.01	0.02	0.01	9.06	0.12	50.94	0.03	0.03	-	0.01	0.33	99.94	90.75
2Ol1-17	40.17	0.02	0.01	0.03	0.01	10.20	0.12	49.46	0.03	0.02	-	0.01	0.34	100.40	89.60
2Ol1-18	39.75	0.03	-	0.02	-	9.66	0.12	49.99	0.02	0.03	-	0.01	0.31	99.93	90.17
2Ol1-19	39.98	0.03	0.01	0.02	0.01	9.27	0.13	49.98	0.02	0.02	-	0.01	0.33	99.79	90.62
2Ol2-1	40.28	0.04	-	0.04	0.01	9.31	0.13	49.59	0.02	0.02	-	0.01	0.33	99.75	90.52
2Ol2-2	39.40	0.03	0.01	0.04	0.01	9.70	0.14	49.59	0.02	0.02	-	0.01	0.34	99.28	90.15
2Ol2-3	40.07	0.03	0.01	0.02	-	9.37	0.13	50.20	0.03	0.02	-	0.01	0.33	100.19	90.59
2Ol2-4	39.28	0.03	0.01	0.03	0.01	9.29	0.14	50.16	0.02	0.02	-	0.01	0.34	99.31	90.69
2Ol2-5	39.18	0.01	-	0.03	-	10.27	0.11	49.41	0.03	0.02	-	0.03	0.32	99.43	89.71
2Ol2-6	39.61	0.02	0.01	0.03	-	10.36	0.13	49.06	0.03	0.03	-	0.01	0.31	99.57	89.60
2Ol2-7	39.35	0.03	0.01	0.01	0.01	10.51	0.15	49.33	0.02	0.03	-	0.02	0.30	99.73	89.22
2Ol2-8	39.80	0.03	0.01	0.02	-	9.82	0.13	49.52	0.03	0.04	-	-	0.29	99.66	90.10
2Ol2-9	39.91	0.02	0.02	0.03	-	9.82	0.12	49.86	0.03	0.03	-	0.02	0.30	100.13	90.12
2Ol2-10	39.67	0.04	0.01	0.03	0.01	9.22	0.14	50.02	0.03	0.03	-	0.01	0.33	99.50	90.64

Continued on next page...

Table F.8 – continued

Sample	SiO_2	TiO_2	Al_2O_3	Cr_2O_3	V_2O_3	FeO tot	MnO	MgO	CaO	Na_2O	K_2O	P_2O_5	NiO	Total	Mg#
2Ol2-11	40.09	0.02	0.01	0.03	0.01	9.74	0.13	49.90	0.03	0.02	-	0.01	0.32	100.28	90.12
2Ol2-12	39.76	0.01	0.02	0.03	-	10.14	0.12	49.05	0.03	0.03	-	0.01	0.34	99.51	89.60
2Ol2-13	39.33	0.04	0.02	0.03	0.01	9.32	0.12	50.12	0.03	0.02	-	0.02	0.31	99.37	90.69
2Ol2-14	39.41	0.03	0.01	0.03	-	9.35	0.12	49.70	0.02	0.02	0.01	0.01	0.33	99.02	90.62
2Ol2-15	39.74	0.03	0.01	0.03	-	9.75	0.15	50.05	0.02	0.03	-	0.02	0.34	100.13	90.17
2Ol2-16	39.12	0.03	0.01	0.03	0.02	9.88	0.14	49.87	0.03	0.02	0.01	0.01	0.32	99.44	90.00
2Ol2-17	38.87	0.04	0.51	-	-	10.44	0.16	48.22	0.02	0.02	-	0.01	0.28	98.56	89.11
2Ol2-18	39.17	0.03	0.01	0.01	0.01	10.56	0.15	49.63	0.03	0.03	-	0.02	0.30	99.91	89.29
2Ol2-19	39.55	0.02	0.02	0.03	0.01	10.06	0.13	49.54	0.03	0.03	-	0.03	0.34	99.77	89.68
2Ol2-20	40.08	0.02	0.02	0.04	-	9.71	0.12	49.90	0.03	0.03	-	0.01	0.31	100.25	90.12
2Ol3-1	38.68	0.04	0.02	0.04	-	9.22	0.12	50.39	0.03	0.02	-	-	0.34	98.89	90.78
2Ol3-2	38.72	0.02	0.01	0.03	-	9.51	0.14	50.16	0.02	0.03	-	0.01	0.32	98.94	90.29
2Ol3-3	39.49	0.03	0.01	0.03	0.01	10.15	0.12	49.35	0.03	0.04	-	-	0.33	99.54	89.68
2Ol3-4	39.46	0.04	0.01	0.03	0.01	9.13	0.13	50.22	0.03	0.02	-	-	0.33	99.39	90.69
2Ol3-5	39.99	0.04	0.01	0.03	-	9.84	0.14	49.76	0.02	0.03	-	0.01	0.32	100.15	90.10
2Ol3-6	39.44	0.02	0.01	0.02	0.01	10.30	0.13	49.33	0.03	0.03	-	-	0.33	99.63	89.66
2Ol3-7	39.26	0.02	0.01	0.02	0.01	9.74	0.12	50.12	0.03	0.02	-	0.02	0.31	99.65	90.24
2Ol3-8	39.90	0.03	-	0.03	-	9.47	0.13	50.08	0.03	0.03	-	0.02	0.33	100.03	90.37
2Ol3-9	39.59	0.03	0.02	0.03	-	10.24	0.12	49.26	0.03	0.03	-	0.03	0.32	99.66	89.63
2Ol3-10	38.45	0.03	0.02	0.03	0.01	9.32	0.13	50.46	0.02	0.02	-	0.01	0.32	98.80	90.58
2Ol3-11	39.29	0.03	0.02	0.03	-	10.14	0.13	49.36	0.03	0.03	-	-	0.33	99.36	89.71
2Ol3-12	39.33	0.04	0.01	0.03	0.01	9.06	0.13	50.57	0.02	0.02	0.01	-	0.32	99.52	90.73
2Ol3-13	39.65	0.02	0.01	0.03	-	9.09	0.14	50.42	0.02	0.04	-	0.02	0.32	99.76	90.69
2Ol3-14	39.49	0.03	0.01	0.03	-	10.13	0.13	49.64	0.03	0.02	-	0.01	0.34	99.83	89.68
2Ol3-15	39.65	0.04	0.01	0.02	-	9.12	0.13	51.21	0.03	0.03	-	-	0.33	100.54	90.75
2Ol3-16	39.48	0.04	0.01	0.04	0.01	9.14	0.14	50.38	0.03	0.02	-	0.01	0.33	99.60	90.71
2Ol3-17	39.74	0.04	0.01	0.03	0.01	9.31	0.11	50.31	0.03	0.02	-	-	0.33	99.91	90.66
2Ol3-18	39.19	0.04	0.01	0.03	0.01	9.26	0.13	50.40	0.02	0.03	-	0.01	0.33	99.42	90.73
2Ol3-19	38.77	0.02	0.01	0.03	0.01	9.23	0.12	49.99	0.03	0.02	-	0.02	0.35	98.59	90.73
2Ol4-1	38.39	0.01	0.01	0.02	-	10.22	0.12	49.37	0.03	0.02	-	0.04	0.34	98.56	89.81
2Ol4-2	38.69	0.02	0.01	0.02	-	9.99	0.17	49.51	0.01	0.01	-	0.01	0.30	98.74	89.76

Continued on next page. . .

Table F.8 – continued

Sample	SiO_2	TiO_2	Al_2O_3	Cr_2O_3	V_2O_3	FeO tot	MnO	MgO	CaO	Na_2O	K_2O	P_2O_5	NiO	Total	Mg#
2Ol4-3	38.61	0.02	0.02	0.01	0.01	10.02	0.13	49.59	0.03	0.03	-	0.01	0.31	98.76	89.81
2Ol4-4	38.56	0.02	0.01	0.02	-	9.73	0.12	49.88	0.03	0.02	-	-	0.31	98.71	90.29
2Ol4-6	38.61	0.02	-	0.03	-	10.29	0.12	49.71	0.04	0.03	-	0.02	0.34	99.19	89.81
2Ol4-7	39.09	0.04	-	0.03	-	9.09	0.12	50.33	0.03	0.03	-	-	0.34	99.08	90.73
2Ol4-8	38.72	0.04	0.01	0.03	-	9.21	0.13	50.26	0.02	0.03	-	-	0.33	98.75	90.75
2Ol4-9	39.06	0.04	0.01	0.03	0.01	9.21	0.13	50.55	0.03	0.03	-	0.01	0.33	99.41	90.75
2Ol4-10	39.13	0.04	0.01	0.02	-	9.22	0.13	50.74	0.02	0.03	0.01	0.01	0.33	99.67	90.75
2Ol4-11	39.86	0.04	0.01	0.02	0.01	9.23	0.12	50.44	0.02	0.03	-	0.01	0.33	100.10	90.66
2Ol4-12	39.46	0.03	-	0.03	0.01	9.12	0.13	50.40	0.01	0.03	-	-	0.32	99.53	90.71
2Ol4-13	39.94	0.03	-	0.02	0.01	9.56	0.12	50.27	0.03	0.02	-	0.02	0.34	100.33	90.39
2Ol4-14	39.54	0.04	0.01	0.03	-	9.08	0.12	49.73	0.03	0.02	-	0.01	0.34	98.93	90.64
2Ol4-15	40.06	0.02	0.01	0.03	-	9.68	0.12	49.81	0.03	0.03	-	0.02	0.32	100.11	90.10
2Ol4-16	39.39	0.03	0.01	0.03	0.01	9.18	0.12	50.16	0.03	0.03	0.01	0.01	0.34	99.30	90.69
2Ol4-17	39.67	0.03	0.02	0.03	0.01	10.08	0.13	49.49	0.03	0.03	-	0.01	0.33	99.84	89.66
2Ol4-18	39.33	0.02	0.01	0.03	0.02	8.18	0.09	50.53	0.03	0.03	-	-	0.38	98.64	91.67
2Ol4-21	39.09	0.03	0.01	0.02	0.01	9.65	0.12	50.02	0.03	0.02	-	-	0.32	99.30	90.24
2Ol4-22	38.36	0.03	0.03	0.02	0.01	9.91	0.13	50.50	0.03	0.03	-	0.03	0.32	99.37	90.14
2Ol4-23	39.51	0.03	0.01	0.02	0.01	9.57	0.12	49.83	0.17	0.14	0.01	0.02	0.32	99.73	90.15
2Ol4-24	38.95	0.04	-	0.01	-	10.28	0.13	49.52	0.02	0.03	-	0.02	0.35	99.34	89.76
2Ol4-25	38.16	0.03	-	-	0.01	9.75	0.18	50.41	0.02	0.02	-	0.02	0.24	98.83	90.39
2Ol5-3	38.47	0.02	-	0.01	0.01	11.66	0.16	48.45	0.02	0.02	-	0.02	0.21	99.02	88.11
2Ol5-4	38.97	0.02	0.02	0.04	0.01	8.79	0.11	50.81	0.03	0.02	-	0.03	0.35	99.19	91.24
2Ol5-5	38.51	0.01	0.02	0.03	0.01	10.17	0.12	49.76	0.03	0.03	-	0.03	0.34	99.04	89.81
2Ol5-6	38.90	0.02	0.01	0.02	0.01	10.20	0.13	49.40	0.03	0.04	-	0.02	0.34	99.07	89.73
2Ol5-7	38.47	0.02	0.02	0.02	0.03	9.51	0.13	50.03	0.02	0.03	-	-	0.31	98.58	90.29
2Ol5-12	39.09	0.01	0.01	0.03	-	8.96	0.12	50.04	0.02	0.04	-	-	0.38	98.69	90.73
2Ol5-13	38.76	0.04	0.01	0.02	0.02	10.15	0.12	49.20	0.03	0.03	-	0.01	0.34	98.72	89.71
2Ol5-15	38.83	0.02	-	0.03	-	10.27	0.15	49.76	0.03	0.02	-	0.01	0.32	99.43	89.76
2Ol5-21	38.84	0.04	0.01	0.03	-	9.32	0.13	49.93	0.03	0.03	-	0.03	0.35	98.71	90.71
average	39.39	0.03	0.02	0.03	0.01	9.66	0.13	49.93	0.03	0.03	0.01	0.02	0.32	99.56	90.22
min	38.16	0.01	0.01	0.01	0.01	8.18	0.09	48.22	0.01	0.01	0.01	0.01	0.21	98.56	88.11

Continued on next page. . .

Table F.8 – continued

Sample	SiO_2	TiO_2	Al_2O_3	Cr_2O_3	V_2O_3	FeO tot	MnO	MgO	CaO	Na_2O	K_2O	P_2O_5	NiO	Total	Mg#
max	40.62	0.05	0.51	0.04	0.03	11.66	0.18	51.21	0.17	0.14	0.01	0.04	0.38	101.08	91.67
2σ	1.08	0.02	0.12	0.01	0.01	1.07	0.03	1.03	0.03	0.03	0.00	0.02	0.04	1.12	1.11
n	89														

Table F.9: Major element compositions of Victor clinopyroxene xenocrysts

Sample	SiO_2	TiO_2	Al_2O_3	Cr_2O_3	V_2O_3	FeO tot	MnO	MgO	CaO	Na_2O	K_2O	P_2O_5	NiO	Total
Cpx-1-1	54.39	0.26	2.07	1.74	0.10	3.18	0.12	15.54	19.09	2.37	0.02	0.01	0.04	98.94
Cpx-1-2	54.37	0.27	2.85	1.46	0.05	3.45	0.12	15.79	17.84	2.55	0.02	-	0.03	98.79
Cpx-1-5	54.24	0.22	1.28	1.21	0.05	3.22	0.08	15.93	20.56	1.70	0.02	0.01	0.03	98.54
Cpx-1-6	54.17	0.11	0.23	1.62	0.05	2.12	0.07	16.36	22.63	1.23	-	0.01	0.03	98.62
Cpx-2-27	54.03	0.22	1.16	1.42	0.07	3.27	0.09	15.66	21.03	1.74	0.02	-	0.03	98.71
Cpx-3-1	54.19	0.18	0.64	2.06	0.06	2.56	0.08	15.88	21.77	1.59	0.01	0.01	0.03	99.08
Cpx-3-2	54.33	0.20	1.83	1.59	0.12	3.05	0.10	16.08	19.53	1.97	0.03	0.01	0.03	98.87
Cpx-3-3	54.38	0.24	0.95	1.52	0.07	3.34	0.10	16.03	20.81	1.67	0.01	0.01	0.01	99.14
Cpx-3-4	54.17	0.11	0.23	1.62	0.05	2.12	0.07	16.36	22.63	1.23	-	0.01	0.03	98.62
Cpx-3-5	54.54	0.24	1.82	1.66	0.06	3.12	0.10	15.78	19.65	2.08	0.02	0.01	0.03	99.11
Cpx-3-6	54.20	0.27	1.59	1.93	0.07	3.14	0.10	15.37	20.00	2.17	0.02	0.01	0.03	98.89
Cpx-3-7	54.44	0.13	0.26	1.95	0.05	2.17	0.07	16.09	22.43	1.46	-	0.01	0.03	99.09
Cpx-3-8	54.45	0.12	0.27	2.04	0.05	2.34	0.07	15.94	22.16	1.56	0.01	0.01	0.03	99.04
Cpx-3-9	54.48	0.11	0.26	2.04	0.05	2.33	0.07	15.89	22.25	1.57	-	-	0.04	99.08
Cpx-3-10	54.40	0.13	0.26	2.06	0.06	2.35	0.07	15.84	22.09	1.59	-	0.01	0.03	98.89
Cpx-3-11	54.35	0.12	0.25	2.01	0.06	2.34	0.07	15.96	22.20	1.56	-	0.02	0.03	98.95
Cpx-3-12	54.40	0.12	0.27	1.97	0.06	2.35	0.08	15.95	22.34	1.58	-	0.01	0.04	99.16
Cpx-3-13	54.26	0.16	0.68	1.38	0.06	2.90	0.09	16.18	21.80	1.37	0.01	0.02	0.03	98.94
Cpx-3-14	54.17	0.11	0.23	1.62	0.05	2.12	0.07	16.36	22.63	1.23	-	0.01	0.03	98.62
Cpx-3-15	54.37	0.11	0.25	1.99	0.05	2.34	0.07	15.89	22.16	1.54	-	-	0.03	98.79
Cpx-3-16	54.17	0.11	0.23	1.62	0.05	2.12	0.07	16.36	22.63	1.23	-	0.01	0.03	98.62
Cpx-3-17	54.51	0.10	0.25	1.98	0.05	2.32	0.07	15.90	22.27	1.58	-	-	0.03	99.07
Cpx-3-18	54.51	0.24	1.30	1.28	0.08	3.19	0.09	15.94	20.72	1.68	0.02	0.01	0.02	99.08
Cpx-3-19	54.70	0.20	2.43	1.34	0.05	3.51	0.12	16.73	17.46	2.27	0.04	-	0.05	98.89
Cpx-3-20	54.59	0.13	0.73	1.52	0.04	1.96	0.06	16.13	22.65	1.30	-	-	0.04	99.17
Cpx-3-21	54.41	0.13	0.74	1.51	0.05	1.96	0.08	16.17	22.74	1.28	0.01	0.01	0.03	99.11
Cpx-3-22	54.04	0.16	0.69	1.39	0.06	2.84	0.09	16.09	21.97	1.40	0.01	0.01	0.02	98.77
Cpx-3-23	54.25	0.11	0.20	1.69	0.06	2.41	0.08	16.02	22.71	1.37	-	0.01	0.02	98.93
Cpx-3-24	54.17	0.11	0.23	1.62	0.05	2.12	0.07	16.36	22.63	1.23	-	0.01	0.03	98.62
Cpx-3-25	54.70	0.23	2.86	1.44	0.05	3.60	0.11	16.32	16.79	2.60	0.03	0.01	0.05	98.80

Continued on next page. . .

Table F.9 – continued

Sample	SiO_2	TiO_2	Al_2O_3	Cr_2O_3	V_2O_3	FeO tot	MnO	MgO	CaO	Na_2O	K_2O	P_2O_5	NiO	Total
Cpx-3-26	54.16	0.23	1.29	1.27	0.07	3.19	0.09	15.95	20.77	1.70	0.02	-	0.02	98.76
Cpx-3-27	54.62	0.22	2.82	1.43	0.04	3.59	0.12	16.42	16.97	2.64	0.03	-	0.04	98.95
Cpx-3-28	54.34	0.23	2.68	1.52	0.05	3.40	0.12	16.00	17.93	2.44	0.03	0.01	0.04	98.78
Cpx-4-1	54.17	0.11	0.23	1.62	0.05	2.12	0.07	16.36	22.63	1.23	-	0.01	0.03	98.62
Cpx-4-2	54.30	0.22	1.23	1.37	0.07	3.35	0.08	16.00	20.61	1.86	0.02	0.01	0.03	99.16
Cpx-4-3	54.35	0.27	2.88	1.37	0.04	3.38	0.10	16.00	17.97	2.55	0.02	0.02	0.04	99.00
Cpx-4-5	54.15	0.22	1.17	1.15	0.06	3.41	0.09	16.12	20.67	1.76	0.02	0.01	0.03	98.84
Cpx-4-6	54.28	0.22	1.18	1.15	0.07	3.39	0.09	15.98	20.63	1.77	0.01	0.02	0.04	98.83
Cpx-4-7	54.29	0.27	2.89	1.40	0.05	3.39	0.12	15.93	18.05	2.54	0.03	0.02	0.04	99.00
Cpx-4-8	54.17	0.11	0.23	1.62	0.05	2.12	0.07	16.36	22.63	1.23	-	0.01	0.03	98.62
Cpx-4-9	54.17	0.11	0.23	1.62	0.05	2.12	0.07	16.36	22.63	1.23	-	0.01	0.03	98.62
Cpx-4-10	53.74	0.21	1.19	1.15	0.06	3.40	0.08	16.04	20.85	1.77	0.01	-	0.02	98.53
Cpx-4-20	53.89	0.26	1.57	1.01	0.06	3.48	0.08	16.17	20.27	1.83	0.02	0.02	0.02	98.67
Cpx-4-22	54.17	0.11	0.23	1.62	0.05	2.12	0.07	16.36	22.63	1.23	-	0.01	0.03	98.62
Cpx-4-23	53.80	0.11	0.26	2.10	0.06	2.35	0.06	16.12	22.03	1.62	-	0.01	0.03	98.55
Cpx-4-24	54.17	0.11	0.23	1.62	0.05	2.12	0.07	16.36	22.63	1.23	-	0.01	0.03	98.62
Cpx-4-25	53.98	0.27	2.83	1.62	0.07	3.41	0.11	15.92	17.90	2.63	0.02	0.01	0.04	98.80
Cpx-4-26	54.44	0.14	0.77	1.59	0.04	2.02	0.06	16.44	22.34	1.37	-	0.01	0.03	99.26
Cpx-4-27	54.27	0.18	2.43	1.33	0.04	3.55	0.12	17.10	17.19	2.29	0.03	-	0.06	98.60
Cpx-4-28	53.86	0.24	1.30	1.29	0.06	3.24	0.10	16.33	20.69	1.72	0.02	0.02	0.02	98.89
Cpx-4-29	54.17	0.11	0.23	1.62	0.05	2.12	0.07	16.36	22.63	1.23	-	0.01	0.03	98.62
Cpx-4-30	54.17	0.11	0.23	1.62	0.05	2.12	0.07	16.36	22.63	1.23	-	0.01	0.03	98.62
Cpx-4-31	54.17	0.11	0.23	1.62	0.05	2.12	0.07	16.36	22.63	1.23	-	0.01	0.03	98.62
Cpx-4-32	53.89	0.26	1.59	1.00	0.05	3.49	0.10	16.29	20.27	1.82	0.02	0.03	0.03	98.85
Cpx-4-33	54.17	0.11	0.23	1.62	0.05	2.12	0.07	16.36	22.63	1.23	-	0.01	0.03	98.62
Cpx-4-34	54.08	0.27	1.69	1.69	0.09	3.26	0.09	15.83	19.75	2.19	0.02	0.01	0.04	99.01
Cpx-4-35	54.58	0.22	2.72	1.39	0.04	3.58	0.12	16.73	16.84	2.54	0.03	0.03	0.05	98.89
Cpx-4-36	54.17	0.11	0.23	1.62	0.05	2.12	0.07	16.36	22.63	1.23	-	0.01	0.03	98.62
Cpx-4-37	53.94	0.23	1.39	1.62	0.08	3.55	0.10	15.60	20.10	2.16	0.01	0.01	0.02	98.81
Cpx-4-38	54.38	0.27	2.88	1.40	0.05	3.35	0.11	15.82	18.00	2.58	0.03	0.01	0.04	98.92
BC24150-Cpx1-1	54.90	0.11	1.32	1.64	0.04	2.62	0.10	16.79	19.87	1.99	0.03	0.02	0.06	99.48

Continued on next page...

Table F.9 – continued

Sample	SiO_2	TiO_2	Al_2O_3	Cr_2O_3	V_2O_3	FeO tot	MnO	MgO	CaO	Na_2O	K_2O	P_2O_5	NiO	Total
BC24150-Cpx1-2	54.59	0.14	0.31	2.54	0.06	2.23	0.06	15.60	21.53	1.99	-	0.01	0.03	99.08
BC24150-Cpx1-3	54.49	0.26	2.47	2.00	0.05	2.63	0.09	16.02	18.03	2.68	0.03	0.02	0.03	98.80
BC24150-Cpx1-4	54.93	0.25	3.15	1.46	0.05	3.34	0.11	15.62	17.37	2.84	0.03	0.04	0.03	99.22
BC24150-Cpx1-5	54.79	0.23	1.10	1.64	0.07	3.28	0.09	15.57	20.17	2.20	0.01	0.02	0.04	99.20
BC24150-Cpx1-6	54.70	0.20	0.88	1.68	0.06	3.03	0.09	15.82	20.82	1.52	0.01	0.03	0.01	98.84
BC24150-Cpx1-7	55.05	0.12	0.30	2.22	0.05	2.24	0.07	15.82	21.73	1.50	-	-	0.02	99.13
BC24150-Cpx1-8	54.75	0.12	0.28	1.72	0.06	2.19	0.07	16.15	22.22	1.24	-	0.03	0.02	98.82
BC24150-Cpx1-9	54.47	0.14	0.79	1.71	0.03	1.95	0.06	15.98	22.14	1.25	-	0.02	0.03	98.57
BC24150-Cpx1-10	54.84	0.11	0.29	1.60	0.07	2.18	0.07	16.17	22.24	1.13	-	0.02	-	98.72
BC24150-Cpx1-11	54.79	0.19	0.80	1.78	0.07	3.03	0.07	15.61	21.02	1.51	0.01	0.01	0.02	98.92
BC24150-Cpx1-12	54.79	0.23	1.86	2.01	0.05	2.81	0.10	16.01	18.92	1.87	0.02	0.02	0.02	98.71
BC24150-Cpx1-13	54.72	0.24	1.42	1.42	0.07	3.25	0.10	15.85	20.10	1.66	0.01	0.02	0.01	98.86
BC24150-Cpx1-14	54.47	0.10	2.08	1.10	0.04	2.12	0.08	15.84	21.75	1.18	0.00	0.02	0.03	98.80
BC24150-Cpx1-15	54.69	0.20	0.97	1.49	0.06	3.10	0.07	15.72	20.83	1.46	0.01	0.04	0.02	98.66
BC24150-Cpx1-16	54.67	0.19	0.85	2.09	0.05	2.69	0.08	15.74	20.95	1.52	0.01	0.02	0.02	98.86
BC24150-Cpx1-17	54.58	0.17	0.71	1.72	0.06	2.87	0.08	15.84	21.33	1.35	0.01	0.03	0.03	98.78
BC24150-Cpx1-18	55.00	0.20	2.64	1.37	0.05	3.55	0.12	16.54	16.99	2.18	0.03	0.02	0.05	98.74
BC24150-Cpx1-19	54.96	0.24	1.37	1.16	0.06	3.37	0.09	15.90	20.43	1.46	0.02	0.01	-	99.08
BC24150-Cpx1-20	55.07	0.11	0.25	1.78	0.05	2.04	0.08	16.34	22.25	1.03	0.01	0.01	0.04	99.05
BC24150-Cpx	55.34	0.20	2.67	1.43	0.05	3.50	0.13	16.70	16.90	2.13	0.03	0.02	0.05	99.15
BC24150-Cpx1-22	54.75	0.22	0.99	1.91	0.07	3.02	0.09	15.64	20.66	1.65	0.01	0.02	0.03	99.06
BC24150-Cpx1-23	54.77	0.21	1.70	1.60	0.06	3.32	0.11	16.06	19.11	1.80	0.02	0.01	0.02	98.80
BC24150-Cpx1-24	55.11	0.22	4.93	0.89	0.06	4.64	0.13	15.14	13.69	3.70	0.01	0.01	0.04	98.53
BC24150-Cpx1-25	54.93	0.19	0.84	1.83	0.06	2.84	0.08	15.83	21.10	1.48	0.01	0.02	0.02	99.23
BC24150-Cpx1-26	54.73	0.28	1.66	1.81	0.06	3.23	0.10	15.50	19.48	1.98	0.02	0.02	0.03	98.91
BC24150-Cpx1-27	54.52	0.28	1.65	1.83	0.06	3.24	0.10	15.46	19.60	1.91	0.02	0.01	0.02	98.70
BC24150-Cpx1-28	54.70	0.21	1.14	1.23	0.06	3.22	0.10	15.91	20.74	1.41	0.02	0.03	0.02	98.77
BC24150-Cpx1-29	54.94	0.12	0.21	1.82	0.03	2.12	0.07	16.20	22.11	1.06	-	0.02	0.02	98.71
BC24150-Cpx1-30	55.14	0.13	1.69	1.08	0.04	3.27	0.11	17.85	18.36	1.24	0.03	0.01	0.04	98.99
BC24150-Cpx1-31	55.12	0.23	1.20	1.53	0.06	2.92	0.09	15.93	20.57	1.56	0.02	0.03	0.04	99.28
BC24150-Cpx1-32	54.70	0.14	0.30	2.50	0.05	2.27	0.07	15.66	21.62	1.60	-	0.02	0.02	98.94

Continued on next page...

Table F.9 – continued

Sample	SiO_2	TiO_2	Al_2O_3	Cr_2O_3	V_2O_3	FeO tot	MnO	MgO	CaO	Na_2O	K_2O	P_2O_5	NiO	Total
BC24150-Cpx1-33	54.93	0.14	0.44	1.50	0.05	2.33	0.09	16.24	22.37	1.06	-	0.01	0.02	99.19
BC24150-Cpx2-1	54.50	0.19	1.08	1.62	0.05	2.89	0.09	15.91	20.83	1.52	0.01	0.02	0.02	98.72
BC24150-Cpx2-2	54.79	0.13	0.36	2.16	0.04	2.19	0.07	15.88	21.84	1.40	-	0.01	0.01	98.88
BC24150-Cpx2-3	54.73	0.26	1.40	1.76	0.06	3.10	0.09	15.54	20.00	1.72	0.01	0.04	0.03	98.72
BC24150-Cpx2-4	55.12	0.24	5.68	0.60	0.05	4.72	0.10	13.57	14.73	3.97	0.01	0.02	0.03	98.85
BC24150-Cpx2-5	55.37	0.18	2.52	1.33	0.05	3.46	0.12	16.51	17.16	2.05	0.03	0.02	0.03	98.83
BC24150-Cpx2-6	55.02	0.24	2.78	1.70	0.05	3.04	0.10	16.02	17.46	2.47	0.03	0.03	0.03	98.96
BC24150-Cpx2-7	54.80	0.29	2.99	1.56	0.06	3.46	0.13	15.45	17.54	2.41	0.02	0.03	0.02	98.75
BC24150-Cpx2-8	54.70	0.24	1.36	1.63	0.06	3.08	0.09	15.69	20.14	1.64	0.01	0.01	0.02	98.68
BC24150-Cpx2-9	54.55	0.27	2.02	1.48	0.07	3.23	0.12	15.74	19.18	1.92	0.02	0.02	0.02	98.65
BC24150-Cpx2-12	54.81	0.14	0.57	1.35	0.07	3.07	0.07	15.69	21.67	1.26	-	0.01	0.01	98.73
BC24150-Cpx2-13	54.76	0.09	2.16	0.75	0.05	2.07	0.08	15.83	21.71	1.34	-	0.04	0.03	98.91
BC24150-Cpx2-14	54.70	0.25	2.80	1.56	0.05	3.31	0.11	15.57	18.08	2.48	0.02	0.03	0.03	99.00
BC24150-Cpx2-15	54.77	0.18	1.89	0.92	0.04	3.54	0.12	17.20	18.60	1.76	0.03	0.01	0.04	99.10
BC24150-Cpx2-16	54.78	0.12	0.31	2.12	0.05	2.33	0.07	15.74	21.92	1.80	-	0.03	0.03	99.29
BC24150-Cpx2-17	54.70	0.22	1.06	1.64	0.06	3.07	0.10	15.59	20.89	1.78	0.01	0.02	0.01	99.14
BC24150-Cpx2-18	54.74	0.14	0.68	1.70	0.04	2.06	0.06	15.90	22.15	1.36	-	0.02	0.01	98.85
BC24150-Cpx2-19	54.71	0.16	0.58	1.52	0.06	3.10	0.07	15.69	21.68	1.31	-	0.03	-	98.90
BC24150-Cpx2-20	54.98	0.11	0.34	2.23	0.05	2.31	0.07	15.59	21.62	1.46	-	0.03	-	98.79
BC24150-Cpx2-21	55.06	0.12	0.29	2.07	0.05	2.39	0.07	15.76	21.85	1.49	-	0.02	0.03	99.20
BC24150-Cpx2-22	54.93	0.22	1.21	1.40	0.07	3.06	0.09	15.86	20.69	1.62	0.02	0.03	0.01	99.20
BC24150-Cpx2-23	54.91	0.24	2.55	1.61	0.06	3.33	0.11	15.84	18.09	2.46	0.03	0.01	0.04	99.26
BC24150-Cpx2-24	54.71	0.12	0.33	1.67	0.05	2.40	0.08	15.82	22.45	1.42	-	0.02	0.02	99.10
BC24150-Cpx2-25	54.90	0.27	2.93	1.49	0.05	3.22	0.10	15.44	18.02	2.53	0.02	0.02	0.03	99.03
BC24150-Cpx2-26	54.52	0.22	1.22	1.16	0.07	3.17	0.10	15.95	20.82	1.61	0.01	0.01	0.01	98.88
BC24150-Cpx2-27	54.81	0.21	1.08	1.14	0.06	3.21	0.08	15.81	21.14	1.53	0.01	0.04	0.02	99.14
BC24150-Cpx2-28	54.86	0.17	0.54	2.09	0.06	2.38	0.07	15.67	21.68	1.51	0.01	0.02	0.01	99.08
BC24150-Cpx2-29	54.67	0.11	2.30	0.94	0.04	2.03	0.08	15.75	21.70	1.39	-	0.02	0.02	99.05
BC24150-Cpx2-30	54.94	0.23	1.38	0.91	0.06	3.40	0.10	15.84	20.48	1.54	0.02	0.01	0.01	98.93
BC24150-Cpx2-31	54.83	0.25	1.84	3.09	0.06	2.58	0.11	15.19	18.82	2.48	0.01	0.02	0.03	99.32
BC24150-Cpx2-32	54.96	0.12	0.62	1.42	0.04	1.93	0.06	16.27	22.62	1.22	-	0.02	0.03	99.31

Continued on next page...

Table F.9 – continued

Sample	SiO_2	TiO_2	Al_2O_3	Cr_2O_3	V_2O_3	FeO tot	MnO	MgO	CaO	Na_2O	K_2O	P_2O_5	NiO	Total
BC24150-Cpx3-1	55.04	0.27	2.97	1.46	0.05	3.35	0.10	15.43	18.07	2.70	0.02	0.03	0.02	99.50
BC24150-Cpx3-2	54.89	0.21	1.21	1.43	0.07	3.24	0.09	15.56	20.62	1.66	0.01	0.02	-	99.01
BC24150-Cpx3-3	55.08	0.24	1.44	1.65	0.06	3.07	0.09	15.58	20.06	1.60	0.02	0.01	-	98.90
BC24150-Cpx3-4	55.32	0.01	1.36	0.94	0.03	2.45	0.10	17.59	20.10	0.86	0.07	0.03	0.06	98.90
BC24150-Cpx3-5	54.65	0.16	3.20	1.85	0.07	1.60	0.06	14.77	20.44	2.04	-	-	0.01	98.86
BC24150-Cpx3-6	54.89	0.24	1.98	2.00	0.05	2.74	0.10	15.97	18.93	1.96	0.03	0.01	0.03	98.92
BC24150-Cpx3-7	54.88	0.28	1.76	1.71	0.06	3.26	0.10	15.44	19.33	1.94	0.02	0.02	0.02	98.83
BC24150-Cpx3-8	55.23	0.32	4.94	0.96	0.06	4.55	0.12	14.06	14.86	3.79	0.01	0.01	0.01	98.93
BC24150-Cpx3-9	54.93	0.22	1.21	1.32	0.07	3.38	0.09	15.52	20.51	1.48	0.01	0.02	0.01	98.77
BC24150-Cpx3-10	55.58	0.26	5.57	0.89	0.06	4.55	0.12	14.10	14.03	4.03	0.01	0.02	-	99.23
BC24150-Cpx3-11	55.46	0.23	4.96	0.85	0.04	4.62	0.12	14.82	14.20	3.61	0.01	0.03	0.04	98.98
BC24150-Cpx3-12	55.18	0.25	2.77	1.68	0.05	3.27	0.11	15.60	17.64	2.44	0.02	0.01	0.03	99.04
BC24150-Cpx3-13	55.23	0.13	1.57	1.59	0.03	3.07	0.13	17.82	17.78	1.52	0.04	-	0.06	98.98
BC24150-Cpx3-14	54.80	0.22	2.00	2.44	0.06	2.53	0.10	15.59	18.99	2.32	0.01	0.01	0.03	99.09
BC24150-Cpx3-15	55.01	0.15	0.33	2.55	0.05	2.22	0.06	15.46	21.34	1.56	-	0.02	0.02	98.79
BC24150-Cpx3-16	54.93	0.26	1.45	1.64	0.06	3.08	0.10	15.62	19.98	1.69	0.02	0.02	0.03	98.87
BC24150-Cpx3-17	54.87	0.14	0.52	1.93	0.06	2.31	0.08	15.87	21.73	1.22	-	0.03	0.02	98.78
BC24150-Cpx3-18	55.10	0.22	1.21	1.21	0.06	3.12	0.09	15.95	20.58	1.57	0.02	0.02	-	99.15
BC24150-Cpx3-19	55.13	0.22	4.13	0.90	0.05	4.42	0.14	15.20	15.32	3.14	0.01	0.02	0.01	98.69
BC24150-Cpx3-20	55.06	0.20	1.93	2.83	0.05	2.26	0.08	14.66	19.53	2.31	-	0.02	0.03	98.95
BC24150-Cpx3-21	55.05	0.19	0.82	1.77	0.05	2.83	0.08	15.63	21.15	1.52	0.01	0.01	0.02	99.13
BC24150-Cpx3-22	55.09	0.23	1.32	1.39	0.07	3.40	0.09	15.50	20.49	1.80	0.01	0.02	0.02	99.42
BC24150-Cpx3-23	55.32	0.18	2.57	1.41	0.04	3.50	0.12	16.52	17.03	2.31	0.03	0.01	0.05	99.10
BC24150-Cpx3-24	55.27	0.20	2.57	1.36	0.05	3.46	0.12	16.42	17.12	2.25	0.03	0.02	0.06	98.93
BC24150-Cpx3-25	54.81	0.25	1.46	1.55	0.06	3.18	0.10	15.48	20.20	1.75	0.02	0.03	0.01	98.88
BC24150-Cpx3-26	55.03	0.25	1.43	1.43	0.07	3.24	0.09	15.70	20.15	1.60	0.02	0.01	-	99.02
BC24150-Cpx3-27	55.35	0.20	2.62	1.39	0.04	3.50	0.12	16.45	16.80	2.21	0.03	0.02	0.03	98.78
BC24150-Cpx3-28	54.86	0.23	1.20	1.40	0.06	3.24	0.09	15.64	20.52	1.56	0.02	0.02	0.02	98.83
BC24150-Cpx3-29	54.96	0.23	1.22	1.32	0.05	3.18	0.09	15.66	20.67	1.50	0.02	0.01	0.02	98.93
BC24150-Cpx3-30	54.93	0.23	1.28	1.44	0.06	3.10	0.09	15.69	20.45	1.79	0.02	0.02	0.01	99.10
BC24150-Cpx3-31	54.86	0.14	0.69	1.85	0.05	2.06	0.06	15.80	21.85	1.48	-	0.02	0.03	98.88

Continued on next page...

Table F.9 – continued

Sample	SiO_2	TiO_2	Al_2O_3	Cr_2O_3	V_2O_3	FeO tot	MnO	MgO	CaO	Na_2O	K_2O	P_2O_5	NiO	Total
BC24150-Cpx3-32	54.87	0.27	1.98	2.02	0.05	2.79	0.11	15.89	18.72	2.10	0.03	0.02	0.03	98.87
BC24150-Cpx3-33	55.09	0.12	0.24	2.38	0.05	2.10	0.07	15.64	21.84	1.56	-	-	0.03	99.11
BC24150-Cpx3-34	54.98	0.26	2.86	1.50	0.06	3.26	0.10	15.48	17.93	2.42	0.03	0.01	0.02	98.90
average	54.65	0.19	1.43	1.59	0.06	2.89	0.09	15.91	20.23	1.81	0.02	0.02	0.03	98.91
min	53.74	0.01	0.20	0.60	0.03	1.60	0.06	13.57	13.69	0.86	0.00	0.01	-	98.53
max	55.58	0.32	5.68	3.09	0.12	4.72	0.14	17.85	22.74	4.03	0.07	0.04	0.06	99.50
2σ	0.77	0.12	2.28	0.78	0.02	1.26	0.04	1.08	4.15	1.16	0.02	0.02	0.02	0.42
n	157													

Table F.10: Major element compositions of Victor orthopyroxene xenocrysts

Sample	SiO_2	TiO_2	Al_2O_3	Cr_2O_3	V_2O_3	FeO tot	MnO	MgO	CaO	Na_2O	K_2O	P_2O_5	NiO	Total	Mg#
o1-4	57.20	0.09	0.68	0.24	0.01	6.09	0.14	34.48	0.62	0.21	-	0.02	0.09	99.87	90.98
o1-5	58.03	0.09	0.69	0.24	-	6.18	0.16	34.40	0.60	0.23	-	0.01	0.09	100.70	90.85
o1-6	58.44	0.12	0.57	0.35	-	4.72	0.12	35.77	0.48	0.15	-	0.01	0.11	100.83	93.11
o1-7	57.92	0.07	0.63	0.27	0.01	5.59	0.12	34.94	0.60	0.15	-	0.02	0.09	100.41	91.76
o1-8	57.79	0.09	0.68	0.22	-	6.13	0.14	34.65	0.62	0.21	-	-	0.10	100.61	90.98
o1-9	57.31	0.10	0.70	0.23	-	6.20	0.15	34.27	0.60	0.22	-	-	0.10	99.87	90.79
o1-10	56.13	0.07	0.88	0.28	0.01	5.59	0.14	35.10	0.60	0.16	0.01	-	0.09	99.02	91.80
o1-15	56.50	0.08	0.64	0.25	0.01	5.53	0.13	34.90	0.57	0.14	-	0.01	0.09	98.85	91.84
o1-16	58.05	0.09	0.69	0.24	-	6.06	0.14	34.42	0.62	0.22	-	0.01	0.10	100.62	91.02
o1-17	58.97	0.09	0.86	0.24	0.02	6.03	0.13	32.99	0.62	0.20	0.01	-	0.11	100.24	90.70
o1-18	57.67	0.08	0.68	0.22	0.01	6.09	0.15	34.54	0.61	0.20	-	0.01	0.10	100.34	91.01
o1-19	56.97	0.09	0.66	0.22	-	6.09	0.14	34.55	0.62	0.20	-	-	0.11	99.66	91.00
o1-21	57.15	0.09	0.68	0.22	-	6.18	0.12	34.49	0.64	0.19	-	0.01	0.09	99.86	90.87
o1-22	57.48	0.09	0.69	0.23	0.01	6.04	0.14	34.40	0.62	0.22	-	0.01	0.10	100.03	91.03
opx1-2	57.18	0.10	0.69	0.22	-	6.13	0.12	34.51	0.61	0.21	0.01	-	0.09	99.87	90.94
opx1-3	56.77	0.09	0.68	0.21	0.01	6.19	0.14	34.24	0.63	0.21	-	0.01	0.10	99.28	90.79
opx1-4	56.24	0.08	0.67	0.22	0.01	6.13	0.14	34.31	0.63	0.23	-	0.02	0.11	98.78	90.89
opx1-5	56.31	0.10	0.68	0.23	0.01	6.22	0.14	34.22	0.58	0.23	-	-	0.10	98.80	90.75
opx1-6	56.88	0.10	0.55	0.34	-	4.78	0.11	35.58	0.45	0.12	-	0.02	0.10	99.02	92.99
opx1-7	56.67	0.07	0.62	0.25	0.01	5.60	0.13	34.95	0.58	0.16	-	-	0.09	99.12	91.76
opx1-9	56.09	0.10	0.67	0.23	0.01	6.21	0.15	34.25	0.59	0.21	0.01	-	0.10	98.62	90.77
opx1-10	56.59	0.07	0.62	0.27	-	5.56	0.13	34.72	0.57	0.15	0.01	0.01	0.08	98.77	91.76
opx1-12	56.71	0.08	0.70	0.28	0.01	6.07	0.13	34.33	0.58	0.21	-	0.02	0.11	99.21	90.98
opx1-13	56.35	0.10	0.69	0.26	-	6.28	0.15	34.49	0.60	0.20	-	0.01	0.10	99.23	90.73
opx1-14	55.97	0.10	0.67	0.23	-	6.18	0.14	34.32	0.62	0.20	0.01	0.02	0.10	98.56	90.83
opx1-15	56.32	0.07	0.64	0.26	0.01	5.58	0.12	34.88	0.58	0.14	-	-	0.09	98.68	91.76
opx1-16	56.67	0.09	0.68	0.23	0.01	6.10	0.14	34.78	0.60	0.21	-	0.02	0.10	99.62	91.05
opx1-17	56.24	0.10	0.69	0.21	0.01	6.08	0.15	34.68	0.62	0.21	-	-	0.10	99.06	91.05
opx1-18	56.04	0.09	0.66	0.21	0.02	6.17	0.15	34.63	0.61	0.20	-	0.02	0.10	98.91	90.91
opx1-19	55.94	0.09	0.67	0.22	0.03	6.15	0.14	34.53	0.61	0.21	0.01	0.01	0.10	98.69	90.92

Continued on next page. . .

Table F.10 – continued

Sample	SiO_2	TiO_2	Al_2O_3	Cr_2O_3	V_2O_3	FeO tot	MnO	MgO	CaO	Na_2O	K_2O	P_2O_5	NiO	Total	Mg#
opx1-20	56.98	0.08	0.65	0.26	-	5.63	0.14	34.92	0.59	0.17	-	-	0.10	99.52	91.71
opx1-21	56.48	0.09	0.68	0.21	0.01	6.22	0.15	34.41	0.62	0.22	-	-	0.10	99.17	90.80
opx2-1	57.28	0.08	0.68	0.22	0.01	6.18	0.15	34.77	0.60	0.22	0.01	-	0.09	100.27	90.93
opx2-7	56.12	0.10	0.65	0.23	0.01	6.18	0.15	34.56	0.62	0.20	0.01	-	0.09	98.91	90.88
opx2-8	57.46	0.09	0.69	0.22	0.02	6.09	0.14	34.72	0.60	0.22	-	-	0.09	100.34	91.05
opx2-9	57.33	0.10	0.68	0.22	0.01	6.09	0.15	34.98	0.60	0.22	-	0.01	0.10	100.48	91.10
opx2-10	57.63	0.08	0.66	0.22	0.01	5.99	0.14	34.76	0.62	0.23	0.01	-	0.11	100.45	91.18
opx2-11	57.77	0.08	0.68	0.22	0.01	5.96	0.15	34.88	0.62	0.23	-	0.01	0.11	100.70	91.25
opx2-12	57.21	0.11	0.69	0.21	-	6.13	0.13	34.74	0.59	0.22	0.01	0.02	0.09	100.13	91.00
opx2-13	57.27	0.10	0.69	0.21	0.01	6.15	0.14	34.89	0.60	0.22	-	-	0.09	100.35	91.01
opx2-14	57.15	0.09	0.67	0.22	-	6.05	0.14	34.67	0.61	0.21	0.01	0.01	0.10	99.89	91.09
opx2-16	56.34	0.11	0.68	0.21	0.01	6.16	0.15	34.43	0.57	0.20	-	0.01	0.08	98.95	90.88
opx2-17	57.07	0.08	0.70	0.23	0.01	6.19	0.14	34.60	0.61	0.23	-	0.01	0.10	99.95	90.88
opx2-18	57.40	0.09	0.67	0.22	0.01	6.15	0.14	34.46	0.61	0.20	-	0.01	0.10	100.04	90.90
opx2-19	57.28	0.08	0.68	0.22	0.01	6.17	0.14	34.70	0.59	0.20	-	0.01	0.09	100.15	90.94
opx2-20	57.34	0.09	0.66	0.26	0.01	5.93	0.13	34.88	0.57	0.19	-	0.01	0.09	100.14	91.30
opx3-1	56.04	0.09	0.68	0.24	0.02	5.94	0.16	34.49	0.56	0.20	-	0.01	0.08	98.51	91.19
opx3-4	56.67	0.09	0.68	0.23	0.01	6.17	0.14	34.59	0.60	0.22	-	0.02	0.10	99.52	90.90
opx3-5	56.39	0.09	0.67	0.24	0.01	6.17	0.14	34.65	0.58	0.22	-	0.01	0.10	99.26	90.92
opx3-6	55.98	0.10	0.80	0.24	0.01	6.11	0.15	34.51	0.60	0.21	-	0.01	0.09	98.78	90.97
opx3-7	55.87	0.09	0.68	0.22	0.01	6.17	0.12	34.47	0.62	0.22	-	0.02	0.10	98.59	90.88
opx3-9	56.67	0.07	0.69	0.22	-	6.13	0.14	34.47	0.61	0.20	-	0.01	0.10	99.30	90.93
opx3-10	56.19	0.08	0.65	0.23	0.02	6.15	0.14	34.48	0.59	0.21	-	0.01	0.10	98.85	90.90
opx3-11	56.61	0.08	0.69	0.21	0.01	6.04	0.14	34.54	0.59	0.22	-	0.01	0.11	99.24	91.07
opx3-12	56.83	0.08	0.67	0.24	0.01	6.13	0.14	34.58	0.59	0.22	-	-	0.10	99.57	90.96
opx3-13	57.33	0.08	0.67	0.23	-	6.19	0.14	34.55	0.58	0.20	-	0.01	0.10	100.07	90.87
opx3-14	56.98	0.10	0.68	0.21	-	6.10	0.13	34.17	0.61	0.21	-	-	0.10	99.28	90.90
opx3-15	56.81	0.09	0.67	0.21	0.02	6.19	0.14	34.19	0.59	0.22	-	0.02	0.09	99.24	90.79
opx3-16	56.55	0.09	0.68	0.24	0.01	6.13	0.13	34.32	0.60	0.22	0.00	0.01	0.09	99.04	90.89
opx3-17	56.81	0.09	0.67	0.21	0.01	6.12	0.13	34.33	0.62	0.21	-	0.02	0.09	99.31	90.91
opx3-20	56.34	0.10	0.71	0.24	0.01	6.17	0.11	34.13	0.60	0.24	-	-	0.09	98.75	90.79

Continued on next page...

Table F.10 – continued

Sample	SiO_2	TiO_2	Al_2O_3	Cr_2O_3	V_2O_3	FeO tot	MnO	MgO	CaO	Na_2O	K_2O	P_2O_5	NiO	Total	Mg#
opx3-21	56.38	0.09	0.65	0.23	0.01	6.00	0.13	34.29	0.63	0.24	-	0.02	0.10	98.78	91.06
opx3-22	56.75	0.09	0.69	0.27	0.01	5.97	0.14	34.21	0.58	0.21	0.00	0.01	0.09	99.01	91.08
opx4-1	56.50	0.09	0.69	0.22	0.02	6.15	0.13	34.46	0.60	0.20	-	-	0.09	99.14	90.90
opx4-2	56.84	0.07	0.69	0.23	0.01	6.05	0.14	34.34	0.62	0.27	-	0.01	0.10	99.37	91.01
opx4-3	56.59	0.10	0.69	0.22	-	6.19	0.14	34.35	0.59	0.20	-	-	0.10	99.16	90.83
opx4-4	57.04	0.09	0.69	0.21	0.01	6.19	0.14	34.57	0.62	0.22	-	-	0.10	99.87	90.87
opx4-5	56.50	0.09	0.72	0.23	0.01	6.09	0.13	34.50	0.61	0.24	-	0.01	0.10	99.22	90.99
opx4-6	56.31	0.09	0.69	0.24	0.02	6.29	0.14	34.52	0.58	0.21	-	0.01	0.08	99.18	90.73
opx4-7	56.13	0.09	0.68	0.21	-	6.21	0.14	34.68	0.60	0.19	-	0.01	0.09	99.04	90.87
opx4-8	56.56	0.09	0.71	0.23	0.01	6.14	0.13	34.51	0.59	0.23	-	0.01	0.10	99.31	90.93
opx4-9	56.89	0.10	0.70	0.23	-	6.26	0.13	34.71	0.60	0.22	-	0.02	0.10	99.95	90.82
opx4-10	56.51	0.10	0.68	0.22	0.02	6.27	0.14	34.63	0.62	0.20	-	0.01	0.09	99.48	90.78
opx4-11	56.95	0.10	0.69	0.25	0.01	6.24	0.13	34.75	0.55	0.21	0.01	0.01	0.10	99.98	90.85
opx4-12	57.06	0.10	0.69	0.26	0.01	6.27	0.14	34.75	0.56	0.20	-	-	0.09	100.12	90.82
opx4-13	56.64	0.09	0.70	0.25	0.01	6.19	0.13	34.74	0.56	0.20	-	0.01	0.10	99.61	90.92
opx4-14	56.90	0.08	0.67	0.21	0.02	6.02	0.13	34.62	0.65	0.24	-	-	0.10	99.61	91.12
opx4-15	57.53	0.09	0.69	0.22	-	6.12	0.15	34.65	0.60	0.22	-	0.01	0.09	100.35	90.99
opx4-16	57.04	0.10	0.68	0.26	0.01	5.88	0.15	34.96	0.56	0.19	-	0.01	0.09	99.92	91.39
opx4-17	57.05	0.09	0.70	0.28	0.01	6.08	0.14	34.68	0.56	0.19	-	-	0.10	99.87	91.05
opx4-18	57.44	0.08	0.69	0.23	-	6.08	0.14	34.71	0.61	0.23	-	-	0.10	100.31	91.05
opx4-19	57.08	0.10	0.70	0.21	0.01	6.31	0.15	34.60	0.59	0.23	-	-	0.09	100.07	90.72
opx4-20	56.96	0.09	0.68	0.22	0.01	6.20	0.14	34.43	0.60	0.20	-	0.01	0.10	99.61	90.83
opx4-21	56.92	0.09	0.67	0.21	0.01	6.21	0.15	34.33	0.61	0.18	0.00	-	0.09	99.47	90.79
opx4-22	57.35	0.12	0.56	0.32	-	4.92	0.14	35.47	0.45	0.18	-	0.01	0.11	99.62	92.78
opx4-23	56.50	0.09	0.67	0.22	0.01	6.22	0.14	34.44	0.62	0.20	-	0.01	0.09	99.20	90.80
opx5-1	56.81	0.08	0.66	0.20	-	6.20	0.14	34.74	0.60	0.20	-	0.01	0.10	99.75	90.91
opx5-2	56.60	0.09	0.71	0.23	0.01	6.09	0.15	34.77	0.61	0.25	-	0.02	0.10	99.61	91.05
opx5-3	56.51	0.09	0.67	0.22	-	6.25	0.14	34.77	0.59	0.20	-	0.01	0.08	99.51	90.85
opx5-4	56.52	0.09	0.69	0.22	0.01	6.19	0.15	34.75	0.61	0.22	-	-	0.09	99.52	90.91
opx5-5	56.94	0.09	0.68	0.21	-	6.09	0.14	34.82	0.62	0.23	-	0.01	0.10	99.92	91.06
opx5-6	56.50	0.10	0.66	0.28	0.01	5.80	0.14	35.17	0.56	0.20	-	0.01	0.09	99.51	91.54

Continued on next page...

Table F.10 – continued

Sample	SiO_2	TiO_2	Al_2O_3	Cr_2O_3	V_2O_3	FeO tot	MnO	MgO	CaO	Na_2O	K_2O	P_2O_5	NiO	Total	Mg#
opx5-7	56.07	0.09	0.66	0.20	0.01	6.27	0.14	34.63	0.61	0.20	-	0.01	0.10	98.99	90.79
opx5-8	56.63	0.07	0.71	0.23	0.01	6.12	0.13	34.63	0.59	0.24	-	0.02	0.10	99.48	90.98
opx5-9	56.87	0.10	0.66	0.22	-	6.21	0.14	34.76	0.60	0.22	-	-	0.10	99.89	90.89
opx5-10	56.48	0.10	0.70	0.21	-	6.28	0.16	34.50	0.56	0.19	-	0.01	0.09	99.29	90.73
opx5-11	55.98	0.09	0.70	0.23	0.01	6.21	0.14	34.42	0.57	0.23	-	0.04	0.09	98.69	90.81
opx5-12	56.73	0.09	0.67	0.21	0.02	6.17	0.15	34.45	0.62	0.20	-	-	0.08	99.37	90.87
opx5-14	56.39	0.09	0.71	0.22	-	6.19	0.15	34.41	0.61	0.22	-	-	0.10	99.08	90.83
opx5-16	56.74	0.09	0.71	0.23	-	6.15	0.14	34.47	0.61	0.21	0.01	0.02	0.07	99.44	90.90
opx5-17	55.88	0.09	0.67	0.23	0.03	6.04	0.14	34.62	0.61	0.21	-	-	0.09	98.60	91.09
opx5-20	56.32	0.09	0.69	0.22	0.01	6.12	0.15	34.43	0.60	0.24	-	0.02	0.09	98.96	90.94
average	56.81	0.09	0.68	0.23	0.01	6.06	0.14	34.59	0.60	0.21	0.01	0.01	0.10	99.52	91.05
min	55.87	0.07	0.55	0.20	-	4.72	0.11	32.99	0.45	0.12	-	0.01	0.07	98.51	90.70
max	58.97	0.12	0.88	0.35	0.03	6.31	0.16	35.77	0.65	0.27	0.01	0.04	0.11	100.83	93.11
2σ	1.15	0.02	0.08	0.05	0.01	0.55	0.02	0.64	0.06	0.05	-	0.01	0.01	1.17	0.84
n	102														

Appendix G

Major element data for Delta xenoliths

All major element data in weight %. "-" indicates not measured or below detection.
2σ is the standard deviation of the mean of 'n' analytical spots per xenolith.
FeO tot as ferrous iron.

Table G.1: Garnet major element compositions of Delta xenoliths

Sample	DEL1-02	DEL1-03	DEL1-05	DEL1-09	DEL1-14	DEL1-18	DEL1-15	DEL1-07	DEL1-04	DEL1-12	DEL1-17
Garnet class	G10	G10	G9	G9	G9	G9	G9	G12	G5	G4	G4
	harzburgite	harzburgite	lherzolite	lherzolite	lherzolite	lherzolite	lherzolite	wehrlite	pyroxenite	pyroxenite	pyroxenite
n	14	22	26	30	18	8	23	24	36	45	38
P_2O_5	0.04	0.05	0.02	0.01	0.04	0.01	0.02	0.01	0.02	0.02	0.01
2σ	0.02	0.02	0.02	0.02	0.02	0.02	0.02	0.02	0.02	0.02	0.02
SiO_2	42.38	42.26	42.55	41.92	41.87	41.27	41.75	41.50	41.13	41.92	41.84
2σ	0.27	0.27	0.36	0.29	0.17	0.28	0.44	0.47	0.48	0.33	0.33
TiO_2	0.01	0.00	0.22	0.05	0.15	0.02	0.00	0.03	0.04	0.04	0.05
2σ	0.02	0.01	0.03	0.03	0.02	0.02	0.01	0.02	0.02	0.03	0.03
Al_2O_3	21.97	22.41	22.93	22.97	20.48	20.95	21.42	22.50	21.40	23.46	23.40
2σ	0.67	0.72	0.30	0.37	0.33	0.54	0.62	0.31	0.59	0.29	0.27
Cr_2O_3	3.41	3.04	1.81	1.51	4.77	4.74	3.98	2.12	3.05	0.78	0.97
2σ	0.77	0.82	0.10	0.43	0.38	0.71	0.80	0.31	0.66	0.04	0.12
V_2O_3	0.01	0.01	0.02	0.01	0.04	0.03	0.02	0.01	0.03	0.02	0.02
2σ	0.01	0.01	0.01	0.01	0.02	0.02	0.01	0.01	0.02	0.01	0.02
FeO	7.87	8.34	7.27	10.78	8.04	8.70	8.14	8.52	13.76	11.33	12.19
2σ	0.09	0.08	0.09	0.36	0.08	0.19	0.08	0.25	0.14	0.23	0.13
MnO	0.59	0.58	0.38	0.62	0.41	0.93	0.56	0.48	0.72	0.40	0.50
2σ	0.03	0.03	0.02	0.06	0.02	0.19	0.03	0.03	0.03	0.03	0.03
NiO	0.00	0.00	0.00	0.00	0.01	0.00	0.00	0.00	0.00	0.00	0.00
2σ	0.01	0.01	0.01	0.01	0.01	0.01	0.01	0.01	0.01	0.01	0.01
MgO	21.40	21.31	21.23	18.56	19.50	18.39	19.65	16.53	15.43	18.48	17.44
2σ	0.44	0.37	0.36	0.38	0.32	0.21	0.44	0.21	0.25	0.26	0.23
CaO	3.45	2.85	4.27	4.76	5.32	6.22	5.17	9.02	5.88	4.68	5.06
2σ	0.53	0.44	0.07	0.16	0.14	0.32	0.44	0.20	0.12	0.11	0.16
Na_2O	0.04	0.04	0.06	0.03	0.04	0.03	0.03	0.02	0.03	0.03	0.02
2σ	0.01	0.02	0.02	0.01	0.02	0.01	0.04	0.01	0.02	0.02	0.02
Total	101.17	100.90	100.76	101.22	100.67	101.29	100.75	100.75	101.50	101.15	101.50
2σ	0.38	0.34	1.03	0.44	0.38	0.51	0.48	0.66	0.78	0.80	0.43

Table G.2: Clinopyroxene major element compositions of Delta xenoliths

Sample	DEL-01	DEL1-04	DEL1-05	DEL1-06	DEL1-09	DEL1-11	DEL1-12	DEL1-15	DEL1-17	DEL1-18
Description	metasomatic	pyroxenite	lherzolite	metasomatic	lherzolite	metasomatic	pyroxenite	lherzolite	pyroxenite	lherzolite
n	6	61	51	2	41	19	36	3	41	4
Na_2O	2.38	0.97	2.18	4.02	1.44	2.76	0.88	1.55	0.51	1.25
2σ	0.29	0.06	0.42	0.24	0.32	0.10	0.07	1.12	0.02	0.06
MgO	14.84	16.32	16.16	13.90	15.89	15.24	16.70	16.36	17.06	16.25
2σ	0.28	0.16	0.57	0.83	0.38	0.17	0.20	1.76	0.12	0.17
Al_2O_3	0.72	1.17	2.67	2.89	2.29	1.78	1.35	1.09	0.85	1.62
2σ	0.22	0.09	0.51	0.07	0.58	0.11	0.12	2.53	0.08	0.14
SiO_2	54.47	54.71	55.18	54.81	54.51	54.87	54.71	55.11	54.93	54.21
2σ	0.40	0.55	0.22	1.65	0.32	0.12	0.36	0.45	0.57	0.69
P_2O_5	0.02	0.02	0.02	0.06	0.02	0.02	0.02	0.02	0.02	0.01
2σ	0.02	0.02	0.02	0.09	0.02	0.01	0.02	0.01	0.02	0.01
CaO	20.18	22.26	19.51	16.75	21.69	18.15	22.40	21.18	23.28	22.30
2σ	0.56	0.23	0.85	0.18	0.65	0.18	0.23	0.92	0.20	0.54
TiO_2	0.13	0.06	0.21	0.14	0.14	0.30	0.08	0.15	0.05	0.02
2σ	0.01	0.02	0.03	0.06	0.07	0.01	0.02	0.38	0.02	0.01
V_2O_3	0.04	0.05	0.05	0.09	0.05	0.04	0.03	0.06	0.03	0.04
2σ	0.02	0.03	0.02	0.07	0.03	0.01	0.02	0.03	0.02	0.01
Cr_2O_3	3.32	0.84	1.00	3.85	1.09	3.56	0.29	1.41	0.23	1.34
2σ	0.26	0.11	0.21	0.61	0.11	0.33	0.03	1.38	0.03	0.05
MnO	0.09	0.09	0.08	0.11	0.07	0.12	0.05	0.09	0.06	0.11
2σ	0.01	0.02	0.02	0.01	0.02	0.01	0.02	0.06	0.02	0.03
FeO	2.39	2.84	2.29	2.91	1.71	2.59	2.26	2.54	2.12	1.42
2σ	0.14	0.09	0.12	0.06	0.13	0.05	0.09	1.40	0.11	0.18
NiO	0.03	0.04	0.04	0.03	0.03	0.05	0.06	0.03	0.05	0.04
2σ	0.01	0.02	0.01	0.00	0.01	0.01	0.01	0.00	0.01	0.01
Total	98.60	99.36	99.41	99.58	98.93	99.49	98.82	99.58	99.18	98.58
2σ	0.61	0.70	0.38	0.80	0.34	0.20	0.41	0.71	0.79	1.35

Table G.3: Olivine major element compositions of Delta xenoliths-1

Sample	DEL1-02	DEL1-03	DEL1-07	DEL1-04	DEL1-09	DEL1-14	DEL1-15	DEL1-18
	harzburgite	harzburgite	wehrlite	pyroxenite	lherzolite	lherzolite	lherzolite	lherzolite
n	40	38	36	17	11	51	40	33
P_2O_5	0.01	0.01	0.00	0.01	0.00	0.01	0.00	0.00
2σ	0.02	0.02	0.01	0.02	0.01	0.01	0.01	0.01
SiO_2	41.18	40.85	40.77	40.03	40.63	40.77	40.89	40.21
2σ	0.86	0.22	0.48	0.27	0.34	0.23	0.56	0.59
TiO_2	0.00	0.00	0.01	0.02	0.01	0.01	0.00	0.00
2σ	0.01	0.01	0.01	0.02	0.02	0.01	0.01	0.01
Al_2O_3	0.01	0.01	0.01	0.01	0.01	0.02	0.01	0.01
2σ	0.01	0.01	0.01	0.01	0.02	0.01	0.01	0.01
Cr_2O_3	0.01	0.01	0.00	0.00	0.00	0.02	0.01	0.00
2σ	0.02	0.02	0.01	0.01	0.01	0.02	0.01	0.01
V_2O_3	0.00	0.00	0.00	0.00	0.00	0.00	0.00	0.00
2σ	0.01	0.01	0.01	0.01	0.01	0.01	0.01	0.01
FeO	7.12	7.40	7.75	14.16	9.67	8.74	7.34	8.02
2σ	0.07	0.06	0.09	0.09	0.21	0.07	0.08	0.16
MnO	0.11	0.11	0.08	0.14	0.11	0.11	0.10	0.23
2σ	0.02	0.02	0.02	0.02	0.02	0.02	0.02	0.02
NiO	0.35	0.35	0.37	0.36	0.39	0.40	0.36	0.31
2σ	0.02	0.02	0.02	0.03	0.03	0.01	0.02	0.07
MgO	51.19	50.73	50.79	46.17	49.41	49.56	50.64	49.95
2σ	0.70	0.32	0.34	0.37	0.44	0.34	0.24	0.55
CaO	0.01	0.00	0.01	0.01	0.01	0.02	0.01	0.01
2σ	0.01	0.01	0.01	0.01	0.01	0.02	0.01	0.01
Na_2O	0.02	0.02	0.01	0.01	0.01	0.02	0.02	0.01
2σ	0.01	0.01	0.01	0.01	0.01	0.01	0.01	0.01
Total	100.00	99.49	99.81	100.94	100.26	99.69	99.38	98.76
2σ	1.18	0.35	0.65	0.42	0.53	0.34	0.56	0.90
Mg#	92.77	92.44	92.12	85.32	90.11	90.99	92.48	91.74

Table G.4: Olivine major element compositions of Delta xenoliths - 2

Sample	DEL1-08	DEL1-10	DEL-01	DEL1-01	DEL1-06	DEL1-11	DEL1-13	DEL1-16
	harzburgite	harzburgite	dunite	harzburgite	harzburgite	dunite	harzburgite	dunite
n	28	131	44	45	53	46	10	38
P_2O_5	0.02	0.00	0.02	0.01	0.01	0.00	0.02	0.00
2σ	0.05	0.01	0.03	0.02	0.02	0.01	0.02	0.01
SiO_2	40.98	40.80	40.36	40.54	41.22	40.93	40.77	41.11
2σ	0.76	0.38	0.87	0.57	0.24	0.15	0.62	0.23
TiO_2	0.00	0.01	0.01	0.00	0.00	0.03	0.00	0.01
2σ	0.01	0.02	0.01	0.01	0.01	0.02	0.01	0.04
Al_2O_3	0.01	0.02	0.01	0.01	0.01	0.02	0.01	1.38
2σ	0.01	0.01	0.01	0.01	0.01	0.01	0.01	8.06
Cr_2O_3	0.01	0.03	0.01	0.00	0.01	0.02	0.01	0.09
2σ	0.01	0.02	0.02	0.01	0.02	0.02	0.02	0.48
V_2O_3	0.00	0.00	0.00	0.00	0.00	0.00	0.00	0.00
2σ	0.01	0.01	0.01	0.01	0.01	0.01	0.01	0.01
FeO	7.48	8.40	7.88	7.64	7.74	8.54	7.42	6.82
2σ	0.09	0.11	0.14	0.23	0.09	0.07	0.08	3.11
MnO	0.13	0.11	0.15	0.13	0.12	0.14	0.17	0.11
2σ	0.02	0.02	0.02	0.03	0.02	0.02	0.03	0.06
NiO	0.24	0.39	0.26	0.35	0.34	0.37	0.34	0.32
2σ	0.02	0.02	0.02	0.06	0.03	0.02	0.02	0.12
MgO	51.11	50.23	49.46	49.79	50.35	49.58	50.65	47.95
2σ	0.33	0.25	0.78	0.73	0.44	0.23	0.53	16.06
CaO	0.00	0.02	0.01	0.01	0.01	0.02	0.01	0.00
2σ	0.01	0.01	0.01	0.01	0.01	0.01	0.01	0.01
Na_2O	0.02	0.02	0.02	0.02	0.02	0.03	0.02	0.11
2σ	0.01	0.01	0.01	0.01	0.01	0.01	0.02	0.56
Total	100.01	100.04	98.20	98.51	99.84	99.69	99.43	98.72
2σ	0.85	0.42	1.58	1.33	0.51	0.27	1.02	5.34
Mg#	92.41	91.42	91.80	92.07	92.06	91.19	92.41	92.74

Table G.5: Orthopyroxene major element compositions of Delta peridotite xenoliths

Sample	DEL1-08	DEL1-10	DEL1-01	DEL1-06	DEL1-13	DEL1-02	DEL1-05	DEL1-09	DEL1-15	DEL1-18
	harzburgite	harzburgite	harzburgite	harzburgite	harzburgite	harzburgite	lherzolite	lherzolite	lherzolite	lherzolite
n	39	5	4	15	22	28	38	17	3	13
Na_2O	0.08	0.13	0.05	0.10	0.12	0.08	0.11	0.03	0.06	0.04
2σ	0.03	0.04	0.01	0.01	0.03	0.02	0.06	0.02	0.01	0.03
MgO	35.68	35.06	34.92	35.24	35.41	35.87	35.69	34.81	35.38	35.27
2σ	0.37	0.18	0.31	0.21	0.35	0.33	0.76	0.24	0.35	0.37
Al_2O_3	0.85	0.58	0.67	0.69	0.59	0.71	0.66	0.79	0.70	0.92
2σ	0.15	0.07	0.03	0.02	0.28	0.04	0.14	0.17	0.01	0.12
SiO_2	57.71	57.25	56.66	58.02	57.74	58.15	58.04	57.29	58.04	57.19
2σ	0.47	1.13	0.48	0.40	0.73	0.40	0.40	0.41	0.19	0.61
P_2O_5	-	-	-	-	-	-	-	-	-	-
2σ	0.01	0.01	0.01	0.01	0.01	0.01	0.01	0.01	-	0.01
CaO	0.15	0.50	0.20	0.22	0.20	0.19	0.37	0.18	0.22	0.21
2σ	0.05	0.01	0.04	0.06	0.08	0.04	0.17	0.10	0.01	0.32
TiO_2	-	0.02	-	0.01	0.01	0.01	0.09	0.06	-	0.01
2σ	0.01	0.02	0.01	0.01	0.01	0.01	0.02	0.03	0.01	0.01
V_2O_3	0.01	-	0.01	0.01	0.01	0.01	0.01	0.01	0.01	0.01
2σ	0.01	0.01	0.02	0.01	0.01	0.01	0.01	0.01	0.01	0.01
Cr_2O_3	0.28	0.35	0.25	0.28	0.29	0.28	0.16	0.18	0.29	0.31
2σ	0.09	0.04	0.04	0.08	0.10	0.05	0.34	0.04	0.02	0.05
MnO	0.12	0.13	0.12	0.13	0.20	0.13	0.11	0.13	0.12	0.18
2σ	0.03	0.02	0.01	0.02	0.03	0.02	0.02	0.02	0.02	0.03
FeO_{tot}	4.62	5.06	4.61	4.73	4.62	4.43	4.61	6.04	4.59	4.72
2σ	0.13	0.02	0.05	0.13	0.08	0.06	0.38	0.09	0.03	0.19
NiO	0.07	0.11	0.08	0.08	0.08	0.08	0.09	0.07	0.07	0.07
2σ	0.02	0.01	0.01	0.01	0.02	0.01	0.02	0.01	0.02	0.01
Total	99.59	99.20	97.57	99.51	99.25	99.93	99.94	99.59	99.48	98.94
2σ	0.56	1.09	0.56	0.57	1.16	0.53		0.35	0.37	0.93

Table G.6: Orthopyroxene major element compositions of Delta pyroxenite xenoliths

Sample	DEL1-04	DEL1-12	DEL1-17
	pyroxenite	pyroxenite	pyroxenite
n	14	20	5
Na_2O	0.03	0.03	0.02
2σ	0.01	0.02	0.01
MgO	33.08	34.50	34.18
2σ	0.30	0.33	0.15
Al_2O_3	0.58	0.57	0.54
2σ	0.05	0.05	0.03
SiO_2	57.06	57.55	57.51
2σ	0.65	0.39	0.39
P_2O_5	-	-	-
2σ	0.01	0.01	0.01
CaO	0.23	0.21	0.19
2σ	0.05	0.03	0.01
TiO_2	0.05	0.05	0.05
2σ	0.02	0.02	0.03
V_2O_3	0.01	0.01	0.01
2σ	0.01	0.02	0.01
Cr_2O_3	0.18	0.06	0.06
2σ	0.04	0.03	0.04
MnO	0.17	0.09	0.12
2σ	0.03	0.02	0.01
FeO_{tot}	8.66	6.76	7.24
2σ	0.07	0.10	0.06
NiO	0.08	0.11	0.09
2σ	0.02	0.01	0.01
Total	100.13	99.94	100.01
2σ	0.66	0.54	0.35

Appendix H

Trace element data for Victor xenocrysts

Data are given in ppm. ”-” indicates below detection.
1σ errors given as the average of the in-run precision for ”n” analyses.

Table H.1: Trace element compositions of Victor G9 xenocrysts - 1

Element	grt1-6	1σ	grt1-11	1σ	grt1-30	1σ	grt1-32	1σ	grt1-35	1σ	grt1-36	1σ	grt2-15	1σ
Li7	0.19	0.07	0.19	0.08	-	0.09	-	0.08	0.06	0.05	0.19	0.11	0.32	0.08
Sc45	90.48	3.70	103.31	4.28	104.35	4.31	105.13	4.33	89.04	3.68	100.22	4.17	94.79	3.97
Ti48	237.63	7.72	105.99	3.48	186.30	6.09	53.46	1.77	254.04	8.30	50.60	1.69	252.24	8.29
V51	194.72	9.09	210.19	9.87	192.18	9.06	201.05	9.52	215.20	10.25	155.80	7.51	208.67	10.11
Ni60	32.57	2.69	25.27	2.21	26.65	2.32	28.65	2.48	34.94	2.98	24.21	2.17	29.15	2.60
Co59	28.67	1.99	28.54	2.02	28.02	1.99	26.95	1.93	30.15	2.17	26.64	1.96	24.59	1.83
Zn64	10.53	1.18	17.34	1.95	9.36	1.12	8.28	1.00	10.29	1.22	9.24	1.14	23.30	2.77
Ga69	6.38	0.48	5.30	0.42	6.52	0.51	5.59	0.44	7.34	0.57	4.17	0.35	5.74	0.46
Rb85	0.19	0.03	0.21	0.03	0.07	0.02	-	0.02	0.06	0.02	0.11	0.02	0.15	0.03
Sr88	1.08	0.11	1.34	0.14	0.55	0.08	0.09	0.03	0.30	0.05	0.51	0.07	2.07	0.19
Y89	13.94	1.05	4.59	0.42	13.95	1.09	4.40	0.39	13.91	1.09	4.35	0.40	6.34	0.55
Zr90	36.24	2.19	12.57	0.96	43.38	2.66	1.49	0.24	37.67	2.31	12.68	0.94	31.98	2.06
Nb93	0.21	0.06	0.35	0.08	0.25	0.10	0.47	0.09	0.35	0.07	0.38	0.08	0.20	0.07
Cs133	0.02	0.01	0.05	0.01	0.01	0.01	-	-	0.01	0.01	0.04	0.01	0.06	0.01
Ba138	2.13	0.19	3.41	0.31	1.36	0.14	-	0.02	0.36	0.05	0.55	0.07	5.64	0.52
La139	0.75	0.09	1.23	0.13	0.26	0.05	0.03	0.02	0.13	0.03	0.19	0.04	0.76	0.09
Ce140	1.88	0.14	2.86	0.21	0.56	0.06	0.18	0.03	0.26	0.03	0.79	0.07	2.84	0.21
Pr141	0.16	0.02	0.18	0.03	0.20	0.03	0.04	0.02	0.06	0.02	0.19	0.03	0.21	0.03
Nd142	0.76	0.10	1.50	0.16	1.35	0.15	0.22	0.06	0.48	0.07	0.97	0.12	1.89	0.18
Sm152	0.60	0.11	0.47	0.12	1.31	0.18	0.18	0.06	0.60	0.10	0.25	0.08	0.94	0.14
Eu153	0.28	0.05	0.16	0.05	0.57	0.08	0.07	0.03	0.25	0.04	0.12	0.03	0.35	0.06
Gd158	1.33	0.21	0.82	0.20	2.20	0.31	-	0.11	1.08	0.19	0.34	0.10	1.29	0.22
Tb159	0.34	0.05	0.16	0.04	0.29	0.05	0.05	0.02	0.28	0.04	0.04	0.02	0.21	0.04
Dy164	1.87	0.23	0.67	0.14	2.09	0.26	0.40	0.11	2.05	0.25	0.49	0.11	1.00	0.17
Ho165	0.46	0.06	0.21	0.04	0.46	0.07	0.15	0.03	0.53	0.07	0.16	0.03	0.28	0.05
Er166	1.39	0.19	0.49	0.12	1.42	0.22	0.70	0.13	1.55	0.21	0.56	0.12	0.73	0.14
Tm169	0.23	0.04	0.13	0.03	0.29	0.05	0.11	0.03	0.28	0.04	0.13	0.03	0.13	0.03
Yb173	1.98	0.25	1.16	0.24	2.12	0.28	0.79	0.16	1.71	0.23	1.13	0.22	0.79	0.19
Lu175	0.27	0.04	0.24	0.04	0.24	0.04	0.14	0.03	0.30	0.04	0.22	0.04	0.18	0.04
Hf180	0.87	0.12	0.17	0.09	0.75	0.13	-	0.05	0.90	0.12	0.25	0.08	0.60	0.11

Continued on next page...

Table H.1 – continued

Element	grt1-6	1σ	grt1-11	1σ	grt1-30	1σ	grt1-32	1σ	grt1-35	1σ	grt1-36	1σ	grt2-15	1σ
Ta181	0.05	0.03	-	0.04	-	0.03	-	0.03	0.05	0.03	-	0.03	-	0.03
Pb208	0.17	0.02	0.25	0.02	0.09	0.02	0.02	0.01	0.05	0.01	0.08	0.01	0.24	0.03
Th232	0.59	0.05	0.88	0.07	0.15	0.03	-	0.01	0.14	0.02	0.28	0.03	0.54	0.05
U238	0.03	0.01	0.04	0.01	0.02	0.01	0.02	-	0.04	0.01	0.07	0.01	0.04	0.01

Table H.2: Trace element compositions of Victor G9 xenocrysts - 2

Element	grt2-18	1σ	grt2-19	1σ	grt2-21	1σ	grt2-32	1σ	grt2-33	1σ	grt3-6	1σ	grt3-9	1σ
Li7	0.14	0.09	-	0.13	-	0.15	0.19	0.09	0.22	0.09	0.24	0.09	-	0.11
Sc45	118.61	4.97	89.43	3.94	89.18	4.05	82.55	3.61	93.02	4.07	167.92	7.15	166.08	7.18
Ti48	197.14	6.52	188.67	6.31	78.58	2.69	184.78	6.19	201.05	6.75	17.84	0.62	22.05	0.77
V51	112.87	5.57	126.29	6.36	179.34	9.14	151.48	7.74	177.92	9.20	70.21	3.70	81.86	4.38
Ni60	23.38	2.17	20.02	2.04	36.93	3.66	23.79	2.35	29.95	2.96	4.14	0.52	5.58	0.70
Co59	27.53	2.08	26.94	2.11	34.20	2.73	28.68	2.29	32.07	2.60	17.48	1.45	21.18	1.80
Zn64	16.20	2.00	14.05	1.84	12.31	1.71	14.83	1.98	23.63	3.18	9.99	1.40	7.58	1.13
Ga69	4.08	0.35	6.53	0.57	7.63	0.68	6.45	0.56	7.37	0.65	0.70	0.09	0.85	0.12
Rb85	0.16	0.03	0.13	0.03	0.12	0.03	0.26	0.04	0.12	0.02	0.39	0.04	0.09	0.02
Sr88	1.72	0.17	1.28	0.15	0.20	0.06	1.06	0.13	1.11	0.13	2.78	0.27	0.68	0.09
Y89	20.49	1.66	22.59	1.90	9.57	0.92	15.87	1.38	16.14	1.43	0.74	0.11	5.97	0.59
Zr90	38.59	2.49	41.77	2.86	2.85	0.47	39.60	2.67	31.57	2.22	1.82	0.25	44.15	3.06
Nb93	0.34	0.08	0.31	0.08	0.14	0.10	0.27	0.07	0.24	0.08	0.34	0.07	0.23	0.08
Cs133	-	0.01	-	0.01	-	0.01	0.02	0.01	0.03	0.01	0.04	0.01	-	0.01
Ba138	2.55	0.25	2.98	0.30	0.96	0.09	2.49	0.26	1.42	0.16	2.55	0.27	1.28	0.15
La139	1.88	0.18	1.72	0.19	0.07	0.05	0.31	0.06	0.55	0.07	1.11	0.12	0.43	0.07
Ce140	4.84	0.35	2.86	0.23	0.10	0.03	1.79	0.15	1.10	0.11	4.83	0.37	0.61	0.07
Pr141	0.32	0.04	0.28	0.04	0.05	0.02	0.18	0.03	0.23	0.04	0.87	0.08	0.17	0.03
Nd142	2.35	0.22	2.25	0.24	0.28	0.09	1.58	0.18	1.48	0.17	4.19	0.35	1.73	0.18
Sm152	1.04	0.15	0.83	0.18	0.19	0.08	1.09	0.17	0.89	0.16	0.83	0.13	4.99	0.48
Eu153	0.33	0.06	0.41	0.08	0.11	0.05	0.41	0.07	0.37	0.07	0.15	0.04	1.49	0.17
Gd158	1.73	0.29	2.01	0.37	0.33	0.15	1.46	0.27	1.49	0.28	0.59	0.15	3.27	0.48
Tb159	0.41	0.06	0.45	0.08	0.13	0.05	0.35	0.06	0.29	0.06	0.06	0.02	0.50	0.08
Dy164	3.21	0.37	3.40	0.45	0.98	0.23	2.20	0.31	2.86	0.37	0.21	0.07	2.24	0.31
Ho165	0.66	0.08	0.85	0.11	0.31	0.07	0.49	0.07	0.60	0.08	0.04	0.02	0.20	0.04
Er166	2.17	0.28	2.36	0.35	1.06	0.24	1.60	0.24	1.76	0.27	0.20	0.06	0.36	0.10
Tm169	0.39	0.06	0.30	0.06	0.23	0.06	0.25	0.05	0.36	0.06	0.09	0.03	0.07	0.03
Yb173	2.80	0.34	2.49	0.41	1.83	0.38	2.17	0.31	1.88	0.30	0.76	0.16	0.32	0.14
Lu175	0.45	0.06	0.41	0.07	0.25	0.07	0.30	0.05	0.46	0.06	0.17	0.03	-	0.03
Hf180	0.68	0.12	0.72	0.14	0.26	0.11	0.64	0.12	0.63	0.12	0.09	0.04	0.52	0.11

Continued on next page...

Table H.2 – continued

Element	grt2-18	1σ	grt2-19	1σ	grt2-21	1σ	grt2-32	1σ	grt2-33	1σ	grt3-6	1σ	grt3-9	1σ
Ta181	-	0.03	0.06	0.04	0.08	0.04	-	0.03	-	0.04	0.08	0.03	-	0.04
Pb208	0.08	0.02	0.10	0.02	-	0.02	0.07	0.02	0.26	0.02	0.23	0.02	0.08	0.01
Th232	0.22	0.04	0.12	0.03	0.03	0.02	0.08	0.02	0.13	0.02	1.19	0.08	9.70	0.44
U238	0.03	0.01	0.02	0.01	0.01	0.01	0.02	-	0.02	-	0.11	0.01	0.02	-

Table H.3: Trace element compositions of Victor G9 xenocrysts - 3

Element	grt3-11	1σ	grt3-12	1σ	grt3-13	1σ	grt3-14	1σ	grt3-15	1σ	grt3-16	1σ	grt3-17	1σ
Li7	-	0.07	0.12	0.08	0.08	0.08	0.25	0.10	-	0.11	0.13	0.11	0.13	0.08
Sc45	88.22	7.03	75.30	6.12	80.22	6.58	83.34	6.88	143.37	6.29	89.64	7.42	81.66	6.85
Ti48	117.99	4.90	54.48	2.32	176.22	7.40	183.26	7.71	62.72	2.15	193.33	8.11	161.90	6.84
V51	223.13	14.10	114.53	7.41	200.67	12.97	198.35	12.92	296.80	15.95	218.66	14.33	177.24	11.77
Ni60	26.38	3.70	7.55	1.41	27.15	4.00	26.27	3.91	29.69	3.10	26.34	3.91	24.38	3.66
Co59	35.29	4.18	30.26	3.65	34.15	4.16	32.41	4.00	23.70	2.05	29.75	3.71	30.92	3.89
Zn64	10.21	1.55	11.34	1.90	11.27	1.95	10.85	1.94	10.60	1.58	19.18	2.78	7.86	1.56
Ga69	5.67	0.61	4.07	0.48	7.10	0.77	6.71	0.75	4.77	0.46	5.75	0.64	5.67	0.63
Rb85	0.16	0.04	0.19	0.05	0.25	0.06	0.29	0.07	0.16	0.03	0.24	0.06	0.10	0.04
Sr88	1.40	0.20	1.12	0.19	1.25	0.21	2.16	0.28	0.69	0.09	3.79	0.39	3.30	0.34
Y89	6.79	0.83	22.19	2.29	15.89	1.73	14.62	1.65	1.55	0.21	7.26	0.90	15.16	1.64
Zr90	31.73	3.14	16.43	1.92	30.28	3.20	18.42	2.18	5.33	0.55	34.82	3.46	25.84	2.68
Nb93	0.49	0.19	-	0.21	-	0.23	0.55	0.19	0.92	0.14	1.01	0.30	0.64	0.23
Cs133	0.02	0.02	-	0.02	-	0.03	-	0.02	-	0.01	-	0.03	-	0.02
Ba138	3.49	0.39	0.88	0.16	3.28	0.39	6.69	0.72	1.77	0.21	3.75	0.43	-	0.09
La139	0.55	0.17	0.28	0.14	0.59	0.17	1.15	0.24	0.64	0.09	0.79	0.22	-	0.15
Ce140	1.18	0.20	0.42	0.12	1.39	0.25	1.01	0.20	1.35	0.13	1.78	0.29	0.59	0.13
Pr141	0.37	0.10	0.31	0.09	0.22	0.08	0.25	0.08	0.25	0.04	0.43	0.11	0.32	0.09
Nd142	2.56	0.49	1.49	0.36	1.18	0.36	0.65	0.26	1.59	0.18	2.91	0.54	1.48	0.35
Sm152	1.28	0.43	1.63	0.43	0.97	0.37	0.42	0.26	0.45	0.11	1.99	0.47	1.24	0.33
Eu153	0.70	0.18	0.56	0.16	0.55	0.16	0.33	0.16	0.10	0.03	0.65	0.18	0.69	0.18
Gd158	2.05	0.53	1.55	0.46	1.40	0.47	1.94	0.59	0.32	0.13	1.30	0.46	1.74	0.50
Tb159	0.19	0.11	0.43	0.13	0.43	0.13	0.31	0.11	-	0.02	0.25	0.13	0.45	0.13
Dy164	1.45	0.41	2.93	0.61	2.42	0.64	2.27	0.57	0.27	0.10	1.65	0.43	2.49	0.55
Ho165	0.31	0.09	0.90	0.18	0.47	0.17	0.54	0.15	0.08	0.04	0.41	0.12	0.66	0.15
Er166	0.77	0.26	2.39	0.52	1.88	0.45	1.58	0.46	0.24	0.09	0.81	0.35	1.48	0.39
Tm169	0.14	0.09	0.63	0.15	0.41	0.14	0.32	0.11	0.06	0.02	0.22	0.10	0.28	0.09
Yb173	1.87	0.55	3.49	0.80	1.30	0.67	2.28	0.65	0.58	0.16	1.75	0.61	1.78	0.57
Lu175	0.33	0.10	0.50	0.15	0.31	0.12	0.45	0.14	0.11	0.03	0.28	0.11	0.35	0.11
Hf180	0.68	0.26	0.59	0.25	0.87	0.33	0.80	0.28	-	0.07	1.22	0.35	-	0.32

Continued on next page...

Table H.3 – continued

Element	grt3-11	1σ	grt3-12	1σ	grt3-13	1σ	grt3-14	1σ	grt3-15	1σ	grt3-16	1σ	grt3-17	1σ
Ta181	0.19	0.11	0.38	0.16	-	0.13	0.30	0.16	0.07	0.03	-	0.14	0.21	0.14
Pb208	-	0.11	-	0.14	-	0.14	-	0.14	0.06	0.01	-	0.13	-	0.12
Th232	2.64	0.27	2.28	0.26	0.61	0.12	0.56	0.14	0.57	0.06	5.22	0.47	1.29	0.14
U238	0.07	0.02	-	0.02	0.06	0.02	0.07	0.02	0.04	0.01	0.07	0.02	0.03	0.01

Table H.4: Trace element compositions of Victor G9 xenocrysts - 4

Element	grt3-18	1σ	grt3-19	1σ	grt3-20	1σ	grt3-21	1σ	grt3-22	1σ	grt3-23	1σ	grt3-24	1σ
Li7	0.27	0.07	-	0.06	0.17	0.08	0.18	0.09	-	0.09	0.15	0.07	0.19	0.08
Sc45	94.80	8.00	92.22	7.90	106.34	9.22	86.80	7.70	85.60	7.74	141.35	6.21	104.13	9.51
Ti48	197.10	8.34	169.97	7.26	59.49	2.60	124.11	5.41	73.89	3.28	57.48	1.98	207.50	9.18
V51	171.21	11.50	170.79	11.63	94.92	6.63	255.43	17.87	232.80	16.60	269.00	14.66	188.36	13.67
Ni60	27.96	4.20	23.81	3.68	13.61	2.29	35.05	5.46	34.92	5.59	29.52	3.11	26.07	4.37
Co59	30.52	3.90	29.66	3.85	29.09	3.85	32.03	4.30	34.30	4.70	22.55	1.99	31.70	4.44
Zn64	16.42	2.41	7.48	1.59	9.78	1.73	10.00	1.79	13.76	2.35	14.12	2.11	18.73	6.95
Ga69	5.50	0.62	4.83	0.56	2.28	0.31	5.82	0.68	7.06	0.84	3.79	0.37	5.08	0.67
Rb85	0.21	0.06	0.17	0.10	0.24	0.06	0.13	0.05	0.18	0.06	0.23	0.04	0.37	0.09
Sr88	2.64	0.32	3.07	1.94	4.28	0.44	4.16	0.43	5.09	0.54	1.08	0.13	7.51	1.42
Y89	14.92	1.62	11.96	1.40	11.43	1.31	4.38	0.61	5.32	0.75	1.95	0.24	10.74	1.35
Zr90	44.81	4.31	38.76	3.80	65.81	6.20	12.20	1.55	3.02	0.74	4.07	0.44	36.97	3.95
Nb93	-	0.25	0.47	0.22	0.55	0.22	0.64	0.23	0.77	0.22	0.44	0.09	0.82	0.22
Cs133	-	0.05	0.06	0.03	-	0.02	0.05	0.02	0.06	0.03	-	0.01	-	0.04
Ba138	1.74	2.47	1.59	0.93	3.20	0.38	2.29	0.29	1.91	0.26	0.89	0.11	4.31	0.86
La139	0.64	1.45	1.49	0.48	1.96	0.33	1.04	0.22	0.53	0.18	0.51	0.07	0.72	0.40
Ce140	1.51	2.93	1.98	0.99	4.20	0.58	1.92	0.31	1.09	0.21	1.40	0.13	1.19	0.39
Pr141	0.27	0.29	0.42	0.12	0.72	0.14	0.33	0.08	0.29	0.09	0.34	0.05	0.41	0.13
Nd142	2.14	1.60	2.65	0.71	4.59	0.77	1.15	0.30	1.03	0.28	2.02	0.21	2.40	0.53
Sm152	2.07	0.46	1.99	0.46	2.91	0.57	0.59	0.25	-	0.24	0.77	0.12	1.60	0.43
Eu153	0.63	0.18	0.87	0.21	0.85	0.21	0.40	0.13	0.29	0.12	0.20	0.05	0.86	0.21
Gd158	2.37	0.59	2.23	0.65	4.57	0.87	1.08	0.43	-	0.38	0.33	0.15	2.00	0.64
Tb159	0.44	0.15	0.51	0.14	0.56	0.14	0.20	0.09	-	0.09	0.08	0.02	0.45	0.14
Dy164	2.73	0.54	2.95	0.58	2.30	0.49	0.99	0.35	1.15	0.33	0.36	0.11	1.97	0.48
Ho165	0.63	0.15	0.50	0.14	0.40	0.12	-	0.12	0.30	0.11	0.07	0.03	0.49	0.14
Er166	1.80	0.43	1.35	0.33	0.92	0.34	0.46	0.26	1.00	0.33	0.24	0.08	1.45	0.37
Tm169	0.30	0.10	-	0.10	-	0.09	0.25	0.09	0.24	0.09	0.08	0.03	-	0.10
Yb173	1.77	0.45	1.41	0.51	1.44	0.49	1.48	0.49	1.54	0.52	0.75	0.16	1.29	0.52
Lu175	0.34	0.10	0.30	0.12	0.26	0.09	0.20	0.09	0.21	0.10	0.10	0.03	0.36	0.10
Hf180	0.66	0.27	0.86	0.28	0.88	0.25	0.55	0.20	-	0.22	0.21	0.06	1.20	0.32

Continued on next page. . .

Table H.4 – continued

Element	grt3-18	1σ	grt3-19	1σ	grt3-20	1σ	grt3-21	1σ	grt3-22	1σ	grt3-23	1σ	grt3-24	1σ
Ta181	0.20	0.11	-	0.16	-	0.13	0.23	0.13	-	0.14	-	0.03	-	0.15
Pb208	0.31	0.11	0.32	0.17	0.32	0.11	-	0.13	-	0.13	0.07	0.02	-	0.13
Th232	4.43	0.37	8.64	0.77	5.73	0.58	10.93	0.97	3.94	0.40	0.21	0.03	5.74	0.56
U238	0.05	0.02	-	0.03	0.10	0.03	0.06	0.03	-	0.02	0.03	0.01	0.07	0.02

Table H.5: Trace element compositions of Victor G9 xenocrysts- 5

Element	grt3-25	1σ	grt3-26	1σ	grt3-27	1σ	grt3-28	1σ	grt3-29	1σ	grt3-31	1σ	grt3-32	1σ
Li7	-	0.10	0.12	0.12	-	0.09	0.16	0.07	0.07	0.07	0.12	0.09	-	0.08
Sc45	104.93	9.74	95.63	9.41	73.92	7.20	91.52	8.95	153.79	6.81	87.73	8.94	153.82	6.85
Ti48	183.24	8.17	234.04	10.84	57.78	2.69	166.05	7.62	55.41	1.91	57.05	2.72	152.33	5.24
V51	289.10	21.25	173.80	13.39	99.67	7.70	195.96	15.18	288.19	15.94	227.53	18.32	272.45	15.30
Ni60	39.15	6.46	18.70	3.95	7.14	1.63	24.42	4.37	28.93	3.12	39.81	7.26	29.13	3.18
Co59	33.89	4.82	31.47	4.79	31.00	4.59	28.79	4.34	22.67	2.04	35.04	5.51	21.71	1.99
Zn64	13.37	2.30	11.46	2.55	6.65	1.59	9.02	1.82	8.74	1.38	10.42	2.11	9.78	1.56
Ga69	6.34	0.78	7.54	1.06	4.93	0.65	6.26	0.81	3.35	0.34	6.48	0.87	3.50	0.36
Rb85	0.21	0.06	-	0.06	0.23	0.07	-	0.05	0.23	0.03	0.07	0.04	0.21	0.03
Sr88	4.28	0.46	2.12	0.40	4.07	0.46	4.05	0.45	0.82	0.11	1.56	0.24	1.20	0.14
Y89	6.16	0.83	17.87	2.44	39.21	4.44	13.65	1.66	0.67	0.12	6.25	0.89	4.41	0.47
Zr90	23.25	2.63	48.76	6.04	11.35	1.66	27.87	3.13	3.30	0.38	4.97	0.94	17.97	1.40
Nb93	0.44	0.18	0.41	0.26	-	0.27	0.53	0.22	0.40	0.09	-	0.19	0.99	0.14
Cs133	-	0.02	-	0.03	-	0.03	-	0.02	-	0.01	-	0.02	0.01	0.01
Ba138	1.66	0.24	0.49	0.19	0.71	0.13	0.93	0.15	1.21	0.15	0.74	0.14	2.07	0.25
La139	-	0.15	-	0.13	0.48	0.17	0.28	0.13	0.22	0.05	0.49	0.13	1.02	0.12
Ce140	0.53	0.13	0.53	0.20	0.35	0.11	0.68	0.15	0.91	0.09	1.25	0.23	3.32	0.29
Pr141	0.23	0.07	0.20	0.11	0.27	0.09	0.27	0.10	0.18	0.03	0.41	0.10	0.50	0.06
Nd142	0.93	0.29	1.21	0.49	1.92	0.43	1.75	0.39	0.86	0.11	2.34	0.49	2.48	0.24
Sm152	0.79	0.29	2.37	0.78	2.38	0.54	1.24	0.39	0.39	0.09	0.88	0.32	0.73	0.12
Eu153	0.47	0.15	0.63	0.30	1.10	0.25	0.59	0.16	0.09	0.03	0.26	0.11	0.27	0.05
Gd158	-	0.44	2.20	0.92	4.06	0.86	1.66	0.51	0.27	0.12	-	0.38	0.96	0.20
Tb159	0.21	0.09	0.57	0.23	0.79	0.20	0.54	0.13	-	0.03	-	0.09	0.14	0.03
Dy164	1.26	0.42	4.57	1.16	6.11	1.03	2.40	0.52	0.16	0.09	1.33	0.34	0.97	0.17
Ho165	0.23	0.10	0.49	0.24	1.30	0.25	0.35	0.14	0.05	0.02	0.30	0.11	0.17	0.04
Er166	1.09	0.33	1.44	0.55	3.86	0.73	2.01	0.45	0.13	0.05	1.08	0.38	0.42	0.10
Tm169	0.24	0.08	-	0.14	0.79	0.16	0.43	0.09	0.06	0.02	0.25	0.10	0.08	0.03
Yb173	1.12	0.46	1.55	0.92	4.46	0.92	1.18	0.54	0.32	0.12	1.41	0.46	0.78	0.16
Lu175	-	0.10	0.42	0.17	0.89	0.18	0.42	0.11	0.07	0.02	0.27	0.10	0.14	0.03
Hf180	0.72	0.33	1.02	0.45	-	0.31	0.61	0.27	0.11	0.05	0.56	0.25	0.39	0.08

Continued on next page. . .

Table H.5 – continued

Element	grt3-25	1σ	grt3-26	1σ	grt3-27	1σ	grt3-28	1σ	grt3-29	1σ	grt3-31	1σ	grt3-32	1σ
Ta181	-	0.14	-	0.23	-	0.16	0.28	0.11	-	0.03	-	0.19	0.09	0.03
Pb208	-	0.11	-	0.13	0.35	0.12	0.27	0.10	0.07	0.01	-	0.13	0.10	0.02
Th232	0.29	0.09	0.31	0.16	0.63	0.14	1.60	0.16	0.51	0.04	7.06	0.68	0.93	0.07
U238	-	0.01	0.06	0.02	-	0.02	0.03	0.02	0.02	-	0.04	0.02	0.03	0.01

Table H.6: Trace element compositions of Victor G9 xenocrysts - 6

Element	grt4-1	1σ	grt4-2	1σ	grt4-3	1σ	grt4-4	1σ	grt4-5	1σ	grt4-6	1σ	grt4-7	1σ
Li7	-	0.12	0.22	0.12	0.13	0.10	0.19	0.10	-	0.10	-	0.14	-	0.11
Sc45	88.02	4.07	127.81	5.92	105.19	4.94	89.51	9.35	121.99	12.91	91.15	9.97	87.26	9.74
Ti48	351.59	12.19	142.09	4.98	315.02	11.05	122.97	5.90	250.52	12.05	57.31	2.87	274.35	13.63
V51	167.35	9.59	203.24	11.82	169.80	10.03	186.20	15.37	303.97	25.46	221.42	19.05	199.90	17.56
Ni60	30.63	3.46	30.94	3.60	31.81	3.76	27.66	5.35	41.29	7.94	40.79	8.09	37.49	7.63
Co59	27.29	2.56	27.53	2.64	24.37	2.39	32.41	5.24	32.87	5.43	34.66	5.88	34.76	6.02
Zn64	12.49	2.06	11.99	2.05	15.49	2.68	9.32	1.92	11.20	2.39	9.72	2.35	15.32	3.24
Ga69	7.03	0.71	4.99	0.53	6.17	0.66	6.06	0.85	6.56	0.93	5.47	0.81	7.22	1.06
Rb85	0.08	0.02	-	0.03	0.07	0.02	0.24	0.07	-	0.06	-	0.07	0.35	0.07
Sr88	0.44	0.07	0.64	0.10	1.44	0.18	1.49	0.24	1.12	0.19	1.78	0.25	3.48	0.45
Y89	16.08	1.64	7.62	0.84	14.07	1.51	9.90	1.35	8.35	1.18	4.98	0.82	12.71	1.74
Zr90	60.46	4.50	25.01	2.04	45.09	3.54	31.87	3.75	39.74	4.58	1.60	0.63	31.32	3.86
Nb93	0.35	0.09	0.34	0.08	0.58	0.12	1.44	0.28	0.69	0.27	0.65	0.23	-	0.31
Cs133	-	0.01	-	0.01	-	0.01	-	0.03	-	0.02	-	0.03	-	0.03
Ba138	1.08	0.14	0.61	0.09	4.57	0.57	1.43	0.24	0.47	0.13	1.20	0.20	2.12	0.32
La139	0.50	0.08	1.37	0.14	1.65	0.20	1.14	0.24	-	0.15	0.89	0.23	1.41	0.25
Ce140	0.48	0.06	1.08	0.12	3.03	0.28	1.60	0.31	0.51	0.13	0.78	0.20	2.69	0.49
Pr141	0.11	0.03	0.13	0.03	0.28	0.04	0.48	0.12	0.25	0.10	-	0.11	0.21	0.09
Nd142	0.77	0.11	1.18	0.16	2.00	0.23	2.30	0.53	0.76	0.28	0.92	0.29	1.78	0.47
Sm152	0.85	0.15	0.80	0.16	1.04	0.17	1.50	0.47	1.30	0.39	0.51	0.26	0.82	0.31
Eu153	0.45	0.08	0.37	0.07	0.43	0.08	0.49	0.19	0.46	0.14	-	0.11	0.44	0.15
Gd158	1.65	0.31	1.32	0.29	1.77	0.34	1.42	0.64	2.41	0.72	-	0.55	1.60	0.65
Tb159	0.40	0.07	0.20	0.05	0.39	0.07	0.38	0.12	0.35	0.13	-	0.14	0.42	0.14
Dy164	2.33	0.35	1.19	0.25	2.48	0.38	1.47	0.43	2.09	0.56	1.54	0.50	2.01	0.55
Ho165	0.59	0.09	0.27	0.06	0.53	0.08	0.39	0.15	0.32	0.12	-	0.14	0.55	0.17
Er166	1.87	0.31	0.69	0.18	1.14	0.23	1.49	0.39	1.44	0.36	-	0.38	1.63	0.48
Tm169	0.31	0.05	0.13	0.04	0.20	0.05	0.20	0.10	0.17	0.10	-	0.12	0.48	0.13
Yb173	1.86	0.34	0.83	0.22	1.50	0.28	-	0.63	1.65	0.58	2.05	0.63	1.64	0.69
Lu175	0.28	0.05	0.12	0.04	0.27	0.05	-	0.12	-	0.11	0.26	0.12	0.34	0.13
Hf180	1.32	0.18	0.51	0.12	0.89	0.16	0.95	0.33	1.36	0.36	0.93	0.29	0.79	0.34

Continued on next page...

Table H.6 – continued

Element	grt4-1	1σ	grt4-2	1σ	grt4-3	1σ	grt4-4	1σ	grt4-5	1σ	grt4-6	1σ	grt4-7	1σ
Ta181	-	0.04	-	0.03	0.10	0.04	-	0.14	-	0.17	0.29	0.14	0.40	0.13
Pb208	0.08	0.02	0.10	0.02	0.10	0.02	-	0.14	-	0.13	0.30	0.15	0.51	0.14
Th232	0.08	0.02	0.52	0.06	1.06	0.08	14.19	1.35	6.19	0.64	9.83	1.00	22.24	2.16
U238	0.01	-	0.01	-	0.04	0.01	-	0.02	0.04	0.02	-	0.02	0.14	0.03

Table H.7: Trace element compositions of Victor G9 xenocrysts - 7

Element	grt4-8	1σ	grt4-9	1σ	grt4-10	1σ	grt4-11	1σ	grt4-12	1σ	grt4-13	1σ	grt4-14	1σ
Li7	0.31	0.15	0.51	0.17	-	0.14	0.21	0.12	0.31	0.13	0.07	0.11	0.27	0.11
Sc45	88.63	4.24	138.36	15.86	99.75	11.59	96.10	11.45	91.83	11.13	108.98	5.25	100.50	12.48
Ti48	347.81	12.29	106.59	5.51	231.51	11.79	190.56	9.87	205.97	10.74	220.92	7.87	65.31	3.50
V51	158.39	9.51	211.25	19.15	200.73	18.39	195.37	18.31	215.00	20.52	185.53	11.30	256.89	25.06
Ni60	33.56	4.04	25.73	5.91	29.14	6.33	33.44	7.42	31.97	7.19	32.92	4.07	39.67	9.10
Co59	26.12	2.61	32.58	5.91	34.69	6.29	33.40	6.23	36.70	6.96	26.75	2.73	36.60	7.13
Zn64	13.67	2.45	17.06	3.83	18.25	3.86	11.36	2.78	11.43	2.64	12.03	2.23	19.19	4.90
Ga69	7.56	0.82	3.58	0.67	7.20	1.10	6.13	0.98	8.48	1.33	7.06	0.78	6.49	1.07
Rb85	-	0.03	0.18	0.09	0.12	0.06	-	0.07	0.19	0.07	0.08	0.02	-	0.07
Sr88	0.53	0.09	2.33	0.40	1.69	0.29	1.75	0.30	0.77	0.15	0.29	0.06	2.46	0.61
Y89	15.97	1.75	7.23	1.25	18.95	2.60	12.61	1.83	16.92	2.38	13.79	1.56	4.68	0.79
Zr90	58.68	4.64	73.18	9.00	37.35	4.63	58.37	7.10	26.34	3.42	22.63	1.97	5.86	1.25
Nb93	0.24	0.07	0.98	0.48	1.21	0.37	0.59	0.27	0.43	0.19	0.44	0.11	0.59	0.24
Cs133	0.02	0.01	-	0.03	-	0.03	-	0.03	-	0.03	-	0.01	-	0.03
Ba138	0.42	0.07	2.71	0.47	3.08	0.47	2.23	0.37	2.02	0.32	1.51	0.21	1.54	0.49
La139	0.34	0.07	0.52	0.22	1.48	0.26	0.88	0.24	1.15	0.19	0.10	0.04	-	0.23
Ce140	0.51	0.06	1.23	0.30	1.81	0.36	1.09	0.25	0.67	0.16	0.30	0.05	0.71	0.23
Pr141	0.08	0.02	0.43	0.14	0.26	0.10	0.30	0.11	0.19	0.09	0.11	0.03	-	0.08
Nd142	0.47	0.09	2.81	0.74	1.83	0.53	1.76	0.52	1.03	0.31	0.72	0.12	0.86	0.31
Sm152	0.69	0.15	2.17	0.75	1.28	0.44	1.87	0.59	0.95	0.35	0.67	0.14	1.08	0.35
Eu153	0.31	0.06	0.79	0.28	0.68	0.21	0.73	0.23	0.54	0.16	0.27	0.07	0.30	0.13
Gd158	1.32	0.30	2.79	0.94	3.29	0.89	2.89	0.75	1.91	0.60	1.34	0.31	0.87	0.38
Tb159	0.27	0.06	-	0.20	0.32	0.11	0.29	0.14	0.42	0.14	0.21	0.05	0.20	0.11
Dy164	2.12	0.35	2.02	0.73	3.39	0.77	2.73	0.70	2.67	0.60	2.13	0.36	0.63	0.36
Ho165	0.45	0.08	-	0.19	0.76	0.21	0.61	0.19	0.52	0.14	0.58	0.09	-	0.12
Er166	1.58	0.29	1.26	0.48	2.62	0.59	1.93	0.51	2.47	0.57	1.73	0.32	0.60	0.31
Tm169	0.26	0.05	-	0.10	0.33	0.13	0.47	0.12	0.45	0.12	0.23	0.05	-	0.11
Yb173	1.86	0.32	1.52	0.74	2.57	0.74	1.39	0.62	2.30	0.56	1.76	0.31	1.12	0.59
Lu175	0.33	0.05	-	0.16	0.39	0.12	0.35	0.13	0.45	0.11	0.33	0.05	-	0.10
Hf180	1.37	0.20	1.27	0.53	0.61	0.35	1.51	0.42	0.76	0.28	0.57	0.14	0.59	0.25

Continued on next page...

Table H.7 – continued

Element	grt4-8	1σ	grt4-9	1σ	grt4-10	1σ	grt4-11	1σ	grt4-12	1σ	grt4-13	1σ	grt4-14	1σ
Ta181	-	0.04	-	0.22	0.38	0.19	-	0.15	0.28	0.13	0.09	0.03	-	0.15
Pb208	0.11	0.02	-	0.17	-	0.14	0.30	0.16	-	0.14	0.06	0.02	0.36	0.13
Th232	0.28	0.04	8.97	1.12	11.57	1.81	1.92	0.32	-	0.11	0.07	0.02	5.91	0.68
U238	0.03	-	0.09	0.04	-	0.03	0.02	0.02	0.07	0.02	0.02	0.01	-	0.02

Table H.8: Trace element compositions of Victor G9 xenocrysts - 8

Element	grt4-15	1σ	grt4-16	1σ	grt4-17	1σ	grt4-18	1σ	grt4-19	1σ	grt4-20	1σ	grt4-21	1σ
Li7	-	0.12	-	0.11	-	0.10	-	0.12	-	0.11	0.16	0.11	-	0.13
Sc45	93.88	11.95	101.95	13.28	92.76	12.37	107.64	14.63	96.84	4.68	132.96	18.45	94.69	13.62
Ti48	213.60	11.49	149.77	8.19	367.90	20.28	163.39	9.15	111.91	4.01	249.47	14.14	180.23	10.47
V51	157.65	15.78	190.82	19.49	217.15	22.64	226.78	24.14	148.40	9.16	195.90	21.34	170.83	19.13
Ni60	30.70	7.30	26.12	6.46	37.15	9.25	45.73	11.58	30.70	3.85	29.71	7.84	23.65	6.69
Co59	33.97	6.79	32.12	6.58	35.98	7.54	37.48	8.03	24.93	2.59	35.49	7.80	33.41	7.59
Zn64	15.80	3.14	23.56	5.45	15.85	3.95	14.30	3.66	16.19	3.04	8.88	2.57	9.78	2.63
Ga69	6.19	1.07	7.22	1.23	7.42	1.29	7.66	1.35	4.37	0.50	6.13	1.12	5.68	1.10
Rb85	-	0.10	0.32	0.09	0.26	0.09	0.55	0.08	0.42	0.06	2.32	0.26	0.25	0.10
Sr88	3.38	0.58	3.80	0.54	4.08	0.56	3.19	0.45	1.27	0.17	2.02	0.34	4.11	0.67
Y89	18.60	2.74	13.21	2.00	16.30	2.46	7.72	1.25	2.27	0.30	12.62	1.99	12.74	2.12
Zr90	29.96	4.04	26.49	3.68	69.05	8.87	20.25	2.94	13.25	1.21	73.97	9.72	40.82	5.94
Nb93	-	0.22	1.23	0.26	-	0.24	-	0.27	1.19	0.18	0.87	0.24	-	0.36
Cs133	-	0.03	-	0.03	-	0.03	-	0.03	0.03	0.01	0.07	0.03	0.06	0.03
Ba138	2.68	0.53	3.00	1.73	2.34	0.39	1.52	0.27	2.22	0.30	2.65	0.32	2.46	0.79
La139	0.37	0.18	0.94	0.99	1.08	0.27	0.56	0.21	0.80	0.11	0.73	0.20	1.45	0.42
Ce140	0.84	0.22	1.79	1.22	1.54	0.33	1.30	0.29	2.15	0.22	1.28	0.29	3.97	0.97
Pr141	0.27	0.09	0.30	0.16	0.15	0.09	0.29	0.09	0.29	0.04	0.29	0.08	0.42	0.15
Nd142	1.39	0.40	1.80	0.60	1.13	0.33	0.85	0.31	1.54	0.19	1.98	0.52	3.39	0.87
Sm152	1.21	0.43	1.02	0.39	1.46	0.46	1.30	0.38	0.45	0.11	1.39	0.47	1.47	0.43
Eu153	0.46	0.16	0.56	0.20	0.52	0.18	0.32	0.13	0.16	0.04	0.80	0.23	0.41	0.17
Gd158	1.75	0.69	3.11	0.81	1.25	0.60	-	0.47	0.53	0.16	2.66	0.76	1.36	0.70
Tb159	0.56	0.16	0.56	0.15	0.35	0.14	-	0.11	0.09	0.03	0.49	0.17	0.49	0.17
Dy164	2.63	0.65	2.31	0.62	2.68	0.67	1.44	0.48	0.44	0.12	2.94	0.72	1.64	0.59
Ho165	0.48	0.17	0.51	0.18	0.50	0.17	0.31	0.13	0.09	0.03	0.61	0.18	0.50	0.16
Er166	1.68	0.50	1.18	0.42	1.94	0.52	1.08	0.38	0.38	0.10	1.13	0.39	1.87	0.60
Tm169	0.43	0.12	0.33	0.12	0.54	0.15	0.33	0.10	0.08	0.03	0.32	0.10	0.39	0.14
Yb173	2.97	0.80	1.90	0.69	1.74	0.65	-	0.65	-	0.15	1.48	0.39	1.85	0.75
Lu175	0.34	0.13	0.37	0.12	0.48	0.14	0.21	0.11	0.11	0.03	-	0.10	0.36	0.10
Hf180	0.61	0.27	0.52	0.31	1.48	0.44	0.64	0.28	0.51	0.11	1.52	0.41	0.86	0.37

Continued on next page. . .

Table H.8 – continued

Element	grt4-15	1σ	grt4-16	1σ	grt4-17	1σ	grt4-18	1σ	grt4-19	1σ	grt4-20	1σ	grt4-21	1σ
Ta181	0.19	0.14	-	0.14	-	0.17	-	0.15	0.09	0.03	-	0.14	-	0.17
Pb208	-	0.12	-	0.16	-	0.25	-	0.13	0.10	0.02	-	0.12	0.38	0.15
Th232	2.69	0.30	1.74	0.45	6.11	0.97	7.99	0.96	0.59	0.05	6.48	0.54	4.41	0.60
U238	-	0.02	-	0.04	-	0.03	-	0.02	0.04	0.01	-	0.02	0.06	0.03

Table H.9: Trace element compositions of Victor G9 xenocrysts - 9

Element	grt4-22	1σ	grt4-23	1σ	grt4-24	1σ	grt4-25	1σ	grt5-1	1σ	grt5-2	1σ	grt5-3	1σ
Li7	0.16	0.10	-	0.13	-	0.10	0.40	0.16	0.10	0.06	0.28	0.07	0.28	0.12
Sc45	107.25	15.62	120.10	17.94	113.44	17.33	114.93	18.02	90.63	4.91	89.20	4.88	123.73	6.03
Ti48	219.58	12.80	49.49	2.97	47.50	2.88	326.79	19.85	109.65	4.91	145.87	6.55	207.32	7.46
V51	219.67	24.97	276.60	32.13	291.44	34.56	268.31	32.55	190.61	17.12	171.21	15.54	214.96	13.46
Ni60	30.38	8.40	39.28	11.14	40.44	11.72	46.31	13.79	35.52	3.55	28.02	3.00	29.44	3.80
Co59	32.88	7.58	37.55	8.88	30.97	7.51	40.89	10.14	31.92	2.61	31.17	2.58	23.89	2.54
Zn64	21.50	5.63	12.00	3.55	10.82	3.21	14.38	4.39	9.72	1.34	8.11	1.35	12.85	2.50
Ga69	7.20	1.36	7.27	1.41	5.87	1.17	8.15	1.65	5.34	0.46	5.75	0.50	5.29	0.61
Rb85	0.25	0.08	0.73	0.14	0.12	0.07	-	0.09	0.21	0.05	-	0.04	0.17	0.03
Sr88	5.80	0.80	6.22	0.88	2.73	0.43	10.49	1.46	1.08	0.22	1.94	0.26	0.97	0.14
Y89	10.69	1.74	2.86	0.61	1.17	0.29	16.66	2.79	7.19	0.88	13.67	1.50	9.11	1.09
Zr90	32.43	4.60	3.09	0.87	6.91	1.31	48.51	7.07	16.30	2.72	23.33	3.80	25.23	2.22
Nb93	-	0.21	-	0.27	0.48	0.22	0.71	0.30	-	0.18	0.66	0.23	0.32	0.09
Cs133	0.10	0.03	-	0.03	-	0.02	-	0.03	-	0.02	-	0.02	0.02	0.01
Ba138	3.92	0.65	2.14	0.39	0.99	0.16	1.37	0.29	1.87	0.17	0.77	0.12	2.48	0.35
La139	0.83	0.22	0.65	0.21	-	0.15	-	0.13	0.79	0.17	0.30	0.14	1.04	0.15
Ce140	1.13	0.27	0.78	0.21	0.32	0.11	0.39	0.14	0.58	0.16	2.05	0.38	2.41	0.25
Pr141	0.25	0.09	0.47	0.13	0.22	0.06	0.22	0.08	0.18	0.07	0.28	0.08	0.25	0.04
Nd142	1.38	0.36	0.93	0.29	0.86	0.27	0.57	0.25	1.15	0.29	1.74	0.34	2.10	0.25
Sm152	0.71	0.31	-	0.26	0.94	0.37	1.04	0.42	1.31	0.31	0.99	0.32	0.79	0.16
Eu153	0.46	0.16	0.15	0.12	0.18	0.12	0.43	0.19	0.47	0.13	0.41	0.12	0.32	0.07
Gd158	1.86	0.61	0.89	0.69	1.26	0.51	1.81	0.73	2.16	0.53	2.21	0.61	1.31	0.29
Tb159	0.47	0.13	-	0.09	-	0.09	0.46	0.16	0.12	0.06	0.32	0.11	0.24	0.06
Dy164	2.13	0.59	-	0.36	-	0.36	2.82	0.81	1.17	0.35	2.35	0.46	1.75	0.31
Ho165	0.51	0.15	0.34	0.12	-	0.09	0.67	0.19	0.36	0.11	0.55	0.14	0.31	0.06
Er166	1.13	0.40	0.78	0.35	-	0.24	2.12	0.55	1.05	0.31	1.70	0.39	1.14	0.24
Tm169	0.38	0.11	-	0.10	0.24	0.11	0.39	0.12	0.21	0.08	0.23	0.09	0.14	0.04
Yb173	1.41	0.56	-	0.62	-	0.51	1.69	0.65	-	0.50	1.49	0.56	0.93	0.22
Lu175	0.25	0.09	0.20	0.10	0.20	0.08	0.38	0.15	0.22	0.09	0.41	0.09	0.15	0.04
Hf180	1.27	0.34	-	0.23	0.30	0.19	0.94	0.41	0.74	0.20	0.70	0.24	0.62	0.12

Continued on next page. . .

Table H.9 – continued

Element	grt4-22	1σ	grt4-23	1σ	grt4-24	1σ	grt4-25	1σ	grt5-1	1σ	grt5-2	1σ	grt5-3	1σ
Ta181	-	0.11	0.19	0.11	-	0.13	-	0.16	0.14	0.12	-	0.14	0.07	0.03
Pb208	-	0.11	-	0.14	-	0.11	-	0.13	-	0.08	-	0.10	0.08	0.02
Th232	3.42	0.45	6.30	0.80	2.33	0.25	0.44	0.12	0.73	0.12	2.55	0.23	0.24	0.03
U238	0.06	0.02	0.07	0.02	0.06	0.02	0.05	0.02	-	0.02	0.04	0.02	0.05	0.01

Table H.10: Trace element compositions of Victor G9 xenocrysts - 10

Element	grt5-4	1σ	grt5-5	1σ	grt5-6	1σ	grt5-7	1σ	grt5-8	1σ	grt5-9	1σ	grt5-10	1σ
Li7	-	0.14	0.27	0.18	-	0.10	-	0.08	-	0.08	0.38	0.09	0.11	0.05
Sc45	84.44	4.71	110.05	6.87	133.01	7.17	91.83	5.05	93.18	5.18	104.85	5.90	91.01	5.00
Ti48	138.38	6.27	220.14	10.37	56.31	2.60	54.22	2.50	183.18	8.38	123.18	5.73	109.06	5.05
V51	192.12	17.63	168.38	15.96	74.73	7.04	210.23	19.79	199.62	19.07	191.74	18.63	227.26	22.31
Ni60	36.30	3.75	39.10	5.36	5.30	1.16	35.61	3.61	23.74	2.68	25.06	2.90	29.30	2.95
Co59	34.76	2.89	26.37	2.69	27.61	2.34	32.26	2.70	30.66	2.61	31.83	2.77	33.02	2.79
Zn64	22.32	2.55	10.20	2.24	6.70	1.34	18.34	2.16	8.54	1.38	9.43	1.58	12.00	1.45
Ga69	6.43	0.55	6.16	0.73	2.41	0.28	5.93	0.50	5.82	0.51	3.18	0.34	5.87	0.48
Rb85	0.88	0.10	0.16	0.10	0.11	0.05	0.20	0.05	0.14	0.05	-	0.06	0.08	0.02
Sr88	3.13	0.36	2.87	0.50	2.01	0.25	2.04	0.25	1.42	0.20	1.92	0.26	0.61	0.09
Y89	7.02	0.88	9.14	1.53	43.12	4.29	5.13	0.69	14.79	1.64	3.82	0.61	4.43	0.55
Zr90	17.14	2.92	26.91	5.20	18.52	3.12	2.24	0.67	35.73	5.81	34.62	5.79	11.43	1.99
Nb93	1.16	0.23	-	0.36	-	0.19	0.83	0.24	0.63	0.22	-	0.23	0.32	0.14
Cs133	-	0.02	-	0.05	-	0.02	0.04	0.02	-	0.02	-	0.02	-	0.01
Ba138	3.57	0.36	2.12	0.40	0.57	0.13	1.64	0.20	0.74	0.13	1.71	0.23	1.16	0.10
La139	1.53	0.32	2.78	0.68	1.31	0.17	0.82	0.22	-	0.13	1.75	0.26	0.20	0.09
Ce140	3.18	0.56	1.61	0.42	0.67	0.17	1.90	0.36	0.94	0.20	1.07	0.23	0.30	0.08
Pr141	0.52	0.10	0.52	0.19	0.23	0.08	0.21	0.06	0.28	0.09	0.30	0.09	0.15	0.05
Nd142	2.27	0.38	2.45	0.68	0.74	0.26	0.74	0.24	1.82	0.35	1.82	0.38	0.77	0.16
Sm152	0.99	0.35	1.08	0.55	0.99	0.28	0.38	0.18	1.14	0.34	1.86	0.41	0.56	0.16
Eu153	0.37	0.11	0.45	0.24	0.37	0.16	0.35	0.10	0.52	0.12	0.65	0.17	0.22	0.07
Gd158	1.38	0.45	3.18	1.20	2.90	0.69	0.98	0.35	2.18	0.50	1.91	0.60	0.94	0.27
Tb159	0.30	0.11	-	0.21	0.60	0.14	-	0.08	0.41	0.11	0.35	0.10	0.14	0.05
Dy164	1.18	0.40	-	0.74	5.77	0.71	0.76	0.25	1.90	0.43	1.31	0.34	1.09	0.23
Ho165	0.30	0.10	-	0.21	1.22	0.21	0.26	0.10	0.47	0.13	0.27	0.09	0.18	0.06
Er166	1.46	0.36	1.12	0.57	4.71	0.70	0.75	0.24	1.86	0.43	0.80	0.28	0.72	0.19
Tm169	0.36	0.10	0.21	0.13	0.83	0.15	0.22	0.08	0.28	0.10	0.49	0.09	0.19	0.06
Yb173	1.63	0.60	1.78	0.87	6.60	0.99	-	0.43	1.72	0.54	1.17	0.40	1.16	0.38
Lu175	0.32	0.12	0.56	0.19	0.93	0.16	0.28	0.09	0.26	0.11	-	0.09	0.14	0.06
Hf180	-	0.33	-	0.21	-	0.26	-	0.18	0.75	0.26	0.70	0.26	0.18	0.14

Continued on next page. . .

Table H.10 – continued

Element	grt5-4	1σ	grt5-5	1σ	grt5-6	1σ	grt5-7	1σ	grt5-8	1σ	grt5-9	1σ	grt5-10	1σ
Ta181	-	0.16	-	0.21	-	0.13	-	0.12	0.28	0.10	0.19	0.13	-	0.08
Pb208	0.31	0.12	-	0.17	0.31	0.19	0.17	0.09	-	0.10	0.21	0.10	-	0.07
Th232	2.24	0.24	2.49	0.41	9.75	1.19	3.48	0.30	1.98	0.20	44.30	2.72	1.55	0.13
U238	0.09	0.02	0.06	0.03	-	0.05	0.08	0.02	-	0.02	-	0.02	0.03	0.01

Table H.11: Trace element compositions of Victor G9 xenocrysts - 11

Element	grt5-11	1σ	grt5-12	1σ	grt5-13	1σ	grt5-14	1σ	grt5-15	1σ	grt5-16	1σ	grt5-17	1σ
Li7	0.34	0.10	0.24	0.14	-	0.09	0.26	0.08	-	0.09	-	0.11	-	0.09
Sc45	96.79	5.50	254.23	12.38	99.52	5.77	115.18	6.68	112.29	6.61	88.75	5.42	106.69	6.43
Ti48	332.43	15.58	37.59	1.39	227.96	10.85	89.78	4.34	121.39	5.93	50.39	2.54	78.25	3.93
V51	187.96	18.84	62.34	4.00	225.76	23.05	312.37	32.43	215.32	22.84	222.83	24.14	229.41	25.33
Ni60	32.28	3.49	11.26	1.58	34.59	3.90	36.55	4.02	21.61	2.68	38.16	4.32	34.62	4.02
Co59	32.20	2.82	23.54	2.56	31.59	2.84	31.83	2.89	30.17	2.80	35.46	3.32	31.90	3.03
Zn64	9.97	1.50	6.05	1.27	12.83	1.88	10.69	1.62	11.72	1.73	13.19	2.02	9.22	1.59
Ga69	5.94	0.53	0.76	0.13	5.92	0.56	5.33	0.51	3.11	0.33	6.41	0.60	4.99	0.49
Rb85	0.12	0.05	-	0.02	-	0.05	-	0.06	0.19	0.05	0.26	0.07	-	0.05
Sr88	0.58	0.12	0.30	0.06	1.34	0.21	0.89	0.16	2.07	0.21	2.00	0.21	3.04	0.35
Y89	16.25	1.82	41.42	4.86	9.89	1.22	1.37	0.37	3.09	0.51	3.70	0.58	0.83	0.28
Zr90	56.90	9.46	71.82	6.08	20.18	3.65	5.79	1.31	31.80	5.73	0.67	0.50	14.60	2.87
Nb93	0.44	0.19	0.25	0.07	1.02	0.27	0.40	0.21	0.76	0.22	0.54	0.24	0.52	0.21
Cs133	-	0.02	0.01	0.01	-	0.02	-	0.02	-	0.02	0.08	0.02	0.06	0.02
Ba138	0.56	0.10	0.01	0.01	3.71	0.39	0.98	0.11	1.48	0.16	1.53	0.16	0.88	0.14
La139	0.39	0.13	0.10	0.03	0.50	0.18	0.33	0.15	0.60	0.18	1.17	0.19	0.26	0.12
Ce140	0.17	0.08	0.51	0.07	0.85	0.21	0.99	0.23	1.04	0.24	1.11	0.20	0.29	0.10
Pr141	0.23	0.06	0.28	0.04	0.30	0.08	-	0.10	0.30	0.09	-	0.07	0.25	0.06
Nd142	1.02	0.24	1.64	0.21	1.25	0.27	0.92	0.29	2.38	0.38	0.70	0.21	1.03	0.26
Sm152	1.19	0.30	2.30	0.32	0.81	0.29	-	0.25	2.17	0.40	0.92	0.26	1.11	0.30
Eu153	0.55	0.12	1.21	0.18	0.31	0.13	-	0.09	0.58	0.16	-	0.10	0.37	0.11
Gd158	2.11	0.52	5.55	0.95	2.21	0.54	0.79	0.36	1.25	0.47	-	0.42	0.88	0.46
Tb159	0.33	0.12	1.35	0.22	0.17	0.10	0.16	0.06	0.45	0.10	-	0.10	-	0.08
Dy164	3.10	0.46	8.97	1.31	1.78	0.41	-	0.23	1.68	0.36	0.87	0.32	0.59	0.26
Ho165	0.73	0.12	1.65	0.23	0.43	0.11	-	0.10	0.41	0.11	0.29	0.10	-	0.08
Er166	1.68	0.36	3.47	0.58	1.29	0.38	-	0.26	-	0.28	0.71	0.31	-	0.22
Tm169	0.24	0.10	0.30	0.06	0.30	0.10	-	0.08	0.19	0.07	0.17	0.08	-	0.08
Yb173	1.29	0.51	1.34	0.26	1.54	0.53	0.92	0.39	-	0.48	1.14	0.47	0.91	0.42
Lu175	0.27	0.09	0.23	0.04	0.33	0.10	0.30	0.07	0.27	0.09	-	0.10	0.21	0.08
Hf180	1.26	0.29	0.66	0.12	0.91	0.27	0.65	0.23	0.68	0.24	0.40	0.24	-	0.26

Continued on next page...

Table H.11 – continued

Element	grt5-11	1σ	grt5-12	1σ	grt5-13	1σ	grt5-14	1σ	grt5-15	1σ	grt5-16	1σ	grt5-17	1σ
Ta181	-	0.10	-	0.03	-	0.14	-	0.14	-	0.12	-	0.15	-	0.11
Pb208	-	0.08	0.03	0.01	-	0.09	-	0.10	0.26	0.09	-	0.24	-	0.08
Th232	0.42	0.08	-	0.01	0.85	0.13	2.90	0.23	4.56	0.27	2.69	0.86	0.72	0.14
U238	0.02	0.02	0.02	-	-	0.02	-	0.02	0.05	0.02	-	0.04	0.04	0.01

Table H.12: Trace element compositions of Victor G9 xenocrysts- 12

Element	grt5-18	1σ	grt5-19	1σ	grt5-20	1σ	grt5-21	1σ	grt5-22	1σ	grt5-23	1σ	grt5-24	1σ
Li7	0.17	0.10	-	0.09	0.47	0.19	0.11	0.11	-	0.11	-	0.10	-	0.10
Sc45	123.45	6.16	99.16	6.11	77.51	3.98	140.27	7.12	129.10	6.66	76.38	5.28	95.47	6.11
Ti48	59.25	2.18	55.01	2.82	63.69	2.37	95.81	3.56	110.54	4.13	246.78	12.88	202.00	10.51
V51	118.73	7.68	220.35	24.86	71.91	4.73	273.50	18.11	226.11	15.19	177.51	20.69	190.25	22.45
Ni60	15.21	2.11	35.71	4.16	5.49	0.87	31.54	4.39	30.54	4.35	24.98	3.84	28.40	3.59
Co59	23.80	2.64	31.87	3.08	22.48	2.54	23.13	2.66	23.21	2.73	30.13	3.23	30.30	3.06
Zn64	15.26	3.14	8.54	1.53	16.88	3.56	13.28	2.90	14.39	3.23	9.99	1.93	10.48	1.82
Ga69	2.90	0.36	6.10	0.58	6.00	0.74	4.15	0.52	4.59	0.59	8.11	0.88	4.95	0.52
Rb85	0.09	0.02	0.22	0.05	0.22	0.04	0.21	0.03	0.14	0.03	-	0.06	-	0.05
Sr88	1.07	0.16	1.59	0.22	1.04	0.16	1.49	0.21	0.85	0.13	1.42	0.45	3.48	0.41
Y89	5.61	0.73	5.43	0.78	45.49	5.59	4.63	0.63	3.08	0.44	15.87	2.24	6.76	0.99
Zr90	29.37	2.64	3.57	0.93	17.36	1.67	40.24	3.65	10.26	1.06	32.08	6.63	26.32	5.28
Nb93	0.36	0.08	-	0.24	0.12	0.05	1.22	0.19	0.76	0.13	0.98	0.44	0.51	0.24
Cs133	0.02	0.01	-	0.02	0.02	0.01	-	0.01	0.03	0.01	-	0.03	0.11	0.03
Ba138	0.86	0.13	0.67	0.13	2.81	0.41	1.59	0.24	0.97	0.16	1.11	0.21	1.13	0.24
La139	0.30	0.06	0.36	0.17	0.39	0.08	0.57	0.09	0.30	0.05	-	0.19	0.42	0.23
Ce140	2.24	0.24	0.55	0.15	1.64	0.18	3.59	0.38	1.59	0.18	0.48	0.16	0.79	0.25
Pr141	0.58	0.07	-	0.06	0.19	0.03	0.76	0.09	0.33	0.05	-	0.08	-	0.10
Nd142	3.39	0.38	0.58	0.22	0.83	0.13	4.17	0.46	1.67	0.21	0.68	0.29	1.18	0.38
Sm152	1.56	0.24	-	0.25	0.75	0.15	1.70	0.25	0.85	0.16	0.81	0.28	0.84	0.33
Eu153	0.45	0.08	0.15	0.08	0.44	0.09	0.46	0.09	0.24	0.06	0.58	0.19	-	0.15
Gd158	2.00	0.41	0.82	0.42	3.21	0.61	1.42	0.31	0.98	0.25	1.66	0.72	0.95	0.49
Tb159	0.26	0.06	0.17	0.08	0.76	0.14	0.17	0.04	0.11	0.04	0.37	0.17	0.33	0.11
Dy164	1.20	0.24	0.69	0.26	7.38	1.14	0.83	0.19	0.62	0.16	1.70	0.53	1.43	0.39
Ho165	0.22	0.05	0.33	0.09	1.63	0.23	0.18	0.04	0.08	0.04	0.61	0.16	0.39	0.12
Er166	0.65	0.16	1.02	0.30	5.06	0.86	0.53	0.14	0.36	0.12	1.59	0.51	0.86	0.31
Tm169	0.11	0.04	0.15	0.09	0.76	0.11	-	0.03	0.09	0.03	0.46	0.11	0.31	0.10
Yb173	0.84	0.20	1.31	0.43	5.00	0.62	0.37	0.14	0.57	0.22	1.91	0.74	-	0.52
Lu175	0.15	0.04	0.28	0.09	0.81	0.10	0.12	0.03	0.15	0.03	0.40	0.15	0.27	0.10
Hf180	0.47	0.11	-	0.22	0.19	0.08	0.68	0.13	0.29	0.09	0.61	0.29	0.74	0.25

Continued on next page...

Table H.12 – continued

Element	grt5-18	1σ	grt5-19	1σ	grt5-20	1σ	grt5-21	1σ	grt5-22	1σ	grt5-23	1σ	grt5-24	1σ
Ta181	-	0.04	-	0.11	-	0.04	0.11	0.03	0.12	0.04	-	0.11	-	0.14
Pb208	0.07	0.01	-	0.09	0.22	0.03	0.09	0.02	0.07	0.01	0.23	0.11	-	0.11
Th232	0.29	0.03	8.44	0.65	0.11	0.02	0.22	0.03	0.07	0.02	1.03	0.49	4.06	0.38
U238	0.10	0.01	0.04	0.02	0.03	0.01	0.07	0.01	0.04	0.01	0.04	0.02	-	0.02

Table H.13: Trace element compositions of Victor G9 xenocrysts - 13

Element	grt5-25	1σ	grt5-26	1σ	grt5-27	1σ	grt5-28	1σ	grt5-29	1σ	grt5-30	1σ	grt5-31	1σ
Li7	-	0.08	-	0.07	-	0.09	-	0.08	0.16	0.10	0.32	0.11	-	0.10
Sc45	97.57	6.29	103.98	6.73	103.01	6.81	86.26	5.87	88.62	6.14	79.82	5.68	106.20	7.54
Ti48	93.71	4.96	183.90	9.81	125.86	6.84	65.70	3.66	182.98	10.27	89.46	5.13	138.03	7.99
V51	273.90	33.00	221.70	27.32	198.23	25.03	209.76	27.12	173.98	23.05	117.30	15.95	191.33	26.58
Ni60	38.87	4.68	33.24	4.12	27.58	3.56	36.06	4.64	26.05	3.56	6.58	1.46	24.83	3.56
Co59	33.95	3.45	30.76	3.17	31.18	3.29	34.16	3.67	30.44	3.35	32.19	3.61	31.54	3.60
Zn64	13.47	2.17	14.50	2.24	9.41	1.71	9.32	1.81	8.20	1.83	14.33	2.56	10.01	2.03
Ga69	7.60	0.74	6.05	0.60	5.55	0.58	6.85	0.71	6.12	0.66	7.22	0.77	6.24	0.69
Rb85	0.53	0.07	-	0.05	0.11	0.05	0.22	0.06	0.17	0.05	-	0.06	0.14	0.05
Sr88	3.42	0.42	2.60	0.32	1.72	0.25	0.46	0.18	3.54	0.43	2.13	0.31	2.11	0.32
Y89	5.43	0.82	10.25	1.40	8.82	1.25	8.44	1.24	16.84	2.34	47.46	6.44	12.74	1.90
Zr90	9.30	2.11	19.19	4.03	41.92	8.69	-	0.55	40.70	8.84	14.38	3.40	31.70	7.25
Nb93	0.51	0.20	0.96	0.24	0.62	0.26	0.48	0.22	1.05	0.26	0.28	0.25	0.56	0.23
Cs133	0.03	0.02	0.02	0.02	-	0.02	0.04	0.02	0.05	0.02	0.04	0.02	-	0.02
Ba138	1.41	0.16	1.67	0.23	1.08	0.17	0.32	0.08	0.87	0.13	0.73	0.15	1.05	0.26
La139	-	0.17	0.36	0.12	-	0.11	-	0.14	0.57	0.19	0.33	0.15	0.25	0.19
Ce140	0.62	0.18	0.74	0.20	0.70	0.20	0.40	0.13	0.43	0.14	0.37	0.13	0.75	0.25
Pr141	0.19	0.08	0.13	0.06	-	0.08	0.15	0.07	0.16	0.07	-	0.06	0.23	0.09
Nd142	0.90	0.26	0.98	0.26	1.66	0.35	0.52	0.19	0.98	0.26	-	0.19	1.16	0.32
Sm152	0.94	0.28	0.91	0.26	1.44	0.35	0.91	0.20	1.19	0.32	0.89	0.29	1.01	0.36
Eu153	0.37	0.13	0.29	0.11	0.44	0.12	-	0.09	0.50	0.13	0.48	0.15	0.37	0.13
Gd158	0.67	0.38	1.31	0.43	1.59	0.51	-	0.41	1.66	0.62	2.07	0.62	1.36	0.50
Tb159	-	0.10	0.26	0.09	0.28	0.10	0.26	0.10	0.56	0.11	0.72	0.15	0.28	0.10
Dy164	-	0.38	1.67	0.36	1.54	0.35	1.14	0.33	2.67	0.47	5.82	0.75	2.10	0.43
Ho165	0.28	0.11	0.47	0.11	0.33	0.10	0.41	0.12	0.60	0.14	1.92	0.25	0.52	0.13
Er166	-	0.34	0.90	0.31	1.09	0.31	1.18	0.37	1.51	0.38	4.40	0.74	1.32	0.39
Tm169	-	0.09	0.25	0.08	0.22	0.08	0.29	0.11	0.24	0.10	0.59	0.13	0.25	0.09
Yb173	0.94	0.49	1.84	0.54	1.42	0.39	1.75	0.51	2.09	0.56	6.24	1.02	1.03	0.57
Lu175	0.20	0.09	0.25	0.08	0.29	0.09	0.27	0.09	0.38	0.12	0.70	0.14	0.30	0.10
Hf180	-	0.24	0.67	0.24	0.62	0.23	0.35	0.19	0.92	0.23	0.79	0.24	0.64	0.27

Continued on next page...

Table H.13 – continued

Element	grt5-25	1σ	grt5-26	1σ	grt5-27	1σ	grt5-28	1σ	grt5-29	1σ	grt5-30	1σ	grt5-31	1σ
Ta181	0.21	0.14	0.18	0.10	-	0.11	0.22	0.10	-	0.10	-	0.14	-	0.12
Pb208	-	0.09	-	0.08	-	0.08	0.33	0.09	-	0.10	-	0.09	-	0.10
Th232	0.55	0.15	0.54	0.12	0.45	0.09	1.81	0.16	1.20	0.17	2.53	0.27	1.84	0.22
U238	-	0.02	0.03	0.01	0.03	0.01	0.05	0.02	0.04	0.02	0.03	0.02	0.05	0.02

Table H.14: Trace element compositions of Victor clinopyroxene xenocrysts - 1

Element	cpx1-2	1σ	cpx1-3	1σ	cpx1-4	1σ	cpx1-8	1σ	cpx1-9	1σ	cpx1-12	1σ	cpx1-20	1σ
Li7	0.13	0.04	0.15	0.04	0.15	0.04	0.14	0.04	0.12	0.04	0.21	0.05	0.14	0.05
Sc45	6.30	0.77	6.45	0.82	6.67	0.88	6.67	0.91	7.05	0.99	7.48	1.08	7.08	1.07
Ti48	266.76	10.81	265.59	10.77	227.76	9.25	227.86	9.27	223.87	9.14	259.68	10.62	225.96	9.29
V51	352.68	28.35	352.97	28.40	336.10	27.11	339.28	27.46	335.87	27.33	342.68	28.05	313.84	25.91
Ni60	71.49	8.56	74.64	9.20	80.86	10.28	81.61	10.71	83.84	11.39	71.89	10.17	78.29	11.44
Co59	14.59	1.59	11.88	1.33	11.16	1.28	11.18	1.31	10.70	1.28	10.82	1.33	11.22	1.42
Zn64	7.12	0.89	8.18	1.06	9.69	1.30	8.23	1.16	8.40	1.20	7.85	1.15	11.59	1.68
Ga69	3.62	0.33	3.54	0.33	3.07	0.30	3.22	0.32	3.02	0.31	4.01	0.40	3.14	0.33
Rb85	-	0.17	-	0.17	-	0.16	-	0.13	0.32	0.13	-	0.11	0.26	0.11
Sr88	91.09	4.97	91.77	5.03	107.71	5.94	112.94	6.26	113.63	6.35	98.26	5.53	104.66	5.95
Y89	2.93	0.29	3.03	0.31	2.95	0.31	2.72	0.27	2.15	0.25	2.72	0.25	2.42	0.25
Zr90	16.42	1.36	16.24	1.35	10.96	1.04	12.01	1.08	10.82	1.00	14.56	1.18	11.31	1.00
Nb93	0.16	0.08	0.28	0.08	0.38	0.11	0.37	0.14	0.20	0.09	0.30	0.08	0.20	0.08
Cs133	-	0.01	-	0.01	0.05	0.02	0.01	0.01	0.02	0.01	0.01	0.01	0.03	0.01
Ba138	0.79	0.08	2.17	0.18	3.19	0.31	0.99	0.26	3.13	0.25	2.25	0.20	3.11	0.26
La139	2.79	0.30	3.59	0.36	4.30	0.46	2.74	0.33	3.14	0.31	1.72	0.20	2.99	0.30
Ce140	6.94	0.64	9.08	0.80	12.35	0.99	9.70	0.96	9.06	0.78	5.88	0.52	6.57	0.58
Pr141	0.95	0.11	1.43	0.15	1.38	0.17	1.26	0.14	1.55	0.16	0.83	0.09	1.03	0.11
Nd142	5.41	0.59	6.05	0.65	6.63	0.83	6.39	0.69	6.73	0.71	4.66	0.50	5.07	0.55
Sm152	0.99	0.16	1.30	0.20	1.40	0.22	1.05	0.17	1.22	0.19	1.06	0.17	1.07	0.17
Eu153	0.32	0.06	0.30	0.05	0.25	0.06	0.30	0.06	0.20	0.06	0.28	0.05	0.33	0.06
Gd158	0.63	0.14	0.51	0.13	0.66	0.18	0.64	0.15	0.74	0.17	0.66	0.14	0.63	0.16
Tb159	0.13	0.04	0.11	0.03	0.12	0.04	0.08	0.04	0.20	0.05	0.10	0.03	0.13	0.04
Dy164	0.63	0.13	0.71	0.13	0.54	0.13	0.65	0.13	0.45	0.13	0.60	0.13	0.45	0.12
Ho165	0.13	0.03	0.12	0.04	0.09	0.03	0.09	0.03	0.10	0.03	0.14	0.03	0.11	0.03
Er166	0.18	0.06	0.20	0.08	0.29	0.08	0.39	0.09	0.28	0.09	0.20	0.06	0.28	0.08
Tm169	0.05	0.02	-	0.02	0.07	0.03	-	0.03	-	0.03	0.06	0.02	-	0.03
Yb173	0.10	0.06	-	0.10	0.26	0.10	0.09	0.08	0.26	0.09	0.18	0.10	0.48	0.08
Lu175	-	0.02	-	0.02	-	0.03	-	0.02	0.05	0.02	-	0.02	-	0.02

Continued on next page. . .

Table H.14 – continued

Element	cpx1-2	1σ	cpx1-3	1σ	cpx1-4	1σ	cpx1-8	1σ	cpx1-9	1σ	cpx1-12	1σ	cpx1-20	1σ
Hf180	0.90	0.15	0.87	0.14	0.72	0.14	0.72	0.13	0.74	0.15	0.92	0.15	0.74	0.13
Ta181	0.09	0.03	0.07	0.03	0.10	0.03	0.06	0.04	0.06	0.04	-	0.03	-	0.02
Pb208	0.11	0.02	0.18	0.02	0.28	0.04	0.09	0.02	0.14	0.03	0.14	0.02	0.10	0.03
Th232	1.51	0.12	7.19	0.39	2.88	0.19	3.99	0.24	0.49	0.06	0.21	0.04	1.11	0.16
U238	0.01	0.01	0.03	0.01	0.03	0.02	0.02	0.01	-	0.01	-	-	0.03	0.02

Table H.15: Trace element compositions of Victor clinopyroxene xenocrysts - 2

Element	cpx1-21	1σ	cpx2-2	1σ	cpx2-6	1σ	cpx2-8	1σ	cpx2-14	1σ	cpx2-21	1σ	cpx3-14	1σ
Li7	0.14	0.05	0.14	0.05	0.20	0.06	0.18	0.05	0.22	0.07	0.21	0.06	0.24	0.08
Sc45	7.78	1.23	7.51	1.24	8.22	1.42	8.29	1.50	8.73	1.66	8.42	1.69	9.73	2.06
Ti48	259.70	10.73	226.23	9.40	254.04	10.62	224.23	9.44	186.51	7.91	234.94	10.03	252.28	10.86
V51	339.57	28.28	312.05	26.25	323.91	27.53	308.63	26.55	302.95	26.38	292.99	25.84	311.93	27.88
Ni60	80.63	12.26	82.88	13.13	79.20	13.09	92.47	16.01	93.09	16.88	104.42	19.90	102.23	20.51
Co59	11.94	1.55	11.68	1.56	11.73	1.61	11.88	1.69	13.04	1.91	12.97	1.97	14.49	2.27
Zn64	9.93	1.50	9.24	1.45	8.75	1.41	11.08	1.84	9.84	1.69	13.25	2.33	11.97	2.20
Ga69	4.04	0.43	3.37	0.37	4.09	0.45	3.84	0.44	3.47	0.41	4.23	0.51	4.27	0.53
Rb85	0.42	0.11	0.89	0.16	-	0.12	-	0.13	0.38	0.11	0.57	0.13	-	0.22
Sr88	104.11	5.98	105.92	6.16	99.67	5.85	95.53	5.69	74.83	4.53	95.54	5.84	94.77	5.89
Y89	2.98	0.28	2.31	0.25	2.66	0.26	2.61	0.25	2.08	0.22	2.83	0.25	2.32	0.28
Zr90	14.62	1.19	11.40	0.97	13.40	1.06	12.21	1.02	8.17	0.74	12.74	1.02	12.56	1.06
Nb93	0.13	0.07	0.19	0.07	0.20	0.09	0.25	0.07	0.31	0.08	0.27	0.09	-	0.06
Cs133	0.02	0.01	-	0.01	-	0.01	-	0.01	-	0.01	0.01	0.01	-	0.01
Ba138	0.86	0.09	0.70	0.08	0.79	0.08	1.54	0.14	1.36	0.14	2.97	0.25	2.16	0.20
La139	1.60	0.19	2.65	0.26	2.06	0.21	2.33	0.24	2.15	0.22	2.85	0.27	1.67	0.19
Ce140	5.30	0.47	6.29	0.55	5.37	0.47	6.90	0.61	7.42	0.65	7.94	0.70	4.55	0.42
Pr141	0.85	0.10	1.00	0.11	0.84	0.09	1.05	0.11	1.12	0.12	1.00	0.11	0.88	0.10
Nd142	3.97	0.44	4.67	0.51	4.54	0.49	5.23	0.56	5.63	0.60	5.16	0.56	3.98	0.45
Sm152	0.91	0.16	1.06	0.18	0.91	0.15	1.23	0.19	1.11	0.18	1.15	0.18	1.11	0.18
Eu153	0.27	0.06	0.27	0.05	0.21	0.05	0.26	0.06	0.29	0.06	0.35	0.06	0.32	0.07
Gd158	0.63	0.16	0.72	0.16	0.80	0.18	0.86	0.18	0.81	0.17	0.94	0.21	0.77	0.19
Tb159	0.14	0.04	0.13	0.03	0.16	0.04	0.10	0.04	0.13	0.03	0.16	0.03	0.12	0.03
Dy164	0.63	0.13	0.64	0.13	0.49	0.12	0.56	0.12	0.51	0.12	0.73	0.12	0.49	0.13
Ho165	0.14	0.03	0.12	0.03	0.15	0.03	0.12	0.03	0.13	0.03	0.13	0.03	0.15	0.04
Er166	0.28	0.08	0.24	0.08	0.38	0.08	0.27	0.07	0.17	0.06	0.19	0.07	0.26	0.08
Tm169	-	0.03	-	0.02	-	0.02	0.06	0.02	0.03	0.02	-	0.02	0.06	0.03
Yb173	0.22	0.09	0.38	0.10	-	0.10	0.21	0.08	0.18	0.07	0.20	0.09	0.20	0.07
Lu175	0.06	0.02	0.02	0.02	0.04	0.02	0.04	0.02	0.05	0.02	0.06	0.02	-	0.02

Continued on next page...

Table H.15 – continued

Element	cpx1-21	1σ	cpx2-2	1σ	cpx2-6	1σ	cpx2-8	1σ	cpx2-14	1σ	cpx2-21	1σ	cpx3-14	1σ
Hf180	0.96	0.15	0.70	0.12	0.88	0.13	0.76	0.12	0.44	0.09	0.72	0.12	0.89	0.14
Ta181	0.08	0.03	0.05	0.02	0.05	0.03	0.09	0.04	-	0.03	0.06	0.03	-	0.03
Pb208	0.16	0.02	0.12	0.02	0.18	0.03	0.11	0.04	0.10	0.02	0.24	0.03	0.12	0.03
Th232	0.38	0.04	1.84	0.12	2.90	0.22	21.33	0.77	0.09	0.02	15.72	0.76	4.84	0.27
U238	-	-	0.01	0.01	0.01	0.01	0.02	0.01	0.01	-	0.03	0.01	0.01	-

Table H.16: Trace element compositions of Victor clinopyroxene xenocrysts - 3

Element	cpx3-19	1σ	cpx3-24	1σ	cpx3-25	1σ	cpx3-28	1σ	cpx4-3	1σ	cpx4-4	1σ	cpx4-7	1σ
Li7	0.31	0.09	0.22	0.08	0.22	0.09	0.36	0.12	0.28	0.09	0.25	0.08	0.34	0.08
Sc45	8.10	1.83	9.71	2.33	9.61	2.46	11.05	3.01	26.26	1.99	26.13	1.99	27.07	2.09
Ti48	195.25	8.47	232.52	10.17	213.77	9.44	225.48	10.04	233.33	13.55	224.97	13.28	233.33	14.00
V51	269.64	24.44	299.18	27.49	262.26	24.45	287.08	27.14	253.72	35.97	260.33	37.82	260.81	38.81
Ni60	152.38	32.24	111.49	24.96	146.92	34.79	117.03	29.48	154.85	19.26	180.07	22.81	171.22	22.18
Co59	15.93	2.59	14.22	2.40	15.75	2.76	14.41	2.62	15.35	1.78	17.34	2.03	16.33	1.96
Zn64	13.06	2.50	10.35	2.11	13.18	2.77	10.81	2.39	14.00	2.32	18.11	2.99	17.30	2.96
Ga69	3.99	0.51	4.00	0.53	4.37	0.60	3.99	0.57	4.73	0.51	5.02	0.54	5.45	0.60
Rb85	-	0.17	-	0.14	-	0.15	-	0.13	0.16	0.04	0.29	0.04	0.11	0.03
Sr88	112.89	7.10	100.48	6.42	107.92	7.01	99.27	6.55	111.63	11.64	114.04	12.11	118.06	12.78
Y89	2.77	0.26	2.59	0.25	3.31	0.30	2.37	0.24	2.88	0.48	2.64	0.45	2.84	0.48
Zr90	7.35	0.68	11.38	0.96	9.48	0.84	11.52	0.95	12.79	3.02	12.43	2.97	12.60	3.07
Nb93	0.22	0.09	0.35	0.06	0.12	0.06	0.26	0.08	0.38	0.13	0.30	0.12	0.27	0.12
Cs133	0.02	0.01	-	0.01	-	0.01	-	0.01	0.03	0.01	0.08	0.01	0.06	0.01
Ba138	0.90	0.09	0.86	0.09	1.01	0.11	0.96	0.11	1.64	0.21	2.38	0.30	0.96	0.14
La139	1.29	0.15	1.34	0.15	1.37	0.16	1.51	0.17	2.40	0.56	2.81	0.65	1.45	0.37
Ce140	4.71	0.44	4.44	0.41	4.33	0.41	4.87	0.46	6.12	1.57	6.10	1.60	4.53	1.23
Pr141	0.81	0.09	0.93	0.10	0.69	0.08	0.83	0.09	0.97	0.19	0.82	0.16	0.92	0.18
Nd142	4.12	0.46	4.23	0.48	4.00	0.46	4.22	0.48	4.45	0.67	4.08	0.63	3.95	0.62
Sm152	1.04	0.17	1.05	0.17	1.22	0.20	1.01	0.17	1.08	0.22	0.92	0.21	1.07	0.21
Eu153	0.40	0.07	0.33	0.07	0.35	0.07	0.29	0.06	0.29	0.09	0.23	0.07	0.41	0.08
Gd158	0.90	0.20	0.71	0.19	0.77	0.20	1.04	0.23	1.43	0.37	0.98	0.26	1.00	0.28
Tb159	0.13	0.03	0.15	0.04	0.11	0.04	0.13	0.04	0.15	0.06	0.19	0.06	0.16	0.05
Dy164	0.64	0.13	0.63	0.14	0.93	0.15	0.82	0.13	0.72	0.21	0.45	0.18	0.72	0.19
Ho165	0.12	0.03	0.12	0.04	0.16	0.04	0.11	0.03	0.17	0.06	-	0.05	0.19	0.06
Er166	0.24	0.07	0.24	0.08	0.24	0.08	0.27	0.09	-	0.15	0.35	0.14	0.33	0.13
Tm169	0.05	0.02	0.07	0.02	0.06	0.03	0.06	0.02	0.07	0.05	0.11	0.04	-	0.04
Yb173	0.21	0.10	0.21	0.10	-	0.11	0.19	0.08	-	0.23	-	0.21	0.42	0.15
Lu175	0.02	0.01	-	0.02	0.03	0.02	0.02	0.02	-	0.05	-	0.04	-	0.03

Continued on next page...

Table H.16 – continued

Element	cpx3-19	1σ	cpx3-24	1σ	cpx3-25	1σ	cpx3-28	1σ	cpx4-3	1σ	cpx4-4	1σ	cpx4-7	1σ
Hf180	0.52	0.10	0.64	0.12	0.74	0.12	0.84	0.13	0.91	0.20	0.71	0.19	0.92	0.20
Ta181	-	0.02	-	0.03	0.06	0.03	0.03	0.02	-	0.07	0.13	0.06	-	0.08
Pb208	0.20	0.03	0.16	0.03	0.14	0.03	0.20	0.03	0.32	0.06	0.30	0.06	0.13	0.06
Th232	5.40	0.29	2.50	0.15	0.44	0.05	1.82	0.13	6.68	0.56	2.13	0.20	3.76	0.34
U238	0.02	0.01	0.01	0.01	0.02	0.01	-	0.01	0.01	0.01	0.05	0.01	0.02	0.01

Table H.17: Trace element compositions of Victor clinopyroxene xenocrysts - 4

Element	cpx4-8	1σ	cpx4-9	1σ	cpx4-12	1σ	cpx4-15	1σ	cpx4-16	1σ	cpx4-17	1σ	cpx4-21	1σ
Li7	0.35	0.09	0.16	0.07	0.33	0.09	0.25	0.07	0.28	0.08	0.37	0.09	0.50	0.10
Sc45	27.42	2.16	27.58	2.21	28.08	2.28	28.35	2.33	26.32	2.24	28.07	2.41	29.35	2.57
Ti48	226.01	13.79	238.33	14.78	235.48	14.85	235.82	15.12	211.12	13.77	233.04	15.45	237.12	15.99
V51	274.54	41.87	286.68	44.79	270.99	43.38	273.59	44.88	267.19	44.91	266.63	45.89	284.51	50.20
Ni60	194.21	25.68	164.74	22.28	172.46	23.83	169.42	23.90	185.38	26.72	163.81	24.14	180.49	27.16
Co59	18.86	2.29	16.12	2.01	15.72	2.00	15.67	2.03	15.52	2.05	15.16	2.04	16.89	2.31
Zn64	27.49	4.71	17.90	3.22	15.56	2.92	19.32	3.66	18.67	3.68	20.52	4.15	18.33	3.84
Ga69	5.66	0.63	5.20	0.59	5.41	0.63	5.61	0.66	5.20	0.63	5.15	0.64	5.88	0.74
Rb85	0.31	0.05	0.30	0.05	-	0.03	0.18	0.03	0.16	0.04	0.08	0.03	0.09	0.03
Sr88	115.11	12.71	108.99	12.26	115.84	13.28	112.26	13.11	114.93	13.67	113.10	13.70	118.82	14.66
Y89	2.61	0.45	2.71	0.47	2.96	0.52	2.50	0.46	2.39	0.45	2.73	0.51	2.62	0.51
Zr90	12.26	3.06	15.12	3.82	13.23	3.43	11.21	2.98	10.68	2.91	13.94	3.84	12.84	3.63
Nb93	0.46	0.14	0.54	0.17	0.32	0.12	0.38	0.11	-	0.14	0.44	0.13	0.31	0.15
Cs133	0.05	0.02	-	0.01	-	0.01	-	0.01	-	0.01	0.02	0.01	-	0.01
Ba138	2.43	0.31	0.82	0.13	0.47	0.07	8.52	1.09	1.16	0.18	1.28	0.19	0.31	0.07
La139	2.05	0.52	1.74	0.45	1.22	0.33	1.62	0.43	1.29	0.37	1.47	0.42	1.52	0.44
Ce140	7.10	1.96	4.26	1.21	4.35	1.27	5.13	1.53	4.10	1.26	4.83	1.51	4.81	1.55
Pr141	0.95	0.19	0.79	0.17	0.81	0.17	0.85	0.18	0.85	0.19	0.84	0.19	0.94	0.21
Nd142	5.11	0.80	4.17	0.68	3.86	0.64	4.35	0.72	3.15	0.56	3.84	0.68	4.05	0.73
Sm152	1.03	0.22	1.35	0.22	1.03	0.22	1.19	0.23	1.08	0.23	0.92	0.22	1.06	0.23
Eu153	0.42	0.09	0.45	0.08	0.37	0.08	0.33	0.07	0.36	0.08	0.27	0.08	0.32	0.09
Gd158	1.29	0.33	1.05	0.29	1.40	0.34	1.17	0.33	1.29	0.34	0.88	0.30	1.34	0.32
Tb159	0.14	0.05	0.16	0.05	0.16	0.05	0.17	0.05	0.17	0.05	0.21	0.06	0.15	0.05
Dy164	0.68	0.19	0.83	0.20	0.70	0.16	0.67	0.17	0.55	0.16	1.03	0.21	0.80	0.22
Ho165	0.18	0.05	0.16	0.05	0.14	0.05	0.16	0.05	0.11	0.05	0.16	0.05	0.14	0.06
Er166	0.30	0.13	-	0.15	0.31	0.17	0.37	0.12	-	0.13	0.48	0.15	-	0.14
Tm169	-	0.05	0.07	0.05	0.09	0.04	0.07	0.04	-	0.04	-	0.04	-	0.05
Yb173	-	0.22	-	0.20	-	0.25	-	0.18	0.35	0.21	0.43	0.19	0.40	0.17
Lu175	0.05	0.04	0.05	0.04	0.06	0.03	0.07	0.04	0.04	0.04	-	0.04	-	0.04

Continued on next page...

Table H.17 – continued

Element	cpx4-8	1σ	cpx4-9	1σ	cpx4-12	1σ	cpx4-15	1σ	cpx4-16	1σ	cpx4-17	1σ	cpx4-21	1σ
Hf180	0.59	0.16	0.79	0.19	0.73	0.18	0.78	0.18	0.60	0.17	0.86	0.19	0.88	0.19
Ta181	-	0.07	0.17	0.06	-	0.07	0.11	0.04	-	0.07	-	0.06	-	0.08
Pb208	0.30	0.06	0.25	0.06	0.25	0.05	0.17	0.05	0.17	0.05	0.21	0.05	0.28	0.06
Th232	2.47	0.24	3.83	0.35	1.55	0.08	0.24	0.05	0.54	0.08	1.07	0.13	4.11	0.41
U238	0.04	0.01	0.07	0.01	-	0.01	-	0.01	-	0.01	0.02	0.01	-	0.01

Table H.18: Trace element compositions of Victor clinopyroxene xenocrysts - 5

Element	cpx4-25	1σ	cpx4-29	1σ	cpx4-31	1σ	cpx4-33	1σ	cpx4-38	1σ
Li7	0.27	0.09	0.29	0.09	0.33	0.10	0.21	0.08	0.42	0.09
Sc45	28.21	2.51	28.78	2.65	29.58	2.73	27.97	2.65	30.06	2.86
Ti48	239.87	16.44	240.21	16.75	227.18	16.10	231.25	16.65	233.71	17.11
V51	300.14	54.24	292.84	54.23	274.15	51.99	275.40	53.50	283.93	56.48
Ni60	164.95	25.36	178.72	28.10	173.34	27.78	176.20	28.83	183.30	30.59
Co59	16.12	2.25	17.01	2.43	15.26	2.21	15.69	2.32	15.52	2.33
Zn64	17.83	3.85	18.27	4.10	15.55	3.62	18.34	4.36	19.01	4.65
Ga69	5.46	0.70	5.44	0.72	5.36	0.72	4.88	0.67	5.01	0.69
Rb85	-	0.02	0.18	0.03	-	0.03	0.10	0.04	-	0.03
Sr88	106.63	13.39	105.95	13.55	111.84	14.54	112.78	14.92	114.91	15.46
Y89	2.81	0.54	2.37	0.50	2.35	0.47	2.77	0.56	2.97	0.60
Zr90	13.73	3.94	12.93	3.82	13.43	4.02	13.63	4.16	13.83	4.29
Nb93	0.37	0.12	-	0.15	0.18	0.12	-	0.11	0.27	0.12
Cs133	0.04	0.01	-	0.01	-	0.02	0.02	0.01	-	0.01
Ba138	0.49	0.09	1.26	0.20	0.30	0.07	0.35	0.08	0.61	0.11
La139	1.46	0.43	1.14	0.36	1.15	0.36	1.15	0.37	1.63	0.51
Ce140	4.13	1.36	3.78	1.29	4.27	1.48	4.22	1.50	4.64	1.68
Pr141	0.79	0.19	0.82	0.20	0.71	0.18	0.60	0.16	0.91	0.22
Nd142	3.48	0.65	3.55	0.68	3.67	0.70	3.39	0.67	3.75	0.74
Sm152	0.91	0.22	1.28	0.29	0.78	0.23	0.97	0.23	1.19	0.24
Eu153	0.27	0.08	0.29	0.08	0.32	0.08	0.26	0.08	-	0.07
Gd158	1.28	0.37	1.00	0.34	0.76	0.27	1.31	0.32	0.88	0.29
Tb159	0.12	0.05	0.31	0.06	0.15	0.05	0.28	0.06	0.17	0.05
Dy164	0.66	0.18	0.65	0.20	0.73	0.20	0.90	0.23	0.53	0.18
Ho165	0.16	0.05	-	0.05	0.16	0.05	0.18	0.06	0.13	0.05
Er166	0.23	0.11	0.30	0.12	0.48	0.17	-	0.14	0.26	0.13
Tm169	-	0.04	0.11	0.04	0.07	0.03	-	0.04	-	0.04
Yb173	0.57	0.19	-	0.22	0.46	0.18	-	0.16	-	0.23
Lu175	-	0.05	0.08	0.05	-	0.04	-	0.04	-	0.03

Continued on next page...

Table H.18 – continued

Element	cpx4-25	1σ	cpx4-29	1σ	cpx4-31	1σ	cpx4-33	1σ	cpx4-38	1σ
Hf180	1.15	0.22	0.95	0.21	0.92	0.20	0.86	0.20	0.69	0.18
Ta181	-	0.07	-	0.07	-	0.06	-	0.08	-	0.06
Pb208	0.19	0.05	0.16	0.06	0.19	0.05	0.22	0.05	0.17	0.05
Th232	5.58	0.55	0.19	0.06	0.25	0.05	0.39	0.08	6.74	0.48
U238	0.02	0.01	0.02	0.01	-	0.01	0.01	0.01	0.02	0.01

Appendix I

Isotopic data for Delta xenoliths

Table I.1: Replicate digestions of GP13

Lab#	P66	P67	P69	published (Pearson et al., 2004)
Sample#	GP13	GP13	GP13	GP13
Os (ppb)	3.74	3.87	3.44	3.58
Ir (ppb)	3.46	3.46	3.14	3.28
Ru (ppb)	-	-	-	6.71
Pt (ppb)	6.39	6.07	6.00	6.65
Pd (ppb)	5.48	4.70	5.61	5.85
Re(ppb)	0.38	0.37	0.38	0.33
$^{187}Os/^{188}Os$	0.12579	0.12576	0.12669	0.1262
2SE	0.00013	0.00009	0.00043	0.002

Table I.2: Replicate analyses of the Durham Osmium Standard (DrOsS)

		$^{187}Os/^{188}Os$	2SE
Accepted Value	Luguet et al. (2008)	0.160924	0.000004
Long-term lab average	Nov 2012- Aug 2013	0.160787	0.000215
Mag 0007 F17	14 March 2013	0.160785	0.000054
Mag 0008 F1	19 March 2013	0.160725	0.000054
Mag 0013 F8	13 April 2013	0.160846	0.000086
Mag 0014 F6	20 April 2013	0.160440	0.000093

Table I.3: Re-Os isotopic compositions and PGE content of olivine from Delta peridotite xenoliths

Sample #	DEL1-01	DEL1-03	DEL1-04	DEL1-07	DEL1-10	DEL1-13
Lab #	PL1	PL2	PL3	PL4	PL5	PL6
Description	dunite	harzburgite	pyroxenite	wehrlite	harzburgite	harzburgite
Olivine Mg#	92.1	92.4	85.3	92.1	91.4	92.4
$^{187}Os/^{188}Os$	0.11812	0.10116	0.11372	0.10222	0.11700	bd
2SE (total)	0.00127	0.00369	0.00391	0.00082	0.00030	bd
$^{187}Re/^{188}Os$	2.62892	4.17808	3.41834	0.61712	0.10276	bd
2σ (total)	0.06347	0.26518	0.25408	0.04264	0.00620	bd
T_{RD} (Ga)	1.43	3.73	2.03	3.59	1.58	-
error (Ga)	0.18	0.49	0.54	0.11	0.04	-
T_{Ma} (Ga)	-0.31	-0.46	-0.32	-9.07	2.32	-
$^{187}Os/^{188}Os_{(i)}$	0.11023	0.08861	0.10345	0.10037	0.11669	-
Os (ppb)	0.727	0.175	0.089	0.143	1.168	bd
2σ	0.034	0.005	0.002	0.001	0.035	bd
Ir (ppb)	0.241	0.295	0.116	0.075	0.408	0.015
2σ	0.078	0.108	0.054	0.020	0.072	0.022
Ru (ppb)	0.986	0.760	0.277	bd	17.379	0.025
2σ	0.182	0.178	0.074	bd	1.016	0.042
Pt (ppb)	0.380	bd	0.722	0.334	6.700	bd
2σ	0.084	bd	0.120	0.038	0.400	bd
Pd (ppb)	0.422	8.769	1.694	0.185	1.322	0.049
2σ	0.188	2.018	0.760	0.074	0.308	0.032
Re (ppb)	0.399	0.148	0.064	0.018	0.035	0.116
2σ	0.150	0.046	0.022	0.006	0.010	0.046
Re/Os	0.55	0.85	0.72	0.13	0.03	-
$(Os/Ir)_N$	2.84	0.54	0.73	1.75	2.68	-
$(Pd/Ir)_N$	1.33	22.43	11.02	1.86	2.45	2.41
$(Pd/Pt)_N$	1.70	-	3.59	0.85	0.30	-
$(Re/Pd)_N$	14.15	0.25	0.56	1.46	0.39	35.89
$(Re/Os)_N$	6.61	10.53	8.58	1.55	0.36	-

Sample #	DEL1-18	DEL1-09	DEL1-14	DEL1-16	DEL1-02	DEL1-11
Lab #	PL7	PL8	PL9	PL10	P19	P20
Description	lherzolite	lherzolite	lherzolite	dunite	harzburgite	dunite
Olivine Mg#	91.7	90.1	90.1	92.7	92.7	91.2
$^{187}Os/^{188}Os$	0.10921	bd	0.11724	0.11052	0.16093	0.18213
2SE (total)	0.00069	bd	0.00100	0.00029	0.00441	0.00190
$^{187}Re/^{188}Os$	0.45858	bd	0.94299	0.12346	0.04416	0.02480
2σ (total)	0.02465	bd	0.05705	0.00621	0.00294	0.00142
T_{RD} (Ga)	2.65	-	1.55	2.47	-	-
error (Ga)	0.09	-	0.14	0.04	-	-
T_{Ma} (Ga)	-48.93	-	-1.44	3.72	-5.20	-8.51
$^{187}Os/^{188}Os_{(i)}$	0.10783	-	0.11441	0.11015	0.16080	0.18206
Os (ppb)	1.087	bd	0.505	1.440	2.294	3.524
2σ	0.035	bd	0.008	0.131	0.452	1.354
Ir (ppb)	0.744	0.014	0.507	1.854	0.025	0.273
2σ	0.170	0.034	0.168	0.278	0.018	0.080
Ru (ppb)	7.053	1.042	1.709	5.887	1.697	0.752
2σ	0.682	0.414	0.354	0.498	0.516	0.710
Pt (ppb)	3.485	bd	0.169	0.593	bd	0.194
2σ	0.350	bd	0.058	0.080	bd	0.062
Pd (ppb)	0.978	0.262	0.175	0.024	0.017	0.019
2σ	0.370	0.136	0.084	0.014	0.012	0.010
Re (ppb)	0.105	0.318	0.100	0.037	0.021	0.018
2σ	0.034	0.120	0.038	0.014	0.008	0.006
Re/Os	0.10	-	0.20	0.03	0.01	0.01
$(Os/Ir)_N$	1.38	-	0.94	0.73	87.00	12.07
$(Pd/Ir)_N$	0.99	14.61	0.26	0.01	0.53	0.05
$(Pd/Pt)_N$	0.43	-	1.59	0.06	-	0.15
$(Re/Pd)_N$	1.61	18.17	8.56	22.81	18.35	14.21
$(Re/Os)_N$	1.15	-	2.37	0.31	0.11	0.06

"bd" and "-" refers to analyses below detection or not applicable.
2SE uncertainties for $^{187}Os/^{188}Os$ include the in-run precision, the uncertainty in the concentration and isotopic composition of the blank and the uncertainty in the spike calibration.
Os concentrations determined by NTIMS. Errors include the in-run precision, uncertainty in the blank concentration and error magnification due to overspiking.
2SE uncertainties for $^{187}Re/^{188}Os$ include in in-run precision, the uncertainty in the concentration and isotopic compositions of the blanks.
PGE and Re concentrations determined by ICP-MS. Errors include the in-run precision and the uncertainty in the blank concentration.
T_{RD}, T_{MA} and γ_{Os} calculations relative to the O-chondrite reservoir ($^{187}Os/^{188}Os = 0.1283$; $^{187}Re/^{188}Os = 0.422$; Walker et al., 2002).
$^{187}Os/^{188}Os_{(i)}$ is the initial isotopic composition calculated at the time of kimberlite eruption (~180 Ma; Januszczak et al., 2013).

Appendix J

Disequilibrium evaluation in Delta and Victor xenoliths

Table J.1: Tests for disequilibrium between two pyroxenes after Grütter (2009)

Sample	Temperature (°C) Ca-in-Opx Brey and Kohler (1990) modified by Nimis and Grutter (2009) if under 900 °C using Nickel and Green (1985) pressure	Difference in Temperature Taylor (1998) - Ca-in-Opx	Disequilibrium between Pyroxenes? for samples with diff more than 90 °C
DEL1-04	815	51	no
DEL1-05	955	11	no
DEL1-09	716	73	no
DEL1-12	786	79	no
DEL1-15	789	85	no
DEL1-17	763	82	no
DEL1-18	719	-25	no
VIC0106	764	9	no
VIC0507	677	56	no
VIC1703	662	3	no
VIC2002	693	-13	no
VIC2001	704	64	no
VIC2302	637	-25	no
VIC2501	760	131	yes
VIC8401	994	36	no

Table J.2: Tests for disequilibrium between clinopyroxene and garnet after Grütter (2009)

Sample	Temperature (°C) Nimis and Grutter (2009)	Difference in Temperature Taylor (1998) - Nimis and Grutter (2009)	Disequilibrium between Cpx-Grt? for samples with diff more than 70 °C
DEL1-04	826	41	no
DEL1-05	972	-6	no
DEL1-09	733	57	no
DEL1-12	829	35	no
DEL1-15	820	54	no
DEL1-17	805	39	no
DEL1-18	688	5	no
VIC0106	752	21	no
VIC0507	717	16	no
VIC1703	671	-6	no
VIC2002	588	92	yes
VIC2001	968	-199	yes
VIC2302	636	-24	no
VIC2501	809	82	yes
VIC8401	1019	11	no

References

Carswell, D. A.: 1991, The garnet-orthopyroxene A1 barometer: problematic application to natural garnet lherzolite assemblages, *Mineralogical Magazine* **55**, 19–31.

Grütter, H. S.: 2009, Pyroxene xenocryst geotherms: Techniques and application, *Lithos* **112S**, 1167–1178.

Januszczak, N., Seller, M. H., Kurszlaukis, S., Murphy, C., Delgaty, J., Tappe, S., Ali, K., Zhu, J. and Ellemers, P.: 2013, A Multidisciplinary Approach to the Attawapiskat Kimberlite Field, Canada: Accelerating the Discovery-to-Production Pipeline, *Proceedings of the 10th International Kimberlite Conference* .

Luguet, A., Pearson, D. G., Jaques, A. L., Smith, C. B., Bulanova, G. P., Carter, G., Roffey, S., Rayner, M. J. and Lorand, J.-P.: 2008, Age constraints on the lithosphere beneath the Halls Creek mobile belt and implications for diamonds of the Argyle lamproite deposit, *9th International Kimberlite Conference Extended Abstracts* **9IKC-A-00263**.

Nickel, K. G. and Green, D. H.: 1985, Empirical geothermobarometry for garnet peridotites and implications for the nature of the lithosphere, kimberlites and diamonds., *Earth and Planetary Science Letters* **73**, 158–170.

Nimis, P. and Grütter, H.: 2009, Internally consistent geothermometers for garnet peridotites and pyroxenites, *Contributions to Mineralogy and Petrology* **159**(3), 411–427.

Pearson, D. G., Irvine, G. J., Ionov, D. A., Boyd, F. R. and Dreibus, G. E.: 2004, Re-Os isotope systematics and platinum group element fractionation during mantle melt extraction: a study of massif and xenolith peridotite suites, *Chemical Geology* **208**, 29–59.

Walker, R. J., Horan, M. F., Morgan, J. W., Becker, H., Grossman, J. N. and Rubin, A. E.: 2002, Comparative ^{187}Re-^{187}Os systematics of chondrites: Implications regarding early solar system processes, *Geochimica et Cosmochimica Acta* **66**(23), 4187–4201.